SAPIENZA
UNIVERSITÀ DI ROMA

PhD in Biochemistry

XXXII Cycle (2016/2019)

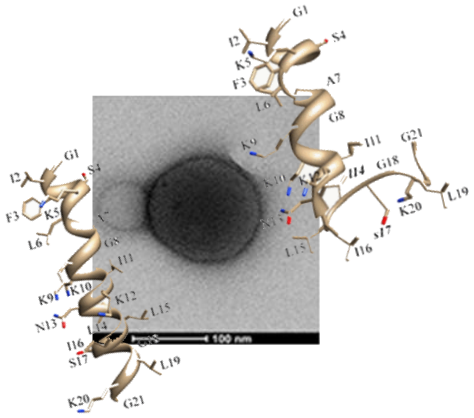

Insights into the mechanism(s) of action and therapeutic applications of Esculentin-1a-derived antimicrobial peptides

Tutor
Prof. Maria Luisa Mangoni

Coordinator
Prof. Stefano Gianni

PhD student
Maria Rosa Loffredo

To my parents

Index

List of papers relevant for this thesis

- **Loffredo MR**, Ghosh A, Harmouche N, Casciaro B, Luca V, Bortolotti A, Cappiello F, Stella L, Bhunia A, Bechinger B, Mangoni ML. **"Membrane perturbing activities and structural properties of the frog-skin derived peptide Esculentin-1a(1-21)NH_2 and its Diastereomer Esc(1-21)-1c: Correlation with their antipseudomonal and cytotoxic activity."** *Biochimica et biophysica Acta* 2017; 1859(12):2327-2339.

- Casciaro B, Lin Q, Afonin S, **Loffredo MR**, de Turris V, Middel V, Ulrich AS, Di YP, Mangoni ML. **"Inhibition of *Pseudomonas aeruginosa* biofilm formation and expression of virulence genes by selective epimerization in the peptide Esculentin-1a(1-21)NH_2."** *FEBS Journal* 2019; 286(19):3874-3891.

- Casciaro B, d'Angelo I, Zhang X, **Loffredo MR**, Conte G, Cappiello F, Quaglia F, Di YP, Ungaro F, Mangoni ML. **"Poly(lactide- co-glycolide) nanoparticles for prolonged therapeutic efficacy of Esculentin-1a-derived antimicrobial peptides against *Pseudomonas aeruginosa* lung infection: *in vitro* and *in vivo* studies."** *Biomacromolecules* 2019; 20(5):1876-1888.

- Casciaro B, Dutta D, **Loffredo MR**, Marcheggiani S, McDermott AM, Willcox MD, Mangoni ML. **"Esculentin-1a derived peptides kill *Pseudomonas aeruginosa* biofilm on soft contact lenses and retain antibacterial activity upon immobilization to the lens surface."** *Peptide Science* 2018; 110:e23074.

- Casciaro B, **Loffredo MR**, Luca V, Verrusio W, Cacciafesta M, Mangoni ML. **"Esculentin-1a derived antipseudomonal peptides: Limited induction of resistance and synergy with Aztreonam."** *Protein and peptide letters* 2018; 25(12):1155-1162.

- Casciaro B, Cappiello F, **Loffredo MR**, Ghirga F, Mangoni ML. **"The potential of frog skin peptides for anti-infective therapies: The case of Esculentin-1a(1-21)NH_2."** *Current medicinal chemistry*. 2019; In press.

List of other papers

- Casciaro B, Calcaterra A, Cappiello F, Mori M, **Loffredo MR**, Ghirga F, Mangoni ML, Botta B, Quaglio D. **"Nigritanine as a new potential antimicrobial alkaloid for the treatment of *Staphylococcus aureus*-induced infections."** *Toxins* 2019; 11(9): E511

- Merlino F, Carotenuto A, Casciaro B, Martora F, **Loffredo MR**, Di Grazia A, Yousif AM, Brancaccio D, Palomba L, Novellino E, Galdiero M, Iovene MR, Mangoni ML, Grieco P. **"Glycine-replaced derivatives of [Pro$_3$, DLeu$_9$]TL, a Temporin L analogue: Evaluation of antimicrobial, cytotoxic and hemolytic activities."** *European journal medicinal chemistry*. 2017 Oct 20; 139:750-761.

- Buommino E, Carotenuto A, Antignano I, Bellavita R, Casciaro B, **Loffredo MR**, Merlino F, Novellino E, Mangoni ML, Nocera FP, Brancaccio D, Punzi P, Roversi D, Ingenito R, Bianchi E, Grieco P. "**The outcomes of decorated prolines in the discovery of antimicrobial peptides from Temporin-L."** *ChemMedChem.* 2019 Jul 3; 14(13):1283-1290.

Abstract

Cationic α-helical antimicrobial peptides (AMPs) hold promise for treatment of the raising multi-drug resistant microbial infections, due to their broad spectrum of activity and membrane-perturbing mechanism of action. Compared to conventional antibiotics, these features make them newsworthy molecules that hardly induce microorganisms to acquire resistance to them.

Among these pathogens, *Pseudomonas aeruginosa* is the most clinically relevant Gram-negative bacterium known to cause serious human infections, e.g. pneumoniae, especially in immune-compromised patients, such as cystic fibrosis (CF) sufferers and keratitis, associated to contact lens (CL) wear. This is due to the unique ability of this pathogen to adhere to different types of inert materials or biological tissues, and to grow in a more resistant and dangerous sessile life form, called biofilm.

Recently, two Esculentin-1a-derived antimicrobial peptides i.e. Esc(1-21) and its D-amino acids containing Esc(1-21)-1c, [Esc peptides], have been fully characterized for their powerful antipseudomonal activity against both planktonic and biofilm forms.

The diastereomer showed a higher bactericidal activity than the all-L isomer against the more dangerous *Pseudomonas* biofilm phenotype; a lower cytotoxicity and higher biostability. However, when tested *in vitro* against the free-living form of this pathogen, it displayed a weaker bactericidal effect.

Here, to investigate the reason accounting for this discrepancy, mechanistic studies on intact bacterial cells were initially carried out. Then to further understand the effect of packing parameters, i.e. composition, charge, shape

and negative intrinsic curvature of membrane phospholipids in the membrane-permeabilizing activity of Esc peptides, leakage assays and circular dichroism spectroscopy analysis were carried out.

Our results have suggested that the weaker *in vitro* antibacterial activity of Esc(1-21)-1c on the planktonic phenotype of the Gram-negative bacterium *P. aeruginosa* is mainly correlated to a slighter ability in permeabilizing both outer and inner bacterial membranes.

Notably, experiments with lipid vesicles have suggested that if electrostatic interactions between negatively-charged membrane phospholipids and positively-charged peptide molecules do play a crucial role in the peptides' membrane perturbing activity, this latter is hampered by the bilayer structure packing parameters including hydrogen bonding and intrinsic curvature, associated to phosphatidylserine (PE), especially for the diastereomer compared to all-L parent peptide.

In parallel, we explored the molecular mechanism underlying the biofilm inhibition activity of Esc peptides when used at dosages below the minimal growth inhibitory concentration (1/8 MIC), by studying the peptides' effect on the expression of key genes involved in the bacterial virulence and motility, as well as the peptide' interaction with the bacterial signaling nucleotide ppGpp. Our findings revealed that the two D-amino acids containing Esc(1-21)-1c, confer the peptide the ability to downregulate the expression of biofilm-associated genes, likely as a result of increased peptide stability and prolonged binding to ppGpp compared to the all-L peptide.

Furthermore, we reported two different applicative strategies to ameliorate the biological properties of these two AMPs: (i) encapsulation in poly(lactide-co-glycolide) (PLGA) nanoparticles; and (ii) covalent conjugation to soft CLs.

In the first case, to enhance the peptides' bioavailability and to optimize their translocation to the target infectious site, Esc peptides were loaded into PLGA nanoparticles (NPs) engineered with polyvinyl alcohol (PVA). The peptides-loaded NPs were found to be more efficient in diffusing through artificial CF mucus and simulated bacterial extracellular matrix compared to the free peptides. Moreover, they were more efficient in inhibiting *P. aeruginosa* growth under both *in vitro* and *in vivo* conditions at long term.

In the second case, Esc peptides were covalently immobilized to hydrogel soft CLs and tested for their ability to reduce bacterial colonization. The antimicrobial CLs were able to cause more than four log reduction in the number of bacterial cells within 20 min and to reduce bacterial adhesion to their surface in 24 hours.

Finally, the ability of both peptides to limit the onset of microbial resistance was also evaluated by exposing *Pseudomonas* strains to multiple cycles of treatment at sub-MIC dosages. Interestingly, in contrast with conventional antibiotics, Esc peptides did not induce resistance in *P. aeruginosa* cells.

Overall, besides providing knowledges on the molecular mode(s) of action the two esculentin-derived AMPs, our data suggest that Esc peptides, particularly Esc(1-21)-1c, have great potential to be developed as novel drugs for treatment and prevention of *P. aeruginosa* pneumonia and keratitis.

Abbreviations

AMP, antimicrobial peptide; ANTS, 8-aminonaphthalene-1,3,6-trisulfonic acid, disodium salt; BAL, bronchoalveolar lavage; CD, circular dichroism; CF, cystic fibrosis; CFU, colony-forming units; CL, contact lens; CTRL control; CV, crystal violet; DH, hydrodynamic diameter; DIC, differential interference contrast; DLS, dynamic light scattering; DMEM, Dulbecco's modified Eagle's medium; DPC dodecylphosphocholine; DPX, p-xylene-bis-pyridinium bromide; DTPA, diethylenetriaminepentaacetic acid; EDC, 1-ethyl-3-(3-dimethylaminopropyl) carbodiimide hydrochloride; EDTA ethyl-enediaminetetraacetic acid; ELISA, enzyme-linked immunosorbent assay; ELS, electrophoretic light scattering; Esc peptides collectively Esc(1-21) and Esc(1-21)-1c; LB, Luria-Bertani broth; LPS, lipopolysaccharide; LTA, lipoteichoic acids; LUV large unilamellar vesicles; MAA, methacrylic acid; MTT, 3-(4,5-dimethylthiazol-2-yl)-2,5-diphenyltetrazolium bromide; NMR, nuclear magnetic resonance; NPs, PVA-engineered PLGA nanoparticles; OD, optical density; PBS, phosphate buffered saline; PDI, polydispersity index; PLGA, poly(lactide-co-glycolide); POPC, 1-palmitoyl-2-oleoyl-sn-glycero-3-phosphocholine; POPE, 1-palmitoyl-2-oleoyl-sn-glycero-3-phosphoethanolamine; POPG, 1-palmitoyl-2-oleoyl-sn-glycero-3-phosphoglycerol; ppGpp guanosine-30,50-bisdiphosphate; PVA, poly(vinyl alcohol); PVD, pyoverdine; QS, quorum sensing; RF, respirable fraction; Rho-Esc, rhodamine-B-labeled Esc peptides; Rho-Esc_NPs, rhodamine-B-labeled Esc(1-21) NPs; RP-HPLC, reverse phase high-performance liquid chromatography; SAB, sodium acetate buffer; SD standard deviation; SDS, sodium-dodecyl sulfate; SEM standard errors of the mean; SILF, simulated interstitial lung fluid; THR, trehalose; TOCL, tetra-oleoyl cardiolipin.

1. Introduction

1.1. THE ANTIMICROBIAL RESISTANCE

In the 1900's the discovery of antibiotics as compounds to treat infections revolutionized the healthcare community. Indeed, antibiotics acquired relevant support for clinical approaches in the surgical procedures, organ transplantation and management of cancer patients [WHO 2014; Reygaert 2018].

Thanks to the antibiotic's discovery and to the rapidity by which they were introduced to the pharmaceutical market, infectious diseases became a public health problem [Michael et al 2014].

Currently, antimicrobial resistance (AMR) has been recognized by The World Health Organization (WHO) as one of the three most important public health threats of the 21st century [WHO 2015]. In accordance with the Centre for Disease Control and Prevention (CDC), the amount of deceased people in USA owing to antibiotic-resistant infections is at least 23,000 per year. Future perspectives are certainly not more optimistic; indeed, new United Kingdom reports estimated that antibiotic resistant infections will cause around 10 million premature deaths per year by 2050, as well as significant economic damage of up to US$3.5 billion per year [OECD 2018].

Interestingly, a recent report outlined a plan of simple rules to reduce the resistance state: better hygiene, fewer and more careful antibiotic prescriptions, quick testing to discriminate bacterial from viral infections and educating the public by media campaigns.

1.1.1. *Mechanisms, origins and evolution in bacteria*

Antimicrobials are compounds endowed with specific activity against microbes, while the antibiotics are antibacterial compounds derived from microorganisms. AMR refers to the lack of susceptibility of microorganisms to a specific compound. It is generally evaluated on the basis of the minimum inhibitory concentration (MIC), i.e. the minimal concentration of compound that can inhibit the growth of that bacterium. The resistance to a specific compound can be due to the inability of this latter to hinder the bacterial growth of or to kill the bacterial species [Kidd et al 2018].

The genotypical resistance can be distinguished in intrinsic, acquired and adaptive. The first one includes mutations in gene(s) causing an altered outer membrane permeability, an over-expression of efflux pumps that extrude the antimicrobial molecules as well as the synthesis of antibiotic-inactivating enzymes [Figure 1] [Reygaert 2018].

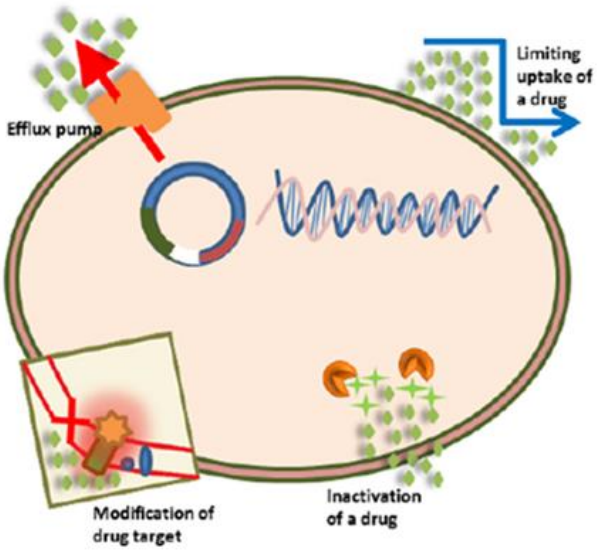

Figure 1. *A schematic representation of the intrinsic antibiotic resistance mechanisms in bacteria [*Reygaert 2018*].*

The acquired resistance can be achieved by two different pathways: vertical evolution or horizontal evolution, whereby *de novo* mutations, involved in the antibiotic sensitivity, are transmitted to the descendants [Figure 2a], or the external antibiotic resistance genes are acquired through horizontal gene transfer (HGT) from another bacterium (donor) [Breidenstein et al 2011] [Figure 2b].

Although the relative contribution of each of these evolutionary paths to the development of clinical bacterial resistance is still unknown, one of the most important factors is the HGT [Henrichfreise et al 2007; Pang et al 2019].

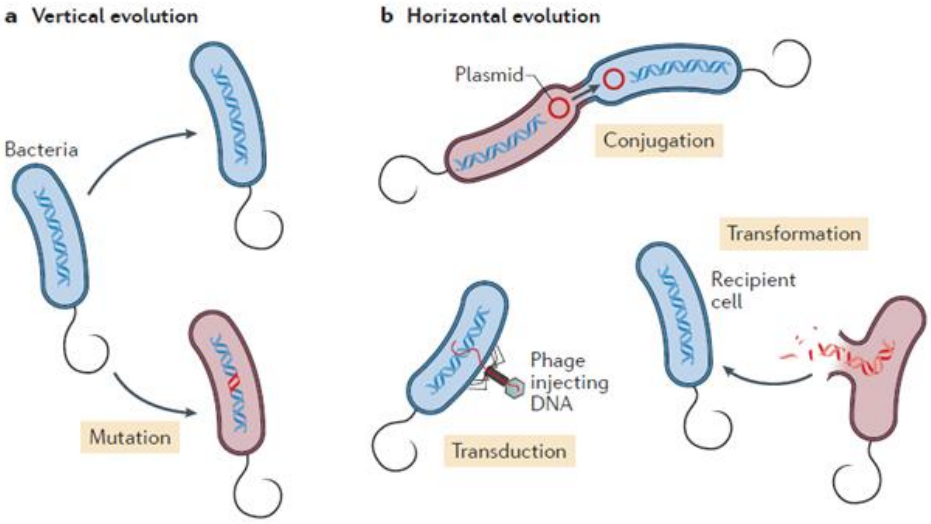

Figure 2. *Mechanisms of acquisition of resistance genes in bacteria. a) Vertical evolution, transmission of the de novo mutations in the bacterial genome to the daughter bacterial cells. The antibiotic-sensitive bacterial cells are depicted in blue, whereas the antibiotic-resistant cells in red icon. b) Horizontal acquisition, also known as horizontal gene transfer (HGT), can involve the phage transduction, conjugation or transformation. All these processes are based on the transmission carriers of resistance mutations and/or genes of mutations (indicated by red DNA routes) from the donor bacterial cell (in red) to the target bacteria (in blue) [Sommer et al 2017].*

The third one is the adaptive resistance. Compared to the intrinsic and acquired resistance mechanisms, the adaptive resistance is dependent on transient alterations in genes and/or protein expression as a response to environmental stimuli or chemical and physical stresses [Sandoval-Motta and Aldana, 2016].

Among environmental stimuli associated with this type of resistance there are antibiotics, pH, heat shock, DNA stress, anaerobiosis, polyamines, cations and nutrient deficiency states and group behavioural adaptations such as biofilm formation and swarming motility [Fernández et al 2011].

Biofilm-mediated resistance to antibiotics (simplified in Figure 3), is a topic that is currently attracting attention. The pathogens involved in the biofilm infections are *Staphylococcus aureus*, *Staphylococcus epidermidis*, *Pseudomonas aeruginosa*, *Burkholderia cepacia* complex and *Haemophilus influenzae*, among others [Folkesson et al 2012; Fernández et al 2011; Bjarnsholt et al 2009].

An important role in adaptive resistance is also given by "persister" cells (PC), subset of phenotypic variants in an isogenic bacterial population that, unlike drug-resistant bacteria, survive the antibiotic attacks by decreasing their metabolism and entering into a non-growing/quiescent state [Lewis 2010].

Generally, PC arise as adaptation to stress environmental factors, including oxidative stress, DNA damage, nutrients and oxygen deprivation, and antibiotics [Wang et al 2017]. Indeed, PC typically increase in stationary-phase cultures and biofilm lifestyle, wherein PCs represent as much as 1% of the total bacterial population [Grassi et al 2017] [Figure 3].

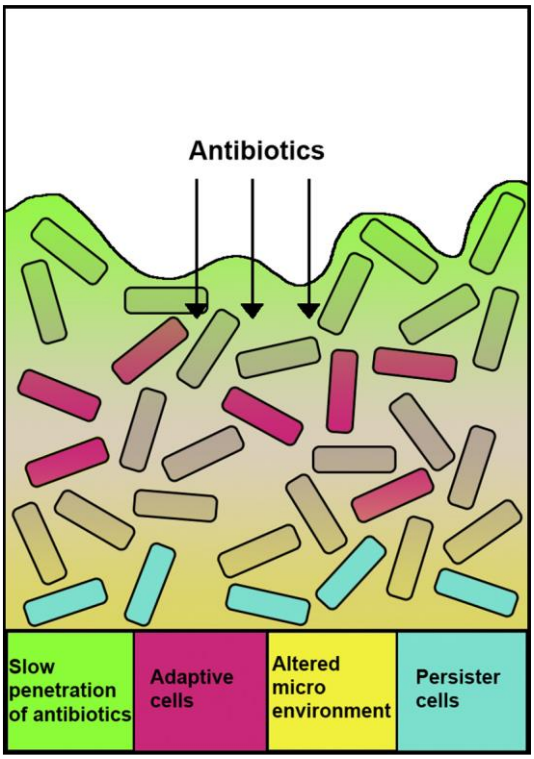

Figure 3. *The biofilm-mediated antibiotic resistance. Limited penetration of antibiotics within the biofilm (green); some biofilm cells exhibit an adaptive response as a result of antibiotic attack (pink); an altered microenvironment in biofilm (yellow) leads to lower growth of bacteria. This results in reduced antibiotic uptake and the emergence of multidrug-susceptibility "persister" cells (in blue). [Pang et al 2019].*

1.2. *PSEUDOMONAS AERUGINOSA* PATHOGEN

One of the human pathogens that most easily acquire resistance to conventional antibiotics is the Gram-negative bacterium *Pseudomonas aeruginosa (P.aeruginosa)*. Pulmonary infections due to *P.aeruginosa* are the main cause of lung decline and death in patients suffering from cystic fibrosis (CF) [Parker et al 2016; Blanc et al 1998; Sadikot et al 2005].

Cystic fibrosis (CF) is a genetic disorder that is caused by recessive mutations in the gene encoding the cystic fibrosis transmembrane conductance regulator

(CTFR), which regulates chloride transport across the airway epithelium and submucosal glands. The most common mutation is a deletion of phenylalanine at position 508, leading to hyperinflammation and formation of a thick and viscous mucus layer with impaired mucocillary clearance. Thus, these conditions predispose the lung of CF patients to a favourable environment for bacterial growth and colonization [Nixon et al 2001; Maurice et al 2018].

Despite aggressive antibiotic treatments, *Pseudomonas* often grows in the CF lung and leads to chronic and recalcitrant infections characterized with robust host inflammatory response [Rudkjøbing et al 2012; Bjarnsholt et al 2009].

P. aeruginosa is among the most virulent opportunistic pathogens capable of surviving in nutrient-poor environments and colonizing biological or abiotic surfaces e.g. medical implants such as catheters, prostheses or contact lenses (CLs), making its eradication even more complex [Willcox 2011].

Among medical devices, CLs wear is one of the most important risk factors for the development of microbial keratitis. This is because *Pseudomonas* can easily colonize the hydrogel or silicone hydrogel lens surface, forming biofilms which can rapidly colonize the cornea tissue, once the CL is placed in the eye [Willcox 2011].

1.2.1. *Pseudomonas aeruginosa* biofilm development

Adaptive antibiotic resistance represents a huge obstacle in the treatment of *Pseudomonas* biofilm infections as compared to the free-swimming, planktonic counterpart of this microbial pathogen [Bhagirath et al 2016, Pletzer et al 2016].

Biofilms are complex sessile communities of microbes found either attached to an inert or living surface and integrated in a self-produced extracellular

matrix as three-dimensional aggregates [Costerton et al 1999; Roy et al 2018]. Exopolysaccharides, proteins, nucleic acids, and other cellular debris, collectively named extra polymeric substances (EPS), are the general constituents of this matrix.

It is known that biofilm formation *in vitro* starts with an irreversible adhesion of planktonic bacterial cells to surfaces favoured by pili and flagella. Type IV pili, for example, are filamentous protein complexes that are of vital importance for the initial attachment of cells as well as for the regular biofilm maturation [Figure 4].

Attachment of cells to a surface is then followed by microcolonies formation, secretion of EPS and biofilm maturation by quorum sensing intercellular communication.

It is notable that in the maturation step, the twitching motility, which is the bacterial movement resulting from extension and retraction of pili including the Type IV, plays a direct role in the cell-to-cell interactions [Skercer and Berg 2001; Giraud et al 2011].

Furthermore, besides swimming and twitching motility, *P. aeruginosa* can also swarm through viscous environments. The swarming is a complex type of motility, depending on flagella, type IV pili and bacterial surfactants, e.g. rhamnolipids which contribute to the early stage of biofilm formation and colonization of adjacent semi-solid surfaces [Overhage et al 2007].

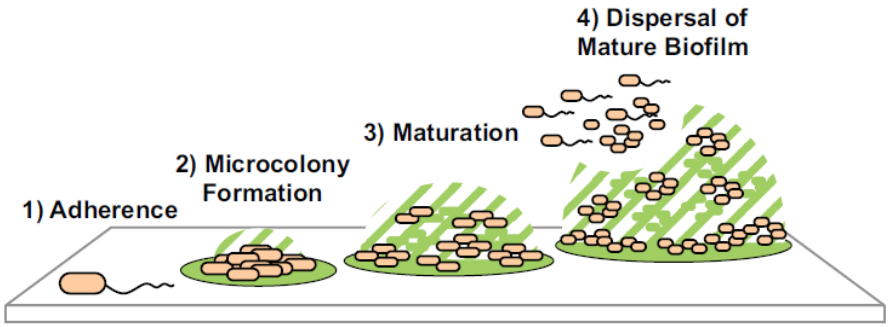

Figure 4. *Biofilm development process. (1) Initial attachment of bacterial cells to a surface. Gene expression changes lead to down-regulation of polar flagella and up-regulation of Type IV pili. Bacteria start to adhere to the surface and to produce extracellular matrix, (2) Microcolonies formation through different cycles of bacterial cell division. The increased expression of Type IV pili and secretion of extracellular matrix components allow a higher attachment of cells to a surface as well as a strong association with other cells leading to protection from the external environment. (3) Development of mature biofilm structure with subpopulations of cells with different morphologies between the external and internal layers of biofilm microcolonies. (4) Dispersion of some cells, which revert to the motile phenotype and dissociate, from the outer surface of the biofilm by quorum-sensing pathway, external signals or physical breakdown [Taylor et al 2014].*

Biofilm differentiation and maturation is a highly regulated program associated to expression of dozens of genes and regulatory circuits. A critical regulatory circuit is the stringent response triggered by the cellular and starvation stress (i.e. nutrients deficiency, carbon source, iron or lipid starvation, heat and oxidative stresses) and mediated by the synthesis of small signalling nucleotides, i.e. the guanosine 5'-diphosphate 3'-diphosphate (ppGpp) and 5'-triphosphate 3'-diphosphate (pppGpp), collectively denoted nucleotide alarmones tetra- and penta-phospate (p)ppGpp [Potrykus and Cashel 2008; Romling et al 2013].

In Gram-negative bacteria the synthesis of these molecules is regulated by global stress response regulator enzymes, RelA and SpoT; while a single bifunctional enzyme Rsh is associated to the Gram-positive bacteria. As

illustrated in Figure 5, in response to amino acid starvation, RelA binds to the ribosome, which is blocked by uncharged tRNA molecules, and triggers the production of cellular alarmones ppGpp. Contrariwise, under other type of stresses including iron starvation, SpoT starts ppGpp synthesis. SpoT is alternatively a bifunctional enzyme that can hydrolyze ppGpp. Subsequently, the rapid intracellular accumulation of the alarmones ppGpp and its following binding to the RNA polymerase, influences the transcription causing a passage from cell growth to survival. Anti-biofilm peptides are able to block the intracellular accumulation of ppGpp [De la Fuente-Nunez et al 2014; Pletzer et al 2016].

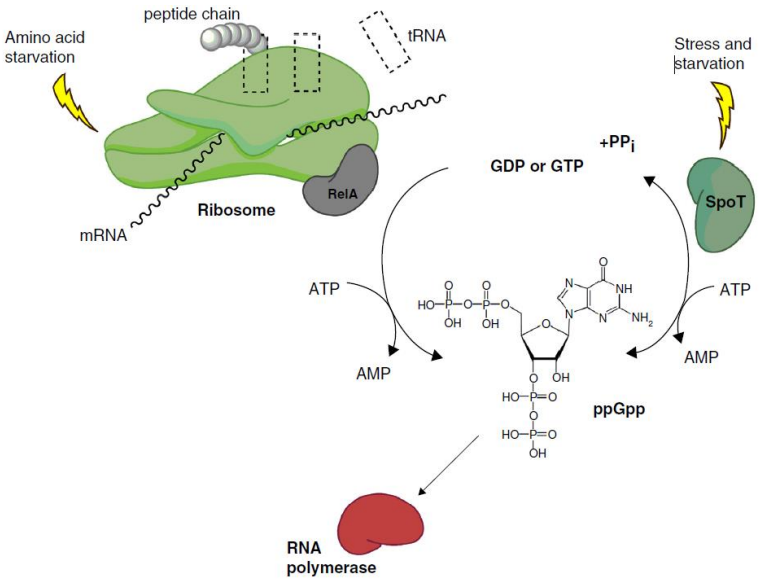

Figure 5. *Stringent response in biofilm formation mediated by alarmones ppGpp. RelA is expressed as a response to amino acid deprivation and binds to the ribosome triggering the synthesis of cellular alarmones ppGpp. Instead, SpoT causes the production of ppGpp as response to iron starvation. ppGpp signalling molecules bind to RNA polymerase, thus influencing the transcription. [Pletzer et al 2016].*

Another global regulatory system involved in the biofilm development is the quorum sensing (QS) that involves cell-to-cell communication.
In *P. aeruginosa*, the principal QS systems are the las, rhl and pqs. They regulate the response of bacterial cells to the surrounding environment through the production of signalling molecules implicated in the expression of several virulence factors including toxins and proteases [De Kievit et al 2001].

Among these virulence factors, an example is the endogenous siderophore pyoverdine (PVD), which acts as both an iron carrier and a virulence-related signalling molecule. Indeed, it has been demonstrated that it is in turn implicated in biofilm control, cell-to-cell communication, and in the expression of other virulence factors, including exotoxin A, exoprotease PrpL, and PVD itself [Imperi et al 2009].

1.3. ANTIMICROBIAL PEPTIDES (AMPs)

Natural antimicrobial peptides (AMPs), also called host defence peptides, are a class of evolutionally conserved components of the innate immunity that are expressed as a first-line of defence against microbial pathogens in many multicellular organisms, ranging from prokaryotes to humans [Zanetti 2004; Powers and Hancock 2003; Zhang and Gallo 2016].

In 1922, Alexander Fleming identified the first human antimicrobial protein, called Lysozyme from nasal mucus, while in 1940s this finding was tarnished by the advent of the "Golden Age of Antibiotics" with the discovery of penicillin.

However, in the 1960s, with the increased emergence of antibiotic resistance, the development of novel therapeutic strategies directed against biofilm-related infections became urgently needed.

The AMPs' discovery began in 1980 when Hans G Boman discovered how the injection of bacterial cells in Cecropia silk moth was able to induce the synthesis of an AMP, called cecropin. [Hultmark et al 1980]. Another relevant breakthrough occured in 1987 when Michale Zasloff and co-workers isolated magainins from the skin of the African frog *Xenopus laevis* [Zasloff 1987].

In 1994 the increased scientific and clinical interest towards AMPs led to the discovery of cathelicidins in the mammalian host defense by Bob Lehrer's group [Gallo et al 1994].

Even if more than 5,000 AMPs have been discovered or synthesized up to date, these likely depict only a tiny part of all gene-encoded antibiotic peptides existing in nature.

Many AMPs are small cationic molecules which act mainly by killing pathogenic bacteria, fungi, viruses and protozoa *via* direct non-receptor mediated membrane damage.

In addition, or in support to their membrane-perturbing activity, AMPs can also have non-membranous targets, interfering with intracellular biochemical processes like the inhibition of nucleic acids, proteins and cell wall synthesis [Brodgen 2005].

Furthermore, besides their well-known antibacterial activity, several AMPs have been characterized as innate immunity modulators anti-diabetic agents and anti-tumor agents. Melittin and NK-2, a bee venom and porcin NK-lysin-derived peptides respectively, have been identified as antitumor molecules. Particularly, while melittin inhibits the tumour cell metastasis by decreasing cell motility and migration, NK-2 allows cancer cell death by interaction with

negatively charged phosphatidylserine (PS) on the tumour cell surface. [Pushpanathan et al 2013].

1.3.1. Structure-function properties

Generally, AMPs are relatively small molecules. They can vary from 6 to 60 amino acid residues with a cationic character at neutral pH.

The target cell selectivity of AMPs is the result of sensitive interplay between structural and functional features, as summarised below.

- ***Peptide's charge:*** It is the sum of all charges of the ionizable groups. Most AMPs are positively charged with a net charge ranging between + 2 to + 9 due to arginine (Arg) and/ or lysine (Lys) residues [Hancock and Sahl 2006]. The positive charge is required for the initial interaction of AMPs with the components of the outer surface of microorganisms (e.g. lipopolysaccharides, LPS, in Gram-negative bacteria or lipoteichoic acids, LTA, in Gram-positive bacteria).

  Some anionic AMPs (AAMPs) (net charge -1 to -7), rich in aspartic or glutamic acids residues, have also shown an antimicrobial efficacy.

  They use metal ions (e.g. Zn^{2+}) to establish salt bridges with the anionic components of microbial membranes [Harris et al 2011]. Their mechanism of action, even if poorly understood, mainly includes translocation across the membrane to specific intracellular targets (e.g. ovine and SAAPs) or pathogen' membranes perturbation *via* pore formation (e.g. cyclotides) or in a carpet-like manner, as in the case of human-β-defensins prior to interact with intracellular targets. However, the mechanisms of their antimicrobial activity are unclear.

Peptide's conformation and sequence: Generally, according to their secondary structures in a membrane-mimicking environment, AMPs are classified in the following groups: (i) α-helical AMPs, such as the cathelicidin LL-37, melittin, magainin [Figure 6B]; (ii) β-stranded peptides connected by two or more disulfide bonds (e.g., defensins and protegrins) [Figure 6A]; (iii) β-hairpin or loop AMPs interconnected by a single disulphide bond and/or cyclization of the peptide backbone (e.g., gramicidin S, thanatin) [Figure 6D]; (iv) linear peptides rich in tryptophan (e.g., indolicidin), proline and arginine (e.g., PR-39), glycine and histidine (e.g., histatins) [Figure 6C]. Most of them are usually unstructured in aqueous solution and adopt an amphiphatic helical conformation in membrane mimetic environment. In the numerous AMPs' sequences, the prevalent amino acid residues are the cationic Lys and Arg, which are fundamental for their electrostatic interaction with the negatively-charged lipid head-groups of microbial membranes at lipid/water interface, as well as the aromatic tryptophan (Trp) which favors AMPs' anchorage into membranes [Shagaghi et al 2018]. Several α-helical AMPs contain glycine (Gly) as first amino acid because it is considered an excellent N-capping residue for α-helices, thus limiting proteolytic degradation by aminopeptidases [Tossi et al 2000]. On the other hand, AMPs rarely contain residues as aspartic acid (Asp) or glutamic acid (Glu).

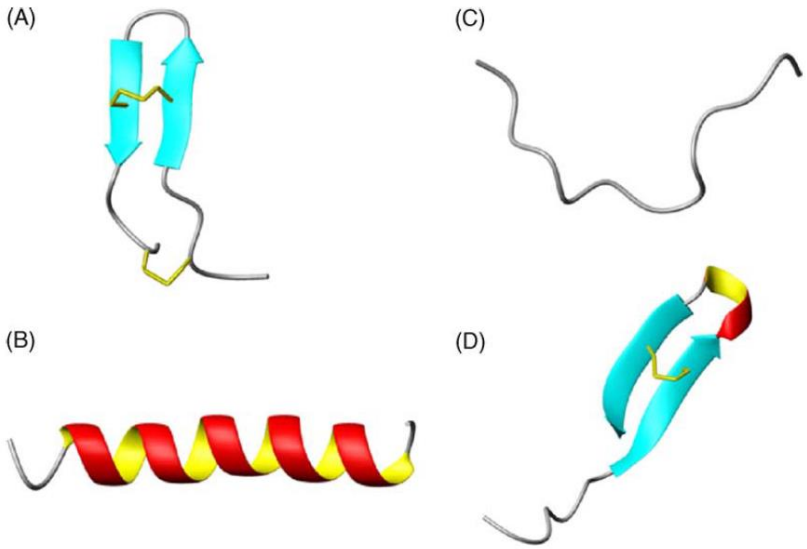

Figure 6. *Structural classes of antimicrobial peptides. (A) β-sheet, tachyplesin I, defensins, protegrins; (B) α-helical structure of human cathelicidin LL-37 or magainin 2; (C) linear extended indolicidin, PR39, histatins; (D) β-hairpin or loop peptides, e.g. thanatin, gramicidin S. In yellow are represented the disulfide bonds [Powers and Hancock 2003].*

- ***Peptide's amphipathicity and hydrophobicity:*** The amphipathicity or hydrophobicity refers to the distribution of hydrophobic and hydrophilic moieties within the peptide sequence. There is a strong correlation between the amphipathic structure of AMPs and their mechanism of action, particularly by van der Waals interactions: the hydrophilic domains of AMPs interact with the negatively-charged membrane components whereas the hydrophobic face interacts with the membrane phospholipids leading to peptides' penetration into the membrane bilayer [Hancock and Chapple 1999; Dathe et al 1997].

  Approximately 50% hydrophobic residues are found in many naturally occurring AMPs [Yeaman and Yount 2003; Tossi et al 2000] and assist their partition into the membrane. Importantly a direct correlation

between and mammalian cell toxicity has been reported [Strandberg et al 2015].

- ***Target cell membrane composition:*** an attractive feature of many AMPs is their cell selectivity i.e., the peptide ability to kill bacterial cells at concentrations significantly lower than those causing damage to cells of the host organism [Hancock and Sahl 2006].

  Since cellular membranes are the primary target for the mechanism of action of AMPs, it is worth mentioning that selectivity results from a different composition between the membrane of eukaryotic cells and bacterial cells [Wang 2017].

  In nature, bacteria can be divided into two groups, Gram-positive and Gram-negative. Gram-positive bacteria are characterized by a thick peptidoglycan and LTA layer (40-80 nm) surrounding the cytoplasmic membrane. Gram-negative bacteria, on the contrary, have a thinner peptidoglycan layer (8 nm thick) adjacent an outer membrane with an asymmetric composition: phospholipids are the main components of the inner leaflet, while the outer layer is mostly made of LPS [Wada et al 2012].

  By contrast, eukaryotic cells only have the plasma membrane, with asymmetric lipid composition in the two leaflets of the bilayer.

  The major components of bacterial membranes include negatively-charged phospholipids. Specifically, in Gram-negatives, both membranes contain phosphatidylglycerol (PG, ~20%) and cardiolipin (CL, ~5%); the content of anionic lipids in Gram-positive bacteria is much higher and PG and CL are again the most important components [Malanovic and Lohner 2016].

Furthermore, the positively charged L-lysyl phosphatidylglycerol, (l-lysyl-PG or LPG) can also be present in the membranes of Gram-positive.

In both bacteria types, the zwitterionic phospholipid is phosphatidylethanolamine (PE), and no sterols are present [Epand et al 2016] [Figure 7]. Obviously, bacterial membrane composition is influenced by specific strain and growth conditions [Bobone and Stella 2019].

Human cells contain cholesterol and have no anionic phospholipids in the outer leaflet of their cell membrane. In comparison with eukaryotic cells, bacterial membranes have more anionic lipids in the outer surface of their bilayers and their transmembrane potential is more negative than that of mammalian cells [Yeaman and Yount 2003].

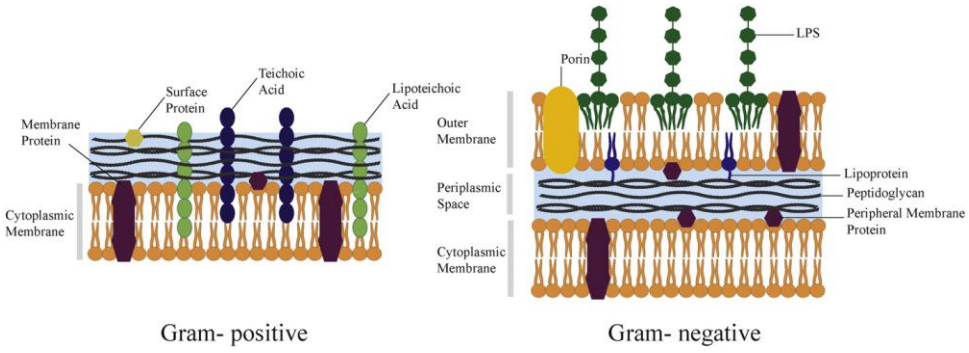

Figure 7. *Schematic representation of the cell wall of Gram-positive and Gram-negative bacteria [Epand et al 2016].*

For these reasons, electrostatic interactions between positively-charged peptide molecules and negatively-charged membrane components of bacterial cells are prevalent.

Greater amounts of “non-bilayer lipids” are contained in the bacterial membranes and are characterized by negative (for PE, CL and phosphatidic acid, PA) or positive (LPG) values for the “intrinsic curvature” [Malanovic and Lohner 2016].

This feature is related to the relative sizes of the phospholipid head-groups and acyl chains: lipids with a cross-sectional area composed by similar head-groups and tails (e.g., phosphatidylcholine PC, PG or PS) have a cylindrical shape and pack well in flat bilayer structures (zero intrinsic curvature). On the contrary, lipids with head-group shorter than the tails, as for PE and PA, favour concave shapes of the monolayer (negative curvature). Lipids with larger polar heads, such as LPG or phosphatidylinositol PI, have positive curvature [Koller and Lohner 2014] [Figure 8].

By investigating interactions between AMPs and different types of model membranes mimicking the composition of natural bilayers is helpful in order to understand the AMPs’ selectivity [Bocchinfuso et al 2011; Savini et al 2018].

As demonstrated by Matsuzaki association of cationic peptides to phospholipid bilayers and their perturbation is enhanced by the presence of anionic lipids [Matsuzaki et al 1989; Russell et al 2010; Golbek et al 2017]; while, the positively charged lipid LPG, contained into Gram positive bacteria, hinders AMP activity [Andra et al 2011].

Although the knowledge regarding the effect of the presence of negative curvature lipids in the bacterial membranes, such as PE, is not yet well-defined, different groups, including Dr. Matsuzaki and Allende showed that PE inhibits pore formation by magainin, melittin,

alamethicin, PMAP23 and mastoparan X [Matsuzaki et al 1998; Allende et al 2005; Bobone et al 2012].

By contrast, other works showed that the presence of PE favours the activity of some AMPs [Schröder-Borm et al 2003; Epand et al 2006; Leite et al 2015].

The inhibition of AMPs' activity by PE can be understood considering that AMPs act by introducing into the head-groups of the membrane phospholipids, triggering a positive curvature strain and, as consequence, a pore-like mechanism of membrane perturbation. In comparison, lipids with a negative intrinsic curvature would hinder this mechanism [Matsuzaki et al 1998; Lee et al 2005].

However, it is difficult to definite an exact role of PE in AMPs' selectivity, and future studies regarding the role of negative curvature will be needed to understand this effect.

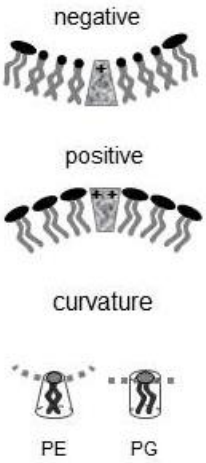

Figure 8. *Molecular shape and curvature strain of primary lipids of bacterial membranes [Lohner 2017].*

1.3.2. Mode of action of cationic AMPs

Most of the cationic AMPs exert their antimicrobial action by inducing an irreversible alteration of the cellular structure and/or function through different and complex mechanisms [Powers and Hancock 2003; Brogden 2005; Jenssen et al 2006; Teixeira et al 2012].

All mechanisms involve key steps such as attraction, attachment and insertion of AMPs into the target cell's membrane, thus causing a lytic or a non-lytic effect [Nijnik and Hancock 2009; Shagaghi et al 2018].

Unlike conventional antibiotics, the initial binding is mediated by electrostatic interactions between the cationic residues of AMPs and the negatively-charged outer envelope of Gram-negative bacteria (i.e. anionic phospholipids and LPS) or the LTA on the Gram-positive bacterial surface [Malanovic and Lohner 2016] [Figure 9, 10].

Once AMPs interact with LPS, divalent cations such as Mg^{2+} and Ca^{2+} bound to LPS are dislocated, thus leading to a local disorder of the outer membrane and promotion of peptide translocation into the cytoplasmic membrane, according to the self-promoted uptake hypothesis [Bechinger and Gorr 2017; Anunthawan et al 2015].

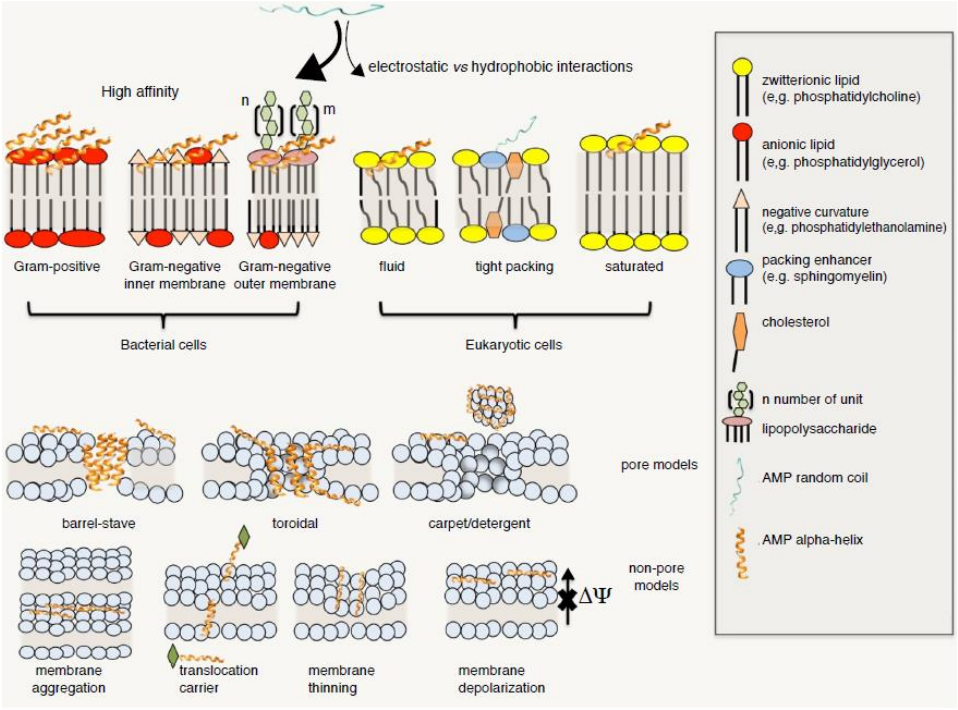

Figure 9. *Molecular basis and general mechanisms of cell selectivity of AMPs [Lee et al 2019].*

In addition to this primary mechanism of action, many AMPs exert immunomodulatory functions. Indeed, AMPs can protect the host by enhancing recruitment or activation of leukocytes and monocytes at the site of infection or by modulating the host-cell responsiveness to Toll-like receptor (TLR) ligands [Figure 10].

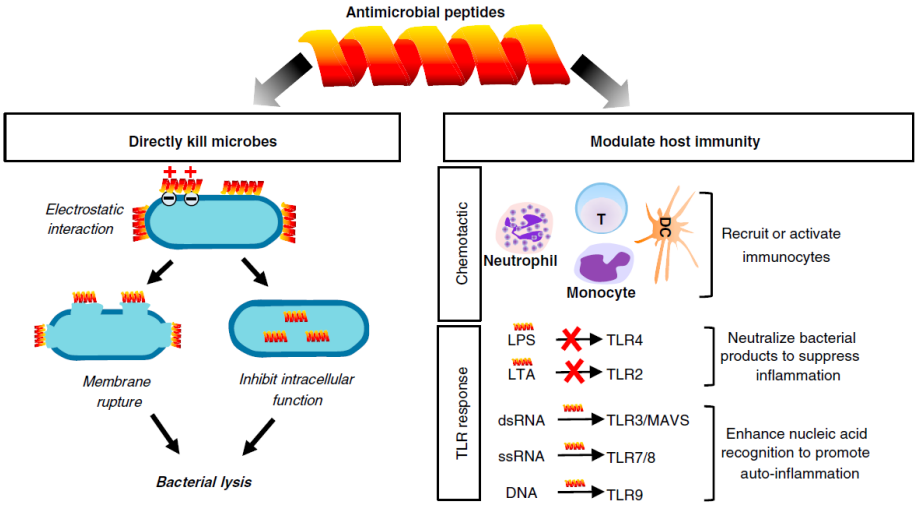

Figure 10. *Biological functions of AMPs. AMPs can bind to bacterial membranes through electrostatic interactions either to permeabilize the membrane or to penetrate the bacterium causing inhibition of intracellular functions. Furthermore, AMPs can also have immunoregulatory functions by recruiting/activating immunocytes or by affecting of Toll-like receptor (TLR) neutralization of microbial products and nucleic acids release upon tissue damage. DC, dendritic cell; LPS, lipopolysaccharide; LTA, lipoteichoic acid; MAVS, mitochondrial antiviral signaling protein. [Zhang and Gallo 2016].*

1.3.2.1. Membrane-permeabilizing AMPs

After AMPs target and bind to the outer membrane of pathogen, the peptides' ability to traverse the lipid bilayer can be influenced by the threshold concentration of the peptide itself, which is usually investigated in experimental protocols as peptide-to-lipid ratio (P/L). This depends on many aspects including, peptide concentration, peptide tendency to self-assemble or to oligomerize, phospholipid membrane composition, fluidity, head group type, as well as pH, temperature and ionic strength [Teixeira et al 2012; Huang 2000].

Generally, at low peptide/lipid ratios AMPs lie parallel to the lipid bilayer, while once high peptide/lipid concentrations are reached, they begin to

penetrate and to dispose themselves perpendicularly to membranes thus causing the formation of transmembrane channels, pores and/or extensive membrane lesions [Brogden 2005; Ciumac et al 2019].

The general models proposed to explain the membranolytic mode of action of AMPs are reported below:

- ***"Barrel-stave"*:** Peptide helices shape a bundle with a central lumen into the bilayer, like a barrel wherein the helical peptides are the staves. The hydrophobic peptide surfaces interact with the fatty acid chains of the membrane phospholipids, while the hydrophilic regions point inward forming the interior region of the channel. The leakage of intracellular components through these pores subsequently causes cell death. It has been noted that a transmembrane pore can be made of a minimum of three molecules. In this model, the membrane does not show significant curvature and the hydration of the membrane remains unchanged [Li et al 2017]. The mechanism of action of alamethicin is defined according to this model [Figure 11 A] [Shagaghi et al 2018; Leitgeb et al 2007; Yang et al 2001].
- ***"Toroidal-pore (worm hole)":*** AMPs helices insert into the bilayer inducing a positive curvature strain in the lipid monolayers (membrane thinning) to bend through the pore wherein the water core is lined by peptide molecules and lipid head groups. Similarly, to the previous model, in toroidal-pore structure the polar faces of the peptides are tied with the polar head groups of the lipids. This type of model has been proposed for AMPs which target intracellular components; pore disintegration would then lead to AMPs translocation into the

cytoplasmic space (i.e. magainins, melittin and protegrins) [Figure 11 C] [Hallock et al 2003; Matsuzaki et al 1996; Yang et al 2001]

- ***"Disordered toroidal pore model":*** Pore formation is more stochastic and involves fewer peptides [Sengupta et al 2008].
- ***"Carpet mechanism"*:** Peptide are electrostatically attracted to the anionic phospholipid head groups covering the membrane surface like a carpet. Once critical threshold concentrations of AMPs have been reached, AMPs form toroidal transient holes in the membrane. This is then followed by membrane micellization in a detergent like manner with collapse of the membrane packing into fragments and cell lysis. Cecropins and ovisprin employ this model [Figure 11 B] [Teixeira et al 2010; Shai 1999; Ciumac et al 2019].
- ***"Membrane thinning/thickening affection model"*:** When the thickness of the bilayer is affected by the presence of the peptides, or the membrane itself is remodelled to form anionic rich domains surrounding the peptide.

On the other hand, some AMPs can permeabilize the membrane by a non-lytic mechanism accompanied by transient pore formation. This includes: (i) aggregate-channels, wherein the peptides form disordered aggregates associated with water molecules, allowing ion diffusion (e.g. cyclic peptide bactenecin) [Hancock and Chapple 1999]; (ii) molecular electroporation, wherein AMPs form an electric field across the membrane thus resulting in pore formation (e.g. oligo-arginine cell-penetrating peptides, CPP) [Figure 11 D] [Cahill 2010]; (iii) sinking-rafts, wherein the amphipathic AMPs bind to particular lipid sites and sink into the bilayer causing transient pores with

peptide translocation to the cytoplasmic membrane (e.g. polyphemusin) [Figure 11 E] [Haney et al 2010].

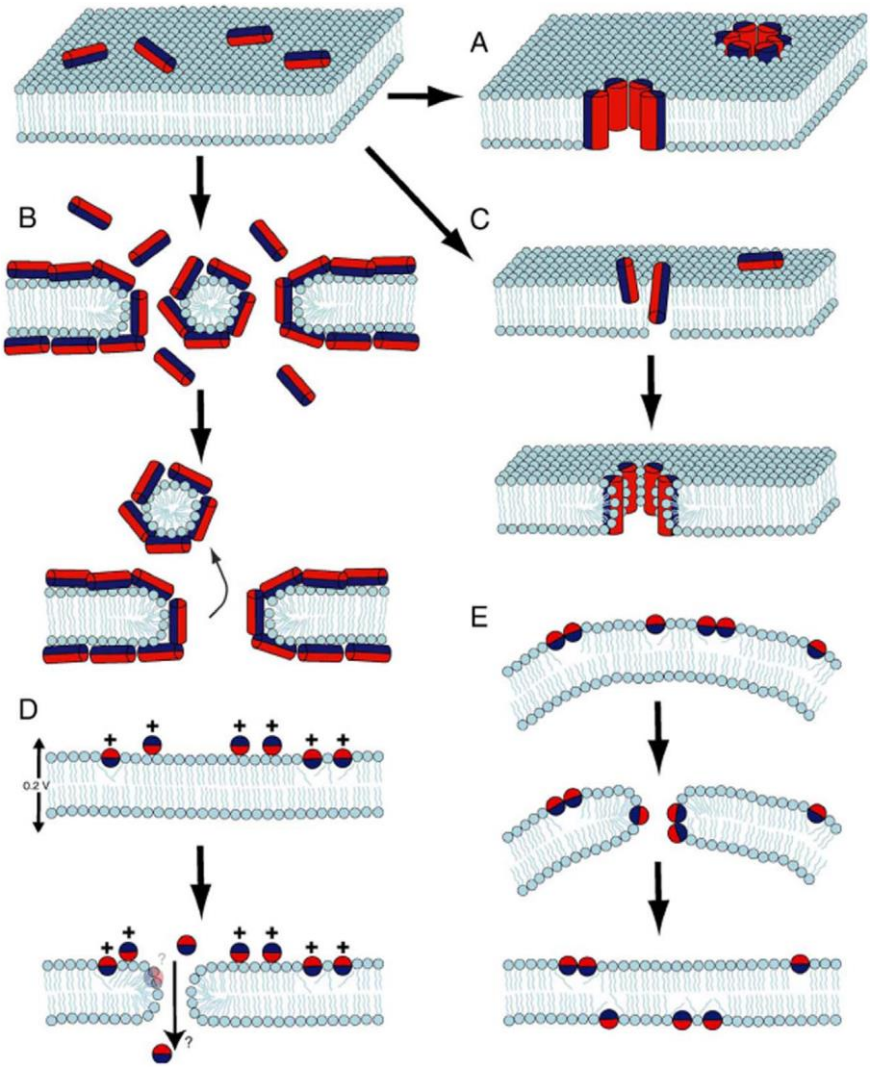

Figure 11. *Mechanisms of action of AMPs. A) barrel-stave, B) carpet, C) toroidal pore, D) molecular electroporation, E) sinking raft. Hydrophilic and hydrophobic surface of peptides are indicated in red and in blue, respectively [Shagaghi et al 2018].*

1.3.2.2. Non-membrane-permeabilizing AMPs: Focus on AMPs-intracellular targets interactions

In the last years the number of reports explaining non-lytic killing mechanisms of AMPs has been quickly augmented [Yeung et al 2011; Mojsoska and Jenssen 2015].

Different evidences seem to indicate that AMPs have single or multiple intracellular targets, including inhibition of protein synthesis, alteration of cytoplasmic membrane septum formation, DNA binding affecting transcription and/or replication, cell wall biosynthesis inhibition and inactivation of enzyme activities [Scocchi 2016] [Figure 12].

Numerous studies with the insect and mammalian proline-rich AMPs (PR-AMPs) have shown that this group inhibits the protein synthesis. Initially, Boman discovered that PR-39 hinders the translation and synthesis of DNA [Boman et al 1993]; later, the PR-AMPs Bac7, was found to interfere with the stress genes expression involved in protein synthesis when used at sub-lethal concentrations [Tomasinsig et al 2004]. Recently, other studies have indicated that binding to ribosome subunits and inhibition of protein synthesis represent additional intracellular targets of PR-AMPs family.

A correlation between DNA binding capability and antimicrobial activity was initially observed with Buforin II. This is a well-known example of AMP that binds DNA after its translocation inside *E. coli* without membrane damage [Park et al 2000].

Furthermore, different AMPs have been found to target components of the cell wall peptidoglycan, e.g. the lantibiotics, a class of post-translationally modified bacteriocins derived from Gram-positive bacteria [Hechard and Sahl 2002]. Despite being membrane-active compounds, many bacteriocins have

the peptidoglycan precursor lipid II as one of the major targets. Since peptidoglycan is absent in eukaryotic cells these peptides have attracted interest for therapeutic field [Willey and Van der Donk 2007].

In recent studies, other membrane-independent mechanisms of microbicidal activity have been reported for AMPs including: (i) the release of autolytic enzymes from lipoteichoic acids by θ-defensins group leading to cell wall breaking [Wilmes, M., 2014]; and (ii) the phosphatidylserine externalization to outer membrane surface with DNA fragmentation and chromatin condensation leading to apoptosis-like death by magainin-2 peptide [Lee and Lee 2014].

Since many studies regarding non-lytic mechanisms of action have not investigated the state of membrane integrity, it is not yet clear whether the killing effect is related only partially or totally to the intracellular action or whether it is triggered by membrane permeabilization.

The activity of AMPs and their related mechanism of action depends on various factors including concentrations of AMPs, bacterial growth phase and bacterial membrane composition. Several AMPs can have two or more inhibitory functions and a peptide that exerts a bactericidal effect via membrane perturbation may also kill microbes by a non-membranolytic manner or viceversa [Hale and Hancock 2007].

For example, Bac7, when used at low concentration it can inhibit bacterial growth by binding to intracellular targets; while if used at several high MIC concentrations it can also kill bacteria through a secondary direct membranolytic mechanism [Podda et al 2006].

Furthermore, several AMPs when used at sub-MIC can act as inhibitors of biofilm formation by opportunistic bacterial pathogens (e.g. *P. aeruginosa*). This could be the result of inhibition of genes expression by specific intracellular signal molecules, i.e. (p)ppGpp which is involved in the control of bacterial motility as well as in the stress-induced biofilm development and maintenance [de la Fuente-Nunez et al 2012; Lin et al 2018]

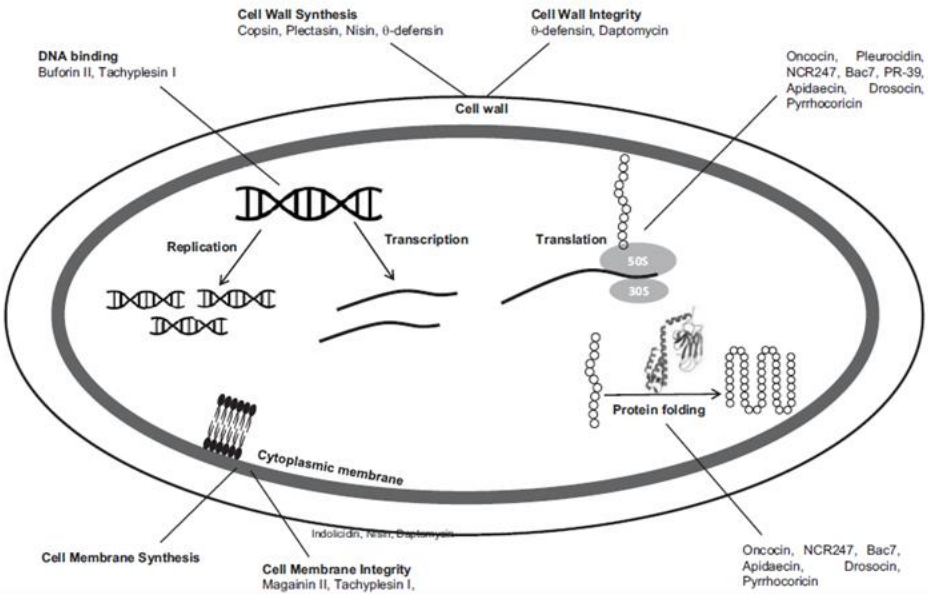

Figure 12. *Illustration of possible targets of membrane-active and non-membrane permeabilizing AMPs [Scocchi 2016].*

1.3.3. AMPs as therapeutic agents

Against the background of rapidly increasing resistance development to conventional antibiotics all over the world, efforts to bring AMPs into clinical use are accelerating.

Interestingly, several AMPs, due to their broad antimicrobial spectrum and high bactericidal activity, are currently evaluated in clinical trials as novel anti-infectives, but also as new pharmacological agents to modulate the immune response, to promote wound healing, and to prevent post-surgical infections [Mahlapuu et al 2016; Lei et al 2019].

To date, only a few AMPs have been approved by the Food and Drug Administration (FDA).

Polymyxins, introduced already in the 1950s, are the most characterized. They are used for intravenous treatment of drug-resistant infections caused by Gram-negative pathogens but are also applied as topicals formulations in the prevention and treatment of local infections.

Furthermore, daptomycin, was approved and marketed in 2003 as an anionic antibacterial peptide for the treatment of skin infections caused by Gram-positive bacteria. This peptide has also shown growth inhibitory effects on typhoid bacillus and *Staphylococcus aureus* with high drug resistance.

To date, as indicated in the Table 1, there are several AMPs under clinical development in different therapeutic areas. They hold promise to confirm the therapeutic advantage of these novel candidates for a market authorization of new AMP-based drugs [Mwangi et al 2019; Mahlapuu et al 2016].

Table 1. *Examples of AMPs in clinical phase of development.*

AMP	Description	Phase	Indication
Pexigan	Analog of magainin (skin of African clawed frog)	Phase III	Infected diabetic foot ulcers
Omiganan	Derived from indolicidin (bovine)	Phase II/III	Catheter infections and rosacea
Lytixar	Synthetic antimicrobial peptidomimetic	Phase I/II	Gran-positive skin infections
Novoexatin	Derived from defensins (humans)	Phase II	Onychomycosis (fungal nail infection)
LL-37	LL-37 (humans)	Phase I/II	Hard-to-heal venous leg ulcers
Iseganan (IB-367)	Derived from protegrin 1 (porcine leukocytes)	Phase III	Oral mucositis in patients receiving radiotherapy for head and neck malignancy

1.4. FROG SKIN AMPs

Among the sources of natural AMPs, amphibian skin is considered one of richest [Conlon 2011].

They are mainly located at high concentrations in dermal serous glands of skin dorsal region of the animal acting as protector agents against invading microorganisms. As reaction to stress or tissue damage, adrenergic stimulation of myocytes, surrounding dermal glands, causes AMPs release of their content onto the skin surface, by a holocrine mechanism [Mangoni 2006; Konig et al 2015; Simmaco et al 1998; Conlon et al 2004].

Since the discovery of magainins from the skin of *Xenopus laevis* [Zasloff 1987] a large number of AMPs has been isolated and characterized from the skin secretion of various Anuran species [Coccia et al 2011; Conlon 2011a].

From various *Rana* genera, many AMPs have been classified into several families, e.g. magainins, temporins, brevinines -1 and -2, ranalexins, ranacyclins, bombinins and esculentins-1 and -2 [Conlon et al 2009; Pantic et al 2017; Mangoni et al 2003; Morikawa et al 1992] on the basis of their structural similarities [Ladram and Nicolas 2016] (Table 2).

Table 2. *Primary structure of some frog-skin AMPs.*

Peptide	**Sequence**	**Genus**
Magainin-1	**GIGKF LHSAG KFGKA FVGEI MKS**	*Xenopus*
Magainin-2	**GIGKF LHSAK KFGKA FVGEI MNS**	*Xenopus*
Bombinin	**GIGAL LSAAK VGLKG LAKGL AEHFA N-NH_2***	*Bombina*
Bombinin H1	**IIGPV LGMVG SALGG LLKKI-NH_2***	*Bombina*
Temporin A	**FLPLI GRVLS GIL-NH_2***	*Rana*
Brevinin-1	**FLPVL AGIAA KVVPA LFCKI TKKC**	*Rana*
Brevinin-2	**GLLDS LKGFA ATAGK CVLQS LISTA SCKLA KTC**	*Rana*
Ranalexin	**FLCCL IKIVP AMICA VTKKC**	*Rana*
Ranaciclin-T	**GALRG CWTKS YPPKP CK-NH_2***	*Rana*
Esculentin-1	**GIFSK LGRKK IKNLL ISGLK NVGKE VGMDV VRTGI DIAGC KIKGE C**	*Rana*
Esculentin-2a	**GILSL VKGVA KLAGK GLAKE GGKFG LELIA CKIAK QC**	*Rana*

**Peptides amidated at their C-terminus.*

1.4.1. Esculentins and Esculentin-1a(1-21)NH_2

Esculentin-1 family is a set of biologically active compounds previously isolated by *Pelophylax lessonae*/*ridibundus* (previously known as *Rana esculenta*) [Conlon 2008] [Figure 13] and afterwards detected also in other different frog species such as the related North American species *Lithobates palustris*/*areolatu* [Basir et al 2000], or obtained by screening skin-derived cDNA libraries [Wang et al 2012; Li et al 2007; Iwakoshi-Ukena et al 2007; Conlon et al 2014].

Figure 13. *A specimen of Pelophylax lessonae/ridibundus*

All members of this family have 46 amino acids with a C-terminal loop stabilized by a disulphide bridge forming an hepta peptide ring [Simmaco et al 1994]. They have a net charge of +5 at neutral pH, an identical 16-46 region and an amphipathic α-helical structure in membrane mimetic environments [Mangoni et al 2015; Wang et al 2016].

The primary structures of some members of esculentis-1 family and their derivatives are showed in Table 3.

Moreover, they are endowed with a broad spectrum of activity against Gram-positive and Gram-negative bacteria, including *P. aeruginosa* and fungal species, such as *Candida albicans* (lethal concentration, LC, ranging from 0.1 to 1.5 μM) with a low toxicity towards mammalian cells [Simmaco et al 1993; Simmaco et al 1994].

After discovering that the fragment isolated from skin secretions of *P. lessonae*/*ridibundus* and corresponding to the 19-46 amino acids of esculentin-1 peptides, was devoid of antimicrobial activity (probably due to its low net positive charge at neutral pH) [Wang et al 2016] the antimicrobial activity of 1-18 portion of the parent full-length peptide was tested.

This synthetic peptide, named esculentin-1b(1-18)NH_2, i.e. Esc(1-18) (Table 3), was amidated at the carboxyl-end (C-terminal) in order to preserve a net positive charge of +5 at neutral pH and to prevent its proteolytic degradation. It showed a lower hemolytic activity and a comparable antimicrobial activity to that of the full-length parent peptide Esculentin-1b [Mangoni et al 2003].

It was also found that Esc(1-18) adopted an α-helical conformation in anionic lipid vesicles. Since the minimum length for a peptide in α-helical structure to span a phospholipid bilayer (~ 30 Å thick) is 20 amino acids [Gamberi et al 2007], a slightly longer analog of esculentin-1a, named escuentin-1a(1-21)NH_2, i.e. Esc(1-21) (Table 3) was subsequently synthesized and characterized for its biological activity.

Esc(1-21) shares the first 20 amino acids with the natural esculentin-1a peptide, followed by a glycinamide at its C-terminus [Islas-Rodriguez et al 2009]. Differently from Esc(1-18) it carries the substitution Leu-11-Ile and three additional C-terminal residues (Leu-Lys-Gly), giving it higher net positive charge (+6) (Table 3).

Esc(1-21) has a strong antimicrobial activity, mainly against Gram-negative bacteria, e.g. *P. aeruginosa* including both free-living and sessile forms of this microbial pathogen. Specifically, it has a similar efficacy against both reference and clinical isolates of *P. aeruginosa* with a MIC of 4 μM and a rapid bactericidal activity (15 min) causing 99.9% bacterial killing at a concentration ranging from 0.5 μM to 1 μM [Luca et al 2013].

Differently, compared to Esc(1-18), a weaker activity against Gram-positive bacterial strains with MIC values ranging from 1 μM to 64 μM [Kolar et al 2015] and a lower toxicity against human erythrocytes [Isla-Rodriguez et al 2009] have been detected.

Recently, further in-depth *in vivo* studies against mouse models of acute *Pseudomonas*-induced pneumonia were also carried out to investigate its antipseudomonal efficacy. An intratracheal administration of Esc(1-21) significantly prolonged survival of mice (25%) compared to vehicle-treated animals [Luca et al 2013].

The *in vivo* activity of this peptide was also examined in mouse models of *Pseudomonas*-induced sepsis, wherein intravenous administration of Esc(1-21) resulted in 40% prolonged survival mice with respect to controls [Luca et al 2013]. Similarly, when the peptide was locally applied to the ocular surface of mouse models of *Pseudomonas*-induced keratitis, it decreased the eye infection degree, thus protecting the cornea from perforation compared to non-treated infected animals [Kolar et al 2015].

Besides displaying antimicrobial properties, Esc(1-21) was found to possess the ability (i) to hamper the secretion of the pro-inflammatory cytokine TNF-α from *P. aeruginosa* LPS-stimulated macrophages and [Di Grazia et al 2015] (ii) to promote migration of lung epithelial cells causing ~ 100% coverage of

the pseudo-"wound" field produced in a monolayer of bronchial epithelial cells within 20 h at a concentration of 10 µM [Cappiello et al 2016]. This is expected to recover the injured bronchial epithelium.

Table 3. *Primary structure of Esculentin-1 analogs and derivatives.*

Peptide	**Sequence[a]**	**Net charge at neutral pH**
Esculentin-1a	**GIFSK LAGKK IKNLL ISGLK NVGKE VGMDV VRTGI DIAGC KIKGE C**	+5
Esculentin-1b	**GIFSK LAGKK LKNLL ISGLK NVGKE VGMDV VRTGI DIAGC KIKGE C**	+5
Esculentin-1a(1-21)NH_2	**GIFSK LAGKK IKNLL ISGLK G-NH_2**	+6
Esculentin-1a(19-46)	**LKNVG KEVGM DVVRT GIDIA GCKIK GEC**	+1
Esculentin-1b(1-18)NH_2	**GIFSK LAGKK LKNLL ISG-NH_2**	+5

[a]*Basic and acidic amino acids are indicated by red and blue letters, respectively.*

**Peptides amidated at their C-terminus.*

1.5. STRATEGIES TO IMPROVE THE THERAPEUTIC POTENTIAL OF ESCULENTIN-1a(1-21)NH_2

Despite the encouraging hallmarks that make AMPs a valid group of compounds for the new generations of antibiotics, Esc(1-21) is not devoid of the limitations common to all them: (i) the susceptibility to proteolytic degradation; (ii) the cytotoxicity at high concentrations and (iii) the limited ability to overcome biological barriers before reaching the site of infection at effective concentrations [Casciaro et al 2017a; Kang et al 2014; Haney et al 2017; Gordon et al 2005; Barreto-Santamaria et al 2019].

Recent research on AMPs has focused on different rational biochemical and computational approaches based on amino acids replacement [Fjell et al 2011; Porto et al 2017; Biswas et al 2019].

Below is a list of some of these approaches:

1.5.1. Modification of the primary structure: Focus on the diastereomer Esc(1-21)-1c

- ✓ Replacement with natural amino acids: Some amino acids have unique properties, such as proline, due to its low propensity to form α-helical structures. A change in the proline content may cause alteration of the peptide conformation with reduction in cytotoxicity [Zhang et al 1999].
- ✓ Acetylation and/or Amidation of N- and C-terminal ends: One common method to enhance the peptide's stability against proteases is the N-acetylation [Nguyen et al 2005; Papo and Shai 2004]. The C-amidation is frequently used to improve peptide efficacy and to decrease its hemolytic activity by

increasing the overall net positive charge of the primary structure of the peptide and by stabilizing its amphipathic helix formation [Kim et al 2011; Nguyen et al 2010].

- ✓ Cyclization by linking the N- and C-terminus: A well-known method to improve both microbicidal activity and serum stability, in comparison to the linear peptide form [Giuliani et al 2007; Oyston et al 2009].
- ✓ Incorporation of D-amino acids and non-natural amino acids: Since host proteases can recognize and hydrolyze natural L-amino acids, incorporation of D-amino acids into the peptide sequence represents a valuable alternative to protect the peptide from proteolytic degradation without affecting the peptide's functionality [Giuliani and Rinaldi 2011]. Moreover, different types of non-natural amino acid are used to increase the α-helix stability as well as the spectrum of activity of AMPs, including β-didehydrophenylalanine [Gupta and Chauhan 2011] and α-aminoisobutyric acid (Aib) [De Zotti et al 2012].

Considering the existence of a direct correlation between the α-helical content of a peptide and its antimicrobial/cytotoxic activity [Zang et al 2016; Huang et al 2014] an analog of Esc(1-21), containing three α-aminoisobutyric acid (Aib) and named [$Aib^{1,10,18}$]-Esc(1-21) was initially synthesized (Table 4). The Aib-Esc(1-21) revealed a higher α-helical content; a higher activity against Gram-positive bacteria but stronger cytotoxicity compared to the parent peptide [Biondi et al 2017].

Subsequently, with the aim to protect Esc(1-21) from proteolytic degradation and to reduce its cytotoxicity, another analog carrying two D-amino acids,

named Esc(1-21)1c, was synthesized. This is because the insertion of D-amino acids, known as "helix breakers" [Grieco et al 2013], should reduce the peptide helical content and therefore its propensity to perturb mammalian membranes [Strahilevitz et al 1994]. The diastereomer was obtained by replacing two L-amino acids i.e., L-Leu^{14} and L-Ser^{17} with the corresponding D-enantiomers [Di Grazia et al 2015] (Table 4).

In contrast with data obtained for the Aib-analog, this diastereomer was found to be less toxic than the parent peptide against circulating mammalian cells (i.e. erythrocytes and macrophages), with a LD_{50} higher than 256 μM compared 64 -150 μM for the all-L peptide [Di Grazia et al 2015; Cappiello et al 2016]. This finding was also supported by circular dichroism (CD) analysis in lysophosphatidylcholine (LPC) which simulates the zwitterionic nature of mammalian cell membranes [Di Grazia et al 2015].

Moreover, in comparison with Esc(1-21), the diastereomer was more stable in the presence of 10% and 30% fresh human serum (less than 50% of peptide was degraded) [Di Grazia et al 2015] and more resistant to the proteolytic cleavage by human and bacterial elastases [Cappiello et al 2016].

Interestingly, although a slightly lower bactericidal activity was estimated for the diastereomer with respect to the all-L peptide against the free-living form of *P. aeruginosa* (minimum bactericidal concentration equal to 4 μM versus 1 μM of the all-L peptide), the introduction of these two residues in the D-configuration made the peptide significantly more efficient in killing the biofilm form of this pathogen at concentrations lower than 25 μM [Di Grazia et al 2015].

This may be due to: (i) the higher stability of the diastereomer and prolonged residence time with respect to the parent peptide; (ii) easier diffusion through the extracellular biofilm matrix.

Beyond antimicrobial effects, in comparison with all-L isomer, Esc(1-21)-1c resulted to have (i) a stronger activity in promoting re-epithelization of a wounded area produced in a monolayer of bronchial epithelial cells with a concentration of 1 μM [Cappiello et al 2016]; (ii) a lower efficacy in inhibiting the pro-inflammatory cytokine TNF-α secretion from LPS-activated macrophages [Cappiello et al 2016], according to studies showing its ~8-fold lower binding affinity to *P. aeruginosa* LPS when compared to Esc(1-21) [Ghosh et al 2016].

Finally, the diastereomer was also tested *in vivo* to assess its pulmonary toxicity, lung inflammatory reaction as well as antipseudomonal activity.

Upon a single intratracheal instillation of 20 μM (2 μg/ml, 0.1 mg/kg) neither significant pulmonary toxicity nor meaningful lung inflammatory response were noted, as supported by the invariant expression level of airways epithelial cells-associated inflammatory genes (e.g. genes encoding for IL-6, IL-10 and TNF-α and NK-kB) [Chen et al 2017].

Furthermore, the diastereomer was found to reduce lung bacterial burden (~ 2 log reduction in the number of viable bacterial cells) in a mouse model after 24 h from *P. aeruginosa* infection [Chen et al 2017].

Table 4. *Primary structure of Esculentin-1 synthetic derivatives*

Peptide	Sequence	Species/origins
Esc(1-21)	**GIFSKLAGKKIKNLLISGLKG-NH_2***	**Synthetic**
[$Aib^{1,10,18}$]-Esc(1–21)	***Aib*IFSK LAGK*Aib* IKNLL IS*Aib*LK G-NH_2***	**Synthetic**
Esc(1-21)-1c	**GIFSKLAGKKIKN*<u>L</u>*LI*<u>S</u>*GLKG-NH_2***	**Synthetic**

Aib indicates α-aminoisobutyric acid residue. The residues in D-configuration are in italics and underlined.

*Peptides amidated at their C-terminus.

1.5.2. Functionalization of biomaterials with Esculentin-1a(1-21)NH_2 and Esc(1-21)-1c [Esc peptides]

Another novel strategy to improve the therapeutic potential of AMPs includes their coating or conjugation to biocompatible materials by means of nanotechnological tools [Brogden and Brogden 2011; Dutta and Willcox 2014; Kamaruzzaman et al 2019].

Nowadays, the usage of nanotechnologies and studies dealing with the conjugation of AMPs to nanoparticulate systems are increasingly growing [Waghu et al 2018]. In fact, thanks to engineered nanoparticles (NPs) it is possible not only to increase the biostability of the peptide, but also to develop pharmaceutical formulations able to protect the drug from the external environment and to reach the target site [d'Angelo et al 2015a; d'Angelo et al 2015b]. In addition, such formulations would minimize the potential side-effects of the drug while increasing its pharmacological effect and limiting the

number of drug administrations [Pham et al 2019; Wang 2017; Anselmo and Mitragori 2016].

Remarkably, the employment of biocompatible and biodegradable materials, such as lipids (e.g., phospholipids, triglycerides, cholesterol, and monoolein); polymers [e.g., cellulose, chitosan, hyaluronic acid, poly lactic-co-glycolic acid (PLGA), and poly lactic acid (PLA)]; [Gutjahr et al 2016] or inorganic particles (such as gold or silver) is becoming more and more encouraging for new therapeutic formulations [Rai et al 2016; Ramesh et al 2016; Ali et al 2016].

Among various NPs produced in recent years, gold nanoparticles (AuNPs) are prominent inorganic nanocarriers used in the field of biomedical sciences [Pietro et al 2016].

In our case, we have demonstrated how chemical conjugation of Esc(1-21) to AuNPs by poly(ethylene glycol) (PEG) linker [AuNPs@Esc(1-21)] is able to increase the peptide's antimicrobial activity by ~15-fold against both free-living and sessile forms of *P. aeruginosa* with respect to the peptide in the free soluble form.

Furthermore, after conjugation to AuNPs, the peptide was found to preserve its membrane-perturbing and wound-healing activities, without being toxic to human keratinocytes, while displaying a higher resistance to trypsin digestion than the free soluble peptide form [Casciaro et al 2017b].

However, in medicine, the use of biopolymers as new tools for nano-application is taking hold [Vhora et al 2015]. Indeed, several studies have reported the PLGA-based NPs application for delivery of bioactive compounds

in the neoplasia or for atherosclerosis treatment [Chai et al 2017; Imanparast et al 2017].

In order to stabilize the surface of NPs and to facilitate their diffusion through the components of lung biobarriers (i.e. the anionic mucus rich in mucins and the negatively-charged biofilm rich in alginate), positively-charged chitosan (CS) and neutral polyvinyl alcohol (PVA) are the most employed stabilizing agents [Madani et al 2018].

Along these lines, the design and development of NPs containing a model cationic AMP, colistin (Col), with a PLGA core and a shell of either CS or PVA, were produced by emulsion/solvent diffusion technique.

Both CS and PVA modified NPs were found to penetrate a bacterial biofilm enhancing the activity of colistin against *P. aeruginosa* biofilm at longer term compared to the free drug.

In the meantime, the Col-loaded NPs-based formulations were embedded into an inert carrier (lactose or mannitol) to obtain nano-embedded microparticles (NEM). This allowed to achieve long-term stable inhalable dry powders by spray-drying in appropriate formulation conditions [D'angelo et al 2015c].

As underlined above, *P. aeruginosa* is also responsible for different types of ocular surface infections, such as keratitis, mainly associated with contact lenses (CLs) wear, due to the ability of this bacterium to rapidly adhere to silicone hydrogel or hydrogel lenses forming biofilms [Borazjani et al 2004].

Among several novel strategies to reduce the onset of CL-associated cornea infections and particularly to prevent their development, the inhibition of bacterial adhesion to the CLs is the most useful [Subedi et al 2018].

In previous studies, the group of Dr. Willcox demonstrated that once the hybrid peptide melimine, corresponding to the active regions of protamine and melittin [Rasul et al 2010], is bound to contact lenses it is able to reduce corneal infection in animal models [Dutta et al 2016]. Furthermore, melimine and its shorter derivative, Mel-4, when immobilised on CLs surface, has been found to be superior to other cationic peptides, including LL-37 and lactoferrin, showing a remarkable inhibition activity against *P. aeruginosa* and *S. aureus* strains [Dutta et al 2016b].

2. AIMs of the work

The principal aims of the present work were:

- To understand whether the discrepancy in the antimicrobial activity between the two Esculentin-derived peptides [Esc peptides] against the free-living form of *P. aeruginosa* strains reflected a different ability in damaging the outer and/or inner membrane of bacterial cells. To this purpose, mechanistic studies on intact bacterial cells as well as on lipid vesicles of different anionic character and intrinsic negative curvature, were performed.

- To verify the existence of possible intracellular targets in the mechanism of antimicrobial activity of Esc peptides when used at sub-MIC.

- To ameliorate the biological properties of Esc peptides and to overcome the general limitations of AMPs. To this goal, two different applicative strategies were used:

    1. Encapsulation of Esc peptides in poly(lactide-co-glycolide) (PLGA) nanoparticles in order to protect the AMPs from proteolytic degradation and to allow their delivery to the target site.

    2. Covalent conjugation of Esc peptides to hydrogel soft contact lenses (CLs) in order to develop novel anti-infective pharmaceuticals to prevent and treat CL-associated ocular infections.

3. Results

3.1 MECHANISM(S) OF ACTION OF ESC PEPTIDES

3.1.1 Focus on the microbial membrane as target

3.1.1.1 Confocal microscopy analysis and killing activity against the mutant *P. aeruginosa* PAO1 *ΔpdvT* strain

To understand whether the discrepancy in antimicrobial activity between the two Esc peptides was due to differences in their ability to interact with the bacterial outer membrane and/or to a difference in binding and subsequent perturbation of the anionic cytoplasmic membrane, the activity of both peptides was initially investigated on a *ΔpvdT* mutant of *P. aeruginosa* PAO1.

PvdT is an inner membrane component of tripartite ATP-binding cassette efflux pumps, namely the PvdRT-OpmQ pump controlling the secretion of the fluorescent siderophore pyoverdine from the periplasmic space to the extracellular medium. Since *ΔpvdT* mutant strain fails to transport PVD across the outer membrane, the siderophore is accumulated in the periplasm [Imperi et al 2009]. The accumulation of PVD in the periplasm causes the bacterial cells to appear fluorescent under a confocal microscope, when PVD is excited at a wavelength of 405 nm. However, in the presence of molecules that disturb the outer membrane, the accumulated PVD is released outside the cell with consequent loss of fluorescence.

To assess the ability of peptides to damage the outer membrane, PAO1 *ΔpvdT* was treated for 15 min with different concentrations of Esc(1-21) and Esc(1-21)-1c and the results were compared to those of colistin, a well-known disrupting agent of LPS-outer membrane.

Upon visualization of cells by confocal microscopy, it was observed that both colistin and Esc(1-21) were able to determine a total loss of fluorescence at concentrations ≤ 4 μM, while the diastereomer Esc(1-21)-1c had a weaker effect with loss of fluorescence only at concentrations ≥ 16 μM [Figure 14 A-D].

Importantly, fluorescence loss by PAO1 *ΔpvdT* in the presence of peptides suggested their ability to destabilize the outer membrane, causing PVD release to the outside of the cell. Furthermore, as shown by confocal microscopy, both peptides did not cause any apparent morphology variations, since the morphology of bacterial cells did not change in the treated samples with respect to untreated control cells [Figure 14 DIC].

In parallel, the effect of peptides on the viability of the *ΔpvdT* mutant was assessed by viable colony-forming units (CFU) counting 15 min after exposure of bacteria to the peptides at concentrations of 0.5, 4, 16 and 32 μM. As reported in Figure 15, the Esc peptides affected the viability of *P. aeruginosa* cells in a dose-dependent manner. Esc(1-21) caused ~ 4 log reduction in the number of viable cells when used at 4 μM compared to colistin and Esc(1-21)-1c that caused ~ 2 log reduction at the same concentration.

Interestingly, total cell mortality (i.e., 0 CFU/mL) was achieved by colistin and Esc(1-21) at the concentrations of 16 μM and 32 μM, respectively, while a significantly weaker killing activity was recorded for Esc(1-21)-1c at the same concentrations.

Thus, confocal microscopy data suggest that the diastereomer has a weaker outer membrane perturbing activity compared to the parent Esc(1-21) and this reflects in a reduced killing activity.

A

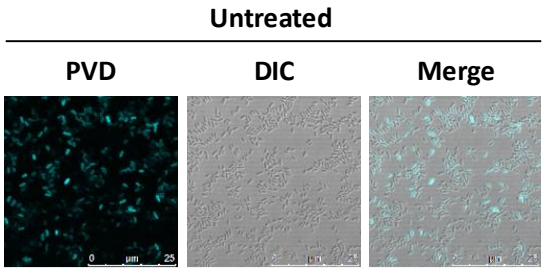
Untreated
PVD
DIC
Merge

B

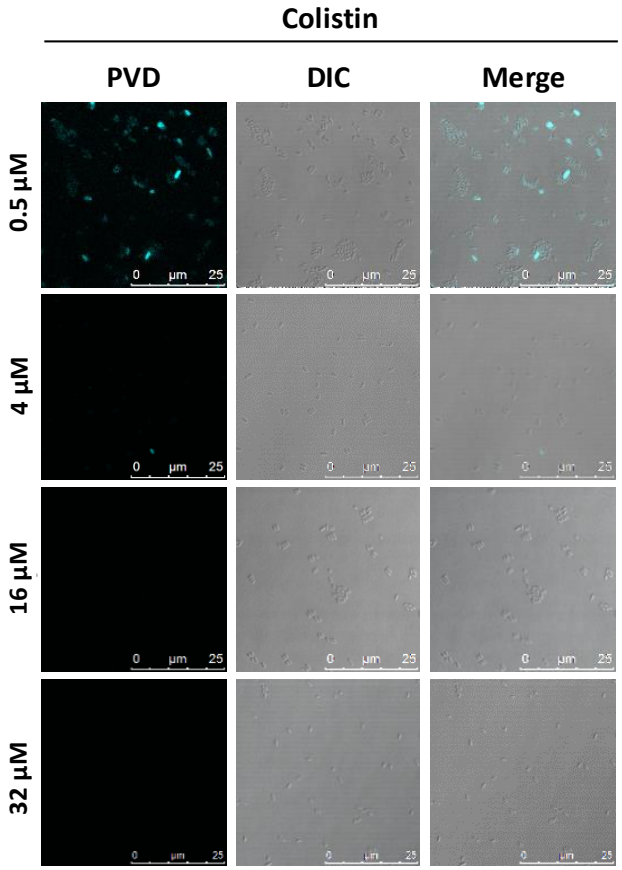
Colistin
PVD
DIC
Merge
0.5 µM
4 µM
16 µM
32 µM

C

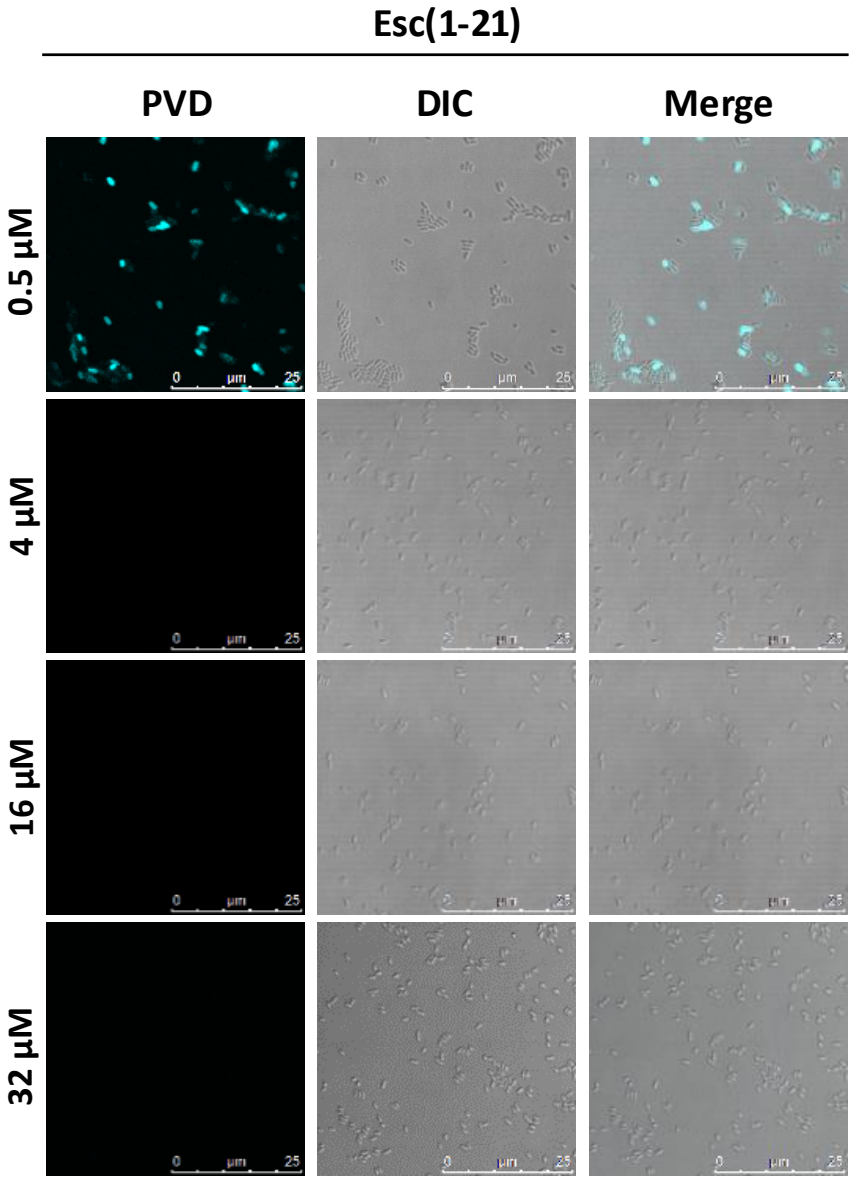

D

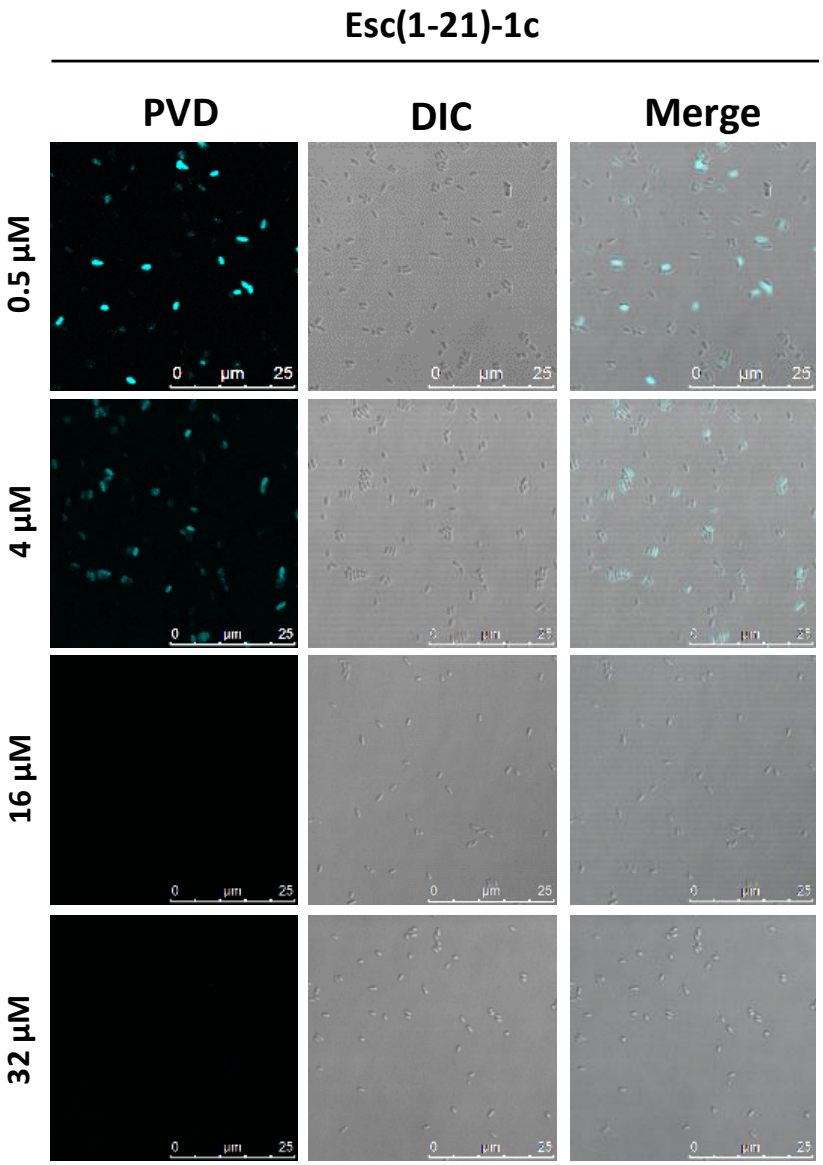

Figure 14. *Panel A-D: Confocal microscopy visualization of the ΔpvdT P. aeruginosa cells upon treatment with Esc peptides and colistin with respect to the untreated control (ctrl) sample (panel A). P. aeruginosa PAO1 ΔpvdT cells (~1x10^9 CFU/ml) were treated with different concentrations of colistin (panel B), Esc(1-21)(panel C) and Esc(1-21)-1c (panel D) for 15 min at 37 °C in phosphate-buffered saline (PBS). Pyoverdine (PVD) emission was visualized after excitation at 405 nm. Representative images of PVD fluorescence, differential interference contrast (DIC) and merged channels are shown. Scale bar, 25 µm.*

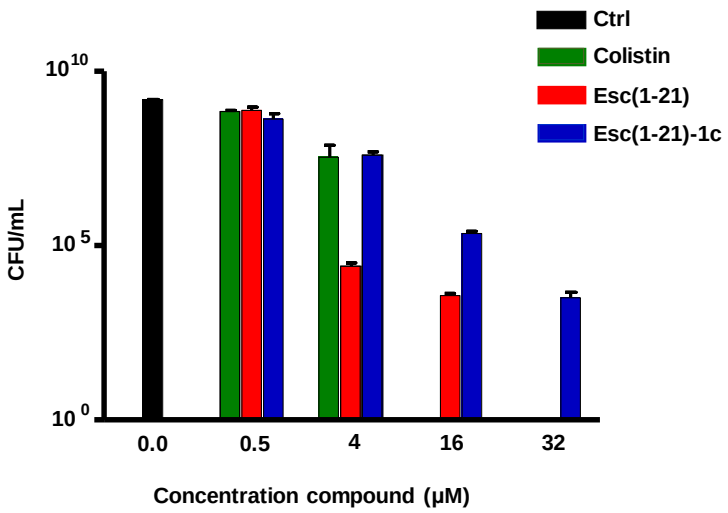

Figure 15. *Effect of peptides on P. aeruginosa PAO1 ΔpvdT cell viability. Bacteria (1x10^9 CFU/ml) were incubated with 0.5, 4, 16 and 32 µM of Esc peptides and colistin in PBS at 37 °C. The number of surviving cells (CFU/ml) was determined after 15 min with respect to the untreated*
control samples (Ctrl). Data are the mean of triplicate samples ± SD from a single experiment, representative of three independent experiments.

3.1.1.2 Cytoplasmic membrane permeabilization

Subsequently, to assess whether this difference reflected a different ability in perturbing the cytoplasmic membrane, a Sytox Green assay was carried out on two different bacterial strains: the reference *P. aeruginosa* PAO1 and the clinical isolate *P. aeruginosa* AA43.

Peptides' activity was evaluated within the first 20 min after peptides addition to bacterial cells, at concentrations ranging from 1 to 32 µM [Figure 16]. Sytox Green (MW 900 Da) is a membrane-impermeant probe, which is excluded from intact cells. In damaged cells, its entrance provokes a rapid increase of fluorescence intensity upon binding to nucleic acids. Basically, the intensity of

the fluorescent signal is tightly correlated to the degree of membrane damage [Luca et al 2013].

As indicated in Figure 16, both Esc peptides were able to destabilize the bacterial membrane of *P. aeruginosa* AA43. A fast kinetics was shown by Esc(1-21) with a total membrane perturbation after 5 min from its addition to the bacteria at 16 μM and 32 μM [Figure 16 A]. Differently, a slighter and slower membrane damage was caused by the diastereomer Esc(1-21)-1c (~40% of membrane injury at the highest peptide concentration of 32 μM within 5 min) [Figure 16 B, 17]. The degree of membrane injury gradually diminished in a dose-dependent manner and became negligible at 1 μM. Differently, at the same time point of 5 min, about 40% of membrane perturbation was caused by 1 μM of Esc(1-21) [Figure 17]. Similar results were obtained with the reference PAO1 and ATCC 27853 strains (data not shown).

These data indicate a significant difference between the two peptides in perturbing the cytoplasmic membrane of intact bacterial cells.

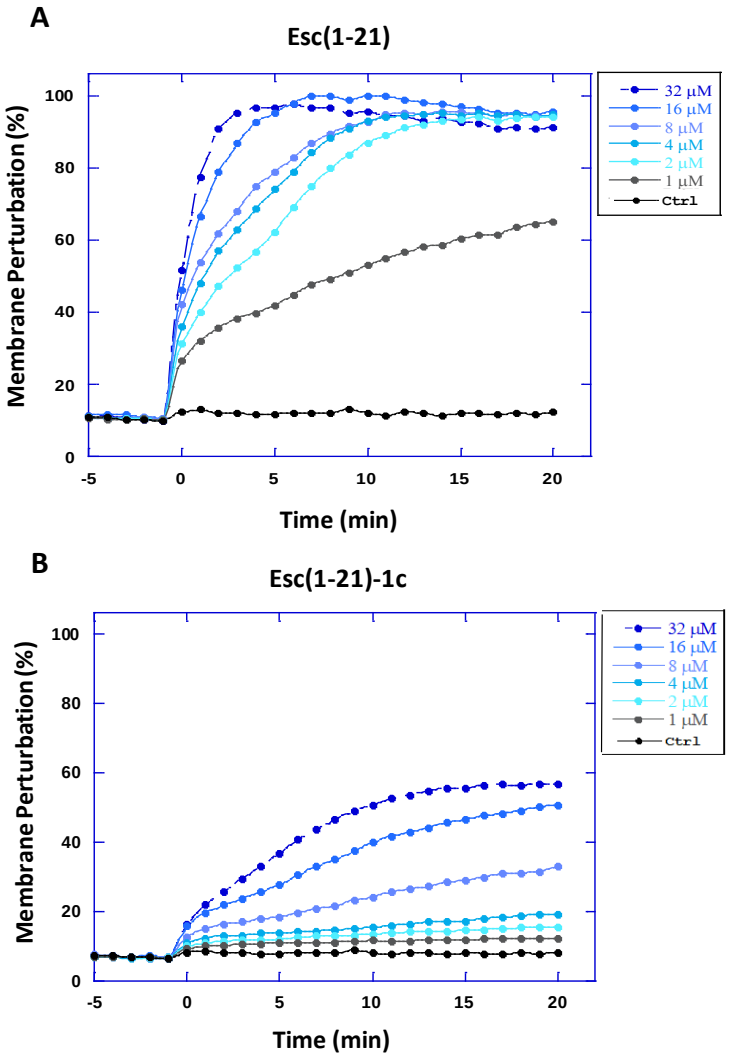

Figure 16. *Kinetics of cytoplasmic membrane permeabilization of the planktonic form of P. aeruginosa AA43. Cells (1×10^7 CFU/ml) were incubated with 1 µM Sytox Green in PBS. Once basal fluorescence reached a constant value, the peptide was added (t=0) at different concentrations and changes in fluorescence (λexc =485 nm, λems= 535 nm) were evaluated for 20 min and plotted as the percentage of membrane perturbation relative to that obtained after treating bacteria with the highest peptide concentration (32 µM) and the addition of 1 mM EDTA+0.5% Triton X-100. Data points represent the mean of triplicate samples from a single experiment, representative of three different experiments. Cells not exposed to the peptide were used as Ctrl.*

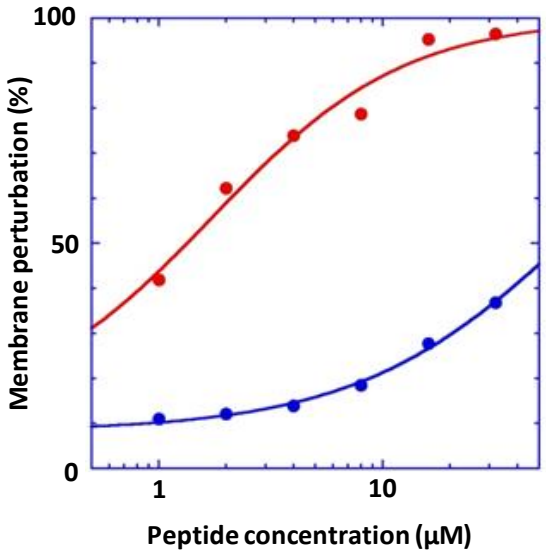

Figure 17. *Dose-dependent response of the cytoplasmic membrane injury of the planktonic form of P. aeruginosa AA43, 5 min after addition of different concentrations of Esc(1-21), red line, and Esc(1-21)-1c, blue line, to the bacterial cells. Data points represent the mean of triplicate samples from a single experiment, representative of three different experiments.*

3.1.1.3 Activity on spheroplasts of *P. aeruginosa*

With the intent to know whether the peptidoglycan layer of the cell wall of *P. aeruginosa* had a role in explaining the different antibacterial and membrane-perturbing activities between Esc(1-21) and its diastereomer, the two peptides were tested against *P. aeruginosa* cells lacking of the cell wall (spheroplasts).

The viability of *P. aeruginosa* PAO1 spheroplasts ($1x10^8$ cells/ml) was evaluated by measuring the reduction of 3(4,5-dimethylthiazol-2yl)2,5-diphenyltetrazolium bromide (MTT) to insoluble formazan, 30 min after peptide addition at different concentrations ranging from 2 to 10 µM.

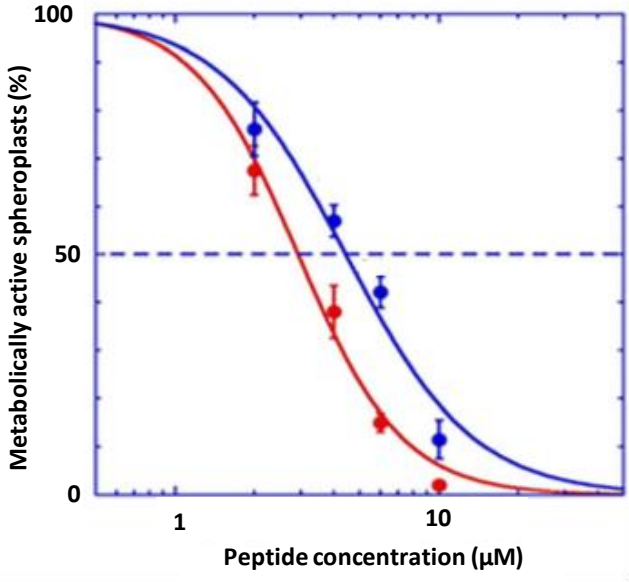

Figure 18. *Viability of spheroplasts of P. aeruginosa PAO1. Spheroplasts viability (1x10^8 CFU/ml) was evaluated by the MTT reduction to insoluble formazan, 30 min after peptide treatment at 37 °C (see Materials and Methods). The effect of Esc(1-21), red line, and its diastereomer, Esc(1-21)1c, blue line, is plotted as percentage with respect to the Ctrl (cells not treated with the peptide). Data represent the mean ± SD of three independent experiments performed in triplicate.*

Overall, as illustrated in Figure 18, no dramatic difference between the two peptides was noted in comparison to their different activity in damaging the inner cytoplasmic membrane. Also in this case, the diastereomer resulted to be the less active molecule.

At the lowest concentration of 2 µM, both peptides caused a limited decrease in metabolic activity of spheroplasts (about 20-35%). However, the reduction in the percentage of metabolically-active cells dropped down to 2% and 12%

for the all-L peptide and its diastereomer, respectively, at the maximum concentration tested, i.e. 10 μM.

3.1.1.4 Leakage assay on large unilamellar vesicles (LUVs) of different composition

To expand our knowledge on the effect of composition, charge, shape and negative intrinsic curvature of membrane phospholipids in the mechanism of action of Esc peptides, leakage assays of lipid vesicles content were performed on large unilamellar vesicles (LUV) loaded with fluorophore/quencher 8-aminonaphthalene-1,3,6-trisulfonic acid/p-xylene-bis-pyridinium bromide, ANTS/DPX solution.

More precisely, LUV made of 1-palmitoyl-2-oleoyl-sn-glycero-3-phosphoethanolamine/1-palmitoyl-2-oleoyl-sn-glycero-3-phosphoglycerol (POPE/POPG) (7:3 mol:mol, 50 μM), 1-palmitoyl-2-oleoyl-sn-glycero-3-phosphoglycerol/ tetra-oleoyl cardiolipin (POPG/TOCL) (8:2 mol:mol, 50 μM) and 1-palmitoyl-2-oleoyl-snglycero-3-phosphocholine/1-palmitoyl-2-oleoyl-sn-glycero-3-phosphoglycerol (POPC/POPG (7:3 mol:mol, 50 μM) were prepared [Leber and al 2018; Lohner 2016] and used for the assay. After peptide addition at increasing concentrations ranging from 0.25 μM to 32 μM, the fluorescence intensity of samples was measured and used to calculate the percentage of probes release, according to what explained in Materials and Methods.

As shown in Figure 19, release of entrapped fluorescence markers from the highly negatively-charged POPG/TOCL LUVs upon addition of Esc(1-21) was observed already at low peptide concentrations ranging from 0.5 μM and 2 μM, with an almost total leakage at 1 μM. In comparison, in the case of Esc(1-

21)-1c, total probe release was achieved at 4 μM. Similar results were found for the less anionic POPC/POPG LUV, with Esc(1-21) and its diastereomer causing complete probe leakage at 2 and 16 μM concentration, respectively.

In contrast, when the two peptides were analyzed on POPE/POPG model membranes that better simulate the composition of the cytoplasmic membrane of Gram-negative bacteria, a significant lower membrane-perturbing activity was shown, with a maximum probe leakage of about 56% and ~ 2% for Esc(1-21) and its diastereomer, respectively, at the highest concentration tested (32 μM).

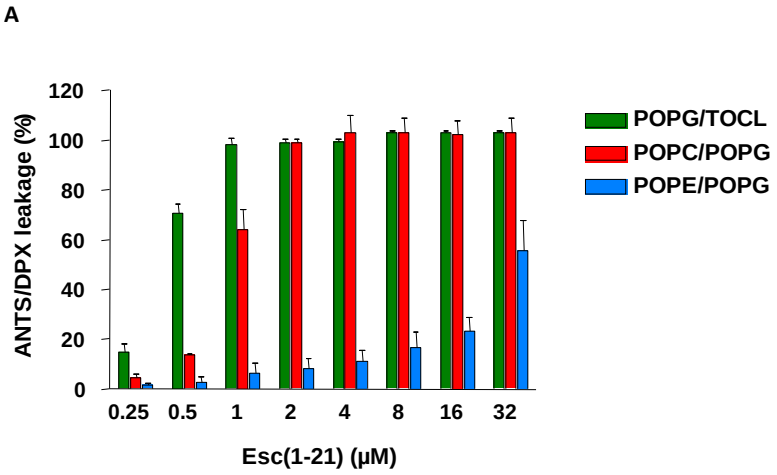

B

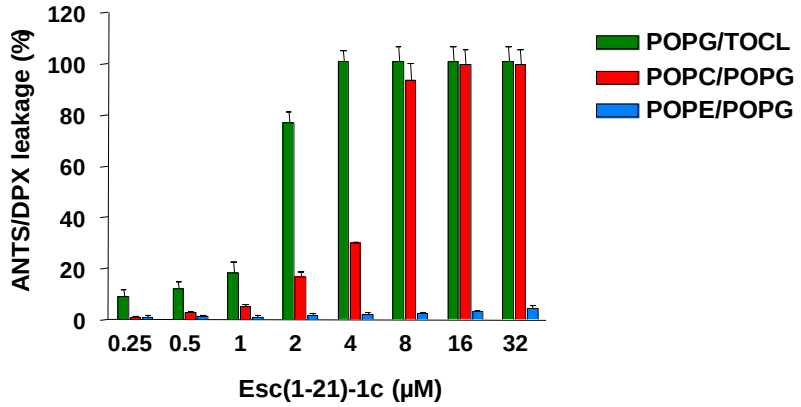

Figure 19. *Effect of different concentrations of Esc(1-21) (panel A) and Esc(1-21)-1c (panel B) on the leakage of ANTS/DPX encapsulated into LUV of different lipid composition. LUVs were used at a final lipid concentration of 50 μM. Fluorescence emission was recorded as a function of time before and after the addition of incremental amounts of peptide, ranging from 0.25 up to 32 μM. The percentage of leakage was calculated according to Eq.: 100x(F-*F_0*)/*F_{max}*-*F_0 *where F is the measured fluorescence,* F_0 *is the initial fluorescence without peptide, and* F_{max} *is the fluorescence corresponding to 100% leakage gained upon addition of 1% Triton X-100 (as explained in the Materials and Methods). Data points are the mean ± SD of three experiments measurements performed in duplicate.*

Overall, when the leakage assays were carried out on the highly anionic POPG/TOCL vesicles, the complete membrane perturbing activity was obtained at a 4-fold lower concentration for the parent Esc(1-21) with respect to the diastereomer. This discrepancy was maintained on POPC/POPG LUVs, although the peptides' concentrations causing the total probes release were slightly higher (2 μM and 16 μM for Esc(1-21) and Esc(1-21)-1c respectively). In contrast, when the peptides were tested on POPE/POPG LUVs, their activity was significantly weaker, and almost lost for the diastereomer.

3.1.1.5 Circular Dichroism (CD) spectroscopy

To analyze the conformation of two Esc peptides in association with membrane-mimicking environments, circular dichroism (CD) spectra were initially recorded in the presence of sodiumdodecylsulfate (SDS) and dodecylphosphocholine (DPC) micelles mimicking the anionic and zwitterionic nature of the bacterial and mammalian cell membranes, respectively [Figure 20].

In all cases, the spectral features typical of alpha helical structure were observed, even though this was less pronounced in the case of Esc(1-21)-1c [Figure 20 B], probably due to the presence of D-amino acids.

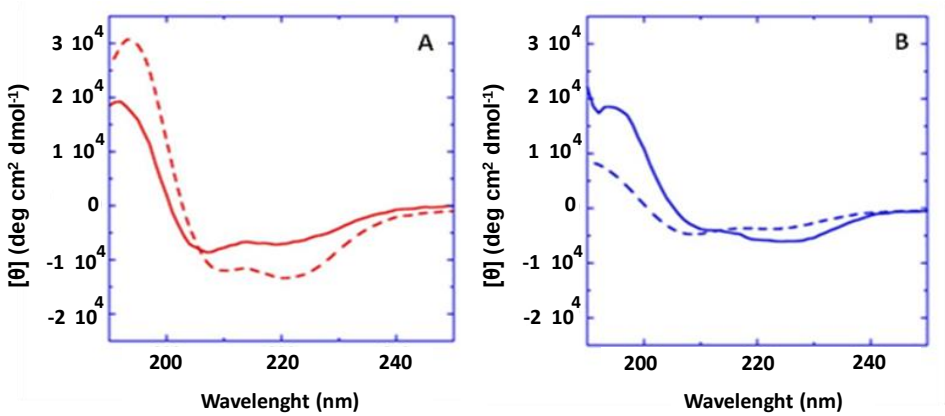

Figure 20. *CD spectra in the presence of SDS and DPC. Circular dichroism spectra of Esc(1-21) (panel A) and Esc(1-21)-1c (panel B), measured in the SDS (broken line) and DPC (solid line) (25 μM peptide, 40 mM SDS or 10 mM DPC).*

Subsequently, the selectivity of AMPs towards membranes with different lipid composition, charge, shape and curvature, was tested by studying the affinity of AMPs to model membranes (i.e. LUVs) mimicking natural phospholipid

bilayers. CD spectra of peptides in the presence of increasing concentrations of liposomes of different compositions were measured and compared to those obtained in phosphate buffer.

In phosphate buffer, at a peptide concentration of 10 µM, both peptides showed a single negative minimum around 200 nm which is a characteristic spectral signature for random coil conformations.

In contrast, with the addition of increasing concentrations of the highly anionic POPG/TOCL vesicles, both peptide isomers exhibited a similar remarkable binding affinity, with two negative minima at 208 nm and 222 nm, which are indicative of α-helical conformation [Figure 21]. Notably, at lipid concentrations ranging from 9 to 12 µM, a significant binding and increase in helicity was recorded [Figure 23 B].

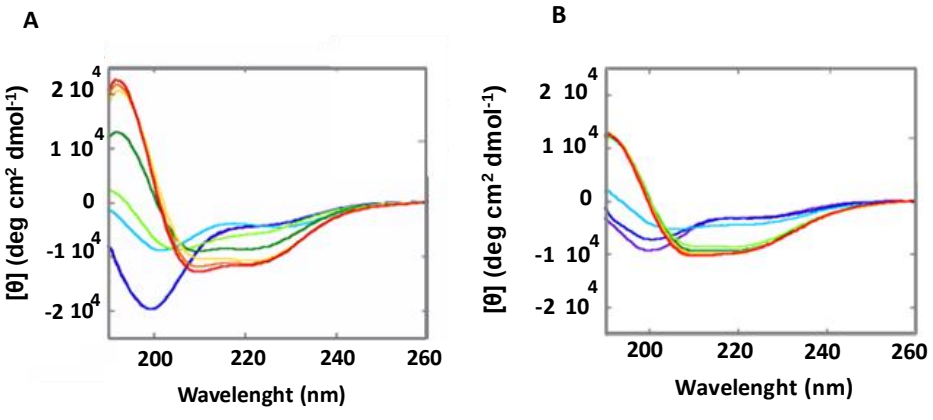

Figure 21. *CD spectroscopy at increasing concentration of POPG/TOCL LUVs. Circular dichroism spectra of Esc(1-21) (panel A) and Esc(1-21)-1c (panel B), measured in the presence of increasing lipid concentrations (POPG/TOCL 8:2 mol:mol). Peptide concentration: 10 µM, lipid concentrations: 3 µM, 6 µM, 9 µM, 12 µM, 15 µM, 20 µM, 30 µM, 40µM and 50 µM. The CD spectra are colored from blue to red, in order of increasing concentrations and following the order of colors in the visible spectrum.*

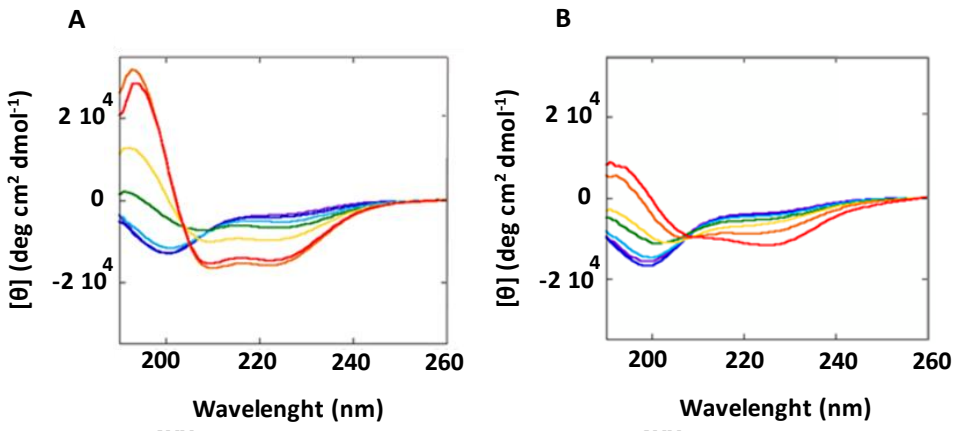

Figure 22. *CD spectroscopy at increasing concentrations of POPE/POPG LUVs. Circular dichroism spectra of Esc(1-21)(panel A) and Esc(1-21)-1c (panel B), measured in the presence of increasing lipid concentrations (POPE/POPG 7:3 mol:mol). Peptide concentration: 10 µM, lipid concentrations: 1 µM, 2 µM, 5 µM, 10 µM, 20 µM, 50 µM, 100 µM, 200 µM, 500 µM and 1 mM. The CD spectra are colored from blue to red, in order of increasing concentrations and following the order of colors in the visible spectrum.*

Differently, according to the leakage results, when the secondary structure of Esc(1-21) and Esc(1-21)-1c was studied in the presence of increasing concentrations of POPE/POPG LUVs, their binding affinity was significantly weaker compared to POPG/TOCL vesicles [Figure 22]. Regardless of the peptide used, substantial enhancement of helicity degree was obtained only at lipid concentrations in the range of 100 µM, even though to a lesser extent in the case of Esc(1-21)-1c [Figure 23 A].

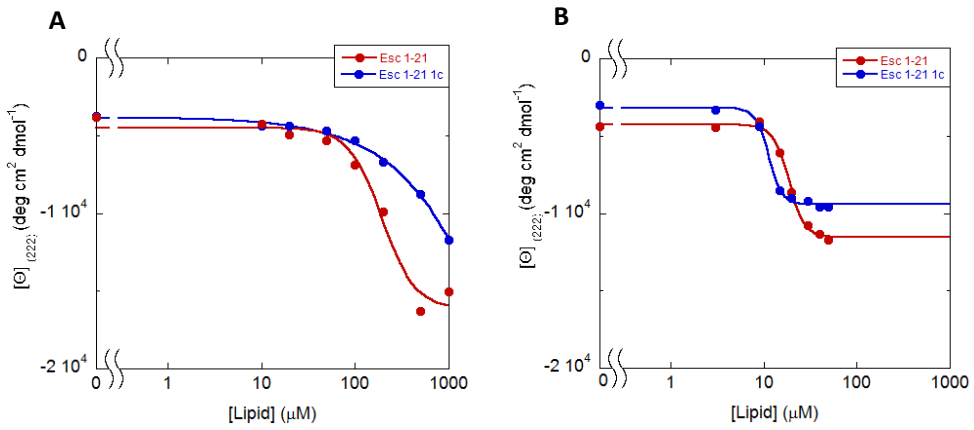

Figure 23. *Mean residue ellipticity ([θ]) at 222 nm as function of lipid concentrations of POPE/POPG LUVs (panel A) and POPG/TOCL LUVsCF (panel B), [peptide] = 10 μM. Esc(1-21) in red and Esc(1-21)-1c in blue.*

3.1.2 Focus on non-membranous targets

3.1.2.1 Identification of intracellular targets in the mechanism of antimicrobial activity of Esc peptides: Antibiofilm activity at dosages below the minimum inhibitory growth concentration (sub-MIC)

To know whether Esc peptides were able to affect the growth of *Pseudomonas* cells when used at sub-MIC levels, their ability to inhibit biofilm formation of *P. aeruginosa* CF clinical isolates was evaluated.

While the diastereomer was able to hinder biofilm growth of *Pseudomonas* strains at all concentrations examined (see attached paper Casciaro et al., 2019), Esc(1-21) seemed to have no activity or rather it stimulated biofilm formation. Notably, since a more marked difference in inhibiting biofilm formation between the two isomers was observed at 1/8 MIC [Figure 24] against the clinical isolate of *P. aeruginosa* AA11, we used this concentration for all the following molecular and non-molecular studies aimed at understanding the underlying mechanism of antibiofilm action [Kaplan 2011].

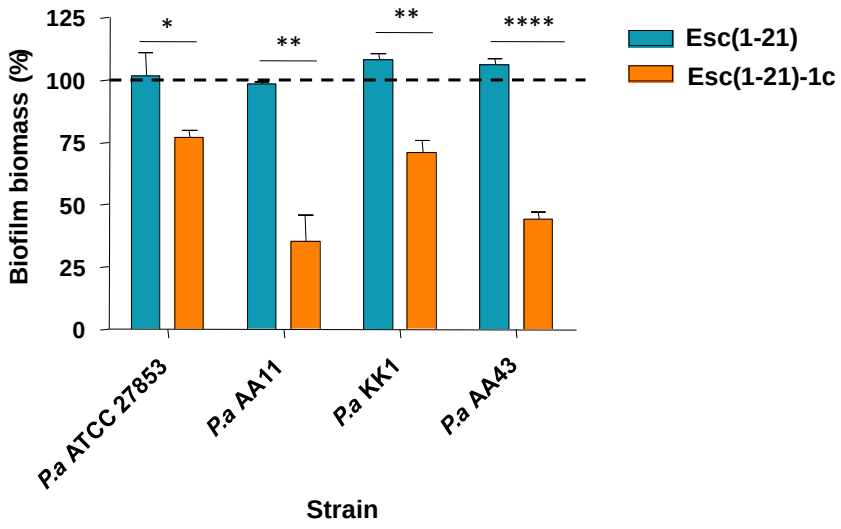

Figure 24. *Biofilm inhibition by Esc peptides at 1/8 MIC on different CF clinical isolates and the reference P. aeruginosa ATCC 27853. After treatment of bacterial cells (5x10^5 cells/ml) for 20 h at 37 °C in humidified environment with Esc peptides at 1/8 MIC, the surface-associated biomass was evaluated by 0.05% crystal violet (CV) staining and the absorbance measured at 590 nm. Data are expressed as percentage of biofilm biomass compared to Ctrl (untreated samples). The results are means ± SEM of three independent experimental repeats. Dotted lines indicate biofilm mass of Ctrl. Statistical significance between the two isomers was calculated by the Student's t-test and reported as *P < 0.05; **P < 0.01; ****P < 0.0001.*

3.1.2.2 Peptides' effect on *P. aeruginosa* motility

In order to investigate whether the inhibition of biofilm formation by Esc peptides was associated with their ability to inhibit bacterial motility, the effect of Esc peptides on the swimming, swarming and twitching *in vitro* motility of the CF clinical isolate *P. aeruginosa* AA11 was studied by evaluating the zone of bacterial growth in 0.3%, 0.5% and 1% agarose plates, respectively (see Materials and Methods) [de la Fuente-Núñez et al 2012].

As reported in Figure 25, while the diastereomer was able to hamper swimming/swarming and twitching motility after overnight incubation at 30°C with bacterial cells, the parent peptide did not have any effect on three types of motility.

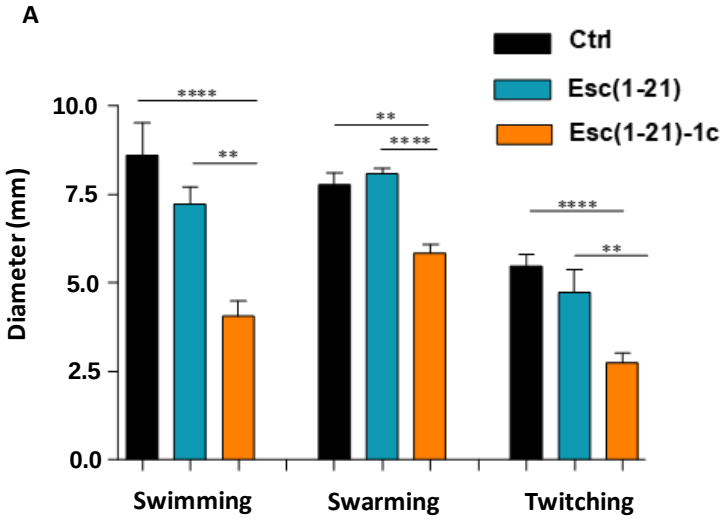

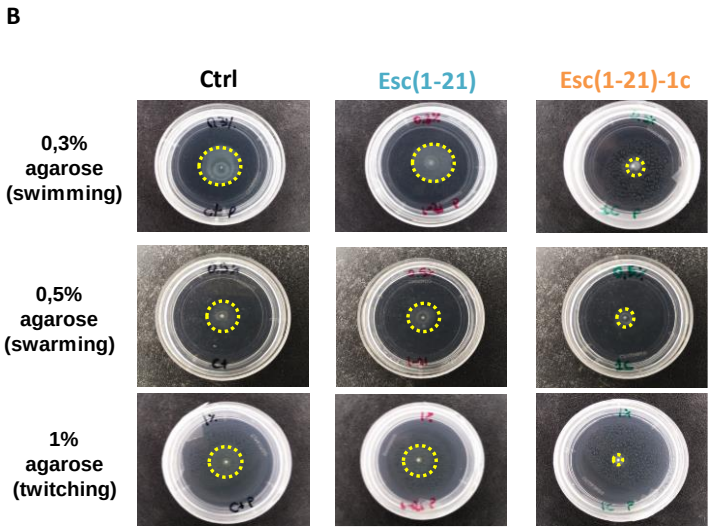

Figure 25. *Esc peptides' effect at 1/8 MIC on the swimming, swarming or twitching motility of P. aeruginosa AA11. (A) Five microliter of bacterial culture grown for 20 h with 1/8 MIC of peptides were inoculated onto plates containing 10% LB supplemented with 0.3%, 0.5% or 1% (for swimming, swarming or twitching motility assays, respectively). Bacterial growth zones were evaluated after incubation at 30 °C for 24 h. Untreated bacteria served as Ctrl samples. The experiments were performed in triplicates with three technical repeats. Data are shown as mean ± SEM. Statistical significance between peptide-treated cells and Ctrl was calculated by the Student's t-test and reported as **P < 0.01; ****P < 0.0001. (B) Representative images of swimming, swarming and twitching motility of P. aeruginosa AA11 strain in the presence of Esc(1-21), Esc(1-21)-1c and Ctrl, after 48h incubation at 30 °C. Dotted circle line indicates the extension zone of bacterial growth. Images are at 1x magnification. All scale bars represent 0.5 cm.*

3.1.2.3 Gene-expression analysis and role of ppGpp nucleotide in biofilm formation

Afterward, to better explore the molecular mechanism underlying the differences between the two Esc peptides in inhibiting bacterial motility, the peptides' effect on the expression of key genes controlling bacterial virulence and motility was evaluated [Winsor et al 2016].

Interestingly, treatment of bacterial cells with the D-amino acid containing diastereomer at 1 μM (a sub-MIC dosage), led to a significant down-regulation

of genes transcription, compared to the level found in bacteria exposed to Esc(1-21) [Figure 26].

The diastereomer was able to inhibit the expression of *fleN*, *fimT* and *fimX* genes, encoding for the flagellar synthesis regulator FleN, the type IV fimbrial biogenesis protein FimT and the twitching motility regulating phosphodiesterase FimX, respectively.

Furthermore, mRNA levels of *lasI* and *lasB* genes, which play a key role in the quorum sensing intercellular communication and in the pathogenicity of *P.aeruginosa* were reduced by about 95% following treatment with the diastereomer Esc(1-21)-1c.

Also the expression of *rhlA* and *rhlB* genes, encoding for rhamnosyltransferase subunits involved in the biosynthesis of rhamnolipids was down-regulated up to ~ 98% [Lin et al 2018].

In addition, treatment of bacteria with Esc(1-21)-1c led to ~ 50% decrease in the mRNA levels encoding for *RpoS*, which affects the production of extracellular alginate and exotoxin A required for the biofilm maintenance [Suh et al 1999].

On the contrary, both Esc peptides did not influence the gene expression of *FliC*, encoding the structural subunit of flagella, B-type flagellin.

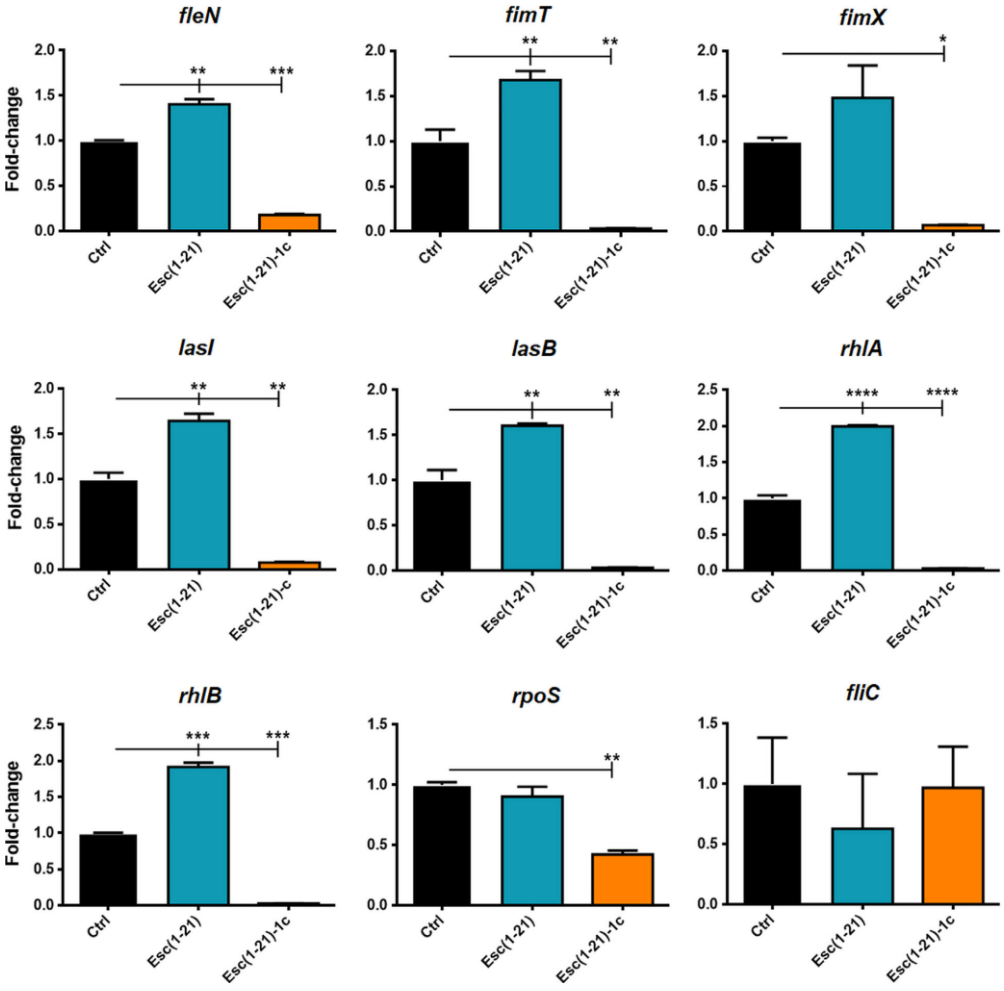

Figure 26. *Effect of Esc peptides on the gene expression of P. aeruginosa AA11. Ten microliters of bacterial culture (1x10^8 cells/ml) were incubated with 1 µM each peptide for 20 h in an orbital shaker at 37 °C. Total RNA was extracted immediately after the incubation. Results are mean ±SEM of three independent experiments. Statistical analyses were carried out by one-way ANOVA and Dunnett's multiple comparisons test. *P < 0.05; **P < 0.01; ***P < 0.001; ****P < 0.0001 compared to untreated control cells, Ctrl (otherwise non-significant).*

It is noteworthy that bacteria under stressful conditions trigger the synthesis of small signalling nucleotides, including guanosine tetraphosphate (ppGpp) that regulates the expression of a plethora of genes controlling biofilm formation

[Xu et al 2016]. Here, the capacity of Esc peptides to target ppGpp was examined by Phosphorus-31 nuclear magnetic resonance (^{31}P-NMR) spectroscopy, as previously done for other AMPs [Berditsch et al 2017]. As highlighted by the ^{31}P-NMR spectra, upon addition of increasing concentrations of peptide, the resonances of the four phosphate groups in ppGpp were shifted by up to 3 ppm upfield, suggesting that the nucleotide part of the molecule was directly involved in the binding to the peptide [Figure 27].

Examination of the spectra revealed that both Esc peptides bound ppGpp in the same way; therefore, the differences between the two isomers could not be attributed to any differential affinity toward ppGpp.

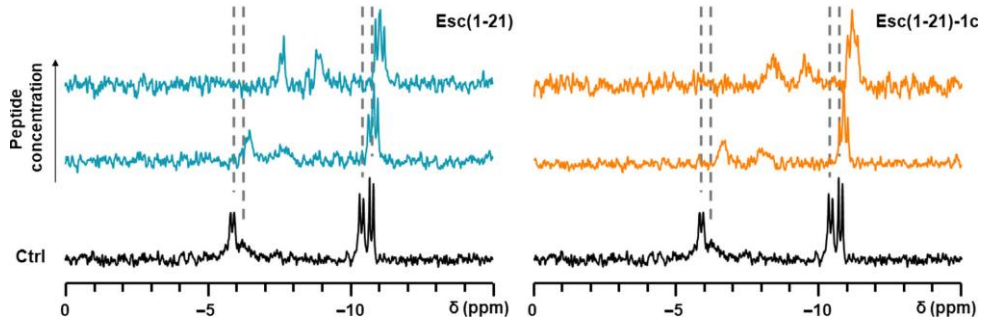

Figure 27. *Interaction of Esc peptides with ppGpp by phosphorus-31 nuclear magnetic resonance (^{31}P-NMR) spectroscopy. Resonances from the four phosphate groups of ppGpp after 2 h incubation with the peptide in aqueous environment (10% D2O) are shifted compared to Ctrl without peptide. Dashed lines indicate the underlying chemical shifts of the nucleotide (without splittings).*

3.2 ENGINEERED NANOPARTICLES (NPs) FOR PROLONGED THERAPEUTIC EFFICACY OF ESC PEPTIDE

To prevent AMPs kidnapping by mucosal and cellular barriers and to favour their translocation across biobarriers, especially in CF patients, poly(lactide-co-glycolide) nanoparticles (PLGA NPs) encapsulated with AMPs were produced as a powerful strategy for pulmonary delivery of Esc peptides at high concentration.

Our engineered PLGA NPs were coated with the stabilizing agent poly(vinyl alcohol) (PVA) in order to provide them with a neutral hydrophilic surface. This was done to prevent NPs aggregation during their formation as well as to assist NPs translocation through the negatively-charged pulmonary barriers e.g. the mucus lining lung epithelium, which is rich in mucins [Ernst et al 2018; Forier et al 2013; Huckaby and Lai 2018; Sahoo et al 2002].

3.2.1 Properties of Esc peptide-loaded NPs

NPs embedded with Esc peptides at a theoretical loading of 2% were successfully prepared by a modified emulsion/solvent diffusion technique [d' Angelo et al 2015]. NPs labeled with rhodamine-B (Rho-Esc) were prepared and used to follow peptide diffusion in simulated mucus/bacterial extracellular matrix (Rho-Esc_NPs). The adopted formulation condition for both peptides led to the formation of a homogeneous population of spherical NPs with a hydrodynamic diameter around 300nm (D_H), as also validated by transmission electron microscopy (TEM) images [Figure 28], a low polydispersity index (PDI), a slight negative ζ -potential and a complete peptide entrapment (Table 5). Representation of the adopted formulation approach is shown in Figure 29.

The cryoprotectant trehalose (THR) was used to lyophilize the Esc peptide-loaded NP formulations in order to preserve the nanostructure integrity (i.e. nanoparticle size and ζ-potential) upon reconstitution in water/saline media; a crucial aspect for drug delivery applications [Fonte et al 2016].

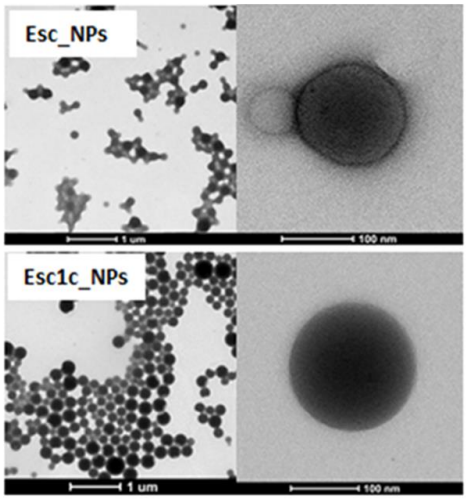

Figure 28. *TEM images of the NPs at different magnifications*

Table 5. *General parameters of Esc peptide-loaded NPs*

	Esc_NPs	Esc1c_NPs
D_H (nm ± SD)	261 ± 1	282 ± 4
PDI (mean ± SD)	0.041 ± 0.020	0.061 ± 0.007
ζ-potential (mV ± SD)	-0.67 ± 0.07	-0.84 ± 0.22
yield of production (% ± SD)	84 ± 2	80 ± 3
actual loading (%[a] ± SD)	2.08 ± 0.047	2.02 ± 0.014
EE[b] (% ± SD)	104 ± 2	101 ± 1

[a]Milligrams of encapsulated Esc peptides per 100 mg of NPs, calculated on the basis of the actual amount of NPs recovered after production (i.e., yield of production). [b]encapsulation efficacy, calculated as actual /theorical loading x 100.

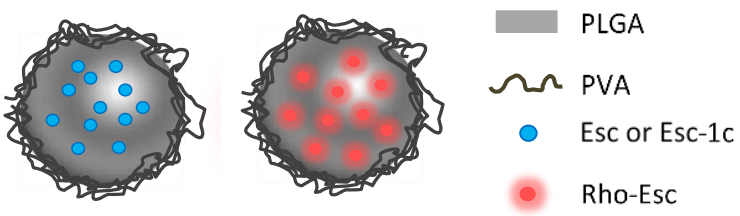

Figure 29. *Representative image of the employed formulation approaches.*

3.2.2 *In vitro* release kinetics

Results of *in vitro* release kinetics of Esc peptides in phosphate-buffered saline (PBS) (pH 7.2) and 37 °C are shown in Figure 30 as a percentage of Esc peptide released from NPs along the time. Both NP formulations displayed a typical biphasic release profile with an initial burst (about 60% of the encapsulated amount released in 3 h) followed by a controlled release of the peptide lasting for about 3 days.

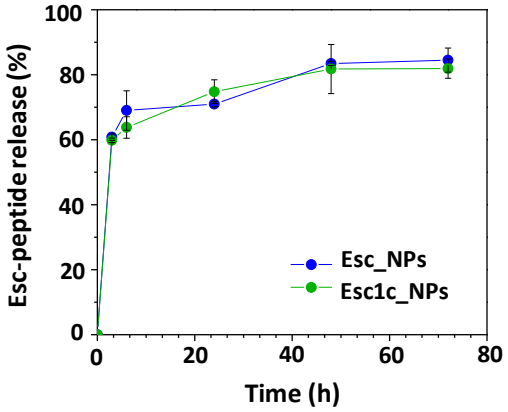

Figure 30. *Esc peptides release profile from the NPs formulation in PBS at pH 7.2 and 37°C. Data are represented as Esc peptide released (%) ± SD of three independent experiments.*

3.2.3 Diffusion of NPs across artificial CF mucus and bacteria biofilm prototype

Studies with NPs containing labeled Rho-Esc were subsequently performed to investigate the ability of NPs to assist the transport of the encapsulated Esc peptide across simulated CF mucus or bacterial extracellular matrix.

The diffusion efficacy of the NPs was investigated by a modified Transwell multi-plate assay (see materials and methods section) and compared to that of free Rho-Esc peptides, for 6 h after depositing the same amount of fluorescent Rho-Esc dispersion on top of the Transwell containing artificial CF mucus or simulated biofilm given by polymannuronic acid [d' Angelo et al 2015].

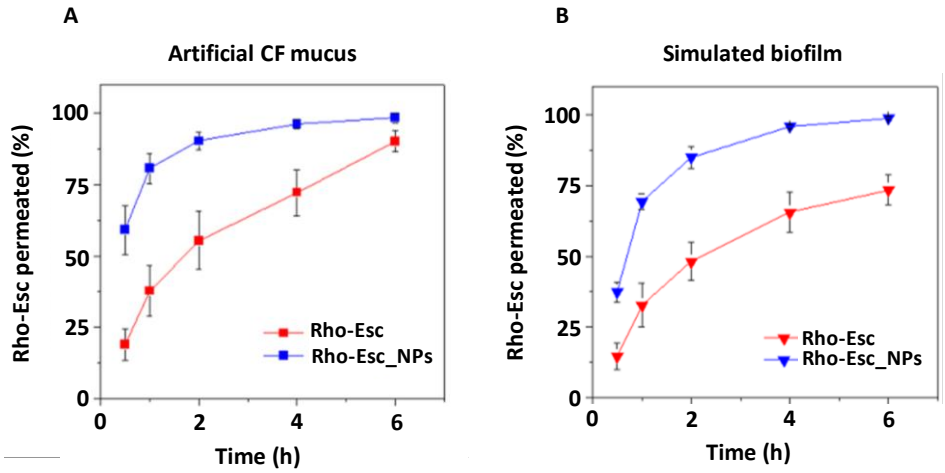

Figure 31. *Diffusion measurements of Esc peptide-loaded fluorescent NPs through simulated CF mucus (A) and bacterial biofilm (B) by the Transwell multiplate assay (see materials and methods). Percentage of permeated kinetics of Rho-Esc both encapsulated inside NPs (Rho-Esc_NPs) and as free form (Rho-Esc) through the acceptor compartments. Data are the mean (± SD) of three independent tests.*

From the analysis of the acceptor medium i.e. simulated interstitial lung fluid (SILF), 2-fold higher percentage of permeated Rho-Esc was found for nano-encapsulated Rho-Esc compared with the free peptide molecule within 1 h (80.7% versus 37.8% for Rho-Esc_NPs and Rho-Esc, respectively) [Figure 31 A].

In parallel, similar diffusion results were observed in simulated bacterial extracellular matrix medium, wherein the amount of permeated peptide in PBS after 1 h was double compared to the free peptide form (69.4% versus 32.7% for Rho-Esc_NPs and Rho-Esc, respectively) [Figure 31 B]. While the total amount of encapsulated Rho-Esc diffused in PBS within 6 h, the percentage of fluorescent free peptide found in the acceptor medium at the same time point was about 70%. This suggested a partial entrapment of the free peptide by alginate of the simulated biofilm [Figure 31 B].

3.2.4 *In vitro* antipseudomonal activity of Esc peptide-loaded NPs

The antibacterial activity of the two Esc peptides-loaded NPs against the planktonic form of the reference strain *P. aeruginosa* ATCC 27853 was determined *in vitro* by evaluating the inhibition of bacterial growth. As shown in Figure 32, while both free peptides caused almost the total inhibition of bacterial growth within a short time interval (24h), this effect was severely inhibited at long-term, causing ~ 40% growth inhibition after 72 hours.

In contrast, Esc peptide-loaded NPs were able to constantly preserve their growth inhibitory efficacy also after 3 days (~ 60% inhibition) compared to the free Esc peptides, despite nano-formulations displayed a lower activity at the shorter time of 24h.

In comparison, no growth inhibition was caused by the bare NPs or the cryoprotectant THR.

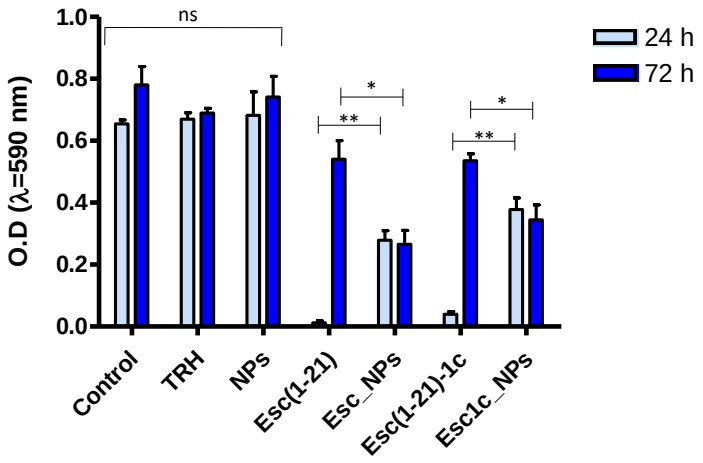

Figure 32. *In vitro antibacterial activity of free Esc peptides, Esc_NPs, Esc1c_NPs, unloaded NPs and cryoprotectant THR after 24 h and 72 h treatment. Aliquots of 100 µl of P. aeruginosa ATCC 27853 (2x10^6 cells/ml) diluted in E^{++} medium were added to 100 µl of free peptide or Esc-loaded NPs [final peptide concentration, 10 and 20 µM for Esc(1-21) and Esc(1-21)1c, respectively] dissolved in the same medium and loaded in a 96-well plate. The absorbance (λ=590nm) was measured after incubation at 37 °C at a short-time (1 day) and a long-time interval (3 days) in comparison with the Ctrl (untreated bacterial cells). The amount of unloaded NPs, THR and Esc peptide-loaded NPs was the same as that present in Esc peptide-loaded NPs. Data are the mean ±SEM of three independent experiments and the statistical significance was evaluated by two ANOVA tests as follows: *, $p < 0.05$; **, $p < 0.01$; ns, non-significant.*

3.2.5 *In Vivo* antimicrobial efficacy of Esc Peptide-loaded NPs

To further explore the antibacterial efficacy of the Esc peptide-loaded NPs with respect to the free peptide, *in vivo* assays on mouse model of acute *P. aeruginosa* lung infection were carried out in collaboration with Prof. Peter Di at Pittsburgh University (US).

A peptide concentration of 0.1 mg/ kg, which was previously found to reduce lung bacterial burden in a mouse model after 24 h from *P. aeruginosa* infection was used [Chen et al 2017]. Samples were intra-tracheally (i.t) instilled 1 h after bacterial challenge, and the number of CFUs in the bronchoalveolar lavage (BAL) and lung homogenate was determined at a longer term (i.e., 36 h) after administration of *Pseudomonas* cells. Bare NPs were also included for comparison [Figure 33].

The data showed that lung bacterial burden was reduced to $\sim 3 \times 10^4$ and $\sim 4.7 \times 10^3$ bacterial cells by Esc(1-21) and Esc(1-21)-1c, respectively, 36 h after lung infection. Nevertheless, when Esc peptide loaded NPs were i.t. instilled, the total lung bacterial burden was significantly lowered (more than 3-log reduction compared to PBS-treated infected animals). Indeed, the total number of CFU (lung homogenate + BAL) dropped down to $\sim 1.8 \times 10^3$ and $\sim 1.1 \times 10^3$ after treatment with Esc_NPs and Esc1c_NPs respectively, compared with the number of CFU in PBS treated infected animals ($\sim 4.4 \times 10^6$) [Figure 33]. As expected, no antimicrobial activity was displayed by the bare NPs or THR.

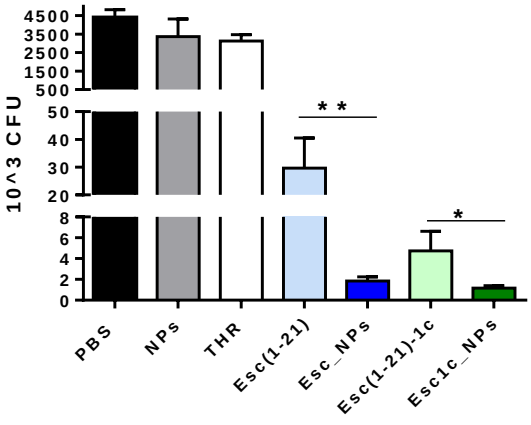

Figure 33. *In vivo antibacterial activity of free Esc peptides, Esc_NPs, Esc1c_NPs, unloaded NPs and cryoprotectant THR in mouse model of acute P. aeruginosa lung infection. Mice were intratracheally (i.t.) inoculated with ~3x10^6 PAO1 cells/mouse. One h after bacterial infection, the free peptide, Esc peptide-loaded NPs (20 µM corresponding to 0.1 mg/kg), unloaded NPs as well as THR dissolved in PBS, were i.t. instilled. The amount of CFU in mouse lung tissue homogenate and bronchoalveolar lavage (BAL) was assessed at 36 h after the bacterial inoculation to estimate the treatment efficacy. The amount of unloaded NPs or THR was the same as that present in Esc peptide-loaded NPs. Results are from three tests and are represented as the mean ± SEM in which n= 5-6 mice for treatment group. The level of statistical significance was calculated by the t-test (* p< 0.05 and ** p< 0.01).*

3.2.6 *In vivo* effect of Esc Peptide-loaded NPs on immune response and pulmonary toxicity

Finally, to investigate the safety of Esc peptide_NPs (at a peptide dosage of 0.1 mg/kg) at the lung level, the amount of inflammatory cells in the BAL of healthy mice was explored after 36 h from the NPs administration.

As reported in Figure 34, treatment with the unloaded and loaded NPs as well as with THR, did not significantly affect the total amount of inflammatory cells in the BAL, compared to the number of cells found in control animals receiving the vehicle PBS. The only exception was given by Esc_NPs, which slightly increased the number of inflammatory cells, hence suggesting that the use of NPs does not induce a significant pro-inflammatory effect at lung.

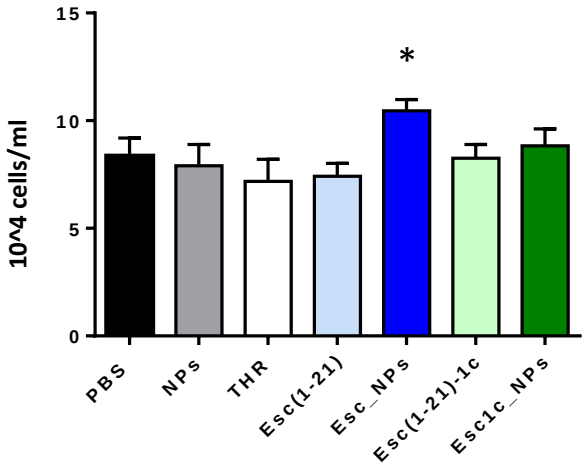

Figure 34. *In vivo evaluation of total inflammatory cell amount in healthy mouse lungs, upon treatment with unloaded and Esc peptide-loaded NPs. After 36 h from i.t. administration of NPs formulations, the total number of inflammatory cells in the BAL of healthy mice was compared to that of PBS-treated animals. Cell numbers in the BAL following treatment with free soluble peptides (0.1 mg/ml) or THR were included for comparison. The amount of unloaded NPs, THR and Esc peptide-loaded NPs was the same as that present in Esc peptide-loaded NPs. Results are the mean ± SEM of three experiments with n=5-6 mice per treatment group. The treatment groups were compared to PBS vehicle control group using t-test and the statistical significance is indicated as follows: p value of < 0.05 (*).*

Furthermore, the effect of NPs instillation on the expression of inflammatory-associated genes (including IL-6, IL-10, or the tumor necrosis factor-α TNF-α and NF-κB) was also assessed in the lungs of mice 36 h from their administration.

Remarkably, no significant difference in the expression of the selected genes was found out in the lungs of healthy mice upon treatment with all different formulations compared to the expression level of mice treated with the vehicle PBS [Figure 35].

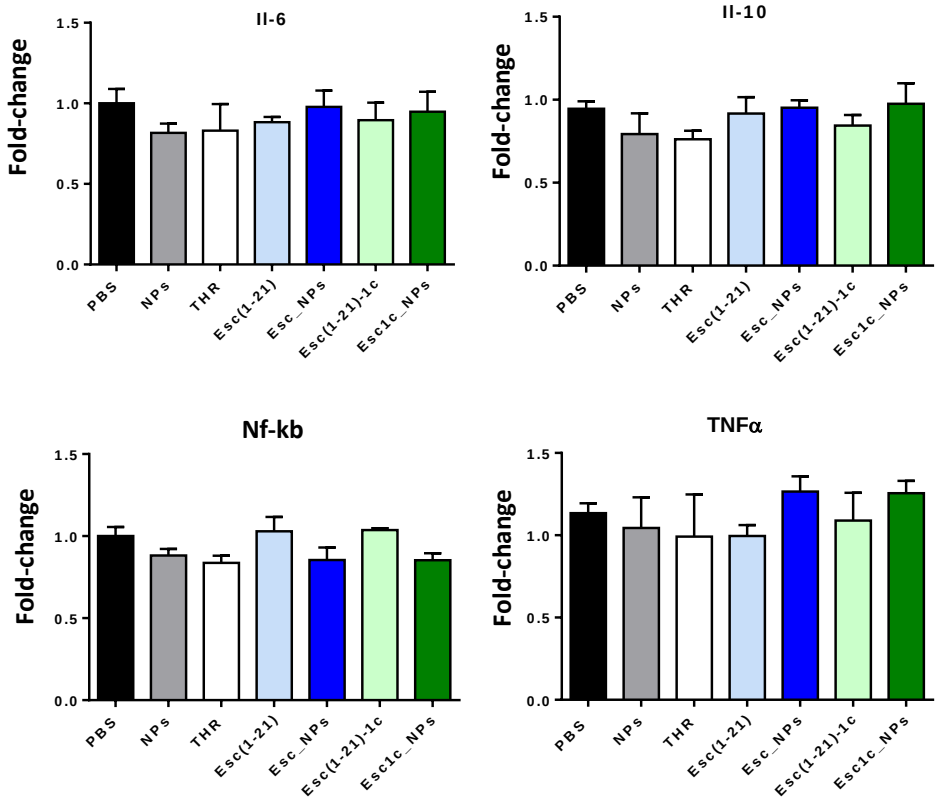

Figure 35. *In vivo effect on the expression of different airway epithelial cell-associated inflammatory genes in healthy mouse, 36 h after treatment with unloaded and Esc peptide-loaded NPs (peptide concentration of 0.1 mg/kg). Gene expression was evaluated by quantitative RT-PCR of total mRNA isolated from lung tissue of treated mice. Mice treated with peptides in the free soluble form or with THR alone were included for comparison. The amount of unloaded NPs, THR and Esc peptide-loaded NPs was the same as that present in Esc peptide-loaded NPs. Results are the mean ± SEM of three experiments with n=5-6 mice per treatment group. No statistically significant difference between groups was noted.*

3.3 IMMOBILIZATION OF ESC PEPTIDES ON HYDROGEL CONTACT LENSES (CLs) TO PREVENT AND/OR TREAT *P. AERUGINOSA*-ASSOCIATED OCULAR SURFACE INFECTONS

Previous studies indicated that Esc(1-21) was able to preserve its antipseudomonal activity in the presence of human basal tears and that it could drastically reduce the infection level in a mouse model of *P. aeruginosa* keratitis [Kolar et al 2015].

Importantly, as mentioned in the Introduction section, microbial keratitis is an infection of the cornea and is mainly associated with contact lens (CL) wear, due to the ability of *Pseudomonas* to strongly adhere to the CL surface, forming biofilms.

One of the most reliable approaches to reduce the risk of CL-associated keratitis is the prevention of bacterial colonization of CLs. Therefore, the conjugation of AMPs to these medical devices could represent an efficient strategy to obtain an antimicrobial surface able to prevent bacterial adhesion and eye infection.

Here, both Esc peptides were covalently bound to the surface of soft contact lenses and their features and biological activity were further investigated.

3.3.1 Covalent immobilization of Esc peptides on CLs and their amino acids quantification

Esc peptides were covalently bound to the surface of hydrogel CLs, via carbodiimide mediated coupling, upon activation of the carboxyl group of methacrylic acid (MAA), present in the lens matrix, by 1-ethyl-3-(3-dimethylaminopropyl) carbodiimide hydrochloride (EDC). CLs activated with

EDC and commercially available CLs were used as process control and control lenses, respectively.

Quantification of peptides immobilized on the CLs surface was determined by amino acids analysis. It revealed no significant difference between the amount of peptide recovered from Esc(1-21) and Esc(1-21)-1c immobilized CL (2.13 ± 0.29 µg and 2.09 ± 0.20 µg respectively). Process control and control lenses had <0.10 µg of peptide associated with them.

3.3.2 Killing activity and inhibition of bacterial adhesion to the surface of Esc peptide-coated CLs

The antipseudomonal activity of the Esc peptides-coated CLs was initially analyzed by evaluating their killing activity against the planktonic form of *P. aeruginosa* ATCC 27853. Interestingly, despite the covalent attachment to the lens, both Esc peptides were able to maintain their antimicrobial activity, causing more than 4 log reduction (99.99% killing) in the number of viable bacterial cells within 20 min incubation with bacteria [Figure 36 A].

Subsequently, the ability of Esc peptide-conjugated CLs to inhibit bacterial adhesion to their surface was evaluated by CFU counting, 24 hours after incubation with bacteria.

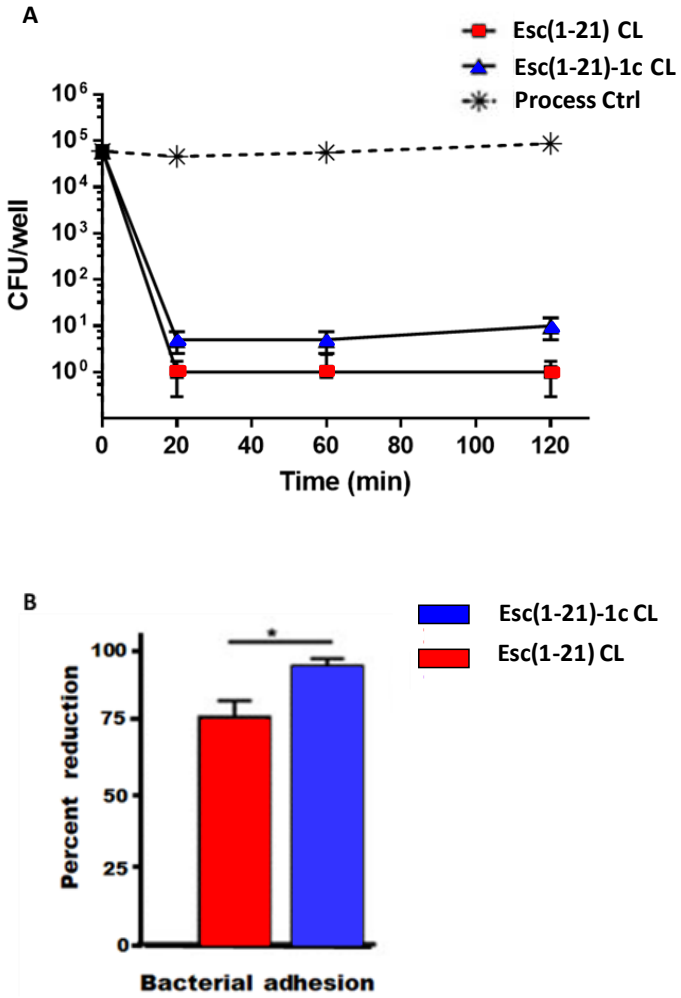

Figure 36. *Antipseudomonal activity of Esc(1-21) and Esc(1-21)-1c-coated CLs. (A) Killing activity of Esc peptides-coated CLs against P. aeruginosa ATCC 27853 (5x10^4 CFU/ml) in PBS at 37 °C. One ml of bacterial suspension was added inside wells of a plate containing Esc-coated CLs, EDC-activated CLs (process Ctrl) or untreated non-coated CLs (Ctrl). At different time intervals, aliquots of all samples were appropriately diluted and plated for CFU counting. (B) Inhibition of bacterial adhesion to Esc peptides-coated CLs with respect to the process control after 24 h incubation in LB medium at 37 °C with a bacterial suspension of 5x10^4 cells/ml. Samples were sonicated to remove bacterial cells from the lens surface and aliquots were diluted and plated for CFU counting. Data are the mean ± SEM of three independent experiments. The level of statistical significance between the two peptides are indicated as follows: *p<0.05, **p<0.01, ***p <0.001*

As indicated in Figure 36 (panel B), both Esc peptides-coated CLs were able to hinder bacterial adhesion to their surface, with a stronger efficacy for the diastereomer Esc(1-21)-1c. In fact, in comparison with the process control or untreated control CLs, ~97% and ~77% reduction in the amount of adherent bacterial cells was observed after 24 hours incubation of *Pseudomonas* with Esc(1-21)-1c and Esc(1-21)-coated CLs, respectively.

3.3.3 Effect of Esc peptide immobilization on CL parameters

Remarkably, as reported in Table 6 peptides conjugation to CLs was not found to affect the CL surface parameters e.g. curvature, diameter and central thickness, the values of which were comparable to those of the commercially available etafilcon A CLs. Furthermore, no optical abnormalities were noticed in the peptide-coated CLs compared to the control lenses, when examined under a Nikon profile projector [Figure 37 A]. Moreover, peptides immobilization to CLs did not provoke any significant change in the CL hydrophobicity, as pointed out by the captive bubble technique for measurements of advancing and receding contact angles [Figure 37 B].

Table 6. *CL parameters of Esc peptide-coated and untreated CLs*

CL Parameters	**CL**			
	Control	**Process control**	**Esc(1-21)**	**Esc(1-21)-1c**
Diameter (mm)	13.89 ± 0.01	13.86 ± 0.02	13.84 ± 0.02	13.86 ± 0.07
Centre thickness (µM)	73.4 ± 4.2	71.8 ± 4.3	72.4 ± 2.1	70.6 ± 3.0

Five CLs (Acuvue 2) for each type of lens coating were randomly selected for the evaluation. The results are indicated as average values ± SD.

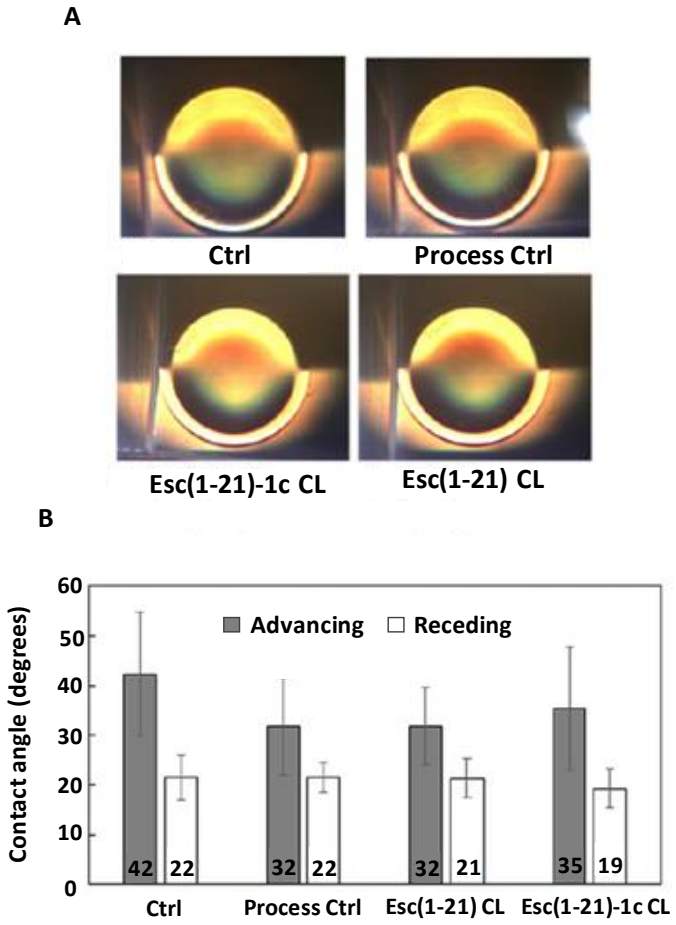

Figure 37. *(A) Representative images of Ctrl, process Ctrl and Esc-peptide immobilized CLs with a Nikon profile projector. The images are representative of five samples. (B) Advancing and receding measurements of contact angle of Ctrl, process Ctrl, Esc (1-21) and Esc(1-21)-1c-immobilized CLs using captive bubble technique. Five CLs (Acuvue 2) for each type of lens coating were selected for the evaluation data (± SD).*

3.3.4 *In vitro* toxicity of Esc peptide-coated CLs

The potential cytotoxicity of Esc peptide-coated CLs was evaluated *in vitro* on murine L929 cells by a direct contact method approved by international organization for standardization (ISO 10993) guidelines for medical devices.

It was assessed on the basis of reactivity grades. This method quantifies the zonal extent of cell damage (0-4 maximum). Negative controls showed mostly healthy cells with no morphological abnormality, whereas positive controls showed that all cells were dead (stained with trypan blue). Both the Esc peptides-immobilized lenses and commercially available etafilcon A lenses gave a minimal response of grade 1 indicating no cytotoxicity, with only few degenerated cells under CL physical contact zone [Figure 38]. Thus, the peptide-immobilized lenses can be considered nontoxic.

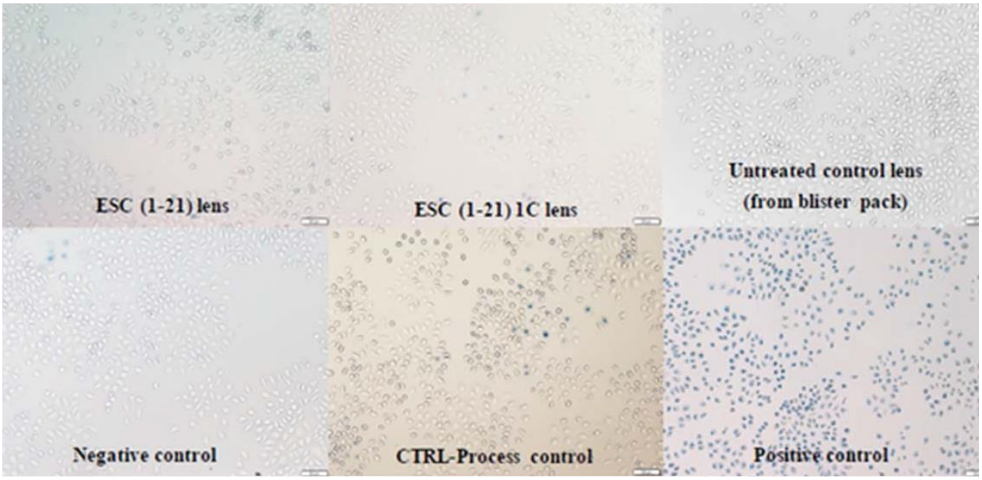

Figure 38. *Representative pictures of the effect of Esc peptide-coated CLs on the vitality of murine L929 cells 24h after incubation. They were estimated by means of bright field and phase contrast microscopy after Trypan Blue staining. Surgical latex gloves and silastic medical grade tubing were used as positive and negative Ctrl, respectively. The pictures are representative of quadruplicate samples.*

4. Discussion

Every year infections caused by multi-drug resistant bacteria provoke millions of deaths and the increasing emergence of bacterial strains resistant to conventional antibiotic therapy has become a worldwide threat for human health.

Pseudomonas aeruginosa is among the most clinically pathogenic bacteria known to cause serious human infections, e.g. pneumoniae, especially in immune-compromised patients or in CF sufferers, as well as keratitis associated to contact lens (CL) wear. This pathogen is difficult to treat, due to its low susceptibility to most available antibiotics and its unique ability to switch from a drug-tolerant planktonic to a more dangerous and treatment-resistant sessile life form, upon adhesion to different types of inert materials or biological tissues.

In this regard, naturally occurring cationic antimicrobial peptides (AMPs) represent an interesting class of gene-encoded molecules endowed with excellent biocompatibility, wide and potent spectrum of antimicrobial activity and immunomodulatory properties [Chen et al 2017; Casciaro et al 2017a; Hilpert et al 2005]. They are promising candidates for the development of new therapeutics mainly due to their mechanism of action, which generally involves the destabilization of the target microbial membrane. However, for a number of AMPs, many evidences point to alternative, non-lytic modes of action, which include AMPs' interactions with specific intracellular molecular targets.

We previously identified a short-sized derivative of the frog-skin AMP esculentin-1a, named Esc(1-21), which was found to quickly kill both free-

living and existing biofilm forms of *P. aeruginosa* with a membrane-perturbing activity as its major killing mechanism [Luca et al 2013]. In contrast with the majority of mammalian AMPs, topical application of Esc(1-21) resulted in a significant reduction of infection in a mouse model of *P. aeruginosa*-induced keratitis [Kolar et al 2015].

By changing the stereochemistry of L-Leu14 and L-Ser17 with the corresponding D-amino acids, we designed a diastereomer of Esc(1-21), namely Esc(1-21)-1c. Compared to the wild-type peptide, Esc(1-21)-1c was characterized by an increased stability, a decreased cytotoxicity and higher efficacy in reducing lung bacterial burden in mouse models of acute *P. aeruginosa* lung infection [Chen et al 2017].

Furthermore, our results indicated that in contrast with clinically-used antibiotics, either Esc(1-21) or its diastereomer were able to limit the induction of resistance in *P. aeruginosa* after 15 cycles of treatment at sub-MIC concentrations, preserving antimicrobial activity in medium mimicking the composition of CF lung mucus (see attached paper Casciaro et al 2018).
However, when tested *in vitro* against the free living form of *P. aeruginosa* strains, the diastereomer Esc(1-21)-1c, although endowed with a potent killing activity, was ~ 4-fold lower than that of the wild-type peptide Esc(1-21).

To understand the reason accounting for this discrepancy, the first aim of the thesis was to test both Esc peptides against *P. aeruginosa* PAO1 *ΔpvdT* mutant strain. PvdT is a protein involved in the export of the pyoverdine, the most important fluorescent siderophore produced by *P. aeruginosa*, from the periplasm to the outside of the bacterial cell. The accumulation of PVD in the periplasm makes the mutant strain fluorescent under a confocal microscope. In

the presence of compounds with the ability to perturb the outer membrane of Gram-negative bacteria, such as the antimicrobial peptide colistin, the PVD inside the cell would be released to the external area with a consequent decrease in the fluorescence signal. This suggest that tested agents determine an outer membrane perturbation with a consequent release of PVD and therefore obscuration of the image under confocal microscopy.

On the whole, confocal microscopy data showed a fluorescence loss in the PAO1 ΔpvdT strain after incubation with both Esc peptides and revealed that the diastereomer is endowed with a weaker perturbing activity of the outer membrane compared to the parent peptide Esc(1-21), in line with the corresponding killing data.

This was consistent with previous results highlighting that the relative binding affinity of Esc(1-21)-1c to *P. aeruginosa* LPS was 8-fold lower in magnitude than Esc(1-21), with a minor marked perturbation of LPS structure caused by the diastereomer with respect to the parent peptide [Ghosh et al 2016].

Furthermore, cytoplasmic membrane permeabilization analysis revealed that the activity of Esc(1-21)-1c was weaker and slower than what recorded for all-L peptide.

Interestingly, when the effect of both peptides was analyzed on bacterial cells devoid of cell wall, i.e. spheroplasts of *Pseudomonas*, only a slightly less pronounced microbicidal activity was observed for the diastereomer in comparison to Esc(1-21).

Based on these findings, we can state that the weaker *in vitro* antibacterial activity of Esc(1-21)-1c on the planktonic phenotype of the Gram-negative

bacterium *P. aeruginosa* is mainly correlated to a weaker ability in permeabilizing both bacterial membranes.

To expand the knowledge on the effect of composition, charge, shape and negative intrinsic curvature of membrane phospholipids in the membrane perturbing activity of Esc peptides, leakage assays and CD spectroscopy analysis were then performed.

The leakage experiments demonstrated that, even though a significant membrane-perturbing activity was shown for both peptides when tested on the highly negatively-charged POPG/TOCL LUVs, Esc(1-21)-1c induced ~ 4-fold lower leakage of vesicles content with respect to the parent peptide. This is in agreement with CD spectroscopy data showing a remarkable binding affinity of both Esc peptides to POPG/TOCL vesicles.

When the anionic character was reduced, as in the case of POPC/POPG LUVs, although the discrepancy between the two peptides was preserved in the same ratio, both of them had a weaker membrane perturbing activity, which is consistent with the lower anionic character of these vesicles. Indeed, this would lead to a less electrostatic interaction between the cationic Esc peptides and POPC/POPG vesicles.

In contrast, the vesicles leakage obtained from POPE/POPG LUVs (with negative “intrinsic curvature”) was significantly weaker for both Esc peptides, and almost lost for the diastereomer. These results are in accordance with the CD spectroscopy data highlighting that the membrane binding of peptides was hindered by the negative intrinsic curvature of PE to a larger extent for the diastereomer compared to the parent peptide.

In summary, our results have suggested that the membrane perturbing activity of the two cationic Esc peptides, is favoured by their electrostatic interaction with the negatively-charged membrane phospholipids, while hampered by the bilayer structure packing parameters including hydrogen bonding and intrinsic negative curvature linked to the presence of PE, although this effect is much more marked for the diastereomer.

Furthermore, we previously demonstrated how replacement of two amino acids with the corresponding D-enantiomers in the C-terminal region of Esc(1-21) was sufficient to obtain a peptide with a reduced α-helical content in line with its reduced ability in destabilizing zwitterionic model membranes as well as in killing mammalian cells (LD_{50} value > 256 μM compared to 64 -150 μM for the all-L peptide) [Di Grazia et 2015].

Importantly, even though the two amino acid substitutions caused a weaker activity of the diastereomer against free-living cells of *P. aeruginosa*, they conferred the peptide a higher potency against the more resistant form of this pathogen, that is its biofilm community [Di Grazia et al 2015].

The greater effectiveness of the diastereomer in killing the more dangerous biofilm state of *Pseudomonas* activity is not in contradiction with its lower antimicrobial efficacy against the planktonic state [Drenkard and Ausubel 2002]. In fact, Esc(1-21)-1c is more resistant to proteases, mainly synthesized by biofilm cells compared to planktonic bacteria [Singh et al 2017]. This would result in an improved residence time of the diastereomer and thus prolonged antimicrobial efficacy in comparison with the all-L peptide which would be quickly degraded. Moreover, recent data have highlighted that D-amino acids can favour the disassembly of extracellular matrix of biofilm cells [Romero et al 2010; Segev-Zarko et al 2015].

The second aim of the thesis consisted in the investigation of possible intracellular targets in the biofilm inhibition activity of Esc peptides when used at concentration below those that hamper bacterial growth.

We first demonstrated that the presence of the two D-amino acids in the Esc(1-21)-1c was able to increase the peptide's efficacy in preventing biofilm formation of *Pseudomonas* already after one day of peptide treatment at sub-MIC.

Three hypotheses could explain this remarkable feature of Esc(1-21)-1c. First, the inhibition of flagella-mediated swimming motility of *P. aeruginosa* cells, as proved by both motility assays showing a reduction in the bacterial swimming diameter, and gene expression analysis showing down-regulation of *fleN* gene which controls flagella amount. This would hinder the bacterial cells from achieving a surface for the initial adhesion or from diffusing into the host tissues wherein *in vivo* biofilm formation begins.

Second, the down-regulation of mRNA level of genes involved in the biosynthesis and function of type IV pili (*fimX* and *fimT*). This would hinder either pili-mediated twitching motility, or microcolony formation and surfaces colonization.

Third, the down-regulation of genes encoding for virulence factors (*rhlA, rhlB, lasB, lasI*) that are essential for quorum sensing systems, such as lasI and rhl systems affecting biofilm maturation and host tissues damage.

Previous studies demonstrated that the expression of a large number of genes involved in biofilm growth was regulated by activation of small signalling nucleotides synthesis, such as (p)ppGpp, as a response to stressful environmental conditions. Bob Hancock's group demonstrated that (p)ppGpp

was the principal target in order to inhibit the biofilm formation by the AMP IDR-1018 peptide [de la Fuente-Nunez et al 2014].

In our case, since P-NMR studies revealed that both Esc peptides interacted similarly though weakly with this nucleotide, the different antibacterial activity may be the consequence of a stronger biostability of the D-amino acids peptide than the all-L isomer.

Specifically, a prolonged interaction of Esc(1-21)-1c with ppGpp would constantly reduce the availability of the alarmone, and this would lead to a gradual down-regulation of ppGpp-mediated signalling pathways controlling bacterial virulence (e.g. quorum sensing lasI and rhl systems).

Overall, a stereospecific mechanism mediated by selective inhibition or activation of other intracellular targets by the two peptides may be involved, though the exact molecular aspects are not yet clear, and they will have to be further investigated.

In summary, we demonstrated for the first time that the presence of only two D-amino acids in Esc(1-21)-1c is sufficient to make it more efficient in inhibiting biofilm formation of *P. aeruginosa* by modulating its virulence genes, likely via peptide-bacterial alarmone ppGpp interaction. This effectiveness is more pronounced compared to the all-L parent peptide likely due to the improved resistance of the D-amino acid containing peptide to bacterial proteases, such as elastases.

Finally, regarding the third aim, novel strategies to improve the therapeutic potential of AMPs were investigated, in particular the Esc peptides' encapsulation into polymeric nanoparticles or coating to biocompatible materials.

Currently, in medicine the use of biopolymers as new tools for nano-application is an innovative strategy, to (i) enhance peptides' bioavailability (ii) to reduce AMPs' cytotoxicity and (iii) to optimize peptides' translocation to the target site of action, e.g. the lung tissue (Klinger et al., 2015). Furthermore, for a better therapeutic compliance and to reduce systemic side effects associated with intravenous injection of drugs, a direct administration of AMPs at lungs can act as promising strategy [Rytting et al 2008].

We successfully designed PVA-engineered PLGA nanoparticles (NPs) for encapsulation and controlled release of Esc(1-21) or its analog Esc(1-21)-1c.

In order to stabilize the surface of the NPs and to ameliorate their diffusion, preventing adhesion of the hydrophobic PLGA to the negatively-charged components of lung biobarriers, i.e. mucus and bacterial alginate, the neutral hydrophobic PVA was employed to coat PLGA NPs [Forier et al 2013; Ernst et al 2018].

Since it is necessary to know appropriate physicochemical properties (e.g. size and surface) of inhaled nanoparticles in order to assist their diffusion through the negatively-charged lung components, the mean hydrodynamic diameter of the present NPs as well as the hydrophilic surface was detected.

Surface engineering of PLGA NPs with partially hydrolyzed grade PVA resulted in an almost neutral ζ-potential, making NPs inert toward the negatively charged mucin and alginate [Din and Zhu 2018].

Indeed, we observed that NPs favored Esc peptides transport through an artificial mucus layer and promoted their penetration inside *P. aeruginosa* biofilm.

Importantly, Esc peptide-loaded NPs displayed a prolonged *in vitro* antimicrobial activity against *P. aeruginosa*, compared to the free Esc peptide. According to the kinetics of peptide release in aqueous environment, the initial burst would act as an attack dose to hinder the growth of a plenty of bacterial cells. Thereafter, the sustained release over time of the Esc peptide would be enough to maintain a constant peptide concentration at the site of action, thus prolonging the antibacterial effect compared to the free Esc peptides.

This would explain the higher antimicrobial activity of Esc peptide-encapsulated NPs along the time, in comparison with the free Esc peptide counterparts.

Furthermore, *in vitro* findings well correlated with the higher *in vivo* efficacy of Esc peptide-loaded NPs than non-encapsulated peptides, causing a significantly lower lung bacterial burden (3-log reduction of CFU compared to vehicle-treated infected animal). Specifically, a 2-fold higher efficacy in killing *Pseudomonas* was detected for Esc1c_NPs compared to all-L peptide-loaded NPs, likely due to the higher *in vivo* stability of Esc(1-21)-1c and its moderate accumulation effect.

Overall, the *in vivo* results have contributed to highlight the usefulness of the NPs in protecting the encapsulated drug as well as in protracting and potentiating its therapeutic efficacy.

Importantly, in line with the reported safety of PLGA NPs for lung delivery, Esc peptide-based nanoformulations were found to be devoid of toxic effect when used *in vivo*.

In summary, this is the first report indicating *in vivo* therapeutic efficacy of AMP-loaded PLGA nanoparticles against *P. aeruginosa* lung infections compared to AMPs in their free soluble form.

With the aim to develop Esc peptides as new ophthalmic pharmaceuticals to treat microbial keratitis associated to CL wearers, we covalently attached Esc peptides to hydrogel CLs, via amide bonding process between MAA of the lens matrix and the amino groups of the peptide.

The total amount of surface tethered peptide (i.e. 2 µg) was enough to achieve an antimicrobial surface able to (i) rapidly kill *Pseudomonas* cells that can be found as contaminants of CLs storage solutions (more than 4-log reduction in the number of bacterial cells), as well as to (ii) inhibit *Pseudomonas* adhesion to CLs after long-term incubation (e.g. 24 hours) under conditions favouring bacterial growth.

Interestingly, according to previous studies dealing with the conjugation of Esc(1-21) or LL-37 to gold NPs [Casciaro et al 2017b; Qin et al 2015] or with the conjugation of melamine to CLs [Dutta et al 2013], our non-directional binding between AMPs and the lens surface did not inhibit the peptides' antimicrobial activity.

This is probably due to the membrane-perturbing mechanism of the two Esc peptides. This would not depend on peptide detachment from the lens surface or its mobility, but rather on its cationicity and amphipathicity.

Furthermore, the immobilization of the two AMPs to CLs did not cause any alteration of CL surface contact angles, measured by captive bubble technique, denoting that the surface hydrophobicity was not changed following surface conjugation with the Esc peptides.

In addition, it is worthwhile noting that Esc peptide immobilization to CLs did not make the lenses toxic toward mammalian cells.

In summary, our results have shown that one of the possible advantages of covalent attachment of AMPs to medical devices is related to the stable peptide association to them, reducing AMPs elution and interaction with the surrounding environment thus minimizing their potential cytotoxicity.

5. Conclusion and Future Perspectives

In this work we showed how the weaker *in vitro* antibacterial activity of Esc(1-21)-1c on the planktonic phenotype of the Gram-negative bacterium *P. aeruginosa* is correlated to its lower tendency in perturbing outer and cytoplasmic bacterial membranes compared to the parent all-L peptide.

It is likely that the lesser membrane perturbing activity of the diastereomer Esc(1-21)-1c in comparison to the all-L peptide is due to its weaker binding to LPS followed by a slower translocation into the target bacterial membrane, the permeability of which would be hindered by charge, shape and negative curvature of the membrane phospholipids.

Altogether, the more efficient diastereomer's propensity in inhibiting biofilm formation of *P. aeruginosa* by modulating the expression of its virulence genes combined with its more efficient wound healing effect, higher biostability and lower *in vivo* toxicity, make it a more attractive candidate for the development of novel antibiotics.

Importantly, encapsulation of Esc peptides into PLGA NPs resulted in an improved *in vitro* and *in vivo* antibacterial activity of AMPs compared to their free soluble counterparts, likely due to peptide protection from proteases and controlled release.

Similarly, both Esc peptides represent encouraging candidates to be developed as ophthalmic formulations and/or for the manufacture of antimicrobial CLs to prevent and or treat *P. aeruginosa* associated ocular infections. The structure of the peptides immobilized to CL as well as their *in vivo* antibacterial activity will be considered in future work.

In addition, further experiments will be carried out to investigate the interesting biological properties of Esc(1-21) analogs, e.g. Esc(1-21)-1c, to better understand the biochemical parameters responsible for their antimicrobial features. Particularly, studies aimed at analyzing other molecular mechanisms underlying the multiple properties of Esc peptides will be investigated.

6. Materials and Methods

6.1. MATERIALS

Synthetic Esc(1-21) [GIFSKLAGKKIKNLLISGLKG-$CONH_2$ MW, 2184], and its diastereomer Esc(1-21)-1c [GIFSKLAGKKIKNlLIsGLKG-$CONH_2$ MW, 2184], as well as rhodamine-labeled Esc peptides (Rho-Esc) were purchased from Biomatik (USA/Canada). Briefly, they were assembled by stepwise solid-phase synthesis using a standard F-moc strategy and purified via reverse-phase high-performance liquid chromatography (RP-HPLC) to a purity of 98%, while the molecular mass was checked by mass spectrometry. The following lipids:1-palmitoyl-2-oleoyl-sn-glycero-3-phosphoethanolamine (POPE); 1-palmitoyl-2-oleoyl-sn-glycero-3-phosphoglycerol (POPG); 1-palmitoyl-2-oleoyl-snglycero-3-phosphocholine (POPC); tetra-oleoyl cardiolipin (TOCL) were obtained from Avanti Polar Lipids (Alabaster, AL, USA).

ANTS (8-aminonaphthalene-1,3,6-trisulfonic acid, disodium salt), bodipy-cadaverine and DPX (p-xylene-bis-pyridinium bromide) were purchased from Molecular Probes (Eugene, OR). Sodiumdodecylsulfate (SDS), dodecylphosphocholine (DPC) were obtained from Cambridge Isotope Laboratories (Tewksbury, MA). Colistin, rhodamine, 3-(4,5-dimethylthiazol-2-yl)-2,5-diphenyltetrazolium bromide (MTT), Crystal violet (CV), PVA (Mowiol 40−88, average Mw ∼205 000 Da, 87−89% hydrolyzed), diethylenetriaminepentaacetic acid (DTPA), DNA from calf thymus, mucin type II from porcine stomach, egg yolk emulsion, and RPMI 1640 amino acid solution were from Sigma-Aldrich Sigma (St. Quentin Fallavier, France). Sytox Green was from Molecular Probes (Invitrogen, Carlsbad, CA, USA).

Guanosine-30,50-bisdiphosphate (ppGpp) was from TriLink BioTechnologies (San Diego, CA, USA). Uncapped PLGA 50:50 (Resomer RG 502H, inherent viscosity 0.16−0.24 dL/g) was purchased from Boehringer Ingelheim (Ingelheim, Germany). Nonacetylated polymannuronic acid (average Mw > 5000 Da) from bacterial alginates was supplied by Carbosynth (U.K.). High-performance liquid chromatography (HPLC) grade acetonitrile, methylene chloride, and 96% ethanol were purchased from Carlo Erba Reagents (Italy). Water (HPLC grade). All other chemicals were reagent grade.

6.2. MICROORGANISMS

P. aeruginosa strains used in the antimicrobial assays were the reference ATCC 27853 and PAO1 [Luca et al 2013]; the clinical isolates *P. aeruginosa* KK1, AA43, AA11, from the strains collection of the Cystic Fibrosis Outpatients Clinic at Hannover Medical School, Germany [Bragonzi et al 2009].

Furthermore, *P. aeruginosa* PAO1 *ΔpvdT* [Imperi et al 2009], kindly provided by Prof. Paolo Visca (Roma Tre University, Rome, Italy), was used for the confocal microscopy analysis and antimicrobial activity.

6.3. MAMMALIANS CELLS

The mouse fibroblast cell lines L929 (NCTC clone 929 ATCC CCL-1) were employed. They were cultured in Dulbecco's modified Eagle's medium (DMEM) supplemented with 10% fetal bovine serum (FBS) (Sigma, Irvine, UK) at 37 °C and 5 % CO_2 in tissue culture treated 25-cm2 and 75-cm^2 flasks.

6.4. METHODS

6.4.1. Studies of mechanism of action

6.4.1.1. Confocal microscopy analysis and killing activity against mutant *P. aeruginosa* PAO1 ΔpvdT strain

P. aeruginosa PAO1 *ΔpvdT* was grown in iron-poor Casamino acids (DCAA) medium, washed twice with PBS and resuspended at OD_{600}=0.5 (corresponding to ~ 1 x 10^9 CFU/ml) and consequently incubated for 15 min at room temperature with different concentrations of colistin, Esc(1-21) or Esc(1-21)-1c. Pyoverdine emission was visualized by using a Leica SP5 confocal laser scanning microscope equipped with a 63x oil immersion objective, employing an excitation of 405 nm. Representative images of pyoverdine fluorescence, differential interference contrast (DIC) and merged channels were taken. In parallel, the effect of peptides on the viability of the mutant *ΔpvdT* was evaluated by CFU counting. Briefly, about 1 x 10^9 CFU/ml were incubated with colistin, Esc(1-21) or Esc(1-21)-1c at different concentrations. Aliquots were taken after 15 min, appropriately diluted in saline, and spread onto LB-agar plates for viable cell counting. After overnight incubation at 37 °C, the number of CFU was determined. Controls were run without peptide and in the presence of peptide solvent (PBS). The bactericidal activity was determined by comparing the number of viable cells between the untreated and the peptide-treated samples.

6.4.1.2. Cytoplasmic membrane permeabilization: Sytox Green assay

To assess the ability of Esc(1-21) to alter the bacterial membrane permeability of planktonic cells of *Pseudomonas*, approximately 1 x 10^6 cells in 100 µl of PBS were mixed with 1 µM Sytox Green (Figure 39) for 5 min in the dark.

After adding the peptide, the increase in fluorescence, caused by the binding of the dye to intracellular DNA, was measured in the microplate reader (Infinite M200, Tecan, excitation and emission wavelengths were 485 and 535 nm, respectively) at 37 °C. The peptide concentrations ranged from 1 to 32 μM. Controls were given by cells not exposed to the peptides, whereas the maximal membrane perturbation was obtained after treating bacteria with the highest peptide concentration (32 μM) followed by the addition of 1 mM ethyl-enediaminetetraacetic acid (EDTA) + 0.5 % Triton X-100 (final concentration) to completely destabilize the LPS-outer membrane and solubilize the phospholipid bilayer of the cytoplasmic membrane [Uccelletti et al 2010]. Samples were run in triplicate and the experiments were performed three times.

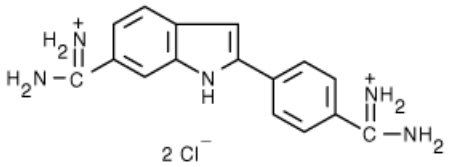

Figure 39*. Chemical structure of Sytox Green*

6.4.1.3. Spheroplasts preparation for 3(4,5-dimethylthiazol-2yl)2,5-diphenyltetrazolium bromide (MTT) assay

Spheroplasts of *P. aeruginosa* PAO1 (1 x 10^8 CFU/ml) were prepared by adapting the procedure published by Sullivan [Sullivan et al 2005]. Briefly, bacteria from a log-phase culture were collected by centrifugation at 3000 ×g and resuspended in an equal volume of 0.01 M phosphate buffer, pH 7.0 (PB). The cells were then pelleted by centrifugation and resuspended in half-volume of 0.5 M sucrose solution in PB (SPB1) to induce plasmolysis. Lysozyme (Sigma) was added to the cell suspension at a final concentration of 50 μg/ml.

After incubation at 37 °C for 90 min with moderate shaking, the sample was diluted 1:1 with PB and EDTA was added to a final concentration of 10 mM. The cell suspension was incubated again at 37 °C for additional 60 min. Thereafter, transition of the rod-shaped bacteria into spheres was determined by light microscopy. When ~80% of the cells were spheroplasted (as visualized by phase-contrast microscopy), the reaction was stopped by pelleting the cells at 500 x g for 15 min. The spheroplasts were then washed in 0.25 M sucrose in phosphate buffer PB (SPB2), centrifuged at 500 x g for 15 min, and resuspended in SPB2. For the antimicrobial assay, 100 µl aliquots of spheroplasts resuspended in SPB2 were treated with Esc(1-21) and its diastereomer for 30 min at 37 °C. After treatment, the effect of Esc peptides on the spheroplasts viability was evaluated by the colorimetric method based on the intracellular reduction of the yellow tetrazolium salt (MTT) to a purple insoluble compound, called formazan, by mitochondrial dehydrogenases (Figure 40 A). The intensity of this colour transformation is directly proportional to the number of metabolically-active cells (Figure 40 B). Briefly, 100 µl of 1 mg/ml MTT were added to the bacterial suspension, transferred into a 96-wells microplate, which was incubated for 90 min at 37 °C. The reduced formazan was then solubilized by the addition of an equal volume of 10% (w/v) SDS, measured in a microplate reader (Infine M 200, Tecan) at 590 nm.

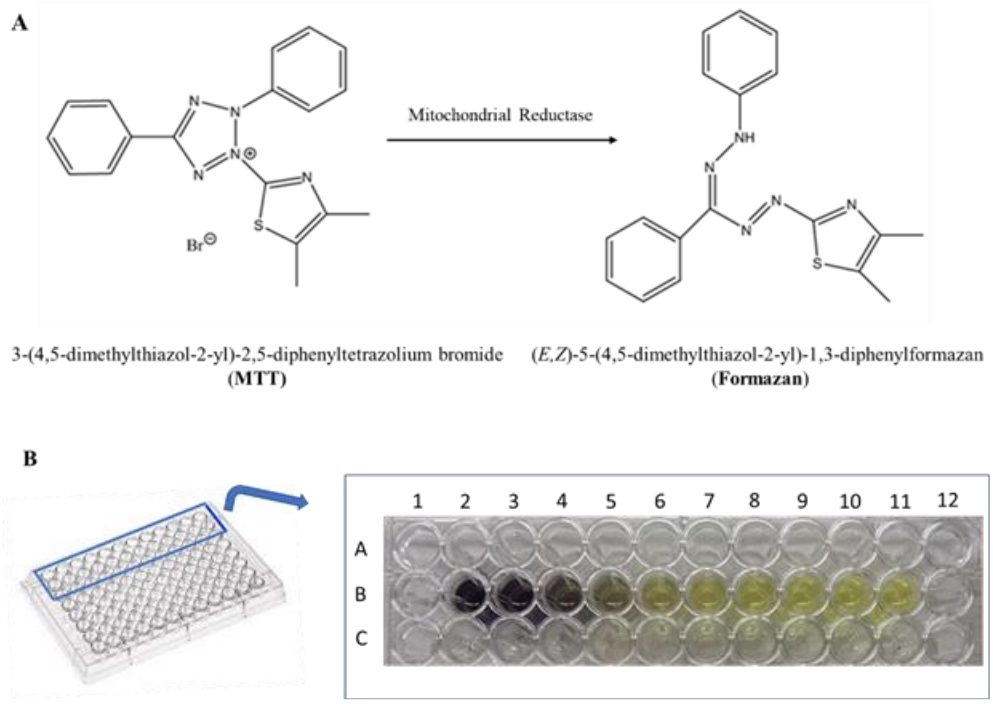

Figure 40. *Reduction of the yellow tetrazolium salt (MTT) to purple insoluble compound, formazan, by metabolically-active cells (A). The intensity of the purple dye is proportional to the number of viable cells. The transparent yellow color in the B11 well corresponds to MTT solution without cells (B).*

6.4.1.4. Preparation of LUVs

Lipid films (20 mg total lipid) of POPG/TOCL, POPC/POPG and POPE/POPG were prepared by dissolving lipids (20 mg of POPE/POPG mixture, 7:3, mol/mol, 20 mg of POPC/POPG, 7:3, mol/mol or POPG/TOCL, 8:2, mol/mol) in chloroform/methanol (2:1, v/v). The solvent was evaporated under reduced argon atmosphere until a thin film was formed. Complete evaporation was ensured by applying a rotary vacuum pump for at least 4 h or over-night at room temperature. Lipid films were then hydrated with HEPES-buffer (10 mM Hepes, 140 mM NaCl, pH 7.4) or with fluorophore/quencher

ANTS/DPX solution (12.5 mM ANTS, 45 mM DPX, 68 mM NaCl, 10 mM HEPES, pH 7.4) for dye-release experiments, following the standard hydration protocol. Subsequently, the dispersions were extruded 25 times through a polycarbonate filter (Millipore-IsoporeTM) of 0.1 μm pore size to obtain LUVs [Zweytick et al 2011]. Non-encapsulated fluorophore and quencher were removed by exclusion chromatography using SephadexTM G-75 gel. LUVs were eluted with HEPES-buffer and the final LUV concentration for dye-release experiments was adjusted to 50 μM. Liposomal lipids were quantified by the determination of lipid phosphorus according to the method described by [Broekhuyse 1968]. NaF was used in place of NaCl for CD experiments, to avoid the high absorption by Clions in the far UV [Kelly et al 2005].

6.4.1.4.1. ANTS/DPX leakage assay

Leakage of ANTS/DPX-loaded LUVs suspension composed of POPG/TOCL, POPC/POPG or POPE/POPG upon incubation with peptides was determined according to Zweytick et al 2011. Briefly, 2 ml of LUV suspension was filled into quartz cuvettes and equilibrated at 37 °C for 5 min. Incremental amounts of peptide solutions prepared in HEPES-buffer were added to the LUV suspension with μ-pipettes and mixed using a magnetic stirrer to achieve final peptide concentrations ranging from 0.25 - 32 μM, corresponding to peptide-to-lipid molar ratios from 1: 200 to ~1:2. Fluorescence measurements were recorded 5 min before and after the addition of incremental amounts of peptides on a Fluorescence Spectrophotometer using an excitation wavelength of λ_{ex} = 360 nm and an emission wavelength λ_{em} = 530 nm. Percentage of leakage was calculated from the fraction of the fluorescence intensity (I_F) according to following equation.

$$I_F = \frac{F - F_0}{F_{max} - F_0}$$

where F is the measured fluorescence, F_0 is the initial fluorescence without peptide, and F_{max} is the fluorescence corresponding to 100% leakage gained by addition of 1% Triton X-100.

6.4.1.4.2. CD spectroscopy

In order to investigate the change in the secondary structure of Esc(1-21) and Esc(1-21)-1c in SDS and DPC micelles, circular dichroism experiments were performed using a Jasco J-815 spectrometer (Jasco International Co., Ltd. Tokyo, Japan) equipped with a Peltier cell holder and temperature controller unit accessory. CD spectra measurements were recorded for both peptides in water (25 μM) and in the presence of different concentrations of SDS (peptide 25 μM, detergent 40 mM), DPC (peptide 25 μM, detergent 10 mM) at 37 °C, or in liposomes of POPE/POPG 7:3 (mol/mol) (peptide 10 μM, lipids up to 1 mM), POPG/TOCL 8:2 (mol/mol) (peptide 10 μM, lipids up to 50 μM) at 25 °C. Both working concentrations of SDS and DPC micelles were previously published as critical micellar concentrations (CMC) [Manzo et al 2013].

The far-UV spectra were scanned over a range of 190-260 nm with 1 nm data interval and averaging over 4 scans. Blank sample spectra were subtracted from the raw data and the CD values were converted to per residue molar ellipticity ([θ]) (deg cm^2 $dmol^{-1}$).

6.4.1.5. Antibiofilm activity

Pseudomonas strains were grown in Luria-Bertani (LB) medium at 37 °C to a mid-log phase. Aliquots (50 µl) of bacteria at a concentration of 1 x 10^6 CFU, appropriately diluted in 10% LB (LB broth diluted 1:10 in water), were added into the wells of a 96-well plate containing 50 µl of diluted LB containing the peptide in serial twofold dilutions. The plate was incubated for 20 h at 37 °C in a humidified incubator. After 20 h, the biofilm biomass was evaluated by CV staining, by adapting the procedure described in [Luca et al 2013]. After the incubation time, peptide-treated wells were washed in PBS, fixed in 99 % methanol for 15 min at room temperature and air-dried. Then, the wells were stained with 200 µl of a CV solution (0.05 % in water). After 20 min, by washing the wells, the excess CV was removed and with addition of 200 µl of 33 % acetic acid the bound CV was dissolved. The absorbance was measured at 600 nm with microplate reader (Infine M 200, Tecan).

6.4.1.5.1. Motility

P. aeruginosa AA11 was grown as described above. In order to simulate the three different types of bacterial motility, aliquots (5 µl) of the bacterial culture grown for 20 h in the presence of each peptide at a sub-MIC level (1/8 MIC) were withdrawn and inoculated in dish plates (3.5 cm) containing diluted LB supplemented with different agarose concentrations, i.e. 0.3%, 0.5% and 1%, plus the peptide at 1/8 MIC. Plates with 0.3%, 0.5% and 1% agarose were used to simulate the three different types of bacterial movement across an aqueous environment (i.e. swimming motility), and across a moist surface of low or moderate viscosity (i.e. swarming or twitching motility, respectively) [Mattick

2002]. After overnight incubation at 30 °C, the diameters of bacterial growth zones were estimated and compared to the control (untreated bacterium).

6.4.1.5.2. Gene expression

About 1×10^8 CFU in mL^{-1} were grown in 10% LB supplemented with each peptide at 1 μM for 20 h at 37 °C. Using TRI Reagent (Sigma-Aldrich) the bacterial RNA was then extracted. A High-Capacity cDNA Reverse Transcription Kit (Applied Biosystems,Waltham, MA, USA) was used to synthesize the complementary DNA (cDNA) and the quantitative data was obtained by Fast SYBR Green Master Mix (Applied Biosystems) and 7900HT Fast Real time PCR (RT-PCR) System (Applied Biosystems). To normalize qPCR results was used the constitutively expressed rplU gene encoding 50S ribosomal as housekeeping gene, whose expression did not change under the described experimental conditions.

6.4.2. PVA-engineered PLGA NPs

6.4.2.1. Synthesis and characterization

Esc peptide-loaded NPs were prepared at 2% theoretical loading (2 mg of peptide per 100 mg of NPs) by a modified emulsion/solvent diffusion technique, as previously described [Ungaro et al 2012]. A water-in-oil emulsion was achieved adding 100 μL of an aqueous Esc peptide solution (2 mg/ml) to 1 mL of PLGA-containing methylene chloride (1% w/v) under vortex mixing (2400 min-1, Heidolph, Germany). The emulsion was then added to 12.5 mL of ethanol (external diffusion phase) to induce polymer precipitation in the form of NPs. NPs dispersion, diluted with aqueous PVA (12.5 mL, 0.01% w/v), was kept under stirring at room temperature for 10 min; afterwards, residual organic solvent was evaporated under vacuum at 30 °C

(Rotavapor®, Heidolph VV2000, Germany). To isolate NPs, the colloidal dispersion, after adjustment to a final volume of 5 mL, were isolated by centrifugation at 7000 rcf for 20 min at 4 °C and the pellet dispersed in ultrapure water. Fluorescent NPs containing Esc(1-21) were prepared to follow peptide diffusion studies in simulated mucus and biofilm (Rho-Esc_NPs). When needed, Esc peptide-loaded NPs were freeze-dried adding THR as cryoprotectant. Just after production, THR was added to the NP dispersion in ultrapure water (NP/THR1:25 w/w), frozen at -80 °C, and freeze-dried for 24 h by a Modulyo freeze-drier (Edwards, U.K.) operating at 0.01 atm and -60 °C.

The hydrodynamic diameter, the polydispersity index, and the ζ-potential of Esc peptide-loaded NPs were determined by dynamic light scattering (DLS) and electrophoretic light scattering (ELS) with a Zetasizer Nano ZS (Malvern Instruments Ltd, U.K.). For ζ-potential analysis, NP aqueous dispersion was diluted in 10 mM NaCl and analyzed in an electrophoresis cell at a fixed potential of ±150 mV. The morphology of Esc peptide-loaded NPs was assessed by TEM.

The actual amount of Esc peptides inside NPs was determined by an indirect or a direct method, as previously reported [d'Angelo et al 2015c]. For the indirect method, after just production, NPs were collected by centrifugation (4◦C, 7000 rcf, 20 min) and the supernatant was analysed for Esc peptide amount by RP-HPLC analysis. For direct method, a dispersion of Esc peptide-loaded NPs in water (4 mg/ml) was centrifuged (7000 rcf for 20 min at 4◦C) and NP pellet freeze-dried for 24 h (0.01 mbar, −80◦C) (Modulyo, Edwards, UK). After freeze-drying, NPs were solubilized in 0.5 mL of acetonitrile and diluted with 1 mL of 30 mM sodium sulfate (pH 3). Upon centrifugation (4◦C, 7000 rcf, 20 min), the samples were analyzed by RP-HPLC, as indicated above.

Results are reported in terms of actual loading (mg of encapsulated Esc peptide per 100 mg of NPs) and encapsulation efficiency (actual loading/theoretical loading x 100).

6.4.2.2. *In Vitro* release kinetics of Esc peptides

Esc peptide-loaded NPs were characterized for the *in vitro* release kinetics in phosphate buffer at pH 7.2 (120 mM NaCl, 2.7 mM KCl, 10 mM phosphate salts). Esc peptide-loaded NPs, appropriately diluted in PBS (4 mg/mL), were incubated in a horizontal-shaking water bath at 40 rpm and 37 °C (ShakeTempSW 22, Julabo Italia, Italy). At scheduled time intervals, samples were centrifuged to isolate NPs, and NP pellet freeze-dried for 24 h. After freeze-drying, Esc peptide content within the NPs was measured by solvent extraction, and the samples analyzed by RP-HPLC, as described above. The amount of Esc peptide, released at each time point, was calculated as the difference between the total amount encapsulated and the amount detected inside the NPs. The results are expressed as percentage of Esc peptide released from NPs (%).

6.4.2.3. *In Vitro* transport of NPs through mucus and biofilm models

The ability of the free peptide to diffuse through artificial mucus and simulated bacterial extracellular matrix was also evaluated by employing Esc(1-21) labeled with rhodamine (Rho-Esc) using a model based on Transwell multiwell plate, as previously reported [d' Angelo et al 2015c]. The artificial mucus was prepared under stirring by adding sterile egg yolk emulsion (25 μL), mucin (25 mg), aqueous DTPA (30 μL at 1 mg/mL), DNA (20 mg), NaCl (25 mg), KCl (11 mg), and RPMI (100 μL) to 5 mL of water [d' Angelo et al 2015c]. The simulated bacterial extracellular matrix consisted of nonacetylated

polymannuronic acid dispersion in water (1% w/v). The diffusion test was carried out on Rho-Esc and compared to that on Rho-Esc-loaded NPs (Rho-Esc_NPs)

Briefly, 75 µL of artificial mucus or polymannuronic acid was transferred in 8 µm pore polycarbonate membrane Transwell inserts submerged in 300 µL of acceptor medium in a 24-well plate. Afterward, 25 µL of a Rho-Esc aqueous solution (1 mg/mL) or 25 µL of a Rho-Esc NP dispersion (5.88 mg/100 µL corresponding to 1 mg/mL of Rho-Esc) was deposited on the top of the artificial mucus or polymannuronic acid layer. SILF, prepared according to the instructions provided by Moss [Moss 1979], or PBS at pH 7.2 was used as acceptor media for mucus or biofilm diffusion experiments, respectively (Figure 41). At scheduled time intervals (from 0 to 6 h), the acceptor medium (i.e., SILF or PBS) was collected and the amount of permeated Rho-Esc was determined by spectrofluorimetric analysis at λex=520 nm/λem=580-640 nm (GloMax Explorer, Promega, Italy). For Rho-Esc_NPs, Rho-Esc was extracted after PLGA matrix degradation in 0.5 N NaOH before analysis. The results are reported as a percentage (%) of permeated Rho-Esc versus the total amount of Rho-Esc.

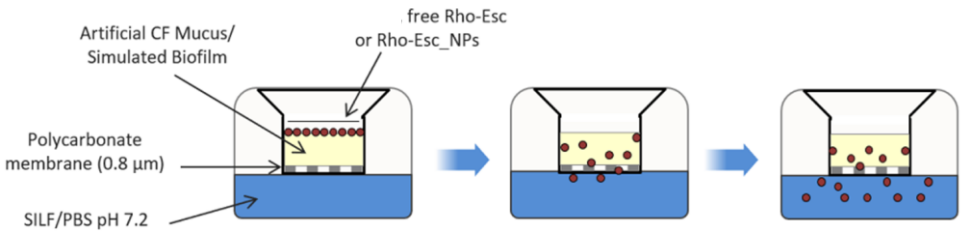

Figure 41. *Schematic drawing of the Transwell multiplate assay.*

6.4.2.4. *In vitro* activity of NPs against *P. aeruginosa*

P. aeruginosa ATCC 27853 was grown in LB medium at 37 °C to a mid-log phase. Upon centrifugation at 3000 x g for 10 min, the bacterial culture was resuspended in minimal medium E [Vogel and Bonner 1956] supplemented with 0.2% glucose, 1 μg/mL vitamin B1 (medium E++) according to [d' Angelo et al 2015c]. It was then diluted in medium E++ and aliquots of 100 μL were added into the wells of a 96-well plate containing 100 μL of dilutions of free peptide or Esc-loaded NPs [final peptide concentration, 10 and 20 μM for Esc(1-21) and Esc(1-21)-1c, respectively] dissolved in the same medium to reach a final cell density of 1 $x10^6$ CFU/mL. It is worth nothing that 10 or 20 μM peptide concentrations were the minimal concentrations of Esc(1-21) or the diastereomer, inhibiting bacterial growth in medium E++ after 20 h. The plate was then incubated at 37 °C, and the absorbance (λ = 590 nm) was measured with a microplate reader (Infinite M200; Tecan, Salzburg, Austria) after a short time (24 h) and long time (72 h) interval. The absorbance value at time zero was subtracted from the corresponding absorbance values at the indicated time points. Unloaded NPs were also tested, and untreated cells used as control.

6.4.2.5. *In Vivo* effect in a murine lung infection model and lung toxicity/ inflammation

An intratracheal (i.t.) inoculation of *P. aeruginosa* PAO1 bacteria (about 3 x 10^6 CFU/mouse) was performed in isoflurane anesthetized mice. One hour after bacterial infection, free peptide and Esc peptide-loaded NPs (at 20 μM corresponding to a peptide dosage of 0.1 mg/kg), and unloaded NPs or THR (in the same amount present in peptide-loaded NPs) were intra-tracheally

administered in 50 µl of PBS. Control mice were instilled with 50 µl of PBS without peptide. To estimate the treatment efficacy, the number of CFU in mouse lungs and bronchoalveolar lavage (BAL) was assessed after 36 h from bacterial instillation [Chen et al 2017]. The mice were anesthetized, the trachea was cannulated, the lungs were washed twice using saline solution, and the BAL samples collected as previously described (Di, 2014). Serial dilutions of BAL and homogenated mouse lungs were spread onto LB-agar plates and incubated overnight at 37 °C, each dilution plated in triplicate, for counting.

As described above, the free peptides, Esc peptide-loaded NPs (at the same concentration used for *in vivo* efficacy studies), as well as unloaded NPs, THR and only PBS (vehicle control), were i.t administered in 50 µl to anesthetized mice. To evaluate the inflammatory effect, after 36 h of treatment mice were anesthetized and sacrificed according to [Di 2014]. The number of inflammatory cells (including macrophages and neutrophils) in the BAL of mice was then counted by a Vision Cell Analyzer automatic cell counter (Nexcelom, Lawrence, MA).

The effect of free Esc peptides, peptide-loaded NPs, unloaded NPs, and THR on the expression of different inflammatory genes or airway epithelial cell-related genes in healthy mice was also evaluated. Total mRNA was isolated from the lung tissue of treated mice using Trizol reagent. Gene expression was performed by quantitative RT-PCR using ABI 7900HT (Applied Biosystems, Foster City, CA) Validation tests of all primers were performed to confirm equivalent PCR efficiencies for the target genes, including IL-6, IL-10, TNF-α, NF-κB, as previously described [Chen et al 2017]. Enzyme-linked immunosorbent assays (ELISA) were performed for quantitative evaluation of

IL-6 (ELISA kit, R&D Systems) and TNF-α (ELISA kit, Invitrogen, ThermoFisher Scientific) from BAL samples.

6.4.3. Covalent immobilization of Esc peptides to CLs and quantification

Etafilcon A soft CLs (Acuvue 2) which contain MAA in the lens matrix were washed and finally soaked in 2 mL of 0.1 M sodium acetate buffer (SAB), pH 5.0 containing EDC for 15 min at 25 °C, to activate the carboxylic group of MAA. After EDC treatment, the lenses were washed and soaked in Esc peptide solution for peptide immobilization (1 mg/mL in PBS) (2 h at 37 °C with gentle shaking). After peptide immobilization, the lenses were washed and soaked in 10% wt/vol sodium chloride overnight. Finally, they were left in PBS for 2 hours to remove the non-covalently peptide attached to lens matrix. CLs treated or not with EDC soaked in PBS (without peptide immobilization) were used as process control or sample control, respectively. The amount of Esc peptide present on the immobilized lens was quantified by amino acid analysis (AAA) according to what explained in Dutta et al 2013. Briefly, lenses were washed in water, and then underwent gas phase hydrolysis 24 h in 6 M HCl at 110 °C (Ajax Finechem Pty Ltd, New South Wales, Australia). After drying the lenses, the amino acids were extracted in 20% acetonitrile in trifluoroacetic acid (Thermo Fisher Scientific, Rockford). The amount of amino acids in the hydrolysates was analyzed using the AccQ-Tag Ultra chemical kit (Waters Corp., Milford). The total amount of Esc peptide binding to lens was regarded as the total amount of amino acids from each lens. Uncoated PBS lenses were used as controls.

6.4.3.1. Antimicrobial activity of Esc-immobilized CLs

P. aeruginosa ATCC 27853 was grown in LB medium at 37 °C until mid-log phase. Aliquots (1 mL) of bacterial culture at concentration of 5 x 10^4 CFU/mL

diluted in PBS was added into the wells of a 24-multiwell plate containing Esc-coated CLs or EDC-activated CLs (process control) or untreated non-coated CLs (control). Aliquots were taken after 20, 60 and 120 min, appropriately diluted and plated on LB-agar plates for CFU counting.

The ability of Esc-coated CLs to inhibit bacterial adhesion was estimated. One mL of bacterial suspension, diluted in LB medium (5 x 10^4 CFU/mL), containing Esc-coated CLs, EDC-activated CLs (process control) or untreated non-coated CLs (control) was grown for 24 h at 37 °C. The lenses were then taken out from the wells and washed with PBS to remove non-adherent bacterial cells. Afterward, they were transferred into Eppendorf tubes containing 500 µl of PBS and sonicated to remove bacterial cells from the lens surface. Finally, aliquots from the Eppendorf tube were withdrawn, diluted and plated on LB-agar plates for CFU counting.

6.4.3.2. Cytotoxicity

In vitro cytotoxicity of the CLs was tested using a direct contact method as outlined in ISO 10993. In detail, murine L929 cells were grown in 24-well cell culture plates until 80% confluence was reached. The peptide-coated CLs, process controls and non-coated controls were taken on the cell monolayer and incubated for 24 h with fresh medium. The cytotoxicity was then assessed by bright field and phase contrast microscopy upon Trypan blue staining.

Cytotoxic responses, i.e. the area of extension of cellular damage, were classified on a scale from 0 to 4 according to ISO guidelines. Silastic medical grade tubes (Dow Corning Corporation, Michigan) and surgical latex gloves (Ansell Medical, Victoria, Australia) were used as positive and negative

controls, respectively. Values of above 1 degree indicate cytotoxic responses under the conditions defined.

6.5. STATISTICAL ANALYSIS

Quantitative data were expressed as the mean ± standard errors of the mean (SEM) or standard deviation (SD). Statistical analysis was carried out by one-way or two-way analysis of variance (ANOVA) and Dunnet's multiple comparisons test or Student's t test with PRISM software (GraphPad, San Diego, CA). Differences with a p value of < 0.05 were considered statistically significant. The levels of statistical significance are indicated in the legend to the figures.

7. References

- Ali, A., H. Zafar, M. Zia, I. Ul Haq, A.R. Phull, J.S. Ali, A. Hussain (2016). Synthesis, characterization, applications, and challenges of iron oxide nanoparticles. Nanotechnol Sci Appl **9**: 49-67.
- Allende, D., S.A. Simon, T.J. McIntosh (2005). Melittin-induced bilayer leakage depends on lipid material properties: evidence for toroidal pores. Biophys J **88**(3): 1828-1837.
- Amini, A., M. Kamali, B. Amini, A. Najafi, A. Narmani, L. Hasani, J. Rashidiani, H. Kooshki, N. Elahi (2018). Bio-barcode technology for detection of *Staphylococcus aureus* protein A based on gold and iron nanoparticles. Int J Biol Macromol **124**: 1256-1263.
- Andra, J., T. Goldmann, C.M. Ernst, A. Peschel, T. Gutsmann (2011) Multiple peptide resistance factor (MprF)-mediated resistance of *Staphylococcus aureus* against antimicrobial peptides coincides with a modulated peptide interaction with artificial membranes comprising lysyl-phosphatidylglycerol. J Biol Chem **286**(21): 18692-18700.
- Anselmo, A.C. and S. Mitragotri (2016). Nanoparticles in the clinic. Bioeng Transl Med **1**(1): 10-29.
- Anunthawan, T., C. de la Fuente-Núñez, R.E.W. Hancock, S. Klaynongsruang (2015). Cationic amphipathic peptides KT2 and RT2 are taken up into bacterial cells and kill planktonic and biofilm bacteria. Biochim Biophys Acta **1848**(6):1352-1358.
- Barreto-Santamaría, A., M.E. Patarroyo, H. Curtidor (2019). Designing and optimizing new antimicrobial peptides: all targets are not the same. Crit Rev Clin Lab Sci 56(6): 351-373.

- Basir, Y.J., F.C. Knoop, J. Dulka, J.M. Conlon (2000). Multiple antimicrobial peptides and peptides related to bradykinin and neuromedin N isolated from skin secretions of the pickerel frog, *Rana palustris.* Biochim et Biophys Acta **1543**(1): 95-105.
- Bechinger, B. and S.U. Gorr (2017). Antimicrobial Peptides: Mechanisms of Action and Resistance. J Dent Res **96**(3): 254-260.
- Berditsch, M., M. Trapp, S. Afonin, C. Weber, J. Misiewicz, J. Turkson, A.S. Ulrich (2017). Antimicrobial peptide gramicidin S is accumulated in granules of producer cells for storage of bacterial phosphagens. Sci Rep **7**: 44324.
- Bhagirath, A.Y., Y. Li, D. Somayajula, M. Dadashi, S. Badr, K. Duan (2016). Cystic fibrosis lung environment and *Pseudomonas aeruginosa* infection. BMC Pulm Med **6**(1): 174.
- Biondi, B., B. Casciaro, A. Di Grazia, F. Cappiello, V. Luca, M. Crisma, M.L. Mangoni (2017). Effects of Aib residues insertion on the structural-functional properties of the frog skin-derived peptide esculentin-1a(1-21)NH2. Amino acids **49**(1): 139-150.
- Biswas, K., H. Ilyas, A. Datta, A. Bhunia (2019). NMR assisted antimicrobial peptide designing: Structure based modifications and functional correlation of a designed peptide VG16KRKP. Curr Med Chem.
- Bjarnsholt, T., P.Ø. Jensen, M.J. Fiandaca, J. Pedersen, C.R. Hansen, C. B. Andersen, T. Pressler, M. Givskov, N Høiby (2009). *Pseudomonas aeruginosa* biofilms in the respiratory tract of cystic fibrosis patients. Pediatr Pulmonol **44**: 547-558.
- Blanc, D.S., C. Petignat, B. Janin, J. Bille, P. Francioli (1998). Frequency and molecular diversity of *Pseudomonas aeruginosa* upon admission and

during hospitalization: a prospective epidemiologic study. Clin Microbiol Infect **4**: 242-247.

- Bobone, S and L., Stella (2019). Selectivity of Antimicrobial Peptides: A Complex Interplay of Multiple Equilibria. Adv Exp Med Biol **1117**: 175-214.
- Bobone, S., D. Roversi, L. Giordano, M. De Zotti, F. Formaggio, C. Toniolo, Y. Park, L. Stella (2012). The lipid dependence of antimicrobial peptide activity is an unreliable experimental test for different pore models. Biochemistry **51**(51): 10124-10126.
- Bocchinfuso, G., S. Bobone, C. Mazzuca, A. Palleschi, L. Stella (2011). Fluorescence spectroscopy and molecular dynamics simulations in studies on the mechanism of membrane destabilization by antimicrobial peptides. Cell Mol Life Sci **68**(13):2281-2301.
- Boman, H.G., B. Agerberth, A. Boman (1993). Mechanisms of action on *Escherichia coli* of cecropin P1 and PR-39, two antibacterial peptides from pig intestine. Infect Immun **61**(7): 2978-2984.
- Borazjani, R.N., B. Levy, D.G. Ahearn (2004). Relative primary adhesion of *Pseudomonas aeruginosa*, *Serratia marcescens* and *Staphylococcus aureus* to HEMA-type contact lenses and an extended wear silicone hydrogel contact lens of high oxygen permeability. Cont Lens Anterior Eyen **27**(1): 3-8.
- Bragonzi, A., M. Paroni, A. Nonis, N. Cramer, S. Montanari, J. Rejman, C. Di Serio, G. Doring, B. Tummler (2009). *Pseudomonas aeruginosa* microevolution during cystic fibrosis lung infection establishes clones with adapted virulence. Am J Respir Crit Care Med **180**: 138-145.

- Breidenstein, E. B., C. de la Fuente-Nunez and R. E. Hancock (2011). "*Pseudomonas aeruginosa*: all roads lead to resistance." Trends Microbiol **19**(8): 419-426.
- Broekhuyse, R.M. (1968). Phospholipids in tissues of the eye. I. Isolation, characterization and quantitative analysis by two-dimensional thin-layer chromatography of diacyl and vinyl-ether phospholipids. Biochim Biophys Acta **152**: 307-315.
- Brogden, K.A. (2005). Antimicrobial peptides: pore formers or metabolic inhibitors in bacteria? Nat Rev Microbiol **3**(3): 238-50.
- Brogden, N.K. and K.A. Brogden (2011). Will new generations of modified antimicrobial peptides improve their potential as pharmaceuticals? Int J Antimicrob Agents **38**(3):217-225.
- Cahill, K. (2010). Molecular electroporation and the transduction of oligoarginines. Phys Biol 7: 16001.
- Cappiello, F., A. Di Grazia, L.A. Segev-Zarko, S. Scali, L. Ferrera, L. Galietta, A. Pini, Y. Shai, Y., Y.P. Di, M.L. Mangoni (2016). Esculentin-1a-Derived Peptides Promote Clearance of *Pseudomonas aeruginosa* Internalized in Bronchial Cells of Cystic Fibrosis Patients and Lung Cell Migration: Biochemical Properties and a Plausible Mode of Action. Antimicrob Agents Chemother **60**(12): 7252-7262.
- Casciaro, B., F. Cappiello, M. Cacciafesta, M.L. Mangoni (2017a). Promising Approaches to Optimize the Biological Properties of the Antimicrobial Peptide Esculentin-1a(1-21)NH2: Amino Acids Substitution and Conjugation to Nanoparticles. Front Chem **5**: 26.
- Casciaro, B., M. Moros, S. Rivera-Fernandez, A. Bellelli, J.M. de la Fuente, M.L. Mangoni (2017b). Gold-nanoparticles coated with the

antimicrobial peptide esculentin-1a(1-21)NH_2 as a reliable strategy for antipseudomonal drugs. Acta biomater **47**: 170-181.

- Chai, Z., X. Hu, X. Wei, C. Zhan, L. Lu, K. Jiang, B. Su, H. Ruan, D. Ran, R.H. Fang, L. Zhang, W. Lu (2017). A facile approach to functionalizing cell membrane-coated nanoparticles with neurotoxin-derived peptide for brain-targeted drug delivery. J Control Release **264**: 102-111.
- Chen, C., M.L. Mangoni, Y.P. Di (2017). *In vivo* therapeutic efficacy of frog skin-derived peptides against *Pseudomonas aeruginosa*-induced pulmonary infection. Sci Rep **7**(1): 8548.
- Ciumac, D., H. Gong, X. Hu, J.R. Lu (2018). Membrane targeting cationic antimicrobial peptides. J Colloid Interface Sci **537**: 163-185.
- Coccia C., A.C. Rinaldi, V. Luca, D. Barra, A. Bozzi, A. Di Giulio, E.C. Veerman, M.L. Mangoni (2011). Membrane interaction and antibacterial properties of two mildly cationic peptide diastereomers, bombinins H2 and H4, isolated from Bombina skin. Eur Biophys J **40**(4): 577-588.
- Conlon J.M., J. Kolodziejek, N. Nowotny (2004). Antimicrobial peptides from ranid frogs: taxonomic and phylogenetic markers and a potential source of new therapeutic agents. Biochim Biophys Acta **1696**(1): 1-14.
- Conlon, J.M. (2008). Reflections on a systematic nomenclature for antimicrobial peptides from the skins of frogs of the family Ranidae. Peptides **29**(10): 1815-1819.
- Conlon, J.M. (2011). Structural diversity and species distribution of host-defense peptides in frog skin secretions. Cell Mol Life Sci **68**(13): 2303-2315.
- Conlon, J.M. (2011). The contribution of skin antimicrobial peptides to the system of innate immunity in anurans. Cell Tissue Res **343**(1): 201-212.

- Conlon, J.M., J. Kolodziejek, M. Mechkarska, L. Coquet, J. Leprince, T. Jouenne, H. Vaudry, P.F. Nielsen, N. Nowotny, J.D. King (2014). Host defense peptides from *Lithobates forreri*, *Hylarana luctuosa*, and *Hylarana signata* (Ranidae): phylogenetic relationships inferred from primary structures of ranatuerin-2 and brevinin-2 peptides. Comp Biochem Physiol Part D Genomics Proteomics **9**: 49-57.
- Conlon, J.M., M.A. Meetani, L. Coquet, T. Jouenne, J. Leprince, H. Vaudry, J. Kolodziejek, N. Nowotny, J.D. King (2009). Antimicrobial peptides from the skin secretions of the New World frogs Lithobates capito and Lithobates warszewitschii (Ranidae). Peptides **30**(10): 1775-1781.
- Costerton, J.W., P.S Stewart, E.P. Greenberg (1999) Bacterial biofilms: a common cause of persistent infections. Science **284**:1318-1322.
- d'Angelo, I., B. Casciaro, A. Miro, F. Quaglia, M.L. Mangoni, F. Ungaro (2015c). Overcoming barriers in *Pseudomonas aeruginosa* lung infections: Engineered nanoparticles for local delivery of a cationic antimicrobial peptide. Colloids Surf B Biointerfaces **135**: 717-725.
- d'Angelo, I., C. Conte, A. Miro, F. Quaglia, F. Ungaro (2015a). Pulmonary drug delivery: a role for polymeric nanoparticles? Curr Top Med Chem **15**(4): 386-400.
- d'Angelo, I., F. Quaglia, F. Ungaro (2015b). PLGA carriers for inhalation: where do we stand, where are we headed? Ther Deliv **6**(10):1139-1144.
- Dathe, M., T. Wieprecht, H. Nikolenko, L. Handel, W.L Maloy, D.L. MacDonald, M. Beyermann, M. Bienert (1997). Hydrophobicity, hydrophobic moment and angle subtended by charged residues modulate antibacterial and haemolytic activity of amphipathic helical peptides. FEBS Lett **403**(2): 208-212.

- De Kievit, T.R., R. Gillis, S. Marx, C. Brown, B.H. Iglewski (2001). Quorum-sensing genes in *Pseudomonas aeruginosa* biofilms: their role and expression patterns. Appl Environ Microbiol **67**(4): 1865-1873.
- de la Fuente-Nunez, C., F. Reffuveille, E.F. Haney, S.K Straus, R.E.W. Hancock (2014). Broad-spectrum anti-biofilm peptide that targets a cellular stress response. PLoS Pathog **10**: e1004152.
- de la Fuente-Núñez, C., V. Korolik, M. Bains, U. Nguyen, E.B. Breidenstein, S. Horsman, S. Lewenza, L. Burrows, R.E.W. Hancock (2012). Inhibition of bacterial biofilm formation and swarming motility by a small synthetic cationic peptide. Antimicrob Agents Chemother **56**(5): 2696-2704.
- De Zotti, M., B. Biondi, Y. Park, K.S. Hahm, M. Crisma, C. Toniolo, F. Formaggio (2012). Antimicrobial lipopeptaibol trichogen GA IV: role of the three Aib residues on conformation and bioactivity. Amino Acids **43**(4): 1761-1777.
- Di Grazia, A., F. Cappiello, H. Cohen, B. Casciaro, V. Luca, A. Pini, Y.P. Di, Y. Shai, M.L. Mangoni (2015). D-Amino acids incorporation in the frog skin-derived peptide esculentin-1a(1-21)NH2 is beneficial for its multiple functions. Amino acids **47**(12): 2505-2519.
- Di, Y.P. (2014). Assessment of pathological and physiological changes in mouse lung through bronchoalveolar lavage. Methods Mol Biol **1105**: 33-42.
- Ding, D. and Q. Zhu (2018). Recent advances of PLGA micro/nanoparticles for the delivery of biomacromolecular therapeutics. Mater Sci Eng **92**: 1041-1060.

- Drenkard, E. and F.M. Ausubel (2002). *Pseudomonas* biofilm formation and antibiotic resistance are linked to phenotypic variation. Nature **416**: 740-743.
- Dutta, D, A.K. Vijay, N. Kumar, M.D. Willcox (2016). Melimine-coated antimicrobial contact lenses reduce microbial keratitis in an animal model. Invest Ophthalmol Vis Sci **57**(13): 5616-5624.
- Dutta, D. and M.D. Willcox (2014). Antimicrobial contact lenses and lens cases: a review. Eye Contact Lens **40**(5): 312-324.
- Dutta, D., N. Cole, N. Kumar, M.D. Willcox (2013). Broad spectrum antimicrobial activity of melimine covalently bound to contact lenses. Invest Ophthalmol Vis Sci **54**(1): 175-182.
- Dutta, D., N. Kumar, M.D. Willcox (2016b). Antimicrobial activity of four cationic peptides immobilised to poly-hydroxyethylmethacrylate. Biofouling **32**(4): 429-438.
- Epand RM, Walker C, Epand RF, Magarvey NA (2016). Molecular mechanisms of membrane targeting antibiotics. Biochim Biophys Acta **1858**(5): 980-987.
- Epand, R.F., M.A. Schmitt, S.H. Gellman, R.M. Epand (2006). Role of membrane lipids in the mechanism of bacterial species selective toxicity by two α/β-antimicrobial peptides. Biochim Biophys Acta **1758**(9):1343-1350.
- Ernst, J., M. Klinger-Strobel, K. Arnold, J. Thamm, A. Hartung, M.W. Pletz, O. Makarewicz, D. Fischer (2018). Polyester-based particles to overcome the obstacles of mucus and biofilms in the lung for tobramycin application under static and dynamic fluidic conditions. Eur J Pharm Biopharm **131**: 120-129.

- Fernández, L., E.B.M. Breidenstein, R.E.W. Hancock (2011). Creeping baselines andadaptive resistance to antibiotics. Drug Resist Updat **14**: 1-21.
- Fjell, C.D., H. Jenssen, W.A. Cheung, R.E.W. Hancock, A. Cherkasov (2011). Optimization of antibacterial peptides by genetic algorithms and cheminformatics. Chem Biol Drug Des **77**(1): 48-56.
- Folkesson, A., L. Jelsbak, L. Yang, H.K. Johansen, O. Ciofu, N. Høiby, S. Molin (2012). Adaptation of *Pseudomonas aeruginosa* to the cystic fibrosis airway: anevolutionary perspective. Nat Rev Microbiol **10**: 841-851.
- Fonte, P., S. Reis, B. Sarmento (2016). Facts and evidences on the lyophilization of polymeric nanoparticles for drug delivery. J Control Release **225**: 75-86.
- Forier, K., A.S. Messiaen, K. Raemdonck, H. Deschout, J. Rejman, F. De Baets, H. Nelis, S.C. De Smedt, J. Demeester, T. Coenye, K. Braeckmans (2013). Transport of nanoparticles in cystic fibrosis sputum and bacterial biofilms by single-particle tracking microscopy. Nanomedicine (Lond) **8**(6): 935-949.
- Gallo, R.L., M. Ono, T. Povsic, C. Page, E. Eriksson E, M. Klagsbrun, M. Bernfield (1994). Syndecans, cell surface heparan sulfate proteoglycans, are induced by a proline-rich antimicrobial peptide from wounds. Proc Natl Acad Sci U S A **91**(23): 11035-9.
- Gamberi, T., D. Cavalieri, F. Magherini, M.L. Mangoni, C. De Filippo, M. Borro, G. Gentile, M. Simmaco, A. Modesti (2007). An integrated analysis of the effects of Esculentin 1–21 on *Saccharomyces cerevisiae*. Biochim Biophys Acta **1774**(6): 688-700.

- Ghosh, A., S. Bera, Y. Shai, M.L. Mangoni, A. Bhunia (2016). NMR structure and binding of esculentin-1a (1-21)NH_2 and its diastereomer to lipopolysaccharide: Correlation with biological functions. Biochim Biophys Acta **1858**(4): 800-812.
- Giraud, C., C.S. Bernard, V. Calderon, L. Yang, A. Filloux, S. Molin, G. Fichant, C. Bordi, S. de Bentzmann (2011). The PprA-PprB two-component system activates CupE, the first non-archetypal *Pseudomonas aeruginosa* chaperone-usher pathway system assembling fimbriae. Environ Microbiol **13**(3): 666-683.
- Giuliani, A. and A.C. Rinaldi (2011). Beyond natural antimicrobial peptides: multimeric peptides and other peptidomimetic approaches. Cell Mol Life Sci **68**(13): 2255-2266.
- Giuliani, A., G. Pirri, S.F. Nicoletto (2007). Antimicrobial peptides: an overview of a promising class of therapeutics. Cent Eur J Biol **2**(1): 1-33.
- Golbek, T.W., J. Franz, J. Elliott Fowler, K.F. Schilke, T. Weidner, J.E. Baio (2017). Identifying the selectivity of antimicrobial peptides to cell membranes by sum frequency generation spectroscopy. Biointerphases **12**(2): 02D406.
- Gordon, Y.J.; E.G. Romanowski, A.M. McDermott (2005). A review of antimicrobial peptides and their therapeutic potential as anti-infective drugs. Curr Eye Res **30**(7): 505-515.
- Grassi, L., M. Di Luca, G. Maisetta, A.C. Rinaldi, S. Esin, A. Trampuz, G. Batoni (2017). Generation of persister cells of *Pseudomonas aeruginosa* and Staphylococcus aureus by chemical treatment and evaluation of their susceptibility to membrane-targeting agents. Front Microbiol **8**: 1917.
- Grieco, P., A. Carotenuto, L. Auriemma, M.R. Saviello, P. Campiglia, I.M. Gomez Monterrey, L. Marcellini, V. Luca, D. Barra, E. Novellino, M.L.

Mangoni (2013). The effect of d-amino acid substitution on the selectivity of temporin L towards target cells: identification of a potent anti-Candida peptide." Biochim Biophys Acta **1828**(2): 652-660.

- Gupta, M. and V.S. Chauhan (2011). De novo design of alpha, betadidehydrophenylalanine containing peptides: from models to applications. Biopolymers **95**(3): 161-173.
- Gutjahr, A., C. Phelip, A.L. Coolen, C. Monge, A.S. Boisgard, S. Paul, B. Verrier (2016). Biodegradable polymeric nanoparticles-based vaccine adjuvants for lymph nodes targeting. Vaccines (Basel) **4**(4).
- Hale, J. D. and R.E.W. Hancock (2007). Alternative mechanisms of action of cationic antimicrobial peptides on bacteria. Expert Rev Anti Infect Ther **5**(6): 951-959.
- Hallock, K.J., D.K. Lee, A. Ramamoorthy (2003). Msi-78, an analogue of the Magainin Antimicrobial Peptides, Disrupts Lipid Bilayer Structure Via Positive Curvature Strain. Biophys J **84**: 3052-3060.
- Hancock, R.E.W. and D.S. Chapple (1999). Peptide antibiotics. Antimicrob Agents Chemother **43**(6): 1317-1323.
- Hancock, R.E.W. and H.G. Sahl (2006) Antimicrobial and host-defense peptides as new anti-infective therapeutic strategies. Nat Biotechnol **24**(12): 1551-1557.
- Haney, E.F., S. Nathoo, H.J. Vogel, E.J. Prenner (2010). Induction of nonlamellar lipid phases by antimicrobial peptides: a potential link to mode of action. Chem Phys Lipids 163: 82-93.
- Haney, E.F., S.C. Mansour, R.E.W. Hancock (2017). Antimicrobial Peptides: An Introduction. Methods Mol Biol **1548**: 3-22.

- Harris, F., S.R. Dennison, D.A. Phoenix (2011) Anionic antimicrobial peptides from eukaryotic organisms and their mechanisms of action. Curr Chem Biol **5**:142-153.
- Hechard, Y. and H.G. Sahl (2002). Mode of action of modified and unmodified bacteriocins from Gram-positive bacteria. Biochimie **84** (5-6): 545-57.
- Henrichfreise, B., I. Wiegand, W. Pfister and B. Wiedemann (2007). "Resistance mechanisms of multiresistant *Pseudomonas aeruginosa* strains from Germany and correlation with hypermutation." Antimicrob Agents Chemother **51**(11): 4062-4070.
- Hilpert, K., R. Volkmer-Engert, T. Walter, R.E.W. Hancock (2005). High-throughput generation of small antibacterial peptides with improved activity. Nat Biotechnol **23**(8): 1008-1012.
- Huang, H.W. (2000). Action of antimicrobial peptides: two-state model. Biochemistry **39**:8347-8352.
- Huang, Y., L. He, G. Li, N. Zhai, H. Jiang, Y. Chen (2014). Role of helicity of alpha-helical antimicrobial peptides to improve specificity. Protein Cell **5**(8): 631-642.
- Huckaby, J.T. and S.K. Lai (2018). PEGylation for enhancing nanoparticle diffusion in mucus. Adv Drug Deliv Rev **124**: 125-139.
- Hultmark, D., H. Steiner, T. Rasmuson, H.G. Boman (1980). Insect immunity. Purification and properties of three inducible bactericidal proteins from hemolymph of immunized pupae of Hyalophora cecropia. Eur J Biochem **106**(1): 7-16.
- Imanparast, F., M.A. Faramarzi, A. Vatannejad, M. Paknejad, B. Deiham, F. Kobarfard, A. Amani, M. Doosti (2017). mZD7349 peptide-conjugated PLGA nanoparticles directed against VCAM-1 for targeted delivery of

simvastatin to restore dysfunctional HUVECs. Microvascular Research **112**: 14-19.

- Imperi, F., F. Tiburzi, P. Visca (2009). Molecular basis of pyoverdine siderophore recycling in *Pseudomonas aeruginosa*. Proc Natl Acad Sci U S A **106**(48): 20440-20445.
- Islas-Rodriguez, A.E., L. Marcellini, B. Orioni, D. Barra, L. Stella, M.L. Mangoni (2009). Esculentin 1-21: a linear antimicrobial peptide from frog skin with inhibitory effect on bovine mastitis-causing bacteria. J Pept Sci **15**(9): 607-614.
- Iwakoshi-Ukena, E., K. Ukena, A. Okimoto, M. Soga, G. Okada, N. Sano, T. Fujii, Y. Sugawara, M. Sumida (2011). Identification and characterization of antimicrobial peptides from the skin of the endangered frog *Odorrana ishikawae*. Peptides **32**(4): 670-676.
- Jenssen, H., P. Hamill, R.E.W. Hancock (2006). Peptide antimicrobial agents. Clin Microbiol Rev **19**:491-511.
- Kamaruzzaman, N.F., L.P. Tan, R.H. Hamdan, S.S. Choong, W.K. Wong, A.J. Gibson, A. Chivu, M.F. Pina (2019). Antimicrobial polymers: The potential replacement of existing antibiotics? Int J Mol Sci **20**(11): E2747.
- Kang, S.J., S.J. Park, T. Mishig-Ochir, B.J. Lee (2014). Antimicrobial peptides: therapeutic potentials. Expert Rev Anti Infect Ther **12**(12) :1477-1486.
- Kaplan, J.B. (2011). Antibiotic-induced biofilm formation. Int J Artif Organs **34**(9): 737-751.
- Kelly, S.M., T.J. Jess, N.C. Price (2005). How to study proteins by circular dichroism, Biochim Biophys Acta **1751**: 119-139.
- Kidd, T. J., R. Canton, M. Ekkelenkamp, H. K. Johansen, P. Gilligan, J. J. LiPuma, S. C. Bell, J. S. Elborn, P. A. Flume, D. R. VanDevanter, V. J.

Waters and G. Antimicrobial Resistance in Cystic Fibrosis International Working (2018). "Defining antimicrobial resistance in cystic fibrosis." J Cyst Fibros **17**(6): 696-704.

- Kim, J.Y., S.C. Park, M.Y. Yoon, K.S. Hahm, Y. Park (2011). C-terminal amidation of PMAP-23: translocation to the inner membrane of Gram-negative bacteria. Amino Acids **40**(1): 183-195.
- Kolar, S.S.N.; V. Luca, H. Baidouri, G. Mannino, A.M. McDermott, M.L. Mangoni (2015). Esculentin-1a(1-21)NH2: a frog skin-derived peptide for microbial keratitis. Cell Mol Life Sci **72**(3): 617-627.
- Koller, D. and K. Lohner (2014). The role of spontaneous lipid curvature in the interaction of interfacially active peptides with membranes. Biochim Biophys Acta **1838**(9): 2250-2259.
- König, E., O.R. Bininda-Emonds, C. Shaw (2015). The diversity and evolution of anuran skin peptides. Peptides **63**: 96-117.
- Ladram, A. and P. Nicolas (2016). Antimicrobial peptides from frog skin: biodiversity and therapeutic promises. Front Biosci **21**: 1341-1371.
- Leber, R., M. Pachler, I. Kabelka, I. Svoboda, D. Enkoller, R. Vácha, K. Lohner, G. Pabst (2018). Synergism of antimicrobial frog peptides couples to membrane intrinsic curvature strain. Biophys J **114**(8): 1945-1954.
- Lee, M.T., W.C. Hung, F.Y. Chen, H.W. Huang (2005) Many-body effect of antimicrobial peptides: on the correlation between lipid's spontaneous curvature and pore formation. Biophys J **89**(6): 4006-4016.
- Lee, W. and D.G. Lee (2014). Magainin 2 induces bacterial cell death showing apoptotic properties. Curr Microbiol **69**(6): 794-801.
- Lee, T.H., V. Hofferek, F. Separovic, G.E. Reid, M.I Aguilar (2019). The role of bacterial lipid diversity and membrane properties in modulating

antimicrobial peptide activity and drug resistance. Curr Opin Chem Biol **52**: 85-92.

- Lei, J., L. Sun, S. Huang, C. Zhu, P. Li, J. He, V. Mackey, D. H. Coy, Q. He (2019). The antimicrobial peptides and their potential clinical applications. Am J Transl Res **11**(7): 3919-3931.
- Leite, N.B., A. Aufderhorst-Roberts, M.S. Palma, S.D Connell, J.R Neto, P.A. Beales (2015). PE and PS lipids synergistically enhance membrane poration by a peptide with anticancer properties. Biophys J **109**(5): 936-947.
- Leitgeb, B., A. Szekeres, L. Manczinger, C. Vágvölgyi, L. Kredics (2007). The history of Alamethicin: a review of the most extensively studied peptaibol. Chem Biodivers **4**:1027-1051.
- Lewis, K., (2010). "Persister cells" Annu Rev Microbiol **64**: 357-372.
- Li, J., J.J. Koh, S. Liu, R. Lakshminarayanan, C.S. Verma, R.W. Beuerman (2017). Membrane Active Antimicrobial Peptides: Translating Mechanistic Insights to Design. Front Neurosci **11**:73.
- Li, J., X. Xu, C. Xu, W. Zhou, K. Zhang, H. Yu, Y. Zhang, Y. Zheng, H.H. Rees, R. Lai, D. Yang, J. Wu (2007). Anti-infection peptidomics of amphibian skin. Mol Cell Proteomics **6**(5): 882-894.
- Lin, Q., B. Deslouches, R.C. Montelaro, Y.P. Di (2018). Prevention of ESKAPE pathogen biofilm formation by antimicrobial peptides WLBU2 and LL37. Int J Antimicrob Agents **52**(5): 667-672.
- Lohner, K. (2017). Membrane-active Antimicrobial Peptides as Template Structures for Novel Antibiotic Agents. Curr Top Med Chem **17**(5): 508-519.
- Luca, V., A. Stringaro, M. Colone, A. Pini, M.L. Mangoni (2013). Esculentin(1-21), an amphibian skin membrane-active peptide with potent

activity on both planktonic and biofilm cells of the bacterial pathogen *Pseudomonas aeruginosa*. Cell Mol Life Sci **70**(15): 2773-2786.

- Madani, F., S.S. Esnaashari, B. Mujokoro, F. Dorkoosh, M. Khosravani, M. Adabi (2018). Investigation of effective parameters on size of paclitaxel loaded PLGA nanoparticles. Adv Pharm Bull **8**(1): 77-84.
- Mahlapuu, M., J. Håkansson, L. Ringstad, C. Björn (2016). Antimicrobial Peptides: An Emerging Category of Therapeutic Agents. Front Cell Infect Microbiol. **6**:194.
- Malanovic, N. and K. Lohner (2016). Antimicrobial peptides targeting gram-positive bacteria. Pharmaceuticals (Basel) **9**(3): 59.
- Mangoni, M.L. (2006). Temporins, anti-infective peptides with expanding properties. Cell Mol Life Sci **63**(9): 1060-1069.
- Mangoni, M.L., D. Fiocco, G. Mignogna, D. Barra, M. Simmaco (2003). Functional characterisation of the 1-18 fragment of esculentin-1b, an antimicrobial peptide from *Rana esculenta*. Peptides **24**(11): 1771-1777.
- Mangoni, M.L., V. Luca, A.M. McDermott (2015). Fighting microbial infections: A lesson from amphibian skin-derived esculentin-1 peptides. Peptides **71**: 286-295.
- Manzo, G., M. Carboni, A.C. Rinaldi, M. Casu, M.A. Scorciapino (2013). Characterization of sodium dodecylsulphate and dodecylphosphocholine mixed micelles through NMR and dynamic light scattering, Magn Reson Chem **51**(2013): 176-183.
- Matsuzaki, K., K.I. Sugishita, N. Ishibe, M. Ueha, S. Nakata, K. Miyajima K, R.M. Epand (1998). Relationship of membrane curvature to the formation of pores by magainin 2. Biochemistry **37**(34): 11856-11863.

- Matsuzaki, K., M. Harada, T. Handa, S. Funakoshi, N. Fujii, H. Yajima, K. Miyajima (1989). Magainin 1-induced leakage of entrapped calcein out of negatively-charged lipid vesicles. Biochim Biophys Acta **981**(1): 130-134.
- Matsuzaki, K., O. Murase, N. Fujii, K. Miyajima (1996). An antimicrobial peptide, magainin 2, induced rapid flip-flop of phospholipids coupled with pore formation and peptide translocation. Biochemistry **35**: 11361-11368.
- Mattick, J.S. (2002). Type IV pili and twitching motility. Annu Rev Microbiol **56**: 289-314.
- Maurice, N.M., B. Bedi, R.T. Sadikot (2018). *Pseudomonas aeruginosa* Biofilms: Host Response and Clinical Implicati ons in Lung Infections. Am J Respir Cell Mol Biol **58**(4): 428-439.
- Michael, C. A., D. Dominey-Howes and M. Labbate (2014). "The antimicrobial resistance crisis: causes, consequences, and management." Front Public Health **2**: 145.
- Mojsoska, B. and H. Jenssen (2015). Peptides and Peptidomimetics for Antimicrobial Drug Design. Pharmaceuticals (Basel) **28**(3): 366-415.
- Morikawa, N., K. Hagiwara, T. Nakajima (1992). Brevinin-1 and -2, unique antimicrobial peptides from the skin of the frog, *Rana brevipoda porsa*. Biochem Biophys Res Commun **189**: 184-190.
- Moss, O.R. (1979). Simulants of lung interstitial fluid. Health Phys **36**: 447-448.
- Mwangi, J., X. Hao, R. Lai, Z.Y. Zhang (2019). Antimicrobial peptides: new hope in the war against multidrug resistance. Zool Res **40**(6): 488-505
- Nguyen, L.T., D.J. Schibli, H.J. Vogel (2005). Structural studies and model membrane interactions of two peptides derived from bovine lactoferricin." J Pept Sci **11**(7): 379-389.

- Nguyen, L.T., J.K. Chau, N.A. Perry, L. de Boer, S.A. Zaat, H.J. Vogel (2010). Serum stabilities of short tryptophan- and arginine-rich antimicrobial peptide analogs. PLoS One **5**(9): e12684.
- Nijnik, A. and R.E.W. Hancock (2009). The roles of cathelicidin LL-37 in immune defences and novel clinical applications. Curr Opin Hematol **16**:41-47.
- Nixon, G.M., D.S. Armstrong, R. Carzino, J.B. Carlin, A Olinsky, C.F. Robertson, K. Grimwood (2001). Clinical outcome after early *Pseudomonas aeruginosa* infection in cystic fibrosis. J Pediatr **138**(5) :699-704.
- OECD Health Policy Studies (2018) "Stemming the Superbug Tide, Just A Few Dollars More" OECD.
- Overhage, J., S. Lewenza, A.K. Marr, R.E.W Hancock (2007). Identification of genes involved in swarming motility using a *Pseudomonas aeruginosa* PAO1 mini-Tn5-lux mutant library. J Bacteriol **189**(5): 2164-2169.
- Oyston, P.C., M.A. Fox, S.J. Richards, G.C. Clark (2009). Novel peptide therapeutics for treatment of infections. J Med Microbiol **58**: 977-987.
- Pang, Z., R. Raudonis, B. R. Glick, T. J. Lin and Z. Cheng (2019). "Antibiotic resistance in *Pseudomonas aeruginosa*: mechanisms and alternative therapeutic strategies." Biotechnol Adv **37**(1): 177-192.
- Pantic, J.M.; I.P. Jovanovic, G.D. Radosavljevic, N.N. Arsenijevic, J.M. Conlon, M.L. Lukic (2017). The Potential of Frog Skin-Derived Peptides for Development into Therapeutically-Valuable Immunomodulatory Agents. Molecules **22**(12).

- Papo, N., and Y. Shai (2004). Effect of drastic sequence alteration and D-amino acid incorporation on the membrane binding behaviour of lytic peptides. Biochemistry **43**(21): 6393-6403.
- Park, C.B.; K.S. Yi, K. Matsuzaki, M.S. Kim, S.C. Kim (2000). Structure-activity analysis of buforin II, a histone H2A-derived antimicrobial peptide: the proline hinge is responsible for the cell penetrating ability of buforin II. Proc Natl Acad Sci U S A **97**(15): 8245-8250.
- Parker, D., D. Ahn, T. Cohen, A. Prince (2016) Innate Immune Signaling Activated by MDR Bacteria in the Airway. Physiol Rev **96**(1): 19-53.
- Pham, T.N., P. Loupias, A. Dassonville-Klimpt, P. Sonnet (2019). Drug delivery systems designed to overcome antimicrobial resistance. Med Res Rev **39**(6): 2343-2396.
- Pietro, P.D., G. Strano, L. Zuccarello, C. Satriano (2016). Gold and silver nanoparticles for applications in theranostics. Curr Top Med Chem **16**(27): 3069-3102.
- Pletzer, D. , S. R. Coleman, R.E.W. Hancock (2017) Anti-biofilm peptides as a new weapon in antimicrobial warfare. Curr Opin Microbiol **33**: 35-40
- Podda, E., M. Benincasa, S. Pacor, F. Micali, M. Mattiuzzo, R. Gennaro, M. Scocchi (2006). Dual mode of action of Bac7, a proline rich antibacterial peptide. Biochim Biophys Acta **1760** (11): 1732-1740.
- Porto, W.F., A.S. Pires, O.L. Franco (2017). Computational tools for exploring sequence databases as a resource for antimicrobial peptides. Biotechnol Adv **35**(3): 337-349.
- Potrykus, K. and M. Cashel (2008). (p)ppGpp: still magical? Annu Rev Microbiol. **62**: 35-51.
- Powers, J.P. and R.E.W. Hancock (2003). The relationship between peptide structure and antibacterial activity. Peptides **24**(11): 1681-1691.

- Pushpanathan M, Gunasekaran P, Rajendhran J. (2013). Antimicrobial peptides: versatile biological properties. Int J Pept **2013**:675391.
- Qin, G.T., A. Lopez, C. Santos, A.M. McDermott, C.Z. Cai (2015). Antimicrobial peptide LL-37 on surfaces presenting carboxylate anions. Biomater Sci **3**: 771.
- Rai, A., S. Pinto, T.R. Velho, A.F. Ferreira, C. Moita, U. Trivedi, M. Evangelista, M. Comune, K.P. Rumbaugh, P.N. Simões, L. Moita, L. Ferreira (2016). One-step synthesis of high-density peptide-conjugated gold nanoparticles with antimicrobial efficacy in a systemic infection model. Biomaterials **85**: 99-110.
- Ramesh, S., M. Grijalva, A. Debut, B.G. de la Torre, F. Albericio, L.H. Cumbal (2016). Peptides conjugated to silver nanoparticles in biomedicine - a "value-added" phenomenon. Biomater Sci **4**(12): 1713-1725.
- Rasul, R., N. Cole, D. Balasubramanian, R. Chen, N. Kumar, M.D. Willcox (2010). Interaction of the antimicrobial peptide melimine with bacterial membranes. Int J Antimicrob Agents **35**(6): 566-72.
- Reygaert, W. C. (2018). "An overview of the antimicrobial resistance mechanisms of bacteria." AIMS Microbiol **4**(3): 482-501.
- Romero, D., C. Aguilar, R. Losick, R. Kolter (2010). Amyloid fibers provide structural integrity to *Bacillus subtilis* biofilms. Proc Natl Acad Sci USA **107**: 2230-2234.
- Romling, U., M.Y. Galperin, M. Gomelsky (2013). Cyclic di-GMP: the first 25 years of a universal bacterial second messenger. Microbiol Mol Biol **77**:1-52.
- Roy, R., M. Tiwari, G. Donelli, V. Tiwari (2018). Strategies for combating bacterial biofilms: A focus on anti-biofilm agents and their mechanisms of action. Virulence **9**(1): 522-554.

- Rudkjøbing, V.B., T.R Thomsen, M. Alhede, K.N. Kragh, P.H. Nielsen, U.R. Johansen, M. Givskov, N. Høiby N, T. Bjarnsholt (2012). The microorganisms in chronically infected end-stage and non-end-stage cystic fibrosis patients. FEMS Immunol Med Microbiol **65**(2): 236-44.
- Russell, A.L., A.M. Kennedy, A.M. Spuches, D. Venugopal, J.B. Bhonsle, R.P. Hicks (2010). Spectroscopic and thermodynamic evidence for antimicrobial peptide membrane selectivity. Chem Phys Lipids **163**(6): 488-497.
- Rytting, E., J. Nguyen, X. Wang, T. Kissel (2008). Biodegradable polymeric nanocarriers for pulmonary drug delivery. Expert Opin Drug Delivery **5**: 629-639.
- Sadikot, R.T., T.S. Blackwell, J.W. Christman, A.S Prince (2005). Pathogen–host interactions in *Pseudomonas aeruginosa* pneumonia. Am J Respir Crit Care Med **171**: 1209-1223.
- Sahoo, S.K., J. Panyam, S. Prabha, V. Labhasetwar (2002). Residual polyvinyl alcohol associated with poly (D, L-lactide-co-glycolide) nanoparticles affects their physical properties and cellular uptake. J Control Release **82**(1): 105-14.
- Sandoval-Motta, S. and M. Aldana (2016). "Adaptive resistance to antibiotics in bacteria: a systems biology perspective." Wiley Interdiscip Rev Syst Biol Med **8**(3): 253-267.
- Savini, F., S. Bobone, D. Roversi, M.L. Mangoni, L. Stella (2018). From liposomes to cells: filling the gap between physicochemical and microbiological studies of the activity and selectivity of host-defense peptides. Pept Sci **110**(5): e24041.

- Scocchi, M., M. Mardirossian, G. Runti, M. Benincasa (2016). Non-Membrane Permeabilizing Modes of Action of Antimicrobial Peptides on Bacteria. Curr Top Med Chem **16**(1):76-88.
- Segev-Zarko, L., R. Saar-Dover, V. Brumfeld, M.L. Mangoni, Y. Shai (2015). Mechanisms of biofilm inhibition and degradation by antimicrobial peptides. Biochem J **468**: 259-270.
- Sengupta, D., H. Leontiadou, A.E. Mark, S.J. Marrink (2008). Toroidal pores formed by antimicrobial peptides show significant disorder. Biochim Biophys Acta **1778**(10): 2308-2317.
- Shagaghi, N., E.A. Palombo, A.H.A. Clayton, M. Bhave (2018). Antimicrobial peptides: biochemical determinants of activity and biophysical techniques of elucidating their functionality. World J Microbiol Biotechnol **34**(4): 62.
- Shai, Y. (1999). Mechanism of the binding, insertion and destabilization of phospholipid bilayer membranes by K-helical antimicrobial and cell non-selective membrane-lytic peptides. Biochim Biophys Acta 1462(1-2): 55-70.
- Simmaco M., G. Mignogna, D. Barra (1998). Antimicrobial peptides from amphibian skin: what do they tell us? Biopolymers **47**(6): 435-450.
- Simmaco, M., G. Mignogna, D. Barra, F. Bossa (1993). Novel antimicrobial peptides from skin secretion of the European frog *Rana esculenta*. FEBS Lett **324**(2): 159-161.
- Simmaco, M., G. Mignogna, D. Barra, F. Bossa (1994). Antimicrobial peptides from skin secretions of *Rana esculenta*. Molecular cloning of cDNAs encoding esculentin and brevinins and isolation of new active peptides. J Biol Chem **269**(16):11956-11961.

- Singh, S., S.K. Singh, I. Chowdhury, R. Singh (2017). Understanding the mechanism of bacterial biofilms resistance to antimicrobial agents. Open Microbiol J **11**: 53-62.
- Skerker, J.M. and H.C. Berg (2001). Direct observation of extension and retraction of type IV pili Proc Natl Acad Sci U S A **98**(12):6901-6904.
- Sommer, M. O. A., C. Munck, R. V. Toft-Kehler and D. I. Andersson (2017). "Prediction of antibiotic resistance: time for a new preclinical paradigm?" Nat Rev Microbiol **15**(11): 689-696.
- Strahilevitz, J., A. Mor, P. Nicolas, Y. Shai (1994). Spectrum of antimicrobial activity and assembly of dermaseptin-b and its precursor form in phospholipid membranes. Biochemistry **33**(36): 10951-10960.
- Strandberg, E., J. Zerweck, D. Horn, G. Pritz, M. Berditsch, J. Bürck, P. Wadhwani, A.S. Ulrich (2015). Influence of hydrophobic residues on the activity of the antimicrobial peptide magainin 2 and its synergy with PGLa. J Pept Sci **21**(5):436-45.
- Subedi, D., A.K. Vijay, M. Willcox (2018). Overview of mechanisms of antibiotic resistance in *Pseudomonas aeruginosa*: an ocular perspective. Clin Exp Optom **101**(2): 162-171.
- Suh, S.J., et al., L. Silo-Suh, D.E. Woods, D.J. Hassett, S.E. West, D.E. Ohman (1999). Effect of rpoS mutation on the stress response and expression of virulence factors in *Pseudomonas* aeruginosa. J Bacteriol **181**(13): 3890-3897.
- Sullivan, C.J., J.L. Morrell, D.P. Allison, M.J. Doktycz (2005). Mounting of *Escherichia coli* spheroplasts for AFM imaging. Ultramicroscopy **105**(1-4): 96-102.

- Taylor, P.K., A.T. Yeung, R.E.W. Hancock (2014). Antibiotic resistance in *Pseudomonas* aeruginosa biofilms: towards the development of novel anti-biofilm therapies. J Biotechnol **191**:121-130.
- Teixeira, V., M.J. Feio, M. Bastos (2012). Role of lipids in the interaction of antimicrobial peptides with membranes. Prog Lipid Res **51**: 149-177.
- Tomasinsig, L.; M. Scocchi, R. Mettulio, M. Zanetti (2004). Genome wide transcriptional profiling of the *Escherichia coli* response to a proline-rich antimicrobial peptide. Antimicrob Agents Chemother **48**(9): 3260-3267.
- Tossi, A., L. Sandri, A. Giangaspero (2000). Amphipathic, alpha-helical antimicrobial peptides. Biopolymers **55**(1): 4-30.
- Uccelletti, D., E. Zanni, L. Marcellini, C. Palleschi, D. Barra, M.L. Mangoni (2010). Anti-*Pseudomonas* activity of frog skin antimicrobial peptides in a *Caenorhabditis elegans* infection model: a plausible mode of action *in vitro* and *in vivo*. Antimicrob Agents Chemother **54**(9): 3853-3860.
- Ungaro, F., I. d'Angelo, C. Coletta, R. d'Emmanuele di Villa Bianca, R. Sorrentino, B. Perfetto, M.A. Tufano, A. Miro, M.I. La Rotonda, F. Quaglia (2012). Dry powders based on PLGA nanoparticles for pulmonary delivery of antibiotics: modulation of encapsulation efficiency, release rate and lung deposition pattern by hydrophilic polymers. J Control Release **157**(1): 149-159.
- Vhora, I., S. Patil, P. Bhatt, A. Misra (2015). Protein- and Peptide-drug conjugates: an emerging drug delivery technology. Adv Protein Chem Struct Biol **98**: 1-55.
- Vogel, H.J. and D.M. Bonner (1956). Acetylornithinase of *Escherichia coli*: partial purification and some properties. J Biol Chem 218: 97-106.

- Wada, A., M. Kono, S. Kawauchi, Y. Takagi, T. Morikawa, K. Funakoshi (2012). Rapid discrimination of Gram-positive and Gram-negative bacteria in liquid samples by using NaOH-sodium dodecyl sulfate solution and flow cytometry. PLoS One 7: e47093.
- Waghu, F.H., S. Joseph, S. Ghawali, E.A. Martis, T. Madan, K.V. Venkatesh, S. Idicula-Thomas (2018). Designing antibacterial peptides with enhanced killing kinetics. Front Microbiol **9**:325.
- Wang, G. (ed) (2017). Antimicrobial peptides: discovery, design and novel therapeutic strategies. CABI Publishing, Cambridge, MA.
- Wang, H., Z. Yu, Y. Hu, H. Yu, R. Ran, J. Xia, D. Wang, S. Yang, X. Yang, J. Liu (2012). Molecular cloning and characterization of antimicrobial peptides from skin of the broad-folded frog, *Hylarana latouchii*. Biochimie **94**(6): 1317-1326.
- Wang, L., C. Hu, L. Shao (2017). The antimicrobial activity of nanoparticles: present situation and prospects for the future. Int J Nanomedicine **12**: 1227-1249.
- Wang, T., I. El Meouche, M.J. Dunlop (2017). Bacterial persistence induced by salicylate via reactive oxygen species. Sci Rep **7**:43839.
- Willcox, M.D. (2011) Review of resistance of ocular isolates of *Pseudomonas aeruginosa* and staphylococci from keratitis to ciprofloxacin, gentamicin and cephalosporins. Clin Exp Optom **94**: 161-168.
- Willey, J.M. and W.A. van der Donk (2007). Lantibiotics: peptides of diverse structure and function. Annu Rev Microbiol **61**: 477-501.
- Winsor, G.L., E.J. Griffiths, R. Lo, B.K. Dhillon, J.A. Shay, F.S. Brinkman (2016). Enhanced annotations and features for comparing thousands of

Pseudomonas genomes in the *Pseudomonas* genome database. Nucleic Acids Res **44**(D1): D646-653.

- World Health Organization. (2014). "Antimicrobial Resistance: Global Report on Surveillance 2014." WHO, Geneva Switzerland. http://www.who.int/drugresistance/documents/surveillancereport/en/.ISBN.
- World Health Organization. (2015) "Global action plan on antimicrobial resistance." WHO.
- Xu, X., H. Yu, D. Zhang, J. Xiong, J. Qiu, R. Xin, X. He, H. Sheng, W. Cai, L. Jiang, K. Zhang, X. Hu (2016). Role of ppGpp in *Pseudomonas aeruginosa* acute pulmonary infection and virulence regulation. Microbiol Res **192**: 84-95.
- Yang, L., T.A. Harroun, T.M. Weiss, L. Ding, H.W. Huang (2001). Barrel-stave model or toroidal model? A case study on melittin pores. Biophys J **81**: 1475-1485.
- Yeaman, M.R. and N.Y. Yount (2003). Mechanisms of antimicrobial peptide action and resistance. Pharmacol Rev **55**(1): 27-55.
- Yeung, A.T., S.L. Gellatly, R.E.W. Hancock (2011). Multifunctional cationic host defence peptides and their clinical applications. Cell Mol Life Sci **68**(13): 2161-2176.
- Zanetti, M. (2004). Cathelicidins, multifunctional peptides of the innate immunity. J Leukoc Biol **75**: 39-48.
- Zasloff, M. (1987) Magainins, a class of antimicrobial peptides from Xenopus skin: isolation, characterization of two active forms, and partial cDNA sequence of a precursor. Proc Natl Acad Sci U S A **84**(15): 5449-5453.

- Zhang, L., R. Benz, R.E.W. Hancock (1999). Influence of proline residues on the antibacterial and synergistic activities of alpha-helical peptides. Biochemistry **38**(25): 8102-8111.
- Zhang, L.J., R.L. Gallo (2016). Antimicrobial peptides. Curr Biol. **26**(1): R14-19.
- Zhang, S.K., J.W. Song, F. Gong, S.B. Li, H.Y. Chang, H.M. Xie, H.W. Gao, Y.X. Tan, S.P. Ji (2016). Design of an alpha-helical antimicrobial peptide with improved cell-selective and potent anti-biofilm activity. Sci Rep **6**:27394.
- Zweytick, D., G. Deutsch, J. Andrä, S.E. Blondelle, E. Vollmer, R. Jerala K. Lohner (2011). Studies on lactoferricin-derived *Escherichia coli* membrane-active peptides reveal differences in the mechanism of N-acylated versus nonacylated peptides. J Biol Chem **286**(24): 212.

8. Acknowledgments

I would like to thank my tutor Prof. Maria Luisa Mangoni for her support, encouragement and for the innumerable precious advices during my PhD course.

I thank all members of my lab group, with whom I spent wonderful years but also shared difficult moments.

I would like to thank all the collaborators:
Prof. Anirban Bhunia (Bose Institute, Kolkata, India) for the spectroscopic analysis of Esc(1-21) and Esc(1-21)-1c;
The group of Institute of Molecular Biosciences, Biophysics Division, Karl-Franzens University Graz, Austria who welcomed me with enthusiasm. In particular, my best thanks to Prof. Karl Lohner and Dr. Nermina Malanovic for their willingness and the valuable suggestions during the preparation of lipid vesicles which were used for the studies on the mechanism of action of antimicrobial peptides.
Prof. Francesca Ungaro and Dr. Ivana d'Angelo, at University "Federico II" (Naples), for making available their knowledge for the preparation of polymeric nanoparticles.
Prof. Lorenzo Stella (University of Tor Vergata, Rome, Italy) for the supervision during the liposomes preparation and the circular dichroism experiments.
Prof. Paolo Visca and Dr. Daniela Visaggio (University Roma 3, Italy), for the confocal spectroscopy data of Esc(1-21) and Esc(1-21)-1c.
Dr. Stefania Marcheggiani (Istituto Superiore di Sanità, Roma) for having made available the space for microbiological research.

Dr. Alessandra Bragonzi (San Raffaele Institute, Milan, Italy) for providing the *P. aeruginosa* clinical isolates.

Finally, I would like to thank my family, my friends and Lorenzo for supporting me in achieving this difficult but at the same time exciting goal.

Appendix: reprint of the papers

BBA - Biomembranes 1859 (2017) 2327–2339

Contents lists available at ScienceDirect

BBA - Biomembranes

journal homepage: www.elsevier.com/locate/bbamem

Membrane perturbing activities and structural properties of the frog-skin derived peptide Esculentin-1a(1-21)NH_2 and its Diastereomer Esc(1-21)-1c: Correlation with their antipseudomonal and cytotoxic activity

Maria Rosa Loffredo[a,1], Anirban Ghosh[b,1], Nicole Harmouche[c], Bruno Casciaro[a], Vincenzo Luca[a], Annalisa Bortolotti[d], Floriana Cappiello[a], Lorenzo Stella[d], Anirban Bhunia[b], Burkhard Bechinger[c], Maria Luisa Mangoni[a,*]

[a] Laboratory affiliated to Pasteur Italia-Fondazione Cenci Bolognetti, Department of Biochemical Sciences, Sapienza University of Rome, Rome, via degli Apuli, 9, 00185, Italy
[b] Department of Biophysics, Bose Institute, P-1/12, CIT Road, Scheme VII (M), Kolkata 700054, India
[c] University of Strasbourg/CNRS, Chemistry Institute, UMR, 7177, 4, rue Blaise Pascal, 67070 Strasbourg, France
[d] University of Rome Tor Vergata, Department of Chemical Sciences and Technologies, 00133, Rome, Italy

ARTICLE INFO

Keywords:
Antimicrobial peptides
Esculentin
Liposomes
Pseudomonas aeruginosa
Spheroplasts
Membrane thinning

ABSTRACT

Antimicrobial peptides (AMPs) represent new alternatives to cope with the increasing number of multi-drug resistant microbial infections. Recently, a derivative of the frog-skin AMP esculentin-1a, Esc(1-21), was found to rapidly kill both the planktonic and biofilm forms of the Gram-negative bacterium *Pseudomonas aeruginosa* with a membrane-perturbing activity as a plausible mode of action. Lately, its diastereomer Esc(1-21)-1c containing two D-amino acids i.e. ^{D}Leu14 and ^{D}Ser17 revealed to be less cytotoxic, more stable to proteolytic degradation and more efficient in eradicating *Pseudomonas* biofilm. When tested *in vitro* against the free-living form of this pathogen, it displayed potent bactericidal activity, but this was weaker than that of the all-L peptide. To investigate the reason accounting for this difference, mechanistic studies were performed on *Pseudomonas* spheroplasts and anionic or zwitterionic membranes, mimicking the composition of microbial and mammalian membranes, respectively. Furthermore, structural studies by means of optical and nuclear magnetic resonance spectroscopies were carried out. Our results suggest that the different extent in the bactericidal activity between the two isomers is principally due to differences in their interaction with the bacterial cell wall components. Indeed, the lower ability in binding and perturbing anionic phospholipid bilayers for Esc(1-21)-1c contributes only in a small part to this difference, while the final effect of membrane thinning once the peptide is inserted into the membrane is identical to that provoked by Esc(1-21). In addition, the presence of two D-amino acids is sufficient to reduce the α-helical content of the peptide, in parallel with its lower cytotoxicity.

1. Introduction

Most living organisms produce gene-encoded antimicrobial peptides (AMPs) as readily available weapons against a wide variety of microbial pathogens [1–3]. The majority of these AMPs are cationic molecules at neutral pH and they adopt an amphipathic α-helical structure in membrane environments [4]. These two remarkable features are fundamental for their broad microbicidal activity, which generally relies on the perturbation of the target cell membrane, thus limiting the induction of resistance [1,5]. Their ability to recognize and distinguish bacterial membranes from those of mammalian cells is based on an initial electrostatic interaction between the positively charged residues of the peptide and the negatively charged membrane phospholipids [6,7]. The latter are much more abundant at the outside of microbial cells when compared to the external leaflet of mammalian cell membranes, which are mostly made of zwitterionic phosphatidylcholine and sphingomyelin [5]. However, in the case of Gram-negative bacteria, before reaching the cytoplasmic membrane (i.e. inner membrane), bacteria need to cross the lipopolysaccharide (LPS)-outer layer in a self-promoted uptake mechanism [8]. Subsequently, the phospholipid bilayer of the inner membrane is destabilized via pore formation or micellization, leading to cell death [9–11]. After membrane passage, inner

* Corresponding author at: Department of Biochemical Sciences, Sapienza University of Rome, Via degli Apuli, 9-00185 Rome, Italy.
E-mail address: marialuisa.mangoni@uniroma1.it (M.L. Mangoni).
[1] The authors equally contributed to the work.

http://dx.doi.org/10.1016/j.bbamem.2017.09.009
Received 21 June 2017; Received in revised form 21 August 2017; Accepted 8 September 2017
Available online 12 September 2017
0005-2736/

targets may also exist for some of the peptides [12,13]. In contrast, conventional antibiotics generally inhibit intracellular biological function(s) upon interaction with a single stereospecific target that can be mutated [14,15], making it easier for the microbes to become resistant to this class of drugs [16,17]. Due to the alarming worldwide emergence of multi-drug resistant (MDR) pathogenic microorganisms [18] and the concomitant decrease in the pharmaceutical industry research pipeline for novel antibiotics, the search for new antimicrobial strategies has become strictly necessary [19–21]. AMPs hold promise for the development of new anti-infective compounds [22–25]. Interestingly, a few years ago we discovered that a short-sized AMP, esculentin-1a(1-21)NH_2, Esc(1-21), derived from a natural AMP of amphibian origin was endowed with: (i) a wide and potent spectrum of activity especially against Gram-negative bacteria [26–28] and (ii) rapid killing kinetics on planktonic and biofilm cells of *Pseudomonas aeruginosa*. It also showed a membrane-perturbing activity as a plausible mode of action [29]. In addition, it was found to have additional non-antimicrobial properties. Among those, the ability (i) to detoxify *P. aeruginosa* LPS [30] and (ii) to induce re-epithelialization of a pseudo-"wound"; a property which is not shown by any traditional antibiotic [30,31].

Furthermore, we recently demonstrated that a diastereomer of Esc (1-21), named Esc(1-21)-1c, containing two D-amino acids i.e. ^{D}Leu14 and ^{D}Ser17 had significant lower cytotoxicity and higher biostability than its all-L isomer [30]. In addition, it was more efficient in promoting clearance of *P. aeruginosa* internalized in bronchial cells as well as in stimulating wound-healing in an *in vitro* bronchial epithelial cells model [32]. However, when tested *in vitro* against the free living form of *P. aeruginosa* strains, even if it displayed a potent killing activity this was weaker than the parent Esc(1-21) [32].

With the aim to understand whether this discrepancy reflected a different ability of the peptides in damaging the cytoplasmic membrane of bacterial cells or a different interaction with the bacterial cell surface, mechanistic studies have been performed on intact bacterial cells, with bacteria devoid of their cell wall (i.e. spheroplasts) as well as micelles mimicking the head group composition and/or surface charge of membranes. In parallel, to verify whether the lower cytotoxicity of the diastereomer in comparison to the all-L peptide reflected a weaker ability in destabilizing zwitterionic membranes, the leakage of a fluorescent marker from neutral lipid vesicles was assessed in comparison to anionic vesicles. Furthermore, by using optical and nuclear magnetic resonance spectroscopies, the secondary structure of the peptides in membrane-mimicking environments has been investigated. Our studies revealed that the weaker *in vitro* antimicrobial activity of the two D-amino acid containing Esc(1-21)-1c in comparison with the all-L Esc(1-21) is mainly associated to a different interaction of the peptide with microbial cell wall components and only partially due to a weaker ability in binding and perturbing anionic membranes. Furthermore, the presence of two D-amino acids was found to be sufficient to reduce the α-helical content of the peptide, in line with its lower cytotoxicity.

2. Materials and methods

2.1. Materials

Synthetic Esc(1-21) and its diastereomer Esc(1-21)-1c (Scheme 1) were purchased from Chematek Spa (Milan, Italy). Each peptide was assembled by stepwise solid-phase synthesis using a standard F-moc strategy and purified via reverse-phase high-performance liquid chromatography (RP-HPLC) to a purity of 98%, while the molecular mass was verified by mass spectrometry. The following lipids: 1-palmitoyl-2-oleoyl-*sn*-glycero-3-phosphoethanolamine (POPE); 1-palmitoyl-2-oleoyl-*sn*-glycero-3-phosphoglycerol (POPG); 1-palmitoyl-2-oleoyl-*sn*-glycero-3-phosphocholine (POPC), POPE-$^{2}H_{31}$ and cholesterol (Cho) were purchased from Avanti Polar Lipids (Alabaster, AL, USA). Sodium-dodecylsulfate (SDS), dodecylphosphocholine (DPC) were obtained from Cambridge Isotope Laboratories (Tewksbury, MA); carboxy-fluorescein (CF), water (HPLC grade), deuterium depleted water (≤ 1 ppm), 3-(4,5-dimethylthiazol-2-yl)-2,5-diphenyltetrazolium bromide (MTT) were from Sigma (St. Quentin Fallavier, France). Sytox Green was from Molecular Probes (Invitrogen, Carlsbad, CA, USA).

2.2. Microorganisms

The following bacterial strains were used for the antimicrobial assays: the standard *P. aeruginosa* PAO1 [29] and the clinical isolate *P. aeruginosa* AA43 from the strains collection of the cystic fibrosis clinic Medizinische Hochschule of Hannover, Germany [33].

2.3. Spheroplasts preparation

Spheroplasts of *P. aeruginosa* PAO1 were prepared by adapting the procedure described in [34]. Briefly, bacteria from a log-phase culture were collected by centrifugation at 3000 × *g* and washed in 0.01 M phosphate buffer, pH 7.0 (PB). The cells were then harvested by centrifugation and resuspended in half-volume of 0.5 M sucrose solution in PB to induce plasmolysis. Lysozyme was added to the cell suspension at a final concentration of 50 μg/ml. After incubation at 37 °C for 90 min with moderate shaking, the sample was diluted 1:1 with PB and ethylenediaminetetraacetic acid (EDTA) was added to a final concentration of 10 mM. The cell suspension was incubated again at 37 °C for additional 60 min. Thereafter, transition of the rod-shaped bacteria into spheres was determined by light microscopy. When ~80% of the cells were spheroplasted (as visualized by phase-contrast microscopy), the reaction was stopped by pelleting the cells at 500 × *g* for 15 min. The spheroplasts were then washed in 0.25 mM sucrose in PB (SPB2), centrifuged at 500 × *g* for 15 min, and resuspended in SPB2.

2.4. Antimicrobial activity

Aliquots of 100 μl of SPB2 containing spheroplasts derived from 1×10^7 intact bacteria were treated with Esc(1-21) and its diastereomer for 30 min at 37 °C. Afterwards, spheroplasts viability was assayed by the reduction of MTT to insoluble formazan. Briefly, 100 μl of 1 mg/ml MTT were added to the bacterial suspension, transferred into a 96-wells microplate, which was incubated for 90 min at 37 °C. The reduced formazan was then solubilized by the addition of an equal volume of 10% (w/v) SDS, measured in a microplate reader (Infine M 200, Tecan) at 590 nm. All assays were performed in triplicate, and the experiments were repeated three times.

2.5. Sytox green assay on intact bacterial cells

The ability of the peptide to alter the membrane permeability of whole *Pseudomonas* cells was assessed by the Sytox Green (~660 Da) assay. Approximately 1×10^6 cells in 100 μl of phosphate buffered

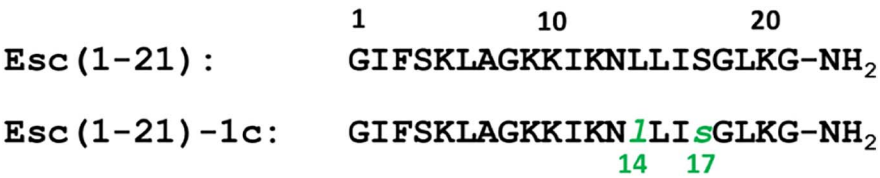

Scheme 1. Amino acid sequence of Esc(1-21) and Esc(1-21)-1c. The D-amino acids at position 14 and 17 are shown in green and in italics.

saline (PBS) were mixed with 1 μM Sytox Green for 5 min in the dark. After adding peptides at different concentrations, the increase of fluorescence, due to the binding of the dye to intracellular DNA, was measured at 37 °C in the microplate reader (Infinite M200). The excitation and emission wavelengths were 485 and 535 nm, respectively. Cells not exposed to the peptides were used as control, whereas the maximal membrane perturbation was obtained after treating bacteria with the highest peptide concentration used (32 μM) followed by the addition of 1 mM EDTA + 0. 5% Triton X-100 (final concentration) to completely destabilize the LPS-outer membrane and to solubilize the cytoplasmic membrane [35]. Samples were run in triplicate and the experiments were performed three times.

2.6. Preparation of large unilamellar vesicles (LUVs)

Lipid films of POPE/POPG and POPC/Cho were prepared by dissolving lipids (2 mg of POPE/POPG mixture, 7:3, mol/mol or 2 mg of POPC/Cho, 1:1, mol/mol) in chloroform/methanol (2:1, v/v). The solvents were then evaporated under reduced argon atmosphere until a thin film was formed. Complete evaporation was ensured by applying a rotary vacuum pump for at least 2 h. The lipid film was then hydrated with a 10 mM phosphate buffer containing 140 mM NaCl and 0.1 mM EDTA, pH 7.4 (buffer A), or with a CF solution at a self-quenching concentration, i.e. 30 mM (for CF leakage experiments) in 10 mM phosphate buffer containing 80 mM NaCl and 0.1 mM EDTA, brought to pH 7.4 with NaOH. The liposome suspension was subjected to 10 freeze and thaw cycles and extruded for 31 times through two stacked polycarbonate membranes with 100 nm pores to obtain LUVs. The free CF (when present) was removed by gel filtration, using a 40 cm Sephadex G-50 at room temperature, equilibrated with buffer A. NaF was used in place of NaCl for CD experiments, to avoid the high absorption by Cl-ions in the far UV [36]. The final lipid concentration was determined by the Stewart phospholipid assay [37].

2.7. CF leakage assay

CF release from LUVs due to membrane permeation induced by the peptide was monitored at 37 °C by the fluorescence increase (excitation = 488 nm; emission = 520 nm). A concentration of lipid vesicles of 200 μM was used and CF leakage after peptide addition at 20 μM was monitored for 30 min. Complete dye release was obtained using 0.1% Triton X-100, which causes total destruction of lipid vesicles [38,39]. The percentage of CF leakage was calculated according to the following formula [40]: leakage (%) = 100(F1 − F0) / (Ft − F0), where F0 represents the fluorescence of intact vesicles, and F1 and Ft denote the intensities of the fluorescence achieved by peptide and Triton X-100 treatment, respectively, at different time points, as indicated. The experiments were performed in duplicate and repeated three times.

2.8. Circular dichroism spectroscopy

In order to investigate the change in secondary structure of Esc(1-21) and Esc(1-21)-1c in SDS and DPC micelles, circular dichroism (CD) experiments were performed using a Jasco J-815 spectrometer (Jasco International Co., Ltd. Tokyo, Japan) with a Peltier cell holder and temperature controller unit accessory. CD spectra were recorded for both the peptides in water (25 μM) and in the presence of different concentrations of SDS (peptide 25 μM, detergent 40 mM), DPC (peptide 25 μM, detergent 10 mM) at 37 °C, or in liposomes of POPE/POPG 7:3 (mol/mol) (peptide 5 or 20 μM, lipids up to 1 mM), at 25 °C. Both working concentrations of SDS and DPC micelles were above previously published critical micellar concentrations (CMC) [41]. The far-UV spectra were scanned over a range of 190–260 nm with 1 nm data interval and averaging over 4 scans. Blank sample spectra were subtracted from the raw data and the CD values were converted to per residue molar ellipticity ([θ]) (deg cm^2 $dmol^{-1}$).

2.9. Solution-state NMR experiments

All solution-state NMR experiments were executed on a Bruker Avance III 700 MHz spectrometer furnished with a CryoProbe at 310 K and/or 335 K. Topspin 3.1 (Bruker Biospin, Rheinstetten, Germany) and SPARKY 3.113 (UCSF) was used for processing and analysis of NMR data [42]. Two-dimensional total correlation (TOCSY) and nuclear Overhauser effect (NOESY) spectra of Esc(1-21) and Esc(1-21)-1c alone (1 mM) and in the presence of perdeuterated d_{25}-SDS (200 mM) and d_{38}-DPC (125 mM) were performed in aqueous solution comprising 10% D_2O (pH ~4.5). All spectra were acquired at 1024 and 512 complex data points along t_2 and t_1 dimensions, respectively, where the States-TPPI-mode was used for quadrature detection in the t_1 dimension [43]. The spectral width was 12 ppm, the offset was adjusted at the water resonance (4.703 ppm) and the relaxation delay was of 2.0 s. TOCSY spectra were acquired using the standard pulse sequence of the pulse sequence library of the Bruker spectrometer, having excitation sculpting for water suppression and spin-lock mixing times of 80 ms (using MLEV-17 mixing scheme), whereas NOESY experiments with 80, 100, 150 and 250 ms mixing time were performed. Sequence-specific resonance assignment was accomplished based on 2D TOCSY and NOESY spectra of peptides in DPC micelles by means of standard assignment procedures [44]. All ^1H chemical shifts were referenced using DSS (2,2-Dimethyl-2-silapentane-5-sulfonate sodium salt) as an internal standard.

2.10. NMR derived structure calculation

The three-dimensional solution NMR structures of Esc(1-21) and Esc (1-21)-1c in DPC micelles were determined using the CYANA 2.1 software [45]. From NOESY spectra of Esc(1-21) and Esc(1-21)-1c in SDS and DPC micelles, NOE cross peak intensities were converted to upper bound distance limits of 3.0, 4.0, and 5.5 Å, corresponding to strong, medium, and weak intensities, respectively. The lower limits for all distance restraints were kept at 2.0 Å. In addition, the dihedral angle constraints were estimated from PREDITOR by means of $C_\alpha H$ chemical shifts and were used for structure calculations with ± 20° variation, from the derived dihedral angle values [46]. Several rounds of structure calculation were performed for iterative refinement using the standard protocol of CYANA 2.1, as described previously [47,48]. Finally, the best 20 structures with lowest target function values were selected, depending upon low RMSD and minimum violation of distance and dihedral angle constraint. The stereochemical nature of the final structures was analyzed using PROCHECK-NMR validation suite [49]. To estimate the convergence of NMR-derived ensemble of structures, NH order parameters (S^2) [50] for both the peptides were calculated.

2.11. Preparation of peptide-loaded liposomes for solid-state NMR spectroscopy

Multilamellar vesicles (MLVs) were prepared by co-solubilization of lipids [POPE:POPE-$^2H_{31}$:POPG (2:1:1)] and peptides at the appropriate lipid-to-peptide molar ratio in chloroform/methanol 2:1 (v/v) to ensure homogenous mixing of the components, followed by solvent evaporation under a stream of nitrogen gas, removal of solvent traces by lyophilisation from a water suspension and then rehydration at h = 0.9 [h = mass of water over the total mass of the system (phospholipids and water)]. To improve sample homogeneity the liposomes were repeatedly vortexed for 40 s, frozen in liquid nitrogen for 30 s and heated in a water bath at 40 °C for 10 min. After 1 to 3 freeze-thaw-vortex cycles, Esc(1-21) and Esc(1-21)-1c embedded in liposomes were obtained.

2.12. Solid-state NMR spectroscopy

^{2}H quadrupole echo experiments [51,52] were acquired with a spectral width of 100 kHz, a recycle delay of 1 s, 25 μs echo delay, 30 ms acquisition time, π/2 pulses of 3.4 μs, and between 50 k and 80 k scans. All samples were investigated at temperatures at least 15 K above the phase transition of the individual lipids of the mixture.

Oriented ^{2}H spectra were obtained from the powder pattern by de-Pakeing [53] thus the splitting can be measured more easily. The de-Paking procedure was performed according to the fast Fourier transform-based deconvolution algorithm [54] and first spectral moments were calculated using the NMR-Depaker software (available from the Launchpad Web site: https://launchpad.net/nmr-friend).

Individual C−^{2}H bond order parameters ($S_{CD}i$) were calculated from quadrupolar splittings as described previously [52,55],

$$S_{CD} = 4^{\Delta\nu_Q}/3^{A_Q} \quad (1)$$

where A_Q is 167 KHz.

2.13. Average acyl chain length measurement

Calculation of acyl chain length is performed according to Douliez et al. [56–60] and can be performed by considering the average projection of each C−C bond along the bilayer normal. This is achieved by connecting the S_{CD} order parameter to the C−C bonds order parameters (S_{CC}), and to sum all the average lengths of the aliphatic chain C−C bonds, projected on the normal to the bilayer. The average length of an aliphatic chain with an even number of carbons is obtained by the following expression:

$$<\text{Lchain}> = \frac{1+\sqrt{1+8S_{mol}}}{4}\left[<l_{C_n\text{-}D}> + 1.,25\cdot\sum_{k=2}^{n}\left(\frac{1}{2}+\frac{S_k^{CC}}{S_{mol}}\right)\right] \quad (2)$$

where $\langle l_{C_n}\text{-D}\rangle$ represents the contribution of the terminal methyl C_n−^{2}H bond, and S_{mol} is the molecular order parameter (taking into account wobbling motions).

By taking n = 14 for DMPC and DMPE and n = 16 for POPC and POPE; S_{mol} = 1, $\langle l_{C_n}\text{-D}\rangle$ is estimated equal to 1.09 Å cos (35,35°) = 0.89 Å, and the angle between the C_n−^{2}H bond and C_{nl}−C_n being 111° the equation reduces to:

$$<\text{Lchain}> = \left[0.\ 89 + 1.,25\cdot\sum_{k=2}^{n}\left(\frac{1}{2}+S_k^{CC}\right)\right] \quad (3)$$

The order parameter S_{CC} can be obtained after considering a fast axial rotation of the methyl group around the C_{nl}−C_n bond; hence, S_{CC} is obtained from measured S_{CD} using the recurring equation $S_n{}^{CC} + S_{n+1}{}^{CC} = -2S_n{}^{CD}$. The order parameter for the nth term can be obtained from:

$$S_n^{CD} = \frac{3\cos^2(111^\circ)\text{-}1}{2}S_n^{CC} \quad (4)$$

The area per lipid A is determined according to de Planque et al., and Nagle [61,62]:

$$A = 2[27.6\,\text{Å}^2/(1.27(0.5+Sp))] \quad (5)$$

where Sp is the average order parameter of the plateau region (carbons 2–6).

2.14. Statistical analysis

Quantitative data were expressed as the mean ± standard deviation (SD). Statistical analysis was performed using Student's *t*-test with the PRISM software (GraphPad, San Diego, CA). Differences were considered to be statistically significant for $p < 0.05$ and are indicated in the legend to figures.

3. Results

3.1. Cytoplasmic membrane perturbation

The diastereomer Esc(1-21)-1c was previously found to display a potent killing activity against the planktonic form of reference and cystic fibrosis strains of *P. aeruginosa* [30]. However, this activity was less pronounced than that of the parent Esc(1-21), as proved by the corresponding minimal bactericidal concentration (MBC) causing 99.9% reduction in the number of viable cells within 30 min, in PBS. This was 4 μM versus 1 μM of Esc(1-21) when tested against a bacterial cell density of 1×10^6 CFU/ml [30].

To assess whether this difference reflected a different perturbation of the cytoplasmic membrane of this pathogen by the two peptides, a Sytox Green assay was carried out on two different bacterial strains: the reference *P. aeruginosa* PAO1 and the clinical isolate *P. aeruginosa* AA43. Sytox Green is a membrane-impermeable probe whose fluorescence intensity rapidly enhances upon binding to nucleic acids of bacterial cells with damaged cytoplasmic membrane; and its fluorescent signal is positively correlated to the level of membrane injury. Note that a significantly higher number of bacterial cells (i.e. 1×10^7 CFU/ml) than that generally used for *in vitro* antimicrobial assays is needed, in order to get a detectable signal [29]. As reported in Fig. 1 for *P. aeruginosa* AA43, both peptides were able to destabilize the bacterial membrane, but with a higher potency and faster kinetics for Esc(1-21) (see also the dose-response relationship after 5 min from peptide addition in the Supplementary Fig. S1). While almost total membrane perturbation was achieved by Esc(1-21) within 5 min (at the concentrations of 16 μM and 32 μM, Fig. 1 and Fig. S1) or 15 min (in the concentration range from 2 μM to 8 μM, Fig. 1), a significantly weaker and slower effect was recorded for Esc(1-21)-1c (Figs. 1 and S1). With reference to the latter, ~40% of membrane damage was caused at the highest peptide concentration of 32 μM within 5 min (Fig. S1). The degree of membrane injury gradually diminished in a dose-dependent manner and became negligible at 1 μM. Differently, ~40% of membrane perturbation was registered at 1 μM of Esc(1-21) at the same time point of 5 min (Fig. S1). Similar results were also found for the reference PAO1 [29] and ATCC 27853 strains (data not shown). These data indicate a significant discrepancy between the two peptides in perturbing the cytoplasmic membrane of intact bacterial cells (i.e. much more than the 4 times ratio observed for the MBC values).

3.2. Activity on spheroplasts of P. aeruginosa

To investigate whether the bacterial cell wall was a barrier that differently interferes with the activity of the two peptides, their effect on *Pseudomonas* cells lacking of cell wall (i.e. spheroplasts) was studied. The reference strain of *P. aeruginosa* PAO1 was employed for this purpose and the peptides' effect on the viability of its spheroplasts (1×10^8 cells/ml) was evaluated by the MTT assay, 30 min after peptide addition at different concentrations, with respect to untreated control cells. As shown in Fig. 2, the percentage of metabolically-active spheroplasts after incubation with the all-L peptide at 2 μM was about 70%, while it dropped down to ~2% at 10 μM, in a dose-dependent manner. In comparison, the activity of the diastereomer on spheroplasts was lower, but the difference was much smaller than what was observed on intact cells: Esc(1-21)-1c was only ~1.5-fold less effective, with an LD_{50} of 4.4 ± 0.5 μM versus 2.9 ± 0.5 μM of Esc(1-21).

3.3. Peptides' effect on LUVs of different composition

To expand our knowledge on the membrane perturbing activities of Esc(1-21) and Esc(1-21)-1c, the leakage of CF entrapped in the water volume inside liposomes made of both anionic and zwitterionic phospholipid bilayers was evaluated. A CF concentration of 30 mM was used to induce self-association and the consequent quenching of the dye

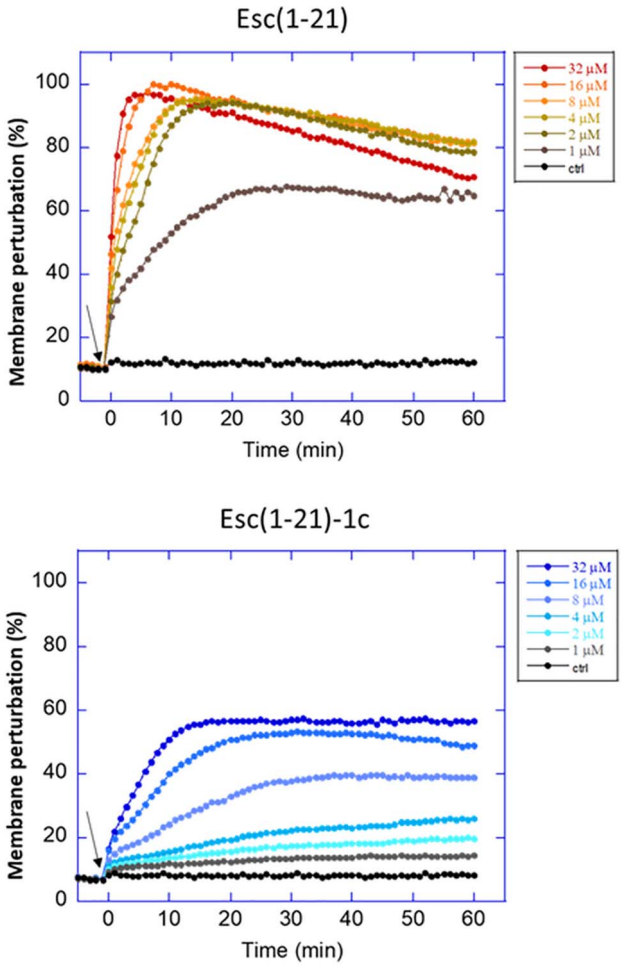

Fig. 1. Kinetics of cytoplasmic membrane permeabilization of the planktonic form of *P. aeruginosa* AA43. Cells (1×10^7 CFU/ml) were incubated with 1 μM Sytox Green in PBS. Once basal fluorescence reached a constant value, the peptide was added (*arrow*, $t = 0$) at different concentrations and changes in fluorescence (λ_{exc} = 485 nm, λ_{ems} = 535 nm) were monitored for 60 min and plotted as the percentage of membrane perturbation relative to that obtained after treating bacteria with the highest peptide concentration (32 μM) and the addition of 1 mM EDTA + 0.5% Triton-× 100. Data points represent the mean of triplicate samples from a single experiment, representative of three different experiments. Cells not exposed to the peptide were used as control (Ctrl).

[63]. After peptide administration, the membrane destabilization leads to probe release and dissociation with a resulting fluorescence increase. Both peptides were tested at a concentration of 20 μM on POPE/POPG liposomes (7:3 mol:mol, 200 μM), which mimic the lipid composition of the anionic membrane of Gram-negative bacteria. After addition to the lipid vesicles, Esc(1-21) gave rise to a 2-fold higher membrane-perturbing activity than the diastereomer, within 30 min (Fig. 3 panel A) and this was consistent with the results on spheroplasts.

When the two isomers were used on zwitterionic liposomes made of POPC/cholesterol (1:1, mol:mol) to simulate the neutral membrane of mammalian cells, a 5-fold lower leakage of entrapped CF was found for the diastereomer in comparison with its all-L counterpart (Fig. 3 panel B) in line with the lower cytotoxicity of Esc(1-21)-1c on mammalian cells [30,32].

3.4. Structural studies by CD and NMR spectroscopy

In parallel, studies aimed at understanding the structural properties of the two peptides were performed by CD and multidimensional solution-state NMR spectroscopy, in the presence of micellar and liposomal membrane mimetics.

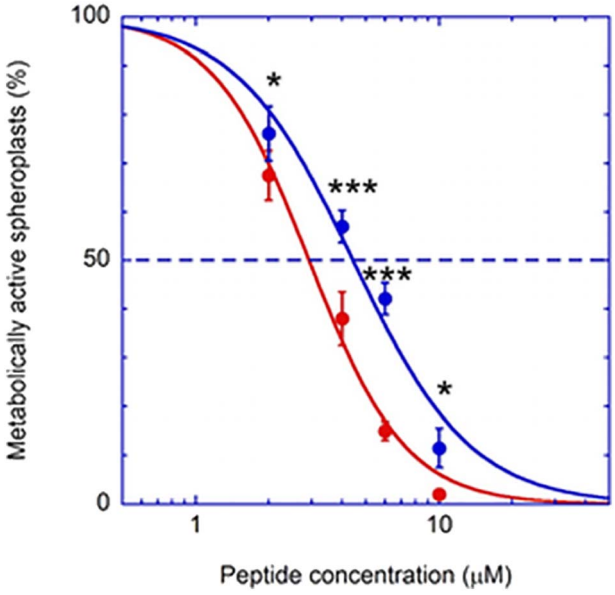

Fig. 2. Effect of different concentrations of Esc(1-21), red line, and its diastereomer, blue line, on the viability of spheroplasts of *P. aeruginosa* PAO1, 30 min after treatment at 37 °C. Cell viability was determined by the MTT reduction to insoluble formazan (see Materials and Methods) and is expressed as percentage with respect to the control (cells not treated with the peptide). Data represent the mean ± SD of three independent experiments performed in triplicate. The level of statistical significance between samples treated with Esc(1-21) and Esc(1-21)-1c are indicated as follows *p < 0.05, ***p < 0.001.

3.4.1. CD

The secondary structure of Esc(1-21) and Esc(1-21)-1c in membranes, and their affinity for lipid bilayers, was initially characterized by CD spectroscopy, in the presence of increasing concentrations of POPE/POPG liposomes (Fig. 4). Their spectra presented a single negative minimum around 200 nm, a characteristic spectral signature for random coil conformations. By contrast, after addition of increasing concentrations of vesicles, the appearance of two negative minima at 208 nm and 222 nm was indicative of α-helical conformations of both peptide isomers, although to a lesser extent in the case of Esc(1-21)-1c (Fig. 4, panels A and B). The change in CD intensity at a fixed wavelength upon binding is directly proportional to the amount of complex formed.

$$[\theta]([L]) = [\theta]_{free} + ([\theta]_{bound} - [\theta]_{free}) \cdot f_{bound} \qquad (6)$$

Here, $[\theta]([L])$, $[\theta]_{free}$ and $[\theta]_{bound}$ are the values of molar ellipticity (in our case at 222 nm) observed at a given lipid concentration $[L]$, in the absence of liposomes, and in the completely bound state, respectively, and f_{bound} is the fraction of membrane-bound peptide [64].

In an ideal water-membrane partition equilibrium, f_{bound} depends on lipid concentration according to the following equation, where K_p is an apparent partition constant [63].

$$f_{bound} = \left(\frac{[L]/K_p}{1 + [L]/K_p} \right) \qquad (7)$$

Combining these two equations, the expected lipid dependence of the molar ellipticity is given by

$$[\theta]([L]) = [\theta]_{free} + ([\theta]_{bound} - [\theta]_{free}) \cdot \left(\frac{[L]/K_p}{1 + [L]/K_p} \right) \qquad (8)$$

In our case, unfortunately, significant binding (and increase in helicity) took place only at lipid concentrations in the 100 μM range (Fig. 4 panels C and D), so that in the experimentally useful range of lipid concentrations (limited to 1 mM by the necessity to avoid

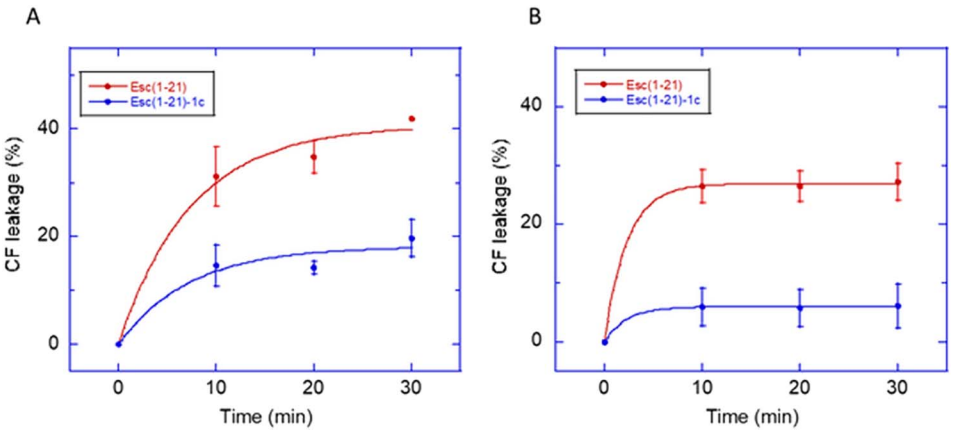

Fig. 3. CF release from POPE/POPG (panel A) and POPC/chol (panel B) LUVs (final lipid concentration 200 μM) within 30 min after addition of peptides (20 μM) at 37 °C. The percentage of leakage was calculated according to the formula: 100(F1 − F0) / (Ft − F0) as explained in the Materials and Methods. Data points are means ± SD of three independent measurements performed in duplicate. The difference between the two peptides was significant ($p < 0.05$).

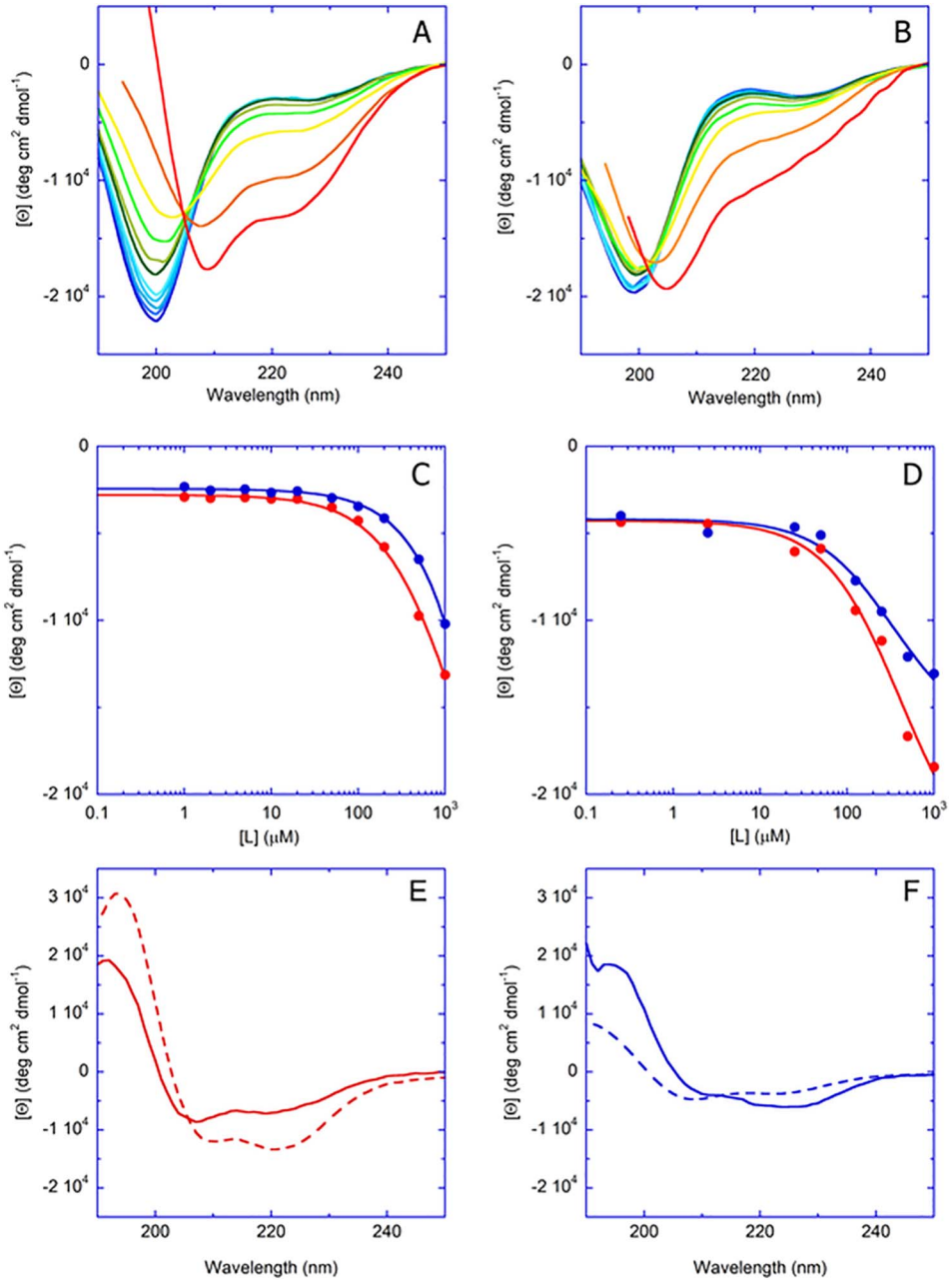

Fig. 4. Top row: Circular dichroism spectra of Esc(1-21) (panel A) and Esc(1-21)-1c (panel B), measured in the presence of increasing lipid concentrations (POPE/POPG 7/3, mol/mol). Peptide concentration: 20 μM, lipid concentrations: 1 μM, 2 μM, 5 μM, 10 μM, 20 μM, 50 μM, 100 μM, 200 μM, 500 μM and 1 mM. The CD spectra are colored from blue to red, in order of increasing concentrations and following the order of colors in the visible spectrum. Middle row: Mean residue ellipticity ([θ]) at 222 nm as function of lipid concentrations, [peptide] = 20 μM (panel C) and [peptide] = 5 μM (panel D), Esc(1-21) in red and Esc (1-21)-1c in blue. Bottom row: Circular dichroism spectra of Esc(1-21) (panel E) and Esc(1-21)-1c (panel F), measured in the presence of SDS (broken line) and DPC (solid line) (25 μM peptide, 40 mM SDS or 10 mM DPC).

scattering artefacts [65]) a plateau was not observed. For this reason, data fitting with the above equation was affected by a large uncertainty on the values of $[\theta]_{bound}$, and thus of K_p. However, the data are sufficient to indicate that the latter constant is of the same order of magnitude for the two peptides (~1 mM), although its value is possibly higher for Esc(1-21)-1c (blue lines).

In order to characterize the conformation of the two peptides when associated to a membrane-mimicking environment, CD spectra were measured in the presence of SDS (broken line) and DPC micelles (solid line), mimicking the anionic and zwitterionic composition of the outer leaflet of the cell membrane of bacteria and mammalian cells, respectively (Fig. 4, panels E, F). In this case, the smaller size of the amphiphilic aggregates reduced light scattering effects, compared to studies in the presence of vesicles. Therefore, surfactant concentrations much higher than the K_p values estimated for POPE/POPG liposomes could be employed, thus favouring peptide association to the micelles. In all cases, the spectral intensities typical of alpha helices were observed, although this was less pronounced in the case of Esc(1-21)-1c (Fig. 4 panel F), probably as a consequence of the presence of D-amino acids. The spectra in SDS exhibited a 222 nm intensity that is more negative than the 208 nm peaks. This finding is often considered indicative of the formation of helical aggregates [66].

3.4.2. NMR studies of Esc(1-21) and Esc(1-21)-1c in SDS and DPC micelles

The conformational transition from random coil to α-helical in the presence of membrane-mimicking environments, as detected by CD spectra, motivated us to explore the peptide structures at atomistic detail by high-resolution solution state NMR spectroscopy. DPC and/or SDS assemble as small size detergent micelles which, in contrast to large liposomes, provide appropriate systems for the structural analysis of AMPs in membrane mimetic environments by multidimensional NMR spectroscopy, due to fast tumbling of the peptide-micellar complex in solution [67,68].

Fig. 5 shows the amide proton region of the one-dimensional ^{1}H NMR spectra of Esc(1-21) and Esc(1-21)-1c in water and in the presence of SDS and DPC micelles. In water, both peptides displayed little dispersion and broad signals in the amide proton region of the spectra whereas in the presence of zwitterionic DPC micelles the spectra were not only well dispersed but also well resolved. The difference in one-dimensional proton spectral pattern demonstrated that micelles induced conformational transformation of both peptides with well-defined secondary structure. Moreover, in the presence of DPC micelles the spectra were better dispersed when compared to their association with SDS micelles, which can be accounted as differential conformational stabilization in the different micellar environment. Unfortunately, due to poor spectral resolution, in SDS micelles for both peptides extensive peak overlap in the fingerprint region of two-dimensional ^{1}H–^{1}H NOESY and TOCSY precludes further analysis of the 2D spectra.

With the help of two-dimensional ^{1}H–^{1}H TOCSY and NOESY spectra, sequential resonance assignment of Esc(1-21) and Esc(1-21)-1c in DPC was performed. It is noteworthy that the NOESY spectra in DPC micelles contained the adequate number of sequential and medium-range NOE cross peaks in comparison to the spectra in aqueous solution (Fig. S2 in SI). Therefore, the lack of diagnostic NOEs for both peptides in aqueous solution confirmed the CD spectral analysis where random coil conformations were observed. Differently, in zwitterionic DPC micelles the peptides adopted a more ordered conformation, as reported below. Intense sequential CαH/HN (i to i + 1) NOEs were observed for all residues of both peptides (Fig. 6A and B). In addition, several medium range CαH/HN (i to i + 2/i + 3/i + 4) NOEs were observed for Esc(1-21) throughout the peptide (Fig. S2 A and Fig. 6A). Furthermore, the presence of medium range NH/NH (i to i + 2) NOE contacts reinforced the α-helical conformation of Esc(1-21). Overall the distribution of medium range CαH/HN (i to i + 3/i + 4) as well as NH/NH (i to i + 2) backbone NOEs throughout the sequence established an α-helical conformation in DPC micelles for Esc(1-21), in good accordance with the CD spectral analysis.

On the other hand, Esc(1-21)-1c in DPC micelles contained less diagnostic CαH/HN (i to i + 2/i + 3/i + 4) NOEs in comparison to Esc (1-21) (Fig. S2 B). Most of the medium range NOEs (i to i + 2/i + 3/i + 4) were observed in the N-terminal G1-N13 region (Fig. 6B). This was also in agreement with the trend in backbone NH/NH (i to i + 2) NOE patterns which showed that most NOEs are in the N terminal region such as I2/F4, F3/K5, S4/L6, K5/A7 while the C-terminal stretch, having D-amino acid mutations at 14th and 17th position contained very few NOEs such as K12/L14, N13/L15 and I16/G18.

The discrepancy in NOE distribution for both peptides indicated that the N-terminal portion was mostly well-organized in the parent peptide while the C-terminal region of Esc(1-21)-1c was relatively unstructured and flexible in zwitterionic DPC micellar environments. This was supported by the trend in the ΔH^{α} values for each residue of Esc(1-21) and Esc(1-21)-1c where the chemical shift deviation of the alpha proton resonances from the reported values of random coil resonances provided information about the secondary structure of the peptide [69]. Here, a helical segment is characteristic of negative chemical shift deviation of ΔH^{α} for consecutive 4 residues while a positive chemical shift deviation is a signature of the beta sheet structure. In our systems in DPC micelles, all the CαH resonances throughout the sequence of Esc(1-21) and Esc(1-21)-1c experienced a downfield trend for the CαH chemical shifts (Fig. S3). This chemical shift deviation is a signature of the

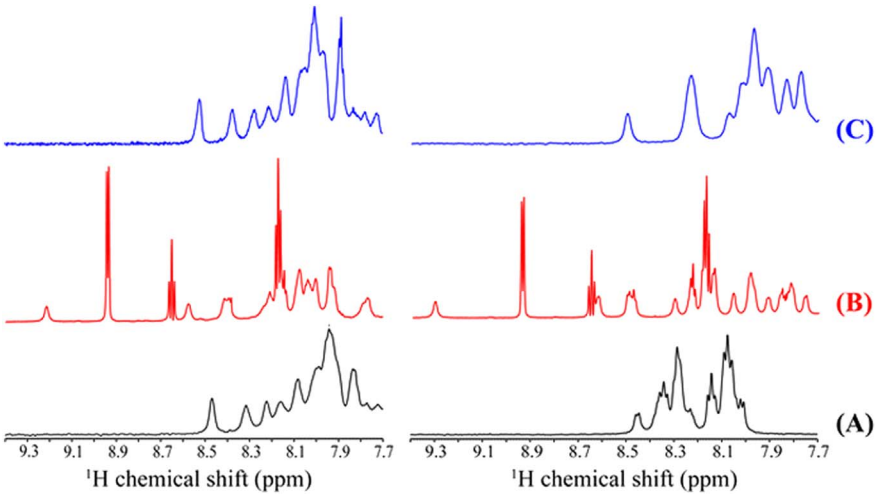

Fig. 5. Amide proton region of ^{1}H NMR spectra of 1 mM Esc(1-21) (left column) and of 1 mM Esc(1-21)-1c (right column) in the absence of detergent (A), and in the presence of (B) 200 mM perdeuterated DPC or (C) 125 mM perdeuterated SDS. The NMR experiments were performed using a Bruker Avance III 700 MHz spectrometer at pH ~4.5 and at 37 °C.

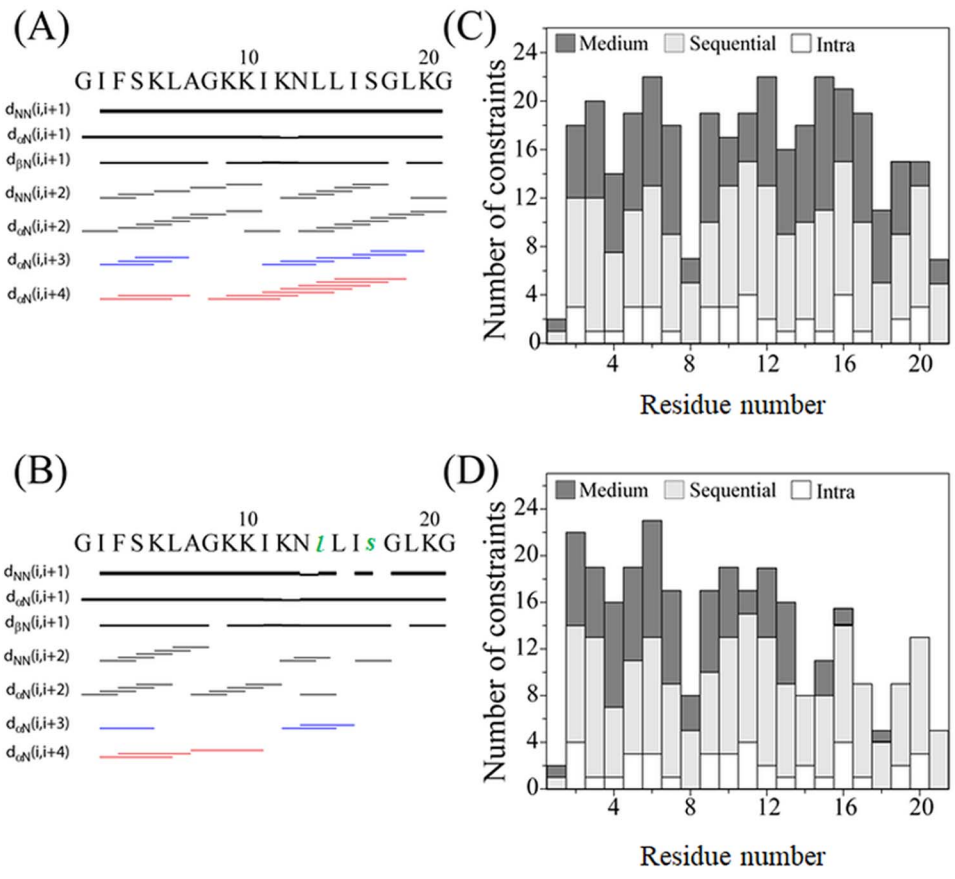

Fig. 6. Summary of NOE contacts of Esc(1-21) and Esc(1-21)-1c peptides in the DPC micelles. Left panel: Bar diagram demonstrating different (sequential, medium range, and long range) NOE contacts of Esc (1–21) (A) and Esc(1–21)-lc (B) in deuterated DPC micelles. The intensity of the NOESY peaks are designated by the thickness of the bars which are assigned as strong, medium, and weak during structure calculation. CαH/NH (i to i + 3) NOEs are marked by blue bars and CαH/NH (i to i + 4) NOEs are marked by red bars. Right panel: A histogram displaying the number and type (intra, sequential, medium) of NOEs of Esc(1-21) (C) and Esc(1-21)-lc (D) as a function of residue number in complex with DPC micelles. The NOESY experiments (mixing time 150 ms) were performed using Bruker Avance III 700 MHz spectrometer with 1 mM peptide in aqueous solution (pH ~4.5) at 37 °C.

predominance of α-helical conformations in DPC micelles. Moreover, it was noted that the overall average chemical shift deviation was little higher in case of Esc(1-21) in comparison to Esc(1-21)-1c. The difference in average chemical shift deviation in the L14-G21 region was almost double for Esc(1-21) in comparison to Esc(1-21)-1c in line with the previous observation from NOESY spectra of both peptides.

3.5. Structure calculations for Esc(1-21) and Esc(1-21)-1c in DPC micelles

The NOESY derived distance constraints in conjunction with angular constrains, obtained from PREDITOR, were used to elucidate the three-dimensional conformations of Esc(1-21) and Esc(1-21)-1c peptides in DPC micellar solution. For structure calculations of Esc(1-21), a total of 190 distance restraints including 38 intra-residue, 85 sequential and 67 medium range constraints were used while in the case of Esc(1-21)-1c 39 intra-residue, 82 sequential and 44 medium range constraints (as a total of 165 NOEs) were available (Table 1). It is also evident that the number of medium range NOE constraints (i to i + 2/i + 3/i + 4) was much less for Esc(1-21)-1c compared to Esc(1-21), which is also reflected in the RMSD from the ensemble of the 20 lowest energy structures, as reported below. The Esc(1-21) conformations converged to a helical structure extending from I2 to G21 with an average root mean square deviation (RMSD) for the backbone atoms (N, Cα, and C′) and the heavy atoms of 0.31 ± 0.13 and 0.67 ± 0.14 Å, respectively. On the other hand, the ensemble of conformations of Esc(1-21)-1c was not precise and diverged especially at the C-terminal residues N13-G18 as designated by RMSD values of 0.96 ± 0.20 and 1.28 ± 0.21 Å for backbone and heavy atoms, respectively. From the Ramachandran plot, it was seen that the backbone dihedral angles (Φ, Ψ) accumulate in the most favoured regions for most of the residues of both Esc(1-21) and Esc(1-21)-lc, respectively.

In DPC micelles, Esc(1-21) adopted mainly α-helical conformations with a tilt at the N-terminal end (Fig. 7 A and B), whereas the central region of the α-helix was straight and amphipathic due to the presence of several polar residues such as K5, K9, K10, N13 and K20, across one face of the helix. In contrast, the other face of the helix consists of the hydrophobic residues I2, F3, L6, A7, I11, L14, L15, I16 and L19. In the N-terminal region of Esc(1-21), I2, F3 and L6 were in close vicinity; thereby facilitating CH_3-π interaction among β-branched side chains and the phenyl ring of the respective residues. Collectively, the amphipathicity of Esc(1-21) was conserved in its structure so that the cumulative hydrophobic and hydrophilic interactions governed the peptide stabilization in DPC micelles. The amphipathic character was also obvious from a representation emphasizing the separation of hydrophobic and hydrophilic residues on opposite sides of the helix.

Table 1
Summarizes the information for the 20 final NMR structures of Esc(1-21) and Esc(1-21)-1c in DPC micelles.

Distance restrains	Esc(1-21)	Esc(1-21)-lc
Intra-residue (i–j = 0)	38	39
Sequential (|i–j| = 1)	85	82
Medium-range (2 ≤ |i–j| ≤ 4)	67	44
Long-range (|i–j| ≥ 5)	0	0
Total	190	165
Angular restraints	40	40
Φ (phi)	20	20
Ψ (psi)	20	20
Distance restraints from violations (≥ 0.3 Å)	0	1
Deviation from mean structure (Å)	0.31 ± 0.13	0.96 ± 0.20
Average back bone to mean structure (G1-N13)	0.08 ± 0.02	
Average heavy atom to mean structure	0.67 ± 0.14	1.28 ± 0.21
Ramachandran plot analysis for ensemble		
% Residues in the most favourable and additionally allowed regions	(98.4 + 1.6) = 100	(90.0 + 6.6) = 96.6
% Residues in the generously allowed Region	0	3.4
% Residues in the disallowed region	0	0

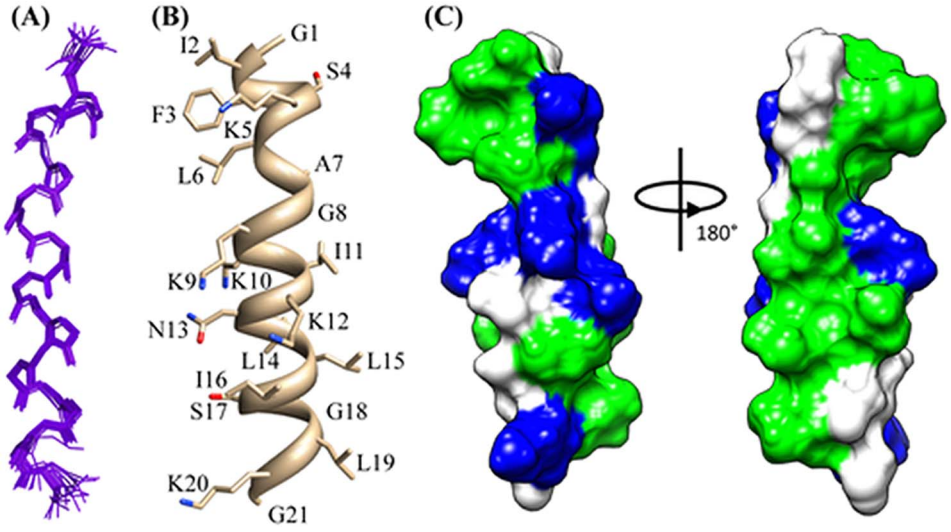

Fig. 7. Three dimensional solution structures of Esc(1-21) in DPC micelles (PDB ID 5XDJ). Superposition of backbone atoms (N, Cα, C′) of the 20 lowest energy conformations of Esc(1–21) (A). Cartoon representation of side chain orientation of a representative NMR structure of Esc(1–21) showing different residues (B). Electrostatic potential surface of Esc(1–21) showing the distribution of polar and non-polar residues (C). The hydrophobic and positively charged amino acid residues are indicated by green and blue, respectively, while all other residues are in white. These images were produced using the PyMOL software.

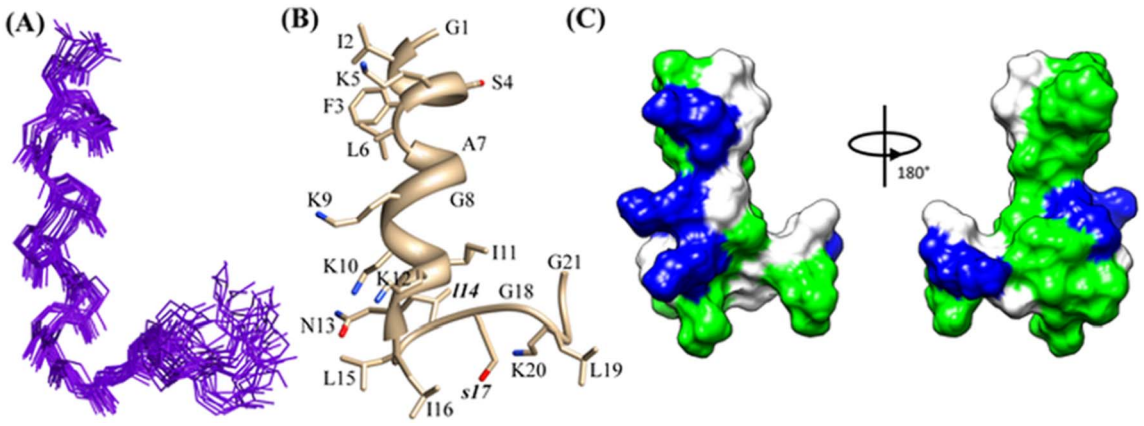

Fig. 8. Three dimensional solution structures of Esc(1-21)-1c in DPC micelles. Superposition of backbone atoms (N, Cα, C′) of the 20 lowest energy conformations of Esc(1-21)-1c (A). Cartoon representation of side chain orientation of a representative NMR structure of Esc(1-21)-lc showing different residues (B). Electrostatic potential surface of Esc(1–21)-1c showing the distribution of polar and non-polar residues (C). The hydrophobic and positively charged amino acid residues are indicated by green and blue, respectively, while all other residues are in white. These images were produced using the PyMOL and Chimera software.

(Fig. 7C).

In contrast, Esc(1-21)-1c in DPC micelles exhibits a partial α-helical conformation only at the N-terminal region between residues I2-N13, with an average backbone RMSD of 0.08 ± 0.02 (Fig. 8). However, the helix breaks after residue N13, likely due to the presence of two D-amino acids ^{D}L14 and ^{D}S17 [70]. It is also worth mentioning that the polar residues K5, K9 and K12 of Esc(1-21)-1c are located on one face of the N-terminal helical region, while the non-polar residues I2, F3, L6, A7 and I11 are on the opposite face of the helix, thereby maintaining an amphipathic character. Therefore, in comparison to Esc(1-21), Esc(1-21)-lc adopts a partial helical conformation only at the N-terminal region (G1-K12) while the C-terminal region (N13-G21) is unstructured and adopts a flexible conformation, which is well supported by the trend in N−H order parameter (S^2) for both peptides (Fig. S3). An order parameter of ~0.8 designates a well-defined backbone conformation, while smaller values indicate disorder. Both peptides exhibited similar trends in the order parameters of the (G1-K12) region, which are almost overlapping. The high order parameters indicate formation of well-defined backbone conformations for both Esc(1-21) and Esc(1-21)-1c. However, due to the incorporation of D-amino acids in the C-terminal part of Esc(1-21)-1c, the order parameter fluctuates in the (N13-G21) segment which supports the existence of poorly defined backbone conformations (Fig. S4). Collectively, close inspection suggests that the main difference between both structures are in the C-terminal region L14-G21 (Fig. 9).

3.6. Membrane disorder induced by both Esc(1-21) and Esc(1-21)-1c

To gain insight into how membrane insertion of these amphiphilic peptides changes the fatty acyl chain packing of phospholipid bilayers, solid-state ^{2}H NMR spectra of membranes encompassing 75 mol% of POPE and 25 mol% of PG lipid were recorded. To assess how the lipid chain mobility and the conformational distribution of the methylene segments is influenced by Esc(1-21) or its diastereomer, the quadrupolar splittings of the ^{2}H NMR spectra were recorded and converted into fatty acyl chain order parameter profiles. The corresponding order parameter profiles of POPE-d_{31} are shown in Fig. 10 and display the characteristic signature of bilayer packing, with a plateau of $|S_{CD}|$ values extending towards the 6th carbon position. The plateau regions exhibit a value of ca. 0.23 for the pure lipid system and of ca. 0.21 for membrane embedded with Esc(1-21) or Esc(1-21)-1c. In both cases, the chain order of the POPE palmitoyl was found to be significantly reduced when compared to the pure lipid sample (Fig. 10). As outlined in the methods section, the ^{2}H NMR order parameters can be converted into the thickness of the acyl chain region of the bilayer ($< L_{chain} >$) and into the area per lipid (A) assuming that these values reflect the distribution of the acyl chain conformation. Therefore, one obtains $< L_{chain} > = 13.4 \pm 0.1$ Å for the pure system and 13.1 ± 0.1 Å upon addition of 2 mol% Esc(1-21) or Esc(1-21)-1c. Although the difference

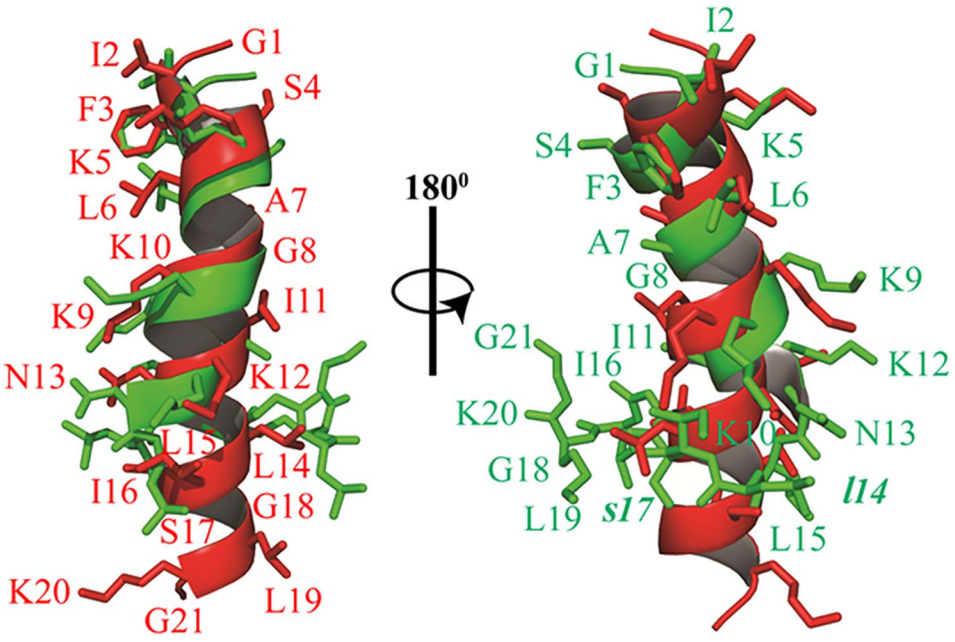

Fig. 9. Overlaid structures of Esc(1-21) (red) and Esc (1-21)-1c (green) in DPC micelles. The N-terminal helical segment (I2-N13) is superimposed nicely with a backbone RMS deviation of 0.482.

in average thickness may appear small, the membrane disordering effects in the direct vicinity of the peptides are probably more pronounced and the decreases in order parameters are significant.

4. Discussion

Recently, the short-sized AMP Esc(1-21) and especially its diastereomer Esc(1-21)-1c have been identified as encouraging candidates for the development of new anti-infective agents, because of their unique properties [30,32]. The diastereomer showed a relevant bactericidal activity against the planktonic form of the bacterial pathogen *P. aeruginosa*, albeit ~4-fold lower than that of Esc(1-21). Here, to investigate the reasons accounting for this difference, the bacterial membrane perturbation was initially assessed by the Sytox Green assay on intact bacterial cells. Similarly to the bactericidal activity, but with a more pronounced difference between the two peptides, a stronger and faster membrane permeabilization was recorded for Esc(1-21). Therefore, it can be stated that the weaker *in vitro* antibacterial activity of Esc(1-21)-1c on the planktonic phenotype of the Gram-negative bacterium *P. aeruginosa*, as compared to Esc(1-21) is mainly associated to a weaker ability in perturbing the bacterial membrane of this pathogen with consequent cell death. In general, such a difference can have three origins [71–73]: a) a different peptide ability in crossing the LPS outer layer and reaching the target bacterial membrane; b) a different affinity for the anionic bacterial membrane; c) differential effects once the peptides are bound to phospholipid bilayers.

Interestingly, when the effect of the two peptides was tested on cells devoid of cell wall i.e. spheroplasts of *Pseudomonas* instead of whole bacterial cells, only a slightly more (1.5-fold) pronounced microbicidal activity was obtained for the wild-type Esc(1-21) with respect to the diastereomer. Similarly, when the two isomers were analyzed on anionic model membranes, the all-L Esc(1-21) was found to induce ~2-fold higher leakage of vesicle contents in comparison to Esc(1-21)-1c. Indeed, CD studies indicated that the affinities of the two peptides for these membranes were only slightly different, while solid-state NMR studies revealed a similar effect of the two peptides on the membrane order parameters. Based on these observations, we can exclude that differences in the antibacterial activity between the two esculentin-derived peptides are mainly due to significant differences in their membrane affinity (hypothesis b) or to a different ability to affect the phospholipid bilayer of the cytoplasmic membrane once inserted into it (hypothesis c). By exclusion, we are led to conclude that the bactericidal activity of the diastereomer against planktonic *P. aeruginosa* cells, compared to the parent peptide, is significantly impaired by a different interaction with the cell wall components, including the LPS outer membrane, which is lacking in spheroplasts. This is in agreement with

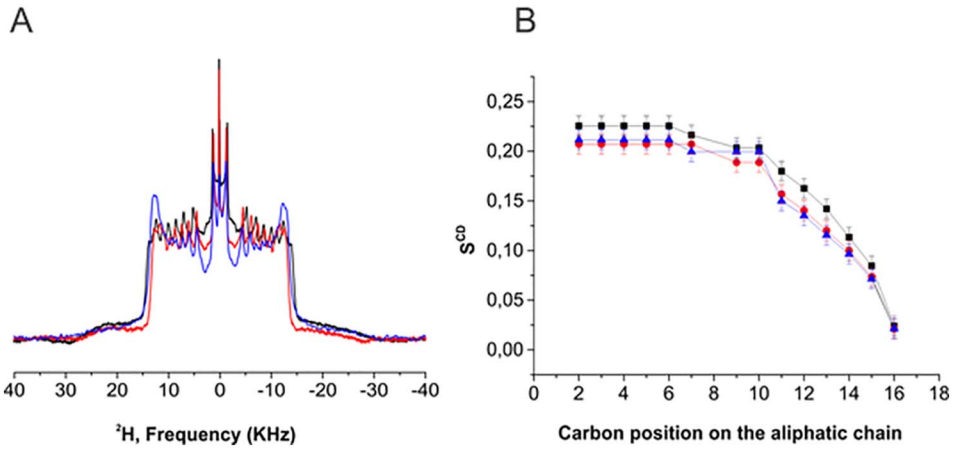

Fig. 10. ^{2}H solid state NMR spectra (A) and the corresponding S_{CD} order parameters profiles (B) of POPE:POPE$^2H_{31}$:POPG (2:1:1) at T = 310 K, in the absence (black line) and presence of 2 mol% Esc(1-21) (red line) and 2 mol% Esc(1-21)-lc (blue line), respectively, with an estimated uncertainty of ± 1%.

previous studies revealing that the relative binding affinity of Esc(1-21)-1c to *P. aeruginosa* LPS is ~8-fold lower in magnitude than Esc(1-21) binding to LPS and that a minor perturbation of LPS structure is caused by the diastereomer when compared to Esc(1-21) [48].

In this work we have also seen how replacement of two amino acids with the corresponding D-enantiomers in the C-terminal region of Esc(1-21) is sufficient to obtain a peptide, Esc(1-21)-1c, with a reduced α-helical content along with a lower tendency in perturbing zwitterionic model membranes. This is in line with its reduced effect on mammalian cells compared to the all-L peptide, as indicated by the corresponding concentrations causing 50% cell death (> 256 μM in comparison to a LD_{50} ranging from 64 μM to 150 μM for the all-L peptide) [30]).

According to the literature, the ease of adopting stable amphipathic three-dimensional folds, which for many peptides is achieved by α-helix formation is an essential factor for AMPs to cause cytotoxicity [74,75]. As demonstrated by solution NMR studies in DPC micelles which simulate the neutral membrane of mammalian cells, an α-helical structure is preserved along the entire amino acid sequence of Esc(1-21), while a highly flexible C-terminal arm is present in Esc(1-21)-1c. This is attributed to the presence of D-amino acids at 14^{th} and 17^{th} position, which break the stereo chemical integrity of the sequence made of L-amino acids. This corroborates well previous structural studies of naturally occurring AMPs e.g. magainin, cytolysin and melittin [76–78].

Interestingly, a remarkable structural difference was observed between the two peptides either in aggregates of LPS, the major component of the outer-membrane of Gram-negative bacteria or in DPC micelles mimicking the lipid composition of the mammalian cell membrane (Fig. S5). The main difference is at the C-terminal region (N13-G18) of Esc(1-21)-lc (Fig. S5 B and Table 1), whose higher flexibility (RMSD = 0.96 ± 0.20 Å) (Table 1) may interfere with the peptide ability to destabilize bacterial and mammalian cell membranes in comparison to the parent Esc(1-21) [32].

Importantly, even though the two amino acid substitutions cause a somewhat weaker activity of the peptide against free-living cells of *P. aeruginosa* [30], a higher potency was shown by Esc(1-21)-1c against the more resistant form of *P. aeruginosa*, that is its biofilm community [30].

Note that the lower antimicrobial activity against the planktonic state of Pseudomonas is not in contradiction with its stronger effectiveness in killing the more dangerous biofilm phenotype [79]. Compared to the all-L peptide, Esc(1-21)-1c is more resistant to proteases which are mainly produced by cells within biofilms and much less by free living bacteria [80]. This may prolong the residence time of the diastereomer and therefore its exposure to the bacterial cells, resulting in a prolonged antimicrobial efficacy in comparison with the all-L peptide, which would be rapidly degraded. In addition, it has been lately demonstrated that D-amino acids can promote the disassembly of the extracellular matrix of biofilm cells [81,82].

Finally, it is worthwhile recalling that the diastereomer showed a reduced cytotoxicity and anti-inflammatory activity [30] than the all-L peptide. This would represent an advantage for the host immune response to bacterial infection at the initial stage.

5. Conclusions

In this work we demonstrated how the cell wall of the free living form of *P. aeruginosa* plays a major role in determining differences in the antibacterial activity between the two esculentin isomers. Most likely, a weaker binding of the diastereomer Esc(1-21)-1c to LPS and presumably slower translocation into the target bacterial membrane account for its weaker activity in comparison to the all-L peptide. The slightly lower ability in binding and perturbing anionic phospholipid bilayers for Esc(1-21)-1c contributes only in a small part to this difference, while the final effect on membrane thinning once the peptide is inserted into the membrane is identical to that provoked by Esc(1-21).

Moreover, we showed how two L- toD- amino acid substitutions in Esc(1-21) led to a lower tendency in perturbing zwitterionic model membranes in line with the lower cytotoxicity of the diastereomer.

In summary, even if Esc(1-21)-1c has a weaker bactericidal activity than the all-L peptide against the planktonic form of Pseudomonas, this still occurs at a low micromolar range [30] and it comes with a significant higher peptide biostability, higher wound-healing activity, less pronounced cytotoxicity and anti-inflammatory property [30]. Overall, these findings represent a valuable compromise for the development of a safer antibacterial agent with an extended in vivo activity. This is supported by our recent *in vivo* efficacy studies on the two selected peptide isoforms [83]. Finally, besides providing information on the structural organization of the two esculentin-derived AMPs, our data may assist in the design of new anti-infective agents with optimized biological properties.

Transparency document

The http://dx.doi.org/10.1016/j.bbamem.2017.09.009 associated with this article can be found, in the online version.

Acknowledgments

This research was supported by Grants from Sapienza University of Rome (Prot. n. C26A14STJZ) (to M.L.M) and by Plan project-II, Bose Institute (to AB). Part of this work was also supported by the Italian Cystic Fibrosis Research Foundation (Project FFC#11/2014 adopted by FFC Delegations from Siena, Sondrio Valchiavenna, Cerea Il Sorriso di Jenny, and Pavia) (to M.L.M.).

The financial contributions of the Agence Nationale de la Recherche (projects MemPepSyn 14-CE34-0001-01 (to B.B.) and the LabEx Chemistry of Complex Systems 10-LABX-0026_CSC), the University of Strasbourg, the CNRS, the Région Alsace and the RTRA International Center of Frontier Research in Chemistry are gratefully acknowledged. M.L.M thanks Alessandra Bragonzi (San Raffaele Institute, Milan, Italy) and Burkhard Tummler (Klinische Forschergruppe, OE 6710, Medizinische Hochschule Hannover, Germany) for the *P. aeruginosa* clinical isolate.

AG thanks Bose Institute for fellowship. AB also would like to acknowledge DBT, Government of India, for infrastructure development fund (BT/PR3106/INF/22/138/2011) to Bose Institute for purchasing a 700 MHz NMR spectrometer with cryoprobe. The calculated structure of the peptides in the presence of DPC was deposited in protein data bank (PDB) with pdb accession code PDB ID 5XDJ. LS acknowledges support by MIUR (grant PRIN 20157WW5EH_007) and Università di Roma “Tor Vergata” (Consolidate the Foundations grant AMPSA).

Appendix A. Supplementary data

Supplementary data to this article can be found online at http://dx.doi.org/10.1016/j.bbamem.2017.09.009.

References

[1] Y. Shai, Mode of action of membrane active antimicrobial peptides, Biopolymers 66 (2002) 236–248.
[2] N. Mookherjee, R.E. Hancock, Cationic host defence peptides: innate immune regulatory peptides as a novel approach for treating infections, Cell. Mol. Life Sci. 64 (2007) 922–933.
[3] H.G. Boman, Peptide antibiotics and their role in innate immunity, Annu. Rev. Immunol. 13 (1995) 61–92.
[4] H. Jenssen, P. Hamill, R.E. Hancock, Peptide antimicrobial agents, Clin. Microbiol. Rev. 19 (2006) 491–511.
[5] R.M. Epand, H.J. Vogel, Diversity of antimicrobial peptides and their mechanisms of action, Biochim. Biophys. Acta 1462 (1999) 11–28.
[6] R.F. Epand, M.A. Schmitt, S.H. Gellman, R.M. Epand, Role of membrane lipids in the mechanism of bacterial species selective toxicity by two alpha/beta-antimicrobial peptides, Biochim. Biophys. Acta 1758 (2006) 1343–1350.
[7] R.M. Epand, R.F. Epand, Bacterial membrane lipids in the action of antimicrobial

agents, J. Pept. Sci. 17 (2011) 298–305.
[8] K.L. Piers, R.E. Hancock, The interaction of a recombinant cecropin/melittin hybrid peptide with the outer membrane of *Pseudomonas aeruginosa*, Mol. Microbiol. 12 (1994) 951–958.
[9] M. Zasloff, Antimicrobial peptides of multicellular organisms, Nature 415 (2002) 389–395.
[10] E.F. Haney, S. Nathoo, H.J. Vogel, E.J. Prenner, Induction of non-lamellar lipid phases by antimicrobial peptides: a potential link to mode of action, Chem. Phys. Lipids 163 (2010) 82–93.
[11] K. Lohner, S.E. Blondelle, Molecular mechanisms of membrane perturbation by antimicrobial peptides and the use of biophysical studies in the design of novel peptide antibiotics, Comb. Chem. High Throughput Screen. 8 (2005) 241–256.
[12] K.A. Brogden, Antimicrobial peptides: pore formers or metabolic inhibitors in bacteria? Nat. Rev. Microbiol. 3 (2005) 238–250.
[13] A. Ghosh, R.K. Kar, J. Jana, A. Saha, B. Jana, J. Krishnamoorthy, D. Kumar, S. Ghosh, S. Chatterjee, A. Bhunia, Indolicidin targets duplex DNA: structural and mechanistic insight through a combination of spectroscopy and microscopy, ChemMedChem 9 (2014) 2052–2058.
[14] H. Bai, Y. Zhou, Z. Hou, X. Xue, J. Meng, X. Luo, Targeting bacterial RNA polymerase: promises for future antisense antibiotics development, Infect. Disord. Drug Targets 11 (2011) 175–187.
[15] J.K. Savjani, A.K. Gajjar, K.T. Savjani, Mechanisms of resistance: useful tool to design antibacterial agents for drug - resistant bacteria, Mini-Rev. Med. Chem. 9 (2009) 194–205.
[16] Y. Carmeli, N. Troillet, G.M. Eliopoulos, M.H. Samore, Emergence of antibiotic-resistant *Pseudomonas aeruginosa*: comparison of risks associated with different antipseudomonal agents, Antimicrob. Agents Chemother. 43 (1999) 1379–1382.
[17] K. Lohner, Membrane-active antimicrobial peptides as template structures for novel antibiotic agents, Curr. Top. Med. Chem. 17 (2017) 508–519.
[18] A.P. Magiorakos, A. Srinivasan, R.B. Carey, Y. Carmeli, M.E. Falagas, C.G. Giske, S. Harbarth, J.F. Hindler, G. Kahlmeter, B. Olsson-Liljequist, D.L. Paterson, L.B. Rice, J. Stelling, M.J. Struelens, A. Vatopoulos, J.T. Weber, D.L. Monnet, Multidrug-resistant, extensively drug-resistant and pandrug-resistant bacteria: an international expert proposal for interim standard definitions for acquired resistance, Clin. Microbiol. Infect. 18 (2012) 268–281.
[19] M.L. Mangoni, Host-defense peptides: from biology to therapeutic strategies, Cell. Mol. Life Sci. 68 (2011) 2157–2159.
[20] C.R. Lee, I.H. Cho, B.C. Jeong, S.H. Lee, Strategies to minimize antibiotic resistance, Int. J. Environ. Res. Public Health 10 (2013) 4274–4305.
[21] A. Nigam, D. Gupta, A. Sharma, Treatment of infectious disease: beyond antibiotics, Microbiol. Res. 169 (2014) 643–651.
[22] D.K. Mercer, D.A. O'Neil, Peptides as the next generation of anti-infectives, Future Med. Chem. 5 (2013) 315–337.
[23] K. Fosgerau, T. Hoffmann, Peptide therapeutics: current status and future directions, Drug Discov. Today 20 (2015) 122–128.
[24] A.A. Kaspar, J.M. Reichert, Future directions for peptide therapeutics development, Drug Discov. Today 18 (2013) 807–817.
[25] P. Kosikowska, A. Lesner, Antimicrobial peptides (AMPs) as drug candidates: a patent review (2003–2015), Expert. Opin. Ther. Pat. 26 (2016) 689–702.
[26] A.E. Islas-Rodriguez, L. Marcellini, B. Orioni, D. Barra, L. Stella, M.L. Mangoni, Esculentin 1-21: a linear antimicrobial peptide from frog skin with inhibitory effect on bovine mastitis-causing bacteria, J. Pept. Sci. 15 (2009) 607–614.
[27] T. Gamberi, D. Cavalieri, F. Magherini, M.L. Mangoni, C. De Filippo, M. Borro, G. Gentile, M. Simmaco, A. Modesti, An integrated analysis of the effects of Esculentin 1-21 on *Saccharomyces cerevisiae*, Biochim. Biophys. Acta 1774 (2007) 688–700.
[28] M.L. Mangoni, V. Luca, A.M. McDermott, Fighting microbial infections: a lesson from amphibian skin-derived esculentin-1 peptides, Peptides 71 (2015) 286–295.
[29] V. Luca, A. Stringaro, M. Colone, A. Pini, M.L. Mangoni, Esculentin(1 − 21), an amphibian skin membrane-active peptide with potent activity on both planktonic and biofilm cells of the bacterial pathogen *Pseudomonas aeruginosa*, Cell. Mol. Life Sci. 70 (2013) 2773–2786.
[30] A. Di Grazia, F. Cappiello, H. Cohen, B. Casciaro, V. Luca, A. Pini, Y.P. Di, Y. Shai, M.L. Mangoni, D-amino acids incorporation in the frog skin-derived peptide esculentin-1a(1-21)NH is beneficial for its multiple functions, Amino Acids 47 (2015) 2505–2519.
[31] A. Di Grazia, F. Cappiello, A. Imanishi, A. Mastrofrancesco, M. Picardo, R. Paus, M.L. Mangoni, The frog skin-derived antimicrobial peptide esculentin-1a(1-21)NH2 promotes the migration of human HaCaT keratinocytes in an EGF receptor-dependent manner: a novel promoter of human skin wound healing? PLoS One 10 (2015) e0128663.
[32] F. Cappiello, A. Di Grazia, L.A. Segev-Zarko, S. Scali, L. Ferrera, L. Galietta, A. Pini, Y. Shai, Y.P. Di, M.L. Mangoni, Esculentin-1a-derived peptides promote clearance of *Pseudomonas aeruginosa* internalized in bronchial cells of cystic fibrosis patients and lung cell migration: biochemical properties and a plausible mode of action, Antimicrob. Agents Chemother. 60 (2016) 7252–7262.
[33] A. Bragonzi, M. Paroni, A. Nonis, N. Cramer, S. Montanari, J. Rejman, C. Di Serio, G. Doring, B. Tummler, *Pseudomonas aeruginosa* microevolution during cystic fibrosis lung infection establishes clones with adapted virulence, Am. J. Respir. Crit. Care Med. 180 (2009) 138–145.
[34] C.J. Sullivan, J.L. Morrell, D.P. Allison, M.J. Doktycz, Mounting of *Escherichia coli* spheroplasts for AFM imaging, Ultramicroscopy 105 (2005) 96–102.
[35] D. Uccelletti, E. Zanni, L. Marcellini, C. Palleschi, D. Barra, M.L. Mangoni, Anti-pseudomonas activity of frog skin antimicrobial peptides in a *Caenorhabditis elegans* infection model: a plausible mode of action *in vitro* and *in vivo*, Antimicrob. Agents Chemother. 54 (2010) 3853–3860.
[36] S.M. Kelly, T.J. Jess, N.C. Price, How to study proteins by circular dichroism, Biochim. Biophys. Acta 1751 (2005) 119–139.
[37] J.C. Stewart, Colorimetric determination of phospholipids with ammonium ferrothiocyanate, Anal. Biochem. 104 (1980) 10–14.
[38] L. Marcellini, M. Borro, G. Gentile, A.C. Rinaldi, L. Stella, P. Aimola, D. Barra, M.L. Mangoni, Esculentin-1b(1-18)—a membrane-active antimicrobial peptide that synergizes with antibiotics and modifies the expression level of a limited number of proteins in *Escherichia coli*, FEBS J. 276 (2009) 5647–5664.
[39] A. Makovitzki, D. Avrahami, Y. Shai, Ultrashort antibacterial and antifungal lipopeptides, Proc. Natl. Acad. Sci. U. S. A. 103 (2006) 15997–16002.
[40] K. Matsuzaki, Why and how are peptide-lipid interactions utilized for self-defense? Magainins and tachyplesins as archetypes, Biochim. Biophys. Acta 1462 (1999) 1–10.
[41] G. Manzo, M. Carboni, A.C. Rinaldi, M. Casu, M.A. Scorciapino, Characterization of sodium dodecylsulphate and dodecylphosphocholine mixed micelles through NMR and dynamic light scattering, Magn. Reson. Chem. 51 (2013) 176–183.
[42] T. Goddard, D.G. Kneller, SPARKY 3, 14 University of California, San Francisco, 2004, p. 15.
[43] M. Piotto, V. Saudek, V. Sklenar, Gradient-tailored excitation for single-quantum NMR spectroscopy of aqueous solutions, J. Biomol. NMR 2 (1992) 661–665.
[44] K. Wuthrich, NMR of Proteins And Nucleic Acids, Wiley, 1986.
[45] P. Guntert, C. Mumenthaler, K. Wuthrich, Torsion angle dynamics for NMR structure calculation with the new program DYANA, J. Mol. Biol. 273 (1997) 283–298.
[46] M.V. Berjanskii, S. Neal, D.S. Wishart, PREDITOR: a web server for predicting protein torsion angle restraints, Nucleic Acids Res. 34 (2006) W63–69.
[47] A. Datta, A. Ghosh, C. Airoldi, P. Sperandeo, K.H. Mroue, J. Jimenez-Barbero, P. Kundu, A. Ramamoorthy, A. Bhunia, Antimicrobial peptides: insights into membrane permeabilization, lipopolysaccharide fragmentation and application in plant disease control, Sci Rep 5 (2015) 11951.
[48] A. Ghosh, S. Bera, Y. Shai, M.L. Mangoni, A. Bhunia, NMR structure and binding of esculentin-1a (1-21)NH2 and its diastereomer to lipopolysaccharide: correlation with biological functions, Biochim. Biophys. Acta 1858 (2016) 800–812.
[49] R.A. Laskowski, J.A. Rullmannn, M.W. MacArthur, R. Kaptein, J.M. Thornton, AQUA and PROCHECK-NMR: programs for checking the quality of protein structures solved by NMR, J. Biomol. NMR 8 (1996) 477–486.
[50] F. Zhang, R. Bruschweiler, Contact model for the prediction of NMR N-H order parameters in globular proteins, J. Am. Chem. Soc. 124 (2002) 12654–12655.
[51] J.H. Davis, K.R. Jeffrey, M. Bloom, M.I. Valic, Quadrupolar echo deuteron magnetic resonance spectroscopy in ordered hydrocarbon chains, Chem. Phys. Lett. 42 (1976) 390–394.
[52] J.H. Davis, The description of membrane lipid conformation, order and dynamics by 2H-NMR, Biochim. Biophys. Acta 737 (1983) 117–171.
[53] M. Bloom, J.H. Davis, A.L. Mackay Mackay, Direct determination of the oriented sample NMR spectrum from the powder spectrum for the systems with local axial symmetry, Chem. Phys. Lett. 80 (1981) 198–202.
[54] M.A. McCabe, S.R. Wassall, Rapid deconvolution of NMR powder spectra by weighted fast Fourier transformation, Solid State Nucl. Magn. Reson. 10 (1997) 53–61.
[55] J. Seelig, Deuterium magnetic resonance: theory and application to lipid membranes, Q. Rev. Biophys. 10 (1977) 353–418.
[56] J.P. Douliez, A. Leonard, E.J. Dufourc, Restatement of order parameters in biomembranes: calculation of C−C bond order parameters from C-D quadrupolar splittings, Biophys. J. 68 (1995) 1727–1739.
[57] L.A. Douliez Jean-Paul, Erick J. Dufourc, Conformational order of DMPC sn-1 versus sn-2 chains and membrane thickness: an approach to molecular protrusion by solid state 2H–NMR and neutron diffraction, J. Chim. Phys. 100 (1996) 18450–18457.
[58] H. Schindler, J. Seelig, Deuterium order parameters in relation to thermodynamic properties of a phospholiped bilayer. A statistical mechanical interpretation, Biochemistry 14 (1975) 2283–2287.
[59] S.L. Grage, S. Afonin, S. Kara, G. Buth, A.S. Ulrich, Membrane thinning and thickening induced by membrane-active amphipathic peptides, Front. Cell. Dev. Biol. 4 (2016) 65.
[60] A. Grelard, P. Guichard, P. Bonnafous, S. Marco, O. Lambert, C. Manin, F. Ronzon, E.J. Dufourc, Hepatitis B subvirus particles display both a fluid bilayer membrane and a strong resistance to freeze drying: a study by solid-state NMR, light scattering, and cryo-electron microscopy/tomography, FASEB J. 27 (2013) 4316–4326.
[61] M.R. de Planque, D.V. Greathouse, R.E. Koeppe 2nd, H. Schafer, D. Marsh, J.A. Killian, Influence of lipid/peptide hydrophobic mismatch on the thickness of diacylphosphatidylcholine bilayers. A 2H NMR and ESR study using designed transmembrane alpha-helical peptides and gramicidin A, Biochemistry 37 (1998) 9333–9345.
[62] J.F. Nagle, Area/lipid of bilayers from NMR, Biophys. J. 64 (1993) 1476–1481.
[63] L. Stella, C. Mazzuca, M. Venanzi, A. Palleschi, M. Didone, F. Formaggio, C. Toniolo, B. Pispisa, Aggregation and water-membrane partition as major determinants of the activity of the antibiotic peptide trichogin GA IV, Biophys. J. 86 (2004) 936–945.
[64] G. Bocchinfuso, S. Bobone, C. Mazzuca, A. Palleschi, L. Stella, Fluorescence spectroscopy and molecular dynamics simulations in studies on the mechanism of membrane destabilization by antimicrobial peptides, Cell. Mol. Life Sci. 68 (2011) 2281–2301.
[65] A.S. Ladokhin, M. Fernandez-Vidal, S.H. White, CD spectroscopy of peptides and proteins bound to large unilamellar vesicles, J. Membr. Biol. 236 (2010) 247–253.
[66] S.Y. Lau, A.K. Taneja, R.S. Hodges, Synthesis of a model protein of defined secondary and quaternary structure. Effect of chain length on the stabilization and formation of two-stranded alpha-helical coiled-coils, J. Biol. Chem. 259 (1984) 13253–13261.
[67] L. Maler, Solution NMR studies of peptide-lipid interactions in model membranes,

Mol. Membr. Biol. 29 (2012) 155–176.
[68] R. Wimmer, L.E. Uggerhoj, Determination of structure and micellar interactions of small antimicrobial peptides by solution-state NMR, Methods Mol. Biol. 1548 (2017) 73–88.
[69] D.S. Wishart, C.G. Bigam, J. Yao, F. Abildgaard, H.J. Dyson, E. Oldfield, J.L. Markley, B.D. Sykes, 1H, 13C and 15N chemical shift referencing in biomolecular NMR, J. Biomol. NMR 6 (1995) 135–140.
[70] P.Y. Chou, G.D. Fasman, Empirical predictions of protein conformation, Annu. Rev. Biochem. 47 (1978) 251–276.
[71] M.L. Mangoni, R.F. Epand, Y. Rosenfeld, A. Peleg, D. Barra, R.M. Epand, Y. Shai, Lipopolysaccharide, a key molecule involved in the synergism between temporins in inhibiting bacterial growth and in endotoxin neutralization, J. Biol. Chem. 283 (2008) 22907–22917.
[72] D. Roversi, V. Luca, S. Aureli, Y. Park, M.L. Mangoni, L. Stella, How many antimicrobial peptide molecules kill a bacterium? The case of PMAP-23, ACS Chem. Biol. 9 (2014) 2003–2007.
[73] F. Savini, V. Luca, A. Bocedi, R. Massoud, Y. Park, M.L. Mangoni, L. Stella, Cell-density dependence of host-defense peptide activity and selectivity in the presence of host cells, ACS Chem. Biol. 12 (2017) 52–56.
[74] E. Gazit, W.J. Lee, P.T. Brey, Y. Shai, Mode of action of the antibacterial cecropin B2: a spectrofluorometric study, Biochemistry 33 (1994) 10681–10692.
[75] Y. Pouny, D. Rapaport, A. Mor, P. Nicolas, Y. Shai, Interaction of antimicrobial dermaseptin and its fluorescently labeled analogues with phospholipid membranes, Biochemistry 31 (1992) 12416–12423.
[76] Y. Shai, Z. Oren, Diastereoisomers of cytolysins, a novel class of potent antibacterial peptides, J. Biol. Chem. 271 (1996) 7305–7308.
[77] R. Saravanan, A. Bhunia, S. Bhattacharjya, Micelle-bound structures and dynamics of the hinge deleted analog of melittin and its diastereomer: implications in cell selective lysis by D-amino acid containing antimicrobial peptides, Biochim. Biophys. Acta 1798 (2010) 128–139.
[78] T. Wieprecht, O. Apostolov, M. Beyermann, J. Seelig, Thermodynamics of the alpha-helix-coil transition of amphipathic peptides in a membrane environment: implications for the peptide-membrane binding equilibrium, J. Mol. Biol. 294 (1999) 785–794.
[79] E. Drenkard, F.M. Ausubel, Pseudomonas biofilm formation and antibiotic resistance are linked to phenotypic variation, Nature 416 (2002) 740–743.
[80] G. Singh, B. Wu, M.S. Baek, A. Camargo, A. Nguyen, N.A. Slusher, R. Srinivasan, J.P. Wiener-Kronish, S.V. Lynch, Secretion of *Pseudomonas aeruginosa* type III cytotoxins is dependent on pseudomonas quinolone signal concentration, Microb. Pathog. 49 (2010) 196–203.
[81] D. Romero, H. Vlamakis, R. Losick, R. Kolter, An accessory protein required for anchoring and assembly of amyloid fibres in *B. subtilis* biofilms, Mol. Microbiol. 80 (2011) 1155–1168.
[82] L. Segev-Zarko, R. Saar-Dover, V. Brumfeld, M.L. Mangoni, Y. Shai, Mechanisms of biofilm inhibition and degradation by antimicrobial peptides, Biochem. J. 468 (2015) 259–270.
[83] C. Chen, M.L. Mangoni, Y.P. Di, *In vivo* therapeutic efficacy of frog skin-derived peptides against *Pseudomonas aeruginosa*-induced pulmonary infection, Sci Rep 7 (2017) 8548.

The FEBS Journal

FEBS PRESS science publishing by scientists

Inhibition of *Pseudomonas aeruginosa* biofilm formation and expression of virulence genes by selective epimerization in the peptide Esculentin-1a(1-21)NH_2

Bruno Casciaro[1,2], Qiao Lin[3], Sergii Afonin[4], Maria Rosa Loffredo[1], Valeriade Turris[2], Volker Middel[5], Anne S. Ulrich[4,6], YuanPu Peter Di[3] and Maria Luisa Mangoni[1]

1 Laboratory affiliated to Pasteur Italia-Fondazione Cenci Bolognetti, Department of Biochemical Sciences, Sapienza University of Rome, Italy
2 Center for Life Nano Science, Istituto Italiano di Tecnologia, Rome, Italy
3 Department of Environmental and Occupational Health, University of Pittsburgh, Pittsburgh, PA, USA
4 Institute of Biological Interfaces (IBG-2), Karlsruhe Institute of Technology (KIT), Karlsruhe, Germany
5 Institute of Toxicology and Genetics (ITG), KIT, Karlsruhe, Germany
6 Institute of Organic Chemistry, KIT, Karlsruhe, Germany

Keywords
amino acids epimerization; antimicrobial peptides; biofilm inhibition; *Pseudomonas aeruginosa*; virulence genes

Correspondence
M. L. Mangoni, Department of Biochemical Sciences, Sapienza University of Rome, Via degli Apuli, 9;00185, Rome
Tel: +39 06 49917693
E-mail: marialuisa.mangoni@uniroma1.it

(Received 29 November 2018, revised 22 March 2019, accepted 28 May 2019)

doi:10.1111/febs.14940

Pseudomonas aeruginosa is a pathogenic bacterium known to cause serious human infections, especially in immune-compromised patients. This is due to its unique ability to transform from a drug-tolerant planktonic to a more dangerous and treatment-resistant sessile life form, called biofilm. Recently, two derivatives of the frog skin antimicrobial peptide esculentin-1a, i.e. Esc (1-21) and its D-amino acids containing diastereomer Esc(1-21)-1c, were characterized for their powerful anti-*Pseudomonal* activity against both forms. Prevention of biofilm formation already in its early stages could be even more advantageous for counteracting infections induced by this bacterium. In this work, we studied how the diastereomer Esc(1-21)-1c can inhibit *Pseudomonas* biofilm formation in comparison to the parent peptide and two clinically-used conventional antibiotics, i.e. colistin and aztreonam, when applied at dosages below the minimal growth inhibitory concentration. Biofilm prevention was correlated to the peptides' ability to inhibit *Pseudomonas* motility and to reduce the production of virulent metabolites, for example, pyoverdine and rhamnolipids. Furthermore, the molecular mechanism underlying these activities was evaluated by studying the peptides' effect on the expression of key genes involved in the virulence and motility of bacteria, as well as by monitoring the peptides' binding to the bacterial signaling nucleotide ppGpp. Our results demonstrate that the presence of only two D-amino acids in Esc(1-21)-1c is sufficient to downregulate ppGpp-mediated expression of biofilm-associated genes, presumably as a result of higher peptide stability and therefore prolonged interaction with the nucleotide. Overall, these studies should assist efficient design and optimization of new anti-infective agents with multiple pharmacologically beneficial properties.

Abbreviations
AMP, antimicrobial peptide; BEC, biofilm eradication concentration; CF, cystic fibrosis; CFU, colony-forming units; Ctrl, control; CV, crystal violet; DAPI, 4′,6-diamidino-2-phenylindole; DIC, differential interference contrast (microscopy); DMSO, dimethyl sulfoxide; Esc peptides, collectively Esc(1-21) and Esc(1-21)-1c; FET, fish embryotoxicity test; hpf, hours postfertilization; LB, Luria-Bertani (medium); LC_{50}, 50% lethal concentration; MIC, minimum inhibitory concentration; NMR, nuclear magnetic resonance (spectroscopy); PBS, phosphate buffered saline; ppGpp, guanosine-3′,5′-bisdiphosphate; QS, quorum sensing.

Introduction

A large variety of microorganisms, including the opportunistic Gram-negative bacterium *Pseudomonas aeruginosa,* have the ability to grow on various types of inert materials or biological tissues, forming multicellular sessile communities known as biofilms [1–3]. It is proposed that biofilm development *in vitro* proceeds through a cycle of distinct stages including a triggering attachment of bacteria to surfaces; an immobilization and formation of micro-colonies accompanied by production of the extracellular matrix [4,5]; a maturation complemented by activation of quorum sensing (QS) intercellular communication. In *P. aeruginosa*, the principal QS circuits are the las, rhl, and pqs. They coordinate the response of bacterial cells to the surrounding environment via the production of signaling molecules. Once production of these molecules has reached a significant level, they activate their regulatory genes to enhance the expression of several virulence factors (e.g. toxins, proteases) [6,7]. Maturation of biofilm is then followed by selected cell death and a matrix degradation process which allows viable cells to dissociate, revert to the planktonic form and proceed with infectious dissemination [8–11].

According to recent studies, *P. aeruginosa* biofilms developed *in vivo* during chronic soft-tissue infections have generally a smaller size than those formed *in vitro*. Here, bacterial cell agglomerates become embedded into the host material and are then continuously exposed to the host's own nutrients flows, as well as an entire range of the circulating communication cues, and to various host defense mechanisms [12,13].

Once established, biofilm communities are very difficult to be eradicated due to their high resistance to the available drugs and their ability to evade the host immune clearance [14–16]. These features explain why biofilm formation is associated with more than 80% of human clinical infections [17–19] including chronic infections of the lung, especially in cystic fibrosis (CF) [20–22], burn wounds, and otitis [17,18,23].

Importantly, even though biofilms represent a serious challenge to the medical field [18,24,25], there are currently no effective treatments for biofilm-related infections, and only limited studies have been conducted to date with the aim to identify novel compounds and therapies capable of selectively eradicating, preventing or inhibiting biofilm growth [26–35].

Naturally occurring cationic antimicrobial peptides (AMPs) hold promise for the development of a new class of antibiotics, due to their biocompatibility, wide spectrum of antimicrobial activity and immunomodulatory properties [24,36–41]. Their main mechanism of action generally involves destabilization of the target microbial membrane, and can also include action on multiple nonmembranous targets (e.g. intracellular enzymes, proteins), altogether making AMPs less prone to induce resistance relative to conventional, single target-directed antibiotics [42,43]. During the past years, we found that a derivative of the frog skin AMP esculentin-1a, named Esc(1-21) (GIFSKLAGKKIKNLLISGLKG-$CONH_2$ [44]), exhibits strong bactericidal activity. Indeed, it is active against both planktonic bacteria and existing biofilms of *P. aeruginosa,* with a membrane-perturbing activity as its major killing mechanism [35,45–47]. However, little is known about its potential to inhibit the formation of *P. aeruginosa* biofilm.

Remarkably, a common concern around the use of AMPs as new therapeutic agents is their high susceptibility to enzymatic degradation by ubiquitous host proteases [38]. One of the strategies pursued to increase AMPs biostability is the selective incorporation of non-natural (e.g. D-epimers) amino acids within the peptide sequence. This is because D-amino acids are not recognized by proteases, thus protecting the peptide from enzymatic cleavage [48,49]. Hence, we recently designed and synthesized a diastereomer of Esc(1-21), namely Esc(1-21)-1c, by replacing two L-amino acids, i.e. Leu^{14} and Ser^{17}, with the corresponding D-enantiomers, and found out that it exhibited better activity than the all-L isomer in eradicating preformed *Pseudomonas* biofilms [50] and also in reducing lung bacterial burden in mouse models of acute *P. aeruginosa* lung infection [41]. Furthermore, Esc(1-21)-1c was shown to be more efficient in promoting migration of airway epithelial cells and preserving anti-*Pseudomonal* activity in artificial sputum medium without inducing resistance [43]. Here, we have studied the ability of this peptide to prevent *Pseudomonas* biofilm formation and explored its underlying molecular mechanisms. These results were compared to those of the all-L parent peptide and demonstrated that the presence of two D-amino acids in Esc(1-21)-1c is sufficient to make this peptide not only more effective in downregulating the expression of virulence factors of *P. aeruginosa,* but also to hinder bacterial motility. This would hamper the formation of a sessile bacterial community. In addition, we also confirmed that the diastereomer exhibits reduced *in vivo* toxicity in a zebrafish (*Danio rerio*) embryo model, demonstrating Esc(1-21)-1c to be a more environmentally friendly and pharmacologically attractive candidate compared to the parent peptide.

Results

Inhibition of biofilm formation

To examine the ability of Esc(1-21) and Esc(1-21)-1c (Esc peptides) in inhibiting biofilm formation when used at dosages below the minimum inhibitory concentration (MIC), we first determined their MICs against the planktonic form of this pathogen (Table 1). The standard strain *P. aeruginosa* ATCC 27853 and clinical isolates (either from early or late stages of chronic lung infection in CF patients) were used for MIC and biofilm formation assays. Furthermore, the minimum peptide concentration causing 95% eradication of biofilm (BEC) formed by the four *P. aeruginosa* strains [50] was included in Table 1. The D-amino acid containing isomer was able to prevent biofilm formation of the selected strains at concentrations ranging from 1/2 to 1/16 MIC (Fig. 1). In contrast, the all-L peptide appeared to have no effect or it slightly stimulated biofilm formation. The only exception was observed at the highest concentration of Esc(1-21), i.e. 1/2 and 1/4 MIC, against AA43 and the reference strain ATCC 27853, where the peptide was able to cause ~ 50% biofilm inhibition. It is notable that the biofilm inhibitory effect by Esc(1-21) and Esc(1-21)-1c was not due to inhibition of planktonic growth, as indicated by the absorbance values from bacterial cultures of the four *P. aeruginosa* strains being challenged with Esc peptides at sub-MICs, compared to untreated control cells (Fig. 2). Next, we analyzed the effect of two clinically-used antibiotics, aztreonam and colistin [51] at their sub-MIC levels (Table 2) on the CF clinical isolates. As indicated in Fig. 3, no inhibition, but rather stimulation of the biofilm formation, primarily for the KK1 strain, was observed for both antibiotics at all concentrations examined. These results are in line with what has been shown for different classes of commonly-used antibiotics [52–54] and even other AMPs [55]. As reported in Fig. 1, higher biofilm formation of *P. aeruginosa* AA43 and AA11 was shown at higher concentrations of Esc(1-21)-1c. Additionally, higher biofilm formation of KK1 and AA11 strains was observed upon treatment with ½ MIC of colistin and aztreonam, respectively, compared to lower antibiotics concentration (Fig. 3). As notes by Kaplan *et al.* [54], some conventional antibiotics can act as inhibitors of biofilm formation at low concentration levels, promoters at higher levels, and once again as inhibitors at still higher concentration. The precise biofilm-modulating action at sub-MIC depends on many factors including the type of antimicrobial agent used, its mode of action, level of persistency and age of the bacterial culture, the bacterial strain and its susceptibility to various classes of antibiotics, etc. Therefore, it does not seem unusual that AMPs can also have inhibitory activity on different bacterial strains which are not linearly dose-dependent (Fig. 1).

Table 1. Antibacterial activity of the Esc peptides against various *P. aeruginosa* strains in the planktonic and biofilm forms

Antibacterial concentrations (μM)				
	Esc(1-21)		Esc(1-21)-1c	
Bacterial strains	MIC	BEC	MIC	BEC
P. aeruginosa ATCC 27853	4	12.5[a]	8	12.5[a]
P. aeruginosa AA11	2	25[a]	8	12.5[a]
P. aeruginosa AA43	2	12.5	4	12.5
P. aeruginosa KK1	4	12.5[a]	8	12.5[a]

The reported MICs are the values obtained from three identical readings out of four independent experiments, and differences by a single dilution step are therefore significant. [a]Data taken from [50].

Peptides' effect on bacterial swimming, swarming and twitching motility

Since a more marked difference in inhibiting biofilm formation between the two isomers was observed against *P. aeruginosa* AA11, especially at 1/8 MIC, we selected this strain for subsequent experiments aimed at understanding the mechanism(s) underlying the inhibition of biofilm formation by Esc(1-21)-1c in comparison to the all-L parent peptide.

It is known that the initial step in the formation of a biofilm community *in vitro* is the adherence of bacterial cells to a surface. This is favored by bacterial movement induced by polar flagella in aqueous environments (swimming motility) [33]. Afterward, bacteria start to proliferate and to produce extracellular polymeric substances in which they remain entrapped. Type IV pili are involved in twitching motility, which is the bacterial movement inside the biofilm community resulting from extension and retraction of pili [56]. It is notable that twitching activity plays a direct role in the cell-to-cell interactions necessary for microcolony formation and for the establishment of cell agglomerates characteristic of mature biofilms [57]. In addition to swimming and twitching motility, *P. aeruginosa* is able to swarm across viscous environments. It is a complex type of motility characterized by a coordinated progression of cells across a semi-solid surface and is dependent on both flagella and type IV pili. Swarming contributes to colonization of surfaces and

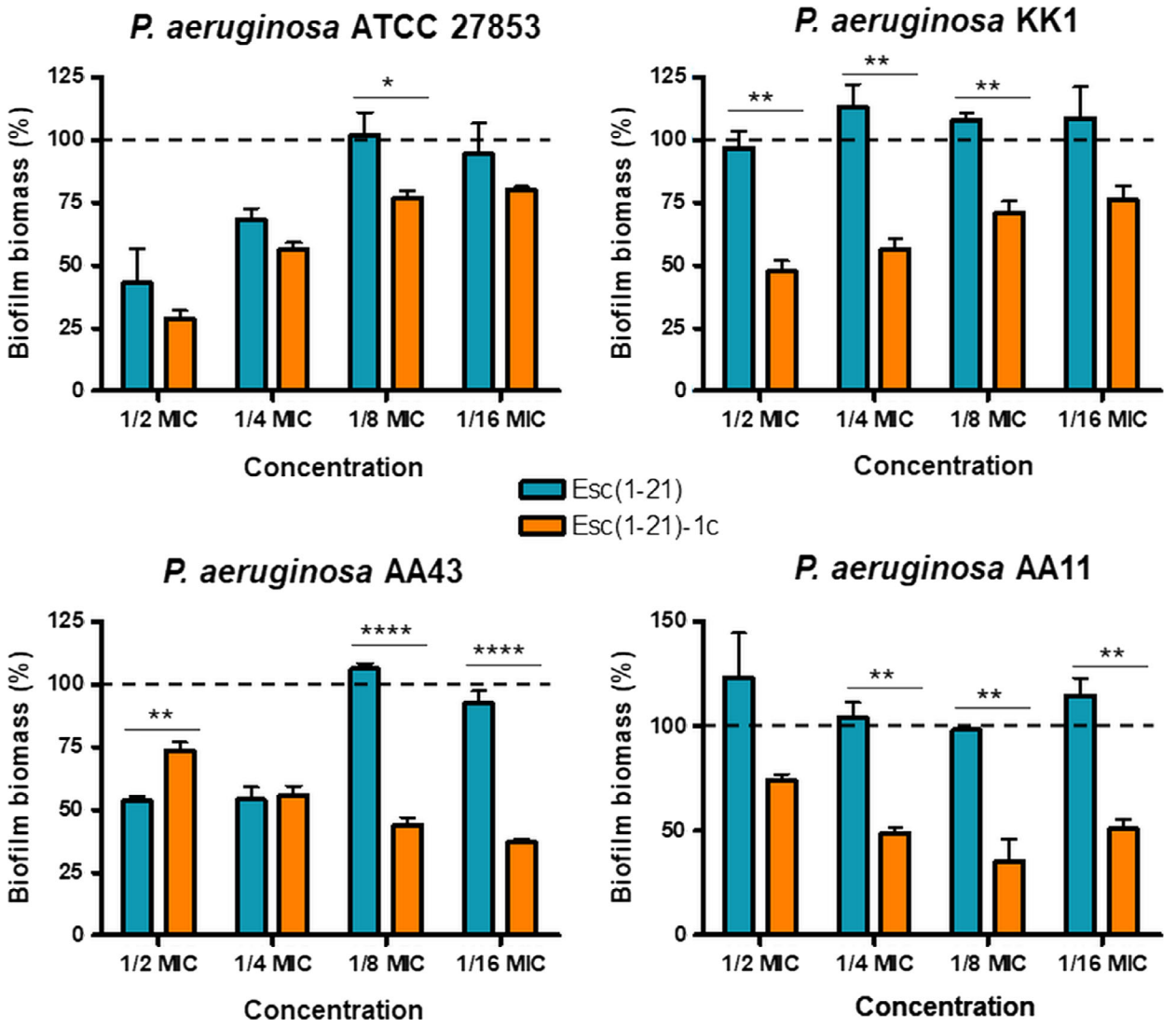

Fig. 1. *P. aeruginosa* bacterial strains were incubated for 20 h in the presence of Esc peptides at concentrations below the MIC (from ½ to 1/16 MIC). Surface-associated biofilm after peptide treatment was evaluated by 0.05% CV staining followed by absorbance measurements at 590 nm. Results are reported as percentage of biofilm biomass with respect to untreated samples. The experiments were performed three times with three technical repeats and the data are reported as mean ± SEM. Dotted line indicates biofilm biomass of untreated bacteria. Statistical significance between the two peptides was determined by the Student's *t*-test. $*P < 0.05$; $**P < 0.01$; $****P < 0.0001$.

plays a crucial role in the early biofilm development [58].

To study whether the inhibition of biofilm formation by Esc peptides was associated to their ability to impede bacterial swimming/swarming and/or twitching motility, AA11 growth was evaluated in 0.3%, 0.5% and 1% agarose plates, respectively, supplemented with the peptide at 1/8 MIC, according to a previously published procedure [33]. The D-amino acid containing peptide markedly decreased swimming, swarming as well as twitching motility, as evident from the significant reduction in the readouts (Fig. 4A). In contrast, the all-L peptide did not influence the three kinds of cell motion until 48 h of co-incubation as shown by representative images of the bacterial growth zones (Fig. 4B). To exclude the possibility that the negligible effect of Esc(1-21) on AA11 motility was due to a lower absolute concentration (i.e. 0.25 μM) compared to that of Esc(1-21)-1c (1 μM), motility assays were also performed at 1 μM for both Esc peptides. However, similar data were obtained (data not shown), confirming that the different behavior between the two peptides cannot be attributed to their different concentrations.

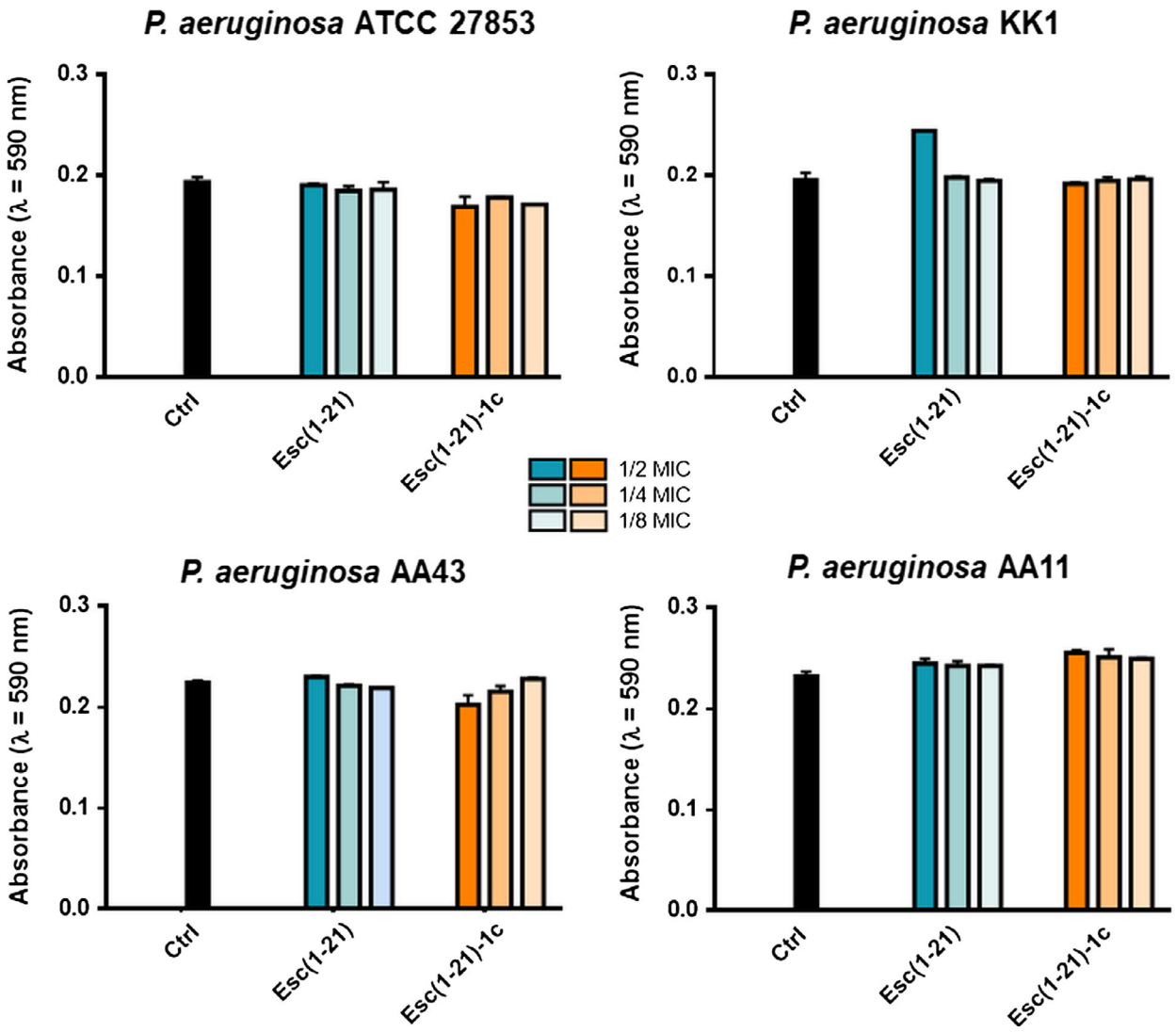

Fig. 2. Bacterial growth of different *P. aeruginosa* strains in the presence of sub-MIC levels of Esc peptides with respect to the untreated control samples (Ctrl). Absorbance of the bacterial culture was measured at 590 nm after 20 h incubation at 37 °C. Data points are the mean ± SEM of three different experiments.

Table 2. Antibacterial activity of aztreonam and colistin against various *P. aeruginosa* strains in the planktonic and biofilm forms

Antibacterial concentrations (μM)				
	Aztreonam		Colistin	
Bacterial strains	MIC	BEC	MIC	BEC
P. aeruginosa ATCC 27853	16	ND	1	6.25
P. aeruginosa AA11	4	ND	2	12.5
P. aeruginosa AA43	32	ND	1	12.5
P. aeruginosa KK1	16	ND	2	12.5

The reported values were obtained from three identical readings out of four independent experiments, and differences by a single dilution step are therefore significant. ND, not determined.

Gene-expression analysis

To specifically address the difference in inhibition of bacterial swimming, swarming and twitching motility by the Esc peptides, we studied the effect of the two peptides on the expression of selected genes known to be involved in the control of bacterial motility and in the biofilm formation [59]. As shown in Fig. 5, when applied at a sub-MIC level (i.e. 1 μM), Esc(1-21)-1c was found to significantly down-regulate the expression of *fleN*, *fimT*, and *fimX* genes, encoding for the flagellar synthesis regulator FleN, the type IV fimbrial biogenesis protein FimT, and the twitching motility regulating phosphodiesterase FimX, respectively. Also

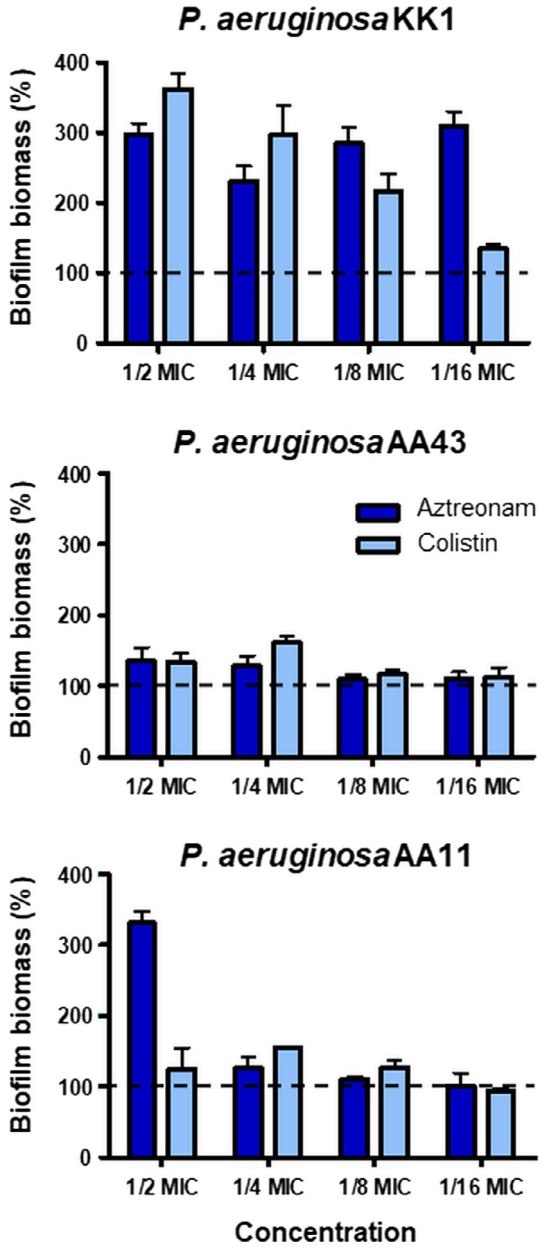

Fig. 3. *P. aeruginosa* bacterial strains were incubated for 20 h in the presence of aztreonam and colistin at concentrations ranging from ½ to 1/16 MIC. Surface-associated biofilm after antibiotic treatment was evaluated by 0.05% CV staining followed by absorbance measurements at 590 nm. Results are reported as percentage of biofilm biomass with respect to untreated samples. The experiments were performed three times with three technical repeats and the data are reported as mean ± SEM. Dotted line indicates biofilm biomass of untreated bacteria.

lasI gene encoding for the quorum sensing molecule acyl-homoserine-lactone synthase as well as *lasB* gene encoding the elastase LasB (pseudolysin precursor involved in the pathogenicity of *P. aeruginosa*) were down-regulated (~ 95% reduction in mRNA levels). In addition, treatment with the non-natural diastereomer led to ~ 98% lowering in the level of mRNA encoding for rhamnosyltransferase subunits, that is, RhlA and RhlB, both being key enzymes in the biosynthesis of rhamnolipids – bacterial surfactants which modulate *P. aeruginosa* swarming motility and biofilm formation/maintenance [60]. Moreover, upon treatment with the non-natural diastereomer, the expression level of *rpoS* gene was reduced by half compared to the level in bacteria exposed to Esc(1-21). This gene is reported

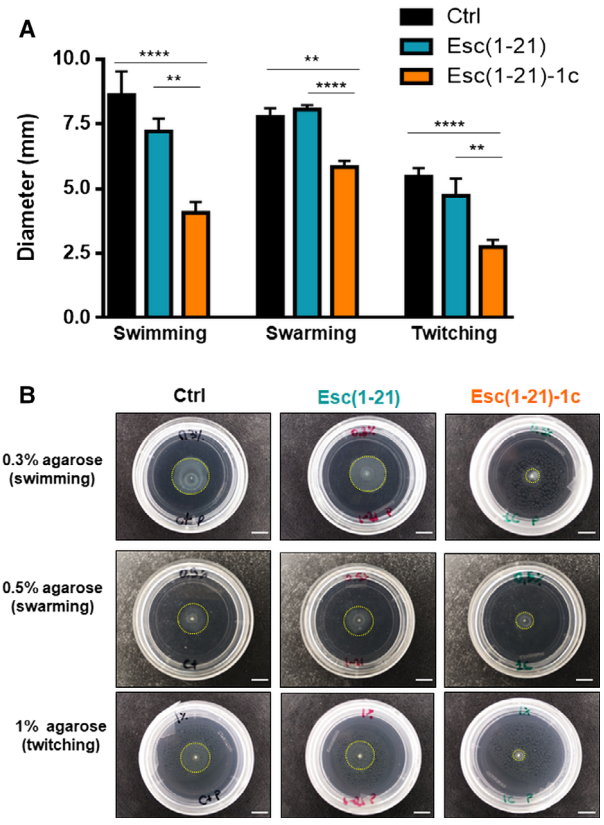

Fig. 4. (A) Effect of Esc(1-21) and Esc(1-21)-1c at 1/8 MIC on the swimming, swarming or twitching motility of *P. aeruginosa* AA11. Bacterial cells were inoculated in 0.3%, 0.5% or 1% agarose plates (for swimming, swarming or twitching motility assays, respectively). Swimming, swarming and twitching zones were determined after 24 h of incubation at 30 °C. Control samples (Ctrl) were plates inoculated with bacteria in the absence of peptide. All experiments were performed in triplicates with three technical repeats and statistical significance was determined using the Student's *t* test. Data are shown as mean ± SEM. $^{**}P < 0.01$; $^{****}P < 0.0001$. (B) Representative images of swimming, swarming and twitching activity of *P. aeruginosa* in the presence of each peptide compared to Ctrl, 48 h after incubation at 30 °C. Dotted circle line indicates the zonal extent of bacterial growth. Images are at 1× magnification. All scale bars represent 0.5 cm.

to affect the production of extracellular alginate, exotoxin A and biofilm formation [61]. In contrast, both peptides did not significantly alter the expression of *fliC* gene (encoding the structural subunit of flagella, B-type flagellin).

Production of pyoverdine and rhamnolipids

We also explored whether the two peptides differentially affected the production of virulence factors i.e, pyoverdine, the primary siderophore of *P. aeruginosa* which facilitates pathogenic growth at the infection site. As reported in Fig. 6A, only Esc(1-21)-1c led to a significant reduction in the amount of siderophore (~ 3-fold lower than that of control samples), corroborating its significant antivirulent activity compared to Esc(1-21). In parallel, the production of rhamnolipids was investigated and found to be significantly reduced after the exposure to Esc(1-21)-1c (Fig. 6B). This is in line with the results of *rhlA* and *rhlB* genes expression profile and with the reduced swarming activity, which is known to be dependent upon the self-produced biosurfactant rhamnolipids [62].

Confocal microscopy

For direct visualization of the peptides' distribution within bacterial cells when used at sub-MIC, we incubated *P. aeruginosa* AA11 with the rhodamine-labeled peptides. Note that conjugation of rhodamine to these peptides did not affect their antimicrobial activity. Indeed, the MICs of Esc(1-21) and Esc(1-21)-1c against *P. aeruginosa* AA11 were equal to 2 and 8 μM, respectively. Examination of the samples revealed that both peptides accumulated at the membrane level mainly at the cell poles and division septa and that they diffused into the cytosol already within the first 5 min (Fig. 7). No pronounced variation was noted between the two isomers, despite a more homogeneous intracellular distribution of the non-natural diastereomer compared to Esc(1-21). The latter appeared to be located mostly on and beneath the plasma membrane. Furthermore, to exclude that rhodamine itself could drive the peptide distribution, bacterial cells were treated with the free dye at the same concentration as labeled peptides. No fluorescence was detected after washes (Fig. 7, control), confirming that rhodamine alone would not enter bacterial cells.

Involvement of ppGpp in peptides' activity

Since an invariant mRNA transcription level was detected for the *fliC* gene, 20 h upon addition of Esc (1-21)-1c, we ruled out a general inhibition of RNA transcription by this peptide. In line with the literature, the bacterial alarmone (p)ppGpp is a nucleotide with a distinctive role in the stress-induced biofilm development and maintenance [63]. We therefore examined the ability of Esc peptides to interact with ppGpp by ^{31}P-NMR, as has been previously described for other AMPs [64]. The ^{31}P-NMR spectra in Fig. 8 shows that the resonances of the four phosphate groups in ppGpp were shifted by up to 3 ppm upfield upon adding increasing amounts of peptide. Interestingly, the α-phosphate resonances experienced the largest shifts, suggesting that the nucleoside part of the molecule is directly involved in binding. At the tested concentrations of up to a 2-fold excess of peptide over nucleotide, we did not observe any co-precipitation and/or concomitant disappearance of the ppGpp NMR signals. Furthermore, in the presence of sub-stoichiometric amounts of peptide, an 8-fold excess of ppGpp showed only a single set of signals, indicating fast exchange between the free and bound forms of ppGpp on the NMR timescale. Therefore, we can rule out an irreversible sequestration of the nucleotide by the peptide as a mechanism of Esc peptides action, which would have led to a broadening and depletion of the ^{31}P-NMR signals, as recently reported for the antibiofilm-active peptide gramicidin S [64]. In the case of Esc peptides, we note that the wild type peptide and its non-natural diastereomer bound ppGpp in virtually the same way, hence the observed difference in their interference with biofilm signaling is not related to any differential affinity toward ppGpp.

In vivo acute toxicity on a zebrafish embryo model

For consideration of pharmacological use of AMPs it is important to demonstrate a high degree of selectivity toward bacteria versus animal cells, both *in vitro* and *in vivo*, to ensure safety. It was previously shown that the diastereomer Esc(1-21)-1c has a lower *in vitro* cytotoxic effect than the all-L peptide on a range of mammalian cell cultures, and that it is harmless to mice, when instilled intra-tracheally [41,50,65]. However, no information on its potential toxicity on other vertebrate organisms is known to date. Zebrafish embryotoxicity tests (FET) generally provide an economic and ethical way of expanding the range of vertebrate *in vivo* safety endpoint evaluations [66]. Here, they were used as a straightforward model to address the safety of Esc peptides in the treatment of *P. aeruginosa* caused airway-associated infections, because the FET

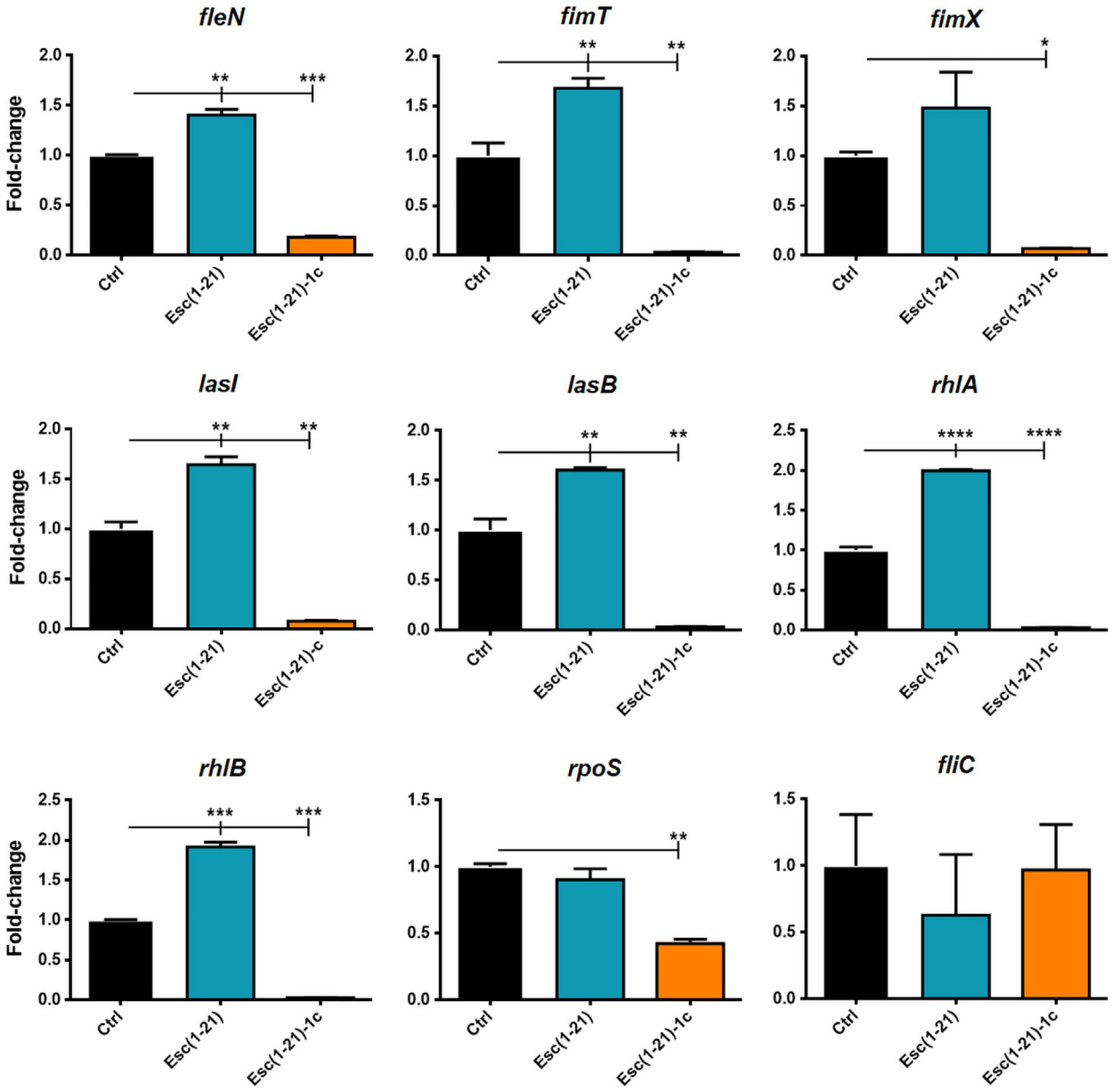

Fig. 5. Effect of Esc peptides on the expression of the following genes in *P. aeruginosa* AA11: *fleN*, flagellar synthesis regulator fleN; *fimT*, type IV fimbrial biogenesis protein FimT; *fimX*, twitching motility regulating phosphodiesterase; *lasI*, autoinducer synthesis protein LasI; *lasB*, elastase LasB; *rhlA*, rhamnosyltransferase chain A; *rhlB*, rhamnosyltransferase chain B; *rpoS* sigma factor RpoS; *fliC*, flagellin type B. Ten microlitre of bacterial planktonic cells culture at a density of 10^8 CFU·mL^{-1} was incubated with 1 μM peptide for 20 h in an orbital shaker at 37 °C. Total RNA was extracted immediately after the incubation. Results are representative of three independent experiments. Data are shown as mean ± SEM. Statistical analyses were performed by one-way ANOVA and Dunnett's multiple comparisons test. *$P < 0.05$; **$P < 0.01$; ***$P < 0.001$; ****$P < 0.0001$ compared to untreated control cells, Ctrl (otherwise nonsignificant).

LC_{50} values of environmental toxicants are known to correlate well with the inhalation LC_{50} values in rodents [67]. Both peptides were tested in a 2-fold dilution series for the whole-organism survival of wild type zebrafish embryos at the 72 hpf stage (Fig. 9). The D-amino acid containing isomer showed an approximately 5-times lower toxicity than the parent peptide (LC_{50} of 123.7 μM and 18.2 μM for Esc(1-21)-1c and Esc(1-21), respectively). Interestingly, the LC_{50} values remained unchanged between 1 and 24 h exposure, suggesting that lethality is caused by a rapid mechanism common to both peptide isomers.

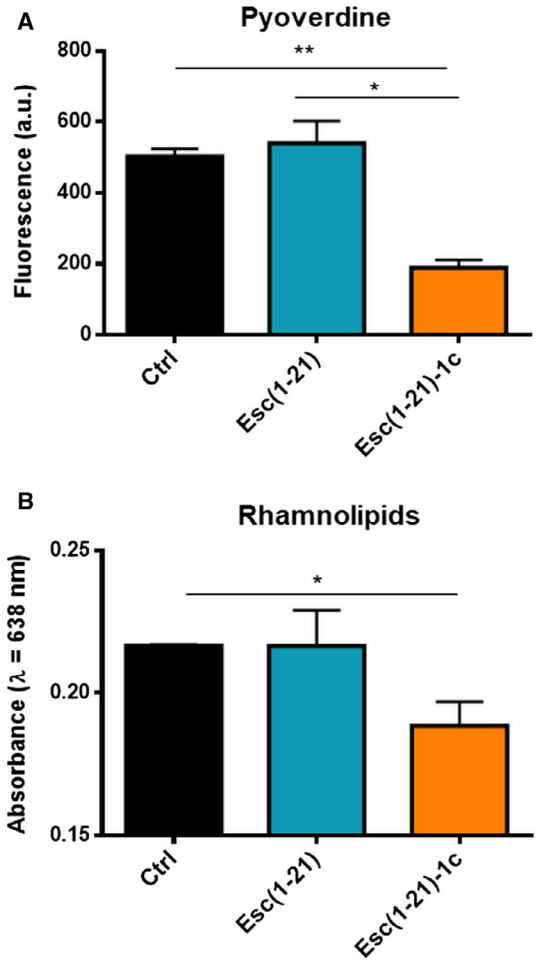

Fig. 6. (A) Effect of Esc peptides on the production of pyoverdine in *P. aeruginosa* AA11 after 20 h incubation, compared to the cells not treated with the peptide (Ctrl). Bacteria were grown in 10% LB in water and pyoverdine was measured in the supernatant of the bacterial culture after 20 h treatment with the peptides at 37 °C. Samples were excited at 400 nm and fluorescence emission was measured at 460 nm and reported as arbitrary units. All values are the mean of three independent experiments ± SEM. Statistical significance was determinesd using the Student's *t* test. $*P < 0.05$; $**P < 0.01$. (B) Effect of Esc peptides on the production of rhamnolipids by *P. aeruginosa* AA11 after 20 h incubation, compared to the bacterial cells not treated with the peptide (Ctrl). Bacteria were grown in 10% LB in water, and rhamnolipids were quantified by colorimetric assay as described in Materials and methods. Absorbance was measured at 638 nm. The values are the mean ± SEM of three independent experiments. Statistical significance was determined using the Student's *t* test. $*P < 0.05$.

Discussion

P. aeruginosa is among the most clinically relevant pathogens leading to chronic biofilm infections that are highly resilient to physical disruption by external stresses and to immune clearance mechanisms [68]. Accordingly, it is challenging to gain insight into the ability of new antimicrobial agents to inhibit the development of sessile communities which protect bacterial cells during infection.

In this study, we first show that the presence of two D-amino acids in the AMP Esc(1-21)-1c is sufficient to significantly enhance its ability to prevent biofilm formation of *Pseudomonas* already within 1 day of peptide treatment at concentrations below those that hamper bacterial growth. The inhibited biofilm formation by Esc(1-21)-1c likely occurs through three different mechanisms. First, by inhibiting flagella-mediated swimming motility of *P. aeruginosa* cells as suggested by either motility assays (showing a reduction in the swimming diameter) or gene expression analysis (showing down-expression of *fleN* gene which controls the number of flagella). This would lead to a smaller number of bacteria to reach the surface for the initial attachment or to diffuse deep into the host tissues where *in vivo* biofilm formation starts [13]. Second, we observed that Esc(1-21)-1c decreased the mRNA level of genes responsible for type IV pili biosynthesis and function. As a result, this would hinder pili-mediated twitching motility (Fig. 4), and therefore also microcolony formation and colonization of surfaces [69]. Third, we were able to demonstrate that Esc(1-21)-1c affects the two major quorum sensing systems, namely the lasI and rhl systems, by down-regulating genes encoding for virulence factors that are essential for biofilm development and host tissues damage, for example, RhlA, RhlB and LasB. In line with these findings is the observed reduced production of important molecules involved in the pathogenicity and in the biofilm architecture of *P. aeruginosa*, such as pyoverdine and rhamnolipids [70].

It is worthwhile emphasizing that both Esc(1-21) and its diastereomer are membrane-active peptides [17,71]. Hence, it is conceivable that they could perturb or destabilize the bacterial membrane at sub-MIC levels without compromising the bacterial viability [72]. The peptide would partition to the inner leaflet of the membrane phospholipid bilayer and diffuse into the cytosol. This is supported by confocal microscopy studies confirming a subcellular localization of the peptides underneath the membrane already after 5 min from their addition to the cells. However, both molecules appeared to be more concentrated at the apical ends and cell septa, where the negatively-charged cardiolipin (to which cationic peptides would have a high binding affinity) resides [73,74]. Most likely, cell poles are initially targeted by Esc peptides which would then translocate across the plasma membrane and distribute into the cytosol.

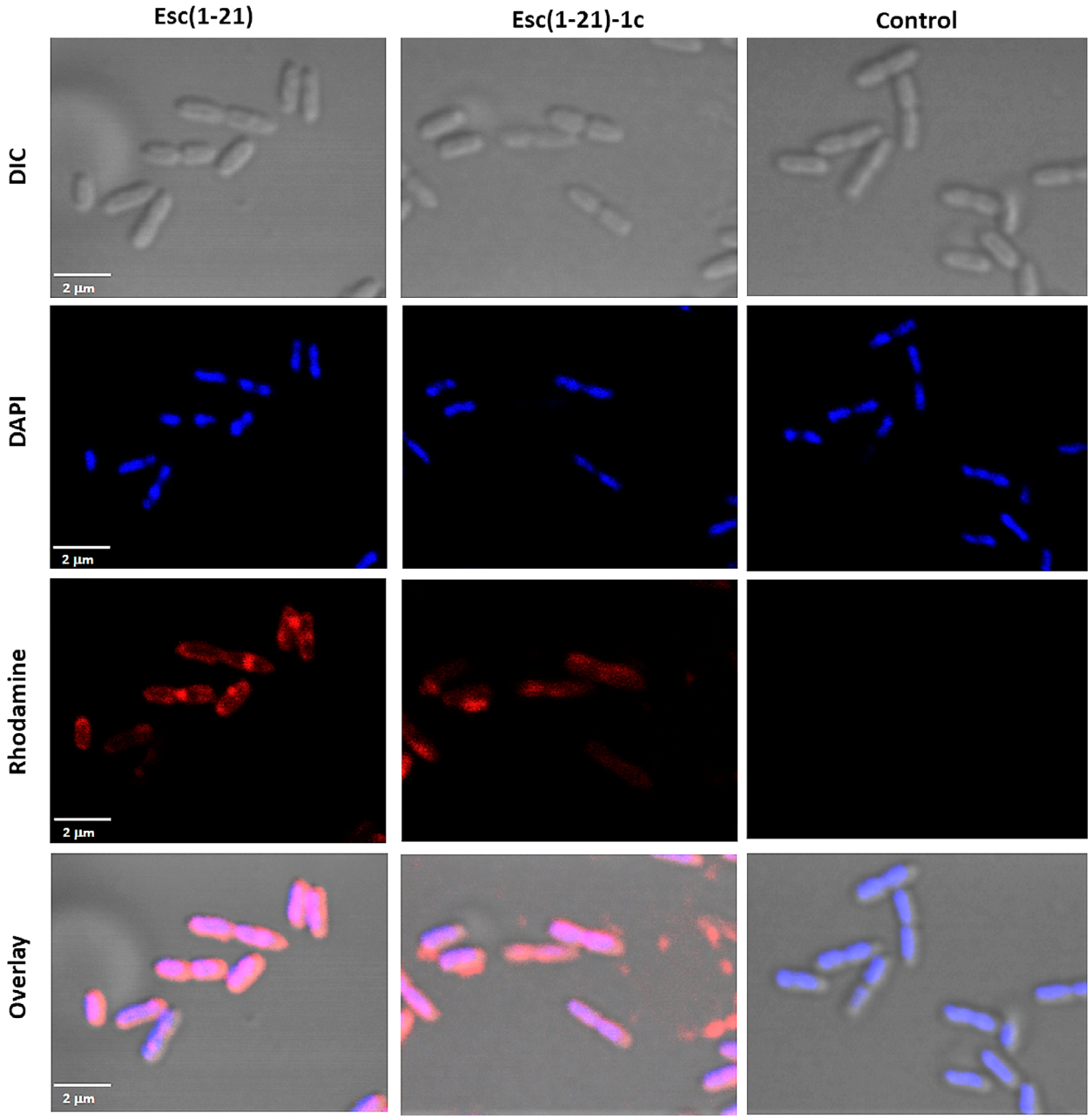

Fig. 7. Confocal images of *P. aeruginosa* cells treated with rhodamine-labeled Esc peptides for 5 min. After peptide treatment, cells were stained with DAPI for DNA detection. DIC shows differential interference contrast images; DAPI shows DNA staining; rhodamine shows signal from labeled peptide and the free dye; overlay shows the merged channels. All images represent confocal single planes taken at the mid-cell height. Control samples are bacterial cells treated with the peptide-free rhodamine.

Previous report indicated that bacterial cells are known to respond to stressful environmental conditions by activating the stringent response [75]. Activation involves synthesis of small signaling nucleotides, guanosine 5′-diphosphate 3′-diphosphate (ppGpp) and guanosine 5′-triphosphate 3′-diphosphate (pppGpp), collectively denoted (p)ppGpp which regulate the expression of a plethora of genes promoting biofilm formation [63,76–79]. Targeting of (p)ppGpp had been described as a major mechanism of biofilm inhibition by the AMP IDR-1018 [80]. In our case, ^{31}P-NMR studies indicated that both Esc peptides interact similarly though weakly with the nucleotide. Based on these data, we hypothesize that the different

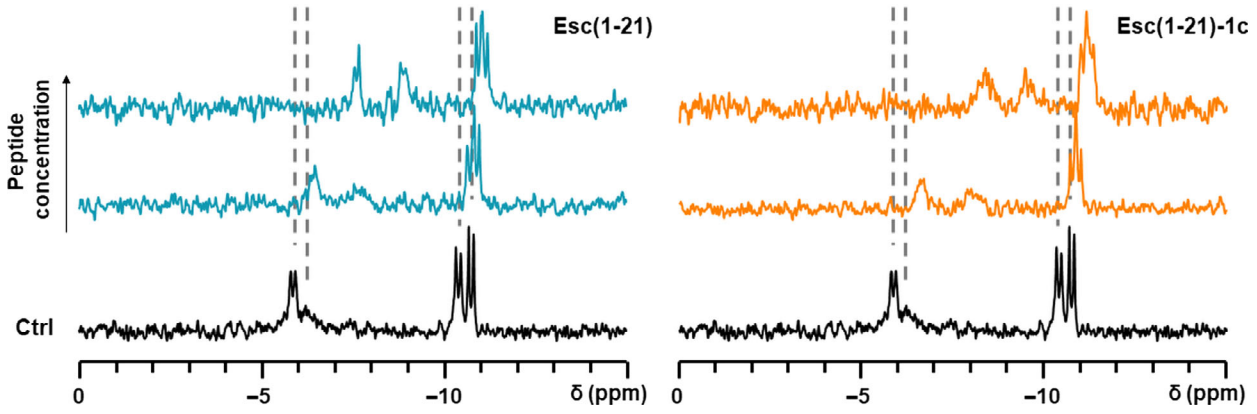

Fig. 8. Interaction of Esc peptides with ppGpp, observed by ^{31}P-NMR spectroscopy. Resonances from the four phosphate groups of ppGpp after 2 h incubation with the peptide in aqueous environment (10% D_2O) are shifted compared to the Ctrl (without peptide). Dashed lines indicate the underlying chemical shifts of the nucleotide (without splittings).

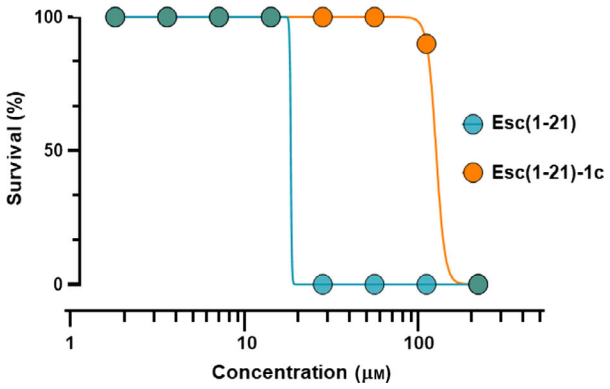

Fig. 9. Survival of zebrafish embryos after peptide treatment at different concentrations. DMSO (0.2%) was used as vehicle and did not cause any toxicity. Data are the average of three independent experiments.

phenotypic outcome of the treatment with the two Esc isomers, within 1 day of bacterial exposure, is the consequence of a higher biostability of the D-amino acids containing diastereomer than the all-L peptide. This would lead to an extended antimicrobial efficacy of Esc(1-21)-1c compared to Esc(1-21) which could be more rapidly degraded by numerous bacterial proteases, for example, elastase, according to earlier studies [50].

As reported by Schafhauser and colleagues, the absence of ppGpp is linked to a reduced expression of *lasI* and *rhl* quorum-sensing associated genes and to a de-repressed expression of *pqsA* [81]. In our case, a prolonged interaction of Esc(1-21)-1c with ppGpp would not just lead to a transient depletion of the alarmone, but rather a constantly reduced availability of the free nucleotides. Hence, (p)ppGpp-mediated signaling pathways, which collectively regulate bacterial virulence (e.g. quorum sensing lasI and rhl systems), would be steadily slowed down. This is consistent with the reduced expression of *lasI* and *rhl* genes in bacterial cells upon exposure to this peptide (Fig. 5), along with the invariant expression levels of *pqsA* and *pqsR* (Fig. 10). A schematic representation of a possible mechanism of bacterial biofilm inhibition by Esc(1-21)-1c is reported in Fig. 11.

Although the exact molecular mechanism is not yet known and would need to be further explored, a stereospecific mechanism mediated by selective inhibition or activation of other intracellular targets by the two peptides may be involved.

Notably, besides a direct reduction of the biofilm biomass or limiting its formation, an additional strategy would be to impede microbial growth in a human host and to delay the emergence of chronic infections. This strategy stands in contrast with the properties of currently used antibiotics, for example, colistin and aztreonam, among others, which do not prevent but rather stimulate biofilm formation of the selected strains at sub-MIC levels (Fig. 3). As described in the literature, only few AMPs have shown the ability either to display a bactericidal activity or to arrest biofilm formation of *P. aeruginosa* [27,33,60]. Among them, LL-37 was reported to inhibit *Pseudomonas* biofilm formation, regardless of its chirality, but no data on the mechanism of action were provided [82].

We have demonstrated here for the first time that the presence of only two D-amino acids in Esc(1-21)-1c is sufficient to confer an ability to prevent biofilm formation of *P. aeruginosa* and to modulate expression of its virulence genes, presumably via an interaction of the peptide with the bacterial alarmone ppGpp. This

activity becomes highly pronounced likely due to the enhanced resistance of the D-amino acid containing peptide to bacterial proteases, for example, elastase [65] and thereby altered pharmacokinetics compared to the all-L parent peptide. Altogether, the enhanced antibiofilm properties of Esc(1-21)-1c combined with its wound healing activity, higher biostability [65] and lower *in vivo* toxicity, when compared to the all-L counterpart, render this peptide a more attractive candidate for the development of novel antibiotics. In addition to other potential indications we envision that these agents will help fight *Pseudomonas* infections, especially in CF subjects where the compromised ability to clear bacteria by mucociliary action favors the establishment of chronic lung bacterial biofilm [83]. In addition to broadening our knowledge on the impact of D-amino acids on the ability of peptide antibiotics to control biofilm formation by interfering with the signal pathways of human pathogens, these studies should assist the design and optimization of new anti-infective agents with multiple therapeutically valuable properties.

Materials and methods

Reagents

Crystal violet (CV), 4′,6-diamidino-2-phenylindole (DAPI), colistin, aztreonam, rhodamine, Mowiol 4-88 and molecular biology grade dimethyl sulfoxide (DMSO), methylene blue solution 1.4% (w:v) in 95% ethanol were purchased from Sigma-Aldrich (St.Luis, MO, USA). Guanosine-3′,5′-bisdiphosphate (ppGpp) was from TriLink BioTechnologies (San Diego, CA, USA). All the other chemicals were reagent grade.

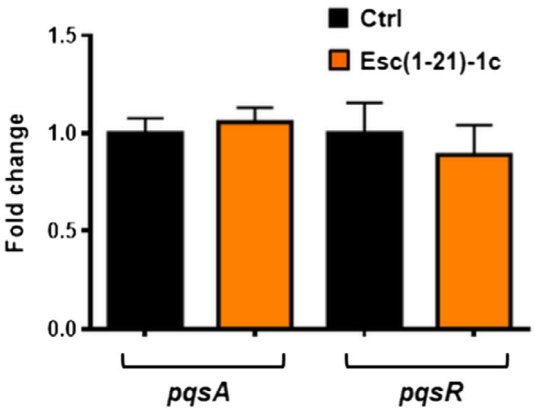

Fig. 10. Effect of Esc(1-21)-1c on the expression of *pqsA* and *pqsR* genes in *P. aeruginosa* AA11. Ten microlitre of bacterial planktonic cells culture at a density of 10^8 CFU·mL^{-1} was incubated with 1 μM peptide for 20 h in an orbital shaker at 37 °C. Total RNA was extracted immediately after the incubation. Results are representative of three independent experiments. Data are shown as mean ± SEM.

Peptides

The synthetic Esc peptides as well as the rhodamine-labeled Esc peptides were purchased from Chematek Spa (Milan, Italy) and synthesized by solid-phase synthesis using standard Fmoc strategy. A purity of 98% was achieved via reverse-phase high-performance liquid chromatography; the molecular mass was verified by mass spectrometry.

Microorganisms

P. aeruginosa strains used in the assays were the reference ATCC 27853 and the CF clinical isolates KK1, AA43 and AA11, from the collection of the Cystic Fibrosis Outpatients Clinic at Hannover Medical School, Germany [84,85].

Determination of antimicrobial activities

Bacteria were grown in Luria-Bertani (LB) medium at 37 °C to a mid-log phase. Susceptibility testing was performed by adapting the microbroth dilution method outlined by the Clinical and Laboratory Standards Institute, using sterile Falcon® 96-well plates. Aliquots (50 μL) of bacteria at a concentration of 1×10^6 colony-forming units (CFU) mL^{-1} in LB broth diluted 1:10 in water (10% LB) were added to 50 μL of diluted LB containing the peptide/antibiotic in serial 2-fold dilutions. Antimicrobial activities were expressed as the minimum inhibitory concentration (MIC), the concentration of peptide at which 100% inhibition of microbial growth is visually observed after 20 h of incubation at 37 °C. In parallel, the minimum concentration of peptides/antibiotics causing 95% eradication of *Pseudomonas* biofilm (BEC) was taken from [50] or determined according to the procedure described in [50].

Biofilm quantification

Pseudomonas strains were allowed to grow in LB medium at 37 °C until reaching an optical density of 0.8 at λ = 590 nm. They were then diluted to 10% LB in water and 50 μL were added into the wells of a 96-well plate containing 50 μL of 2-fold serial dilutions of peptides/antibiotics in 10% LB, to reach a final cell density of 5×10^5 CFU·mL^{-1}. The plate was then

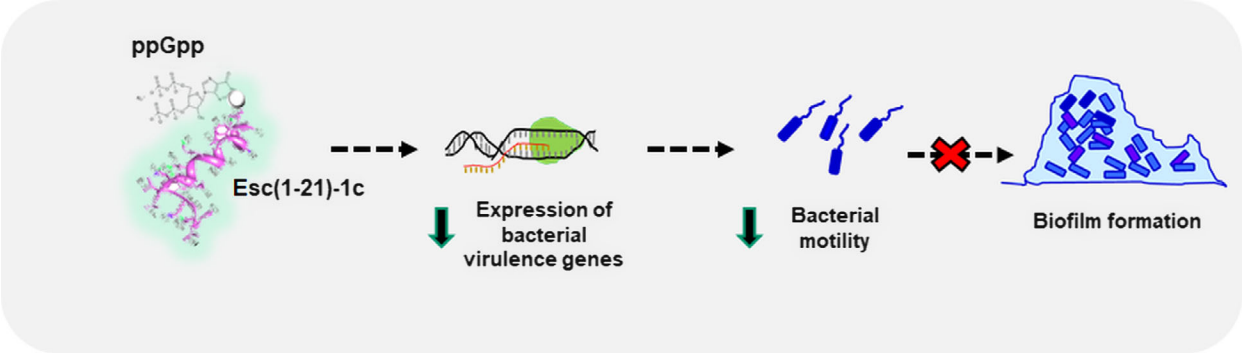

Fig. 11. Cartoon representing one possible mechanism of bacterial biofilm inhibition activity by Esc(1-21)-1c. Prolonged peptide interaction with ppGpp reduces the availability of free nucleotides, lowering expression of virulence genes (including those controlling bacterial motility) which leads to preventative inhibition of biofilm formation. Peptide structure modified from [71].

incubated for 20 h at 37 °C in a humidified incubator. After 20 h, the bacterial biomass was evaluated by CV staining, as already reported [45].

Motility assays

P. aeruginosa AA11 was allowed to grow as described above. For swimming, swarming and twitching assays, 5 μL aliquots of the bacterial culture grown for 20 h in the presence of each peptide at a sub-MIC level (1/8 of MIC) were inoculated onto 3.5 cm dish plates containing 10% LB medium supplemented with 0.3%, 0.5% and 1% agarose plus the peptide at 1/8 MIC. Plates with 0.3%, 0.5% and 1% agarose were used to, respectively, simulate bacterial movement across an aqueous environment (i.e. swimming motility) or across a moist surface of low and moderate viscosity (i.e. swarming and twitching motility, respectively) [86]. The diameters of the swimming, swarming and twitching zones were determined after an incubation at 30 °C for 24 h.

Gene expression analysis

P. aeruginosa AA11 (1×10^8 cells mL^{-1}) was incubated in 10% LB supplemented with each peptide at a concentration of 1 μM for 20 h at 37 °C. Total bacterial RNA was extracted using TRI Reagent® (Sigma-Aldrich). The cDNA was synthesized by High-Capacity cDNA Reverse Transcription Kit (Applied Biosystems, Waltham, MA, USA). Fast SYBR Green Master Mix (Applied Biosystems) and 7900HT Fast Real-Time PCR System (Applied Biosystems) were used for quantification. The constitutively expressed *rplU* gene encoding 50S ribosomal protein was used as housekeeping gene to normalize qPCR data. Note that the expression of *rplU* gene did not vary under the described experimental conditions. Fold change was calculated by ΔΔCT values. Primer sequences are listed in Table 3.

Production of pyoverdine

P. aeruginosa AA11 cells (5×10^5 CFU·mL^{-1}) were grown with mild agitation in 10% LB supplemented with each peptide at a concentration of 1 μM, for 20 h at 37 °C. The relative concentration of pyoverdine was quantified in the supernatants by measurement of the fluorescence intensity at 460 nm after excitation at 400 nm with a Tecan Infinite M200 microplate reader [87].

Production of rhamnolipids

The production of rhamnolipids was evaluated according to [88]. Briefly, *P. aeruginosa* AA11 (1×10^8 CFU·mL^{-1}) in 10% LB (5 mL) was incubated for 20 h at 37 °C with 1 μM of Esc(1-21) and Esc(1-21)-1c and then centrifuged at 3000 ***g*** for 5 min. The supernatant was filtered (with 0.1 μm filter) to remove suspended cells and the pH was adjusted to 2.3 ± 0.2 using 1 N HCl. The supernatant was mixed with 4 mL of ethyl acetate for rhamnolipids extraction. The nonmiscible mixture was vortexed and centrifuged (1 min at 100 ***g***) to allow phase separation. The upper organic phase was collected in a glass reaction tube, and the extraction procedure was repeated two more times. The collected organic phases were dried with a SpeedVac concentrator for the lipid quantification. The dry extract was dissolved in 4 mL chloroform and mixed with 400 μL methylene blue solution. The tubes were vortexed for 5 min and

Table 3. Sequence of primers

Gene	Primer sequence	
fleN	Forward	5′-TGTTCGCCAAACTGACCA-3′
	Reverse	5′-GTATACGGCTCGCTGTTTCT-3′
fimT	Forward	5′-CGCTTGCAAAGAAGGAAAGG-3′
	Reverse	5′-CCTTCCGCAGAGCAGAAA-3′
fimX	Forward	5′-CCTGGCCTATATCCATCTCAAC-3′
	Reverse	5′-ACTGTTCACGCATCAGTCC-3′
lasI	Forward	5′-GGCGCGAAGAGTTCGATAAA-3′
	Reverse	5′-CCATCTCGTCGATGACACTAAC-3′
lasB	Forward	5′-CAACCAGAAGATCGGCAAGTA-3′
	Reverse	5′-GTTCATGTCGACGGTGATGA-3′
rhlA	Forward	5′-CGAGACCGTCGGCAAATAC-3′
	Reverse	5′-GCACCTGGTCGATGTGAAA-3′
rhlB	Forward	5′-CTCACGAGAAGTACGGGATTC-3′
	Reverse	5′-CTCGGGCACGTTGAACT-3′
rpoS	Forward	5′-CGGCGAGTTGGTCATCATCAAACA-3′
	Reverse	5′-ATCGATTGCCCTACCTTGACCTGTC-3′
fliC	Forward	5′-GTCAACACGAACATTGCTTCCC-3′
	Reverse	5′-TTGCTGCCGACCTGGTAAGAAC-3′
pqsA	Forward	5′-GACCGGCTGTATTCGATTC-3′
	Reverse	5′-GCTGAACCAGGGAAAGAAC-3′
pqsR	Forward	5′-CTGATCTGCCGGTAATTGG-3′
	Reverse	5′-ATCGACGAGGAACTGAAGA-3′
rplU	Forward	5′-CGCAGTGATTGTTACCGGTG-3′
	Reverse	5′-AGGCCTGAATGCCGGTGATC-3′

subsequently incubated at room temperature to stain the lipids and allow phase separation. Then, 1 mL of the lower phase was mixed with 500 μL of 0.2 N HCl and phase separation was achieved by centrifugation (1 min at 100 ***g***). The mixture was left 10 min at room temperature; then 200 μL of the upper acidic phase was transferred in a 96-well microplate and the absorbance was measured at 638 nm with a Tecan Infinite M200 microplate reader.

Confocal fluorescence microscopy

Bacterial cells (1×10^8 CFU·mL^{-1}) in 10% LB were incubated for 5 min at 37 °C with 5 μM of rhodamine-labeled Esc peptides. Afterward, cells were washed with phosphate buffered saline (PBS) and seeded on round glass coverslips for about 30 min at 37 °C. Samples were then washed with PBS and fixed with 4% formaldehyde for 10 min at room temperature. Subsequently, they were washed with PBS, stained with 10 μg·mL^{-1} of DAPI for 30 min at room temperature, for DNA detection. The coverslips were placed on a glass slide with a drop of mounting medium Mowiol 4-88 and visualized under a fluorescence confocal microscope (Olympus iX83-FV1200). DAPI and rhodamine-labeled peptides were visualized using laser excitation at 405 and 559 nm, respectively. All images were taken using a 60× NA 1.35 objective with zoom 3×.

Phosphorus-31 nuclear magnetic resonance (^{31}P-NMR) spectroscopy

Freshly prepared stock solutions of Esc peptides and ppGpp in 10% D_2O (pH 7.2) were combined in NMR tubes and adjusted to a final volume of 600 μL. A constant concentration of 0.5 mM ppGpp was maintained in all samples, whereas the amount of peptides was varied over a range of concentrations, from an excess of peptide (2:1 mol/mol) to an excess of nucleotide (1:8 mol/mol). To probe for binding, aggregation, and potentially even precipitation, each NMR sample was allowed to remain without perturbation at ambient temperature for at least 2 h. Proton-decoupled ^{31}P-NMR spectra were acquired on a Bruker (Karlsruhe, Germany) AVANCE 400 MHz spectrometer operating at a ^{31}P frequency of 161.974 MHz. The experiments were performed without temperature control (room temperature) using a standard Bruker 5 mm BB-PABBO probe. For ^{1}H decoupling, a WALTZ16 pulse sequence was used. A total of 3500 scans were accumulated for each spectrum, with an interpulse delay of 2 s. Spectra were processed with TopSpin 3.5 (Bruker), using line broadening of 5 Hz.

Acute toxicity in zebrafish embryos

All experimental procedures were performed in accordance with the Organization for Economic Cooperation and Development Test Guideline [89] and German animal protection standards. Freshly hatched wild-type *D. rerio* embryos were obtained from the European Zebrafish Resource Center at Karlsruhe Institute of Technology. Fertilized eggs (6 hpf, hours postfertilization) were washed once with E3 medium to avoid any microorganism contamination. Then 20 eggs per well (6-well plate) were raised in 4 mL E3 medium at 28 °C until 72 hpf. For toxicity evaluation, the embryos were transferred into flat-bottom glass vials, containing embryonic medium E3 (15–20 embryos per vial). The volume in each bottle was adjusted to 980 μL, and peptides were added as a single 20 μL aliquot in 10% DMSO in serial 2-fold dilutions. Toxicity was expressed as the LC_{50} – the calculated concentration of peptide at which 50% of the embryos die – after visual viability readout at 1, 3 and 24 h (the values did not change) of incubation at room temperature. Each LC_{50} value is the average of three independent experiments.

Statistical analysis

Statistical analyses were performed by one-way analysis of variance and Dunnett's multiple comparisons test or Student's *t* test. Data are expressed as mean ± standard errors of the mean (SEM). Statistical significance is achieved at $P < 0.05$.

Acknowledgements

This work was supported by grants from Sapienza University of Rome (projects RM116154C8434109 and RM11816436113D8A) and the Italian Cystic Fibrosis Foundation (project FFC#11/2014 adopted by FFC Delegations from Siena, Sondrio Valchiavenna, Cerea Il Sorriso di Jenny, and Pavia and project FFC 15/2017 Adopted by Delegations of Palermo, Vittoria, Ragusa, Siracusa, Catania Mascalucia, Messina, Gruppo di Sostegno di Tremestieri). M.L.M thanks Alessandra Bragonzi (San Raffaele Institute, Milan, Italy) and Burkhard Tummler (Klinische Forschergruppe, OE 6710, Medizinische Hochschule Hannover, Germany) for the *P. aeruginosa* clinical isolates. S.A. and A.S.U. thank the Deutsche Forschungsgemeinschaft for grant (INST 121384/58-1 FUGG). This research was also partly supported by the National Institutes of Health awards R01 HL-125128 and AI-133351.

Author contributions

MLM designed the study and wrote the first draft of the manuscript; BC and QL were responsible for the antimicrobial and gene expression studies, analyzed the results, and contributed to the writing of the article. SA performed NMR and *in vivo* studies and contributed to the writing of the manuscript; MRL partially performed the *in vitro* antimicrobial assays. VT performed the confocal microscopy analysis.VM contributed to the *in vivo* experiments. YPD contributed to some of the experimental designs, to the writing of the article and to purchasing of reagents. ASU critically reviewed the manuscript and contributed to reagents. All authors approved the final version of the manuscript. All authors are grateful to John P. Mayer (University of Colorado, Boulder, US) for his careful reading and revision of the whole manuscript.

Conflict of interest

The authors declare that they have no conflicts of interest with the contents of this article.

References

1 Stoodley P, Sauer K, Davies DG & Costerton JW (2002) Biofilms as complex differentiated communities. *Annu Rev Microbiol* **56**, 187–209.
2 Rasamiravaka T, Labtani Q, Duez P & El Jaziri M (2015) The formation of biofilms by *Pseudomonas aeruginosa*: a review of the natural and synthetic compounds interfering with control mechanisms. *Biomed Res Int* **2015**, 759348.
3 Moradali MF, Ghods S & Rehm BH (2017) *Pseudomonas aeruginosa* lifestyle: a paradigm for adaptation, survival, and persistence. *Front Cell Infect Microbiol* **7**, 39.
4 Lopez D, Vlamakis H & Kolter R (2010) Biofilms. *Cold Spring Harb Perspect Biol* **2**, a000398.
5 Romero D, Aguilar C, Losick R & Kolter R (2010) Amyloid fibers provide structural integrity to *Bacillus subtilis* biofilms. *Proc Natl Acad Sci USA* **107**, 2230–2234.
6 Pearson JP, Gray KM, Passador L, Tucker KD, Eberhard A, Iglewski BH & Greenberg EP (1994) Structure of the autoinducer required for expression of *Pseudomonas aeruginosa* virulence genes. *Proc Natl Acad Sci USA* **91**, 197–201.
7 El-Shaer S, Shaaban M, Barwa R & Hassan R (2016) Control of quorum sensing and virulence factors of *Pseudomonas aeruginosa* using phenylalanine arginyl beta-naphthylamide. *J Med Microbiol* **65**, 1194–1204.
8 Hall-Stoodley L & Stoodley P (2002) Developmental regulation of microbial biofilms. *Curr Opin Biotechnol* **13**, 228–233.
9 Webb JS, Thompson LS, James S, Charlton T, Tolker-Nielsen T, Koch B, Givskov M & Kjelleberg S (2003) Cell death in *Pseudomonas aeruginosa* biofilm development. *J Bacteriol* **185**, 4585–4592.
10 Webb JS, Givskov M & Kjelleberg S (2003) Bacterial biofilms: prokaryotic adventures in multicellularity. *Curr Opin Microbiol* **6**, 578–585.
11 Karatan E & Watnick P (2009) Signals, regulatory networks, and materials that build and break bacterial biofilms. *Microbiol Mol Biol Rev* **73**, 310–347.
12 Sonderholm M, Kragh KN, Koren K, Jakobsen TH, Darch SE, Alhede M, Jensen PO, Whiteley M, Kuhl M & Bjarnsholt T (2017) *Pseudomonas aeruginosa* aggregate formation in an alginate bead model system exhibits *in vivo*-like characteristics. *Appl Environ Microbiol* **83**, e00113–e00117.
13 Bjarnsholt T, Alhede M, Alhede M, Eickhardt-Sorensen SR, Moser C, Kuhl M, Jensen PO & Hoiby N (2013) The *in vivo* biofilm. *Trends Microbiol* **21**, 466–474.
14 Pestrak MJ, Chaney SB, Eggleston HC, Dellos-Nolan S, Dixit S, Mathew-Steiner SS, Roy S, Parsek MR, Sen CK & Wozniak DJ (2018) *Pseudomonas aeruginosa* rugose small-colony variants evade host clearance, are

hyper-inflammatory, and persist in multiple host environments. *PLoS Pathog* **14**, e1006842.
15 Romling U & Balsalobre C (2012) Biofilm infections, their resilience to therapy and innovative treatment strategies. *J Intern Med* **272**, 541–561.
16 Pang Z, Raudonis R, Glick BR, Lin TJ & Cheng Z (2019) Antibiotic resistance in *Pseudomonas aeruginosa*: mechanisms and alternative therapeutic strategies. *Biotechnol Adv* **37**, 177–192.
17 Davies D (2003) Understanding biofilm resistance to antibacterial agents. *Nat Rev Drug Discov* **2**, 114–122.
18 Fux CA, Costerton JW, Stewart PS & Stoodley P (2005) Survival strategies of infectious biofilms. *Trends Microbiol* **13**, 34–40.
19 Akers KS, Cardile AP, Wenke JC & Murray CK (2015) Biofilm formation by clinical isolates and its relevance to clinical infections. *Adv Exp Med Biol* **830**, 1–28.
20 Govan JR & Deretic V (1996) Microbial pathogenesis in cystic fibrosis: mucoid *Pseudomonas aeruginosa* and *Burkholderia cepacia*. *Microbiol Rev* **60**, 539–574.
21 Filkins LM & O'Toole GA (2015) Cystic fibrosis lung infections: polymicrobial, complex, and hard to Treat. *PLoS Pathog* **11**, e1005258.
22 Silva Filho LV, Ferreira Fde A, Reis FJ, Britto MC, Levy CE, Clark O & Ribeiro JD (2013) *Pseudomonas aeruginosa* infection in patients with cystic fibrosis: scientific evidence regarding clinical impact, diagnosis, and treatment. *J Bras Pneumol* **39**, 495–512.
23 Kostakioti M, Hadjifrangiskou M & Hultgren SJ (2013) Bacterial biofilms: development, dispersal, and therapeutic strategies in the dawn of the postantibiotic era. *Cold Spring Harb Perspect Med* **3**, a010306.
24 Casciaro B, Cappiello F, Cacciafesta M & Mangoni ML (2017) Promising approaches to optimize the biological properties of the antimicrobial peptide esculentin-1a(1-21)NH_2: amino acids substitution and conjugation to nanoparticles. *Front Chem* **5**, 26.
25 Arciola CR, Campoccia D & Montanaro L (2018) Implant infections: adhesion, biofilm formation and immune evasion. *Nat Rev Microbiol* **16**, 397–409.
26 Johansson EM, Crusz SA, Kolomiets E, Buts L, Kadam RU, Cacciarini M, Bartels KM, Diggle SP, Camara M, Williams P *et al.* (2008) Inhibition and dispersion of *Pseudomonas aeruginosa* biofilms by glycopeptide dendrimers targeting the fucose-specific lectin LecB. *Chem Biol* **15**, 1249–1257.
27 Junker LM & Clardy J (2007) High-throughput screens for small-molecule inhibitors of *Pseudomonas aeruginosa* biofilm development. *Antimicrob Agents Chemother* **51**, 3582–3590.
28 Kolodkin-Gal I, Romero D, Cao S, Clardy J, Kolter R & Losick R (2010) D-amino acids trigger biofilm disassembly. *Science* **328**, 627–629.
29 Lu TK & Collins JJ (2007) Dispersing biofilms with engineered enzymatic bacteriophage. *Proc Natl Acad Sci USA* **104**, 11197–11202.
30 Muh U, Schuster M, Heim R, Singh A, Olson ER & Greenberg EP (2006) Novel *Pseudomonas aeruginosa* quorum-sensing inhibitors identified in an ultra-high-throughput screen. *Antimicrob Agents Chemother* **50**, 3674–3679.
31 Riera E, Macia MD, Mena A, Mulet X, Perez JL, Ge Y & Oliver A (2010) Anti-biofilm and resistance suppression activities of CXA-101 against chronic respiratory infection phenotypes of *Pseudomonas aeruginosa* strain PAO1. *J Antimicrob Chemother* **65**, 1399–1404.
32 Valle J, Da Re S, Henry N, Fontaine T, Balestrino D, Latour-Lambert P & Ghigo JM (2006) Broad-spectrum biofilm inhibition by a secreted bacterial polysaccharide. *Proc Natl Acad Sci USA* **103**, 12558–12563.
33 de la Fuente-Nunez C, Korolik V, Bains M, Nguyen U, Breidenstein EB, Horsman S, Lewenza S, Burrows L & Hancock RE (2012) Inhibition of bacterial biofilm formation and swarming motility by a small synthetic cationic peptide. *Antimicrob Agents Chemother* **56**, 2696–2704.
34 Segev-Zarko L, Saar-Dover R, Brumfeld V, Mangoni ML & Shai Y (2015) Mechanisms of biofilm inhibition and degradation by antimicrobial peptides. *Biochem J* **468**, 259–270.
35 Casciaro B, Dutta D, Loffredo MR, Marcheggiani S, McDermott AM, Willcox MD & Mangoni ML (2018) Esculentin-1a derived peptides kill *Pseudomonas aeruginosa* biofilm on soft contact lenses and retain antibacterial activity upon immobilization to the lens surface. *Peptide Science* **110**, e23074.
36 Hilpert K, Volkmer-Engert R, Walter T & Hancock RE (2005) High-throughput generation of small antibacterial peptides with improved activity. *Nat Biotechnol* **23**, 1008–1012.
37 Hancock RE & Sahl HG (2006) Antimicrobial and host-defense peptides as new anti-infective therapeutic strategies. *Nat Biotechnol* **24**, 1551–1557.
38 Fjell CD, Hiss JA, Hancock RE & Schneider G (2012) Designing antimicrobial peptides: form follows function. *Nat Rev Drug Discov* **11**, 37–51.
39 Easton DM, Nijnik A, Mayer ML & Hancock RE (2009) Potential of immunomodulatory host defense peptides as novel anti-infectives. *Trends Biotechnol* **27**, 582–590.
40 Cherkasov A, Hilpert K, Jenssen H, Fjell CD, Waldbrook M, Mullaly SC, Volkmer R & Hancock RE (2009) Use of artificial intelligence in the design of small peptide antibiotics effective against a broad spectrum of highly antibiotic-resistant superbugs. *ACS Chem Biol* **4**, 65–74.

41 Chen C, Mangoni ML & Di YP (2017) *In vivo* therapeutic efficacy of frog skin-derived peptides against *Pseudomonas aeruginosa*-induced pulmonary infection. *Sci Rep* **7**, 8548.
42 Peschel A & Sahl HG (2006) The co-evolution of host cationic antimicrobial peptides and microbial resistance. *Nat Rev Microbiol* **4**, 529–536.
43 Casciaro B, Loffredo MR, Luca V, Verrusio W, Cacciafesta M & Mangoni ML (2018) Esculentin-1a derived antipseudomonal peptides: limited induction of resistance and synergy with aztreonam. *Protein Pept Lett* **25**, 1155–1162.
44 Islas-Rodriguez AE, Marcellini L, Orioni B, Barra D, Stella L & Mangoni ML (2009) Esculentin 1-21: a linear antimicrobial peptide from frog skin with inhibitory effect on bovine mastitis-causing bacteria. *J Pept Sci* **15**, 607–614.
45 Luca V, Stringaro A, Colone M, Pini A & Mangoni ML (2013) Esculentin(1-21), an amphibian skin membrane-active peptide with potent activity on both planktonic and biofilm cells of the bacterial pathogen *Pseudomonas aeruginosa*. *Cell Mol Life Sci* **70**, 2773–2786.
46 Kolar SS, Luca V, Baidouri H, Mannino G, McDermott AM & Mangoni ML (2015) Esculentin-1a (1-21)NH_2: a frog skin-derived peptide for microbial keratitis. *Cell Mol Life Sci* **72**, 617–627.
47 Mangoni ML, Luca V & McDermott AM (2015) Fighting microbial infections: a lesson from amphibian skin-derived esculentin-1 peptides. *Peptides* **71**, 286–295.
48 Li H, Anuwongcharoen N, Malik AA, Prachayasittikul V, Wikberg JE & Nantasenamat C (2016) Roles of d-amino acids on the bioactivity of host defense peptides. *Int J Mol Sci* **17**, e1023.
49 Grieco P, Carotenuto A, Auriemma L, Saviello MR, Campiglia P, Gomez-Monterrey IM, Marcellini L, Luca V, Barra D, Novellino E *et al.* (2013) The effect of d-amino acid substitution on the selectivity of temporin L towards target cells: identification of a potent anti-*Candida* peptide. *Biochim Biophys Acta* **1828**, 652–660.
50 Di Grazia A, Cappiello F, Cohen H, Casciaro B, Luca V, Pini A, Di YP, Shai Y & Mangoni ML (2015) D-Amino acids incorporation in the frog skin-derived peptide esculentin-1a(1-21)NH_2 is beneficial for its multiple functions. *Amino Acids* **47**, 2505–2519.
51 Izadpanah M & Khalili H (2015) Antibiotic regimens for treatment of infections due to multidrug-resistant Gram-negative pathogens: an evidence-based literature review. *J Res Pharm Pract* **4**, 105–114.
52 Davies J, Spiegelman GB & Yim G (2006) The world of subinhibitory antibiotic concentrations. *Curr Opin Microbiol* **9**, 445–453.
53 Andersson DI & Hughes D (2014) Microbiological effects of sublethal levels of antibiotics. *Nat Rev Microbiol* **12**, 465–478.
54 Kaplan JB (2011) Antibiotic-induced biofilm formation. *Int J Artif Organs* **34**, 737–751.
55 Marina Berditsch SA, Vladimirova T, Wadhwani P & Ulrich AS (2012) Antimicrobial peptides can enhance the risk of persistent infections. *Front Immunol* **3**, 222.
56 Skerker JM & Berg HC (2001) Direct observation of extension and retraction of type IV pili. *Proc Natl Acad Sci USA* **98**, 6901–6904.
57 Giraud C, Bernard CS, Calderon V, Yang L, Filloux A, Molin S, Fichant G, Bordi C & de Bentzmann S (2011) The PprA-PprB two-component system activates CupE, the first non-archetypal *Pseudomonas aeruginosa* chaperone-usher pathway system assembling fimbriae. *Environ Microbiol* **13**, 666–683.
58 Overhage J, Lewenza S, Marr AK & Hancock RE (2007) Identification of genes involved in swarming motility using a *Pseudomonas aeruginosa* PAO1 mini-Tn5-lux mutant library. *J Bacteriol* **189**, 2164–2169.
59 Winsor GL, Griffiths EJ, Lo R, Dhillon BK, Shay JA & Brinkman FS (2016) Enhanced annotations and features for comparing thousands of *Pseudomonas* genomes in the *Pseudomonas* genome database. *Nucleic Acids Res* **44**, D646–D653.
60 Lin Q, Deslouches B, Montelaro RC & Di YP (2018) Prevention of ESKAPE pathogen biofilm formation by antimicrobial peptides WLBU2 and LL37. *Int J Antimicrob Agents* **52**, 667–672.
61 Suh SJ, Silo-Suh L, Woods DE, Hassett DJ, West SE & Ohman DE (1999) Effect of rpoS mutation on the stress response and expression of virulence factors in *Pseudomonas aeruginosa*. *J Bacteriol* **181**, 3890–3897.
62 Caiazza NC, Shanks RM & O'Toole GA (2005) Rhamnolipids modulate swarming motility patterns of *Pseudomonas aeruginosa*. *J Bacteriol* **187**, 7351–7361.
63 Xu X, Yu H, Zhang D, Xiong J, Qiu J, Xin R, He X, Sheng H, Cai W, Jiang L *et al.* (2016) Role of ppGpp in *Pseudomonas aeruginosa* acute pulmonary infection and virulence regulation. *Microbiol Res* **192**, 84–95.
64 Berditsch M, Trapp M, Afonin S, Weber C, Misiewicz J, Turkson J & Ulrich AS (2017) Antimicrobial peptide gramicidin S is accumulated in granules of producer cells for storage of bacterial phosphagens. *Sci Rep* **7**, 44324.
65 Cappiello F, Di Grazia A, Segev-Zarko LA, Scali S, Ferrera L, Galietta L, Pini A, Shai Y, Di YP & Mangoni ML (2016) Esculentin-1a-derived peptides promote clearance of *Pseudomonas aeruginosa* internalized in bronchial cells of cystic fibrosis patients and lung cell migration: biochemical properties and a plausible mode of action. *Antimicrob Agents Chemother* **60**, 7252–7262.
66 Lee KY, Jang GH, Byun CH, Jeun M, Searson PC & Lee KH (2017) Zebrafish models for functional and toxicological screening of nanoscale drug delivery systems: promoting preclinical applications. *Biosci Rep* **37**, BSR20170199.

67 Ducharme NA, Reif DM, Gustafsson JA & Bondesson M (2015) Comparison of toxicity values across zebrafish early life stages and mammalian studies: implications for chemical testing. *Reprod Toxicol* **55**, 3–10.
68 Singh S, Singh SK, Chowdhury I & Singh R (2017) Understanding the mechanism of bacterial biofilms resistance to antimicrobial agents. *Open Microbiol J* **11**, 53–62.
69 Chow L, Lin PC, Chang JS, Chu PY, Lee PK, Chen SN, Cheng YM, Lee JC, Chang JY & Liu TW (2012) Differences in the frequencies of K-ras c12-13 genotypes by gender and pathologic phenotypes in colorectal tumors measured using the allele discrimination method. *Environ Mol Mutagen* **53**, 22–31.
70 Skariyachan S, Sridhar VS, Packirisamy S, Kumargowda ST & Challapilli SB (2018) Recent perspectives on the molecular basis of biofilm formation by *Pseudomonas aeruginosa* and approaches for treatment and biofilm dispersal. *Folia Microbiol (Praha)* **63**, 413–432.
71 Loffredo MR, Ghosh A, Harmouche N, Casciaro B, Luca V, Bortolotti A, Cappiello F, Stella L, Bhunia A, Bechinger B *et al.* (2017) Membrane perturbing activities and structural properties of the frog-skin derived peptide Esculentin-1a(1-21)NH_2 and its diastereomer Esc(1-21)-1c: correlation with their antipseudomonal and cytotoxic activity. *Biochim Biophys Acta* **1859**, 2327–2339.
72 Powers JP, Martin MM, Goosney DL & Hancock RE (2006) The antimicrobial peptide polyphemusin localizes to the cytoplasm of *Escherichia coli* following treatment. *Antimicrob Agents Chemother* **50**, 1522–1524.
73 Renner LD & Weibel DB (2011) Cardiolipin microdomains localize to negatively curved regions of *Escherichia coli* membranes. *Proc Natl Acad Sci USA* **108**, 6264–6269.
74 Swain J, El Khoury M, Kempf J, Briee F, Van Der Smissen P, Decout JL & Mingeot-Leclercq MP (2018) Effect of cardiolipin on the antimicrobial activity of a new amphiphilic aminoglycoside derivative on *Pseudomonas aeruginosa*. *PLoS ONE* **13**, e0201752.
75 Potrykus K & Cashel M (2008) (p)ppGpp: still magical? *Annu Rev Microbiol* **62**, 35–51.
76 Srivatsan A & Wang JD (2008) Control of bacterial transcription, translation and replication by (p)ppGpp. *Curr Opin Microbiol* **11**, 100–105.
77 Costerton JW, Stewart PS & Greenberg EP (1999) Bacterial biofilms: a common cause of persistent infections. *Science* **284**, 1318–1322.
78 Hauryliuk V, Atkinson GC, Murakami KS, Tenson T & Gerdes K (2015) Recent functional insights into the role of (p)ppGpp in bacterial physiology. *Nat Rev Microbiol* **13**, 298–309.
79 Petchiappan A & Chatterji D (2017) Antibiotic resistance: current perspectives. *ACS. Omega* **2**, 7400–7409.
80 de la Fuente-Nunez C, Reffuveille F, Haney EF, Straus SK & Hancock RE (2014) Broad-spectrum anti-biofilm peptide that targets a cellular stress response. *PLoS Pathog* **10**, e1004152.
81 Schafhauser J, Lepine F, McKay G, Ahlgren HG, Khakimova M & Nguyen D (2014) The stringent response modulates 4-hydroxy-2-alkylquinoline biosynthesis and quorum-sensing hierarchy in *Pseudomonas aeruginosa*. *J Bacteriol* **196**, 1641–1650.
82 Dean SN, Bishop BM & van Hoek ML (2011) Susceptibility of *Pseudomonas aeruginosa* biofilm to alpha-helical peptides: D-enantiomer of LL-37. *Front Microbiol* **2**, 128.
83 Drenkard E & Ausubel FM (2002) *Pseudomonas* biofilm formation and antibiotic resistance are linked to phenotypic variation. *Nature* **416**, 740–743.
84 Bragonzi A, Paroni M, Nonis A, Cramer N, Montanari S, Rejman J, Di Serio C, Doring G & Tummler B (2009) *Pseudomonas aeruginosa* microevolution during cystic fibrosis lung infection establishes clones with adapted virulence. *Am J Respir Crit Care Med* **180**, 138–145.
85 Lore NI, Cigana C, De Fino I, Riva C, Juhas M, Schwager S, Eberl L & Bragonzi A (2012) Cystic fibrosis-niche adaptation of *Pseudomonas aeruginosa* reduces virulence in multiple infection hosts. *PLoS ONE* **7**, e35648.
86 Mattick JS (2002) Type IV pili and twitching motility. *Annu Rev Microbiol* **56**, 289–314.
87 Deziel E, Comeau Y & Villemur R (2001) Initiation of biofilm formation by *Pseudomonas aeruginosa* 57RP correlates with emergence of hyperpiliated and highly adherent phenotypic variants deficient in swimming, swarming, and twitching motilities. *J Bacteriol* **183**, 1195–1204.
88 Tsiry Rasamiravaka OMV & El Jaziri M (2016) Procedure for rhamnolipids quantification using methylene-blue. *Bio Protocol* **6**. https://doi.org/10.21769/BioProtoc.21783
89 OECD (2013) 236 – Fish Embryo Acute Toxicity (FET) Test. *OECD Guidelines for the Testing of Chemicals. Organization for Economic Cooperation and Development*.

Article

Cite This: *Biomacromolecules* XXXX, XXX, XXX−XXX

pubs.acs.org/Biomac

Poly(lactide-*co*-glycolide) Nanoparticles for Prolonged Therapeutic Efficacy of Esculentin-1a-Derived Antimicrobial Peptides against *Pseudomonas aeruginosa* Lung Infection: in Vitro and in Vivo Studies

Bruno Casciaro,[†,‡,#] Ivana d'Angelo,[§,#] Xiaoping Zhang,[∥] Maria Rosa Loffredo,[†] Gemma Conte,[§,⊥] Floriana Cappiello,[†] Fabiana Quaglia,[⊥] Yuan-Pu Peter Di,[∥] Francesca Ungaro,*[,⊥] and Maria Luisa Mangoni*[,†]

[†]Laboratory affiliated to Pasteur Italia-Fondazione Cenci Bolognetti, Department of Biochemical Sciences "A. Rossi Fanelli", Sapienza University of Rome, via degli Apuli, 9, 00185 Rome, Italy

[‡]Center for Life Nano Science, Istituto Italiano di Tecnologia, 00161 Rome, Italy

[§]Di.S.T.A.Bi.F., University of Campania "Luigi Vanvitelli", Via Vivaldi 43, 81100 Caserta, Italy

[∥]Department of Environmental and Occupational Health, University of Pittsburgh, Pittsburgh, Pennsylvania 15260, United States

[⊥]Department of Pharmacy, University of Naples Federico II, Via D Montesano 49, 80131 Naples, Italy

Supporting Information

ABSTRACT: Due to their excellent in vitro activity against multidrug resistant bacteria, antimicrobial peptides (AMPs) hold promise for treatment of *Pseudomonas aeruginosa* lung infections in cystic fibrosis (CF) sufferers. In this work, poly(lactide-*co*-glycolide) (PLGA) nanoparticles for lung delivery of AMPs deriving from the frog-skin esculentin-1a, namely, Esc(1-21) and Esc(1-21)-1c (Esc peptides), were successfully developed. Improved peptide transport through artificial CF mucus and simulated bacterial extracellular matrix was achieved in vitro. The formulations were effectively delivered through a liquid jet nebulizer already available to patients. Notably, Esc peptide-loaded nanoparticles displayed an improved efficacy in inhibiting *P. aeruginosa* growth in vitro and in vivo in the long term. A single intratracheal administration of Esc peptide-loaded nanoparticles in a mouse model of *P. aeruginosa* lung infection resulted in a 3-log reduction of pulmonary bacterial burden up to 36 h. Overall, results unravel the potential of PLGA nanoparticles as a reliable delivery system of AMPs to lungs.

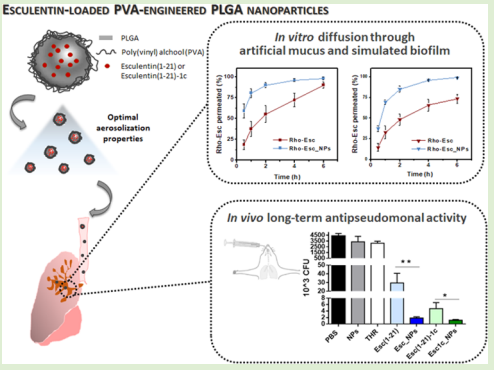

INTRODUCTION

Pseudomonas aeruginosa is the most common pulmonary bacterial pathogen in cystic fibrosis (CF) sufferers where it provokes severe lung tissue damage with failure of respiratory functions.[1−3] It is hard to eradicate, due to its low susceptibility to most available antibiotics[4,5] and ability to form sessile communities named biofilms that are resistant to a large variety of environmental stresses.[6−8] Therefore, the discovery of new anti-infective compounds is highly requested and natural antimicrobial peptides (AMPs) are currently under investigation as novel therapeutics.[9,10] We previously identified a short-sized derivative of the frog-skin AMP esculentin-1a, namely, Esc(1-21), which quickly kills the free-living and biofilm lifestyle of *P. aeruginosa* with a membrane-perturbing mechanism that makes these peptides less disposed to induce resistance.[11−13] Subsequently, we designed a diastereomer of Esc(1-21), by changing the stereochemistry of L-Leu[14] and L-Ser[17] with the corresponding D-amino acids, that is, Esc(1-21)-1c.[14] As compared to the wild-type peptide, Esc(1-21)-1c was characterized by increased stability, decreased cytotoxicity,[14] and a pronounced efficiency in promoting migration of bronchial epithelial cells, which may result in effective recovery of the bronchial epithelium integrity.[15] This is a remarkable feature considering the impaired wound healing activity in the lungs of CF patients.[16] Furthermore, upon a single intratracheal (i.t.) administration in a mouse model of *P. aeruginosa* lung infection, the diastereomer was more potent than Esc(1-21) in decreasing the number of lung bacterial cells.[17]

Although chemical modification of the AMP scaffold can be regarded as a useful strategy to improve in vitro/in vivo peptide stability, local treatment of pulmonary infections with AMPs is still hampered by some biobarriers imposed by lungs, especially in CF patients, e.g., bronchial obstruction with sticky mucus and intrapulmonary bacterial biofilm.[18] To overcome these issues, inhaled formulations able to deliver intact AMPs in conductive airways and to assist their transport across biobarriers, thus preventing AMP kidnapping by mucosal and cellular barriers, are highly desirable.[19] In particular, polymeric

Received: December 28, 2018
Revised: April 2, 2019

DOI: 10.1021/acs.biomac.8b01829
Biomacromolecules XXXX, XXX, XXX−XXX

nanoparticles (NPs) have emerged as a powerful approach to localize and concentrate drugs at the site of infection, while reducing systemic adverse effects.[19−23]

Among biodegradable polyesters, poly(lactide-*co*-glycolide) (PLGA)[20,24] have been extensively studied fulfilling also safety concerns.[25−29] In recent years, PLGA nanoparticles have been designed and developed for lung delivery of different types of drugs, proteins, peptides (e.g., extendin-4), genes, siRNA, and vaccines.[25,30−33] They are expected to ameliorate the therapeutic efficacy of the encapsulated drug by (i) protecting it from interaction with extracellular components, (ii) increasing the amount of drug deposited in lungs, and (iii) prolonging the drug residence time in situ and therefore its pharmacological effect.[34] However, to the best of our knowledge, no reports have been published so far for delivery of controlled release NPs containing AMPs to the pulmonary region.

Here, we developed PLGA nanoparticles containing the AMP Esc(1-21) or its diastereomer Esc(1-21)-1c (i.e., Esc peptides) and coated them with the stabilizing agent poly(vinyl alcohol) (PVA). This was done to prevent the aggregation of our engineered PVA−PLGA nanoparticles (NPs) and to provide them a neutral hydrophilic surface to favor the translocation through biological barriers, e.g., lung mucus.[35,36] NPs loaded with Esc peptides were fully characterized in terms of nanoparticle size, surface properties, release kinetics, and peptide diffusion through an artificial CF mucus and bacterial barrier. In parallel, we studied aerosol performance of the NP dispersion upon delivery from the most advanced nebulizers available to CF patients. From a translational perspective, in vitro antipseudomonal activity was also assessed. More importantly, preclinical studies were carried out upon i.t. instillation of Esc peptide-loaded NPs in a mouse model of acute *Pseudomonas* lung infection to assess their antimicrobial activity as well as in healthy mice to evaluate their safety profile.

EXPERIMENTAL SECTION

Materials. Uncapped PLGA 50:50 (Resomer RG 502H, inherent viscosity 0.16−0.24 dL/g) was from Boehringer Ingelheim (Ingelheim, Germany). PVA (Mowiol 40−88, average M_w ∼205 000 Da, 87−89% hydrolyzed), diethylenetriaminepentaacetic acid (DTPA), DNA from calf thymus, mucin type II from porcine stomach, egg yolk emulsion, and RPMI 1640 amino acid solution were purchased from Sigma-Aldrich. Nonacetylated polymannuronic acid (average M_w > 5000 Da) from bacterial alginates was supplied by Carbosynth (U.K.). High-performance liquid chromatography (HPLC) grade acetonitrile, methylene chloride, and 96% ethanol were purchased from Carlo Erba Reagents (Italy). Ultrapure water was produced from potable water by the Purelab Option-Q (Elga Labwater, Italy) apparatus and employed throughout the study. All other salts and reagents were of analytical grade or better.

Rhodamine-labeled PLGA (PLGA-Rhod) was synthesized under inert nitrogen or argon atmosphere and dry conditions, as we previously reported.[37] Briefly, the terminal hydroxyl group of RG 502H was changed into azide by two-step azidation with mesyl chloride activation and it was subsequently coupled with rhodamine-B. ^{1}H NMR analysis was used to confirm the product chemical structure. The final conversion degree of the PLGA azide in PLGA-Rhod is, within the limits of experimental error, higher than 95%. Synthetic Esc(1-21) [GIFSKLAGKKIKNLLISGLKG-CONH$_2$ MW, 2184], Esc(1-21)-1c [GIFSKLAGKKIKNlLIsGLKG-CONH$_2$ MW, 2184], and rhodamine-labeled Esc peptides (Rho-Esc) were purchased from Biomatik (Delaware). They were assembled by stepwise solid-phase synthesis using a standard F-moc strategy. Peptides were purified to 98% via reverse-phase high-performance liquid chromatography (RP-HPLC), and the molecular mass was checked by mass spectrometry.

Quantitative Analysis of Esc Peptides. Esc peptides were quantified by RP-HPLC analysis, as previously reported.[35] Briefly, the HPLC system consisted of a SIL-10ADvp auto-injector, a LC-10ADvp liquid chromatograph, a SPD-10Avp UV−vis detector, and a C-R6 integrator from Shimadzu (Japan). The quantitative analysis was carried out on a wide-pore C18 reversed-phase column (Jupiter 5 μm, 250 × 4.6 mm, 300 Å, Phenomenex) in isocratic elution mode. A mixture of acetonitrile and sodium sulfate (30 mM) adjusted at pH 3 with phosphoric acid (75:25 v/v), delivered at a flow rate of 1 mL/min, was used as the mobile phase. The detection wavelength was fixed at 214 nm. Calibration curves were obtained by plotting the peak area versus the concentration of Esc(1-21) or Esc(1-21)-1c standard solutions in water. The linearity of the response was verified over the concentration range 5−500 μg/mL ($r^2 \geq 0.999$).

Nanoparticle Production. Esc peptide-loaded NPs at a theoretical loading of 2% (2 mg of peptide per 100 mg of NPs) were prepared by emulsion/solvent diffusion, as previously reported with some modifications.[24,38] Briefly, an aqueous solution of the selected Esc peptide (100 μL) was added to a solution of PLGA in methylene chloride (1 mL, 1% w/v) under vortex mixing at a speed of 2400 rpm (Reax top, Heidolph, Germany). The resulting water-in-oil emulsion was poured in 12.5 mL of ethanol (diffusion phase) to induce polymer precipitation in the form of NPs. The NP dispersion was diluted with aqueous PVA (12.5 mL, 0.1% w/v), kept under magnetic stirring for 10 min at room temperature, and rotary-evaporated (Rotavapor, Heidolph VV 2000, Germany) under vacuum at 30 °C to remove any residual organic solvent. After adjustment to a final volume of 5 mL, the colloidal dispersion was centrifuged at 7000 rcf for 20 min at 4 °C (Hettich Zentrifugen, Universal 16R) to isolate NPs and the pellet dispersed in ultrapure water.

Fluorescently labeled NPs were employed for in vitro aerosolization studies and to follow NP diffusion in artificial mucus/bacterial extracellular matrix. Briefly, NPs containing either Esc(1-21) (i.e., Esc_ Fluo-NPs) or Esc(1-21)-1c (Esc1c_Fluo-NPs) were prepared using PLGA-Rhod in the organic phase at 10% w/w with respect to the total PLGA amount. Control NPs containing Esc(1-21) labeled with rhodamine-B (Rho-Esc) were also prepared for peptide diffusion studies in simulated mucus and biofilm (Rho-Esc_NPs).

When needed, Esc peptide-loaded NPs were freeze-dried adding trehalose (THR) as cryoprotectant. Just after production, THR was added to the NP dispersion in ultrapure water (NP/THR1:25 w/w), frozen at −80 °C, and freeze-dried for 24 h by a Modulyo freeze-drier (Edwards, U.K.) operating at 0.01 atm and −60 °C.

Nanoparticle Characterization. The hydrodynamic diameter (D_H), the polydispersity index (PDI), and the ζ-potential of Esc peptide-loaded NPs were determined by dynamic light scattering (DLS) and electrophoretic light scattering (ELS) with a Zetasizer Nano ZS (Malvern Instruments Ltd, U.K.). For ζ-potential analysis, NP aqueous dispersion was diluted in 10 mM NaCl and analyzed in an electrophoresis cell at a fixed potential of ±150 mV. Results are reported as the mean ± standard deviation (SD) of three measurements performed on three different batches (n = 9).

The morphology of Esc peptide-loaded NPs was analyzed by transmission electron microscopy (TEM) with a FEI Tecnai G2 200 kV s-Twin microscope equipped with a 4 K camera (ThermoFisher Scientific). Sample analysis was performed upon air drying of 10 μL nanoparticle dispersions in water (3 mg/mL) mounted on 200 mesh copper grids coated with carbon film (Ted Pella Inc., Nanovision, Italy).

Fixed aqueous layer thickness (FALT) measurements were performed by monitoring the influence of ionic strength on particle surface charge. Briefly, different amounts of a stock NaCl solution were added to a NP aqueous dispersion (0.5 mg/mL) and the ζ-potential of the samples was determined. A plot of ln(ζ) against k (k = 3.3 C$^{0.5}$, where k^{-1} is the Debye length) gives the thickness of the polymer layer in nanometer as the slope of linear regression.[39]

DOI: 10.1021/acs.biomac.8b01829
Biomacromolecules XXXX, XXX, XXX−XXX

The actual loading of Esc peptides inside NPs was determined by either an indirect or a direct method, as previously reported.[35] Just after production, an indirect measurement of the Esc peptide amount encapsulated inside NPs was achieved by RP-HPLC analysis of the supernatant of the NP dispersions after centrifugation. For direct measurement, an aqueous dispersion of Esc peptide-loaded NPs (1 mL, 4 mg/mL) was centrifuged at 7000 rcf for 20 min at 4 °C (Hettich Zentrifugen, Universal 16R) and the NP pellet freeze-dried for 24 h at −80 °C and 0.1 mbar (LyoQuest, Telstar, Italy). Esc peptide content within the NPs was measured by solvent extraction, upon dissolution of freeze-dried NPs in 500 μL of acetonitrile and subsequent dilution with 1 mL of 30 mM sodium sulfate, (pH 3). Upon centrifugation (4 °C, 7000 rcf, 20 min), the samples were analyzed by RP-HPLC, as indicated above. Data were obtained from three different batches ($n = 6$) and reported in terms of actual loading (milligrams of encapsulated Esc peptide per 100 mg of NPs) and encapsulation efficiency (actual loading/theoretical loading × 100) ± SD.

In Vitro Release Kinetics of Esc Peptides. These experiments were performed in phosphate buffer at pH 7.2 (120 mM NaCl, 2.7 mM KCl, 10 mM phosphate salts, PBS). Upon appropriate dilution in PBS (4 mg/mL), Esc peptide-loaded NPs were incubated in a horizontal-shaking water bath (ShakeTemp SW 22, Julabo Italia, Italy) operating at 40 rpm and 37 °C. At different time intervals, samples were centrifuged at 7000 rcf for 20 min at 4 °C to remove the release medium and to isolate NPs. The NP pellet was freeze-dried for 24 h. Esc peptide content within the NPs was measured by solvent extraction, upon NP dissolution in 500 μL of acetonitrile and subsequent dilution with 1 mL of 30 mM sodium sulfate, pH 3. Samples were centrifuged (4 °C, 7000 rcf, 20 min) and then analyzed by RP-HPLC, as reported above. The amount of Esc peptide released at each time point was calculated as the difference between the total amount encapsulated and the amount detected inside the NPs. Triplicate experiments were performed for each time point of release kinetics, and the results are reported as percentage of Esc peptide released from NPs (%) ± SD along the time.

In Vitro Interactions of Nanoparticles with Mucin and Alginates. The interactions of Esc peptide-loaded NPs with the main components of mucus and *P. aeruginosa* extracellular matrix, that is, mucin and alginates, respectively, were assessed by turbidimetric measurements. For NP/mucin interactions, experiments were performed by the mucin/particle method.[22] Briefly, a saturated aqueous solution of mucin was achieved through dispersion of excess of the protein in water (0.08% w/v), under stirring overnight, followed by centrifugation and collection of the mucin-containing supernatant. Then, 10 μL of a water dispersion of Esc peptide-loaded NPs (corresponding to 1 mg of NPs) was poured into 1 mL of the mucin dispersion. After vortex mixing (Reax top, Heidolph, Germany), the turbidity of the samples was measured at time 0 and after incubation at 37 °C for different time intervals (30−60 min). In the case of NP/alginate interactions, NPs scattering at 650 nm were assessed in the presence of a nonacetylated polymannuronic acid dispersion in water (1% w/v). The absorbance (ABS) measurements at 650 nm were carried out by a spectrophotometer (Shimadzu 1204, Shimadzu, Italy) equipped with a 0.1 cm quartz cell (Hellma Italia, Italy). As controls, the saturated mucin solution (without NPs), the polymannuronic acid dispersion (without NPs), and the Esc peptide-loaded NP dispersions in water were analyzed. Triplicate experiments were performed, and the results are reported as absorbance at 650 nm ± SD along the time. The size and the ζ-potential of the NP dispersions in mucin were also investigated by DLS and ELS, as described above.

In Vitro Transport of Nanoparticles through Mucus and Biofilm Models. The penetration of fluorescent Esc peptide-loaded NPs (i.e., Esc_Fluo-NPs and Esc1c_Fluo-NPs) through artificial mucus and simulated bacterial extracellular matrix was also followed. The artificial mucus was prepared as previously reported[35] under stirring by adding sterile egg yolk emulsion (25 μL), mucin (25 mg), aqueous DTPA (30 μL at 1 mg/mL), DNA (20 mg), NaCl (25 mg), KCl (11 mg), and RPMI (100 μL) to 5 mL of water. The simulated bacterial extracellular matrix consisted of the same nonacetylated polymannuronic acid dispersion in water (1% w/v) employed for NP/alginate interactions.

A previously developed model based on the Transwell multiwell plate[35] was used for the diffusion experiments and suitably adjusted for studies with a simulated bacterial barrier. Briefly, 75 μL of artificial mucus or polymannuronic acid was transferred in 8 μm pore polycarbonate membrane Transwell inserts submerged in 300 μL of acceptor medium in a 24-well plate. Afterward, a NP dispersion in water (25 μL, 20 mg/150 μL) was deposited on the artificial mucus/polymannuronic acid layer. Simulated interstitial lung fluid (SILF) or PBS at pH 7.2 was used as acceptor media for mucus or biofilm diffusion experiments, respectively. SILF was carefully prepared according to the instructions provided by Moss.[40] At scheduled time intervals (from 0 to 24 h), the acceptor medium was collected and centrifuged at 9000 rcf for 20 min at 4 °C to isolate NPs. The NP pellet was suspended in 50 μL of water, diluted with 450 μL of 0.5 N NaOH, and stirred for 1 h to degrade the PLGA matrix. The amount of NPs in the resulting solution was quantified by spectrofluorimetric analysis at λ_{ex} 520 nm/λ_{em} 580−640 nm (GloMax Explorer, Promega, Italy). Calibration curves were derived by analyzing serial dilutions of Esc peptide-loaded Fluo-NP standard solutions prepared from a stock of NPs degraded in 0.5 M NaOH. The linearity of the response was analyzed at the concentration range 2−200 μg/mL ($r^2 \geq 0.999$). Each experiment was run in triplicate. Control experiments were carried out by depositing unloaded fluorescent NPs (made of PLGA-Rhod) on the top of the layer. Triplicate experiments were performed, and the results are reported as percentage (%) of total NPs permeated over time ± SD.

The ability of the free peptide to diffuse through both models of mucus and bacterial extracellular matrix was also evaluated by employing Esc(1-21) labeled with rhodamine (Rho-Esc). The diffusion test was carried out on Rho-Esc and compared to that on Rho-Esc-loaded NPs (Rho-Esc_NPs). Briefly, 25 μL of a Rho-Esc aqueous solution (1 mg/mL) or 25 μL of a Rho-Esc NP dispersion (5.88 mg/100 μL corresponding to 1 mg/mL of Rho-Esc) was added on the top of the artificial mucus or polymannuronic acid layer. At scheduled time intervals (from 0 to 6 h), the acceptor medium (i.e., SILF or PBS) was collected and the amount of permeated Rho-Esc was determined by spectrofluorimetric analysis at λ_{ex} 520 nm/λ_{em} 580−640 nm (GloMax Explorer, Promega, Italy). For Rho-Esc_NPs, Rho-Esc was extracted after NP degradation in NaOH as described above before analysis. Triplicate experiments were performed, and the results are reported as a percentage (%) of permeated Rho-Esc versus the total amount of Rho-Esc ± SD.

In Vitro Aerosol Performance of Nanoparticles. In vitro aerosolization properties of fluorescently labeled Esc peptide-loaded NPs prepared employing PLGA-Rhod (i.e., Esc_Fluo-NPs or Esc1c_Fluo-NPs) were investigated after delivery from either a jet nebulizer (PARI TurboBOY, PARI GmbH, Germany) or a vibrating mesh nebulizer (Aeroneb Go, Aerogen Ltd., Ireland). The study was carried out by a Next Generation Impactor (NGI) (Copley Scientific, U.K.) in line with the standard methodology for nebulizer systems with sampling at 15 L/min and insertion of a filter in a micro-orifice collector (MOC), as dictated by the *Comité Européen de Normalization*.[33] Briefly, 1 mL of water dispersion of fluorescent NPs was transferred to the reservoir of the nebulizer and the aerosol was drawn at 15 L/min through the impactor for 5 min, until dry.

The amount of NPs remaining inside the nebulizer chamber, deposited on the seven NGI collection cups and in the induction port, was quantitatively recovered in 0.5 M NaOH. After stirring at room temperature for 1 h, the amount of Esc peptide-loaded fluorescent NPs in the resulting solutions was determined by spectrofluorimetric analysis at λ_{ex} 520 nm/λ_{em} 580−640 nm (GloMax Explorer, Promega, Italy), as previously reported.[33] Calibration curves were derived by analyzing serial dilutions of a stock of fluorescent NPs after degradation in 0.5 M NaOH, as described above. Each experiment was done in triplicate. The emitted dose (ED) was measured as the difference between the initial amount of NPs and the amount remaining in the nebulizer reservoir. The experimental mass median

DOI: 10.1021/acs.biomac.8b01829
Biomacromolecules XXXX, XXX, XXX−XXX

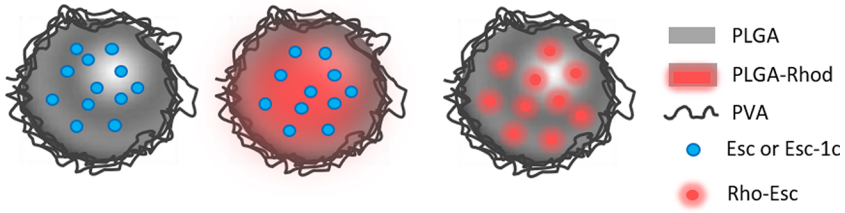

Figure 1. Sketched representation of the adopted formulation approach.

Table 1. Size, PDI, ζ-Potential, Yield of Production, Actual Loading of Esc Peptide-Loaded NPs and Encapsulation Efficiency

	D_H (nm ± SD)	PDI (mean ± SD)	ζ-potential (mV ± SD)	yield of production (% ± SD)	actual loading (%[a] ± SD)	EE[b] (% ± SD)
Esc_ NPs	261 ± 1	0.041 ± 0.020	−0.67 ± 0.07	84 ± 2	2.08 ± 0.047	104 ± 2
Esc1c _ NPs	282 ± 4	0.061 ± 0.007	−0.84 ± 0.22	80 ± 3	2.02 ± 0.014	101 ± 1

[a]Milligrams of encapsulated Esc peptide per 100 mg of NPs, calculated on the basis of the actual amount of NPs recovered after production (i.e., yield of production). [b]Encapsulation efficiency, calculated as actual loading/theoretical loading × 100.

aerodynamic diameter (MMADexp) and the geometric standard deviation (GSD) were calculated following the guidelines of the European Pharmacopoeia. They were obtained by deriving a plot of the cumulative mass of particles present in each collection cup (and expressed as a percent of the total mass recovered in the impactor) versus the cutoff diameter of the respective stage. The fine particle fraction (FPF) was calculated by comparing the amount of NPs deposited on stages 3−7 (MMADexp < 5.39 μm) to the initial amount loaded into the nebulizer chamber, whereas the respirable fraction (RF) referred to the total amount recovered from the NGI.

In Vitro Activity of Nanoparticles against *P. aeruginosa*. *P. aeruginosa* ATCC 27853 was grown at 37 °C in Luria Bertani (LB) medium until an optical density (OD) of 0.8 (λ = 590 nm) was reached. The bacterial culture was centrifuged at 3000*g* for 10 min, washed in PBS, and resuspended in minimal medium E[41] supplemented with 0.2% glucose, 1 μg/mL vitamin B1 (medium E^{++}) according to ref 35. It was then diluted to a concentration of 2 × 10^6 colony-forming units (CFU)/mL in medium E^{++}, and aliquots of 100 μL were added to 100 μL of free peptide or Esc-loaded NPs [final peptide concentration, 10 and 20 μM for Esc(1-21) and Esc(1-21)-1c, respectively] dissolved in the same medium in a 96-well plate. Note that 10 or 20 μM peptide concentrations were the minimal concentrations of Esc(1-21) or the diastereomer, inhibiting bacterial growth in medium E^{++} after 20 h. The plate was incubated at 37 °C, and the absorbance (λ = 590 nm) of each well was measured with a microplate reader (Infinite M200; Tecan, Salzburg, Austria) after a short time (24 h) and long time (72 h) interval. The absorbance of each sample at time zero was subtracted from the corresponding absorbance values at the indicated time points. Unloaded NPs were also tested, and untreated cells served as control.

Animals. Wild-type C57BL/6J female mice were purchased from The Jackson Laboratory (Bar Harbor, ME). All mice were maintained in a specific pathogen-free facility at the University of Pittsburgh. Animal studies were carried out on age- and gender-matched adult mice that were maintained in ventilated microisolator cages. All experiments involving animals were approved by the University of Pittsburgh IACUC.

Therapeutic Efficacy in a Murine Lung Infection Model. *P. aeruginosa* (PAO1) that is sensitive to both Esc(1-21) and Esc(1-21)-1c was used for generating *P. aeruginosa*-induced respiratory infection in mouse lungs according to methods previously described.[17] Intratracheal (i.t.) inoculation of PAO1 bacteria at a concentration of ∼3 × 10^6 CFU/mouse was performed in isoflurane anesthetized mice. One hour after bacterial infection, the free peptides, Esc peptide-loaded NPs (at a peptide concentration of 20 μM corresponding to 0.1 mg/kg), as well as unloaded NPs or THR (in the same amount present in peptide-loaded NPs) were i.t. instilled in 50 μL of PBS. Mice instilled with only PBS (50 μL) were used as vehicle controls. The number of CFU in mouse lungs and bronchoalveolar lavage (BAL) was determined at 36 h after bacterial instillation to evaluate the treatment efficacy.[17] Mice (5−6 animals/group) were sacrificed at the selected end point with 2.5% tribromoethanol (Avertin) as anesthesia. The mouse lungs were lavaged using saline (2 × 1 mL) through cannulated trachea; the BAL was collected, and the lung tissue homogenized. Serial 10-fold dilutions of both BAL and homogenated mouse lungs were plated in triplicate on LB agar plates and the bacterial numbers enumerated after the bacteria-containing plates were incubated at 37 °C overnight.

Lung Toxicity/Inflammation in Healthy Mice. Free peptides, Esc peptide-loaded NPs (at the same peptide concentration used for the in vivo efficacy studies, 20 μM), as well as unloaded NPs or THR (in the same amount present in peptide-loaded NPs), and PBS only (vehicle control) in 50 μL were i.t. administered into anesthetized mice. Mice after 36 h of treatment were anesthetized and sacrificed according to the protocol previously described.[42] The total number of inflammatory cells (including macrophages, neutrophils, and minimal number or occasional lymphocytes) in the BAL of mice was counted by a Vision Cell Analyzer automatic cell counter (Nexcelom, Lawrence, MA). A differential cell count was manually performed for every mouse in the in vivo experiment to define their profile.

The effect of free Esc peptides, peptide-loaded NPs, unloaded NPs, and THR on the expression of different airway epithelial cell-associated inflammatory genes in healthy mice was evaluated. Total mRNA isolation was performed using the lung tissue from the treated mice. Gene expression was analyzed by quantitative RT-PCR using ABI 7900HT (Applied Biosystems, Foster City, CA). Validation tests of all primers were performed to confirm equivalent PCR efficiencies for the target genes, including IL-6, IL-10, TNF-α, NF-κB, as previously described.[17] Fold changes in mRNA expression were calculated using the ΔΔCT method and were normalized to the housekeeping gene β-glucuronidase.[17] Enzyme-linked immunosorbent assays (ELISA) were performed for quantitative evaluation of IL-6 (ELISA kit, R&D Systems) and TNF-α (ELISA kit, Invitrogen, ThermoFisher Scientific) from BAL samples.

Data Analysis. Quantitative data were obtained from independent experiments and represented as the mean ± SD or standard errors of the mean (SEM). Statistical analysis was carried out by two-way analysis of variance (ANOVA) or Student's *t*-test with PRISM software (GraphPad, San Diego, CA). Differences with a *p* value of <0.05 were considered statistically significant.

RESULTS

Overall Properties of Esc Peptide-Loaded Nanoparticles. NPs encapsulating either Esc(1-21) (Esc_NPs) or Esc(1-21)-1c (Esc1c_NPs) were successfully achieved by a modified emulsion/solvent diffusion technique. To quantify the amount of NPs transported through simulated lung-lining fluids or deposited throughout the NGI, fluorescently labeled

DOI: 10.1021/acs.biomac.8b01829
Biomacromolecules XXXX, XXX, XXX−XXX

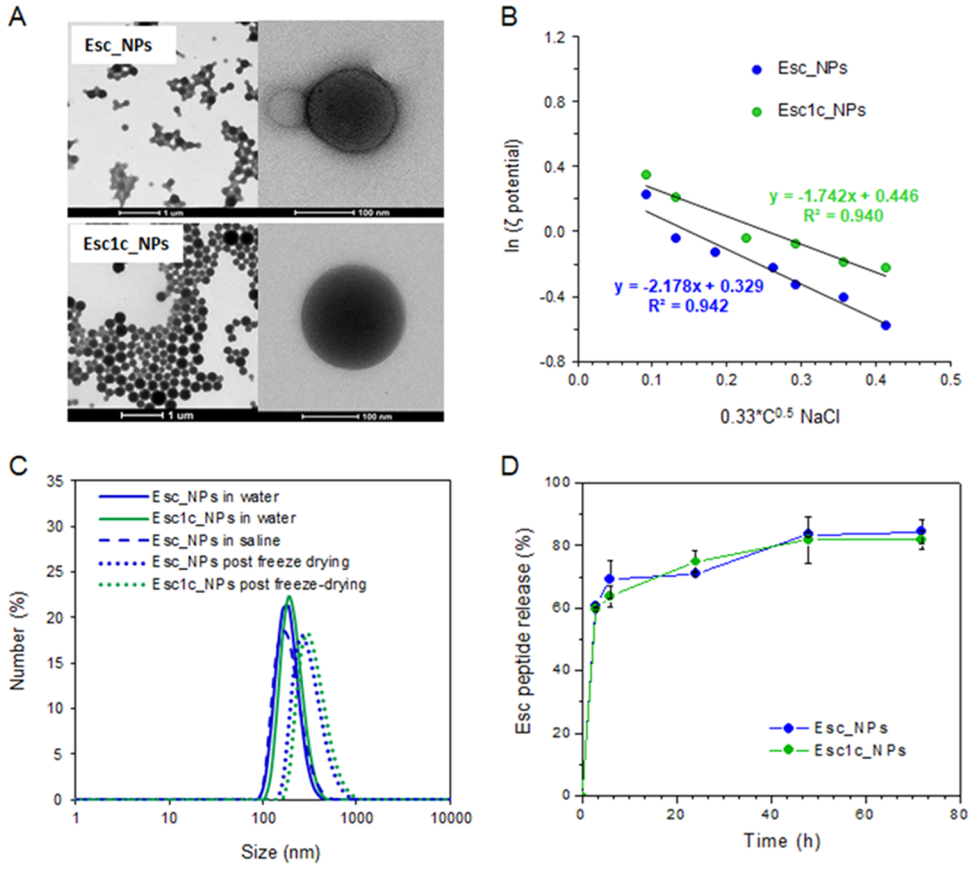

Figure 2. Overall properties of the developed Esc peptide-loaded NPs. (A) TEM images of the NPs at different magnifications (field is representative of the sample). (B) FALT measurements of the PVA shell thickness. The slopes of the linear regressions indicate the corresponding shell thickness in nanometers. (C) Size distribution by number of NPs just after production and upon reconstitution in water/saline of the trehalose-containing freeze-dried powders. (D) Release kinetics of Esc(1-21) and Esc(1-21)-1c from the corresponding NPs in PBS at pH 7.2 and 37 °C. Data are expressed as Esc peptide released (%) ± SD (n = 3).

NPs were prepared using PLGA-Rhod (i.e., Esc_Fluo-NPs and Esc1c_Fluo-NPs). For transport experiments, Rho-Esc was also employed. A sketched representation of the adopted concept is shown in Figure 1.

The overall properties of Esc peptide-loaded NPs are listed in Table 1. Regardless of the Esc peptide encapsulated, the formulation conditions allowed the achievement of NPs with a D_H lower than 300 nm, a low PDI (≤0.061), a slight negative ζ-potential, and a complete peptide entrapment.

TEM analysis confirmed a homogeneous population of spherical NPs with a mean size around 250 nm (Figure 2A, left panels). When images are taken at higher magnification (Figure 2A, right panels), a core−shell structure is suggested, especially for Esc_NPs. Nevertheless, the presence of a PVA shell on the surface of both Esc peptide-loaded NPs was confirmed by FALT measurements performed by monitoring the influence of ionic strength of the dispersing medium on particle surface charge. According to the Gouy−Chapmann theory, the ζ-potential decreased with increasing of the ionic strength of the medium (Figure 2B). Data fitting by linear regression indicates that a shell around 2 nm (1.74−2.18 nm) is formed on the surface of the NPs, independently on the encapsulated peptide.

The possibility to produce long-term stable nanoparticle-based dry powders by freeze-drying the NP dispersion in the presence of the cryoprotectant THR to be reconstituted in water for aerosolization was also investigated. Of note, DLS measurements performed upon dissolution of THR in water indicated no significant variation of D_H and PDI (≤0.1) of the resulting NP dispersion with respect to the control fresh nanosuspensions (Figure 2C). The NP ζ-potential remained substantially unchanged upon freeze-drying as well (data not shown). Conceiving this system for aerosolization, the effect of saline on NP size was also investigated. Of note, no significant change in Esc_NPs size was observed (Figure 2C). Similar results were achieved with Esc1c_NPs in saline (data not shown). Neither the addition of PLGA-Rhod nor the use of Rho-Esc affected NP size and surface properties (data not shown), which are known to govern NP interactions with lung-lining fluids and their aerosolization properties.

Results of in vitro release kinetics studies in PBS (pH 7.2) and 37 °C are shown in Figure 2D as a percentage of Esc peptide released along the time. Both NP formulations displayed a typical biphasic release profile with an initial burst (about 60% of the encapsulated amount released in 3 h) followed by a controlled release of the peptide lasting for about 3 days.

In Vitro Interactions of NPs with Mucin and Alginates. The interactions of Esc peptide-loaded NPs (both Esc_NPs and Esc1c_NPs) with mucin, the main component of airway mucus, were investigated by measuring the scattering at 650 nm (ABS) of a NP dispersion in mucin over time.[35] Whereas the ABS of the reference mucin dispersion was always around zero (0.020−0.025 arbitrary

DOI: 10.1021/acs.biomac.8b01829
Biomacromolecules XXXX, XXX, XXX−XXX

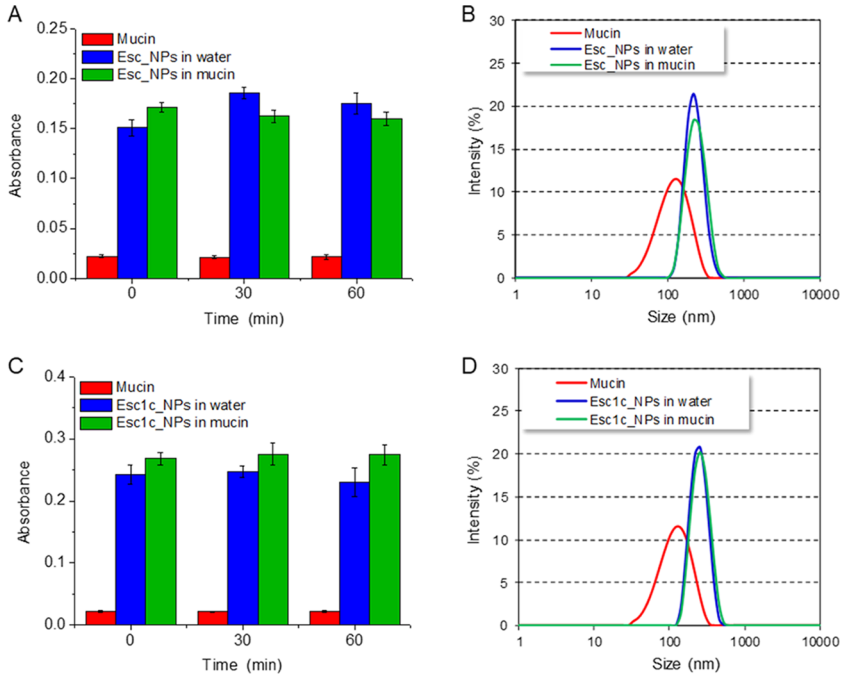

Figure 3. In vitro evaluation of mucin interactions with Esc peptide-loaded NPs. (A–C) Scattering at 650 nm of Esc_NPs and Esc1c_NPs (1 mg/mL) in the presence of mucin over time. Scattering at 650 nm of mucin and Esc peptide-loaded NP dispersion in water are evaluated as controls. Results are from three independent experiments and represented as the mean ± SD. (B–D) Size distribution by intensity of Esc_NPs and Esc1c_NPs (1 mg/mL) in the presence of mucin evaluated by DLS. The size distribution profiles of mucin and Esc peptide-loaded NP dispersion in water are reported as control.

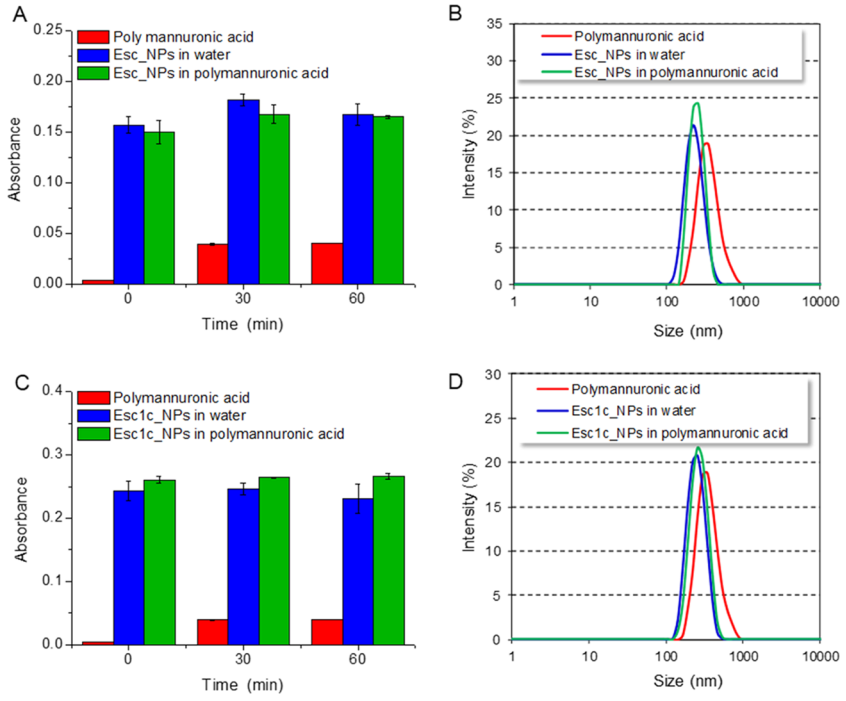

Figure 4. In vitro evaluation of Esc peptide-loaded NP interactions with polymannuronic acid. (A–C) Scattering at 650 nm of Esc_NPs and Esc1c_NPs (1 mg/mL) in the presence of polymannuronic acid over time. Scattering at 650 nm of the polymer dispersion and Esc peptide-loaded NP dispersion in water are reported as controls. Results are from three independent experiments and represented as the mean ± SD. (B–D) Size distribution by intensity of Esc_NPs and Esc1c_NPs (1 mg/mL) in the presence of polymannuronic acid evaluated by DLS. The size distribution profiles of polymannuronic acid and Esc peptide-loaded NP dispersion in water are reported as controls.

units), higher values of ABS were achieved at each time point upon NP addition. In each case, no differences in the ABS values for NP dispersions in water and in mucin were observed up to 1 h (Figure 3A–C). This result was confirmed by DLS analysis of Esc peptide-loaded NPs in the presence of mucin, indicating no change in the size distributions of NPs when mucin was added to the NP dispersion (Figure 3B–D).

DOI: 10.1021/acs.biomac.8b01829
Biomacromolecules XXXX, XXX, XXX–XXX

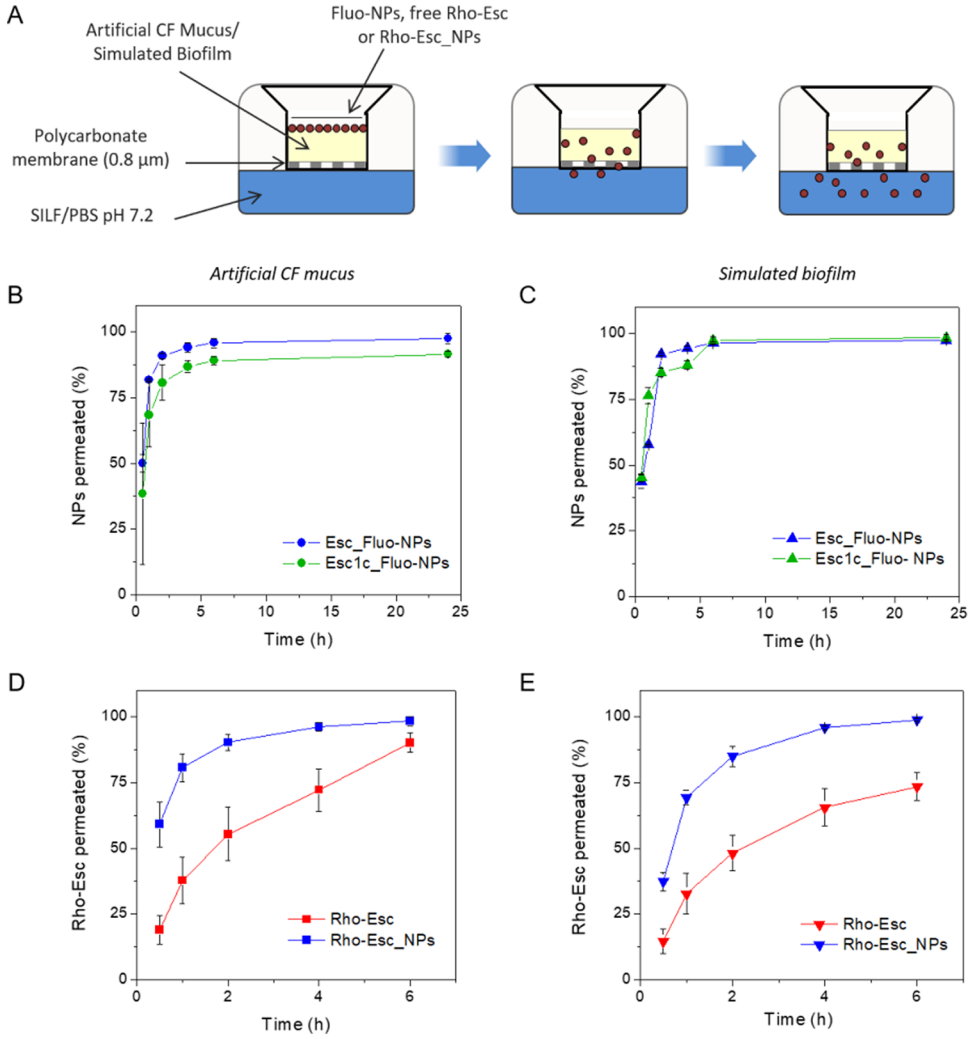

Figure 5. Transport of Esc peptide-loaded fluorescent NPs through artificial CF mucus and simulated bacterial extracellular matrix was evaluated by the Transwell multiplate assay: (A) Schematic drawing of the experimental setup; (B–C) percent of Esc peptide-loaded Fluo-NPs diffused through the artificial mucus layer and the simulated bacterial matrix as a function of time; (D, E) percent of Rho-Esc (either in the free or encapsulated form) diffused through the artificial mucus layer and the simulated bacterial extracellular matrix along the time. Results are represented as the mean ± SD calculated from three different batches (n = 6).

Considering the ability of *P. aeruginosa* to produce biofilm, where extracellular matrix is mainly based on bacterial alginates, the interactions of NPs with these polysaccharides, and, in particular, with nonacetylated polymannuronic acid detached from bacteria, were also evaluated as described for mucin interaction studies (Figure 4). Again, both NP scattering at 650 nm (Figure 4A–C) and NP size distribution by intensity were not affected by polymannuronic acid (Figure 4B–D).

In Vitro Transport of NPs through Simulated Mucus and Bacterial Extracellular Matrix Models. The ability of NPs to diffuse across artificial CF mucus or simulated bacterial extracellular matrix was also evaluated by a modified Transwell multiplate assay (Figure 5A).[35]

Regardless of the encapsulated Esc peptide, NPs easily diffused across the artificial mucus layer. After 1 h, NP percentages as high as 80 and 70%, for Esc_Fluo-NPs and Esc1c_Fluo-NPs, respectively, were found in the acceptor medium (Figure 5B). Similar percentages of NPs permeated through simulated bacterial extracellular matrix, being around 68% after 1 h for both Esc_Fluo-NPs and Esc1c_Fluo-NPs (Figure 5C). After 6 h, all NPs deposited on the donor medium were found in the acceptor compartment.

To confirm the ability of NPs to assist the diffusion of the entrapped Esc peptide through mucus and alginates, studies were performed also with NPs containing labeled Rho-Esc and the results were compared to those of free Rho-Esc (Figure 5D,E). After depositing the same amount of Rho-Esc on the artificial mucus layer, the percent of Rho-Esc permeated through the medium after 1 h was 2-fold higher in the case of nanoencapsulated Rho-Esc compared with the free molecule (80.7 versus 37.8% for Rho-Esc_NPs and Rho-Esc, respectively) (Figure 5D). Similarly, the percent of Rho-Esc permeated through the simulated bacterial extracellular matrix after 1 h doubled when the peptide was entrapped inside NPs (69.4 versus 32.7% for Rho-Esc_NPs and Rho-Esc, respectively) (Figure 5E). About 100% of the initial amount of Rho-Esc diffused in PBS in 6 h, as observed for Esc_Fluo-NPs. On the other hand, the free peptide seemed to be partially trapped by alginate, with the percentage of Rho-Esc in PBS after 6 h as low as 73.5% (Figure 5E).

DOI: 10.1021/acs.biomac.8b01829
Biomacromolecules XXXX, XXX, XXX–XXX

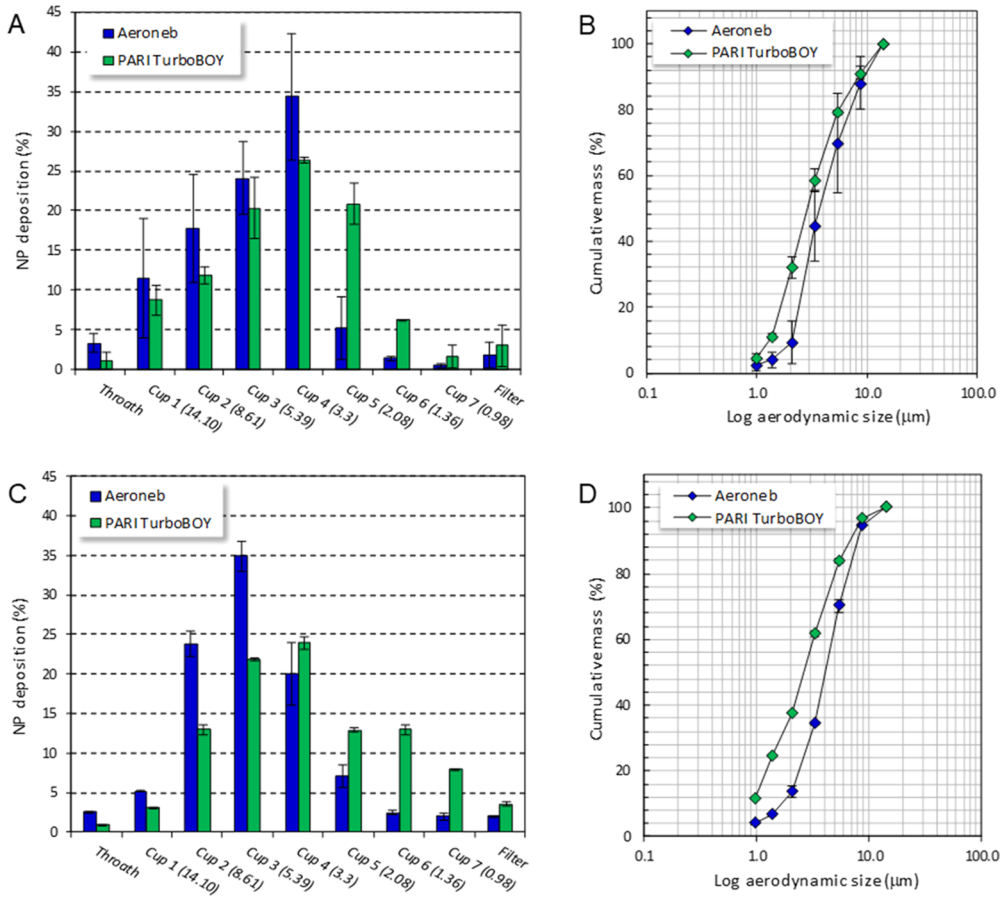

Figure 6. In vitro aerosol performance of Esc peptide-loaded NPs upon delivery through the Aeroneb Go or PARI TurboBOY nebulizers. (A–C) NGI deposition pattern of Esc_Fluo-NPs and Esc1c_Fluo-NPs, respectively; (B–D) Cumulative mass of particle recovered as a function of the cutoff diameter of the NGI stages of Esc_Fluo-NPs and Esc1c_Fluo-NPs, respectively. Results are represented as the mean ± SD calculated from three different batches (n = 6).

Table 2. Fine Particle Characteristics of the Aerosol Clouds Obtained upon Delivery of Esc Peptide-Loaded NPs through the Two Nebulizer Systems[a]

formulation	nebulizer	MMADexp (μm ± SD)	GSD (±SD)	FPF (% ± SD)	RF (% ± SD)
Esc_Fluo-NPs	aeroneb	3.89 ± 0.35	2.40 ± 2.16	27.6 ± 5.6	65.6 ± 17.1
	PARI TurboBOY	3.14 ± 0.08	2.40 ± 0.06	36.9 ± 1.5	75.2 ± 2.4
Esc1c_Fluo-NPs	aeroneb	3.79 ± 0.06	2.27 ± 0.01	29.1 ± 0.7	66.4 ± 1.9
	PARI TurboBOY	2.66 ± 0.01	2.58 ± 0.01	41.0 ± 0.1	79.6 ± 0.9

[a]MMADexp = experimental mass median aerodynamic diameter; GSD = geometrical standard deviation; FPF = fine particle fraction; RF = respirable fraction.

In Vitro Aerosol Performance of NPs. In view of a possible usage of the NPs as inhaled formulations for nebulization, the aerosolization properties of Esc peptide-loaded NPs were investigated in vitro by a Next Generation Impactor (NGI), in line with the *Comité Européen de Normalization* standard methodology for nebulizer systems. Results after delivery from the Aeroneb Go vibrating mesh nebulizer and the PARI TurboBoy jet nebulizer are reported in Figure 6.

When the NGI is operated at 15 L/min without the preseparator and with an internal filter below the MOC, the seven cups produce cutoff diameters in the range 14.1–0.98 μm (Figure 6A,C). The deposition patterns of Esc_Fluo-NPs and Esc1c_Fluo-NPs throughout the NGI cups are shown in Figure 6A,C, respectively. In both cases, very low percentages of NPs were deposited in the throat and cup 1 (always lower than 8% of the emitted dose), with 68–80% of the emitted dose recovered from Cups 3–7 ($MMAD_{exp}$ < 5.39 μm). Nevertheless, differences were apparent between the jet nebulizer and the Aeroneb Go vibrating mesh nebulizer. The cumulative droplet size distributions of the NP dose emitted after aerosolization from the nebulizers are depicted in Figure 6B,D. The best fit line was from logarithmic linear regression (r^2 > 0.96). As expected, by the same value of GSD, both Esc peptide-loaded NP formulations displayed a lower $MMAD_{exp}$ and, consequently, higher FPF and RF values when delivered through the PARI TurboBOY nebulizer compared with the Aeroneb Go (Table 2).

In Vitro Antimicrobial Activity of Esc Peptide-Loaded NPs. The antimicrobial activity of Esc peptide-loaded NPs was evaluated in vitro by monitoring the growth of the reference strain *P. aeruginosa* ATCC 27853 at 37 °C. Their

DOI: 10.1021/acs.biomac.8b01829
Biomacromolecules XXXX, XXX, XXX–XXX

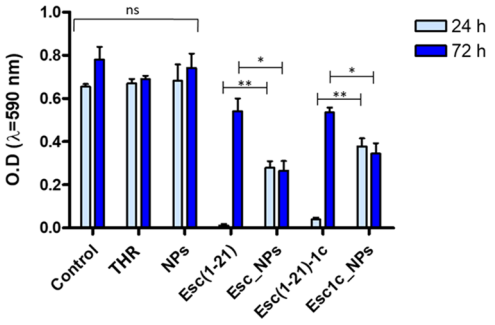

Figure 7. Effect of free Esc peptides, THR, Esc_NPs, Esc-1c_NPs, and unloaded NPs on the growth of *P. aeruginosa* ATCC 27853 (expressed as OD) after 24 and 72 h treatments in comparison with the control sample (untreated bacterial cells). Results are from three independent experiments and represented as the mean ± SEM. The level of statistical significance between groups was evaluated by the two ANOVA tests as follows: *, $p < 0.05$; **, $p < 0.01$; ns, not significant.

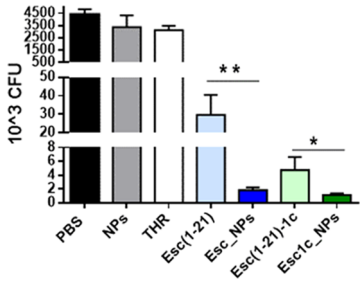

Figure 8. Comparison among unloaded NPs, THR, Esc peptides, and peptides-loaded NPs (final peptide concentration, 0.1 mg/kg) on the CFU numbers of *P. aeruginosa* in mouse lungs (BAL+ lung tissue homogenate) at 36 h after lung infection. Animals were i.t. inoculated with ~3×10^6 PAO1 cells. All formulations were i.t. administered 1 h after the bacterial challenge. The amount of unloaded NPs or THR was the same as that present in Esc peptide-loaded NPs. Results are from three independent experiments and represented as the mean ± SEM with $n = 5-6$ mice per treatment group. The mean of peptide-treated infected mice versus animals treated with the corresponding peptide-loaded NPs was compared by the *t*-test. The levels of statistical significance are *p* values of <0.05 (*) and <0.01 (**).

antipseudomonal potency was compared to that of the free peptides, the unloaded NPs, the cryoprotectant used for freeze-drying of NPs, i.e., THR, and untreated cells (control). As reported in Figure 7, the growth inhibitory activity of the free peptides was highly potent within a short time (24 h) but it was partially lost after 72 h (from ~97% growth inhibition after 1 day to ~38% inhibition after 3 days). In contrast, despite Esc peptide-loaded NPs showed a lower antibacterial activity than that of the free soluble Esc peptides at the shorter time (24 h); they were able to constantly preserve the inhibition of bacterial growth (~60% inhibition) up to 72 h. In comparison, no antimicrobial activity was displayed by the unloaded NPs or THR.

Efficacy of Esc Peptide-Loaded Nanoparticles in a Mouse Model of Acute *P. aeruginosa* Lung Infection. In the light of the promising in vitro antimicrobial activity, the therapeutic potential of the developed Esc peptide-loaded NPs was further investigated in vivo, in a mouse model of acute *P. aeruginosa* lung infection. A peptide concentration of 0.1 mg/kg, which was previously found to reduce lung bacterial burden in a mouse model after 24 h from *P. aeruginosa* infection,[17] was used. Samples were i.t. instilled 1 h after the bacterial challenge, and the number of CFUs in BAL and lung homogenate was determined at a longer term (i.e., 36 h) after administration of *Pseudomonas* cells.

We first excluded any intrinsic antimicrobial activity of unloaded NPs or the inert carrier employed for freeze-drying, i.e., THR. As indicated in Figure 8, no appreciable alteration in the number of bacterial cells was found upon treatment with NPs or THR in comparison with PBS-treated control animals. In contrast, lung bacterial burden was reduced to ~3×10^4 and ~4.7×10^3 bacterial cells by Esc(1-21) and Esc(1-21)-1c, respectively, 36 h after lung infection. Nevertheless, when Esc-loaded NPs were i.t. instilled, the total lung bacterial burden was significantly lowered (more than 3-log reduction compared with PBS-treated infected animals; $p < 0.0001$), 36 h after infection. The total number of CFU (lung homogenate + BAL) dropped down to ~1.8×10^3 and ~1.1×10^3 after treatment with Esc_NPs and Esc1c_NPs (Figure 8), respectively, compared with the number of CFU in PBS-treated infected animals (~4.4×10^6). Remarkably, this antimicrobial activity was ~17-fold or ~4-fold stronger than that displayed when the same concentration of free soluble Esc(1-21) or Esc(1-21)-1c was i.t. administered (Figure 8).

Effect of Nanoparticles on Immune Response and Pulmonary Toxicity in Healthy Mice. To investigate the impact of NPs loaded or not with each peptide (with a dosage of 0.1 mg/kg) on lung inflammation at the time point used for evaluation of antimicrobial activity, we assessed the recruitment of inflammatory cells into the lung lumen of healthy mice, 36 h after i.t. instillation of samples. The total number of BAL cells was determined. The effect of THR alone was also included. As previously found for each individual peptide,[17] the exposure to the polymeric NPs as well as to THR did not significantly change the total number of cells recovered from BAL, compared with vehicle control of PBS-treated mice (Figure 9), highlighting that NPs do not induce any proinflammatory effect. A slight increase in the number of inflammatory cells was only noted for the Esc_NPs (Figure 9). There was no significant change regarding the expression of

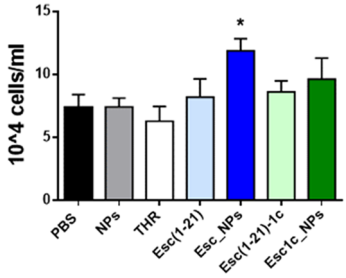

Figure 9. In vivo effect of unloaded NPs and Esc peptide-loaded NPs (final peptide concentration, 0.1 mg/kg) on total inflammatory cell numbers in healthy mouse lungs, 36 h after their i.t. administration, compared with the lungs from the vehicle control PBS-treated mice. The cell numbers in the BAL, 36 h after i.t. instillation of peptides in their soluble free form (0.1 mg/kg) or THR were included for comparison. The amount of unloaded NPs or THR was the same as that present in Esc peptide-loaded NPs. Results are from three independent experiments and represented as the mean ± SEM with $n = 5-6$ mice per treatment group. The mean of the PBS vehicle control group was compared by the *t*-test to all other treatment groups. The levels of statistical significance are *p* values of <0.05 (*).

DOI: 10.1021/acs.biomac.8b01829
Biomacromolecules XXXX, XXX, XXX−XXX

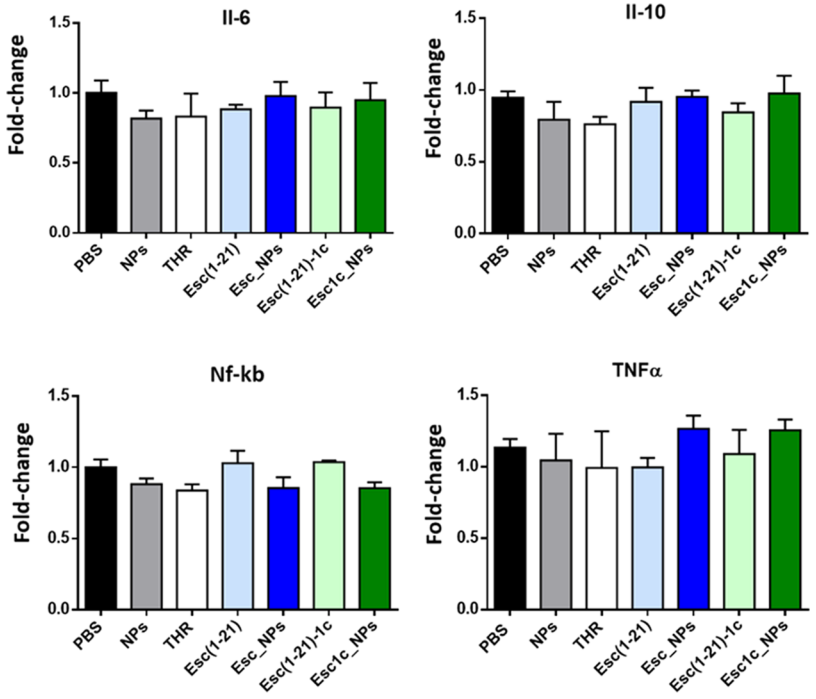

Figure 10. In vivo expression of different inflammatory genes in the lungs of healthy mice 36 h after i.t. instillation of unloaded NPs or Esc peptide-loaded NPs (peptide concentration of 0.1 mg/kg) compared with the PBS vehicle control mice. Mice i.t. instilled with free peptides or THR alone were used for comparison. The amount of unloaded NPs or THR was the same as that present in Esc peptide-loaded NPs. Results are from three independent experiments and represented as the mean ± SEM with n = 5−6 mice per treatment group. No statistical significance among groups.

inflammation-associated genes (including IL-6, IL-10, or the tumor necrosis factor-α TNF-α and NF-κB) in the lungs of treated mice at 36 h after instillation of all formulations (Figure 10). These results indicate a safe use of our NPs for AMP delivery at lungs. Note also that these findings were supported by the invariant production of the proinflammatory cytokine IL-6 at the protein level, in the BAL of mice at 36 h after i.t. administration of the peptides or their encapsulated form, compared with healthy mice receiving PBS as the vehicle control (Figure S1). TNF-α expression was too low to be detected (under the ELISA detection limit) and therefore was not plotted. Furthermore, no significant changes in the production of IL-6 and TNF-α were also observed in the BAL of infected mice, after treatment with either each tested peptide in its soluble free form or peptide-loaded NPs (Figure S2).

DISCUSSION

In recent years, encapsulation of AMPs inside nanoparticles has emerged as a promising overture to circumvent some of the major drawbacks to their appearance on the market. Indeed, polymeric nanoparticles can (i) enhance peptides' bioavailability by protecting them from enzymatic degradation, (ii) reduce AMPs' cytotoxic effect by masking their interaction with extracellular components, and (iii) optimize peptides' translocation to specific airway tissue/cell.[43] As far as lung infections are concerned, pulmonary delivery of nanoparticles represents an ideal strategy for direct administration of AMPs at lungs, thus overcoming poor patient adherence to the therapy and systemic side effects related to intravenous administration.[30] Nevertheless, the identification of appropriate physicochemical properties of inhaled nanoparticles is imperative to increase their residence time in the lungs without being entrapped in the negatively charged bronchial mucus.

In this work, we successfully designed PVA-engineered PLGA nanoparticles (NPs) for effective encapsulation and controlled release of the frog-skin-derived peptide Esc(1-21) or its diastereomer Esc(1-21)-1c. The incorporation into the carrier system of a hydrophilic shell (PVA) was attempted to reduce the adhesion of the hydrophobic PLGA to airway mucus and alginates.[44−46] According to the experimental procedure followed for NP preparation, PVA is adsorbed on the surface of PLGA, forming an interconnected network with the polymer at the interface.[47]

Meanwhile, an appropriate cryoprotectant (THR) was selected to produce a stable dry product, that is, lyophilized NPs, to be reconstituted in the appropriate medium before nebulization. The freeze-drying conditions let us obtain stable lyophilized NPs, with preserved nanostructure integrity (i.e., nanoparticle size and ζ-potential upon redispersion in aqueous media), a crucial aspect for drug delivery applications.[48] The aqueous dispersion of NPs displayed very promising aerosolization properties, indicating that the formulation well fits a liquid jet nebulizer already available to the patients, i.e., PARI TurboBOY, allowing NP administration and deposition at lungs.

However, for airway mucus penetration, the influence of nanoparticle size and surface needs to be considered. Mucus acts as a physical filtering barrier for particles with a bigger size than the mesh-spacing of the mucin network.[49] Similarly, the mesh size of the bacterial extracellular matrix seems to be the major factor playing a role in the selection of particles able to get through such a barrier.[50] The pore size in airway mucus gels from CF sufferers has been estimated to range from 100 to 400 nm using electron microscopy.[51] The mean hydrodynamic diameter of the present NPs, along with the hydrophilic surface, will likely assist their diffusion through lung mucus. Furthermore, surface engineering of PLGA nanoparticles with

DOI: 10.1021/acs.biomac.8b01829
Biomacromolecules XXXX, XXX, XXX−XXX

partially hydrolyzed grade PVA resulted in an almost neutral ζ-potential, making NPs inert toward the negatively charged mucin, the main component of airway mucus, and alginate, an important molecule for *P. aeruginosa* biofilm formation.[52,53] In fact, our results confirmed the ability of NPs to diffuse through an artificial mucus layer and/or a simulated bacterial barrier without interacting with the major components of the lung mucus or the extracellular matrix of *P. aeruginosa* biofilm communities. Results are in line with those of Popov and colleagues, which highlighted how coating with PVAs that are less than 95% hydrolyzed may aid nanoparticle penetration through mucus.[54] We also previously observed that PVA-engineered PLGA nanoparticles assisted colistin transport through artificial mucus and promoted nanoparticle penetration inside *P. aeruginosa* biofilm.[35]

Importantly, Esc peptide-loaded NPs displayed a prolonged in vitro antimicrobial activity against *P. aeruginosa*, compared with the free peptide. According to the kinetics of peptide release in aqueous environment, the initial burst would act as an attack dose to inhibit the growth of a consistent number of bacterial cells. Afterward, the gradual release of the peptide over time would be enough to maintain a constant concentration of the peptide at the site of action, prolonging its antibacterial activity in comparison with the free peptides. This would explain the higher antimicrobial activity of peptide-loaded NPs in the long term, in comparison with the free peptide counterparts.

Remarkably, our in vitro findings well correlate with the in vivo efficacy data showing a significantly lower lung bacterial burden (3-log reduction of CFU compared with vehicle-treated infected animals), after i.t. instillation of Esc peptide-loaded NPs than that found when nonencapsulated peptides were used. A more potent (∼2-fold higher) efficacy in killing *Pseudomonas* was exhibited by Esc1c_NPs in comparison with the all-L peptide-loaded NPs, presumably due to the higher in vivo biostability of Esc(1-21)-1c and its gradual accumulation effect, once released from the NPs.

Notably, a 17-fold or 4-fold reduction in the number of lung *Pseudomonas* cells was determined by Esc_NPs or Esc1c_NPs, compared with the bacterial clearance following i.t. instillation of the corresponding peptides in their soluble free form. The more pronounced difference in the total number of lung CFU after treatment with the free Esc(1-21) and its encapsulated form, compared with CFU values obtained when Esc(1-21)-1c and Esc1c_NPs were administered, is reasonable, considering the higher resistance of the free diastereomer to lung proteases (e.g., elastase).[15] This would lengthen their residence time/antimicrobial activity with respect to that of the free all-L Esc(1-21) that may be quickly degraded, leading to a higher number of surviving bacteria. Overall, the results of the current in vivo efficacy studies have contributed to emphasize the effectiveness of the produced NPs in protecting the encapsulated drug as well as in protracting and potentiating their therapeutic efficacy. Moreover, in vivo toxicity data have suggested that our NPs can be safely used in vivo, as no pathophysiological conditions were observed in healthy mice at the same time point selected for the evaluation of their in vivo antimicrobial efficacy. This is in line with the growing body of the literature supporting the safety of PLGA for lung delivery.[28,55,56] To the best of our knowledge, this is the first report showing an improved in vivo therapeutic efficacy of AMP-loaded PLGA nanoparticles, upon pulmonary delivery for treatment of bacterial lung infections.

CONCLUSIONS

Fundamental achievements for development of advanced nanocarriers for AMP delivery at lungs encompass the following: (i) efficient encapsulation of the peptide in its integer form, (ii) nebulization of the formulation in units suitable for alveolar deposition, (iii) improved penetration across mucus and bacterial barriers to guide the peptide to the site of action upon simple treatment regimens, and (iv) a controlled release to keep constant the drug level in the lung environment for extended periods of time. Here, engineered PLGA nanoparticles effectively entrapping therapeutically relevant AMPs have been successfully developed. Because of their optimal size, morphology, and neutral/hydrophilic surface, the developed NPs are aerosolizable and do not have mucoadhesive properties nor do they interact with components of the extracellular matrix of *Pseudomonas* biofilm, i.e., polymannuronic acid, which can prevent NPs from reaching the target bacterial cells. Importantly, encapsulation of AMPs in NPs resulted in improved activity of AMPs against *P. aeruginosa*, both in vitro and in vivo likely due to peptide protection and gradual release over time. In summary, our data provide the first evidence of the success of PVA-engineered PLGA nanoparticles as valuable nanocarriers to assist the delivery of AMPs in the conductive airways as well as to extend and increase their therapeutic effect against *P. aeruginosa* lung infections compared with AMPs in their free soluble form.

ASSOCIATED CONTENT

Supporting Information

The Supporting Information is available free of charge on the ACS Publications website at DOI: 10.1021/acs.biomac.8b01829.

Histograms showing the production of the proinflammatory cytokine IL-6 in the BAL of healthy mice (Figure S1) and the production of IL-6 and TNF-α in the BAL of mice after infection (Figure S2) (PDF)

AUTHOR INFORMATION

Corresponding Authors

*E-mail: francesca.ungaro@unina.it (F.U.).

*E-mail: marialuisa.mangoni@uniroma1.it. Phone: +39 0649917693 (M.L.M.).

ORCID

Fabiana Quaglia: 0000-0001-6223-0782

Maria Luisa Mangoni: 0000-0002-5991-5868

Author Contributions

#B.C. and I.d. contributed equally to this work.

Author Contributions

The manuscript was written through contributions of all authors. All authors have given approval to the final version of the manuscript.

Notes

The authors declare no competing financial interest.

ACKNOWLEDGMENTS

This work was supported by grants from Sapienza University of Rome (Research Project 2018, N. RM11816436113D8A) and the Italian Cystic Fibrosis Foundation (project FFC #15/2017 Adopted by Delegations of Palermo, Vittoria, Ragusa, Siracusa, Catania Mascalucia, Messina, Gruppo di Sostegno di Tremestieri). Dr. Floriana Cappiello is grateful to Pasteur-Italia

DOI: 10.1021/acs.biomac.8b01829
Biomacromolecules XXXX, XXX, XXX−XXX

Istituto Fondazione Cenci Bolognetti, as a postdoctoral fellow holder of this Institute. Dr. Gemma Conte is an Italian Cystic Fibrosis Foundation fellowship holder (Project FFC #23/2017). This work was also supported by NIH Awards (R01 HL-125128 and AI-133351).

■ ABBREVIATIONS

AMP, antimicrobial peptide; BAL, bronchoalveolar lavage; CF, cystic fibrosis; DLS, dynamic light scattering; D_H, hydrodynamic diameter; DTPA, diethylenetriaminepentaacetic acid; ED, emitted dose; ELISA, enzyme-linked immunosorbent assay; ELS, electrophoretic light scattering; Esc_ Fluo-NPs, rhodamine-labeled NPs loaded with Esc(1-21); Esc1c_Fluo-NPs, rhodamine-labeled NPs loaded with Esc(1-21)-1c; FPF, fine particle fraction; GSD, geometric standard deviation; $MMAD_{exp}$, median aerodynamic diameter; MOC, micro-orifice collector; NGI, Next Generation Impactor; NPs, PVA-engineered PLGA nanoparticles; OD, optical density; PDI, polydispersity index; PLGA, poly(lactide-*co*-glycolide); PLGA-Rhod, rhodamine-labeled PLGA; PVA, poly(vinyl alcohol); RF, respirable fraction; Rho-Esc, rhodamine-labeled Esc peptides; Fluo-NPs, fluorescent NPs; RP-HPLC, reverse-phase high-performance liquid chromatography; SILF, simulated interstitial lung fluid; THR, trehalose

■ REFERENCES

(1) Bjarnsholt, T.; Jensen, P. O.; Fiandaca, M. J.; Pedersen, J.; Hansen, C. R.; Andersen, C. B.; Pressler, T.; Givskov, M.; Hoiby, N. *Pseudomonas aeruginosa* biofilms in the respiratory tract of cystic fibrosis patients. *Pediatr. Pulmonol.* **2009**, *44*, 547−558.

(2) Sorde, R.; Pahissa, A.; Rello, J. Management of refractory *Pseudomonas aeruginosa* infection in cystic fibrosis. *Infect. Drug Resist.* **2011**, *4*, 31−41.

(3) Bhagirath, A. Y.; Li, Y.; Somayajula, D.; Dadashi, M.; Badr, S.; Duan, K. Cystic fibrosis lung environment and *Pseudomonas aeruginosa* infection. *BMC Pulm. Med.* **2016**, *16*, No. 174.

(4) Ciofu, O.; Tolker-Nielsen, T.; Jensen, P. O.; Wang, H.; Hoiby, N. Antimicrobial resistance, respiratory tract infections and role of biofilms in lung infections in cystic fibrosis patients. *Adv. Drug Delivery Rev.* **2015**, *85*, 7−23.

(5) Cabot, G.; Zamorano, L.; Moya, B.; Juan, C.; Navas, A.; Blazquez, J.; Oliver, A. Evolution of *Pseudomonas aeruginosa* antimicrobial resistance and fitness under low and high mutation rates. *Antimicrob. Agents Chemother.* **2016**, *60*, 1767−1778.

(6) Drenkard, E.; Ausubel, F. M. *Pseudomonas* biofilm formation and antibiotic resistance are linked to phenotypic variation. *Nature* **2002**, *416*, 740−743.

(7) Stewart, P. S.; Costerton, J. W. Antibiotic resistance of bacteria in biofilms. *Lancet* **2001**, *358*, 135−138.

(8) Taylor, P. K.; Y eung, A. T.; Hancock, R. E. Antibiotic resistance in *Pseudomonas aeruginosa* biofilms: towards the development of novel anti-biofilm therapies. *J. Biotechnol.* **2014**, *191*, 121−130.

(9) Mahlapuu, M.; Hakansson, J.; Ringstad, L.; Bjorn, C. Antimicrobial peptides: An emerging category of therapeutic agents. *Front. Cell. Infect. Microbiol.* **2016**, *6*, No. 194.

(10) Hamley, I. W. Small bioactive peptides for biomaterials design and therapeutics. *Chem. Rev.* **2017**, *117*, 14015−14041.

(11) Luca, V.; Stringaro, A.; Colone, M.; Pini, A.; Mangoni, M. L. Esculentin(1-21), an amphibian skin membrane-active peptide with potent activity on both planktonic and biofilm cells of the bacterial pathogen *Pseudomonas aeruginosa*. *Cell. Mol. Life Sci.* **2013**, *70*, 2773−2786.

(12) Casciaro, B.; Cappiello, F.; Cacciafesta, M.; Mangoni, M. L. Promising approaches to optimize the biological properties of the antimicrobial peptide Esculentin-1a(1-21)NH_2: Amino acids substitution and conjugation to nanoparticles. *Front. Chem.* **2017**, *5*, No. 26.

(13) Casciaro, B.; Dutta, D.; Loffredo, M. R.; Marcheggiani, S.; McDermott, A. M.; Willcox, M. D.; Mangoni, M. L. Esculentin-1a derived peptides kill *Pseudomonas aeruginosa* biofilm on soft contact lenses and retain antibacterial activity upon immobilization to the lens surface. *Biopolymers* **2017**, No. e23074.

(14) Di Grazia, A.; Cappiello, F.; Cohen, H.; Casciaro, B.; Luca, V.; Pini, A.; Di, Y. P.; Shai, Y.; Mangoni, M. L. D-Amino acids incorporation in the frog skin-derived peptide esculentin-1a(1-21)NH_2 is beneficial for its multiple functions. *Amino Acids* **2015**, *47*, 2505−2519.

(15) Cappiello, F.; Di Grazia, A.; Segev-Zarko, L. A.; Scali, S.; Ferrera, L.; Galietta, L.; Pini, A.; Shai, Y.; Di, Y. P.; Mangoni, M. L. Esculentin-1a-derived peptides promote clearance of *Pseudomonas aeruginosa* internalized in bronchial cells of cystic fibrosis patients and lung cell migration: Biochemical properties and a plausible mode of action. *Antimicrob. Agents Chemother.* **2016**, *60*, 7252−7262.

(16) Trinh, N. T.; Bardou, O.; Prive, A.; Maille, E.; Adam, D.; Lingee, S.; Ferraro, P.; Desrosiers, M. Y.; Coraux, C.; Brochiero, E. Improvement of defective cystic fibrosis airway epithelial wound repair after CFTR rescue. *Eur. Respir. J.* **2012**, *40*, 1390−1400.

(17) Chen, C.; Mangoni, M. L.; Di, Y. P. In vivo therapeutic efficacy of frog skin-derived peptides against *Pseudomonas aeruginosa*-induced pulmonary infection. *Sci. Rep.* **2017**, *7*, No. 8548.

(18) Boegh, M.; Nielsen, H. M. Mucus as a barrier to drug delivery - understanding and mimicking the barrier properties. *Basic Clin. Pharmacol. Toxicol.* **2015**, *116*, 179−186.

(19) Lim, Y. H.; Tiemann, K. M.; Hunstad, D. A.; Elsabahy, M.; Wooley, K. L. Polymeric nanoparticles in development for treatment of pulmonary infectious diseases. *Wiley Interdiscip. Rev.: Nanomed. Nanobiotechnol.* **2016**, *8*, 842−871.

(20) Moreno-Sastre, M.; Pastor, M.; Salomon, C. J.; Esquisabel, A.; Pedraz, J. L. Pulmonary drug delivery: a review on nanocarriers for antibacterial chemotherapy. *J. Antimicrob. Chemother.* **2015**, *70*, 2945−2955.

(21) Dombu, C. Y.; Betbeder, D. Airway delivery of peptides and proteins using nanoparticles. *Biomaterials* **2013**, *34*, 516−525.

(22) Kuzmov, A.; Minko, T. Nanotechnology approaches for inhalation treatment of lung diseases. *J. Controlled Release* **2015**, *219*, 500−518.

(23) Nordström, R.; Malmsten, M. Delivery systems for antimicrobial peptides. *Adv. Colloid Interface Sci.* **2017**, *242*, 17−34.

(24) Ungaro, F.; d'Angelo, I.; Coletta, C.; d'Emmanuele di Villa Bianca, R.; Sorrentino, R.; Perfetto, B.; Tufano, M. A.; Miro, A.; La Rotonda, M. I.; Quaglia, F. Dry powders based on PLGA nanoparticles for pulmonary delivery of antibiotics: modulation of encapsulation efficiency, release rate and lung deposition pattern by hydrophilic polymers. *J. Controlled Release* **2012**, *157*, 149−159.

(25) d'Angelo, I.; Quaglia, F.; Ungaro, F. PLGA carriers for inhalation: where do we stand, where are we headed? *Ther. Delivery* **2015**, *6*, 1139−1144.

(26) Debnath, S. K.; Saisivam, S.; Omri, A. PLGA ethionamide nanoparticles for pulmonary delivery: Development and in vivo evaluation of dry powder inhaler. *J. Pharm. Biomed. Anal.* **2017**, *145*, 854−859.

(27) Tang, J.; Li, J.; Li, G.; Zhang, H.; Wang, L.; Li, D.; Ding, J. Spermidine-mediated poly(lactic-co-glycolic acid) nanoparticles containing fluorofenidone for the treatment of idiopathic pulmonary fibrosis. *Int. J. Nanomed.* **2017**, *12*, 6687−6704.

(28) Semete, B.; Booysen, L.; Lemmer, Y.; Kalombo, L.; Katata, L.; Verschoor, J.; Swai, H. S. In vivo evaluation of the biodistribution and safety of PLGA nanoparticles as drug delivery systems. *Nanomedicine* **2010**, *6*, 662−671.

(29) Ventola, C. L. Progress in nanomedicine: Approved and investigational nanodrugs. *Pharm. Ther.* **2017**, *42*, 742−755.

(30) Rytting, E.; Nguyen, J.; Wang, X.; Kissel, T. Biodegradable polymeric nanocarriers for pulmonary drug delivery. *Expert Opin. Drug Delivery* **2008**, *5*, 629−639.

DOI: 10.1021/acs.biomac.8b01829
Biomacromolecules XXXX, XXX, XXX−XXX

(31) Lee, C.; Choi, J. S.; Kim, I.; Oh, K. T.; Lee, E. S.; Park, E. S.; Lee, K. C.; Youn, Y. S. Long-acting inhalable chitosan-coated poly(lactic-co-glycolic acid) nanoparticles containing hydrophobically modified exendin-4 for treating type 2 diabetes. *Int. J. Nanomed.* **2013**, *8*, 2975−2983.
(32) Ding, D.; Zhu, Q. Recent advances of PLGA micro/nanoparticles for the delivery of biomacromolecular therapeutics. *Mater. Sci. Eng., C* **2018**, *92*, 1041−1060.
(33) d'Angelo, I.; Costabile, G.; Durantie, E.; Brocca, P.; Rondelli, V.; Russo, A.; Russo, G.; Miro, A.; Quaglia, F.; Petri-Fink, A.; Rothen-Rutishauser, B.; Ungaro, F. Hybrid lipid/polymer nanoparticles for pulmonary delivery of siRNA: Development and fate upon in vitro deposition on the human epithelial airway barrier. *J. Aerosol Med. Pulm. Drug Delivery* **2018**, *31*, 170−181.
(34) El-Sherbiny, I. M.; El-Baz, N. M.; Yacoub, M. H. Inhaled nano- and microparticles for drug delivery. *Global Cardiol. Sci. Pract.* **2015**, *2015*, No. 2.
(35) d'Angelo, I.; Casciaro, B.; Miro, A.; Quaglia, F.; Mangoni, M. L.; Ungaro, F. Overcoming barriers in *Pseudomonas aeruginosa* lung infections: Engineered nanoparticles for local delivery of a cationic antimicrobial peptide. *Colloids Surf., B* **2015**, *135*, 717−725.
(36) Madani, F.; Esnaashari, S. S.; Mujokoro, B.; Dorkoosh, F.; Khosravani, M.; Adabi, M. Investigation of effective parameters on size of Paclitaxel loaded PLGA nanoparticles. *Adv. Pharm. Bull.* **2018**, *8*, 77−84.
(37) Maiolino, S.; Moret, F.; Conte, C.; Fraix, A.; Tirino, P.; Ungaro, F.; Sortino, S.; Reddi, E.; Quaglia, F. Hyaluronan-decorated polymer nanoparticles targeting the CD44 receptor for the combined photo/chemo-therapy of cancer. *Nanoscale* **2015**, *7*, 5643−5653.
(38) d'Angelo, I.; Parajo, Y.; Horvath, A.; Keri, G.; La Rotonda, M. I.; Alonso, M. J. Improved delivery of angiogenesis inhibitors from PLGA:poloxamer blend micro- and nanoparticles. *J. Microencapsulation* **2010**, *27*, 57−66.
(39) Conte, C.; Fotticchia, I.; Tirino, P.; Moret, F.; Pagano, B.; Gref, R.; Ungaro, F.; Reddi, E.; Giancola, C.; Quaglia, F. Cyclodextrin-assisted assembly of PEGylated polyester nanoparticles decorated with folate. *Colloids Surf., B* **2016**, *141*, 148−157.
(40) Moss, O. R. Simulants of lung interstitial fluid. *Health Phys.* **1979**, *36*, 447−448.
(41) Vogel, H. J.; Bonner, D. M. Acetylornithinase of *Escherichia coli*: partial purification and some properties. *J. Biol. Chem.* **1956**, *218*, 97−106.
(42) Di, Y. P. Assessment of pathological and physiological changes in mouse lung through bronchoalveolar lavage. *Methods Mol. Biol.* **2014**, *1105*, 33−42.
(43) Klinger-Strobel, M.; Lautenschlager, C.; Fischer, D.; Mainz, J. G.; Bruns, T.; Tuchscherr, L.; Pletz, M. W.; Makarewicz, O. Aspects of pulmonary drug delivery strategies for infections in cystic fibrosis–where do we stand? *Expert Opin. Drug Delivery* **2015**, *12*, 1351−1374.
(44) Huckaby, J. T.; Lai, S. K. PEGylation for enhancing nanoparticle diffusion in mucus. *Adv. Drug Delivery Rev.* **2018**, *124*, 125−139.
(45) Forier, K.; Messiaen, A. S.; Raemdonck, K.; Deschout, H.; Rejman, J.; De Baets, F.; Nelis, H.; De Smedt, S. C.; Demeester, J.; Coenye, T.; Braeckmans, K. Transport of nanoparticles in cystic fibrosis sputum and bacterial biofilms by single-particle tracking microscopy. *Nanomedicine* **2013**, *8*, 935−949.
(46) Ernst, J.; Klinger-Strobel, M.; Arnold, K.; Thamm, J.; Hartung, A.; Pletz, M. W.; Makarewicz, O.; Fischer, D. Polyester-based particles to overcome the obstacles of mucus and biofilms in the lung for tobramycin application under static and dynamic fluidic conditions. *Eur. J. Pharm. Biopharm.* **2018**, *131*, 120−129.
(47) Sahoo, S. K.; Panyam, J.; Prabha, S.; Labhasetwar, V. Residual polyvinyl alcohol associated with poly (D,L-lactide-co-glycolide) nanoparticles affects their physical properties and cellular uptake. *J. Controlled Release* **2002**, *82*, 105−114.
(48) Fonte, P.; Reis, S.; Sarmento, B. Facts and evidences on the lyophilization of polymeric nanoparticles for drug delivery. *J. Controlled Release* **2016**, *225*, 75−86.
(49) Murgia, X.; Loretz, B.; Hartwig, O.; Hittinger, M.; Lehr, C. M. The role of mucus on drug transport and its potential to affect therapeutic outcomes. *Adv. Drug Delivery Rev.* **2018**, *124*, 82−97.
(50) Forier, K.; Messiaen, A. S.; Raemdonck, K.; Nelis, H.; De Smedt, S.; Demeester, J.; Coenye, T.; Braeckmans, K. Probing the size limit for nanomedicine penetration into *Burkholderia multivorans* and *Pseudomonas aeruginosa* biofilms. *J. Controlled Release* **2014**, *195*, 21−28.
(51) Duncan, G. A.; Jung, J.; Hanes, J.; Suk, J. S. The mucus barrier to inhaled gene therapy. *Mol. Ther.* **2016**, *24*, 2043−2053.
(52) Nivens, D. E.; Ohman, D. E.; Williams, J.; Franklin, M. J. Role of alginate and its O acetylation in formation of *Pseudomonas aeruginosa* microcolonies and biofilms. *J. Bacteriol.* **2001**, *183*, 1047−1057.
(53) Hentzer, M.; Teitzel, G. M.; Balzer, G. J.; Heydorn, A.; Molin, S.; Givskov, M.; Parsek, M. R. Alginate overproduction affects *Pseudomonas aeruginosa* biofilm structure and function. *J. Bacteriol.* **2001**, *183*, 5395−5401.
(54) Popov, A.; Enlow, E.; Bourassa, J.; Chen, H. Mucus-penetrating nanoparticles made with "mucoadhesive" poly(vinyl alcohol). *Nanomedicine* **2016**, *12*, 1863−1871.
(55) Aragao-Santiago, L.; Hillaireau, H.; Grabowski, N.; Mura, S.; Nascimento, T. L.; Dufort, S.; Coll, J. L.; Tsapis, N.; Fattal, E. Compared in vivo toxicity in mice of lung delivered biodegradable and non-biodegradable nanoparticles. *Nanotoxicology* **2016**, *10*, 292−302.
(56) Dailey, L. A.; Jekel, N.; Fink, L.; Gessler, T.; Schmehl, T.; Wittmar, M.; Kissel, T.; Seeger, W. Investigation of the proinflammatory potential of biodegradable nanoparticle drug delivery systems in the lung. *Toxicol. Appl. Pharmacol.* **2006**, *215*, 100−108.

DOI: 10.1021/acs.biomac.8b01829
Biomacromolecules XXXX, XXX, XXX−XXX

PeptideScience
THE AMERICAN PEPTIDE SOCIETY JOURNAL

Special Issue: Emerging Peptide Science in Italy

Guest Editors: Dr Giancarlo Morelli (Università di Napoli "Federico II"), Prof. Paolo Rovero (Università di Firenze) and Prof. Claudio Toniolo (Università di Padova)

EDITORIAL

REVIEWS

ARTICLES

PeptideScience
THE AMERICAN PEPTIDE SOCIETY JOURNAL

Special Issue: Emerging Peptide Science in Italy

Guest Editors: Dr Giancarlo Morelli (Università di Napoli "Federico II"), Prof. Paolo Rovero (Università di Firenze) and Prof. Claudio Toniolo (Università di Padova)

Conformational properties, membrane interaction, and antibacterial activity of the peptaibiotic chalciporin A: Multitechnique spectroscopic and biophysical investigations on the natural compound and labeled analogs
Barbara Biondi, Cristina Peggion, Marta De Zotti, Chiara Pignaffo, Annalisa Dalzini, Marco Bortolus, Simona Oancea, Geta Hilma, Annalisa Bortolotti, Lorenzo Stella, Jens Z. Pedersen, Victoria N. Syryamina, Yuri D. Tsvetkov, Sergei A. Dzuba, Claudio Toniolo and Fernando Formaggio, *Peptide Science* 2018, doi: 10.1002/bip.23083

Crystallographic insights into the self-assembly of KLVFF amyloid-beta peptides
Andrea Pizzi, Valentina Dichiarante, Giancarlo Terraneo and Pierangelo Metrangolo, *Peptide Science* 2018, doi: 10.1002/bip.23088

From self-assembled peptide-ynes to peptide polyacetylenes and polydiacetylenes
Giulia Marafon, Maria Angela Motta, Claudio Toniolo and Alessandro Moretto, *Peptide Science* 2018, doi: 10.1002/pep2.24036

Synthesis and structure analysis of ferrocene-containing pseudopeptides
Gaetano Angelici, Marcin Górecki, Gennaro Pescitelli, Nicola Zanna, Magda Monari and Claudia Tomasini, *Peptide Science* 2018, doi: 10.1002/bip.23072

Insights on the structure-activity relationship of peptides derived from Sticholysin II
Aline Lima de Oliveira, Eduardo Maffud Cilli, Uris Ros, Edson Crusca Jr, María Eliana Lanio, Carlos Alvarez, Shirley Schreier, Thelma Agular Pertinhez and Alberto Spisni, *Peptide Science* 2018, doi: 10.1002/bip.23097

Structure-activity studies of peptidomimetics based on kinase-inhibitory region of suppressors of cytokine signaling 1
Sara La Manna, Laura Lopez-Sanz, Marilisa Leone, Paola Brandi, Pasqualina Liana Scognamiglio, Giancarlo Morelli, Ettore Novellino, Carmen Gomez-Guerrero and Daniela Marasco, *Peptide Science* 2018, doi: 10.1002/bip.23082

Esculentin-1a derived peptides kill Pseudomonas aeruginosa biofilm on soft contact lenses and retain antibacterial activity upon immobilization to the lens surface
Bruno Casciaro, Debarun Dutta, Maria Rosa Loffredo, Stefania Marcheggiani, Alison M McDermott, Mark DP Willcox and Maria Luisa Mangoni, *Peptide Science* 2018, doi: 10.1002/bip.23074

Effect of targeted minimal sequence variations on the structure and biological activities of the human cathelicidin LL-37
Sabrina Pacor, Filomena Guida, Daniela Xhindoli, Monica Benincasa, Renato Gennaro and Alessandro Tossi, *Peptide Science* 2018, doi: 10.1002/pep2.24087

Peptide modulators of Rac1/Tiam1 protein-protein interaction: An alternative approach for cardiovascular diseases
Alessandro Contini, Nicola Ferri, Raffaella Bucci, Maria Giovanna Lupo, Emanuela Erba, Maria Luisa Gelmi and Sara Pellegrino, *Peptide Science* 2018, doi: 10.1002/bip.23089

PeptideScience
THE AMERICAN PEPTIDE SOCIETY JOURNAL

Special Issue: Emerging Peptide Science in Italy

Guest Editors: Dr Giancarlo Morelli (Università di Napoli "Federico II"), Prof. Paolo Rovero (Università di Firenze) and Prof. Claudio Toniolo (Università di Padova)

Selective detection of α4β1 integrin (VLA-4)-expressing cells using peptide-functionalized nanostructured materials mimicking endothelial surfaces adjacent to inflammatory sites
Rossella De Marco, Arianna Greco, Natalia Calonghi, Samantha D. Dattoli, Monica Baiula, Santi Spampinato, Pierre Picchetti, Luisa De Cola, Michele Anselmi, Francesca Cipriani and Luca Gentilucci, *Peptide Science* 2018, doi: 10.1002/bip.23081

Deciphering RGDechi peptide-$\alpha_5\beta_1$ integrin interaction mode in isolated cell membranes
Luigi Russo, Biancamaria Farina, Annarita Del Gatto, Daniela Comegna, Sonia Di Gaetano, Domenica Capasso, Annamaria Liguoro, Gaetano Malgieri, Michele Saviano, Roberto Fattorusso and Laura Zaccaro, *Peptide Science* 2018, doi: 10.1002/pep2.24065

A selective $\alpha_v\beta_5$ integrin antagonist hidden into the anophelin family protein cE5 from the malaria vector *Anopheles gambiae*
Sonia Di Gaetano, Annarita Del Gatto, Luciano Pirone, Daniela Comegna, Laura Zaccaro, Michele Saviano, Bruno Arcà, Domenica Capasso and Emilia Pedone, *Peptide Science* 2018, doi: 10.1002/pep2.24054

Potential therapeutics of Alzheimer's diseases: New insights into the neuroprotective role of trehalose-conjugated beta sheet breaker peptides
Giuseppe Di Natale, Stefania Zimbone, Francesco Bellia, Marianna F. Tomasello, Maria L. Giuffrida, Giuseppe Pappalardo and Enrico Rizzarelli, *Peptide Science* 2018, doi: 10.1002/pep2.24083

Design, synthesis, and conformational studies of [DOTA]-Octreotide analogs containing [1,2,3]tiazolyl as a disulfide mimetic
Chiara Testa, Debora D'Addona, Mario Scrima, Anna Maria Tedeschi, Anna Maria D'Ursi, Claire Bernhard, Franck Denat, Claudia Bello, Paolo Rovero, Michael Chorev and Anna Maria Papini, *Peptide Science* 2018, doi: 10.1002/pep2.24071

The several facets of Trichogin GA IV: High affinity Tb(III) binding properties. A spectroscopic and molecular dynamics simulation study
Emanuela Gatto, Maria Elena Palleschi, Beatrice Zangrilli, Marta De Zotti, Benedetta Di Napoli, Antonio Palleschi, Claudia Mazzuca, Fernando Formaggio, Claudio Toniolo and Mariano Venanzi, *Peptide Science* 2018, doi: 10.1002/pep2.24081

Synthesis and biological activity of an Anderson polyoxometalate bis-functionalized with a Bombesin-analog peptide
Daniele Ventura, Andrea Calderan, Claudia Honisch, Silke Krol, Simona Serrati, Marcella Bonchio, Mauro Carraro and Paolo Ruzza, *Peptide Science* 2018, doi: 10.1002/pep2.24047

Received: 3 August 2017 | Revised: 14 September 2017 | Accepted: 4 October 2017

DOI: 10.1002/bip.23074

ORIGINAL ARTICLE

WILEY PeptideScience

Esculentin-1a derived peptides kill *Pseudomonas aeruginosa* biofilm on soft contact lenses and retain antibacterial activity upon immobilization to the lens surface

Bruno Casciaro[1] | Debarun Dutta[2] | Maria Rosa Loffredo[1] | Stefania Marcheggiani[3] | Alison M McDermott[4] | Mark DP Willcox[2] | Maria Luisa Mangoni[1]

[1]Laboratory affiliated to Pasteur Italia-Fondazione Cenci Bolognetti, Department of Biochemical Sciences, Sapienza University of Rome, Rome, Italy

[2]School of Optometry and Vision Science, University of New South Wales, Sydney, Australia

[3]Department of Environment and Health, Istituto Superiore di Sanità, Rome, Italy

[4]Department of Applied Sciences, Northumbria University, Newcastle upon Tyne, United Kingdom

Correspondence
Maria Luisa Mangoni, Department of Biochemical Sciences, Sapienza University of Rome, via degli Apuli, 9-00185 Rome, Italy.
Email: marialuisa.mangoni@uniroma1.it

Funding Information
Grant sponsor: Sapienza Università di Roma; National Health and Medical Research Council, Grant number: APP107620

Abstract

Contact lens (CL) wear is a risk factor for development of microbial keratitis, a vision threatening infection of the eye. Adverse events associated with colonization of lenses, especially by the multi-drug resistant and biofilm forming bacterium *Pseudomonas aeruginosa* remain a major safety issue. Therefore, novel strategies and compounds to reduce the onset of CL-associated ocular infections are needed. Recently, the activity of the frog skin-derived antimicrobial peptide Esc(1-21) and its diastereomer Esc(1-21)-1c was evaluated against both planktonic and sessile forms of this pathogen. Furthermore, Esc(1-21) was found to significantly reduce the severity of *P. aeruginosa* keratitis in a mouse model and preserve antipseudomonal activity in the presence of human basal tears. Here, we have analyzed the activity of the peptides on *P. aeruginosa* biofilm formed on soft CLs. Microbiological assays and scanning electron microscopy analysis indicated that the peptides were able to disrupt the bacterial biofilm, with the diastereomer having the greater efficacy (up to 85% killing vs no killing at 4 μM for some strains). Furthermore, upon covalent immobilization to the CL, the two peptides were found to cause more than four log reduction in the number of bacterial cells within 20 minutes and to reduce bacterial adhesion to the CL surface (77%–97% reduction) in 24 hours. Importantly, peptide immobilization was not toxic to mammalian cells and did not affect the lens characteristics. Overall, our data suggest that both peptides have great potential to be developed as novel pharmaceuticals for prevention and treatment of CL-associated *P. aeruginosa* keratitis.

KEYWORDS
antimicrobial peptides, contact lens, keratitis, *Pseudomonas aeruginosa*

1 | INTRODUCTION

Microbial keratitis is a severe sight-threatening event and can rapidly progress to corneal perforation within 2–3 days. [1] The use of soft contact lenses (CL), one of the most popular ways to correct vision disorders, accounts for approximately 12%–66% of all microbial keratitis cases.[2] This is mainly due to the colonization of lenses by microorganisms, such as Gram-positive and Gram-negative bacteria, including the ubiquitous *Pseudomonas aeruginosa*.[3–5] Indeed, *P. aeruginosa* is the most frequently isolated bacterium from CL-associated microbial keratitis[6,7] accounting for ≥70% of all isolates. *P. aeruginosa* has the capacity to rapidly adhere to silicone hydrogel or hydrogel lenses forming sessile communities, that are called biofilms.[8] In addition, it can invade or directly kill host cells leading to damage and possible perforation of the corneal tissue resulting in vision loss.[9,10] Invasion and cell death is a result of the production of bacterial virulence factors[10–13] and the recruitment/activation of host defense cells, primarily neutrophils, which contribute to the clinical manifestations of the disease.[14]

Abbreviations: AMP, antimicrobial peptide; CFU, colony-forming unit; CL, contact lens; DMEM, Dulbecco's modified Eagle's medium; EDC, 1-ethyl-3-(3-dimethylaminopropyl) carbodiimide hydrochloride; LB, Luria–Bertani broth; MAA, methacrylic acid; MTT, 3-(4,5-dimethylthiazol-2-yl)-2,5-diphenyltetrazolium bromide; PBS, phosphate buffered saline; SAB, sodium acetate buffer.

Risk factors for microbial keratitis include: (*i*) extended wear of CL; (*ii*) CL wear while swimming; (*iii*) improper storage and disinfection of lenses with tap water or home-made solutions; (*iv*) wear of cosmetic CL, especially if purchased online or from roadside shops.[3,15–17] Importantly, newer lens materials, care regimes, and wear modalities have not reduced the incidence and severity of infections.[18] Coupled with the global decrease of pathogen susceptibility to traditional antibiotics (eg ciprofloxacin),[19–21] there is a significant need for novel approaches to prevent and treat CL-associated keratitis. Among them, the development of agents that are active against bacterial biofilms formed on CLs is highly desirable. Furthermore, prevention of bacterial growth in the first place and/or bacterial attachment to CL, so that bacteria cannot be transferred from lens to eye, represents a realistic goal. This could consist of providing an innate immune-like functionality to lenses, by incorporating antimicrobial molecules.

Membrane-active antimicrobial peptides (AMPs) hold particular promise in this regard.[22] Previous studies performed with the hybrid peptide melimine (corresponding to the active regions of protamine from salmon sperm and melittin from bee venom[23]) showed that peptide-coated lenses were able to reduce corneal infection in animal models.[24] Melimine and a shorter derivative called Mel-4 have been shown to be superior to other cationic peptides (LL-37 and lactoferricin) when bound to CLs.[25] However, with the exception of melimine, only a limited number of naturally-occurring AMPs or derivatives have been reported to exhibit signs of clinical benefit once administered to the ocular surface of infected eyes.

Esculentins are a family of α-helical membrane-active AMPs from amphibian skin with a wide spectrum of antimicrobial activity.[26–28] We recently demonstrated that esculentin-1a(1–21)NH_2 [Esc(1–21)], corresponding to the first 20 amino acids of the native esculentin-1a followed by a glycinamide residue at the C-terminus, is a novel AMP with potent activity against both free-living and sessile forms of *P. aeruginosa*.[29,30] In contrast with the majority of mammalian AMPs, the antipseudomonal activity of Esc(1–21) is preserved at high salt concentrations as well as in the presence of human basal tears.[31] In addition, topical application resulted in a significant reduction of infection in a mouse model of *P. aeruginosa* keratitis compared to vehicle-treated animals.[31] Furthermore, it was recently discovered that the diastereomer of Esc(1–21), that is Esc(1–21)-1c, containing two D-amino acids at positions 14 and 17, has significantly lower cytotoxicity and higher biostability than the all-L isomer in physiological environments.[30,32]

Here, we first investigated and compared the ability of these two esculentin-1a derivatives to disrupt *P. aeruginosa* biofilm formed on soft CL. Both reference strains and clinical isolates of *P. aeruginosa* were used and a higher anti-biofilm activity was recorded for the diastereomer. Furthermore, we covalently bound the two peptides to hydrogel soft CL and demonstrated that the diastereomer-coated CLs were more efficient in reducing *Pseudomonas* adhesion to the lens surface, while retaining antibacterial activity without being toxic to mammalian cells or affecting the lens surface parameters.

To the best of our knowledge, these are the first studies showing the ability of derivatives of a frog-skin AMP to both kill Pseudomonas biofilm formed on the surface of a medical device, that is a soft CL, and to preserve antibacterial activity upon covalent attachment to the CL surface, without altering the CL surface parameters.

2 | MATERIALS AND METHODS

2.1 | Peptides

Synthetic Esc(1–21) and Esc(1–21)-1c (Esc peptides) were purchased from Biomatik (USA/Canada). Briefly, each peptide was assembled by stepwise solid-phase synthesis and purified via reverse-phase high-performance liquid chromatography to a purity of 98% using a gradient of acetonitrile in 0.1% aqueous trifluoroacetic acid (from 28% to 100% in 30 minutes) at a flow rate of 1.0 mL/min. The product was obtained by lyophilization of the appropriate fraction. The molecular mass was verified by Electron Spray Ionization Mass Spectrometry.

2.2 | Bacteria

The following bacterial strains were used for the antimicrobial assays: the reference strain *P. aeruginosa* ATCC 27853 and human clinical isolates from keratoconjunctivitis (kindly provided by Dr. Anna Rita Blanco, at SIFI, Catania, Italy) *P. aeruginosa* R1 and *P. aeruginosa* 1Rm.[31]

2.3 | Mammalian cells

L929 mouse fibroblast cells (NCTC clone 929 ATCC CCL-1) were maintained in Dulbecco's modified Eagle's medium (DMEM) (Sigma, Irvine, UK) in tissue culture treated T25 and T75 flasks. The media was supplemented with 10% fetal bovine serum (Sigma, Irvine, UK) and the cells were maintained at 37°C and 5% CO_2 in a humidified incubator.

2.4 | Antipseudomonal activity against preformed biofilm on soft CLs

The reference strain and the clinical isolates were grown at 37 °C in Luria–Bertani broth (LB) to mid-log phase (optical density of 0.8 at 590 nm). With the help of tweezers, silicone hydrogel narafilcon A soft CL (1-Day ACUVUE TruEye) were removed from the manufacturer's containers, and washed thrice in phosphate buffered saline (PBS). The lenses were then immersed into wells of a 24-multiwell plate, each well containing 1 mL of bacterial inoculum in 1/10 LB at a concentration of 5×10^4 colony-forming units (CFU)/mL. The plate was then incubated in a humidified incubator at 37 °C at 125 rpm to allow biofilm formation on the surface of both lens sides. After 20 hours of incubation, each lens was washed thrice with PBS to remove any non-adherent planktonic cells. The lenses were then transferred into wells of a new 24-multiwell plate, each well containing serial dilutions of Esc(1–21) and Esc(1–21)-1c in PBS. For positive controls, the lenses were immersed in sterile PBS. The new plate was then incubated at 37 °C for 2 hours with gentle shaking (125 rpm). After peptide treatment, each lens was washed thrice in PBS and transferred into wells of another 24-multiwell plate, each well containing 350 μL of 0.5 mg/mL of 3-(4,5-dimethylthiazol-2-yl)-2,5-diphenyltetrazolium bromide (MTT, from Sigma Aldrich, Milan, Italy) in Hank's solution (136 mM NaCl; 0.34 mM Na_2HPO_4; 0.44 mM KH_2PO_4; 5.4 mM KCl; 4.1 mM $NaHCO_3$,

pH 7.2, supplemented with 5.5 mM D-glucose) as previously reported.[29] The killing of biofilms was determined as a function of the inhibition of MTT reduction to insoluble formazan crystals by bacterial reductases. The plate was incubated again for 2 hours (125 rpm) at 37 °C. Formazan crystals were solubilized by the addition of acidified isopropanol. During overnight incubation at room temperature the resulting purple color was absorbed by the lens. Afterward, each lens was soaked in absolute ethanol (500 μL in each well) to decolor it. Aliquots of 100 μL were finally transferred to the wells of a 96-multiwell plate and absorbance was measured at 590 nm using a microplate reader (Infine M 200, Tecan). Untreated bacterial cells in PBS were the control. Percentage of killing was calculated according to the formula: [1 - (Abs of treated samples - Abs of blank/Abs of control samples-Abs of blank)] × 100, where the blank was the solvent PBS.

2.5 | Scanning electron microscopy

CLs on which biofilm was formed, as described above, were either used directly or treated with 16 μM of Esc(1–21) or Esc(1–21)-1c dissolved in PBS for 2 hours and prepared for electron microscopy analysis, as follows: each lens was washed thrice with PBS and fixed with 1% glutaraldehyde in PBS for 1 hour at room temperature. Afterward, each lens was cut into four pieces and dehydrated through a graded series of ethanol (30%, 50%, 75%, and 95% vol/vol in water). Finally, all samples were air-dried (overnight) at room temperature and after gold coating, they were observed with a Philips XL 30 CP instrument.

2.6 | Covalent immobilization of esculentin-1a derivatives to CLs

The immobilization process of Esc peptides to CLs was conducted according to the method explained earlier with hydrogel CLs.[33] Briefly, the peptides were diluted in sterile PBS at a concentration of 1 mg/mL. With the help of sterile tweezers, etafilcon A soft CLs (Acuvue 2) which contain methacrylic acid (MAA) in the lens matrix, were removed from the blister packs, washed thrice with PBS and twice with 0.1 M sodium acetate buffer, pH 5.0 (SAB). Afterward, they were soaked in 2 mL SAB containing 2 mg/mL of 1-ethyl-3-(3-dimethylaminopropyl) carbodiimide hydrochloride (EDC) for 15 minutes at 25 °C to activate the carboxylic group of MAA present in the etafilcon A lens. After EDC treatment, the lenses were washed thrice with PBS and soaked in 350 μL of 1 mg/mL Esc(1–21) or Esc(1–21)-1c in PBS for peptide immobilization (2 hours at 37 °C with gentle shaking). After peptide immobilization, the lenses were washed thrice with PBS and immersed in 10% wt/vol sodium chloride overnight. Afterward, they were left in PBS for 2 hours to extract any non-covalently attached peptide remaining within the lens matrix. CLs treated or not with EDC without peptide immobilization were used as process control or control, respectively.

2.7 | Amino acid analysis to determine amount of immobilized AMP

The amount of AMP present on the immobilized lens was quantified by amino acid analysis (AAA) which is detailed in Dutta et al.[33] Briefly, lenses were washed in Milli-Q® (Millipore Corp., Billerica) water, and then underwent 24 hours gas phase hydrolysis in 6 M HCl (Ajax Finechem Pty Ltd, New South Wales, Australia) at 110 °C. Lenses were then dried and amino acids extracted in 20% acetonitrile in trifluoroacetic acid (Themo Fisher Scientific, Rockford). The amount of amino acids in the hydrolysates was analyzed using the AccQ-Tag Ultra chemistry kit (Waters Corp., Milford). As the amino acid asparagine is hydrolyzed to aspartic acid, the amount of this was regarded as the respective original type of amino acid. The sum of all the amino acids derived from each lens was regarded as total amount of AMP attachment. None of the peptides contain cysteine and tryptophan amino acids which are not analyzed by this method. Triplicates were used for each type of peptide immobilized lenses and uncoated PBS soaked lens was used as control.

2.8 | Antimicrobial activity of Esc-coated CLs

The ability of Esc-coated CLs to kill *P. aeruginosa* cells was assessed against the reference strain *P. aeruginosa* ATCC 27853. In detail, *P. aeruginosa* was grown at 37 °C until mid-log phase. Bacterial cells were then diluted to 5×10^4 CFU/mL in PBS. One mL of the bacterial suspension was transferred into wells of a 24-multiwell plate, each well containing Esc-coated CLs or the EDC-activated CLs (process control) or untreated non-coated CLs (control). Aliquots at 20, 60, and 120 minutes were withdrawn and plated on LB-agar plates for CFU counting.

In parallel, to assess the ability of Esc-coated CLs to inhibit bacterial growth and adhesion, the peptide-coated CLs were incubated in 1 mL of LB containing 5×10^4 bacterial cells for 24 hours at 37 °C. Afterward, aliquots from the supernatant were diluted and plated on LB-agar plates for CFU counting. Successively, with the help of sterile tweezers, the lenses were taken out from the wells and washed thrice with PBS to remove non-attached bacterial cells. They were then transferred into eppendorf tubes containing 500 μL of PBS and then sonicated to remove bacterial cells from the lens surface. Aliquots from the eppendorf tube were withdrawn and plated on LB-agar plates for counting.

2.9 | CL parameters measurements

Esc immobilized CLs were tested for any change in physical parameters. Five CLs (Acuvue 2; base curve 8.3, diameter 14.0 and power −4.00Ds) for each type of lens coating were randomly selected for this evaluation. CLs soaked overnight in PBS were used as controls and lenses treated with EDC without peptide immobilization were used as process controls. Lenses were immersed in PBS at ambient temperature (20 °C ± 2 °C) for 24 hours prior to testing. Centre thicknesses of lenses were measured by a Heidenhain soft CL thickness gage according to ISO:18369-3, 9339-2 and American National Standard ANSI Z80.20–1998 protocols. Sagittal depth was calculated by profile projector following ISO:18369-3 and ANSI Z80.20–1998 protocols. The diameters of lenses were measured following the ISO: 18369-3 and 9338 protocols in a wet cell by means of a Nikon profile projector with horizontal *x*–*y* table and digital position readout. Base curve equivalents were calculated from the measured lens diameters, center thickness, and sagittal depth measurements. All procedures were repeated in order to obtain five independent measurements for each lens and the values were then averaged. CL hydrophobicity was determined

through dynamic water contact angle measurement using a captive bubble method[33,34] and a contact angle goniometer (Rame-Hart, Inc NRL USA, Model no. 200-F1). The angle between bubble and lens surface was measured with a 50 mm Cosmicar Television Lens (Japan). Advancing and receding contact angle was calculated by Image J software. A minimum of eight measurements were made on five samples of each CL and then averaged.

2.10 | Cytotoxicity

In vitro cytotoxicity of the CLs was determined using a direct contact method as outlined in ISO 10993—biological evaluation of medical devices. The ISO standard in vitro cytotoxicity results are important for approval and validation with regulatory authorities of CL care products. As per the guideline, murine L929 cells were grown in 24-well cell culture plates (GreinerBio One, Frickenhauser, Germany) to 80% confluence, and peptide-coated CLs, process controls or non-coated controls were placed directly on the cell monolayer and incubated for 24 hours with fresh medium. A minimum of three samples was used for each type of CLs. Afterward, cytotoxicity was evaluated using bright field and phase contrast microscopy after Trypan blue staining. Cytotoxic responses, that is zone of extent of cell damage, were graded on a scale of 0–4 as per ISO guidelines. Silastic medical grade tubing (Dow Corning Corporation, Michigan) and samples of surgical latex gloves (Ansell Medical, Victoria, Australia) were used as a negative and positive control, respectively. Grades of above 1 are suggestive of cytotoxic responses under the conditions specified.

2.11 | Statistical analysis

The statistical analyses were performed using Student's *t* test with PRISM software (GraphPad, San Diego, California) and the differences were considered to be statistically significant for $P < .05$. The levels of statistical significance are indicated in the legend to the figures. Differences between CL types in terms of metrological parameters and AAA were determined using Wilcoxon Signed-Ranked test. Statistical significance was set at 5%.

3 | RESULTS

3.1 | Killing activity against *P. aeruginosa* biofilm formed on soft CL

As shown in Figure 1, Esc(1–21) displayed a dose-dependent antibiofilm activity causing more than 50% killing of *P. aeruginosa* ATCC 27853 biofilm, 2 hours after treatment at a concentration of 32 μM, while this activity was lost at 4 μM. In comparison, the diastereomer was more active causing ~90% and 35% biofilm eradication at 32 μM and 4 μM, respectively. When tested against the two clinical isolates, Esc(1–21) increased its killing activity at all concentrations used, with the exception of 4 μM against *P. aeruginosa* R1 (0% killing). However, the antibiofilm activity of Esc(1–21) was weaker than that of Esc(1–21)-1c against all the strains, and this difference was more pronounced at the lowest concentration of 4 μM.

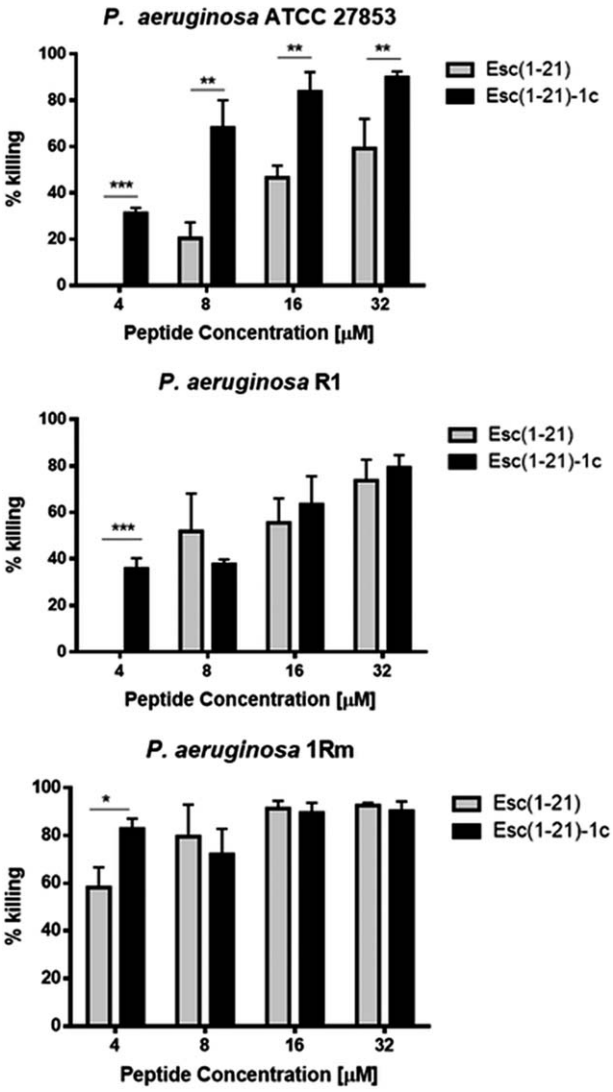

FIGURE 1 Killing activity of Esc(1–21) and Esc(1–21)-1c against different *P. aeruginosa* strains grown as biofilms after 2 hours treatment. Data points are the mean ± SEM of three independent experiments. The levels of statistically significant differences between the two peptides are indicated as follows $^{*}P < .05$, $^{**}P < .01$, $^{***}P < .001$

3.2 | Scanning electron microscopy

The activity of the peptides on Pseudomonas biofilm formed on both sides of soft CLs was next explored by SEM analysis. Figure 2A highlights the effect of the diastereomer on the reference strain of *P. aeruginosa* ATCC 27853, 2 hours after treatment at 16 μM (a peptide concentration causing almost 80% biofilm death). As pointed out by the left panels, a clear biofilm community developed on the concave and the convex side of the lens, 20 hours after incubation with the bacteria. In comparison, when this biofilm was treated with the diastereomer, it appeared disaggregated with a lower cell density on both lens sides, presumably due to the killing action of the peptide and detachment of dead bacteria from the lens surface (Figure 2A, right side). The diastereomer was able to provoke a remarkable change in the morphology of bacterial cells, most of which appeared emptied of their content and with a wrinkled surface. The damage induced by this peptide on

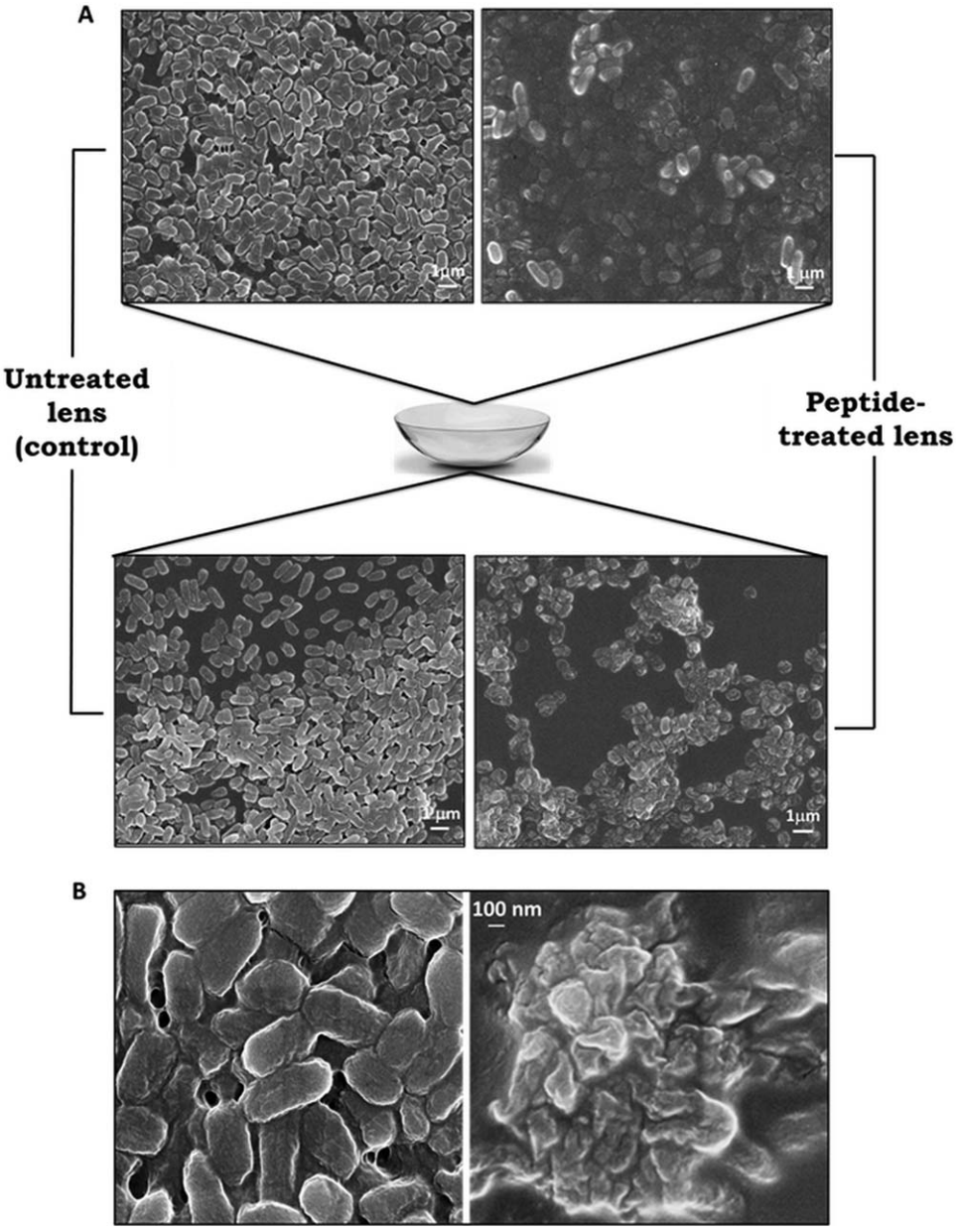

FIGURE 2 Panel (A) SEM of *P. aeruginosa* ATCC 27853 biofilm formed on CL (left side) and after 2 hours treatment with Esc(1–21)-1c at 16 μM (right side). Images are representative of triplicate samples. Panel (B) higher magnification view to show the effect of Esc(1–21)-1c on the morphology of biofilm cells formed on CL (right side) with respect to the untreated biofilm (left side). Representative of triplicate samples

the microbial cell surface was better visualized at 10-fold higher magnification (×100), as reported in Figure 2 (panel B). Overall, this effect was similar to that previously described for the all-L Esc(1–21) on *Pseudomonas* biofilm formed by the same bacterial strain on the peg surface of a Calgary Biofilm Device.[29]

3.3 | Peptides immobilized on CLs and their quantification

Esc(1–21) and Esc(1–21)-1c were immobilized to hydrogel soft CLs (see Materials and Methods) and their amount bound was 2.13 ± 0.29 μg and 2.09 ± 0.20 μg total amino acids, respectively. Process control and control lenses had <0.10 μg of peptide associated with them. There was no significant difference between the amount of peptide recovered from Esc(1–21) and Esc(1–21)-1c immobilized CL ($P > .05$).

3.4 | Bactericidal activity of Esc-immobilized CLs

The antimicrobial activity of the two Esc peptides after immobilization to hydrogel soft CLs was initially studied by measuring the bactericidal activity of Esc-coated CLs against *P. aeruginosa* ATCC 27853 in 1 mL of physiologic solution.

As indicated in Figure 3A, the antipseudomonal activity of both peptides was preserved upon covalent binding to CLs causing a >4 log

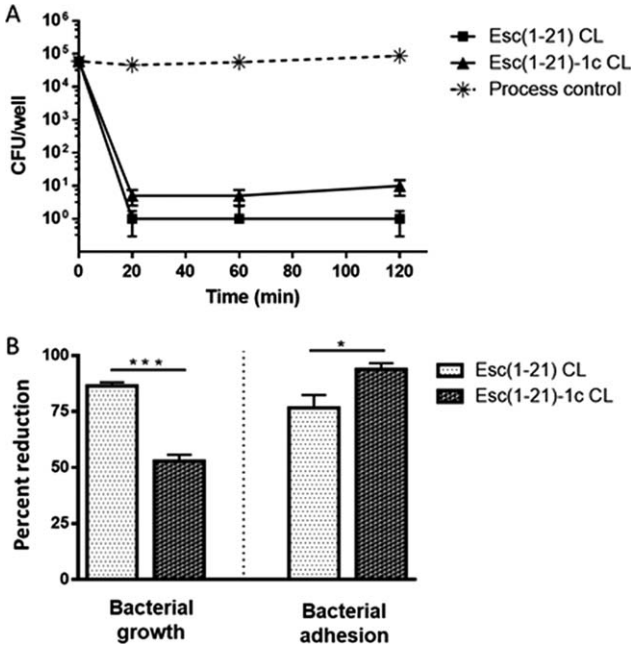

FIGURE 3 Antipseudomonal activity of Esc(1–21) and Esc(1–21)-1c modified CLs. Panel (A) bactericidal activity of peptide-coated CLs against the planktonic form of *P. aeruginosa* ATCC 27853 in comparison to the process control during 2 hours incubation in PBS at 37 °C ($P < .001$). Panel (B) effect of peptide-coated CLs on bacterial growth (left side) or bacterial adhesion on the CL surface (right side) with respect to the process control, 24 hours after incubation in LB medium at 37 °C. The percent reduction was normalized to that of the process control (0% reduction). Data are the mean ± SEM of three independent experiments. The level of statistical significance between the two peptides are indicated as follows $^{*}P < .05$, $^{**}P < .01$, $^{***}P < .001$

reduction in the number of viable bacterial cells (>99.99% killing) within 20 minutes of treatment in PBS with the diastereomer and an even higher bacterial mortality when the all-L peptide-coated CLs were used. This behavior is in accordance with the slightly lower activity of the diastereomer against the planktonic form of *P. aeruginosa*.[30] Taking into account the amount of peptide conjugated to the CL (~2.1 μg), and the volume used for the experiment (1 mL), the "effective" concentration of both peptides was ~1 μM. Importantly, when the bactericidal activity of the peptides in their soluble free form was tested at 1 μM against the same inoculum of bacterial cells in PBS, a lower efficacy was detected with ~99.9% and 90% killing for Esc(1–21) and Esc(1–21)-1c, respectively, within 20 minutes (data not shown).

3.5 | Effect of Esc-immobilized CLs on the inhibition of bacterial growth and adhesion to the lens surface

The ability of Esc-coated CLs to inhibit growth and adhesion of *P. aeruginosa* ATCC 27853 to the lens surface under conditions favoring bacterial replication (eg undiluted LB culture medium) was analyzed up to 24 hours. Both types of immobilized CLs were found to inhibit growth of *P. aeruginosa* with the all-L Esc(1–21)-coated CL having a higher efficacy. Indeed, 86% and 52% reduction in the number of bacterial cells was observed after 24 hours incubation of Pseudomonas culture with Esc(1–21) and Esc(1–21)-1c-coated CLs, respectively, compared to the number found in the medium containing process controls (Figure 3B, left side).

TABLE 1 CL parameters with and without peptide coating ($n = 5$, mean ± SD)

CL	Diameter (mm)	Centre thickness (μm)
Control	13.89 ± 0.01	73.4 ± 4.2
Process control	13.86 ± 0.02	71.8 ± 4.3
Esc(1–21)	13.84 ± 0.02	72.4 ± 2.1
Esc(1–21)-1c	13.86 ± 0.07	70.6 ± 3.0

In parallel, the number of *Pseudomonas* cells attached to the lens surface was evaluated. As indicated in Figure 3B (right side), immobilization of both peptides to hydrogel soft CLs significantly impaired bacterial adhesion to their surface and presumably biofilm formation, after 24 hours incubation with the bacterial culture in LB. Interestingly, in this case, the diastereomer was observed to be more efficient causing approximately 1.56 log (ie 97%) reduction in the number of adherent bacterial cells with respect to the process control. In comparison, a lower potency was manifested by the all-L Esc(1–21) CLs with an

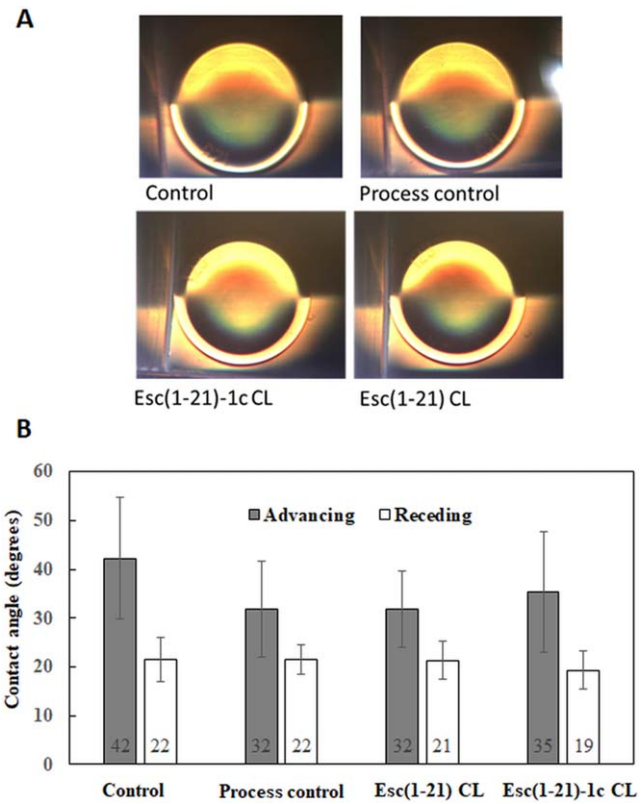

FIGURE 4 Panel (A) a representative photograph of a randomly selected control, process control, and Esc(1–21)-1c and Esc(1–21) CLs with a Nikon profile projector ($n = 5$). Panel (B) contact angle (degrees) measured on control, process control, Esc(1–21)-1c and Esc(1–21) CLs by captive bubble technique ($n = 5$). Data displayed at the base of the bars indicate advancing and receding contact angles in degrees

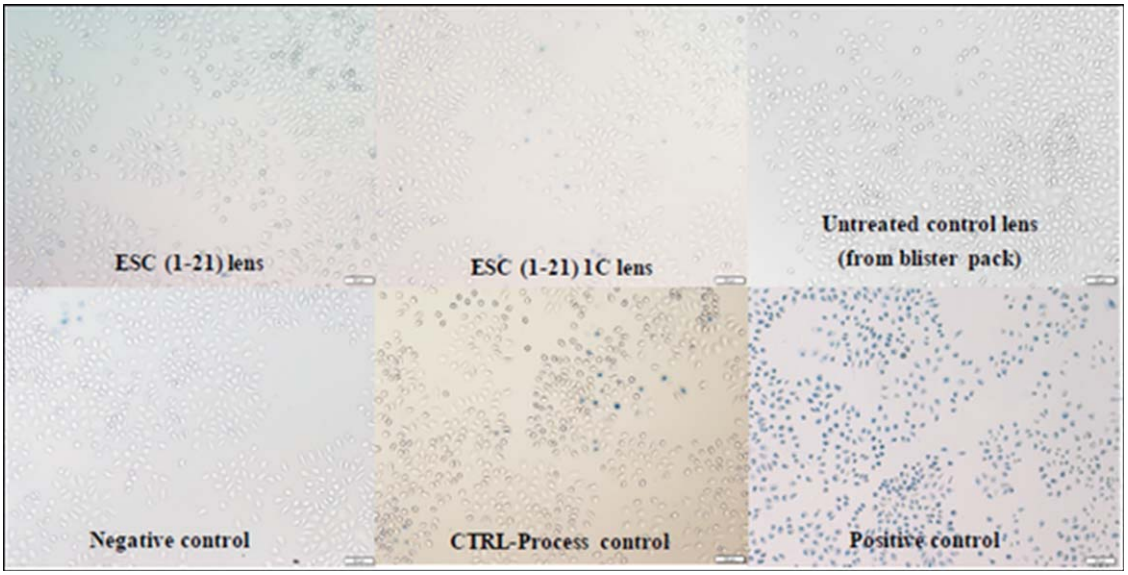

FIGURE 5 Representative images of the effect of Esc-coated CLs on the viability of murine L929 cells after 24 hours incubation. They were assessed by means of bright field and phase contrast microscopy after Trypan Blue staining. Positive and negative controls were surgical latex gloves and silastic medical grade tubing, respectively. Images are representative of quadruplicate samples

average of 77% of reduction in bacterial adhesion compared to the process control. The untreated control CLs gave similar results as those found for the process control and therefore are not shown.

3.6 | Effect of peptide immobilization on CL parameters

The commercially available Etafilcon-A CL had a mean diameter of 13.89 ± 0.01 mm, a central thickness of 73.4 ± 4.2 μm and calculated base curve of 8.1 ± 0.0 mm following soaking in PBS (Table 1). After coating with either peptide, there was no statistically significant difference in any of the lens parameters ($P > .05$). While examining with a Nikon profile projector, no detectable optical abnormality was found in the peptide immobilized lenses and each appeared identical to untreated CLs (Figure 4A). Advancing and receding contact angle measurement by captive bubble technique revealed that there was no statistically significant difference ($P > .05$) between the control, and Esc (1–21)-1c and Esc (1–21) CL (Figure 4B).

3.7 | Cytotoxicity of peptide immobilized lenses

The *in vitro* cytotoxicity results were assessed based on reactivity grades for direct contact test.

This is based on a standard key, which quantifies the zonal extent of cell damage (0–4 maximum). Negative controls showed mostly healthy cells with no morphological abnormality, whereas positive controls showed that all cells were dead (stained with trypan blue). Both the Esc(1–21)-1c and Esc (1–21) immobilized lenses and commercially available etafilcon A lenses showed a minimal response of grade 1. This indicated no cytotoxicity, with only few degenerated cells under CL physical contact zone (Figure 5). Thus, the peptide-immobilized lenses are considered to be nontoxic.

4 | DISCUSSION

Nowadays, CL-associated microbial keratitis is mainly treated by topical administration of fluoroquinolones.[35] However, there is alarming evidence that *P. aeruginosa* strains are developing resistance to antimicrobial components of CL care solutions[21,36] increasing the chance for development of keratitis and thus complicating the treatment options.[5,37–39] Here, for the first time we provide evidence of the killing activity of the frog skin derived AMP Esc(1–21) and its diastereomer Esc(1–21)-1c on *P. aeruginosa* biofilm formed on a medical device that is a narafilcon A soft CL.

With the aim to develop these peptides as new ophthalmic pharmaceuticals, we first evaluated their ability to eradicate *Pseudomonas* biofilm built on soft CLs by one reference strain (*P. aeruginosa* ATCC 27853) and two drug-resistant clinical isolates from ocular infections (ie *P. aeruginosa* R1 and *P. aeruginosa* 1Rm). Noteworthy, the number of bacteria isolated from CL storage cases has been reported to range from 1 to 6 × 10^4 CFU/case.[21,40] Therefore, in order to reproduce a more realistic level of bacteria to which CLs can be exposed, an inoculum size of 5 × 10^4 CFU/mL was used for biofilm formation. In our case, the highest level of biofilm biomass on CL was obtained when bacterial growth was performed in 1/10 LB medium compared to ½ or undiluted LB (data not shown) after 20 hours incubation with mild agitation.

A greater antibiofilm activity was displayed by the diastereomer Esc(1–21)-1c in line with what was found against the biofilm form of *P. aeruginosa* strains from cystic fibrosis patients.[30] As detailed by SEM analysis and in agreement with previous studies on Esc(1–21), bacterial cells in the sessile community appeared like “ghosts” emptied of their intracellular content 2 hours after peptide treatment.

Covalent attachment of esculentin-1a derivatives to biomaterials such as hydrogel CLs was effective at achieving an antimicrobial surface which was active against *P. aeruginosa* causing more than a four log reduction in the number of bacterial cells. Importantly, the killing activity

displayed by the antimicrobial CLs was higher than that displayed by the same concentration of the peptides in their soluble free form. During the immobilization process, the MAA of the lens matrix was activated with EDC and the peptides immobilized via amide bonding. This likely resulted in random orientation of the Esc peptides on the lens surface. Interestingly, such non-directional coupling of the selected AMPs to the lens surface does not affect their antipseudomonal activity, in line with what was previously found when Esc(1–21) or LL-37 was conjugated to gold nanoparticles[41,42] or melimine tethered to CLs.[25,33] This is presumably due to the membrane-perturbing mechanism of bactericidal activity of the two Esc isoforms, which would not require peptide detachment from the lens surface. In addition, this mechanism would not depend on the peptide's mobility, but rather on the peptide's cationicity and amphipathicity. One could speculate that this latter characteristic is likely preserved upon immobilization, thus allowing the peptide to penetrate and destabilize the bacterial membrane, as well. Indeed, according to the literature, the amphipathic character of a polypeptide, generally resulting from the adoption of an α-helix structure is a crucial prerequisite for membrane interactions and perturbation of the hydrophobic core of phospholipid bilayers.[43,44]

In this study, the amount of surface tethered peptide (ie 2 μg) was enough to reach adequate concentration to (*i*) rapidly kill *Pseudomonas* that can be found as a contaminant of CLs storage solutions, as well as to (*ii*) inhibit *Pseudomonas* growth and its adhesion to CLs after a long-term incubation (eg 24 hours) under conditions favoring bacterial replication. The amount of Esc peptide associated with lenses was less than that was found in a previous study with melimine and Mel4 immobilized lenses.[33] However, Esc immobilized CL showed excellent results, likely partly due to its higher amphipathicity compared to melimine and Mel4; which are essentially a chain of highly cationic amino acids.[45] This study also revealed that peptide immobilization did not alter CL surface contact angles measured by captive bubble technique signifying that the surface hydrophobicity has not changed following surface treatment with the Esc peptides. This is particularly important since *P. aeruginosa* is known to attach on hydrophobic CL surfaces more readily than hydrophilic ones. In comparison, earlier results with melimine immobilization showed decrease in hydrophobicity. This difference was probably due to the fact that the total amount of Esc peptides recovered from CL in this study was much less than that of melimine, and the Esc peptides have an overall lower cationicity compared to melimine.

Furthermore, it is worthwhile noting that immobilization of the two AMPs to CLs did not change the lens parameters and did not make the lenses harmful to mammalian cells. One of the advantages of covalent attachment of AMPs to medical devices is related to the stable peptide association to them, limiting AMP elution and interaction with the surrounding tissue followed by potential cytotoxicity. Previous studies proved that binding/inclusion of antibiotics or metals (ie silver) on the surface of CLs or lens cases was effective in reducing bacterial colonization.[3,46–48] Small molecule mimics of AMPs, named ceragenins were able to prevent bacterial colonization of CLs, upon covalent binding to them.[46] Further, lenses coated with the designed AMP melimine have been shown (*i*) to be safely worn by rabbits for 22 days and by humans for 1 day; (*ii*) to inhibit bacterial colonization *in vitro* and *in vivo*,[33,45] and (*iii*) to reduce microbial keratitis in a rabbit model of CL wear.[24]

It should be emphasized that besides displaying antimicrobial activities, AMPs are also endowed with immunomodulatory properties, for example wound-healing activity, which may speed up the recovery process from an infectious agent by restoring the integrity of the damaged tissue.[49] This makes AMPs even more attractive molecules over classical antibiotics.[50–52]

Despite this, only a few studies have reported beneficial effects on the antibacterial/antibiofilm activity of AMPs once applied to the ocular surface, mainly because of their toxicity to the corneal epithelium. Among them, Esc(1–21) was found to display a potent efficacy in reducing the level of infection in a mouse model of *Pseudomonas*-induced keratitis after dropwise administration only three times daily, for 5 days post-infection.[31] Furthermore, it retained its antimicrobial effectiveness in the presence of human tears,[31] making it unlikely that the Esc-immobilized CLs lose antimicrobial efficacy once put into the human eye.

5 | CONCLUSIONS

In summary, we have demonstrated that a derivative of the frog skin AMP esculentin-1a, that is Esc(1–21) as well as its diastereomer represent encouraging candidates to be developed as ophthalmic formulations and/or for the manufacture of antimicrobial CLs to prevent and/or treat *P. aeruginosa* associated ocular surface infections, with the diastereomer being more efficacious against the more resistant sessile form of this pathogen. This may be due to a prolonged residence time of the diastereomer compared to the all-L peptide, because of its higher resistance to bacterial proteases which are mainly produced by bacterial cells in biofilm communities.[53] Therefore, this would prolong the exposure time of the diastereomer to the biofilm cells, resulting in a higher antimicrobial efficacy in comparison with the all-L peptide, which could be rapidly degraded. The structure of the peptides immobilized to CL as well as their in vivo antibacterial activity will be considered in future work.

ACKNOWLEDGMENTS

This work was supported by grants from Sapienza University, an NHMRC development grant (APP107620) and an ARC discovery grant (DP160101664) from the Australian Government. The authors thank Australian Proteome Analysis Facility for helping with amino acid analysis, and Dr. Klaus Ehrmann and Ms. Indrani Perera of Brien Holden Vision Institute for helping with contact lens parameter measurements.

CONFLICT OF INTERESTS

The authors declare that they have no conflict of interest.

ORCID

Maria Luisa Mangoni http://orcid.org/0000-0002-5991-5868

REFERENCES

[1] E. Karsten, S. L. Watson, L. J. Foster, *Open Ophthalmol. J.* **2012**, *6*, 110.

[2] D. Dutta, N. Cole, M. Willcox, *Mol. Vis.* **2012**, *18*, 14.

[3] M. Shayani Rad, B. Khameneh, Z. Sabeti, S. A. Mohajeri, B. S. Fazly Bazzaz, *Curr. Eye Res.* **2016**, *41*, 1286.

[4] N. Konda, S. R. Motukupally, P. Garg, S. Sharma, M. H. Ali, M. D. Willcox, *Optom. Vis. Sci.* **2014**, *91*, 47.

[5] I. Biswal, B. S. Arora, D. Kasana, Neetushree, *J. Clin. Diagn. Res.* **2014**, *8*, DC26.

[6] E. H. Yildiz, S. Airiani, K. M. Hammersmith, C. J. Rapuano, P. R. Laibson, A. S. Virdi, T. Hongyok, E. J. Cohen, *Cornea* **2012**, *31*, 1097.

[7] J. G. Hoddenbach, S. S. Boekhoorn, R. Wubbels, W. Vreugdenhil, J. Van Rooij, A. J. Geerards, *Graefes Arch. Clin. Exp. Ophthalmol.* **2014**, *252*, 299.

[8] R. N. Borazjani, B. Levy, D. G. Ahearn, *Cont. Lens Anterior Eye* **2004**, *27*, 3.

[9] M. D. Willcox, *Optom. Vis. Sci.* **2007**, *84*, 273.

[10] S. M. Fleiszig, J. P. Wiener-Kronish, H. Miyazaki, V. Vallas, K. E. Mostov, D. Kanada, T. Sawa, T. S. Yen, D. W. Frank, *Infect. Immun.* **1997**, *65*, 579.

[11] L. D. Hazlett, *DNA Cell Biol.* **2002**, *21*, 383.

[12] S. S. Twining, S. E. Kirschner, L. A. Mahnke, D. W. Frank, *Invest. Ophthalmol. Vis. Sci.* **1993**, *34*, 2699.

[13] H. Zhu, R. Bandara, T. C. Conibear, S. J. Thuruthyil, S. A. Rice, S. Kjelleberg, M. Givskov, M. D. Willcox, *Invest. Ophthalmol. Vis. Sci.* **2004**, *45*, 1897.

[14] A. Sy, M. Srinivasan, J. Mascarenhas, P. Lalitha, R. Rajaraman, M. Ravindran, C. E. Oldenburg, K. J. Ray, D. Glidden, M. E. Zegans, S. D. McLeod, T. M. Lietman, N. R. Acharya, *Invest. Ophthalmol. Vis. Sci.* **2012**, *53*, 267.

[15] D. Dutta, J. Ozkan, M. D. Willcox, *Optom. Vis. Sci.* **2014**, *91*, 570.

[16] D. V. Seal, C. M. Kirkness, H. G. Bennett, M. Peterson, Keratitis Study Group, *Cont. Lens Anterior Eye* **1999**, *22*, 49.

[17] E. K. Mela, I. P. Giannelou, J. X. Koliopoulos, S. P. Gartaganis, *Eye Contact Lens* **2003**, *29*, 207.

[18] M. D. Willcox, http://www.clspectrum.com/issues/2011/april-2011/microbiology-and-contact-lens-wear (**2011**).

[19] R. Maviglia, R. Nestorini, M. Pennisi, *Curr. Drug Targets* **2009**, *10*, 895.

[20] M. D. Willcox, *Clin. Exp. Optom.* **2011**, *94*, 161.

[21] L. B. Szczotka-Flynn, Y. Imamura, J. Chandra, C. Yu, P. K. Mukherjee, E. Pearlman, M. A. Ghannoum, *Cornea* **2009**, *28*, 918.

[22] E. Guani-Guerra, T. Santos-Mendoza, S. O. Lugo-Reyes, L. M. Teran, *Clin. Immunol.* **2010**, *135*, 1.

[23] R. Rasul, N. Cole, D. Balasubramanian, R. Chen, N. Kumar, M. D. Willcox, *Int. J. Antimicrob. Agents* **2010**, *35*, 566.

[24] D. Dutta, A. K. Vijay, N. Kumar, M. D. Willcox, *Invest. Ophthalmol. Vis. Sci.* **2016**, *57*, 5616.

[25] D. Dutta, N. Kumar, *M. D. P. Willcox*, *Biofouling* **2016**, *32*, 429.

[26] M. L. Mangoni, D. Fiocco, G. Mignogna, D. Barra, M. Simmaco, *Peptides* **2003**, *24*, 1771.

[27] A. E. Islas-Rodriguez, L. Marcellini, B. Orioni, D. Barra, L. Stella, M. L. Mangoni, *J. Pept. Sci.* **2009**, *15*, 607.

[28] B. Biondi, B. Casciaro, A. Di Grazia, F. Cappiello, V. Luca, M. Crisma, M. L. Mangoni, *Amino Acids* **2017**, *49*, 139.

[29] V. Luca, A. Stringaro, M. Colone, A. Pini, M. L. Mangoni, *Cell Mol. Life Sci.* **2013**, *70*, 2773.

[30] A. Di Grazia, F. Cappiello, H. Cohen, B. Casciaro, V. Luca, A. Pini, Y. P. Di, Y. Shai, M. L. Mangoni, *Amino Acids* **2015**, *47*, 2505.

[31] S. S. Kolar, V. Luca, H. Baidouri, G. Mannino, A. M. McDermott, M. L. Mangoni, *Cell Mol. Life Sci.* **2015**, *72*, 617.

[32] F. Cappiello, A. Di Grazia, L. A. Segev-Zarko, S. Scali, L. Ferrera, L. Galietta, A. Pini, Y. Shai, Y. P. Di, M. L. Mangoni, *Antimicrob. Agents Chemother.* **2016**, *60*, 7252.

[33] D. Dutta, N. Cole, N. Kumar, M. D. Willcox, *Invest. Ophthalmol. Vis. Sci.* **2013**, *54*, 175.

[34] M. L. Read, P. B. Morgan, J. M. Kelly, C. Maldonado-Codina, *J. Biomater. Appl.* **2011**, *26*, 85.

[35] N. Gangopadhyay, M. Daniell, L. Weih, H. R. Taylor, *Br. J. Ophthalmol.* **2000**, *84*, 378.

[36] European Center for Disease Prevention and Control. Annual Report of the European Antimicrobial Resistance Surveillance Network (EARS-Net). ISSN 2363–2666, ISBN 978-92-9498-029-8, doi 10.2900/6928, Stockholm, **2015**.

[37] C. Lakkis, S. M. Fleiszig, *J. Clin. Microbiol.* **2001**, *39*, 1477.

[38] G. M. Bruinsma, M. Rustema-Abbing, H. C. van der Mei, C. Lakkis, H. J. Busscher, *J. Antimicrob. Chemother.* **2006**, *57*, 764.

[39] N. Rajkumari, N. V. John, P. Mathur, M. C. Misra, *J. Glob. Infect. Dis.* **2014**, *6*, 182.

[40] M. Ustunturk, Z. Zeybek, *Wien Klin. Wochenschr.* **2012**, *124*, 17.

[41] B. Casciaro, M. Moros, S. Rivera-Fernandez, A. Bellelli, J. M. de la Fuente, M. L. Mangoni, *Acta Biomater.* **2017**, *47*, 170.

[42] G. T. Qin, A. Lopez, C. Santos, A. M. McDermott, C. Z. Cai, *Biomater. Sci.* **2015**, *3*, 771.

[43] E. Gazit, W. J. Lee, P. T. Brey, Y. Shai, *Biochemistry* **1994**, *33*, 10681.

[44] Y. Pouny, D. Rapaport, A. Mor, P. Nicolas, Y. Shai, *Biochemistry* **1992**, *31*, 12416.

[45] M. D. Willcox, E. B. Hume, Y. Aliwarga, N. Kumar, N. Cole, *J. Appl. Microbiol.* **2008**, *105*, 1817.

[46] X. Gu, J. D. Jennings, J. Snarr, V. Chaudhary, J. E. Pollard, P. B. Savage, *Invest. Ophthalmol. Vis. Sci.* **2013**, *54*, 6217.

[47] N. Malakooti, C. Alexander, C. Alvarez-Lorenzo, *J. Pharm. Sci.* **2015**, *104*, 3386.

[48] B. S. Fazly Bazzaz, B. Khameneh, M. M. Jalili-Behabadi, B. Malaekeh-Nikouei, S. A. Mohajeri, *Cont. Lens Anterior Eye* **2014**, *37*, 149.

[49] M. L. Mangoni, A. M. McDermott, M. Zasloff, *Exp. Dermatol.* **2016**, *25*, 167.

[50] B. Casciaro, F. Cappiello, M. Cacciafesta, M. L. Mangoni, *Front Chem.* **2017**, *5*, 26.

[51] U. Piotrowska, M. Sobczak, E. Oledzka, *Chem. Biol. Drug Des.* **2017**, [Epub ahead of print]

[52] B. Mishra, S. Reiling, D. Zarena, G. Wang, *Curr. Opin. Chem. Biol.* **2017**, *38*, 87.

[53] G. Singh, B. Wu, M. S. Baek, A. Camargo, A. Nguyen, N. A. Slusher, R. Srinivasan, J. P. Wiener-Kronish, S. V. Lynch, *Microb. Pathog.* **2010**, *49*, 196.

How to cite this article: Casciaro B, Dutta D, Loffredo MR, et al. Esculentin-1a derived peptides kill *Pseudomonas aeruginosa* biofilm on soft contact lenses and retain antibacterial activity upon immobilization to the lens surface. *Peptide Science*. 2018;110: e23074. https://doi.org/10.1002/bip.23074

Send Orders for Print-Reprints and e-prints to reprints@benthamscience.ae

Protein & Peptide Letters, **2018**, *25*, 1-8 1

RESEARCH ARTICLE

Esculentin-1a Derived Antipseudomonal Peptides: Limited Induction of Resistance and Synergy with Aztreonam

Bruno Casciaro[a,†], Maria Rosa Loffredo[a,†], Vincenzo Luca[a], Walter Verrusio[b], Mauro Cacciafesta[b] and Maria Luisa Mangoni[a,*]

[a]*Laboratory affiliated to Pasteur Italia-Fondazione Cenci Bolognetti, Department of Biochemical Sciences, Sapienza University of Rome, via degli Apuli, 9, 00185, Rome, Italy;* [b]*Department of Cardiovascular, Respiratory, Nephrological, Anesthesiological and Geriatric Sciences, Sapienza University of Rome, Rome, Viale del Policlinico 155, 00161, Rome, Italy*

ARTICLE HISTORY

Received: December 22, 2017
Revised: May 11, 2018
Accepted: October 10, 2018

DOI:
10.2174/0929866525666181101104649

Abstract: ***Background*:** The massive use of antibiotics has led to the selection of resistant bacterial strains that are difficult to eradicate. Among these, *Pseudomonas aeruginosa* most frequently colonizes and infects the airways of cystic fibrosis patients. Cationic Antimicrobial Peptides (AMPs) represent interesting molecules for the development of new antimicrobial agents. Thanks to their mechanism of action that involves the permeabilization of the bacterial cytoplasmic membrane, the induction of resistance is quite limited.

***Objective*:** The evaluation of the capability of two frog-skin derived AMPs, *i.e.* Esc(1-21) and its diastereomer Esc(1-21)-1c, to induce resistance in *P. aeruginosa* and synergize with aztreonam.

***Method*:** The induction of resistance was evaluated after 15 cycles of exposure to non-inhibitory growth concentrations of antibiotics and peptides. Subsequently, the Minimal Inhibitory Concentration (MIC) was calculated and compared to that obtained before drug exposure. Furthermore, MICs of AMPs and antibiotics were evaluated in Artificial Sputum Medium (ASM). Finally, the ability of the two peptides to synergize with aztreonam was determined by the checkerboard titration method.

Results: *P. aeruginosa* acquired resistance to antibiotics, as evidenced by the increased MICs compared to the initial ones (from 8 to 128-fold higher), while no change in MICs was observed after multiple treatments with the Esc-peptides. In addition, both peptides showed significantly lower MICs than aztreonam in ASM. Finally, the diastereomer Esc(1-21)-1c had the ability to synergize with aztreonam in inhibiting growth and in killing *Pseudomonas* cells.

***Conclusion*:** Both peptides represent promising candidates for the development of new antipseudomonal compounds, which do not induce resistance.

Keywords: Antibiotic resistance, *Pseudomonas aeruginosa*, synergism, esculentin-1a, cystic fibrosis, aztreonam.

1. INTRODUCTION

Microbial resistance has increasingly become a worldwide threat to human health especially in immunocompromised subjects [1]. Even more serious is the situation of patients suffering from some diseases, such as Cystic Fibrosis (CF) [2]. Indeed, the lungs of CF sufferers are repeatedly colonized by Gram-positive and Gram-negative bacteria due to the presence of a sticky and dehydrated mucus that allows the entrapment and accumulation of microorganisms easing their growth and establishment of chronic infections [3]. One of the bacteria that colonize the respiratory tract of CF patients is the ubiquitous Gram-negative *Pseudomonas aeruginosa* [4, 5]. This is because *P. aeruginosa* possesses a high ability to adapt to hostile environmental conditions including nutrition shortages and hypoxia by switching to the biofilm mode of growth. This latter provides tolerance to the inflammatory defense mechanism, to antibiotic therapy and to the anaerobic sputum coating the airways epithelia [6, 7].

In addition, it produces several virulence factors that increase its pathogenicity [8]. The most common antibiotics used for treatment of *Pseudomonas* respiratory infections encompass aminoglycosides [9], fluoroquinolones [10] and the monobactam aztreonam [11], all of which act on stereospecific targets [12, 13]. However, *P. aeruginosa* holds an intrinsic resistance to these antimicrobials due to the presence of an outer-membrane barrier, multidrug efflux transporters as well as endogenous mechanisms of drug inactivation [14]. In the last years, both intravenous and nebulized cationic peptides named polymyxins (*e.g.* colistin), whose antibacterial activity is exerted through binding to the

*Address correspondence to this author at the Laboratory affiliated to Pasteur Italia-Fondazione Cenci Bolognetti, Department of Biochemical Sciences Sapienza University of Rome, via degli Apuli, 9,00185, Rome, Italy; Tel: +39 0649917693; E-mail: marialuisa.mangoni@uniroma1.it
†*The authors equally contributed to the work.*

0929-8665/18 $58.00+.00

Lipopolysaccharide (LPS)-outer membrane of Gram-negative bacteria, have been largely used [15-17]. Nevertheless, resistance to colistin has also been disclosed presumably due to modifications of the LPS moieties [18, 19].

For these reasons, new antibacterial compounds with alternative mechanisms of action are highly needed. Gene-encoded Antimicrobial Peptides (AMPs) represent a valid alternative. They are a class of natural molecules endowed with a wide spectrum of microbial targets (*e.g.* bacteria, viruses, fungi and parasites) [20-24], and with immunomodulatory functions [25-27] that make them even more attractive molecules.

Both cationicity and amphipathicity are two crucial factors for their mechanism of microbial killing, which generally consists in the perturbation of the target cytoplasmic membrane through local breakages formation or through membrane disintegration in a carpet-like manner [28].

Another important aspect of membrane-active AMPs for the generation of new therapeutic agents is their ability to synergize with conventional antibiotics, reducing their effective dosage.

Recently, we characterized a derivative of the frog skin AMP esculentin-1a, *i.e.* Esculentin-1a(1-21)NH_2 [Esc(1-21), GIFSKLAGKKIKNLLISGLKG-NH_2] [29], and its diastereomer carrying two D-amino acids (*i.e.* Leu14 e Ser17) named Esc(1-21)-1c [30]. Both peptides were found to be active against *P. aeruginosa* strains, although the all-L peptide was more efficient against the planktonic form of this pathogen, with a concentration causing 99.9% bacterial killing of 1 μM compared to 4 μM of the diastereomer Esc(1-21)-1c [31]. Yet, Esc(1-21)-1c exhibited a stronger bactericidal activity against the more dangerous biofilm form of *P. aeruginosa*; it was less susceptible to proteolytic degradation and less cytotoxic to mammalian cells than the all-L Esc(1-21) [31].

In this work, we first analyzed the ability of the two esculentin-1a derivatives (Esc peptides) to induce or not resistance in *P. aeruginosa* in comparison with representative drugs of the most commonly used classes of antibiotics (*i.e.* aztreonam, ciprofloxacin, tobramycin and colistin). In parallel, we analyzed the antibacterial activity of the selected compounds in an acidic and poor nutrient medium, mimicking the composition of CF lung mucus [32]. Finally, we investigated the existence of a synergistic anti-pseudomonal activity of the two Esc peptides, in comparison with the commercially available peptide colistin, when combined with the monobactam aztreonam.

To the best of our knowledge the results of our experiments are the first evidence showing that (i) the frog-skin derived Esc peptides do not induce resistance in *P. aeruginosa* after multiple cycles of treatment; (ii) they display antipseudomonal activity in a medium mimicking the composition of CF lung mucus and (iii) the presence of only two D-amino acids in the sequence of Esc(1-21) is sufficient to confer the peptide a synergistic bactericidal activity against *P. aeruginosa* when combined with aztreonam.

2. MATERIALS AND METHODS

2.1. Peptides

Synthetic Esc(1-21) and Esc(1-21)-1c (Esc peptides) were purchased from Chematek Spa (Milan, Italy). They were assembled by stepwise solid-phase synthesis using a standard F-moc strategy. The purification was made *via* Reverse-Phase High-Performance Liquid Chromatography (RP-HPLC) to a purity of 98% and the molecular mass was verified by mass spectrometry.

2.2. Materials

Colistin, tobramycin, ciprofloxacin and aztreonam were from Sigma-Aldrich (St. Luis, MO). Sytox Green was obtained from Molecular Probes (Invitrogen, Carlsbad, CA, USA). Artificial sputum medium (ASM) was prepared, according to [32]: all components were purchased from Sigma-Aldrich (St. Luis, MO).

2.3. Bacterial Strains

For microbiological assays, the reference strain *P. aeruginosa* PAO1 and the CF clinical isolates *P. aeruginosa* AA43, AA11 and TR67 were used. These CF strains were chosen from the strains collection of the CF clinic Medizinische Hochschule of Hannover, Germany [33].

2.4. Determination of Minimal Inhibitory Concentration

P. aeruginosa PAO1 and *P. aeruginosa* AA43 were allowed to grow in Luria-Bertani (LB) medium at 37 °C until reaching an optical density of 0.8 at 590 nm and were then diluted in Mueller-Hinton (MH) broth. Aliquots of 50 μL of the diluted bacterial culture containing 1 x 10^5 cells were added to 50 μL of MH containing serial two-fold dilutions of drugs, in a 96-well plate. The plates were then incubated for 16 h at 37 °C and minimal inhibitory concentration (MIC) was defined as the concentration of drug at which 100 % inhibition of microbial growth was observed. ASM diluted 1:10 in water was used to determine the MIC of the tested compounds as described above.

2.5. Induction of Resistance

To evaluate the induction of resistance, multiple exposures of the bacterial suspension to serial two-fold dilutions of the tested compounds (peptide or conventional antibiotics) were performed using a diluted inoculum (1:10.000 in MH) of the bacterial culture grown at ½ MIC.

After 15 cycles, bacteria were grown for two passages in a drug-free medium. Note that the duration of each cycle was dependent on the time needed for a visible turbidity of the wells containing sub-MIC drug concentrations (~ 2-3 days). Afterwards, the standard MIC assay was carried out as described above. The final MICs were compared to the initial ones and graphed as fold increase in MIC.

2.6. Membrane Perturbation Assay

Bacterial cells were grown at 37 °C in LB medium until reaching an optical density of 0.8 at 590 nm. Afterwards,

samples were centrifuged for 10 minutes at 1400 x *g* and resuspended in Phosphate Buffered Saline (PBS) at a concentration of $1x10^7$ *colony-forming units* (CFU)/mL. The membrane impermeable probe Sytox Green was added at a concentration of 1 µM. Ninty-five µl of the bacterial suspension were then loaded into the wells of a 96-well plate and 5 µl of peptides were added to achieve a final concentration of 64, 16 or 4 µM. After peptide addition, the fluorescence was monitored at 37 °C in a microplate reader (Infinite M200; Tecan, Salzburg, Austria) at excitation and emission wavelengths of 485 and 535 nm, respectively.

2.7. Synergistic Effect Between Cationic Peptides and Aztreonam

Effects of drugs combinations in inhibiting bacterial growth were determined by the checkerboard titration method by adding combinations of two compounds in a serial-two fold dilution to wells of a 96-well plate containing 1 x 10^6 CFU/mL of the clinical isolate AA43 in a final volume of 100 µL of 10% MH. The ranges of drug concentrations were from 2 to 0.03 µM (*i.e.* 4.4 to 0.07 µg/mL) for both Esc(1-21) and Esc(1-21)-1c; from 1 to 0.015 µg/mL for colistin and from 32 to 0.25 µg/mL for aztreonam. The plates were incubated for 24 h at 37 °C at 125 rpm and the Fractional Inhibitory Concentration (FIC) index for combination of two compounds was calculated according to the formula:

$$\text{FIC index} = FIC_A + FIC_B = A / MIC_A + B / MIC_B$$

where A and B are the MICs of drug A and drug B in the combination, while MIC_A and MIC_B represent the MIC values of the compounds alone. As reported in [34], the FIC indices were interpreted as follows: FIC ≤0.5, synergy; 0.5 <FIC ≤ 1, additivity, 1 < FIC ≤ 2, no interaction, FIC >2, antagonism.

To evaluate the synergism in killing *P. aeruginosa,* an aliquot from the well with the lowest FIC value (FIC well) and from the wells containing each single compound at the corresponding concentration in the combination (FIC well) was withdrawn, diluted and plated for CFU counting. Results were interpreted by the effect of the combination in comparison with the most active single drug alone. As reported in [35] synergism was defined as a ≥ 100-fold increase in killing at 24 h by the combination of drugs with respect to the most active single compound.

3. RESULTS

3.1. Esc peptides do not Induce Resistance Unlike Conventional Antibiotics

To investigate whether an extended exposure of *P. aeruginosa* to Esc(1-21) and Esc(1-21)-1c elicited resistance to them, repeated treatments at serial two-fold dilutions of each peptide were performed and compared to the results of four representative drugs of the most commonly used classes of antibiotics (*i.e.* ciprofloxacin, tobramycin, colistin and aztreonam). Either a reference strain of *P. aeruginosa* (PAO1) or a CF clinical isolate (AA43) were used.

As indicated in Figure **1**, after 15 cycles of exposure to colistin, ciprofloxacin, aztreonam and tobramycin and subsequent growth in drug-free medium (see experimental method) the MIC of these compounds was found to be from 8-fold to 128-fold higher than the initial value, indicating the induction of resistance. In contrast, after multiple exposures to Esc(1-21), the MIC did not change. Similar results were detected for Esc(1-21)-1c and therefore are not shown.

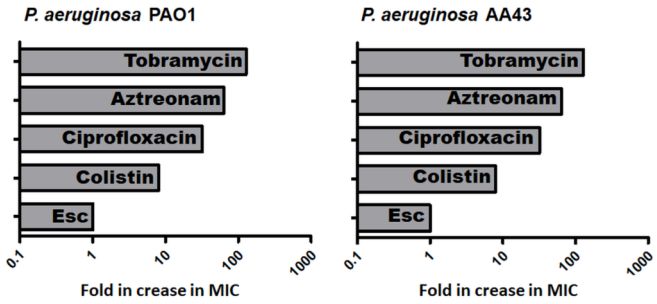

Figure 1. Fold increase in MIC of aztreonam, tobramycin, ciprofloxacin, colistin and Esc(1-21) (Esc) against *P. aeruginosa* PAO1 and the CF clinical isolate *P. aeruginosa* AA43 after 15 cycles of treatment.

3.2. The Acquisition of Resistance to Tobramycin and Ciprofloxacin Slightly Affects the Membrane Perturbation Elicited by the Esc Peptides

Tobramycin and ciprofloxacin are the two most common antibiotics used in clinical practice for treatment of *P. aeruginosa* pulmonary infections. To assess whether the acquisition of bacterial resistance to these antibiotics led to a different susceptibility to the membrane perturbation caused by the two Esc peptides, Sytox Green assays were performed on the clinical isolate AA43 using three different concentrations of Esc(1-21) and Esc(1-21)-1c (4 µM, 16 µM and 64 µM). Sytox Green is a fluorescent probe whose fluorescence intensity increases when it binds to intracellular DNA. The probe does not enter the cell if the membrane is intact; therefore, the increase in fluorescence is proportional to the membrane damage and the resulting binding to DNA. As indicated in Figure **2**, a faster and stronger membrane perturbing activity was recorded for Esc(1-21) on the wild-type AA43 in comparison to its diastereomer, in agreement with what shown in [36]. However, when the two peptides were tested against the Tobramycin-resistant (TOB-res) and Ciprofloxacin-resistant (CIP-res) AA43, two different trends were observed. A prolonged exposure to ciprofloxacin made the AA43 strain more susceptible to the membrane perturbing activity induced by both Esc(1-21) and Esc(1-21)-1c, at all concentrations used, as pointed out by the higher fluorescence intensity than that of the wild-type strain. The same trend was also observed when AA43 strain, repeatedly exposed to tobramycin (TOB-res strain) was treated with Esc(1-21) at 64 µM and 16 µM; in contrast, when 4 µM Esc(1-21) was used on the TOB-res strain, a slightly slower membrane perturbing activity was obtained in comparison to the wild-type AA43. When the diastereomer Esc(1-21)-1c was used, much slower and less pronounced membrane perturbation in the TOB-res strain was observed at all peptide concentrations used (Figure **2**).

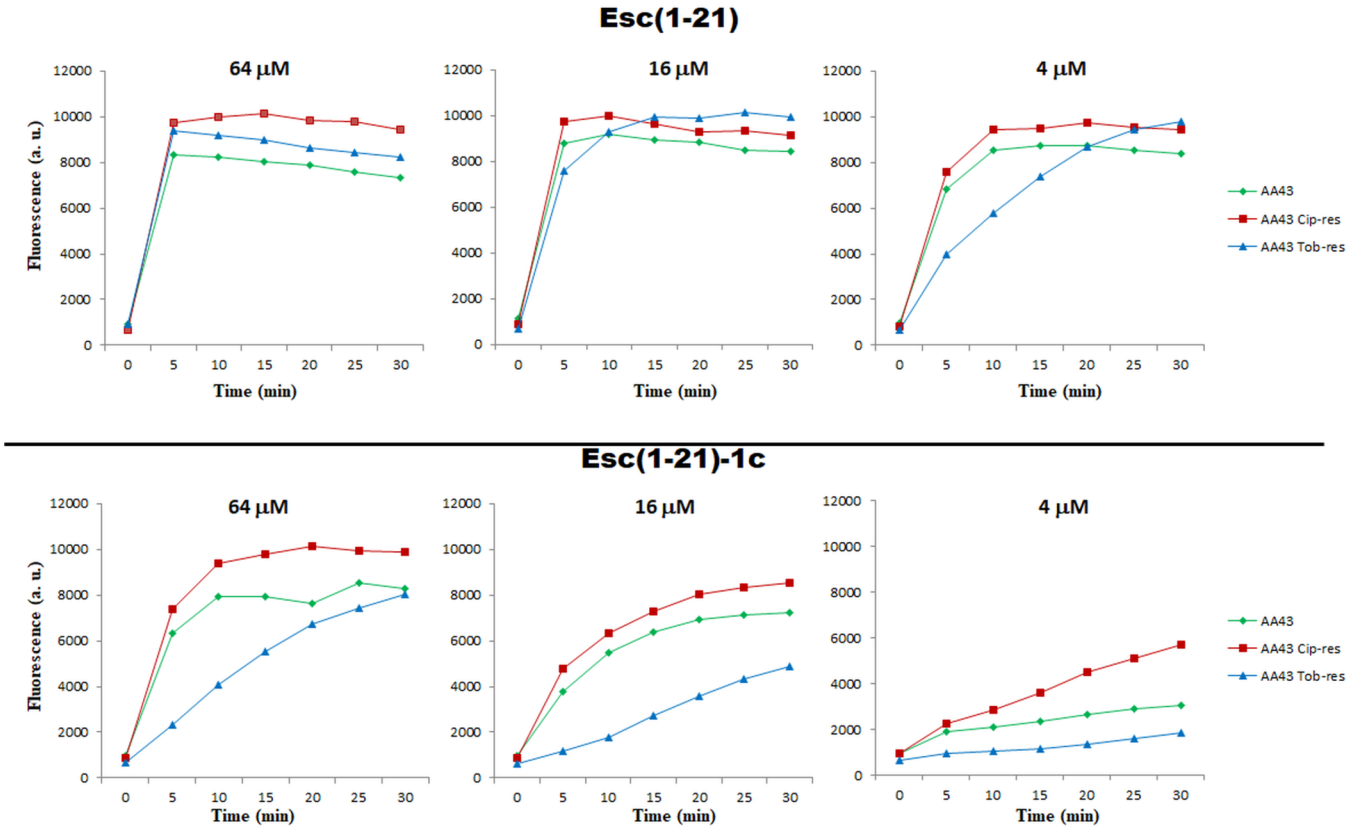

Figure 2. Kinetics of cytoplasmic membrane permeabilization of Esc(1-21) and Esc(1-21)-1c on *P. aeruginosa* AA43 wild-type (green line); AA43 TOB-res (blue line) and AA43 CIP-res strains (red line). Cells ($1x10^7$ CFU/mL) were incubated with 1 µM of Sytox Green and treated with the peptide at 64, 16 and 4 µM for 30 minutes. Changes in fluorescence (λ exc = 485 nm, λ ems = 535 nm) were monitored and expressed as arbitrary units. Data were taken from a single experiment representative of three independent experiments. (*The color version of the figure is available in the electronic copy of the article*).

Table 1. Antipseudomonal activity of Esc(1-21), Esc(1-21)-1c, colistin and aztreonam against the reference strain *P. aeruginosa* PAO1 and the CF clinical isolates AA11, AA43 and TR67 after 16-20 h at 37 °C in 10% ASM.

MIC (µg/mL)*				
Strain	**Esc(1-21)**	**Esc(1-21)-1c**	**Colistin**	**Aztreonam**
***P. aeruginosa* PAO1**	4.4	4.4	0.5	32
***P. aeruginosa* AA11**	4.4	8.8	0.5	2
***P. aeruginosa* AA43**	8.8	35.2	0.25	128
***P. aeruginosa* TR67**	2.2	0.5	0.125	4

*Values are those obtained from at least two readings out of three independent experiments.

3.3. Determination of MICs in Artificial Sputum Medium

To get insight whether the antimicrobial activity of the peptides was affected by low pH, *e.g.* the acidic environment coating the airways of CF sufferers, their MIC was tested in ASM against a panel of CF clinical isolates. Both the currently used peptide colistin and the "last generation drug" aztreonam were also included for comparison. Interestingly, against almost all the strains, the AMPs were found to be stronger than aztreonam as evidenced by the lowest MIC values ranging from 0.125 to 35.2 µg/mL for the AMPs and from 2 to 128 µg/mL for aztreonam (Table **1**).

3.4. Esc(1-21)-1c Synergizes with Aztreonam in Inhibiting and Killing *P. aeruginosa* AA43 Cells

To evaluate a possible synergistic effect of Esc(1-21) and Esc(1-21)-1c when combined with aztreonam, 96-well synergy plates were prepared as described in materials and methods. The combination aztreonam plus colistin was also assayed for comparison. As shown in Table **2**, the FIC values of colistin and Esc(1-21) in combination with aztreonam were equal to 0.53 and 0.56 respectively, indicating the presence of an additive effect (additivity for $0.5 < FIC \leq 1$). Dif-

ferently, when Esc(1-21)-1c at 1/16 MIC (0.06 μM corresponding to 0.14 μg/mL) was analyzed in the presence of aztreonam at ¼ MIC (73.5 μM corresponding to 32 μg/mL) a FIC of 0.31 was detected, highlighting the existence of a synergistic effect between the two drugs in inhibiting *P. aeruginosa* growth.

Table 2. Effect of Esc peptides/colistin in combination with the monobactam aztreonam on the inhibition of *P. aeruginosa* AA43 growth.

Drug Combination	FIC*
Colistin + aztreonam	0.53
Esc(1-21) + aztreonam	0.56
Esc(1-21)-1c + aztreonam	0.31

*The values are those obtained from at least two readings out of three independent experiments according to the formula of FIC index= $FIC_A + FIC_B = A / MIC_A + B / MIC_B$. A synergistic effect is considered for a FIC ≤ 0.5.

To further verify whether the combination aztreonam + Esc(1-21)-1c also synergized in the bactericidal activity, the number of viable bacterial cells was counted and related to the number of CFU after treatment with each individual compound at the concentration used in the combination (Figure **3**). As reported in Figure 3, while a number of ~ 2 x 10^8 CFU/mL or ~ 2 x 10^7 CFU/mL was counted after 24 h incubation with 1/16 MIC of Esc(1-21)-1c or ¼ MIC of aztreonam respectively, the number of viable cells recorded from the combination aztreonam + Esc(1-21)-1c was reduced to ~ 2 x 10^4 CFU/mL. Since the ratio between the number of CFU of the most active compound (*i.e.* aztreonam at 32 μg/mL) and the number of CFU from the combination [Esc(1-21)-1c + aztreonam] was significantly greater than 100 (~1000), this underlined the existence of a synergistic bactericidal activity.

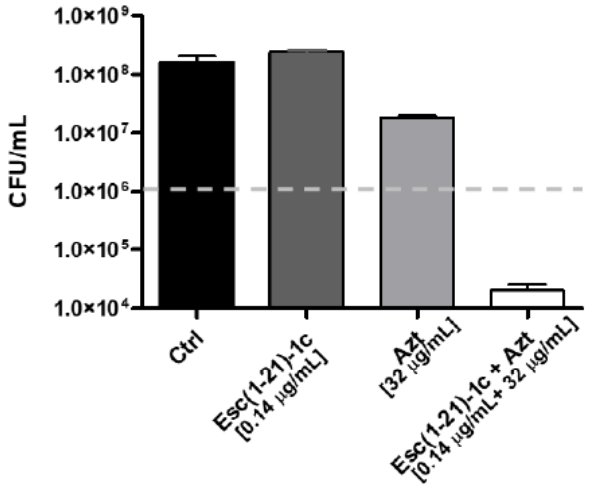

Figure 3. Effect of Esc(1-21)-1c and aztreonam on the number of viable bacterial cells (CFU/mL) 24 h after treatment with each compound alone or their combination. The peptide and aztreonam were used at a concentration of 1/16 MIC and ¼ MIC, respectively. The dotted line indicates the initial number of viable counts. Values are the mean of three different experiments ± SD.

4. DISCUSSION

The ability of *P. aeruginosa* to tolerate minimal nutritional requirements as well as adverse conditions has allowed this bacterium to persist in both community and hospitals [5, 37, 38].

Unfortunately, prolonged exposure to traditional antibiotics is leading to an increasing selection of *P. aeruginosa* "superbugs". This is mainly due to the ability of this bacterium to rapidly develop resistance to multiple classes of antibiotics even during the course of therapy [39]. This can occur through the acquisition of resistance genes on mobile genetic elements or through mutational processes that alter the drug target or the expression of proteins/drug inactivating enzymes [15].

Macfarlane and colleagues [40] have demonstrated a role of the PhoP-PhoQ Two-Component regulatory System (TCS) in the development of resistance to aminoglycosides [41]. In particular, in Mg^{2+} starvation, the sensor protein PhoQ auto-phosphorylates a conserved histidine residue and then activates the transcription factor PhoP by a phosphotransfer reaction. PhoP-PhoQ upregulates the expression of the outer-membrane porin OprH in *P. aeruginosa*, leading to OM modification [42-44]. These changes are also involved in the resistance mechanisms to polymyxin B [45]. Indeed, OprH binds to the divalent cation-binding sites of LPS, making these sites unavailable for polymyxin binding. In addition, the activation of PhoP-PhoQ triggers the indirect activation of the PmrA-PmrB TCS, which controls the synthesis and transfer of phosphoethanolamine and 4-amino-4-deoxy-L-arabinose, respectively, to LPS [46]. This modification results in a reduction of the overall negative charge of the LPS-outer membrane, making bacterial cells less susceptible to the activity of membrane active cationic peptides [43, 47].

4.1. Induction of Resistance

In this work, we have shown for the first time that both Esc peptides do not induce resistance in *P. aeruginosa* strains (either reference or clinical isolate) that have been repeatedly exposed to them, as proved by the unchanged MICs even after 15 cycles of treatment. This is likely due to the membrane-perturbing mechanism of Esc peptides, which should make it difficult for the bacteria to acquire resistance. Indeed, this would require a drastic change in the lipid composition of the microbial membrane and could not happen without provoking a lethal damage to the bacteria. In contrast, after multiple exposures to the currently used peptide colistin or to those antibiotic molecules belonging to different classes (*i.e.,* tobramycin, ciprofloxacin and aztreonam) *P. aeruginosa* is able to acquire resistance to them, as indicated by the significantly increased MICs, up to 128-fold higher than the initial value, in the case of tobramycin (Figure **1**). This is in line with the trend of activity already described in the literature for several conventional antibiotics against different Gram-negative bacterial species (*Escherichia coli, Acinetobacter baumannii* and *Klebsiella pneumonia*) [48].

Nevertheless, a limited induction of bacterial resistance to AMPs has been reported [49, 50]. As an example, Kubicek-Sutherland and colleagues highlighted the selection of resistant *Staphylococcus aureus* strains after serial passages in the presence of increasing concentrations of the human

cathelicidin AMP, LL-37, PR-39 or wheat germ histones [51]. Hein-Kristensen and colleagues reported the development of resistance in *Escherichia coli* to α-Peptide/β-Peptoid peptidomimetic [52], while Yechiel Shai and coworkers described the relationship between the peptide structure and the ability to induce resistance by activation of PhoP-PhoQ in *Salmonella* [53].

Another relevant finding of our work is that the antimicrobial effectiveness and membrane perturbation activity of the two Esc peptides were not significantly affected by pretreatment of bacteria with traditional antibiotics. Indeed, an invariable MIC value was detected for Esc(1-21) and its diastereomer when tested against *P. aeruginosa* AA43 strains that had acquired resistance to tobramycin and ciprofloxacin (data not shown).

As demonstrated by the Sytox Green assay (Figure **2**), the kinetics of membrane perturbation caused by the two peptides on the CIP-res AA43 strain was comparable to that of the wild type. In contrast, a slower and weaker membrane perturbation was displayed by Esc(1-21)-1c against the TOB-res strain. This is presumably due to changes in the OM composition (upon prolonged exposure to tobramycin) that may affect the activity of the two Esc peptides to a different extent.

4.2. Activity in Mucus Mimicking Environment

Prolonged antibiotic therapy often occurs for treatment of chronic and persistent infections such as those in the airways of CF patients. The airways of these subjects are covered by an acidic and sticky mucus, which contributes to the impairment of antibiotics function [54]. We demonstrated that both Esc peptides and colistin maintained their antipseudomonal activity, even in an acidic medium mimicking the mucus composition of CF airways. As highlighted by the lowest MIC values in ASM, AMPs were more efficient in inhibiting growth of *Pseudomonas* cells than the new generation antibiotic aztreonam (Table **1**) [55].

4.3. Synergistic Activity

As reported in the literature, the combination of antiinfective agents represents a promising strategy to expand their antimicrobial spectrum and to ameliorate their therapeutic outcome, reducing the selection of resistant strains [56-58]. Although synergy between antibiotics belonging to different classes is pretty rare, cases of synergy between AMPs and conventional antibiotics have been discovered. Among them, the synergistic activity between BMAP-28 and CRAMP in combination with vancomycin [59, 60]. Furthermore, synergistic and additive effects between the dendrimeric peptide M33 and aztreonam were reported against *P. aeruginosa* multi-drug resistant strains with FICs of 0.5 and 1 respectively [34].

In our experiments, both Esc(1-21) and colistin showed an additive effect when combined with aztreonam (FIC of 0.56 and 0.53, respectively). However, a clear and strong synergism in inhibiting the growth of *P. aeruginosa* was detected when the diastereomer Esc(1-21)-1c (at 1/16 MIC) was combined with aztreonam. More importantly, besides displaying a synergistic effect in inhibiting the growth of *Pseudomonas* cells, the two drugs were also able to synergize in the bactericidal activity. Indeed, >100-fold reduction in the number of viable bacteria was observed after 24 h treatment with Esc(1-21)-1c + aztreonam, at their sub-MIC, compared to the number of surviving microorganisms, 24 h after incubation with each drug alone. It is conceivable that membrane-disturbing AMPs act as helper agents at their sub-MICs favoring the intracellular influx of drugs, *e.g.,* aztreonam, and leading to the reduction of their effective dosage. The different outcome between the two Esc peptides could be related to the existence of intracellular chiral targets on which the diastereomer (but not the all-L peptide) can act to boost the antimicrobial effect of aztreonam. Nevertheless, we cannot rule out that the synergistic effect may in part be the consequence of an extended bioavailability of the diastereomer compared to the all-L Esc(1-21) which would be degraded faster.

CONCLUSION

In contrast with conventional antibiotics and the currently used peptide colistin, our Esc peptides do not induce resistance in *P. aeruginosa* cells and preserve their effectiveness on *P. aeruginosa* strains previously exposed to traditional antibiotics, *e.g.* ciprofloxacin and tobramycin, although with a slight different kinetics of membrane perturbation. Furthermore, they exhibit antimicrobial activity in an acidic CF-mucus mimicking environment, while the presence of only two D-amino acids can confer the peptide a synergistic antipseudomonal activity in combination with aztreonam.

In conclusion, we can state that our Esc peptides represent attractive molecules not only for the development of single-peptide based new anti-pseudomonal agents but also for the development of novel combinatorial therapies with traditional drugs.

ETHICS APPROVAL AND CONSENT TO PARTICIPATE

Not applicable.

HUMAN AND ANIMAL RIGHTS

No animals/humans were used for studies that are the basis of this research.

CONSENT FOR PUBLICATION

Not applicable.

CONFLICT OF INTEREST

The authors declare no conflict of interest, financial or otherwise.

ACKNOWLEDGEMENTS

This work was supported by grants from Sapienza University of Rome and the Italian Cystic Fibrosis Foundation (project FFC#11/2014 adopted by FFC Delegations from Siena, Sondrio Valchiavenna, Cerea Il Sorriso di Jenny, and Pavia and project FFC 15/2017 Adopted by Delegations of Palermo, Vittoria, Ragusa, Siracusa, Catania Mascalucia, Messina, Gruppo di Sostegno di Tremestieri). M.L.M thanks Alessandra Bragonzi (San Raffaele Institute, Milan, Italy)

and Burkhard Tummler (Klinische Forschergruppe, OE 6710, Medizinische Hochschule Hannover, Germany) for the *P. aeruginosa* clinical isolates.

REFERENCES

[1] Michael, C.A.; Dominey-Howes, D.; Labbate, M. The antimicrobial resistance crisis: Causes, consequences, and management. *Front. Public Health,* **2014**, *2*, 145.

[2] Stefani, S.; Campana, S.; Cariani, L.; Carnovale, V.; Colombo, C.; Lleo, M.M.; Iula, V.D.; Minicucci, L.; Morelli, P.; Pizzamiglio, G.; Taccetti, G. Relevance of multidrug-resistant *Pseudomonas aeruginosa* infections in cystic fibrosis. *Int. J. Med. Microbiol.,* **2017**, *307*(6), 353-362.

[3] Doring, G.; Flume, P.; Heijerman, H.; Elborn, J.S. Treatment of lung infection in patients with cystic fibrosis: Current and future strategies. *J. Cyst. Fibros,* **2012**, *11*(6), 461-479.

[4] Lund-Palau, H.; Turnbull, A.R.; Bush, A.; Bardin, E.; Cameron, L.; Soren, O.; Wierre-Gore, N.; Alton, E.W.; Bundy, J.G.; Connett, G.; Faust, S.N.; Filloux, A.; Freemont, P.; Jones, A.; Khoo, V.; Morales, S.; Murphy, R.; Pabary, R.; Simbo, A.; Schelenz, S.; Takats, Z.; Webb, J.; Williams, H.D.; Davies, J.C. *Pseudomonas aeruginosa* infection in cystic fibrosis: Pathophysiological mechanisms and therapeutic approaches. *Expert Rev. Respir. Med.,* **2016**, *10*(6), 685-697.

[5] Klockgether, J.; Tummler, B. Recent advances in understanding *Pseudomonas aeruginosa* as a pathogen. *F1000Res.,* **2017**, *6*, 1261.

[6] Hoffmann, N.; Rasmussen, T.B.; Jensen, P.O.; Stub, C.; Hentzer, M.; Molin, S.; Ciofu, O.; Givskov, M.; Johansen, H.K.; Hoiby, N. Novel mouse model of chronic *Pseudomonas aeruginosa* lung infection mimicking cystic fibrosis. *Infect. Immun.,* **2005**, *73*(4), 2504-2514.

[7] Jelsbak, L.; Johansen, H.K.; Frost, A.L.; Thogersen, R.; Thomsen, L.E.; Ciofu, O.; Yang, L.; Haagensen, J.A.; Hoiby, N.; Molin, S. Molecular epidemiology and dynamics of *Pseudomonas aeruginosa* populations in lungs of cystic fibrosis patients. *Infect. Immun.,* **2007**, *75*(5), 2214-2224.

[8] Gellatly, S.L.; Hancock, R.E. *Pseudomonas aeruginosa*: New insights into pathogenesis and host defenses. *Pathog. Dis.,* **2013**, *67*(3), 159-173.

[9] Kotra, L.P.; Haddad, J.; Mobashery, S. Aminoglycosides: Perspectives on mechanisms of action and resistance and strategies to counter resistance. *Antimicrob. Agents Chemother.,* **2000**, *44*(12), 3249-3256.

[10] Aldred, K.J.; Kerns, R.J.; Osheroff, N. Mechanism of quinolone action and resistance. *Biochemistry,* **2014**, *53*(10), 1565-1574.

[11] Matsen, J.M.; Bosso, J.A. The use of aztreonam in the cystic fibrosis patient. *Pediatr. Infect. Dis. J.,* **1989**, *8*(9 Suppl), S117-119.

[12] Hoiby, N. Recent advances in the treatment of *Pseudomonas aeruginosa* infections in cystic fibrosis. *BMC Med.,* **2011**, *9*, 32.

[13] Waglechner, N.; Wright, G.D. Antibiotic resistance: It's bad, but why isn't it worse? *BMC Biol.,* **2017**, *15*(1), 84.

[14] Poole, K. *Pseudomonas aeruginosa*: Resistance to the max. *Front. Microbiol.,* **2011**, *2*, 65.

[15] Morita, Y.; Tomida, J.; Kawamura, Y. Responses of *Pseudomonas aeruginosa* to antimicrobials. *Front. Microbiol.,* **2014**, *4*, 422.

[16] Gurjar, M. Colistin for lung infection: An update. *J. Intensive Care,* **2015**, *3*(1), 3.

[17] Sabuda, D.M.; Laupland, K.; Pitout, J.; Dalton, B.; Rabin, H.; Louie, T.; Conly, J. Utilization of colistin for treatment of multidrug-resistant *Pseudomonas aeruginosa*. *Can. J. Infect. Dis. Med. Microbiol.,* **2008**, *19*(6), 413-418.

[18] Bakthavatchalam, Y.D.; Pragasam, A.K.; Biswas, I.; Veeraraghavan, B. Polymyxin susceptibility testing, interpretative breakpoints and resistance mechanism: An update. *J. Glob. Antimicrob. Resist.,* **2017**, *12*, 124-136.

[19] Srinivas, P.; Rivard, K. Polymyxin resistance in gram-negative pathogens. *Curr. Infect. Dis. Rep.,* **2017**, *19*(11), 38.

[20] Chatterjee, M.; Anju, C.P.; Biswas, L.; Kumar, V.A.; Mohan, C.G.; Biswas, R. Antibiotic resistance in *Pseudomonas aeruginosa* and alternative therapeutic options. *Int. J. Med. Microbiol.,* **2016**, *306*(1), 48-58.

[21] Casciaro, B.; Dutta, D.; Loffredo, M.R.; Marcheggiani, S.; McDermott, A.M.; Willcox, M.D.; Mangoni, M.L. Esculentin-1a derived peptides kill *Pseudomonas aeruginosa* biofilm on soft contact lenses and retain antibacterial activity upon immobilization to the lens surface. *Biopolymers,* **2017** (ahead of print).

[22] Merlino, F.; Carotenuto, A.; Casciaro, B.; Martora, F.; Loffredo, M.R.; Di Grazia, A.; Yousif, A.M.; Brancaccio, D.; Palomba, L.; Novellino, E.; Galdiero, M.; Iovene, M.R.; Mangoni, M.L.; Grieco, P. Glycine-replaced derivatives of [Pro(3),DLeu(9)]TL, a temporin L analogue: Evaluation of antimicrobial, cytotoxic and hemolytic activities. *Eur. J. Med. Chem.,* **2017**, *139*, 750-761.

[23] Casciaro, B.; Moros, M.; Rivera-Fernandez, S.; Bellelli, A.; de la Fuente, J.M.; Mangoni, M.L. Gold-nanoparticles coated with the antimicrobial peptide esculentin-1a(1-21)NH2 as a reliable strategy for antipseudomonal drugs. *Acta Biomater.,* **2017**, *47*, 170-181.

[24] Di Giampaolo, A.; Luzi, C.; Casciaro, B.; Bozzi, A.; Mangoni, M.L.; Aschi, M. P-113 peptide: New experimental evidences on its biological activity and conformational insights from molecular dynamics simulations. *Biopolymers,* **2014**, *102*(2), 159-167.

[25] Fabisiak, A.; Murawska, N.; Fichna, J. LL-37: Cathelicidin-related antimicrobial peptide with pleiotropic activity. *Pharmacol. Rep.,* **2016**, *68*(4), 802-808.

[26] Cappiello, F.; Casciaro, B.; Kolar, S.S.; Baidouri, H.; McDermott, A.M.; Mangoni, M.L. Methods for *in vitro* analysis of antimicrobial activity and toxicity of anti-keratitis peptides: Bacterial viability in tears, MTT, and TNF-alpha release assays. *Methods Mol. Biol.,* **2017**, *1548*, 395-409.

[27] Cappiello, F.; Di Grazia, A.; Segev-Zarko, L. A.; Scali, S.; Ferrera, L.; Galietta, L.; Pini, A.; Shai, Y.; Di, Y. P.; Mangoni, M. L. Esculentin-1a-derived peptides promote clearance of *Pseudomonas aeruginosa* internalized in bronchial cells of cystic fibrosis patients and lung cell migration: Biochemical properties and a plausible mode of action. *Antimicrob. Agents Chemother.,* **2016**, *60*(12), 7252-7262.

[28] Shai, Y. Mechanism of the binding, insertion and destabilization of phospholipid bilayer membranes by alpha-helical antimicrobial and cell non-selective membrane-lytic peptides. *Biochim. Biophys. Acta,* **1999**, *1462*(1-2), 55-70.

[29] Luca, V.; Stringaro, A.; Colone, M.; Pini, A.; Mangoni, M.L. Esculentin(1-21), an amphibian skin membrane-active peptide with potent activity on both planktonic and biofilm cells of the bacterial pathogen *Pseudomonas aeruginosa*. *Cell Mol. Life Sci.,* **2013**, *70*(15), 2773-2786.

[30] Casciaro, B.; Cappiello, F.; Cacciafesta, M.; Mangoni, M. L. Promising approaches to optimize the biological properties of the antimicrobial peptide Esculentin-1a(1-21)NH_2: Amino acids substitution and conjugation to nanoparticles. *Front. Chem.,* **2017**, *5*, 26.

[31] Di Grazia, A.; Cappiello, F.; Cohen, H.; Casciaro, B.; Luca, V.; Pini, A.; Di, Y.P.; Shai, Y.; Mangoni, M.L. D-Amino acids incorporation in the frog skin-derived peptide esculentin-1a(1-21)NH_2 is beneficial for its multiple functions. *Amino Acids,* **2015**, *47*(12), 2505-2519.

[32] Kirchner, S.; Fothergill, J.L.; Wright, E.A.; James, C.E.; Mowat, E.; Winstanley, C. Use of artificial sputum medium to test antibiotic efficacy against *Pseudomonas aeruginosa* in conditions more relevant to the cystic fibrosis lung. *J. Vis. Exp.,* **2012**, (64), e3857.

[33] Bragonzi, A.; Paroni, M.; Nonis, A.; Cramer, N.; Montanari, S.; Rejman, J.; Di Serio, C.; Doring, G.; Tummler, B. *Pseudomonas aeruginosa* microevolution during cystic fibrosis lung infection establishes clones with adapted virulence. *Am. J. Respir. Crit. Care Med.,* **2009**, *180*(2), 138-145.

[34] Pollini, S.; Brunetti, J.; Sennati, S.; Rossolini, G.M.; Bracci, L.; Pini, A.; Falciani, C. Synergistic activity profile of an antimicrobial peptide against multidrug-resistant and extensively drug-resistant strains of Gram-negative bacterial pathogens. *J. Pept. Sci.,* **2017**, *23*(4), 329-333.

[35] Lorian, V. *Antibiotics in laboratory medicine,* 4th ed.; Williams & Wilkins: Baltimore, **1996**, pp. 1-23.

[36] Loffredo, M.R.; Ghosh, A.; Harmouche, N.; Casciaro, B.; Luca, V.; Bortolotti, A.; Cappiello, F.; Stella, L.; Bhunia, A.; Bechinger, B.; Mangoni, M.L. Membrane perturbing activities and structural properties of the frog-skin derived peptide Esculentin-1a(1-21)NH_2 and its diastereomer Esc(1-21)-1c: Correlation with their antipseudomonal and cytotoxic activity. *Biochim. Biophys. Acta,* **2017**, *1859*(12), 2327-2339.

[37] Azzopardi, E.A.; Azzopardi, E.; Camilleri, L.; Villapalos, J.; Boyce, D.E.; Dziewulski, P.; Dickson, W.A.; Whitaker, I.S. Gram negative wound infection in hospitalised adult burn patients-systematic review and metanalysis. *PLoS One,* **2014**, *9*(4), e95042.

[38] Mulcahy, L.R.; Isabella, V.M.; Lewis, K. *Pseudomonas aeruginosa* biofilms in disease. *Microb. Ecol.,* **2014**, *68*(1), 1-12.

[39] Fair, R.J.; Tor, Y. Antibiotics and bacterial resistance in the 21st century. *Perspect. Medicin. Chem.,* **2014**, *6*, 25-64.

[40] Macfarlane, E.L.; Kwasnicka, A.; Hancock, R.E. Role of *Pseudomonas aeruginosa* PhoP-phoQ in resistance to antimicrobial cationic peptides and aminoglycosides. *Microbiology,* **2000**, *146*(Pt 10), 2543-2554.

[41] Gellatly, S. L.; Needham, B.; Madera, L.; Trent, M. S.; Hancock, R. E. The *Pseudomonas aeruginosa* PhoP-PhoQ two-component regulatory system is induced upon interaction with epithelial cells and controls cytotoxicity and inflammation. *Infect. Immun.,* **2012**, *80*(9), 3122-3131.

[42] McPhee, J.B.; Bains, M.; Winsor, G.; Lewenza, S.; Kwasnicka, A.; Brazas, M.D.; Brinkman, F.S.; Hancock, R.E. Contribution of the PhoP-PhoQ and PmrA-PmrB two-component regulatory systems to Mg^{2+}-induced gene regulation in *Pseudomonas aeruginosa*. *J. Bacteriol.,* **2006**, *188*(11), 3995-4006.

[43] Olaitan, A.O.; Morand, S.; Rolain, J.M. Mechanisms of polymyxin resistance: Acquired and intrinsic resistance in bacteria. *Front. Microbiol.,* **2014**, *5*, 643.

[44] Chevalier, S.; Bouffartigues, E.; Bodilis, J.; Maillot, O.; Lesouhaitier, O.; Feuilloley, M.G.J.; Orange, N.; Dufour, A.; Cornelis, P. Structure, function and regulation of *Pseudomonas aeruginosa* porins. *FEMS Microbiol. Rev.,* **2017**, *41*(5), 698-722.

[45] Macfarlane, E.L.; Kwasnicka, A.; Ochs, M.M.; Hancock, R.E. PhoP-PhoQ homologues in *Pseudomonas aeruginosa* regulate expression of the outer-membrane protein OprH and polymyxin B resistance. *Mol. Microbiol.,* **1999**, *34*(2), 305-316.

[46] Raetz, C.R.; Reynolds, C.M.; Trent, M.S.; Bishop, R.E. Lipid A modification systems in gram-negative bacteria. *Annu. Rev. Biochem.,* **2007**, *76*, 295-329.

[47] Nikaido, H. Molecular basis of bacterial outer membrane permeability revisited. *Microbiol. Mol. Biol. Rev.,* **2003**, *67*(4), 593-656.

[48] Jahnsen, R.D.; Haney, E.F.; Franzyk, H.; Hancock, R.E. Characterization of a proteolytically stable multifunctional host defense peptidomimetic. *Chem. Biol.,* **2013**, *20*(10), 1286-1295.

[49] Hong, J.; Hu, J.; Ke, F. Experimental induction of bacterial resistance to the antimicrobial peptide tachyplesin I and investigation of the resistance mechanisms. *Antimicrob. Agents Chemother.,* **2016**, *60*(10), 6067-6075.

[50] Baltz, R.H. Daptomycin: Mechanisms of action and resistance, and biosynthetic engineering. *Curr. Opin. Chem. Biol.,* **2009**, *13*(2), 144-151.

[51] Kubicek-Sutherland, J.Z.; Lofton, H.; Vestergaard, M.; Hjort, K.; Ingmer, H.; Andersson, D.I. Antimicrobial peptide exposure selects for *Staphylococcus aureus* resistance to human defence peptides. *J. Antimicrob. Chemother.,* **2017**, *72*(1), 115-127.

[52] Hein-Kristensen, L.; Franzyk, H.; Holch, A.; Gram, L. Adaptive evolution of *Escherichia coli* to an alpha-peptide/beta-peptoid peptidomimetic induces stable resistance. *PLoS One,* **2013**, *8*(9), e73620.

[53] Shprung, T.; Peleg, A.; Rosenfeld, Y.; Trieu-Cuot, P.; Shai, Y. Effect of PhoP-PhoQ activation by broad repertoire of antimicrobial peptides on bacterial resistance. *J. Biol. Chem.,* **2012**, *287*(7), 4544-4551.

[54] Mesaros, N.; Nordmann, P.; Plesiat, P.; Roussel-Delvallez, M.; Van Eldere, J.; Glupczynski, Y.; Van Laethem, Y.; Jacobs, F.; Lebecque, P.; Malfroot, A.; Tulkens, P. M.; Van Bambeke, F. *Pseudomonas aeruginosa:* Resistance and therapeutic options at the turn of the new millennium. *Clin. Microbiol. Infect.,* **2007**, *13*(6), 560-578.

[55] Jorth, P.; McLean, K.; Ratjen, A.; Secor, P.R.; Bautista, G.E.; Ravishankar, S.; Rezayat, A.; Garudathri, J.; Harrison, J.J.; Harwood, R.A.; Penewit, K.; Waalkes, A.; Singh, P.K.; Salipante, S.J. Evolved aztreonam resistance is multifactorial and can produce hypervirulence in *Pseudomonas aeruginosa*. *mBio,* **2017**, *8*(5).

[56] Wu, X.; Li, Z.; Li, X.; Tian, Y.; Fan, Y.; Yu, C.; Zhou, B.; Liu, Y.; Xiang, R.; Yang, L. Synergistic effects of antimicrobial peptide DP7 combined with antibiotics against multidrug-resistant bacteria. *Drug Des. Devel. Ther.,* **2017**, *11*, 939-946.

[57] Tabbene, O.; Azaiez, S.; Di Grazia, A.; Karkouch, I.; Ben Slimene, I.; Elkahoui, S.; Alfeddy, M.N.; Casciaro, B.; Luca, V.; Limam, F.; Mangoni, M.L. Bacillomycin D and its combination with amphotericin B: Promising antifungal compounds with powerful antibiofilm activity and wound-healing potency. *J. Appl. Microbiol.,* **2016**, *120*(2), 289-300.

[58] Tabbene, O.; Di Grazia, A.; Azaiez, S.; Ben Slimene, I.; Elkahoui, S.; Alfeddy, M.N.; Casciaro, B.; Luca, V.; Limam, F.; Mangoni, M.L. Synergistic fungicidal activity of the lipopeptide bacillomycin D with amphotericin B against pathogenic *Candida* species. *FEMS Yeast Res.,* **2015**, *15*(4), fov022.

[59] Orlando, F.; Ghiselli, R.; Cirioni, O.; Minardi, D.; Tomasinsig, L.; Mocchegiani, F.; Silvestri, C.; Skerlavaj, B.; Riva, A.; Muzzonigro, G.; Saba, V.; Scalise, G.; Zanetti, M.; Giacometti, A. BMAP-28 improves the efficacy of vancomycin in rat models of gram-positive cocci ureteral stent infection. *Peptides,* **2008**, *29*(7), 1118-1123.

[60] Mishra, N.M.; Briers, Y.; Lamberigts, C.; Steenackers, H.; Robijns, S.; Landuyt, B.; Vanderleyden, J.; Schoofs, L.; Lavigne, R.; Luyten, W.; Van der Eycken, E.V. Evaluation of the antibacterial and antibiofilm activities of novel CRAMP-vancomycin conjugates with diverse linkers. *Org. Biomol. Chem.,* **2015**, *13*(27), 7477-7486.

Send Orders for Reprints to reprints@benthamscience.net

Current Medicinal Chemistry, **2019,** *26,* **1-14**

REVIEW ARTICLE

The Potential of Frog Skin Peptides for Anti-Infective Therapies: The Case of Esculentin-1a(1-21)NH_2

Bruno Casciaro[a,b,*], Floriana Cappiello[a], Maria Rosa Loffredo[a], Francesca Ghirga[b] and Maria Luisa Mangoni[a,*]

[a]*Laboratory affiliated to Pasteur Italia-Fondazione Cenci Bolognetti, Department of Biochemical Sciences, Sapienza University of Rome, Rome, via degli Apuli, 9,00185, Italy;* [b]*Center for Life Nano Science@Sapienza, Istituto Italiano di Tecnologia, Viale Regina Elena 291, 00161 Rome, Italy*

ARTICLE HISTORY

Received: October 11 2018
Revised: June 25 2019
Accepted: July 16 2019

DOI:
10.2174/0929867326666190722095408

Abstract: Antimicrobial peptides (AMPs) are the key effectors of the innate immunity and represent promising molecules for the development of new antibacterial drugs. However, to achieve this goal, some problems need to be overcome: (i) the cytotoxic effects at high concentrations; (ii) the poor biostability and (iii) the difficulty in reaching the target site. Frog skin is one of the richest natural storehouses of AMPs and over the years, many peptides have been isolated from it, characterized and classified into several families encompassing temporins, brevinins, nigrocins and esculentins. In this review, we summarized how the isolation/characterization of peptides belonging to the esculentin-1 family drove us to the design of an analogue, *i.e.* esculentin-1a(1-21)NH_2, with a powerful antimicrobial action and immunomodulatory properties. The peptide had a wide spectrum of activity, especially against the opportunistic Gram-negative bacterium Pseudomonas aeruginosa. We described the structural features and the *in vitro*/*in vivo* biological characterization of this peptide as well as the strategies used to improve its biological properties. Among them: (i) the design of a diastereomer carrying D-amino acids in order to reduce the peptide's cytotoxicity and improve its half-life; (ii) the covalent conjugation of the peptide to gold nanoparticles or its encapsulation into poly(lactide- co-glycolide) nanoparticles; and (iii) the peptide immobilization to biomedical devices (such as silicon hydrogel contact lenses) to obtain an antibacterial surface able to reduce microbial growth and attachment. Summing up the best results obtained so far, this review traces all the steps that led these frog-skin AMPsto the direction of peptide-based drugs for clinical use.

Keywords: Antimicrobial peptides, Pseudomonas aeruginosa, innate immunity, gold nanoparticles, contact lenses, D-amino acids, wound healing.

1. INTRODUCTION

1.1. Antimicrobial Peptides and Innate Immunity

Antimicrobial peptides (AMPs) are key components of the innate immunity and act as a first line of defense against pathogenic microorganisms [1, 2]. They are evolutionally conserved molecules produced by all living organisms, such as bacteria, insects, amphibians, plants and mammals [3, 4] . A significant boost in this field of research occurred in the '80s starting from the discovery of the insect cecropins by Hans Boman, the human α-defensins by Robert Lehrer and magainins by Michael Zasloff [5-7]. Nowadays, AMPs are considered very interesting molecules for the development of a new generation of drugs. This is due to their wide spectrum of activity (ranging from Gram-positive and Gram-negative bacteria, viruses, fungi and parasites) [8]; low molecular weight (2-50 kDa) [9]; quick response to infections, which is faster than the generation time of microbes (20-30 minutes) and activation of the adaptive immunity [10-12]. In mammals, AMPs are generally synthesized by those body sites that are exposed to the external environment (*e.g.* the skin, gastro-

*Address correspondence to these authors at the Center for Life Nano Science@Sapienza, Istituto Italiano di Tecnologia, Viale Regina Elena 291, Italy; Tel: +39 0649917687;
E-mail: bruno.casciaro@uniroma1.it
Department of Biochemical Sciences, Sapienza University of Rome, *via* degli Apuli, 9,00185, Rome, Italy;
Tel: +39 0649917693; E-mail: marialuisa.mangoni@uniroma1.it

0929-8673/19 $58.00+.00

intestinal and respiratory tracts) as well as by circulating white cells, where they are stored in granules to help killing of phagocytized microorganisms [13-16]. They are gene-encoded and ribosomally made as pre-propeptides of 60-170 amino acids consisting of an N-terminal signal for recognition of the endoplasmic reticulum; an anionic pro-segment which is followed by the cationic peptide (at the C-terminal portion) that acquires antimicrobial activity upon endo-proteolytic cleavage [17, 18]. Pre-propeptides usually undergo a post-translational modification encompassing glycosylation, C-terminal amidation, halogenation, hydroxylation, cyclization, amino acid isomerization or N-terminal acetylation [15, 19-21].

AMPs expression can be constitutive or inducible upon inflammation or infections and is controlled by NF-kB transcription factors, through a Toll-like receptor-mediated signaling transduction cascade, which is activated by microbial components, *e.g*. lipopolysaccharides, LPS, from the cell wall of Gram-negative bacteria [22].

In the past years, besides displaying an antimicrobial activity, AMPs from higher eukaryotes have been characterized for their immunomodulatory properties, as coordinators of innate and adaptive host-defense responses. Indeed, they can act as signaling mediators influencing host cell processes like immune cell differentiation; cytokines release; chemotaxis; LPS neutralization; angiogenesis and wound-healing [23-26].

1.2. Antimicrobial Peptides: General Features and Classification

Despite their substantial differences in chain length, sequence and conformation, most AMPs share: (i) a positive net charge (from +2 to +9) at neutral pH due to the presence of basic residues; (ii) an amphipathic character in a membrane-mimicking environment due to the presence of approximately 30% of hydrophobic residues in their sequences; and (iii) a random coil conformation in aqueous solution [27-29]. Depending on their secondary structure, AMPs are generally classified into four families: α-helix peptides, β-sheets peptides, extended/random-coil peptides and hairpin-loop peptides [30, 31].

This review mainly focuses on the structural/biological properties of a linear cationic peptide derived from a frog-skin AMP [esculentin-1a(1-21)NH_2, Esc(1-21)] with a membrane perturbing activity. Either the membranolytic mechanism of action or the features of esculentin1 AMPs are described in the paragraphs below.

1.3. Mechanisms of Action of Membranolytic Cationic Peptides

The interaction of cationic AMPs with biological membranes cannot be correctly predicted because it depends on a combination of biochemical/biophysical properties of AMPs, including size, cationicity, amphipathicity, distribution of cationic residues and oligomeric state [32].

Before reaching the target cytoplasmic membrane, AMPs interact with the negatively charged components of the microbial cell surface. In the case of Gram-positive bacteria, they involve teichoic acids of the peptidoglycan layer, while in Gram-negative bacteria, AMPs initially interact with the LPS-outer membrane. After translocation to the periplasmic space, AMPs can perturb the plasma membrane according to one of the following proposed models. In the "barrel-stave model", AMPs are inserted perpendicularly to the plane of the phospholipid bilayer, forming a pore like a barrel with the hydrophobic surfaces of the helices interacting with the fatty acid chains of the membrane phospholipids, while the hydrophilic surfaces point towards the lumen. This would cause the leakage of intracellular components and subsequent cell death [33, 34]. The "toroidal pore model" resemble the aforementioned mechanism but AMPs are always in contact with the phospholipid head groups [35]. The "carpet-like model" involves the coverage of the membrane by AMPs and, after a threshold concentration has been reached, the membrane is solubilized in a detergent-like manner [36, 37].

1.4. Frog-skin Antimicrobial Peptides

Frog skin is considered one of the richest natural sources of AMPs, with about 1,000 molecules in the Antimicrobial Peptide Database [38-40]. They are stored at high concentrations in dermal glands, mainly located in the dorsal region of the animal, and are released through a holocrine mechanism, upon injury or stress [41, 42]. Many AMPs have been isolated from the skin secretion of various *Anuran species* and classified into several families based on their common features and structure, such as brevinins, nigrocins, temporins, esculentins, and magainins [43-46]. Ranid frogs produce their own unique set of peptides, with the exception of the wood frog *Rana sylvatica* (reclassified as *Lithobates sylvaticus*) from where only a single AMP, *i.e*. brevinin1SY was isolated [47]. Importantly, individual family members have a specific primary structure that rarely is found in other frog species, even if phylogenetically closed, while a synergistic effect in

the biological activity has been discovered among the numerous AMPs produced by each single frog specimen [48, 49].

The principal function of frog skin AMPs is to protect the animal from invading microorganisms [50, 51]. However, as for other animal groups *e.g*. mammals, also frog skin AMPs have shown multiple properties, which make them attractive candidates for the clinical development of new antimicrobial drugs. Among them, an antitumor and antiviral activity as well as the ability to act as anti-diabetic agents [52-54].

2. ESCULENTIN-1 FAMILY

The peptide described in this review is a derivative of an AMP belonging to the Esculentin-1 family, a set of bioactive compounds secreted by *Pelophylax lessonae/ridibundus* (previously classified as *Rana esculenta* [55]) and subsequently identified also in the closely related North American species, *Lithobates palustris* [56] and *L. areolatus* [57]. Over the years, several peptides appertaining to this family have been isolated from the skin secretion of different frog species (originally classified in the *Rana* genus) or deduced by the screening of skin-derived cDNA libraries (Table **1**) [56-63].

All members of this family consist of 46 amino acids with a C-terminal hepta-membered ring stabilized by a disulfide bridge. The peptides isolated from *P, lessonae/ridibundus* (esculentin-1, esculentin-1a and -1b) have a net charge of +5 at neutral pH, an identical 16-46 region and an amphipathic α-helical structure in membrane-mimicking environments [64-66]. Furthermore, they have a broad spectrum of action against Gram-positive and Gram-negative bacteria, including *Pseudomonas aeruginosa* and fungal species, such as *Candida albicans* with lethal concentrations (LC, the minimum peptide concentration that inhibits microbial growth in agarose plates), ranging from 0.1 to 1.5 μM. They also display low toxicity towards mammalian cells [64, 65]. Table **1** shows the primary structure of some members of esculentins-1 family and their derivatives.

Since a little amount of esculentin-1 peptide could be recovered from the skin secretions of *P. lessonae/ridibundus*, analogues of this peptide were produced by recombinant expression, in *Escherichia coli,* of a fusion protein, which is sequestered in inclusion bodies [67]. Two analogues were produced by inserting the peptide sequence at the N-terminus of the protein gamma aminobutyric acid (GABA) transaminase. The first analog, named esculentin-C, consisted of 47 amino acids and carried a C-terminal disulfide bridge, the substitution Met28Leu and an additional Met at position 47, for cyanogen bromide cleavage of the recombinant fusion protein. The second analog, named esculentin-L was a linear 47-amino acids peptide with the same primary structure of esculentin-C but with two additional substitutions (Cys40Ser and Cys46Ser) to avoid the formation of the disulfide bridge (Table **1**). Both esculentin-analogues displayed a similar activity to that of the natural esculentin-1a against several bacterial strains, indicating that the presence of a disulfide bridge at the C-terminal region is not essential for the antimicrobial potency of this peptide [67]. Interestingly, esculentin-L and -C showed a strong activity against plant pathogens. Since they both share the N-terminal sequence Gly-Ile-Phe-Ser with a defensin subfamily from spinach [68], the idea of using these peptides to enhance plant defense against pathogens was therefore pursued. The peptide esculentin-C was transgenically expressed in *Nicotiana tabacum*: it was detected in the intercellular fluid as secretion product and subsequently tested against several phytopathogens [69]. It turned out to be harmless to plants and to confer them greater resistance to bacterial and fungal infections [69].

A fragment corresponding to the 19-46 portion of esculentin-1 peptides was also isolated from the skin secretions of *P. lessonae/ridibundus*. It was devoid of antimicrobial activity, presumably due to its low net positive charge (+1 *versus* +5 of the whole molecule) at neutral pH [65]. Interestingly, its high similarity with the toxin ponericin G isolated from the venom of the ant *Pachycondyla goeldii* [70] suggested that this portion had an insecticidal function. However, since no antimicrobial activity was obtained for this fragment, the 1-18 portion was chemically synthesized and analyzed for its antimicrobial activity. The synthetic peptide, Esculentin-1b(1-18)NH_2, *i.e*. Esc(1-18), Table **1**, was amidated at the C-terminus to maintain a net charge of +5 at neutral pH and to increase its resistance to carboxypeptidases [71]. It showed similar antimicrobial activity to that of its parent full-length peptide (LC values ranging from 0.1 to 1.5 μM), but a lower hemolytic activity [71]. Esc(1-18) was found to adopt an α-helical conformation in lipid vesicles mimicking the anionic character of microbial membranes. Since the minimum length for an α-helix peptide to span a phospholipid bilayer is about 20 amino acids, a longer analog of esculentin-1a, named esculentin-1a(1-21)NH_2 [Esc(1-21), Table **1**] was further synthesized and characterized for its biological properties.

3. ESCULENTIN-1a(1-21)NH_2

3.1. Structural Properties and *In Vitro/In Vivo* Biological Activities

The secondary structure of Esc(1-21) was first analyzed by circular dichroism (CD) spectroscopy in 10 mM sodium phosphate buffer (pH 7.4) or in a suspension of lipid vesicles composed of phosphatidylethanolamine/phosphatidylglycerol (PE/PG, 7:3, w:w) to mimic the lipid composition of microbial membranes. The peptide was found to assume a disordered conformation in aqueous solution, while it adopted an α-helical structure in association with model membranes [72] and with an amphipathic character [73]. Similar results were also obtained in lysophosphatidylcholine, which mimics the zwitterionic composition of eukaryotic cells, as well as in LPS [74]. The antimicrobial activity of Esc(1–21) was tested *in vitro* by the inhibition zone assay against several bacteria strains (*e.g. Staphylococcus aureus, Staphylococcus epidermidis, Streptococcus agalactiae, Streptococcus dysgalactiae, Klebsiella pneumoniae, P. aeruginosa, E. coli*) with LC values ranging from 0.65 to 3.2 μM, with the only exception of *S. aureus* (LC= 14 μM) [72]. Note that *streptococci* are among the most common mastitis-causing pathogens in dairy cattle [75]. Clinical and subclinical mastitis are two major forms of inflammation of the mammary glands in response to bacterial invasion. They are characterized by a decrease in the production of milk and alterations in its composition (decrease of proteins, lactose contents, fat, and increase in leucocytes counts). Esc(1-21) was also tested *in vivo* in mastitis-infected cows, by evaluating the leucocyte counts in the milk and by direct clinical inspection. Importantly, intramammary infusion of peptide-supplemented physiological solution gave rise to a regression of the disease, with a clinical improvement rate of 100%, within 5-days of treatment and without causing any irritant effects to the animals [72].

Further in-depth studies revealed that the peptide had a strong activity also against the Gram-negative bacterium *P. aeruginosa.* Specifically, Esc(1-21) resulted to have a potent antipseudomonal activity against both planktonic and sessile forms of this bacterium with a minimum inhibitory concentration (MIC) of 4 μM [76]. The ability of Esc(1-21) to damage the cytoplasmic membrane of planktonic cells of *P. aeruginosa* was first evaluated by the Sytox Green assay and confirmed by scanning electron microscopy. When treated with the peptide, *Pseudomonas* cells appeared with a wrinkled surface and emptied of their content [60]. Considering that *P. aeruginosa* is one of the most prevalent lung microbial pathogens, especially in cystic fibrosis (CF) patients [77], where it causes a serious lung tissue damage, the ability of the peptide to stimulate lung epithelial cells migration and presumably to recover the injured bronchial epithelium, was also investigated. This was performed by an *in vitro* pseudo-"wound" healing assay on bronchial epithelial cells expressing either a functional or a mutated CF transmembrane conductance regulator CFTR [78]. Esc(1-21) induced ~100 % coverage of the pseudo-"wound" field within 20 h at a concentration of 10 μM [79]. Its antipseudomonal activity was also tested *in vivo*, in mouse models of acute *Pseudomonas*-induced pneumonia: intra-tracheal administration of Esc(1-21) significantly prolonged survival of mice (25%) with respect to the vehicle-treated animals [76]. The *in vivo* efficacy of this peptide was then evaluated in mouse models of *Pseudomonas*-induced sepsis and keratitis. In the first case, intravenous administration of Esc(1-21) resulted in 40% prolonged survival of mice with respect to the controls [76]. In the second case, when the peptide was topically administered in a drop-wise fashion, it significantly reduced severity of infection, compared to non-treated eyes developing a serious cornea perforation [80].

4. HOW TO ENHANCE THE ANTIPSEUDOMONAL THERAPEUTIC POTENTIAL OF ESC(1-21)?

Despite the encouraging results mentioned above, it has to be taken into account that Esc(1-21) is not exempted from the limitations common to all AMPs: (i) low biostability; (ii) cytotoxicity at high concentrations; and (iii) difficulty in reaching the site of infection at active concentrations [81]. To circumvent these drawbacks, different biochemical approaches were followed: (i) changes in the primary structure of Esc(1-21) by amino acids substitution; and (ii) functionalization of biomaterials, upon peptide conjugation/incorporation into nanoparticles or immobilization to biomedical devices such as silicon hydrogel soft contact lenses (CLs) (Fig. **1**).

4.1. Modification of the Primary Structure: Analogs of Esc(1-21)

Modification of the primary structure of a peptide is one of the most widely used biochemical approaches to analyze the structure-function relationship of bioactive peptides. The sequence can be modified by the addition/replacement of amino acids with other natural/unnatural residues, but also by the introduction of non-peptide sequences, *i.e.* glycotriazole and lipid

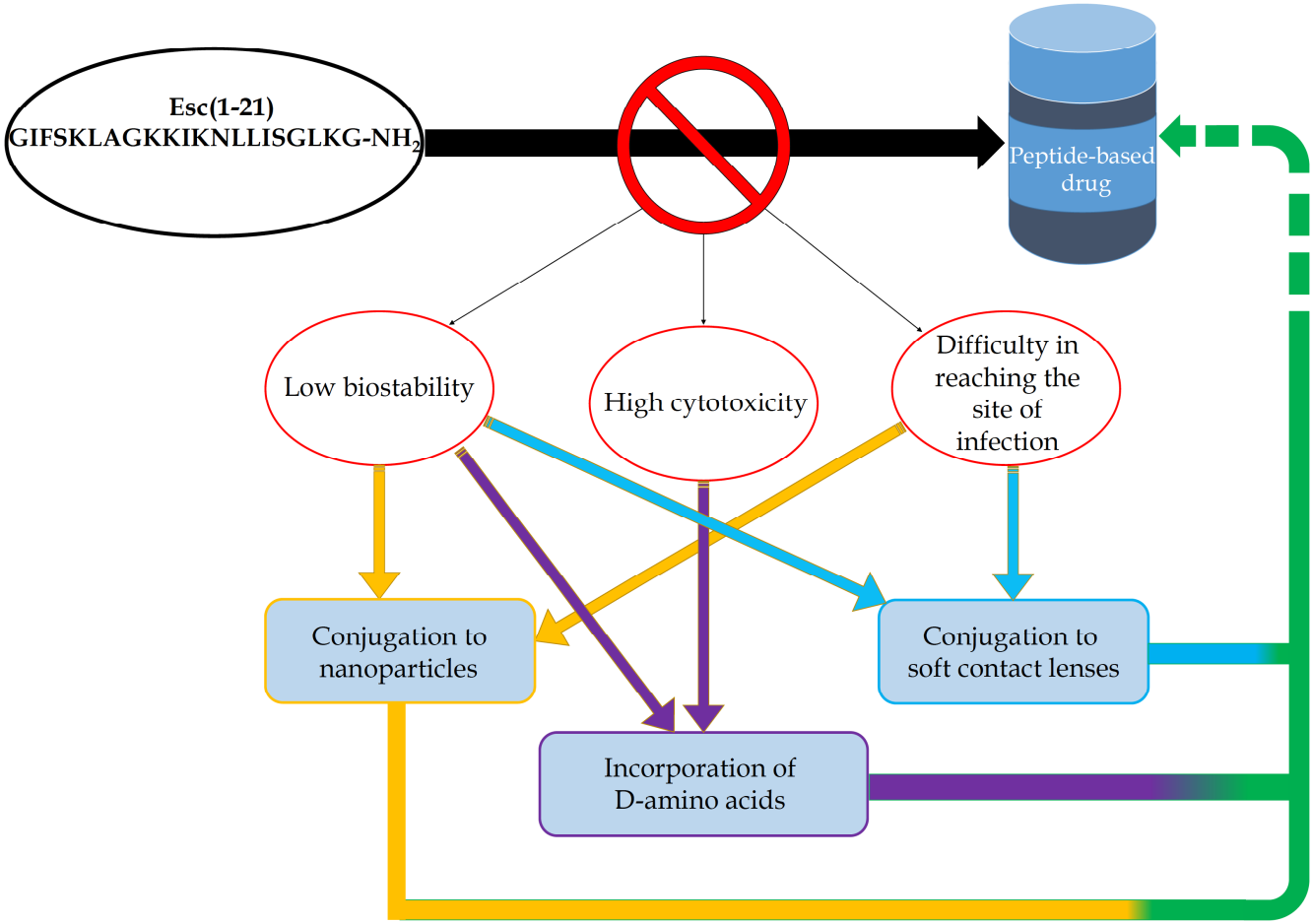

Fig. (1). Schematic representation of the drawbacks hampering peptide-based drugs development and the four examples used to circumvent them.

moieties [82-85]. In terms of structure-function relationship, it is well known that there is a direct correlation between the α-helical content of a peptide and its antimicrobial activity/cytotoxicity [50, 86-89]. This is supported by findings of Esc(1-21). In fact, as previously demonstrated, the insertion of three α-aminoisobutyric acid (Aib) residues in the primary structure of this peptide led to the production of an analog (*i.e.*, [Aib^{1,10,18}]-Esc(1–21)NH_2, see Table **1**) with a higher α-helical content and therefore higher cytotoxicity compared to the parent peptide [88]. It is also well documented that the insertion of D-amino acids, known as "helix breakers", into the primary structure of an α-helix peptide would result in a reduction of its helical content along with a reduction in its harmful effects to mammalian cells. In the case of Esc(1-21), a diastereomer, named Esc(1-21)-1c, was designed by replacing two amino acids (*i.e.* L-Leu14 and L-Ser17) with the respective D-enantiomers [74]. As expected, the less-helical diastereomer was significantly less toxic when tested against mammalian cell lines (*i.e.* lung epithelial cells, macrophages, bronchial epithelial cells) with an LD_{50} > 256 μM versus 64-128 μM of Esc(1-21) [74, 79]. However, a 4-fold lower activity was assessed for the diastereomer with respect to the all-L peptide against the planktonic form of *P. aeruginosa* with a minimum bactericidal concentration of 4 μM [74].

More detailed mechanistic studies have suggested that *Pseudomonas* cell wall plays a key role in the antimicrobial activity of the two isomers. The weaker activity of the diastereomer could be attributed to its lower binding affinity to LPS. This would slow down the translocation of the peptide into the target plasma membrane. In support of this, when the two peptides were tested against *Pseudomonas* spheroplasts, which are devoid of the cell wall, a similar antibacterial activity was recorded; furthermore, both peptides had an identical effect on the membrane thinning [73].

In contrast, when they were tested against the biofilm form of *Pseudomonas*, Esc(1-21)-1c became more active with a concentration causing 95% of killing equal to 12.5 *versus* 25 μM of the all-L peptide

Table 1. List of the primary structures of Esculentin-1 analogs and derivatives.

Peptide	Sequence	Species/Origin
Esculentin-1	GIFSK LGRKK IKNLL ISGLK NVGKE VGMDV VRTGI DIAGC KIKGE C	*P. lessonae/ridibundus*
Esculentin-1a	GIFSK LAGKK IKNLL ISGLK NVGKE VGMDV VRTGI DIAGC KIKGE C	*P. lessonae/ridibundus*
Esculentin-1b	GIFSK LAGKK LKNLL ISGLK NVGKE VGMDV VRTGI DIAGC KIKGE C	*P. lessonae/ridibundus*
Esculentin-1OG1	GLFSK FAGKG IKNFL IKGVK HIGKE VGMDV IRTGI DVAGC KIKGE C	*Odorrana grahami*
Esculentin-1ISA	GIFSK FAGKG IKNLL VKGVK NIGKE VGMDV IRTGI DIAGC KIKGE C	*Odorrana grahami*
Esculentin-1LSa	GIFK* **GKK WLNSI IKGIK TVGKD VAGDV IRTGL DIASC KIKHE C	*Lithobates luctuosa*
Esculentin-1B	GIFSK LAGKK LKNLL ISGLK NVGKE VGMDV VRTGI DIAGC KIKGE C	*Lithobates saharica*
Esculentin-1ARa	GIFSK INKKK AKTGL FNIIK TVGKE AGMDV IRAGI DTISC KIKGE C	*Lithobates areolatus*
Esculentin-1ARb	GLFPK FNKKK VKTGI FDIIK TVGKE AGMDV LRTGI DVIGC KIKGE C	*Lithobates areolatus*
Esculentin-PLa	GLFPK INKKK AKTGV FNIIK TVGKE AGMDL IRTGI DTIGC KIKGE C	*Lithobates palustris*
Esculentin-1GN	GLFSK KGGKG GKSWI KGVFK GIKGI GKEVG GDVIR TGIEI AACKI KGEC	*Hylarana guentheri*
Esculentin-C	GIFSK LAGKK LKNLL ISGLK NVGKE VGLDV VRTGI DIAGC KIKGE CM	Recombinant expression
Esculentin-L	GIFSK LAGKK LKNLL ISGLK NVGKE VGLDV VRTGI DIAGS KIKGE SM	Recombinant expression
Esculentin-1b(1-18)NH_2, Esc(1-18)	GIFSK LAGKK LKNLL ISG-NH_2*	Synthetic
Esculentin-1a(1-21)NH_2, Esc(1-21)	GIFSK LAGKK IKNLL ISGLK G-NH_2*	Synthetic
[Aib^{1,10,18}]-Esculentin-1a (1–21)NH_2	*Aib*IFSK LAGK*Aib* IKNLL IS*Aib*LK G-NH_2*	Synthetic
Esculentin-1a(1-21)-1cNH_2, Esc(1-21)-1c	GIFSK LAGKK IKN*l*L I*s*GLK G-NH_2*	Synthetic

Aib represents α-aminoisobutyric acid residue. The residues in D-configuration are italicized and in lower case.
*Peptides amidated at their C-terminus.

[74]. This may be due to the (i) higher biostability of Esc(1-21)-1c and prolonged residence time in comparison with Esc(1-21); (ii) easier diffusion through the extracellular biofilm matrix; and (iii) higher efficacy in disassembling the biofilm matrix.

Importantly, compared to the clinically-used antibiotics (*e.g.*, tobramycin, ciprofloxacin, aztreonam) [90] either Esc(1-21) or its diastereomer were able to limit the induction of resistance in *P. aeruginosa*, after 15 cycles of treatment at sub-MIC concentrations [91]. The usage of sub-MIC concentrations is of remarkable importance in the case of infections. Indeed, it has been demonstrated that sub-inhibitory antibiotic concentrations can trigger not only the development of microbial resistance to AMPs, but also an increased production of virulence factors by the pathogen along with the formation of biofilm communities [92-95]. In contrast, Esc(1-21)-1c has been recently found to inhibit bacterial biofilm formation when used at sub-MIC concentrations by downregulating some key genes involved in *P. aeruginosa* mobility and pathogenicity [96]. However, we cannot ignore those studies showing the ability of selected AMPs to induce resistance in bacteria [97, 98].

Besides antimicrobial properties, the diastereomer Esc(1-21)-1c was also found to be more active in pro-

moting re-epithelialization of a wounded area produced in a monolayer of bronchial epithelial cells, with an optimal concentration of 1 μM [79]. Moreover, in line with the lower binding affinity to LPS, Esc(1-21)-1c was less efficient in inhibiting the secretion of the pro-inflammatory cytokine TNF-α from LPS-activated macrophages compared to the all-L-peptide (30% *vs* 90% at 20 μM) [74]. This was likely due the weaker effect of Esc(1-21)-1c in disassembling LPS aggregates into smaller-size particles compared to the all-L isomer. LPS monomers would then interact with LPS-binding receptors triggering the secretion of pro-inflammatory cytokines [74].

Moreover, the effects of the diastereomer on the lung inflammatory response, pulmonary toxicity and infection were evaluated *in vivo* and compared to those of the all-L isomer [68]. When the peptides were intratracheally instilled at 20 μM (2 μg/mouse, 0.1 mg/kg), lung inflammatory reaction was negligible as highlighted by the invariant expression of airways epithelial cells-associated inflammatory genes (*i.e.* genes encoding for IL-6, IL-10, TNF-α, and NF-kB) after 24 hours. Importantly, no significant pulmonary toxicity was recorded, as supported by the unchanged expression of the clara cell secretory protein, which is a relevant biomarker for lung epithelial permeability [99], compared to control (vehicle-treated) mice. With reference to the *in vivo* antimicrobial activity, the diastereomer was found to be significantly more active than the all-L peptide, presumably due to its prolonged residence time, causing about 2 log reduction in lung bacterial burden after 24 h from infection [100]. Overall, these promising *in vitro* and *in vivo* data have contributed to make Esc(1-21)-1c a valid alternative for the development of a new antipseudomonal drug.

4.2. Functionalization of Biomaterials

Another interesting approach to enhance the therapeutic potential of AMPs is represented by its coating or conjugation to a biocompatible material by means of nanotechnological techniques. Nowadays, studies dealing with the conjugation of AMPs to nanoparticulate systems are exponentially growing [101-104].

Gold nanoparticles (AuNPs), for example, are among the most applied inorganic nanocarriers in the field of biomedical sciences due to their easy synthesis in a wide range of shapes and sizes; simple usage in combination with different types of molecules and chemical inertia [105]. For all these reasons, AuNPs were chosen for conjugation to Esc(1-21) *via* a poly(ethylene glycol) (PEG) linker [AuNPs@Esc(1-21)] (See Fig. **2**). About 2 μg of peptide were added to 20 pmol of AuNPs and the amount of conjugated Esc(1-21) was equal to 16 molecules per NP [106] The obtained AuNPs@Esc(1-21) were tested against the planktonic and biofilm forms of *P. aeruginosa* and the results were compared to those of the free peptide

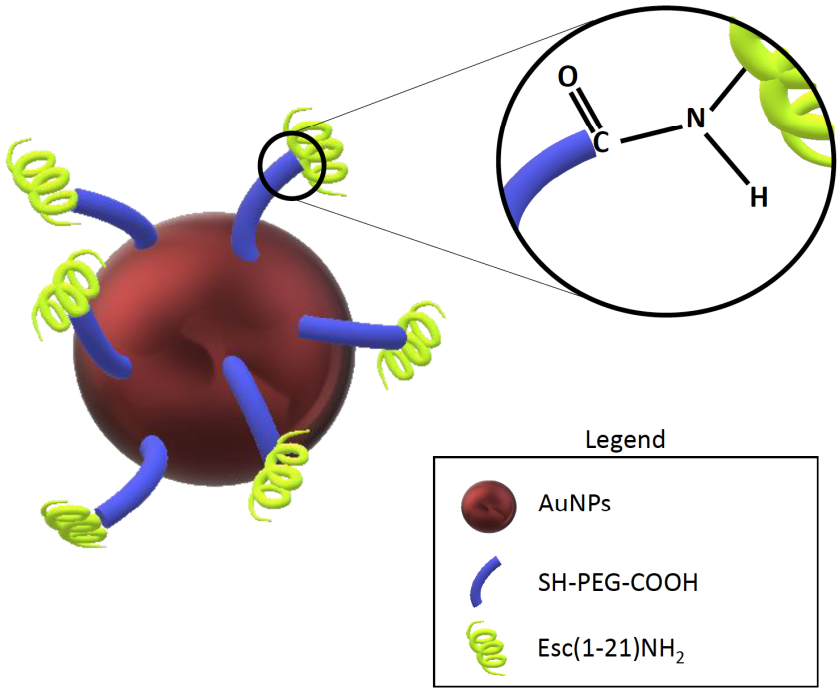

Fig. (2). Representation of the chemical bond between the peptide molecules and the PEG present on the surface of the gold nanoparticles.

[106]. The peptide-based gold nanoformulation enhanced the antipseudomonal activity of the membrane-active Esc(1-21) by approximately 15-fold. Interestingly, this chemical conjugation did not affect the mechanism of action of the peptide. This was demonstrated by fluorimetric assay and scanning/transmission electron microscopy, showing the same membrane-perturbing effects as for the free Esc(1-21). Furthermore, peptide conjugation to AuNPs increased the peptide stability. In fact, 2 hours after treatment with trypsin, the free peptide lost almost its activity while the peptide-coated NPs retained their antipseudomonal power, presumably due to the higher resistance of Esc(1-21) to enzymatic degradation upon its coating. Remarkably, the peptide-coated AuNPs did not precipitate along the time and the formulation was found to preserve its antimicrobial activity up to 3 months from its preparation suggesting that the peptide is not detached from the NPs surface. Furthermore, AuNPs@Esc(1-21) were non-toxic to human keratinocytes and maintained the peptide's ability to stimulate cell migration in the pseudo-"wound" healing assays [106]. Taken all together, these biological features make AuNPs@Esc(1-21) attractive candidates for their future development as new nanoscale formulations likely for treatment of topical (dermatological) epithelial infections.

As stated in paragraph 3.1, *P. aeruginosa* is the etiological agent of recurrent and resistant microbial infections affecting the lungs and the eyes [107]. In CF sufferers, the presence of a thick and dry mucus covering the airway epithelia, accelerates the onset of infections that conventional antibiotics are unlikely to eradicate. In a translational point of view, we recently developed nanoformulations based on poly(lactide-co-glycolide) (PLGA) NPs and loaded with Esc(1-21) or Esc(1-21)-1c [Esc peptides]. They were engineered with the stabilizing agent poly-vinyl alcohol in order to modulate their surface properties preventing NPs aggregation and/or improving NPs diffusion through the lung mucus [108]. Note that PLGA is considered one of the most suitable biodegradable polymers for drug delivery due to its safety and high biocompatibility [109-112]. These nanoformulations were fully characterized in terms of nanoparticles size, zeta potential and encapsulation efficiency [113]. Interestingly, they were found to facilitate the peptide's traslocation through artificial CF mucus and simulated bacterial extracellular matrix. Furthermore, they showed an improved efficacy in inhibiting *P. aeruginosa* growth *in vitro* and *in vivo* at long term, with a 3-log reduction in the number of Pseudomonas cells in the lungs of a mouse model of acute *P. aeruginosa* lung infection, up to 36 h from a single intratracheal administration.

As mentioned above, *P. aeruginosa* is responsible for different types of ocular surface infections, including keratitis. This is an infection of the cornea and is mainly associated with the usage of contact lenses (CLs) that *P. aeruginosa* can easily colonize forming biofilms. Therefore, a useful strategy to prevent the development of cornea infection is the inhibition of bacterial adhesion to the CLs [114].

The two Esc peptides were immobilized on hydrogel etafilcon A soft CLs which contain methacrylic acid (MAA) in their matrix. MAA provides COOH-groups for conjugation with primary amine groups of the peptides after their activation with EDC. The obtained peptide-coated CLs (2 μg peptide/each lens) were first analyzed for their effects on the lens properties. The chemical conjugation was innocuous as demonstrated by the invariant values of lens diameters and central thickness, with respect to the control (non-activated CLs) and process control samples (EDC-activated CLs but without peptide) [115]. When the antimicrobial activity of the AMP-coated CLs was evaluated against the planktonic form of *P. aeruginosa,* both peptides caused at least 99.99% killing of bacterial cells within 20 minutes of treatment in phosphate buffer saline with a higher efficacy for the all-L peptide-coated CLs. Furthermore, the ability of Esc-coated CLs to inhibit adhesion of *P. aeruginosa* to the lens surface under conditions favoring bacterial replication (*e.g*. rich culture medium) was analyzed up to 24 hours. The results showed that both peptide-coated CLs were able to inhibit bacterial adhesion to the CL surface (~75% for all-L peptide *vs* ~90% inhibition for the diastereomer), compared to process control lens [115]. Remarkably, peptide conjugation to CLs, did not make them toxic to mammalian cells. Indeed, when cytotoxicity of the coated-CLs was assessed *in vitro* by a direct contact test following the instructions of ISO 10933, after 24 h incubation, the lenses were harmless to mammalian cells, *e.g*. murine fibroblasts, with a degree of reactivity equal to 1 in a scale from 0 to 4 in which a degree of reactivity greater than 2 is considered to be toxic [115]. Overall, this type of conjugation revealed to be an interesting model of functionalization of a surface of a biomedical device.

CONCLUSION

AMPs represent an attractive class of bioactive molecules that in recent years have been re-evaluated for their promising biological properties. Nevertheless,

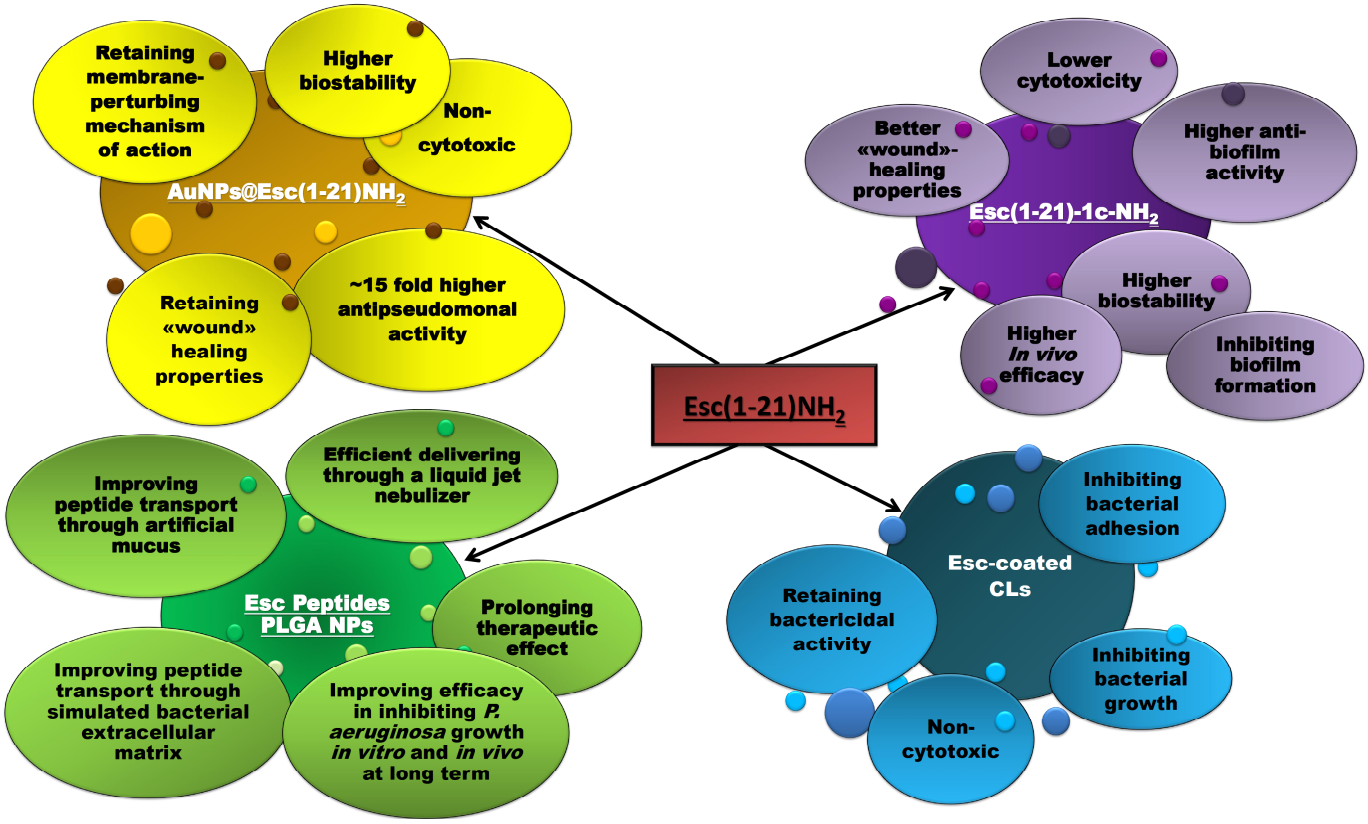

Fig. (3). Schematic representation of the biological advantages of Esc(1-21) upon D-amino acids incorporation or conjugation to gold/PLGA nanoparticles as well as to soft contact lenses.

additional studies are demanded to expand our knowledge on the pharmacological profiles of these compounds and to find new strategies to overcome their intrinsic limitations. Here, we described the history of Esc(1-21), from its isolation, characterization and optimization. In addition, we reported four examples showing how different biochemical and nanotechnological approaches can ameliorate the biological profile of this peptide (Fig. **3**) and that may assist the development of other AMPs as new anti-infective agents.

FUTURE PERSPECTIVES

Future studies will aim at characterizing further biological properties of Esc peptides as well as at refining the already produced nanoformulations for a more efficacious local administration to treat ocular/lung/skin microbial infections. Importantly, the long-term stability of these formulations will be evaluated, with the purpose to yield a product that can better enter into clinical trials

CONSENT FOR PUBLICATION

Not applicable.

FUNDING

This work was supported by grants from Sapienza University of Rome (projects **RM116154C8434109** and **RM11816436113D8A**) and the Italian Cystic Fibrosis Foundation (project FFC 15/2017 Adopted by Delegations of Palermo, Vittoria, Ragusa, Siracusa, Catania Mascalucia, Messina, Gruppo di Sostegno di Tremestieri).

CONFLICT OF INTEREST

The authors declare no conflict of interest, financial or otherwise.

ACKNOWLEDGEMENTS

We are grateful to prof. Andrea Bellelli (Sapienza University of Rome) for the support given for the achievement of some results summarized in this review.

REFERENCES

[1] Boto, A.; Pérez de la Lastra, J.M.; González, C.C. The road from host-defense peptides to a new generation of antimicrobial drugs. *Molecules,* **2018**, *23*(2)E311 [http://dx.doi.org/10.3390/molecules23020311] [PMID: 29389911]

[2] Ageitos, J.M.; Sánchez-Pérez, A.; Calo-Mata, P.; Villa, T.G. Antimicrobial peptides (AMPs): Ancient compounds that represent novel weapons in the fight against bacteria. *Biochem. Pharmacol.,* **2017**, *133*, 117-138. [http://dx.doi.org/10.1016/j.bcp.2016.09.018] [PMID: 27663838]

[3] Maróti, G.; Kereszt, A.; Kondorosi, E.; Mergaert, P. Natural roles of antimicrobial peptides in microbes, plants and animals. *Res. Microbiol.,* **2011**, *162*(4), 363-374. [http://dx.doi.org/10.1016/j.resmic.2011.02.005] [PMID: 21320593]

[4] Tang, S.S.; Prodhan, Z.H.; Biswas, S.K.; Le, C.F.; Sekaran, S.D. Antimicrobial peptides from different plant sources: Isolation, characterisation, and purification. *Phytochemistry,* **2018**, *154*, 94-105. [http://dx.doi.org/10.1016/j.phytochem.2018.07.002] [PMID: 30031244]

[5] Faye, I.; Lindberg, B.G. Towards a paradigm shift in innate immunity-seminal work by Hans G. Boman and coworkers. *Philos. Trans. R. Soc. Lond. B Biol. Sci.,* **2016**, *371*(1695), 371. [http://dx.doi.org/10.1098/rstb.2015.0303] [PMID: 27160604]

[6] Lehrer, R.I. Primate defensins. *Nat. Rev. Microbiol.,* **2004**, *2*(9), 727-738. [http://dx.doi.org/10.1038/nrmicro976] [PMID: 15372083]

[7] Berkowitz, B.A.; Bevins, C.L.; Zasloff, M.A. Magainins: a new family of membrane-active host defense peptides. *Biochem. Pharmacol.,* **1990**, *39*(4), 625-629. [http://dx.doi.org/10.1016/0006-2952(90)90138-B] [PMID: 1689576]

[8] Steckbeck, J.D.; Deslouches, B.; Montelaro, R.C. Antimicrobial peptides: new drugs for bad bugs? *Expert Opin. Biol. Ther.,* **2014**, *14*(1), 11-14. [http://dx.doi.org/10.1517/14712598.2013.844227] [PMID: 24206062]

[9] Sharma, K.; Aaghaz, S.; Shenmar, K.; Jain, R. Short Antimicrobial Peptides. *Recent Pat Antiinfect Drug Discov,* **2018**, *13*(1), 12-52. [http://dx.doi.org/10.2174/1574891X13666180628105928] [PMID: 29952266]

[10] Pasupuleti, M.; Schmidtchen, A.; Malmsten, M. Antimicrobial peptides: key components of the innate immune system. *Crit. Rev. Biotechnol.,* **2012**, *32*(2), 143-171. [http://dx.doi.org/10.3109/07388551.2011.594423] [PMID: 22074402]

[11] Ganz, T. Defensins: antimicrobial peptides of innate immunity. *Nat. Rev. Immunol.,* **2003**, *3*(9), 710-720. [http://dx.doi.org/10.1038/nri1180] [PMID: 12949495]

[12] Brogden, K.A.; Ackermann, M.; McCray, P.B. Jr.; Tack, B.F. Antimicrobial peptides in animals and their role in host defences. *Int. J. Antimicrob. Agents,* **2003**, *22*(5), 465-478. [http://dx.doi.org/10.1016/S0924-8579(03)00180-8] [PMID: 14602364]

[13] Boman, H.G. Antibacterial peptides: key components needed in immunity. *Cell,* **1991**, *65*(2), 205-207. [http://dx.doi.org/10.1016/0092-8674(91)90154-Q] [PMID: 2015623]

[14] Hancock, R.E.; Diamond, G. The role of cationic antimicrobial peptides in innate host defences. *Trends Microbiol.,* **2000**, *8*(9), 402-410. [http://dx.doi.org/10.1016/S0966-842X(00)01823-0] [PMID: 10989307]

[15] Zasloff, M. Antimicrobial peptides of multicellular organisms. *Nature,* **2002**, *415*(6870), 389-395. [http://dx.doi.org/10.1038/415389a] [PMID: 11807545]

[16] Mangoni, M.L.; McDermott, A.M.; Zasloff, M. Antimicrobial peptides and wound healing: biological and therapeutic considerations. *Exp. Dermatol.,* **2016**, *25*(3), 167-173. [http://dx.doi.org/10.1111/exd.12929] [PMID: 26738772]

[17] Bals, R. Epithelial antimicrobial peptides in host defense against infection. *Respir. Res.,* **2000**, *1*(3), 141-150. [http://dx.doi.org/10.1186/rr25] [PMID: 11667978]

[18] Huang, H.W.; Charron, N.E. Understanding membrane-active antimicrobial peptides. *Q. Rev. Biophys.,* **2017**, *50*e10 [http://dx.doi.org/10.1017/S0033583517000087] [PMID: 29233222]

[19] Mangoni, M.L.; Papo, N.; Saugar, J.M.; Barra, D.; Shai, Y.; Simmaco, M.; Rivas, L. Effect of natural L- to D-amino acid conversion on the organization, membrane binding, and biological function of the antimicrobial peptides bombinins H. *Biochemistry,* **2006**, *45*(13), 4266-4276. [http://dx.doi.org/10.1021/bi052150y] [PMID: 16566601]

[20] Nicolas, P.; El Amri, C. The dermaseptin superfamily: a gene-based combinatorial library of antimicrobial peptides. *Biochim. Biophys. Acta,* **2009**, *1788*(8), 1537-1550. [http://dx.doi.org/10.1016/j.bbamem.2008.09.006] [PMID: 18929530]

[21] Wang, G. Post-translational modifications of natural antimicrobial peptides and strategies for peptide engineering. *Curr. Biotechnol.,* **2012**, *1*(1), 72-79. [http://dx.doi.org/10.2174/2211550111201010072] [PMID: 24511461]

[22] Thaiss, C.A.; Levy, M.; Itav, S.; Elinav, E. Integration of innate immune signaling. *Trends Immunol.,* **2016**, *37*(2), 84-101. [http://dx.doi.org/10.1016/j.it.2015.12.003] [PMID: 26755064]

[23] Hemshekhar, M.; Anaparti, V.; Mookherjee, N. Functions of cationic host defense peptides in immunity. *Pharmaceuticals (Basel),* **2016**, *9*(3), E40. [http://dx.doi.org/10.3390/ph9030040] [PMID: 27384571]

[24] Davidson, D.J.; Currie, A.J.; Reid, G.S.; Bowdish, D.M.; MacDonald, K.L.; Ma, R.C.; Hancock, R.E.; Speert, D.P. The cationic antimicrobial peptide LL-37 modulates dendritic cell differentiation and dendritic cell-induced T cell polarization. *J. Immunol.,* **2004**, *172*(2), 1146-1156. [http://dx.doi.org/10.4049/jimmunol.172.2.1146] [PMID: 14707090]

[25] Afacan, N.J.; Yeung, A.T.; Pena, O.M.; Hancock, R.E. Therapeutic potential of host defense peptides in antibiotic-resistant infections. *Curr. Pharm. Des.,* **2012**, *18*(6), 807-819. [http://dx.doi.org/10.2174/138161212799277617] [PMID: 22236127]

[26] Mookherjee, N.; Hancock, R.E. Cationic host defence peptides: innate immune regulatory peptides as a novel approach for treating infections. *Cell. Mol. Life Sci.,* **2007**, *64*(7-8), 922-933. [http://dx.doi.org/10.1007/s00018-007-6475-6] [PMID: 17310278]

[27] Rinaldi, A.C. Antimicrobial peptides from amphibian skin: an expanding scenario. *Curr. Opin. Chem. Biol.,* **2002**, *6*(6), 799-804. [http://dx.doi.org/10.1016/S1367-5931(02)00401-5] [PMID: 12470734]

[28] Hancock, R.E.; Sahl, H.G. Antimicrobial and host-defense peptides as new anti-infective therapeutic strategies. *Nat. Biotechnol.,* **2006**, *24*(12), 1551-1557. [http://dx.doi.org/10.1038/nbt1267] [PMID: 17160061]

[29] Powers, J.P.; Hancock, R.E. The relationship between peptide structure and antibacterial activity. *Peptides,* **2003**, *24*(11), 1681-1691.

[http://dx.doi.org/10.1016/j.peptides.2003.08.023] [PMID: 15019199]

[30] Mojsoska, B.; Jenssen, H. Peptides and peptidomimetics for antimicrobial drug design. *Pharmaceuticals (Basel),* **2015**, *8*(3), 366-415. [http://dx.doi.org/10.3390/ph8030366] [PMID: 26184232]

[31] Mahlapuu, M.; Håkansson, J.; Ringstad, L.; Björn, C. Antimicrobial peptides: an emerging category of therapeutic agents. *Front. Cell. Infect. Microbiol.,* **2016**, *6*, 194. [http://dx.doi.org/10.3389/fcimb.2016.00194] [PMID: 28083516]

[32] Hall, K.; Aguilar, M.I. Surface plasmon resonance spectroscopy for studying the membrane binding of antimicrobial peptides. *Methods Mol. Biol.,* **2010**, *627*, 213-223. [http://dx.doi.org/10.1007/978-1-60761-670-2_14] [PMID: 20217624]

[33] Ehrenstein, G.; Lecar, H. Electrically gated ionic channels in lipid bilayers. *Q. Rev. Biophys.,* **1977**, *10*(1), 1-34. [http://dx.doi.org/10.1017/S0033583500000123] [PMID: 327501]

[34] Zhang, L.; Rozek, A.; Hancock, R.E. Interaction of cationic antimicrobial peptides with model membranes. *J. Biol. Chem.,* **2001**, *276*(38), 35714-35722. [http://dx.doi.org/10.1074/jbc.M104925200] [PMID: 11473117]

[35] Brogden, K.A. Antimicrobial peptides: pore formers or metabolic inhibitors in bacteria? *Nat. Rev. Microbiol.,* **2005**, *3*(3), 238-250. [http://dx.doi.org/10.1038/nrmicro1098] [PMID: 15703760]

[36] Shai, Y. Mode of action of membrane active antimicrobial peptides. *Biopolymers,* **2002**, *66*(4), 236-248. [http://dx.doi.org/10.1002/bip.10260] [PMID: 12491537]

[37] Bechinger, B.; Gorr, S.U. Antimicrobial peptides: mechanisms of action and resistance. *J. Dent. Res.,* **2017**, *96*(3), 254-260. [http://dx.doi.org/10.1177/0022034516679973] [PMID: 27872334]

[38] Conlon, J.M. Structural diversity and species distribution of host-defense peptides in frog skin secretions. *Cell. Mol. Life Sci.,* **2011**, *68*(13), 2303-2315. [http://dx.doi.org/10.1007/s00018-011-0720-8] [PMID: 21560068]

[39] Wang, G.; Li, X.; Wang, Z. APD3: the antimicrobial peptide database as a tool for research and education. *Nucleic Acids Res.,* **2016**, *44*(D1), D1087-D1093. [http://dx.doi.org/10.1093/nar/gkv1278] [PMID: 26602694]

[40] Xu, X.; Lai, R. The chemistry and biological activities of peptides from amphibian skin secretions. *Chem. Rev.,* **2015**, *115*(4), 1760-1846. [http://dx.doi.org/10.1021/cr4006704] [PMID: 25594509]

[41] Mangoni, M.L. Temporins, anti-infective peptides with expanding properties. *Cell. Mol. Life Sci.,* **2006**, *63*(9), 1060-1069. [http://dx.doi.org/10.1007/s00018-005-5536-y] [PMID: 16572270]

[42] Conlon, J.M. The contribution of skin antimicrobial peptides to the system of innate immunity in anurans. *Cell Tissue Res.,* **2011**, *343*(1), 201-212. [http://dx.doi.org/10.1007/s00441-010-1014-4] [PMID: 20640445]

[43] Conlon, J.M.; Kolodziejek, J.; Nowotny, N. Antimicrobial peptides from the skins of North American frogs. *Biochim. Biophys. Acta,* **2009**, *1788*(8), 1556-1563. [http://dx.doi.org/10.1016/j.bbamem.2008.09.018] [PMID: 18983817]

[44] Pantic, J.M.; Jovanovic, I.P.; Radosavljevic, G.D.; Arsenijevic, N.N.; Conlon, J.M.; Lukic, M.L. The potential of frog skin-derived peptides for development into therapeutically-valuable immunomodulatory agents. *Molecules,* **2017**, *22*(12), E2071. [http://dx.doi.org/10.3390/molecules22122071] [PMID: 29236056]

[45] Park, J.M.; Jung, J.E.; Lee, B.J. Antimicrobial peptides from the skin of a Korean frog, *Rana rugosa*. *Biochem. Biophys. Res. Commun.,* **1995**, *209*(2), 775. [http://dx.doi.org/10.1006/bbrc.1995.1567] [PMID: 7733950]

[46] Conlon, J.M.; Kolodziejek, J.; Nowotny, N. Antimicrobial peptides from ranid frogs: taxonomic and phylogenetic markers and a potential source of new therapeutic agents. *Biochim. Biophys. Acta,* **2004**, *1696*(1), 1-14. [http://dx.doi.org/10.1016/j.bbapap.2003.09.004] [PMID: 14726199]

[47] Matutte, B.; Storey, K.B.; Knoop, F.C.; Conlon, J.M. Induction of synthesis of an antimicrobial peptide in the skin of the freeze-tolerant frog, *Rana sylvatica*, in response to environmental stimuli. *FEBS Lett.,* **2000**, *483*(2-3), 135-138. [http://dx.doi.org/10.1016/S0014-5793(00)02102-5] [PMID: 11042268]

[48] Yan, H.; Hancock, R.E. Synergistic interactions between mammalian antimicrobial defense peptides. *Antimicrob. Agents Chemother.,* **2001**, *45*(5), 1558-1560. [http://dx.doi.org/10.1128/AAC.45.5.1558-1560.2001] [PMID: 11302828]

[49] Rosenfeld, Y.; Barra, D.; Simmaco, M.; Shai, Y.; Mangoni, M.L. A synergism between temporins toward Gram-negative bacteria overcomes resistance imposed by the lipopolysaccharide protective layer. *J. Biol. Chem.,* **2006**, *281*(39), 28565-28574. [http://dx.doi.org/10.1074/jbc.M606031200] [PMID: 16867990]

[50] Merlino, F.; Carotenuto, A.; Casciaro, B.; Martora, F.; Loffredo, M.R.; Di Grazia, A.; Yousif, A.M.; Brancaccio, D.; Palomba, L.; Novellino, E.; Galdiero, M.; Iovene, M.R.; Mangoni, M.L.; Grieco, P. Glycine-replaced derivatives of [Pro^3,$DLeu^9$]TL, a temporin L analogue: Evaluation of antimicrobial, cytotoxic and hemolytic activities. *Eur. J. Med. Chem.,* **2017**, *139*, 750-761. [http://dx.doi.org/10.1016/j.ejmech.2017.08.040] [PMID: 28863356]

[51] Mangoni, M.L.; Grazia, A.D.; Cappiello, F.; Casciaro, B.; Luca, V. Naturally occurring peptides from *Rana temporaria*: Antimicrobial properties and more. *Curr. Top. Med. Chem.,* **2016**, *16*(1), 54-64. [http://dx.doi.org/10.2174/1568026615666150703121403] [PMID: 26139114]

[52] Musale, V.; Casciaro, B.; Mangoni, M.L.; Abdel-Wahab, Y.H.A.; Flatt, P.R.; Conlon, J.M. Assessment of the potential of temporin peptides from the frog Rana temporaria (Ranidae) as anti-diabetic agents. *Journal of peptide science: an official publication of the European Peptide Society., 24*(2)**2018**,

[53] Marcocci, M.E.; Amatore, D.; Villa, S.; Casciaro, B.; Aimola, P.; Franci, G.; Grieco, P.; Galdiero, M.; Palamara, A.T.; Mangoni, M.L.; Nencioni, L. The amphibian antimicrobial peptide temporin B inhibits *In vitro* herpes simplex virus 1 infection. *Antimicrob. Agents Chemother.,* **2018**, *62*(5), e02367. [http://dx.doi.org/10.1128/AAC.02367-17] [PMID: 29483113]

[54] Musale, V.; Abdel-Wahab, Y.H.A.; Flatt, P.R.; Conlon, J.M.; Mangoni, M.L. Insulinotropic, glucose-lowering, and beta-cell anti-apoptotic actions of peptides related to esculentin-1a(1-21).NH_2. *Amino Acids,* **2018**, *50*(6), 723-734. [http://dx.doi.org/10.1007/s00726-018-2551-5] [PMID: 29549522]

[55] Conlon, J.M. Reflections on a systematic nomenclature for antimicrobial peptides from the skins of frogs of the family Ranidae. *Peptides,* **2008**, *29*(10), 1815-1819. [http://dx.doi.org/10.1016/j.peptides.2008.05.029] [PMID: 18585417]

[56] Basir, Y.J.; Knoop, F.C.; Dulka, J.; Conlon, J.M. Multiple antimicrobial peptides and peptides related to bradykinin and neuromedin N isolated from skin secretions of the pickerel frog, *Rana palustris*. *Biochim. Biophys. Acta,* **2000**, *1543*(1), 95-105. [http://dx.doi.org/10.1016/S0167-4838(00)00191-6] [PMID: 11087945]

[57] Ali, M.F.; Lips, K.R.; Knoop, F.C.; Fritzsch, B.; Miller, C.; Conlon, J.M. Antimicrobial peptides and protease inhibitors in the skin secretions of the crawfish frog, *Rana areolata*. *Biochim. Biophys. Acta,* **2002**, *1601*(1), 55-63. [http://dx.doi.org/10.1016/S1570-9639(02)00432-6] [PMID: 12429503]

[58] Wang, H.; Yu, Z.; Hu, Y.; Yu, H.; Ran, R.; Xia, J.; Wang, D.; Yang, S.; Yang, X.; Liu, J. Molecular cloning and characterization of antimicrobial peptides from skin of the broad-folded frog, *Hylarana latouchii*. *Biochimie,* **2012**, *94*(6), 1317-1326. [http://dx.doi.org/10.1016/j.biochi.2012.02.032] [PMID: 22426384]

[59] Li, J.; Xu, X.; Xu, C.; Zhou, W.; Zhang, K.; Yu, H.; Zhang, Y.; Zheng, Y.; Rees, H.H.; Lai, R.; Yang, D.; Wu, J. Anti-infection peptidomics of amphibian skin. *Mol. Cell. Proteomics,* **2007**, *6*(5), 882-894. [http://dx.doi.org/10.1074/mcp.M600334-MCP200] [PMID: 17272268]

[60] Iwakoshi-Ukena, E.; Ukena, K.; Okimoto, A.; Soga, M.; Okada, G.; Sano, N.; Fujii, T.; Sugawara, Y.; Sumida, M. Identification and characterization of antimicrobial peptides from the skin of the endangered frog *Odorrana ishikawae*. *Peptides,* **2011**, *32*(4), 670-676. [http://dx.doi.org/10.1016/j.peptides.2010.12.013] [PMID: 21193000]

[61] Marenah, L.; Flatt, P.R.; Orr, D.F.; Shaw, C.; Abdel-Wahab, Y.H. Skin secretions of *Rana saharica* frogs reveal antimicrobial peptides esculentins-1 and -1B and brevinins-1E and -2EC with novel insulin releasing activity. *J. Endocrinol.,* **2006**, *188*(1), 1-9. [http://dx.doi.org/10.1677/joe.1.06293] [PMID: 16394170]

[62] Conlon, J.M.; Meetani, M.A.; Coquet, L.; Jouenne, T.; Leprince, J.; Vaudry, H.; Kolodziejek, J.; Nowotny, N.; King, J.D. Antimicrobial peptides from the skin secretions of the new world frogs *Lithobates capito* and *Lithobates warszewitschii* (Ranidae). *Peptides,* **2009**, *30*(10), 1775-1781. [http://dx.doi.org/10.1016/j.peptides.2009.07.011] [PMID: 19635516]

[63] Conlon, J.M.; Kolodziejek, J.; Mechkarska, M.; Coquet, L.; Leprince, J.; Jouenne, T.; Vaudry, H.; Nielsen, P.F.; Nowotny, N.; King, J.D. Host defense peptides from *Lithobates forreri*, *Hylarana luctuosa*, and *Hylarana signata* (Ranidae): phylogenetic relationships inferred from primary structures of ranatuerin-2 and brevinin-2 peptides. *Comp. Biochem. Physiol. Part D Genomics Proteomics,* **2014**, *9*, 49-57. [http://dx.doi.org/10.1016/j.cbd.2014.01.002] [PMID: 24463457]

[64] Simmaco, M.; Mignogna, G.; Barra, D.; Bossa, F. Novel antimicrobial peptides from skin secretion of the European frog *Rana esculenta*. *FEBS Lett.,* **1993**, *324*(2), 159-161. [http://dx.doi.org/10.1016/0014-5793(93)81384-C] [PMID: 8508915]

[65] Simmaco, M.; Mignogna, G.; Barra, D.; Bossa, F. Antimicrobial peptides from skin secretions of *Rana esculenta*. Molecular cloning of cDNAs encoding esculentin and brevinins and isolation of new active peptides. *J. Biol. Chem.,* **1994**, *269*(16), 11956-11961. [PMID: 8163497]

[66] Wang, Y.; Zhang, Y.; Lee, W.H.; Yang, X.; Zhang, Y. Novel peptides from skins of amphibians showed broad-spectrum antimicrobial activities. *Chem. Biol. Drug Des.,* **2016**, *87*(3), 419-424. [http://dx.doi.org/10.1111/cbdd.12672] [PMID: 26452973]

[67] Ponti, D.; Mignogna, G.; Mangoni, M.L.; De Biase, D.; Simmaco, M.; Barra, D. Expression and activity of cyclic and linear analogues of esculentin-1, an anti-microbial peptide from amphibian skin. *Eur. J. Biochem.,* **1999**, *263*(3), 921-927. [http://dx.doi.org/10.1046/j.1432-1327.1999.00597.x] [PMID: 10469159]

[68] Segura, A.; Moreno, M.; Molina, A.; García-Olmedo, F. Novel defensin subfamily from spinach (*Spinacia oleracea*). *FEBS Lett.,* **1998**, *435*(2-3), 159-162. [http://dx.doi.org/10.1016/S0014-5793(98)01060-6] [PMID: 9762899]

[69] Ponti, D.; Mangoni, M.L.; Mignogna, G.; Simmaco, M.; Barra, D. An amphibian antimicrobial peptide variant expressed in *Nicotiana tabacum* confers resistance to phytopathogens. *Biochem. J.,* **2003**, *370*(Pt 1), 121-127. [http://dx.doi.org/10.1042/bj20021444] [PMID: 12435273]

[70] Orivel, J.; Redeker, V.; Le Caer, J.P.; Krier, F.; Revol-Junelles, A.M.; Longeon, A.; Chaffotte, A.; Dejean, A.; Rossier, J. Ponericins, new antibacterial and insecticidal peptides from the venom of the ant *Pachycondyla goeldii*. *J. Biol. Chem.,* **2001**, *276*(21), 17823-17829. [http://dx.doi.org/10.1074/jbc.M100216200] [PMID: 11279030]

[71] Mangoni, M.L.; Fiocco, D.; Mignogna, G.; Barra, D.; Simmaco, M. Functional characterisation of the 1-18 fragment of esculentin-1b, an antimicrobial peptide from *Rana esculenta*. *Peptides,* **2003**, *24*(11), 1771-1777. [http://dx.doi.org/10.1016/j.peptides.2003.07.029] [PMID: 15019209]

[72] Islas-Rodriguez, A.E.; Marcellini, L.; Orioni, B.; Barra, D.; Stella, L.; Mangoni, M.L. Esculentin 1-21: a linear antimicrobial peptide from frog skin with inhibitory effect on bovine mastitis-causing bacteria. *J. Pept. Sci.,* **2009**, *15*(9), 607-614. [DOI: 10.1002/psc.1148] [PMID: 19507197]

[73] Loffredo, M.R.; Ghosh, A.; Harmouche, N.; Casciaro, B.; Luca, V.; Bortolotti, A.; Cappiello, F.; Stella, L.; Bhunia, A.; Bechinger, B.; Mangoni, M.L. Membrane perturbing activities and structural properties of the frog-skin derived peptide Esculentin-1a(1-21)NH_2 and its Diastereomer Esc(1-21)-1c: Correlation with their antipseudomonal and cytotoxic activity. *Biochim. Biophys. Acta Biomembr.,* **2017**, *1859*(12), 2327-2339. [http://dx.doi.org/10.1016/j.bbamem.2017.09.009] [PMID: 28912103]

[74] Di Grazia, A.; Cappiello, F.; Cohen, H.; Casciaro, B.; Luca, V.; Pini, A.; Di, Y.P.; Shai, Y.; Mangoni, M.L. D-Amino acids incorporation in the frog skin-derived peptide esculentin-1a(1-21)NH2 is beneficial for its multiple functions. *Amino Acids,* **2015**, *47*(12), 2505-2519. [http://dx.doi.org/10.1007/s00726-015-2041-y] [PMID: 26162435]

[75] Klaas, I.C.; Zadoks, R.N. An update on environmental mastitis: Challenging perceptions. *Transbound. Emerg. Dis.,* **2018**, *65*(Suppl. 1), 166-185. [http://dx.doi.org/10.1111/tbed.12704] [PMID: 29083115]

[76] Luca, V.; Stringaro, A.; Colone, M.; Pini, A.; Mangoni, M.L. Esculentin(1-21), an amphibian skin membrane-active peptide with potent activity on both planktonic and biofilm cells of the bacterial pathogen *Pseudomonas aeruginosa*. *Cell. Mol. Life Sci.,* **2013**, *70*(15), 2773-2786. [http://dx.doi.org/10.1007/s00018-013-1291-7] [PMID: 23503622]

[77] Parkins, M.D.; Somayaji, R.; Waters, V.J. Epidemiology, biology, and impact of clonal *Pseudomonas aeruginosa* infections in cystic fibrosis. *Clin. Microbiol. Rev.,* **2018**, *31*(4)e00019-18 [http://dx.doi.org/10.1128/CMR.00019-18] [PMID: 30158299]

[78] Cappiello, F.; Casciaro, B.; Mangoni, M.L. A novel *in vitro* wound healing assay to evaluate cell migration. *Journal of visualized experiments : JoVE.,* **2018**, *133*. [http://dx.doi.org/10.3791/56825]

[79] Cappiello, F.; Di Grazia, A.; Segev-Zarko, L.A.; Scali, S.; Ferrera, L.; Galietta, L.; Pini, A.; Shai, Y.; Di, Y.P.; Mangoni, M.L. Esculentin-1a-derived peptides promote clearance of *Pseudomonas aeruginosa* internalized in bronchial cells of cystic fibrosis patients and lung cell migration: biochemical properties and a plausible mode of action. *Antimicrob. Agents Chemother.,* **2016**, *60*(12), 7252-7262. [PMID: 27671059]

[80] Kolar, S.S.N.; Luca, V.; Baidouri, H.; Mannino, G.; McDermott, A.M.; Mangoni, M.L. Esculentin-1a(1-21)NH2: a frog skin-derived peptide for microbial keratitis. *Cell. Mol. Life Sci.,* **2015**, *72*(3), 617-627. [http://dx.doi.org/10.1007/s00018-014-1694-0] [PMID: 25086859]

[81] Casciaro, B.; Cappiello, F.; Cacciafesta, M.; Mangoni, M.L. Promising approaches to optimize the biological properties of the antimicrobial peptide Esculentin-1a(1-21)Nh_2: amino acids substitution and conjugation to nanoparticles. *Front Chem.,* **2017**, *5*, 26. [http://dx.doi.org/10.3389/fchem.2017.00026] [PMID: 28487853]

[82] Jia, F.; Wang, J.; Peng, J.; Zhao, P.; Kong, Z.; Wang, K.; Yan, W.; Wang, R. D-amino acid substitution enhances the stability of antimicrobial peptide polybia-CP. *Acta Biochim. Biophys. Sin. (Shanghai),* **2017**, *49*(10), 916-925. [http://dx.doi.org/10.1093/abbs/gmx091] [PMID: 28981608]

[83] Saint Jean, K.D.; Henderson, K.D.; Chrom, C.L.; Abiuso, L.E.; Renn, L.M.; Caputo, G.A. Effects of hydrophobic amino acid substitutions on antimicrobial peptide behavior. *Probiotics Antimicrob. Proteins,* **2018**, *10*(3), 408-419. [http://dx.doi.org/10.1007/s12602-017-9345-z] [PMID: 29103131]

[84] Junior, E.F.C.; Guimarães, C.F.R.C.; Franco, L.L.; Alves, R.J.; Kato, K.C.; Martins, H.R.; de Souza Filho, J.D.; Bemquerer, M.P.; Munhoz, V.H.O.; Resende, J.M.; Verly, R.M. Glycotriazole-peptides derived from the peptide HSP1: synergistic effect of triazole and saccharide rings on the antifungal activity. *Amino Acids,* **2017**, *49*(8), 1389-1400. [http://dx.doi.org/10.1007/s00726-017-2441-2] [PMID: 28573520]

[85] Albada, H.B.; Prochnow, P.; Bobersky, S.; Langklotz, S.; Schriek, P.; Bandow, J.E.; Metzler-Nolte, N. Tuning the activity of a short arg-trp antimicrobial Peptide by lipidation of a C- or N-terminal lysine side-chain. *ACS Med. Chem. Lett.,* **2012**, *3*(12), 980-984. [http://dx.doi.org/10.1021/ml300148v] [PMID: 24900420]

[86] Zhang, S.K.; Song, J.W.; Gong, F.; Li, S.B.; Chang, H.Y.; Xie, H.M.; Gao, H.W.; Tan, Y.X.; Ji, S.P. Design of an α-helical antimicrobial peptide with improved cell-selective and potent anti-biofilm activity. *Sci. Rep.,* **2016**, *6*, 27394. [http://dx.doi.org/10.1038/srep27394] [PMID: 27271216]

[87] Huang, Y.; He, L.; Li, G.; Zhai, N.; Jiang, H.; Chen, Y. Role of helicity of α-helical antimicrobial peptides to improve specificity. *Protein Cell,* **2014**, *5*(8), 631-642. [http://dx.doi.org/10.1007/s13238-014-0061-0] [PMID: 24805306]

[88] Biondi, B.; Casciaro, B.; Di Grazia, A.; Cappiello, F.; Luca, V.; Crisma, M.; Mangoni, M.L. Effects of Aib residues insertion on the structural-functional properties of the frog skin-derived peptide esculentin-1a(1-21)NH_2. *Amino Acids,* **2017**, *49*(1), 139-150. [http://dx.doi.org/10.1007/s00726-016-2341-x] [PMID: 27726008]

[89] Buommino, E.; Carotenuto, A.; Antignano, I.; Bellavita, R.; Casciaro, B.; Loffredo, M.R.; Merlino, F.; Novellino, E.; Mangoni, M.L.; Nocera, F.P.; Brancaccio, D.; Punzi, P.; Roversi, D.; Ingenito, R.; Bianchi, E.; Grieco, P. The Outcomes of decorated prolines in the discovery of antimicrobial peptides from Temporin-L. *Chem. Med. Chem.,* **2019**, *14*(13), 1283-1290. [http://dx.doi.org/10.1002/cmdc.201900221] [PMID: 31087626]

[90] Izadpanah, M.; Khalili, H. Antibiotic regimens for treatment of infections due to multidrug-resistant Gram-negative pathogens: An evidence-based literature review. *J. Res. Pharm. Pract.,* **2015**, *4*(3), 105-114. [http://dx.doi.org/10.4103/2279-042X.162360] [PMID: 26312249]

[91] Casciaro, B.; Loffredo, M.R.; Luca, V.; Verrusio, W.; Cacciafesta, M.; Mangoni, M.L. Esculentin-1a derived antipseudomonal peptides: limited induction of resistance and synergy with aztreonam. *Protein Pept. Lett.,* **2018**, *25*(12), 1155-1162. [http://dx.doi.org/10.2174/0929866525666181101104649] [PMID: 30381056]

[92] Davies, J.; Spiegelman, G.B.; Yim, G. The world of subinhibitory antibiotic concentrations. *Curr. Opin. Microbiol.,* **2006**, *9*(5), 445-453. [http://dx.doi.org/10.1016/j.mib.2006.08.006] [PMID: 16942902]

[93] Andersson, D.I.; Hughes, D. Microbiological effects of sublethal levels of antibiotics. *Nat. Rev. Microbiol.,* **2014**, *12*(7), 465-478. [http://dx.doi.org/10.1038/nrmicro3270] [PMID: 24861036]

[94] Kaplan, J.B. Antibiotic-induced biofilm formation. *Int. J. Artif. Organs,* **2011**, *34*(9), 737-751. [http://dx.doi.org/10.5301/ijao.5000027] [PMID: 22094552]

[95] Berditsch, M.; Afonin, S.; Vladimirova, T.; Wadhwani, P.; Ulrich, A.S. Antimicrobial peptides can enhance the risk of persistent infections. *Front. Immunol.,* **2012**, *3*, 222. [http://dx.doi.org/10.3389/fimmu.2012.00222] [PMID: 22870073]

[96] Casciaro, B.; Lin, Q.; Afonin, S.; Loffredo, M.R.; de Turris, V.; Middel, V.; Ulrich, A.S.; Di, Y.P.; Mangoni, M.L. Inhibition of *Pseudomonas aeruginosa* biofilm formation and expression of virulence genes by selective epimerization in the peptide Esculentin-1a(1-21)NH_2. *FEBS J.,* **2019**. [http://dx.doi.org/10.1111/febs.14940] [PMID: 31144441]

[97] Peschel, A.; Sahl, H.G. The co-evolution of host cationic antimicrobial peptides and microbial resistance. *Nat. Rev. Microbiol.,* **2006**, *4*(7), 529-536. [http://dx.doi.org/10.1038/nrmicro1441] [PMID: 16778838]

[98] Hong, J.; Hu, J.; Ke, F. experimental induction of bacterial resistance to the antimicrobial peptide Tachyplesin I and investigation of the resistance mechanisms. *Antimicrob. Agents Chemother.,* **2016**, *60*(10), 6067-6075.

[http://dx.doi.org/10.1128/AAC.00640-16] [PMID: 27480861]

[99] St Helen, G.; Holland, N.T.; Balmes, J.R.; Hall, D.B.; Bernert, J.T.; Vena, J.E.; Wang, J.S.; Naeher, L.P. Utility of urinary Clara cell protein (CC16) to demonstrate increased lung epithelial permeability in non-smokers exposed to outdoor secondhand smoke. *J. Expo. Sci. Environ. Epidemiol.,* **2013**, *23*(2), 183-189. [http://dx.doi.org/10.1038/jes.2012.68] [PMID: 22805990]

[100] Chen, C.; Mangoni, M.L.; Di, Y.P. *In vivo* therapeutic efficacy of frog skin-derived peptides against Pseudomonas aeruginosa-induced pulmonary infection. *Sci. Rep.,* **2017**, *7*(1), 8548. [http://dx.doi.org/10.1038/s41598-017-08361-8] [PMID: 28819175]

[101] Rai, A.; Pinto, S.; Velho, T.R.; Ferreira, A.F.; Moita, C.; Trivedi, U.; Evangelista, M.; Comune, M.; Rumbaugh, K.P.; Simões, P.N.; Moita, L.; Ferreira, L. One-step synthesis of high-density peptide-conjugated gold nanoparticles with antimicrobial efficacy in a systemic infection model. *Biomaterials,* **2016**, *85*, 99-110. [http://dx.doi.org/10.1016/j.biomaterials.2016.01.051] [PMID: 26866877]

[102] Torres, L.M.F.C.; Almeida, M.T.; Santos, T.L.; Marinho, L.E.S.; de Mesquita, J.P.; da Silva, L.M.; Dos Santos, W.T.P.; Martins, H.R.; Kato, K.C.; Alves, E.S.F.; Liao, L.M.; de Magalhães, M.T.Q.; de Mendonça, F.G.; Pereira, F.V.; Resende, J.M.; Bemquerer, M.P.; Rodrigues, M.A.; Verly, R.M. Antimicrobial alumina nanobiostructures of disulfide- and triazole-linked peptides: Synthesis, characterization, membrane interactions and biological activity. *Colloids Surf. B Biointerfaces,* **2019**, *177*, 94-104. [http://dx.doi.org/10.1016/j.colsurfb.2019.01.052] [PMID: 30711763]

[103] Dutta, D.; Willcox, M.D. Antimicrobial contact lenses and lens cases: a review. *Eye Contact Lens,* **2014**, *40*(5), 312-324. [http://dx.doi.org/10.1097/ICL.0000000000000056] [PMID: 25083781]

[104] Kamaruzzaman, N.F.; Tan, L.P.; Hamdan, R.H.; Choong, S.S.; Wong, W.K.; Gibson, A.J.; Chivu, A.; Pina, M.F. Antimicrobial polymers: the potential replacement of existing antibiotics? *Int. J. Mol. Sci.,* **2019**, *20*(11)E2747 [http://dx.doi.org/10.3390/ijms20112747] [PMID: 31167476]

[105] Elahi, N.; Kamali, M.; Baghersad, M.H. Recent biomedical applications of gold nanoparticles: A review. *Talanta,* **2018**, *184*, 537-556. [http://dx.doi.org/10.1016/j.talanta.2018.02.088] [PMID: 29674080]

[106] Casciaro, B.; Moros, M.; Rivera-Fernández, S.; Bellelli, A.; de la Fuente, J.M.; Mangoni, M.L. Gold-nanoparticles coated with the antimicrobial peptide esculentin-1a(1-21)NH_2 as a reliable strategy for antipseudomonal drugs. *Acta Biomater.,* **2017**, *47*, 170-181. [http://dx.doi.org/10.1016/j.actbio.2016.09.041] [PMID: 27693686]

[107] Ciofu, O.; Tolker-Nielsen, T. Tolerance and resistance of *Pseudomonas aeruginosa* biofilms to antimicrobial agents-How *P. aeruginosa* Can Escape Antibiotics. *Front. Microbiol.,* **2019**, *10*, 913. [http://dx.doi.org/10.3389/fmicb.2019.00913] [PMID: 31130925]

[108] d'Angelo, I.; Casciaro, B.; Miro, A.; Quaglia, F.; Mangoni, M.L.; Ungaro, F. Overcoming barriers in *Pseudomonas aeruginosa* lung infections: Engineered nanoparticles for local delivery of a cationic antimicrobial peptide. *Colloids Surf. B Biointerfaces,* **2015**, *135*, 717-725. [http://dx.doi.org/10.1016/j.colsurfb.2015.08.027] [PMID: 26340361]

[109] d'Angelo, I.; Quaglia, F.; Ungaro, F. PLGA carriers for inhalation: where do we stand, where are we headed? *Ther. Deliv.,* **2015**, *6*(10), 1139-1144. [http://dx.doi.org/10.4155/tde.15.37] [PMID: 26606854]

[110] Debnath, S.K.; Saisivam, S.; Omri, A. PLGA ethionamide nanoparticles for pulmonary delivery: development and *in vivo* evaluation of dry powder inhaler. *J. Pharm. Biomed. Anal.,* **2017**, *145*, 854-859. [http://dx.doi.org/10.1016/j.jpba.2017.07.051] [PMID: 28826144]

[111] Tang, J.; Li, J.; Li, G.; Zhang, H.; Wang, L.; Li, D.; Ding, J. Spermidine-mediated poly(lactic-*co*-glycolic acid) nanoparticles containing fluorofenidone for the treatment of idiopathic pulmonary fibrosis. *Int. J. Nanomedicine,* **2017**, *12*, 6687-6704. [http://dx.doi.org/10.2147/IJN.S140569] [PMID: 28932114]

[112] Semete, B.; Booysen, L.; Lemmer, Y.; Kalombo, L.; Katata, L.; Verschoor, J.; Swai, H.S. *In vivo* evaluation of the biodistribution and safety of PLGA nanoparticles as drug delivery systems. *Nanomedicine (Lond.),* **2010**, *6*(5), 662-671. [http://dx.doi.org/10.1016/j.nano.2010.02.002] [PMID: 20230912]

[113] Casciaro, B.; d'Angelo, I.; Zhang, X.; Loffredo, M.R.; Conte, G.; Cappiello, F.; Quaglia, F.; Di, Y.P.; Ungaro, F.; Mangoni, M.L. Poly(lactide- co-glycolide) Nanoparticles for Prolonged Therapeutic Efficacy of Esculentin-1a-Derived Antimicrobial Peptides against Pseudomonas aeruginosa Lung Infection: *in Vitro* and *in Vivo* Studies. *Biomacromolecules,* **2019**, *20*(5), 1876-1888. [http://dx.doi.org/10.1021/acs.biomac.8b01829] [PMID: 31013061]

[114] Subedi, D.; Vijay, A.K.; Willcox, M. Overview of mechanisms of antibiotic resistance in *Pseudomonas aeruginosa*: an ocular perspective. *Clin. Exp. Optom.,* **2018**, *101*(2), 162-171. [http://dx.doi.org/10.1111/cxo.12621] [PMID: 29044738]

[115] Casciaro, B.; Dutta, D.; Loffredo, M.R.; Marcheggiani, S.; McDermott, A.M.; Willcox, M.D.; Mangoni, M.L. Esculentin-1a derived peptides kill Pseudomonas aeruginosa biofilm on soft contact lenses and retain antibacterial activity upon immobilization to the lens surface. *Biopolymers,* **2017**, *110*(5)e23074 [http://dx.doi.org/10.1002/bip.23074] [PMID: 29086910]

European Journal of Medicinal Chemistry 139 (2017) 750–761

Contents lists available at ScienceDirect

European Journal of Medicinal Chemistry

journal homepage: http://www.elsevier.com/locate/ejmech

Research paper

Glycine-replaced derivatives of [Pro^3,DLeu^9]TL, a temporin L analogue: Evaluation of antimicrobial, cytotoxic and hemolytic activities

Francesco Merlino [a, 1], Alfonso Carotenuto [a, 1], Bruno Casciaro [b], Francesca Martora [c], Maria Rosa Loffredo [b], Antonio Di Grazia [b], Ali M. Yousif [d], Diego Brancaccio [a], Luciana Palomba [c], Ettore Novellino [a], Massimiliano Galdiero [c], Maria Rosaria Iovene [c], Maria L. Mangoni [b, **], Paolo Grieco [a, *]

[a] Department of Pharmacy, University of Naples 'Federico II', Naples, 80131, Italy
[b] Department of Biochemical Sciences, Laboratory Affiliated to Pasteur Institute Italia-Fondazione Cenci Bolognetti, Sapienza University of Rome, Rome, 00185, Italy
[c] Department of Experimental Medicine, Università della Campania 'Luigi Vanvitelli', Naples, 80138, Italy
[d] Department of Chemistry, University of Texas at Dallas, 800 W. Campbell Rd., Richardson, TX, 75080, United States

ARTICLE INFO

Article history:
Received 4 July 2017
Received in revised form
3 August 2017
Accepted 19 August 2017
Available online 21 August 2017

Keywords:
Antimicrobial peptides
Temporin L analogues
SAR study
Spectroscopy studies

ABSTRACT

In this study we designed and synthesized a new library of antimicrobial peptides correlated to [Pro^3,DLeu^9]TL **1**, a temporin L derivative devoid of cytolytic effects *in vitro*, and investigated the correlation between the α-helical content of the compounds and their antibacterial, cytotoxic and hemolytic activities. We systematically replaced Gly in position 10 of reference peptide with several amino acids. Structure-activity relationship studies of these analogues were performed by means of antimicrobial and cytotoxicity assays along with CD spectroscopy analyses. NMR analysis was also accomplished for compound **10**. As well, the most promising peptides were additionally evaluated for their activity against some clinical strains isolated from human skin and for their mechanism of action by studying the kinetics of membrane perturbation of some representative microbial strains. We identified novel analogues with interesting properties that make them attractive lead compounds for potential topical applications.

1. Introduction

The emergence of antibiotic-resistant bacterial strains is not a new phenomenon [1,2]. In fact, the discovery of antimicrobial drugs has contributed to reduce the mortality, but not the persistence of infectious diseases. The resistance to currently-used antibiotics is rapidly increasing and the lack of alternative antibiotic strategies is a crucial feature in fighting the infections caused by such bacteria [3,4]. Several of these pathogens, also known as 'superbugs' [5], are Gram-negative bacteria and resistant of up 50% against carbapenems, *e.g. Enterobacteriaceae* (*Escherichia coli* and *Klebsiella* related species), in some developing countries [6]. Together, only few new antibiotics against Gram-positive bacteria (such as recent lipoglycopeptide [7,8], cephalosporin [1,9] and oxazolidinone [10] derivatives) are becoming clinically available in recent years [11], whereas no new class of antibiotics for the treatment of Gram-negative bacteria infections has been introduced during the last four decades [12,13]. Moreover, the use and misuse of preexisting antibiotics and resulting development of specific mechanisms of resistance have plagued their own therapeutic use, prompting for the pursuit of alternative antimicrobial agents [14].

In this regard, antimicrobial peptides (AMPs), virtually existing in all species of life [15], exert killing activity on a large number of invading microorganisms [16]. Belonging to the host's innate defense system, they represent the most ancient and fast-acting elements against microbial pathogens [17]. To date, these AMPs are promising candidates for a new generation of anti-infective agents. Indeed, AMPs prove to be successful *versus* multi-drug resistant bacteria and have low propensity to induce resistance, in contrast with other antimicrobial drugs [18]. Their biological activity can originate from direct killing of pathogenic microbes or indirectly by modulating the innate immune system [19,20]. In particular, such

* Corresponding author.
** Corresponding author.
E-mail addresses: marialuisa.mangoni@uniroma1.it (M.L. Mangoni), paolo.grieco@unina.it (P. Grieco).
[1] These authors contributed equally.

http://dx.doi.org/10.1016/j.ejmech.2017.08.040
0223-5234/

natural compounds may interact with bacterial cell membrane, or intracellular paths (synthesis, modulation and folding of proteins) by diverse mechanisms [21]. Although some AMPs are able to cross the cell membrane and interfere with cellular components [22], cell membrane disruption seems to be the main mode of action [23–26]. Due to their chemical and biological instability, representing one of the major hurdles, only few AMPs are currently in clinical trials [27].

The amphibian temporins represent one of the largest families (around 100 members) and are among the smallest-sized AMPs (10–16 amino acid residues) found in nature to date. These amphibian peptides have an amide group at the C-terminal and present only 1 or 2 basic residues in their whole sequence [28]. Temporins are known to be particularly active against Gram-positive bacteria, with minimal inhibitory concentrations (MIC) ranging from 2.5 to 20 μM [29,30]. The exception is given by the isoform L (temporin L, TL), H-Phe-Val-Gln-Trp-Phe-Ser-Lys-Phe-Leu-Gly-Arg-Ile-Leu-NH_2, as it is also active against Gram-negative bacteria and yeast strains [28]. Most of the temporins are practically non-hemolytic, but the highly potent TL kills human erythrocytes at microbicidal concentrations as well [31]. Therefore, for further development as broad spectrum antibiotic, it is necessary to increase its therapeutic index, referred to as the ratio between the concentration of hemolytic activity (minimum hemolytic concentration, MHC) and antimicrobial activity (MIC), MHC/MIC for bacteria over erythrocytes [32]. Recent studies, focused on the structure-activity relationships of both native TL and some synthetic analogues were performed in our multidisciplinary group [33], and clearly revealed the existence of a straight correlation between the hemolytic activity of TL and derivatives and their α-helix content [34]. No relation has been found with the antimicrobial activity, though.

On the tail of such evidences, we identified an interesting TL analogue, [Pro^3, $DLeu^9$]TL **1**, practically devoid of cytolytic effects *in vitro*, which preserved yet the effectiveness of the native peptide against the yeast *Candida albicans* [33,34]. In this compound the simultaneous substitution of Gln^3 and Leu^9 with proline and D-leucine, respectively, produced additional effects in breaking the α-helical content of TL, discerning activity between eukaryotic and prokaryotic membranes, as well as in the peptides' stability. In sum, these chemical modifications leading to compound **1** preserved damages on the microbial membrane of most of the bacterial and Candida strains, and significantly reduced toxicity on human erythrocytes and keratinocytes [35].

With such potential lead peptide sequence in hand, we provided a structure-activity relationship (SAR) study by single-point modification in order to broaden and improve its antimicrobial efficacy without altering the non-cytolytic character. In particular, we synthesized a novel series of derivatives (**2**–**12**, Table 1) since we envisaged modifying the conformation at the C-terminal region of **1** by replacing Gly in position 10. In fact, on the tail of our previous study [35] that emphasized effects of D amino acids in the sequence of [Pro^3]TL, such residue along with stereoinversion of Leu^9 can play a main role in the peptide toxicity. Hence, we pursued a SAR investigation considering Gly^{10} as key residue to be replaced with appropriate amino acids. Among them, we selected those characterized by (i) the propensity to disrupt helicity [Pro, hydroxyproline (Hyp) and an unconventional amino acid, 2-aminoindane-2-carboxylic acid (Aic)]; (ii) a positive charge or an indole ring in their side chain (Lys and Trp, respectively); and (iii) hydrophobic side chain [norleucine (Nle)]. In all of these residues, both L and D isomers were used (except for the non-chiral Aic). The designed compounds were analyzed by means of antimicrobial and cytotoxicity assays combined with CD spectroscopy. Additionally, the most promising peptides were evaluated for their activity against some clinical strains isolated from human skin as well as for their mechanism of antimicrobial activity by studying the kinetics of membrane perturbation on some representative reference microbial strains. Human serum biostability properties were also investigated and detailed conformational analysis on an interesting derivative was finally performed by solution NMR technique.

2. Results

2.1. Biological activity

2.1.1. Antimicrobial activity

The primary structures of the designed temporin L analogues are reported in Table 1. The amino acid substitutions were made on the peptide sequence [Pro^3,$DLeu^9$]TL **1**, recently discovered in our laboratories and regarded as a starting point for further developments. The activity against some reference bacterial and Candida strains was evaluated by the broth microdilution assay to determine the MIC. As indicated in Table 2, the peptide **2** in which the residue of Gly^{10} was replaced with Pro, with the intent to reduce the α-helix conformation at the C-terminal region of **1**, showed a similar activity of the parent peptide **1,** with a slight increase in activity against the Gram-negative bacterial strain of *Acinetobacter baumannii* ATCC 19606, and a slight lower reduction in activity on *Escherichia coli* D21. Differently, an increased activity against Gram-positive bacteria was recorded, as indicated by the lower MICs ranging from 1.56 μM to 3.125 μM, in comparison with those found for **1** (MICs from 3.125 μM to 12.5 μM). In addition, the activity towards the two *Candida* strains considered in this study,

Table 1
Peptide sequences of Gly^{10}-replaced [Pro^3,$DLeu^9$]TL **1** analogues.

Cmpd	Sequence[a]
[Pro^3,$DLeu^9$]TL (**1**)[b]	Phe-Val-Pro-Trp-Phe-Ser-Lys-Phe-DLeu-**Gly**^{10}-Arg-Ile-Leu-NH_2
2	Phe-Val-Pro-Trp-Phe-Ser-Lys-Phe-DLeu-**Pro**^{10}-Arg-Ile-Leu-NH_2
3	Phe-Val-Pro-Trp-Phe-Ser-Lys-Phe-DLeu-**DPro**^{10}-Arg-Ile-Leu-NH_2
4	Phe-Val-Pro-Trp-Phe-Ser-Lys-Phe-DLeu-**Hyp**^{10}-Arg-Ile-Leu-NH_2
5	Phe-Val-Pro-Trp-Phe-Ser-Lys-Phe-DLeu-**DHyp**^{10}-Arg-Ile-Leu-NH_2
6	Phe-Val-Pro-Trp-Phe-Ser-Lys-Phe-DLeu-**Nle**^{10}-Arg-Ile-Leu-NH_2
7	Phe-Val-Pro-Trp-Phe-Ser-Lys-Phe-DLeu-**DNle**^{10}-Arg-Ile-Leu-NH_2
8	Phe-Val-Pro-Trp-Phe-Ser-Lys-Phe-DLeu-**Lys**^{10}-Arg-Ile-Leu-NH_2
9	Phe-Val-Pro-Trp-Phe-Ser-Lys-Phe-DLeu-**DLys**^{10}-Arg-Ile-Leu-NH_2
10	Phe-Val-Pro-Trp-Phe-Ser-Lys-Phe-DLeu-**Trp**^{10}-Arg-Ile-Leu-NH_2
11	Phe-Val-Pro-Trp-Phe-Ser-Lys-Phe-DLeu-**DTrp**^{10}-Arg-Ile-Leu-NH_2
12	Phe-Val-Pro-Trp-Phe-Ser-Lys-Phe-DLeu-**Aic**^{10}-Arg-Ile-Leu-NH_2

[a] Residue variations compared to **1** are highlighted in bold.
[b] Already described in literature [35].

Table 2
Antimicrobial activity of peptide **1** and related designed compounds **2**–**12**.

	MIC (μM)[a]											
	1	**2**	**3**	**4**	**5**	**6**	**7**	**8**	**9**	**10**	**11**	**12**
Gram-negative bacteria												
A. baumannii ATCC 19606	12.5	6.25	50	6.25	25	6.25	6.25	3.125	6.25	3.125	3.125	3.125
E. coli D21	12.5	25	50	25	25	25	25	12.5	12.5	25	25	>50
P. syringae pv tabaci 1918	12.5	12.5	50	12.5	>50	6.25	3.125	6.25	12.5	1.56	3.125	1.56
P. aeruginosa ATCC 27853	50	50	>50	50	>50	50	50	12.5	12.5	>50	50	>50
Gram-positive bacteria												
B. megaterium Bm11	3.125	1.56	3.125	1.56	3.125	3.125	1.56	3.125	3.125	1.56	3.125	1.56
S. aureus Cowan I	12.5	3.125	>50	6.25	>50	3.125	3.125	6.25	12.5	3.125	3.125	1.56
S. epidermidis ATCC 12228	6.25	3.125	25	6.25	50	3.125	3.125	3.125	3.125	1.56	1.56	1.56
Yeasts												
C. albicans ATCC 10231	3.125	1.56	3.125	3.125	3.125	3.125	3.125	1.56	1.56	3.125	3.125	6.25
C. crusei ATCC 6258	3.125	1.56	3.125	1.56	3.125	3.125	1.56	1.56	1.56	3.125	3.125	6.25

[a] Each MIC value is the average of at least three independent experiments.

resulted to be 2-fold higher. When Pro^{10} was replaced by the corresponding enantiomer DPro, generating the compound **3**, there was a substantial loss of activity towards both Gram-negative and Gram-positive bacterial strains, except for *Bacillus megaterium* Bm11. However, the anticandidal activity remained almost unchanged with respect to **1**. Peptide **4**, characterized by the presence of a Hyp residue in the same position, showed an activity towards Gram-negative bacteria which was comparable to that of derivative **2**, while the activity on Gram-positive bacterial strains was decreased by half compared to that of **2**, except for *B. megaterium* Bm11. In addition, the anticandidal activity of peptide **4** resulted slightly increased compared to compound **1**. Peptide **5**, which has a residue of DHyp in position 10, had a similar activity profile to that seen for the derivative **3** towards both Gram-negative and Gram-positive bacteria. Again, the anticandidal potency turned out to be equal to that of **3** and to that of the reference peptide, **1**. Following these indications, we decided to replace the residue of Gly^{10} with Nle, characterized by an aliphatic side chain (compound **6**). When tested against Gram-negative bacteria, **6** resulted to have comparable activity to that of **1** and **2**, except for *Pseudomonas syringae* pv tabaci 1918 on which it resulted more active (6.25 μM). Differently, its activity was higher than that of **1** towards Gram-positive bacteria and its MICs were comparable to those of **2**. Surprisingly, by replacing the Nle with its isomer D, the resulting peptide **7** did not show a reduction in activity as previously seen for the compounds **3** and **5**, both containing D amino acids at position 10. Interestingly, **7** showed also a stronger activity than **1** against some Gram-negative bacterial strains, *i.e. A. baumannii* ATCC 19606 and *P. syringae* pv tabaci 1918. Furthermore, it maintained a similar potency to that of **6** when tested against Gram-positive bacteria. No significant variations in activity were found on the Candida strains. Replacement of the Gly^{10} residue with a residue of Lys, which has a positively charged side chain **8**, allowed a substantial improvement in activity against *P. aeruginosa* ATCC 27853, and the Gram-positive bacteria. The derivative **9**, characterized by the presence of a DLys residue, did not show a reduction in activity as demonstrated for derivatives **3** and **5**. This result suggests that the nature of the side chain of the amino acid in position 10, rather than its chirality, is more important for the antimicrobial activity of the peptide. The derivatives **10** and **11** that have a residue of Trp and DTrp in position 10, respectively, had a similar profile of activity between them. Interestingly, their activity against the Gram-negative *P. syringae* pv tabaci 1918 (MICs of 1.56–3.125 μM) was better than that found for all the peptides analyzed in this study, except for compound **7** that showed a MIC of 3.125 μM against this strain. Finally, the derivative **12**, characterized by the presence in position 10 of an unconventional amino acid Aic, a dialkylglycine derivative devoid of chirality, displayed a good antimicrobial activity towards the Gram-negative bacterial strains of *A. baumannii* ATCC 19606 and *P. syringae* pv tabaci 1918, but the best activity was manifested against the whole panel of Gram-positive bacteria strains, with MICs values comparable to those of **10** and **11**. Notably, this latter compound was the only one displaying a reduced activity against Candida.

2.1.2. Cytotoxicity towards human keratinocytes

The toxic effect of all the synthesized peptides was evaluated on nucleated human cells (*i.e.* keratinocytes) that are the most representative cells of the skin layer, which is often colonized by Candida cells as well as by Gram-positive or Gram-negative bacterial species such as *Staphylococcus aureus* and *P. aeruginosa*, respectively (Table 3). The cytotoxicity was studied by the 3-(4,5-dimethylthiazol-2-yl)-2,5-diphenyltetrazolium bromide (MTT) assay and expressed as percentage of inhibition of MTT reduction to its insoluble formazan crystals by mitochondrial dehydrogenases relative to that of untreated control cells. As reported in Table 3, the cytotoxic effect of **1** after 24 h treatment at the concentrations of 12.5 μM and 25 μM, ranged from 20% to 57%, respectively. Compounds **9** and **10** were selected as the peptides with an overall higher antibacterial/anticandidal activity and lower cytotoxicity up to a concentration of 25 μM in comparison to **1** (about 30% *vs* 57% of **1** at 25 μM). Differently, when they were tested at 50 μM, their toxicity was only slightly lower than that of compound **1**. Note that all peptides resulted to be harmless at a concentration range from 1.56 μM to 6.25 μM with the only exception of **7** and **11** which caused about 15% cell death at 6.25 μM (data not shown).

2.1.3. Antibacterial activity and mechanism of action of peptides ***9*** *and* ***10***

The mechanism of action underlying the antimicrobial activity of those peptides (*i.e.* **9** and **10**) endowed with an overall higher antibacterial/anticandidal activity and lower cytotoxicity in comparison to **1** was then investigated on three reference strains, *i.e.* the Gram-positive *S. epidemidis* ATCC 12228, the Gram-negative *A. baumannii* ATCC 19606 and the yeast *C. albicans* ATCC 10231.

We first assessed the ability of the synthetic temporin analogues to affect the bacterial membrane permeability at the MIC value and compared it with that of the well-known membrane-active reference naturally-occurring peptide TL. To this aim, we monitored the intracellular influx of SYTOX Green (SG), a membrane impermeant fluorescent nucleic acid stain (Fig. 1). As reported in Fig. 1, all peptides were able to perturb the membrane permeability of the

Table 3
Cytotoxic effect of TL analogues **1**–**12** at different concentrations on HaCaT cells after 24 h of treatment.

Cytotoxic Effect (%)[a]												
[peptide] (μM)	**1**	**2**	**3**	**4**	**5**	**6**	**7**	**8**	**9**	**10**	**11**	**12**
12.5	20.63 ± 2.66	16.15 ± 3.51	0***	2.76 ± 2.42**	0***	12.25 ± 1.44**	39.96 ± 2.50***	49.30 ± 2.88***	0***	0***	19.21 ± 1.44	45.54 ± 1.15***
25	57.52 ± 3.99	77.06 ± 3.03**	0***	84.72 ± 2.55***	0***	65.86 ± 6.11	72.81 ± 0.82**	66.86 ± 2.81*	28.22 ± 3.52***	32.1 ± 2.21**	35.34 ± 5.99**	88.72 ± 3.30***
50	91.58 ± 3.85	96.61 ± 1.29	0***	98.81 ± 1.06*	0***	99.76 ± 1.43*	96.64 ± 1.15	96.79 ± 1.24	87.9 ± 1.07	89.3 ± 0.8	96.77 ± 0.81	92.84 ± 2.07

[a] The cytotoxic effect was expressed as percentage of inhibition of MTT reduction to its insoluble formazan crystals by mitochondrial dehydrogenases relative to that of untreated control cells (0% inhibition). See Materials and Methods for additional details. The values are the mean ± SD of three independent experiments. The levels of statistical significance between the analogues and the parent peptide **1** are indicated as follows *$p < 0.05$, **$p < 0.01$, ***$p < 0.001$.

reference strains as pointed out by the increase of the dye fluorescence intensity with respect to the negative control (peptide-untreated bacterial cells). In all cases, although a different kinetics of membrane perturbation was assessed within the first 30 min of peptide treatment, both **9** and **10** achieved the same fluorescence signal of TL in 1 or 2 h of treatment (Fig. 1). More precisely, on the Gram-positive bacterium *S. epidermidis*, **10** had a similar kinetics of membrane perturbation to that of TL, but a slower kinetic was recorded for **9** within the first 30 min.

Differently, on the Gram-negative bacterium *A. baumannii*, the two peptides **9** and **10** were able to perturb the bacterial membrane with a slower kinetics than that of TL, while this difference was less pronounced against *C. albicans.* However, in all studied cases, the analogue **10** displayed a faster membrane-perturbing activity than **9**.

*2.1.4. Antibacterial activity of peptides **9** and **10** against clinical microbial isolates*

Taking into account that replacement of Gly^{10} with DLys or Trp (compounds **9** and **10**, respectively) led to a slight increase in activity against Gram-positive bacterial species with a reduced cytotoxicity compared to **1**, we further analyzed their activity also against bacterial clinical isolates (Table 4). Clinical isolates, multisensitive to common antibiotics (both Gram-positive and Gram-negative bacteria), were screened to assess the activity of selected peptides towards bacteria which have not yet developed any resistance. When tested compounds showed an antibacterial activity against sensitive isolates, we proceeded to test antibiotic resistant strains. Considering Gram-negative bacteria, **10** showed no efficacy against two different strains of multisensitive *E. coli* or against *P. aeruginosa* or *K. pneumonia*. **9** was instead active, but only against *E. coli* with an MIC of 25 μM, therefore, we reckoned there was no sufficient activity to test clinical resistant isolates. The behavior of both peptides was considerably different when tested against Gram-positive bacterial clinical isolates, therefore, confirming a stronger activity of temporins against Gram-positive bacteria. As indicated in Table 4, the antimicrobial activity of the peptides confirmed that **10** had the highest efficacy against the Gram-positive clinical isolates, with an MIC of 6.25 μM *vs* 12.5 μM of the parent **1** peptide. Interestingly, similar concentrations (generally between 6.25 μM and 12.5 μM) were also effective against isolates presenting wide multidrug resistance profiles. This is of paramount importance when considering the potential use of temporins as antimicrobials to combat the emergence of antibiotic resistant strains. In particular, **10** exhibited an improved activity compared to **1** against all tested isolates. The Gram-positive bacteria used in the study were showing resistance to beta-lactams, macrolides and methicillin.

Finally, we also tested clinical isolates of *C. albicans* and confirmed the results obtained in the previous experiment using laboratory adapted strains of Candida spp. (Tables 2 and 4).

*2.1.5. Hemolytic assay of peptides **9** and **10***

To expand our knowledge also on the potential cytotoxic effect of the selected peptides on human cells, we decided to investigate their effect also on circulating blood cells (*i.e.* erythrocytes). The results of the hemolytic activity shown in Table 5 indicate that as for **1**, both **9** and **10** were practically devoid of hemolytic activity at their antimicrobial concentrations. Only compound **10** showed 20% and 37% hemolytic activity at the highest concentrations of 25 μM and 50 μM, respectively.

*2.1.6. Stability of peptides **9** and **10** in human serum*

Considering the potential of AMPs to be developed as therapeutically suitable antimicrobial agents, we investigated human

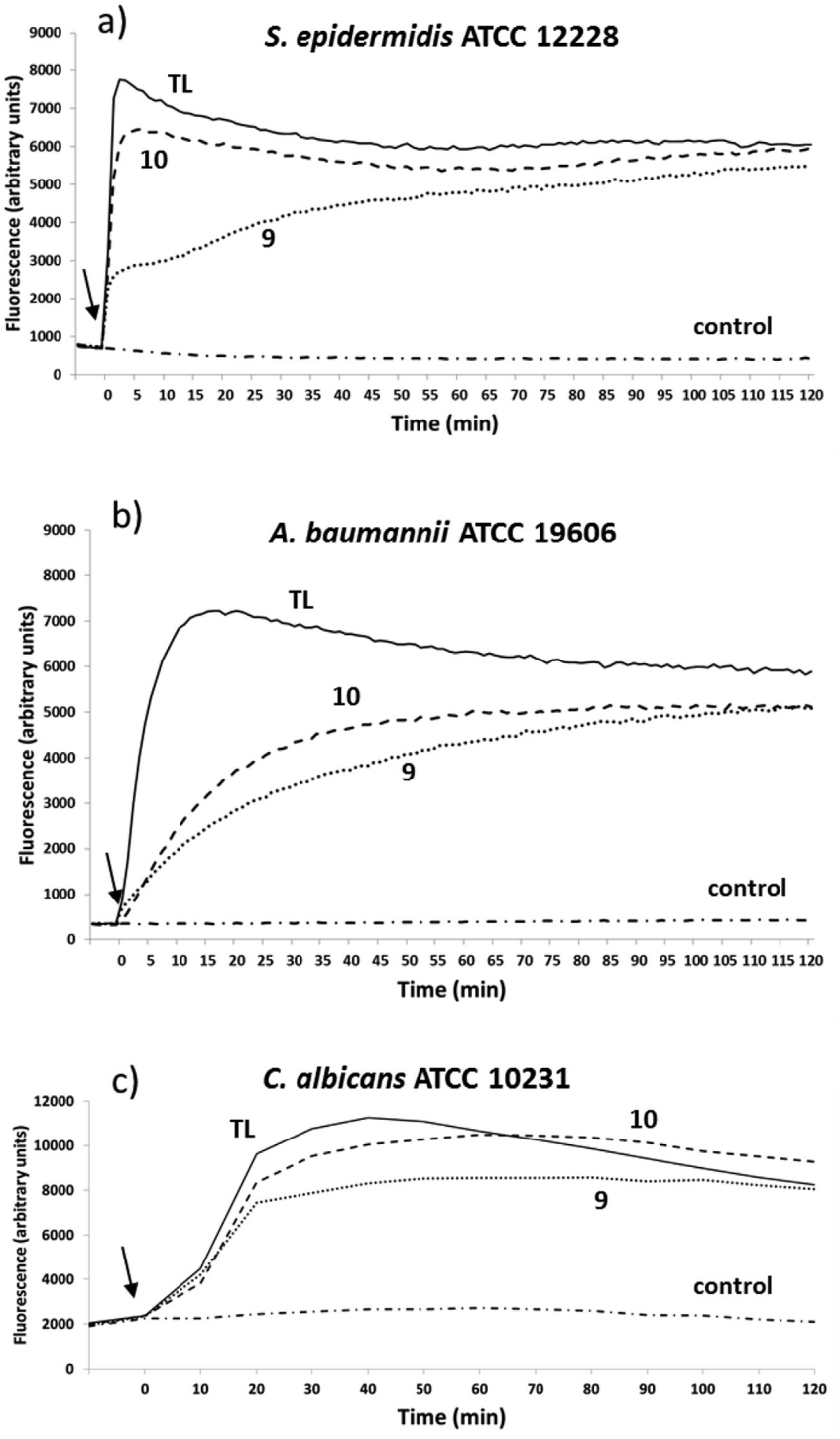

Fig. 1. Kinetics of membrane permeabilization of a) the Gram-positive *S. epidermidis* ATCC 12228, b) the Gram-negative *A. baumannii* ATCC 19606, and c) the yeast *C. albicans* ATCC 10231 induced by the addition of compounds TL, **9** and **10** (*arrow*, $t = 0$). Samples were incubated with 1 μM SYTOX Green (SG) in buffer as described in the Experimental Section and changes in fluorescence were monitored. Peptide concentrations used were equal to the MIC. Control is given by microbial cells without peptide. Values correspond to one representative experiment of three.

serum stability of most promising peptides **9** and **10**. The biostability of both peptides **9** and **10** in biological fluids, along with their precursor peptide **1**, was studied in the presence of 90% fresh human serum within 120 min. The data revealed that both peptides were less degraded, compared to the parent compound **1**, demonstrating higher stability (Fig. 2). More precisely, ~80% of peptide **10** was detected after 45 min of incubation. In comparison, at the same time interval the non-degraded amount of **1** was ~45%. At the longer incubation time of 120 min, the amount of non-degraded **9** (~40%) and **10** (~50%) was approximately two-fold and three-fold higher than that of **1** (~20%), respectively. These results pointed out that such single-point modifications may be useful in the optimization process or in the synthesis of more stable TL derivatives.

Table 4
Antibacterial activity of peptide **1** and its analogues **9** and **10** against human clinical isolates.

	MIC (μM)[a]		
	1	**9**	**10**
Gram-negative bacteria			
E. coli multisensitive 1	50	25	50
E. coli multisensitive 2	50	25	50
P. aeruginosa multisensitive	>50	>50	>50
K. pneumonia multisensitive	>50	50	>50
Gram-positive bacteria			
S. aureus multisensitive	12.5	12.5	6.25
S. aureus (β-lactamase resistant)	12.5	25	6.25
S. aureus (macrolid resistant)	12.5	25	6.25
S. aureus (methicillin resistant) (MRSA1)	12.5	25	6.25
S. aureus (methicillin resistant) (MRSA2)	12.5	12.5	6.25
Yeasts			
C. albicans 1	25	12.5	25
C. albicans 2	25	12.5	25

[a] Each MIC value is the average of at least three independent experiments.

Table 5
Hemolytic activity of compound **1** and its derivatives **9** and **10** on human erythrocytes.

Hemolysis (%)			
[peptide] (μM)	**1**	**9**	**10**
50	21(±4)	7(±4)*	37(±1)**
25	7(±3)	5(±3)	20(±3)**
12.5	6(±3)	5(±2)	7(±1)
6.25	3(±2)	1(±2)	4(±2)
3.125	1(±1)	0(±1)	2(±1)

Values are the mean ± SD of three independent experiments. The levels of statistical significance between the analogues and the parent peptide **1** are indicated as follows: **$p < 0.01$.

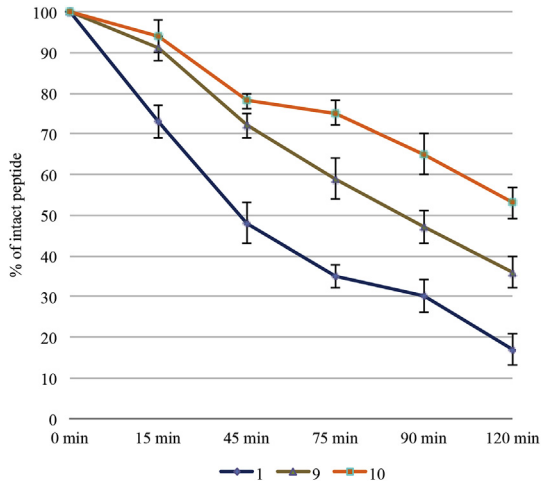

Fig. 2. Percentage of intact peptides **1**, **9** and **10** detected at known time intervals after incubation in fresh 90% human serum (200 μM) at 37 ± 1 °C and RP-HPLC analysis [performed on a Phenomenex Kinetex column (4.6 mm × 150 mm, 5 μm, C18), linear gradient from 10 to 90% MeCN (0.1% TFA) in water (0.1% TFA) over 20 min, flow rate of 1 mL/min, and absorbance detection at 220 nm]. The percentage was calculated by the peak area of the RP-HPLC chromatograms relative to those of the corresponding ones at 0 min (set as 100%). Experiments were performed in triplicate.

2.2. Structural studies

2.2.1. CD analyses

To explore the conformational changes of TL analogues synthesized in this study, we performed CD spectroscopy studies in water, sodium dodecylsulphate (SDS), dodecylphosphocholine (DPC), and DPC/SDS 9:1 micelle solutions. These micelles were used as rough mimetics of bacterial, mammalian, and yeast membranes, respectively. CD spectra in water revealed the presence of disordered conformers for all compounds with a minimum close to 200 nm (data not shown). In contrast, in DPC (Fig. 3a), DPC/SDS 9:1 (Fig. 3b) and SDS (Fig. 3c) membrane mimetic solutions (MMs), CD spectra indicated more structured peptides. Helical content was predicted from CD spectra using an in-house developed program (Table 6). The helical content of peptide **1** is included for comparison. In many cases, two minima close to 208 and 222 nm were obtained, indicating helical propensity. Notably, exceptions were given by **3** and **5** CD spectra in SDS (and SDS/DPC), which showed almost flat curves, and **11,** which showed a broad maximum around 215 nm in all MMs. According to the inversion of configuration at residue 10, the analogues bearing a D residue showed a reduction in the percentage of helicity compared to the corresponding L analogues in the MMs (about 50%).

Comparing the CD spectra acquired in SDS and DPC/SDS 9:1 solution, they were very similar for all peptides and the helical content observed in both SDS and DPC/SDS 9:1 was about 10–30% less compared to DPC.

2.2.2. NMR analysis of peptide ***10***

Considering the very interesting antimicrobial activity of compound **10**, in particular against gram-positive human clinical isolates, its low cytotoxic and hemolytic effects, and its faster membrane-perturbing activity compared to **9** either against Gram-positive and Gram-negative bacteria or Candida cells it was also investigated by NMR spectroscopy. Due to the very similar behavior of this peptide in the presence of SDS and DPC/SDS micelles, as manifested by CD analysis (Fig. 3d and Table 6), NMR spectroscopy was performed only in SDS and DPC micellar solutions. Complete ^{1}H NMR chemical shift assignments were effectively achieved for the peptide according to the Wüthrich procedure [36] (see Supporting Information, Tables S2–S3).

Peptide **10** in DPC solution exhibited NMR spectral features pointing to helical propensity. Upfield shift of the Hα NMR signals (see Supporting Information, Fig. S12), low values of the exchange rates and temperature coefficients of many amide protons (Table S2), and diagnostic NOEs (Table S4) indicated that many residues are in a helical conformation. Structure calculation gave an ensemble of 10 structures (Fig. 4a) satisfying the NMR-derived constraints (violations smaller than 0.10 Å). Backbone is well defined, apart the last two N-terminal residues, with an rmsd = 0.28 Å. A distorted (type IV) β-turn centered on residues Pro^{3}-Trp^{4} can be observed at the N-terminus followed by an α-helix from Trp^{4} to Lys^{7}, by a distorted type II β-turn centered on residues Phe^{8}-DLeu^{9} and again by an α-helix from residue 10 to 13 (Fig. 4a). Also, the side chains are well defined (rmsd all heavy atom of residues 3–13 = 0.80 Å, Fig. 4c).

Regarding SDS solution, diagnostic NMR parameters observed for **10** also indicated some conformational propensity toward helical or turn structures but with higher flexibility. In fact, the number of diagnostic NOEs (Table S4) is less compared to those obtained in DPC solution and only amide protons of residues Ser^{6}, Lys^{7}, and Ile^{12} showed exchange rates and temperature coefficients indicating that they were shielded from the solvent (Table S3). Calculated structures, shown in Fig. 4b, are clearly less defined compared to those obtained in DPC solution (rmsd backbone heavy

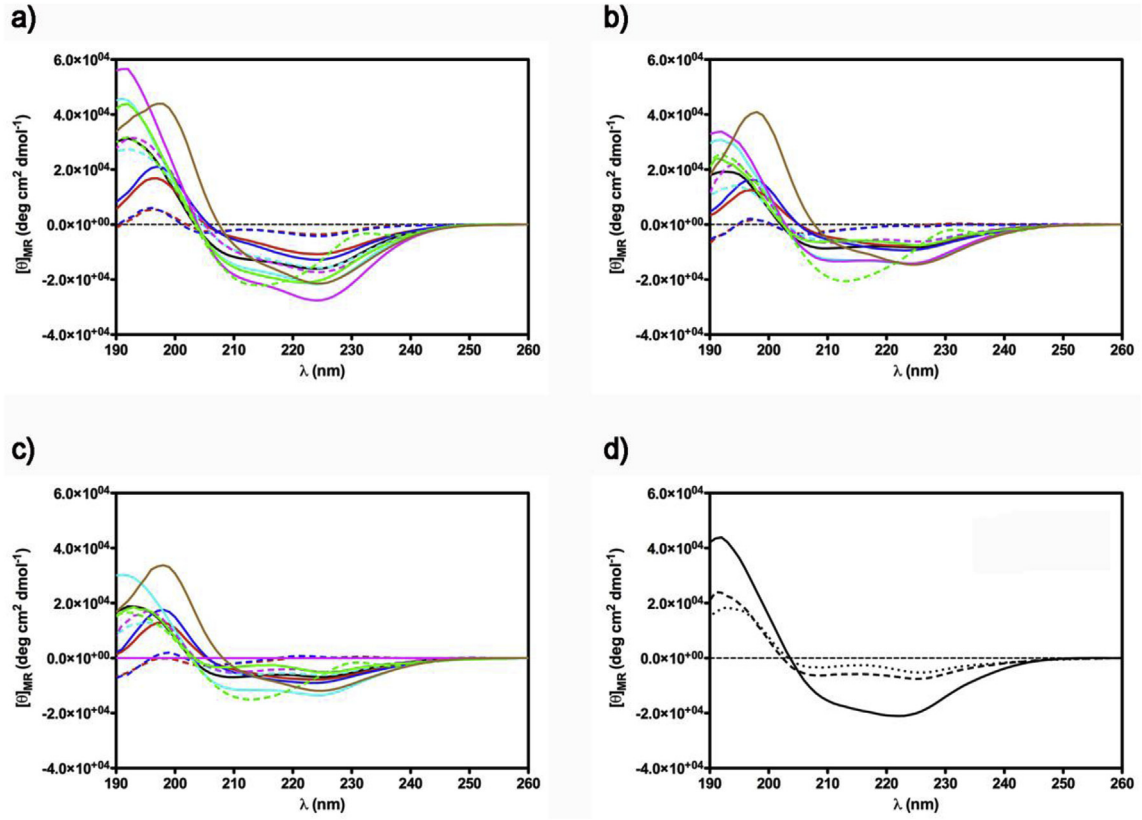

Fig. 3. CD spectra of peptide **1** and its analogues **2**–**12** in a) DPC; b) SDS/DPC; c) SDS (**1**, black solid line; **2**, red solid line; **3**, red dashed line; **4**, blue solid line; **5**, blue dashed line; **6**, cyan solid line; **7**, cyan dashed line; **8**, magenta solid line; **9**, magenta dashed line; **10**, green solid line; **11**, green dashed line; **12**, brown solid line); d) CD spectra of **10** in DPC (solid line), SDS/DPC (dashed line), and SDS (dotted line). (For interpretation of the references to colour in this figure legend, the reader is referred to the web version of this article.)

Table 6
α-Helix percentage of TL-analogues.

Peptide	DPC	DPC-SDS	SDS
1	42	29	23
2	15	15	13
3	8	0.4	0.1
4	18	15	15
5	9	0.3	1
6	51	45	40
7	30	22	19
8	61	46	39
9	30	18	14
10	50	22	19
11	40	23	18
12	18	11	6

atoms of residues 4–13 = 0.51 Å). Secondary structure elements observable in the **10** structures obtained in DPC solution are still present but in equilibrium with more disordered conformations (Fig. 4b). A peculiar aspect of these structures is the position of Trp^{10} side chain which is inserted between the two positively charged side chains of Lys^{7} and Arg^{11} (Fig. 4d) in accordance with some experimental data as the downfield shift of many proton resonances of Arg^{11} (Table S3) and a few NOE contacts between side chain protons of Trp^{10} and Arg^{11} (Table S4).

3. Discussion

In a previous study, we reported the effects of the replacement of cationic and hydrophobic residues of the native TL on its antimicrobial and hemolytic activities [33]. We demonstrated that the nature of cationic residues can differently modify the antimicrobial/hemolytic activity of this peptide, without changing its helical content. In contrast, we found there is direct correlation between the percentage of peptide's helicity and its toxicity on human red blood cells. Furthermore, we identified a TL analogue, [Pro^{3},$DLeu^{9}$]TL **1**, practically devoid of cytolytic effect *in vitro* and with the ability to preserve the effectiveness of the native peptide TL against *C. albicans* [35]. In addition, we observed that replacement of Gly^{10} with a leucine residue almost abrogated the antimicrobial efficacy of TL causing a dramatic enhancement of hemolysis [33].

Starting from these results, we used peptide **1** as the template to design a series of peptides, aimed at optimizing pharmacodynamics and pharmacokinetic properties. Thus, in the context to explore the role played by Gly^{10}, we performed a SAR study using 11 different analogues, containing different amino acids. They were chosen for their propensity to disrupt helicity (Pro, Hyp, Aic); for containing a positive charge in the side chain (Lys); for having a hydrophobic side chain (Nle), or an indole ring (Trp), all in L and D configurations, except for Aic residue (Table 1).

By examining the antimicrobial activities reported in Table 2, most of synthesized peptides showed antibacterial activity and all are endowed with high anticandidal activity. As long as antibacterial activity is considered, effects due to both the residue configuration and chemical properties are observed.

With reference to the effect of the configuration of residue 10, the activities of the peptides containing both L and D forms of the selected amino acids are mostly similar, with the exception of Pro and Hyp, in which a pronounced reduction of the antibacterial

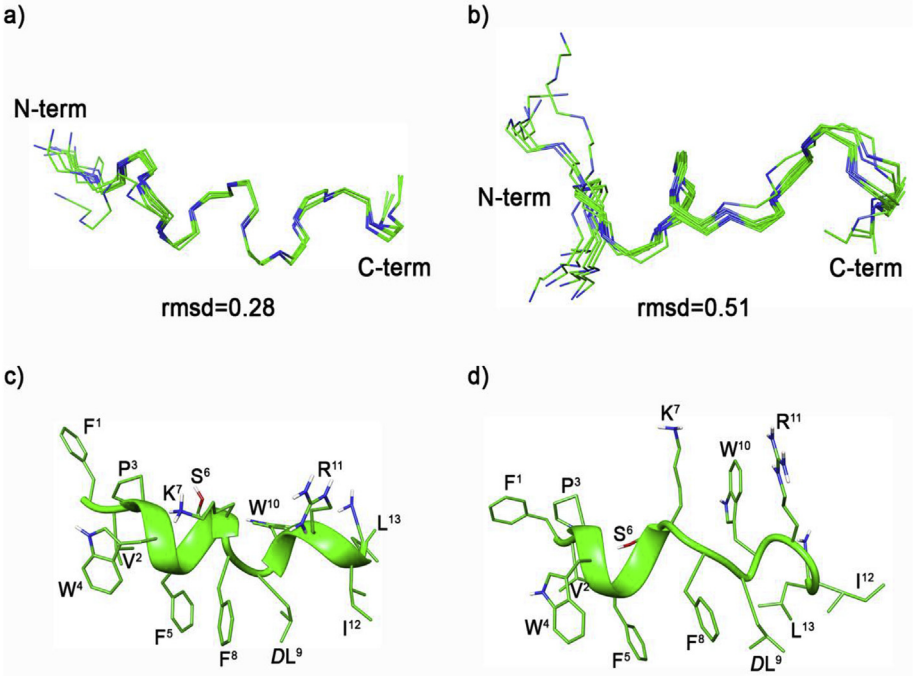

Fig. 4. Superposition of the 10 lowest energy conformers of **10** in DPC (a), and SDS (b). Structures were superimposed using the backbone heavy atoms of residues 4–13. Only heavy backbone atoms are shown for clarity. Lowest energy conformer of **10** in DPC (c), and SDS (d). Backbone atoms were evidenced as a ribbon. Heavy atoms are shown with different colors (carbon, green; nitrogen, blue; oxygen, red). (For interpretation of the references to colour in this figure legend, the reader is referred to the web version of this article.)

activity is observed upon the inversion of configuration from L to D. Considering the conformational results (Fig. 3, and Table 6), a significant reduction of the helical content is appreciable passing from the L to the D configuration (about 50%) of residue 10, with a complete loss of the helix only in peptides containing Pro or Hyp. Therefore, the diminished antibacterial activity of those compounds containing either DPro or DHyp (**3** and **5**, respectively) suggest that the helical content influences, in some extent, the antibacterial activity of the peptide. Interestingly, both peptides containing these D amino acids preserve the anticandidal activity indicating that such activity is not influenced by the peptide conformation around residue 10 in accordance with previous data of D-scan analysis on [Pro^3]TL [35].

With reference to the residue type replacing Gly^{10} in **1**, position 10 was found to be quite tolerant. In more details, an aromatic residue at position 10 is generally preferred for activity against Gram-positive bacteria compared to aliphatic or positively-charged residues. This is supported by the lower MICs of compounds **10**, **11**, and **12** in comparison with those of **1**. Considering the activity against Gram-negative bacteria, a different target cell selectivity is obtained. In fact, a (D/L)Lys residue (**8** and **9**) is preferred against *E. coli* D21 and *P. aeruginosa* ATCC 27853, while D/L aromatic residues are preferred against *P. syringae* pv tabaci 1918. Furthermore, a certain preference for (D/L)Lys residue is also observed for the anticandidal activity.

Regarding the toxicity on keratinocytes (Table 3), the less toxic compounds at any peptide concentration were the derivatives **3** and **5**, which are ineffective to kill these cells. This agrees with the described relationship between helicity and toxicity of TL derivatives already reported by us [37]. The potent antibacterial compounds **9** and **10** showed a weak toxicity against keratinocytes at their MICs, and this was lower than that shown by the parent compound **1**. By combining their anticandidal and antibacterial activities and low cytotoxicity, these peptides are promising candidates as antimicrobial agents for topical treatment. These peptides were also selected for their activity against clinical isolates from human skin as well as for studying their hemolytic capacity and mechanism of antimicrobial activity. As shown in Table 5, both **9** and **10** showed a good safety profile and proved to be devoid of haemolytic activity at their antimicrobial concentrations. Furthermore, they resulted to be more resistant to proteolytic degradation by circulating proteases than the parent peptide **1**, as pointed out by their higher biostability in human serum. Indeed, about 40% and 50% of non-degraded **9** and **10**, respectively, were obtained after 120 min incubation with 90% human serum, in comparison with 20% of **1**. This is an important issue, considering that most AMPs have a short half-life (~1 h) [38].

AMPs, in general, are intended to eliminate bacteria through a membrane damaging activity, although some intracellular targets have been described. Indeed, independent of their mode of action, AMPs engage different interactions on their way to reach the desired target (the cytoplasmic membrane or intracellular targets). The peptides' ability to perturb the microbial membrane permeability as shown by the intracellular influx of SG might reflex differences in the peptide translocation through the cell wall of bacteria or Candida. Adsorption of cationic peptides to the bacterial surface is generally mediated by electrostatic interactions between positively-charged amino acids of the peptide and the negatively-charged cell-wall components such as the lipotechoic acid (LTA) of Gram-positive, lipopolysaccharides (LPS) of Gram-negative bacteria or sialic acids of Candida. In our case, the overall slower membrane-perturbing activity of peptide **9** in comparison with **10** could be in part due to a different interaction with the microbial cell wall components (which may restrict its translocation to the target cytoplasmic membrane) [39,40]. However, we cannot exclude that a weaker interaction of the peptide with the cytoplasmic membrane (presumably due to its lower α-helical content) can also contribute to reduce its kinetics of membrane perturbation. Importantly, as indicated by the results shown in Fig. 1, the kinetic of membrane perturbation by the TL analogues is faster than the

time needed by circulating proteases to completely degrade them, suggesting the potential usage of these peptides also for systemic application.

We also observed for Gram-negative clinical isolated strains a difference in peptides concentration exhibiting antimicrobial activity (Table 4): while *E. coli* was moderately susceptible to peptide **9** we could not observe any antibacterial effect on *P. aeruginosa* and *K. pneumonia*. This effect could be due to the different content and relative percentages of lipids on the plasma membrane of different bacteria. In fact, *E. coli* contains a large proportion of zwittertonic phosphatidylethanolamine (PE) and anionic phosphatidylglycerol (PG), but is lacking cardiolipin (CL), which is present in *P. aeruginosa* [41]. Recent biophysical studies testing the membranotropic activity of myxinidin, a peptide derived from the mucus of the Atlantic hagfish, on two different model biomembranes, composed by DOPE/DOPG (80/20% mol) and DOPE/DOPG/CL (65/23/12% mol), and mimicking the membrane of *E. coli* and *P. aeruginosa*, respectively, showed a complete different behavior in its interaction with CL containing vesicles [42]. The biophysical analysis deeply correlated with the different antimicrobial activity exerted on the living bacterial species by myxinidin. Most laboratory bacterial strains have been subcultured for many years after their initial isolation which could have conducted to the loss of important pathophysiological features. Several genomic and phenotypic alterations are added up during laboratory passages, but despite these differences, microbiological research activities are largely founded on laboratory-adapted strains. Our results pointed out the efficacy of **9** and **10**, which retain most of their activity also against fresh clinical isolates. Moreover, both peptides are efficacious not only against sensitive clinical isolates, but also against *S. aureus* clinical isolates showing different drug-resistance profiles, such as resistance to beta-lactams, methicillin and macrolides.

Also, research on *Candida* pathogenesis and antimicrobials uses laboratory-adapted strains that have been subcultured multiple times since their first isolation, and thus, they may not be suitable infections from current clinically relevant strains. Fungal modifications have been shown to occur under different growth conditions and affect major virulence factors. Candida virulence factors repertoire has been shown to influence colonization, infection of the human host, as well as survival in a changing environment. These factors include adhesins, biofilm formation, morphological transition from yeast to filamentous form (hyphae or pseudohyphae), hydrolytic enzyme production (mainly secreted aspartyl proteinases and phospholipases), and phenotypic switching [43]. Our results show that the concentrations required for inhibiting growth of clinical isolates of *C. albicans* are in the range of 12.5–25 μM, which is between four- and eight-fold higher than the concentration needed against laboratory strains. Nevertheless, we need to consider that clinical isolates represent a heterogeneous population of different morphological stages of the fungus including budding yeast, pseudohyphae, and true hyphae as opposed to the genotypic and phenotypic stability of laboratory adapted stains usually used for antimicrobial studies.

Finally, considering the faster membrane-perturbing activity of **10** compared to **9** either against Gram-positive and Gram-negative bacteria or Candida cells, its higher activity against clinical isolates, this derivative was also investigated by solution NMR for a detailed conformational analysis. This analysis demonstrated that **10** in DPC has a well defined helical structure along almost the entire peptide sequence interrupted by two turns in the presence of the Pro and DLeu residues (Fig. 4a). In SDS micelle solution, **10** is much more flexible than in DPC (Fig. 4b). Furthermore, in this solution, **10** shows a particular disposition of the Trp^{10} side chain, which is close to the Arg^{11} and in the same direction of Lys^{7} side chains (Fig. 4d). The interactions between Arg and Trp are of particular interest in AMPs [44]. In fact, these interactions make the entry of Arg into the hydrophobic environment inside a lipid bilayer energetically more favorable. The Arg is effectively shielded from the highly hydrophobic nature of the bilayer by associating with a Trp residue. In conclusion, the presence of this bulky hydrophobic residue in position 10, may account for the improved antibacterial activity of the lead compound **1**, without altering its anticandidal potency neither enhancing its cytotoxicity, despite the increased α-helical content in DPC.

3.1. Conclusions

In this study, we demonstrated that a selective amino acid substitution in position 10 of the peptide sequence of **1**, a TL derivative discovered previously in our laboratory, resulted in the design of better antibacterial and anticandidal peptides with desired biological and biophysical properties.

In particular, we discovered novel synthetic peptides endowed of antimicrobial activity not only against laboratory strains but also against clinical isolates. Through a series of *in vitro* molecular and cellular studies, the peptides identified as **9** and **10** exhibited potent antibacterial activity with a low toxicity towards eukaryotic cells at their antimicrobial concentrations. The data suggest that these peptides, especially peptide **10**, have the characteristics desired to be good candidates in the development of novel antimicrobial agents for topic applications.

4. Methods

4.1. Chemistry

Materials and general methods. N^{α}-Fmoc-protected amino acids, Fmoc-Phe, Fmoc-Val, Fmoc-Pro and Fmoc-DPro, Fmoc-Trp(Boc) and Fmoc-DTrp(Boc), Fmoc-Ser(*t*Bu), Fmoc-Lys(Boc) and Fmoc-DLys(Boc), Fmoc-Leu and Fmoc-DLeu, Fmoc-Gly, Fmoc-Arg(Pbf), Fmoc-Nle and Fmoc-DNle, all were purchased from GL Biochem Ltd (Shanghai, China). Other unconventional N^{α}-Fmoc-amino acids, namely Fmoc-Hyp(*t*Bu) and Fmoc-DHyp(*t*Bu), were purchased from Sigma-Aldrich, and Fmoc-Aic was acquired by Chem-Impex. Coupling reagents such as *N,N,N′,N′*-tetramethyl-*O*-(1*H*-benzotriazol-1-yl)uronium hexafluorophosphate (HBTU) and 1-hydroxybenzotriazole (HOBt), as well as the Rink amide resin used, all were commercially obtained by GL Biochem Ltd (Shanghai, China). *N,N*-diisopropylethylamine (DIEA), piperidine, and trifluoroacetic acid (TFA) were purchased from Iris-Biotech GMBH. Moreover, peptide synthesis solvents and reagents, such as *N,N*-dimethylformamide (DMF), dichloromethane (DCM), diethyl ether (Et_2O), water and acetonitrile (MeCN) for HPLC, were reagent grade acquired from commercial sources (Sigma-Aldrich and VWR) and used without further purification.

Purification of peptides **2**–**12** was performed by RP-HPLC (Shimadzu Preparative Liquid Chromatograph LC-8A) equipped with a preparative column (Phenomenex Kinetex C18 column, 5 μm, 100 Å, 150 × 21.2 mm) using linear gradients of MeCN (0.1% TFA) in water (0.1% TFA), from 10 to 90% over 30 min, with a flow rate of 10 mL/min and UV detection at 220 nm. Final products were obtained by lyophilization of the appropriate fractions after removal of the MeCN by rotary evaporation. The purity of peptides **2**–**12** was ascertained using analytical UHPLC (Shimadzu Nexera Liquid Chromatograph LC-30AD) performed on a C18-bonded Kinetex reverse-phased column from Phenomenex (5 μm, 100 Å, 150 × 4.6 mm) with a flow rate of 1 mL/min using linear gradients of MeCN (0.1% TFA) in water (0.1% TFA), from 10 to 90% over 15 min. Analytical UHPLC analyses showed peptides **2**–**12** were purified to >97% (see Supporting Information, Figs. S1–11), and the correct

molecular weights were confirmed by ESI/MS (API 2000, Applied Biosystems).

Peptide synthesis. The synthesis of peptides **2**–**12** was performed in a stepwise fashion via solid-phase peptide strategy (SPPS) as elsewhere reported [45]. In particular, each peptide was constructed on the Rink amide resin (0.1 mmol from 0.64 mmol/g of loading substitution) as solid support. The resin, stored as Fmoc-protected on the primary amine of the rink amide linker, was first swollen in DMF for 30 min, then treated with 20% piperidine in DMF solution (5 min × 1, 25 min × 1). Peptide bond formation by the coupling with the first residue N^{α}-Fmoc-Leu (3 equiv) was achieved by using 3-fold excess of HBTU and HOBt, in the presence of a 6-fold excess of DIEA. Deprotection of the N^{α}-Fmoc was carried out by treatment with 20% piperidine in DMF solution (5 min × 1, 25 min × 1) as described above. After each coupling and Fmoc-deprotection step, the peptide resin was washed with DMF (3 × 2 mL), DCM (3 × 2 mL) and DMF (3 × 2 mL), and reactions were monitored by the Kaiser and Chloranil tests as colorimetric assays for the detection of solid-phase bound primary and secondary amines, respectively. The peptide sequences of **1** and its derivatives **2**–**12** were thereby assembled. The N-terminal Fmoc group was deblocked, as previously explained, and the peptide-resin was thoroughly washed with DCM (5 × 2 mL) and dried under argon to yield dried peptide-resin. Peptides **2**–**12** were released from the resin and cleaved by their protecting groups simultaneously by using a cocktail of 95:2.5:2.5 TFA/TIS/H_2O at rt for 3 h. The resin was removed by filtration and crude peptides were recovered by precipitation with chilled anhydrous Et_2O as white to pale beige-colored amorphous solids.

4.2. Biology

Microorganisms. The strains used for the antimicrobial assays were the following: the Gram-negative bacteria *Acinetobacter baumannii* ATCC 19606, *Escherichia coli* D21, *Pseudomonas aeruginosa* ATCC 27853, *Pseudomonas syringae* pv tabaci 1918 NCPPB; the Gram-positive bacteria *Bacillus megaterium* Bm11, *Staphylococcus aureus* Cowan I, *Staphylococcus epidermidis* ATCC 12228 and the yeasts *Candida albicans* ATCC 10231 and *Candida crusei* ATCC 6258. Human clinical isolates of *E. coli*, *P. aeruginosa, K. pneumonia, S. aureus, and C. albicans* were obtained from patients hospitalized at the Medical School of the University of Campania "Luigi Vanvitelli" where antibiotic susceptibility testing was carried out following the recommendations of the Clinical Laboratory Standards Institute (CLSI).

Antimicrobial assay. Susceptibility testing was performed by adapting the microbroth dilution method outlined by the Clinical and Laboratory Standards Institute, using sterile 96-well plates (Falcon NJ, USA). Aliquots (50 μl) of bacteria in mid-log phase at a concentration of 2×10^6 colony-forming units (CFU)/mL in culture medium (Mueller-Hinton, MH) were added to 50 μl of MH broth containing the peptide in serial 2-fold dilutions in water [46]. Peptide dilutions ranged from 0.1 to 50 μM. The same procedure was followed with yeast strains, but using 3.5×10^4 cells/mL in Winge medium [47]. Antimicrobial activities were expressed as the minimal inhibitory concentration (MIC), the concentration of peptide at which 100% inhibition of microbial growth is visually observed after 18–20 h of incubation at 37 °C (30 °C for yeasts). Each MIC value is the average of at least three independent experiments.

Hemolytic assay. The hemolytic activity was measured on human red blood cells (from volunteers) as reported previously [33]. Briefly, aliquots of a human erythrocyte suspension in 0.9% (w/v) NaCl were incubated with serial two-fold dilutions of the peptide (dissolved in water prior to use) for 40 min at 37 °C with gentle mixing. The samples were then centrifuged 5 min at 900×*g* and the absorbance of the supernatant was measured at 415 nm using the microplate reader (Infinite M200; Tecan, Salzburg, Austria). Complete lysis was measured by suspending erythrocytes in distilled water.

Cytotoxic Activity. The effect of the peptides on the viability of the immortalised human keratinocyte (HaCaT) cell line was determined by the inhibition of MTT reduction to insoluble formazan, by mitochondrial reductases [48,49]. Cells were suspended in Dulbecco's modified Eagle's medium (DMEM; Sigma) supplemented with glutamine (4 mM) and 2% heat-inactivated fetal bovine serum without antibiotics. They were plated in triplicate wells at 4×10^4 cells/well [96-well plates (Falcon) were used]. After 24 h at 37 °C in a 5% CO_2 atmosphere, the medium was replaced with 100 μl fresh DMEM supplemented with the peptide at different concentrations. The plate was then incubated for 24 h at 37 °C in a 5% CO_2 atmosphere. Afterwards, the medium was removed and replaced with Hank's buffer (136 mM NaCl; 0.34 mM Na_2HPO_4; 0.44 mM KH_2PO_4; 5.4 mM KCl; 4.1 mM $NaHCO_3$, pH 7.2, supplemented with 5.5 mM D-glucose) containing 0.5 mg/mL MTT. After 4 h incubation, the formazan crystals were dissolved by adding 100 μl of acidified isopropanol and viability was determined by absorbance measurements at 570 nm using the microplate reader (Infinite M200) Percentage of cytotoxicity was equal to [1-(Abs of treated samples-Abs of blank/Abs of control samples-Abs of blank)] × 100 where Abs of blank and control samples correspond to the absorbance of solvent and untreated control cells, respectively.

Membrane-perturbing assay. The peptides' ability to perturb the membrane of bacterial or Candida cells was assessed by the SG assay in microtiter plates. Briefly, about 1×10^6 microbial cells in 100 μL of phosphate buffered saline (PBS, for bacteria) or 0.01 M sodium phosphate buffer (NaPB, for yeasts) containing 1 μM SG were added to each well. Afterwards, peptide was added to achieve a final concentration equal to the MIC. For control samples, peptide solvent (water) was used. After adding peptides, membrane perturbation was monitored at 37 °C or 30 °C (for bacteria or Candida cells, respectively) by measuring the increase in fluorescence with the microplate reader. The excitation and emission wavelengths were 485 and 535 nm, respectively. Fluorescence was measured every minute for 120 min (in the case of bacteria) or every 10 min, in the case of *C. albicans,* as previously described [50].

Plasma Stability Assay. Human plasma was collected from healthy adult volunteers. Water and MeCN were obtained from commercial suppliers and used without further purification. Analytical RP-UHPLC was performed on a Shimadzu Nexera equipped with a Phenomenex Kinetex column (C18, 4.6 mm × 150 mm, 5 μm) and H_2O (0.1% TFA) and MeCN (0.1% TFA) as eluents. Serum stability was evaluated by modification of elsewhere described methods [51]. In particular, the human serum was allocated into a 1.5 mL Eppendorf tube and temperature-equilibrated at 37 ± 1 °C for 15 min. Peptides **1**, **9** and **10** in sterile water (2 mM) were then mixed with the human serum to make a final concentration of 0.2 mM (90% serum) and the resulting reaction solution was incubated at 37 ± 1 °C. Aliquots of the reaction solutions were taken at known time intervals (0 min, 15 min, 45 min, 75 min, 90 min, 120 min), subjected to serum proteins precipitation by addition of MeCN (double volume respect to the aliquot). The cloudy reaction sample was cooled (4 °C) for 15 min and then spun at 13 000 rpm for 10 min to pellet the precipitated serum proteins. The supernatant was then analyzed by RP-UHPLC by using a linear elution gradient from 10 to 90% MeCN (0.1% TFA) in water (0.1% TFA) over 20 min. A flow rate of 1 mL/min was used, absorbance was detected at 220 nm, and the analysis was performed at room temperature.

4.3. Conformational analyses

Circular dichroism. All CD spectra were recorded using a JASCO J710 spectropolarimeter at 25 °C with a cell of 1 mm path length. The CD spectra were acquired in the range 260–190 nm, 1 nm bandwidth, 4 accumulations, and 100 nm/min scanning speed. The CD spectra of peptide **1** and derivatives, at a concentration of 100 μM, were performed in water (unbuffered solution), in SDS (20 mM), DPC (20 mM), or DPC/SDS 18/2 mM micellar solutions. An in-house program based on the $[\theta]_{MR}$ values at 195, 208, and 222 nm was used to extract the helical contents. Only $[\theta]_{MR}$ value at 195 nm was used to calculate helical percentage for peptide **11**.

NMR spectroscopy. The samples for NMR spectroscopy were prepared by dissolving the appropriate amount of **10** in 0.55 mL of ^1H_2O, 0.05 mL of ^2H_2O to obtain a concentration of 1–2 mM peptides and 200 mM SDS-d_{25} or DPC-d_{38}. The NMR experiments were performed at pH 5.0. NH exchange studies were performed by dissolving peptides in 0.60 mL of ^2H_2O and 200 mM SDS-d_{25} or DPC-d_{38}. NMR spectra were recorded on a Varian Unity INOVA 700 MHz spectrometer equipped with a z-gradient 5 mm triple-resonance probe head. All the spectra were recorded at a temperature of 25 °C. The spectra were calibrated relative to TSP (0.00 ppm) as internal standard. One-dimensional (1D) NMR spectra were recorded in the Fourier mode with quadrature detection. Two-dimensional (2D) DQF-COSY [52,53], TOCSY [54], and NOESY [55] spectra were recorded in the phase-sensitive mode using the method from States [56]. Data block sizes were 2048 addresses in t_2 and 512 equidistant t_1 values. A mixing time of 70 ms was used for the TOCSY experiments. NOESY experiments were run with mixing times in the range of 150–300 ms. The water signal was suppressed by gradient echo [57]. The 2D NMR spectra were processed using the NMRPipe package [58]. Before Fourier transformation, the time domain data matrices were multiplied by shifted $\sin^2$ functions in both dimensions, and the free induction decay size was doubled in F1 and F2 by zero filling. The qualitative and quantitative analysis of DQF-COSY, TOCSY, and NOESY spectra were obtained using the interactive program package XEASY [59]. $^3J_{HN\text{-}H\alpha}$ couplings were difficult to measure probably because of a combination of small coupling constants and broad lines. The temperature coefficients of the amide proton chemical shifts were calculated from 1D ^{1}H NMR and 2D TOCSY experiments performed at different temperatures in the range 298–320 K by means of linear regression.

Structural Determinations. The NOE-based distance restraints were obtained from NOESY spectra collected with a mixing time of 200 ms. The NOE cross peaks were integrated with the XEASY program and were converted into upper distance bounds using the CALIBA program incorporated into the program package DYANA [60]. Only NOE derived constraints were considered in the annealing procedures. An error tolerant target function (tf type 3) was used to account for the peptide intrinsic flexibility. For each examined peptide, an ensemble of 200 structures was generated with the simulated annealing of the program DYANA. Then, 100/200 structures were chosen, whose interproton distances best fitted NOE derived distances, and refined through successive steps of restrained and unrestrained energy minimization calculations using the Discover algorithm (Accelrys, San Diego, CA) and the consistent valence force field [61]. The minimization lowered the total energy of the structures; no residue was found in the disallowed region of the Ramachandran plot. The final structures were analyzed using the InsightII program (Accelrys, San Diego, CA). Graphical representations were carried out with the InsightII program. The root-mean-squared-deviation analysis between energy-minimized structures was carried out with the program MOLMOL [62]. The PROMOTIF program was used to extract details on the location and types of structural secondary motifs [63].

4.4. Statistical analyses

Quantitative data were expressed as the mean ± SD. The statistical analyses were performed using Student's *t*-test with the PRISM software (GraphPad, San Diego, CA). Differences were considered to be statistically significant for $p < 0.05$. The levels of statistical significance are indicated in the legend to figures.

Abbreviations

Abbreviations used for amino acids and designation of peptides follow the rules of the IUPAC-IUB Commission of Biochemical Nomenclature in *J. Biol. Chem.* 1972, *247*, 977–983. Amino acid symbols denote L-configuration unless indicated otherwise. The following additional abbreviations are used:

1D and 2D, one- and two-dimensional; Aic, 2-aminoindane-2-carboxylic acid; AMPs, antimicrobial peptides; CL, cardiolipin; DIEA, diisopropylethylamine; DMEM, Dulbecco's modified Eagle's medium; DPC, dodecylphosphocholine; DQF-COSY, double quantum filtered correlated spectroscopy; ESI, Electrospray ionization; Fmoc, 9-fluorenyl-methoxycarbonyl; Hyp, hydroxyproline; LC-MS, liquid chromatography-mass spectrometry; LTA, lipotechoic acid; MMs, membrane mimetic solutions; MTT, 3-(4,5-dimethylthiazol-2-yl)-2,5-diphenyltetrazolium bromide; Nle, norleucine; Pbf, 2,2,4,6,7-pentamethyl-dihydrobenzo-furan-5-sulfonyl; PE, phosphatidylethanolamine; PG, phosphatidylglycerol; RP-HPLC, reversed-phase high performance liquid chromatography; SDS, sodium dodecylsulphate; SG, SYTOX Green; SPPS, solid-phase peptide synthesis; *t*Bu, *tert*-butyl; TIS, triisopropylsilane; TL, temporin-L; TOCSY, total correlated spectroscopy; TSP, 3-(trimethylsilanyl)propionic acid.

Notes

The authors declare no competing financial interest.

Acknowledgments

This work was supported by grants from Regione Campania, Progetti Retrospettivi Coerenti con la Misura 3.5 del FET Campania 2007-2013 (art.41 del Reg. (CE) 1198/2006); and Finanziamento della ricerca di Ateneo - Università degli Studi di Napoli Federico II - Annualità 2016.

Appendix A. Supplementary data

Supplementary data related to this article can be found at http://dx.doi.org/10.1016/j.ejmech.2017.08.040.

References

[1] J. Davies, D. Davies, Origins and evolution of antibiotic resistance, Microbiol. Mol. Biol. Rev. 74 (2010) 417–433.
[2] S.C. Davis, Annual Report of the Chief Medical Officer, Infections and the Rise of Antimicrobial Resistance, vol. 2, 2011.
[3] C. Lee Ventola, The antibiotic resistance crisis. Part 1: causes and threats, Pharm. Ther. 40 (2015) 277–283.
[4] M.T. Osterholm, Emerging infectious diseases, Postgrad. Med. 100 (1996) 15–26.
[5] A. Cherkasov, K. Hilpert, H. Jenssen, C.D. Fjell, M. Waldbrook, S.C. Mullaly, R. Volkmer, R.E. Hancock, Use of artificial intelligence in the design of small peptide antibiotics effective against a broad spectrum of highly antibiotic-resistant superbugs, ACS Chem. Biol. 4 (2009) 65–74.
[6] N. Woodford, D.W. Wareham, B. Guerra, C. Teale, Carbapenemase-producing Enterobacteriaceae and non-Enterobacteriaceae from animals and the environment: an emerging public health risk of our own making? J. Antimicrob.

Chemother. 69 (2013) 287–291.
[7] L.C.A.D. Saravolatz, G.E. Stein, L.B. Johnson, Telavancin: a novel lipoglycopeptide, Clin. Infect. Dis. 49 (2009) 1908–1914.
[8] R.E. Mendes, D.J. Farrell, H.S. Sader, R.N. Jones, Oritavancin microbiologic features and activity results from the surveillance program in the United States, Clin. Infect. Dis. 54 (2012) 203–213.
[9] H. Moisan, M. Pruneau, F. Malouin, Binding of ceftaroline to penicillin-binding proteins of *Staphylococcus aureus* and *Streptococcus pneumoniae*, J. Antimicrob. Chemother. 65 (2010) 713–716.
[10] R.G. Wunderink, M.S. Niederman, M.H. Kollef, A.F. Shorr, M.J. Kunkel, A. Baruch, W.T. Mcgee, A. Reisman, J. Chastre, Linezolid in methicillin-resistant *Staphylococcus aureus* nosocomial pneumonia: a randomized, controlled study, Clin. Infect. Dis. 54 (2012) 621–629.
[11] L. Morata, J. Mensa, A. Soriano, New antibiotics against gram-positives: present and future indications, Curr. Opin. Pharmacol. 24 (2015) 45–51.
[12] Y. Tor, R. Fair, Antibiotics and bacterial resistance in the 21st century, Perspect. Med. Chem. 6 (2014) 25–64.
[13] R. Maviglia, R. Nestorini, M. Pennisi, Role of old antibiotics in multidrug resistant bacterial infections, Curr. Drug Targets 10 (2009) 895–905.
[14] L.C.A.D.S. Tavares, C.S.F. Silva, V.C.D. Souza, V.L.D. Silva, C.G. Diniz, M.O. Santos, Strategies and molecular tools to fight antimicrobial resistance: resistome, transcriptome, and antimicrobial peptides, Front. Microbiol. 4 (2013) 412, 1–11.
[15] N. Mookherjee, R.E.W. Hancock, Cationic host defence peptides: innate immune regulatory peptides as a novel approach for treating infections, Cell. Mol. Life Sci. 64 (2007) 922–933.
[16] A.T.Y. Yeung, S.L. Gellatly, R.E.W. Hancock, Multifunctional cationic host defence peptides and their clinical applications, Cell. Mol. Life Sci. 68 (2011) 2161–2176.
[17] R.E. Hancock, Cationic peptides: effectors in innate immunity and novel antimicrobials, Lancet Infect. Dis. 1 (2001) 156–164.
[18] D. Heimlich, A. Harrison, K. Mason, Host antimicrobial peptides in bacterial homeostasis and pathogenesis of disease, Antibiotics 3 (2014) 645–676.
[19] G. Diamond, N. Beckloff, A. Weinberg, K. Kisich, The roles of antimicrobial peptides in innate host defense, Curr. Pharm. Des. 15 (2009) 2377–2392.
[20] R.E.W. Hancock, H.-G. Sahl, Antimicrobial and host-defense peptides as new anti-infective therapeutic strategies, Nat. Biotechnol. 24 (2006) 1551–1557.
[21] K.A. Brogden, Antimicrobial peptides: pore formers or metabolic inhibitors in bacteria? Nat. Rev. Microbiol. 3 (2005) 238–250.
[22] S.C.B.C.A.T. Henriques, M.N. Melo, M.A.R.B. Castanho, Cell-penetrating peptides and antimicrobial peptides: how different are they? Biochem. J. 399 (2006) 1–7.
[23] R.E. Hancock, R. Lehrer, Cationic peptides: a new source of antibiotics, Trends Biotechnol. 16 (1998) 82–88.
[24] H. Jenssen, P. Hamill, R.E.W. Hancock, Peptide antimicrobial agents, Clin. Microbiol. Rev. 19 (2006) 491–511.
[25] M.R. Yeaman, Mechanisms of antimicrobial peptide action and resistance, Pharmacol. Rev. 55 (2003) 27–55.
[26] T. Koprivnjak, A. Peschel, Bacterial resistance mechanisms against host defense peptides, Cell. Mol. Life Sci. 68 (2011) 2243–2254.
[27] K.E. Greber, M.G. Dawgul, Antimicrobial peptides under clinical trials, Curr. Top. Med. Chem. 17 (2016) 620–628.
[28] M.L. Mangoni, A.C. Rinaldi, A.D. Giulio, G. Mignogna, A. Bozzi, D. Barra, M. Simmaco, Structure-function relationships of temporins, small antimicrobialpeptides from amphibian skin, Eur. J. Biochem. 267 (2000) 1447–1454.
[29] M.L. Mangoni, Temporins, anti-infective peptides with expanding properties, Cell. Mol. Life Sci. 63 (2006) 1060–1069.
[30] M.L. Mangoni, Y. Shai, Temporins and their synergism against Gram-negative bacteria and in lipopolysaccharide detoxification, Biochim. Biophys. Acta Biomembr. 1788 (2009) 1610–1619.
[31] A.C. Rinaldi, M.L. Mangoni, A. Rufo, C. Luzi, D. Barra, H. Zhao, P.K. Kinnunen, A. Bozzi, A.D. Giulio, M. Simmaco, Temporin L: antimicrobial, haemolytic and cytotoxic activities, and effects on membrane permeabilization in lipid vesicles, Biochem. J. 368 (2002) 91–100.
[32] Y. Chen, C.T. Mant, S.W. Farmer, R.E.W. Hancock, M.L. Vasil, R.S. Hodges, Rational design of helical antimicrobial peptides with enhanced activities and specificity/therapeutic index, J. Biol. Chem. 280 (2005) 12316–12329.
[33] M.L. Mangoni, A. Carotenuto, L. Auriemma, M.R. Saviello, P. Campiglia, I. Gomez-Monterrey, S. Malfi, L. Marcellini, D. Barra, E. Novellino, P. Grieco, Structure–activity relationship, conformational and biological studies of temporin L analogues, J. Med. Chem. 54 (2011) 1298–1307.
[34] A. Carotenuto, S. Malfi, M.R. Saviello, P. Campiglia, I. Gomez-Monterrey, L.M. Mangoni, L.M.H. Gaddi, E. Novellino, P. Grieco, A different molecular mechanism underlying antimicrobial and hemolytic actions of temporins A and L, J. Med. Chem. 51 (2008) 2354–2362.
[35] P. Grieco, A. Carotenuto, L. Auriemma, M.R. Saviello, P. Campiglia, I. Gomez-Monterrey, L. Marcellini, V. Luca, D. Barra, E. Novellino, M.L. Mangoni, The effect of d-amino acid substitution on the selectivity of temporin L towards target cells: identification of a potent anti-Candida peptide, Biochim. Biophys. Acta Biomembr. 1828 (2013) 652–660.
[36] K. Wütrich, NMR of Proteins and Nucleic Acids, John Wiley & Sons, Inc, New York, 1986.
[37] M.R. Saviello, S. Malfi, P. Campiglia, A. Cavalli, P. Grieco, E. Novellino, A. Carotenuto, New insight into the mechanism of action of the temporin antimicrobial peptides, Biochemistry 49 (2010) 1477–1485.
[38] D. Knappe, P. Henklein, R. Hoffmann, K. Hilpert, Easy strategy to protect antimicrobial peptides from fast degradation in serum, Antimicrob. Agents Chemother. 54 (2010) 4003–4005.
[39] Y. Rosenfeld, D. Barra, M. Simmaco, Y. Shai, M.L. Mangoni, A synergism between temporins toward gram-negative bacteria overcomes resistance imposed by the lipopolysaccharide protective layer, J. Biol. Chem. 281 (2006) 28565–28574.
[40] M.L. Mangoni, R.E. Epand, Y. Rosenfeld, A. Peleg, D. Barra, R.M. Epand, Y. Shai, Lipopolysaccharide, a key molecule involved in the synergism between temporins in inhibiting bacterial growth and in endotoxin neutralization, J. Biol. Chem. 283 (2008) 22907–22917.
[41] R.F. Epand, P.B. Savage, R.M. Epand, Bacterial lipid composition and the antimicrobial efficacy of cationic steroid compounds (Ceragenins), Biochim. Biophys. Acta Biomembr. 1768 (2007) 2500–2509.
[42] L. Lombardi, M.I. Stellato, R. Oliva, A. Falanga, M. Galdiero, L. Petraccone, G. D'Errico, A.D. Santis, S. Galdiero, P.D. Vecchio, Antimicrobial peptides at work: interaction of myxinidin and its mutant WMR with lipid bilayers mimicking the *P. aeruginosa* and *E. coli* membranes, Sci. Rep. 7 (2017) 44425.
[43] R.A. Calderone, W.A. Fonzi, Virulence factors of Candida albicans, Trends Microbiol. 9 (2001) 327–335.
[44] D.I. Chan, E.J. Prenner, H.J. Vogel, Tryptophan- and arginine-rich antimicrobial peptides: structures and mechanisms of action, Biochim. Biophys. Acta Biomembr. 1758 (2006) 1184–1202.
[45] P. Grieco, A. Carotenuto, L. Auriemma, A. Limatola, S.D. Maro, F. Merlino, M.L. Mangoni, V. Luca, A.D. Grazia, S. Gatti, P. Campiglia, I. Gomez-Monterrey, E. Novellino, A. Catania, Novel α-MSH peptide analogues with broad spectrum antimicrobial activity, PLoS One 8 (2013) e61614.
[46] L. Marcellini, M. Borro, G. Gentile, A.C. Rinaldi, L. Stella, P. Aimola, D. Barra, M.L. Mangoni, Esculentin-1b(1-18) - a membrane-active antimicrobial peptide that synergizes with antibiotics and modifies the expression level of a limited number of proteins in *Escherichia coli*, FEBS J. 276 (2009) 5647–5664.
[47] P. Valenti, P. Visca, G. Antonini, N. Orsi, Antifungal activity of ovotransferrin towards genus Candida, Mycopathologia 89 (1985) 169–175.
[48] A.D. Grazia, F. Cappiello, A. Imanishi, A. Mastrofrancesco, M. Picardo, R. Paus, M.L. Mangoni, The frog skin-derived antimicrobial peptide Esculentin-1a(1-21)NH2 promotes the migration of human HaCaT keratinocytes in an EGF receptor-dependent manner: a novel promoter of human skin wound healing? PLoS One 10 (2015) http://dx.doi.org/10.1371/journal.pone.0128663.
[49] A.D. Grazia, V. Luca, Li-av T. Segev-Zarko, Y. Shai, Y.M.L. Mangoni, Temporins A and B Stimulate migration of HaCaT keratinocytes and kill intracellular *Staphylococcus aureus*, Antimicrob. Agents Chemother. 58 (2014) 2520–2527.
[50] V. Luca, M. Olivi, A.D. Grazia, C. Palleschi, D. Uccelletti, M.L. Mangoni, Anti-Candida activity of 1–18 fragment of the frog skin peptide esculentin-1b: *in vitro* and *in vivo* studies in a *Caenorhabditis elegans* infection model, Cell. Mol. Life Sci. 71 (2013) 2535–2546.
[51] M.E. Mercurio, S. Tomassi, M. Gaglione, R. Russo, A. Chambery, S. Lama, P. Stiuso, S. Cosconati, E. Novellino, S.D. Maro, A. Messere, Switchable protecting strategy for solid phase synthesis of DNA and RNA interacting nucleopeptides, J. Org. Chem. 81 (2016) 11612–11625.
[52] U. Piantini, O.W. Soerensen, R.R. Ernst, ChemInform abstract: multiple quantum filters for elucidating NMR coupling networks (Anwendung auf die Anregung von 1,3-Dibrom-butan), Chem. Inf. 14 (1983).
[53] D. Marion, K. Wüthrich, Application of phase sensitive two-dimensional correlated spectroscopy (COSY) for measurements of 1H-1H spin-spin coupling constants in proteins, Biochem. Biophys. Res. Commun. 113 (1983) 967–974.
[54] L. Braunschweiler, R. Ernst, Coherence transfer by isotropic mixing: application to proton correlation spectroscopy, J. Magn. Reson. 53 (1983) 521–528, 10.
[55] J. Jeener, B.H. Meier, P. Bachmann, R.R. Ernst, Investigation of exchange processes by two-dimensional NMR spectroscopy, J. Chem. Phys. 71 (1979) 4546–4553.
[56] D. States, R. Haberkorn, D. Ruben, A two-dimensional nuclear overhauser experiment with pure absorption phase in four quadrants, J. Magn. Reson. 48 (1982) 286–292.
[57] T. Hwang, A. Shaka, Water suppression that works. Excitation sculpting using arbitrary wave-forms and pulsed-field gradients, J. Magn. Reson. Ser. A 112 (1995) 275–279.
[58] F. Delaglio, S. Grzesiek, G. Vuister, G. Zhu, J. Pfeifer, A. Bax, NMRPipe: a multidimensional spectral processing system based on UNIX pipes, J. Biomol. NMR 6 (1995).
[59] C. Bartels, T.-H. Xia, M. Billeter, P. Güntert, K. Wüthrich, The program XEASY for computer-supported NMR spectral analysis of biological macromolecules, J. Biomol. NMR 6 (1995) 1–10.
[60] P. Güntert, C. Mumenthaler, K. Wüthrich, Torsion angle dynamics for NMR structure calculation with the new program Dyana, J. Mol. Biol. 273 (1997) 283–298.
[61] J.R. Maple, U. Dinur, A.T. Hagler, Derivation of force fields for molecular mechanics and dynamics from ab initio energy surfaces, Proc. Natl. Acad. Sci. 85 (1988) 5350–5354.
[62] R. Koradi, M. Billeter, K. Wüthrich, MOLMOL: a program for display and analysis of macromolecular structures, J. Mol. Graph. 14 (1996) 51–55.
[63] E.G. Hutchinson, J.M. Thornton, PROMOTIF-A program to identify and analyze structural motifs in proteins, Protein Sci. 5 (2008) 212–220.

ChemPubSoc Europe

DOI: 10.1002/cmdc.201900221

CHEMMEDCHEM Full Papers

The Outcomes of Decorated Prolines in the Discovery of Antimicrobial Peptides from Temporin-L

Elisabetta Buommino[+],[a] Alfonso Carotenuto[+],[a] Ignazio Antignano,[a] Rosa Bellavita,[a] Bruno Casciaro,[b, f] Maria Rosa Loffredo,[b] Francesco Merlino,[a] Ettore Novellino,[a] Maria Luisa Mangoni,[b] Francesca Paola Nocera,[e] Diego Brancaccio,[a] Pasqualina Punzi,[c] Daniela Roversi,[c] Raffaele Ingenito,[c] Elisabetta Bianchi,*[c] and Paolo Grieco*[a, d]

Previously, we identified a potent antimicrobial analogue of temporin L (TL), [Pro^3]TL, in which glutamine at position 3 was substituted with proline. In this study, a series of analogues in which position 3 is substituted with non-natural proline derivatives, was investigated for correlations between the conformational properties of the compounds and their antibacterial, cytotoxic, and hemolytic activities. Non-natural proline analogues with substituents at position 4 of the pyrrolidine ring were considered. Structure–activity relationship (SAR) studies of these analogues were performed by means of antimicrobial and cytotoxicity assays along with circular dichroism (CD) and NMR spectroscopic analyses for selected compounds. The most promising peptides were additionally evaluated for their activity against some representative veterinary microbial strains to compare with those from human strains. We identified novel analogues with interesting properties that make them attractive lead compounds.

Introduction

The growing development of antibiotic resistance poses a major human health concern.[1,2] Although antimicrobial agents have saved lives of millions of people, their inappropriate and intensive use in both veterinary and human medicine as well as in food animals, has promoted the emergence of antimicrobial resistance (AMR) and a greater risk of untreatable infections.[3,4] Diseases caused by drug-resistant bacteria may transfer their resistance to drug-susceptible bacteria that ultimately may act as reservoir of resistance to pathogenic organisms.[5] During the last decades, free movement of people and goods around the world as well as the intensive international transport of livestock have contributed even more to AMR. Moreover, the emergence of AMR coincides with a decline in the rate of development of new antimicrobial agents.[6] In fact, only a few novel antibiotics against Gram-positive bacteria have become available in recent years,[7] such as the new cephalosporins ceftobiprole and ceftaroline, active against methicillin-resistant *Staphylococcus aureus* (MRSA), and the oxazolidinone tedizolid, which is active against clinically relevant pathogens such as MRSA, methicillin-susceptible *S. aureus* (MSSA), and various *Streptococcus* species.[8,9]

In contrast, treating Gram-negative bacterial infections is more challenging because of the rapid antimicrobial resistance they develop. Indeed, no new class of drugs has been introduced during the last four decades.[10,11] Moreover, it has been estimated that most of the antibiotics currently used for common human and animal infections will be useless within five to ten years, thus moving back to a pre-antibiotic era when infections caused high morbidity and mortality.[12]

In this context, antimicrobial peptides (AMPs), present in all life forms,[13] exert killing activity on a large number of microorganisms.[14] Belonging to the host's innate defense system, they represent the most ancient and fast-acting elements against microbial pathogens.[15] These AMPs are promising candidates for a new generation of anti-infective agents in both human and veterinary medicine. AMPs are short and generally positively charged peptides,[16,17] many of which have the ability to kill microbial pathogens directly, whereas others act indirectly by modulating the host defense systems.[18–20] Many

[a] Dr. E. Buommino,[+] Prof. A. Carotenuto,[+] Dr. I. Antignano, Dr. R. Bellavita, Dr. F. Merlino, Prof. E. Novellino, Dr. D. Brancaccio, Prof. P. Grieco
Department of Pharmacy, University of Naples "Federico II", Naples 80131 (Italy)
E-mail: paolo.grieco@unina.it

[b] Dr. B. Casciaro, Dr. M. R. Loffredo, Prof. M. L. Mangoni
Department of Biochemical Sciences, Laboratory affiliated to Pasteur Institute Italia–Fondazione Cenci Bolognetti, Sapienza University of Rome, Rome 00185 (Italy)

[c] Dr. P. Punzi, Dr. D. Roversi, Dr. R. Ingenito, Dr. E. Bianchi
Peptide Chemistry Unit, IRBM S.p.A., via Pontina km 30600, Pomezia 00071 (Italy)
E-mail: e.bianchi@irbm.com

[d] Prof. P. Grieco
Centro Interuniversitario di Ricerca sui Peptidi Bioattivi (CIRPEB), University of Naples "Federico II", Naples 80134 (Italy)

[e] Dr. F. P. Nocera
Department of Veterinary Medicine and Animal Production, University of Naples "Federico II", Naples 80137 (Italy)

[f] Dr. B. Casciaro
Center for Life Nano Science, Istituto Italiano di Tecnologia, Rome 00161 (Italy)

[+] These authors contributed equally to this manuscript.

Supporting information and the ORCID identification number(s) for the author(s) of this article can be found under: https://doi.org/10.1002/cmdc.201900221.

AMPs display rapid antimicrobial activity by disrupting the physical integrity of the microbial membrane and/or by translocating across the membrane into the cytoplasm of bacteria to act on intracellular targets.[21] Only a few AMPs are currently in clinical trials because of their low metabolic stability, which generally represents the limit of therapeutic peptides.[22,23] The amphibian peptides, temporins, are one of the largest families (around 100 members) and are among the smallest-sized AMPs (10–16 amino acid residues) found in nature. They are C-terminally amidated, and only one or two basic residues are present.[24] Temporins are known to be particularly active against Gram-positive bacteria, with minimal inhibitory concentrations (MIC) ranging from 2.5 to 20 μM.[25,26] An exception is the isoform L (temporin L, TL), Phe-Val-Gln-Trp-Phe-Ser-Lys-Phe-Leu-Gly-Arg-Ile-Leu-NH_2 (**1**), as it is also active against Gram-negative bacteria and yeast strains.[24] Most of the temporins are practically non-hemolytic, but the highly potent TL kills human erythrocytes at microbicidal concentrations as well.[27] Therefore, for further development as a broad-spectrum antibiotic, it is necessary to increase its therapeutic index, referred to as the ratio between the concentration of hemolytic activity (minimum hemolytic concentration, MHC) and antimicrobial activity (MIC), MHC/MIC.[28] Studies focused on the structure–activity relationships of both native TL and some synthetic analogues revealed a tight correlation between their hemolytic activity and α-helical content,[29] whereas a lesser correlation was found between α-helical content and antimicrobial activity.[30] Previously, we identified an interesting TL analogue, [Pro^3]TL (**2**), through the replacement of glutamine at position 3 with proline. [Pro^3]TL (**2**) showed a 2- to 5-fold lower in vitro cytolytic effect than that of natural TL (**1**), while maintaining antimicrobial effectiveness against both bacteria and yeasts.[29,30]

Considering this prominent result, we designed a focused library of derivatives in which the pyrrolidine group was decorated with various chemical functionalities at position 4 of the ring (Table 1 and Figure 1) to accomplish an extensive structure– and conformation–activity relationship study. Such compounds were analyzed by antimicrobial and cytotoxicity assays on both human bacterial strains and some veterinary bacterial strains in order to compare both activities. Conformational analysis by CD spectroscopy was performed for all compounds, while NMR spectroscopy was carried out only for selected analogues.

Table 1. Peptide sequences of synthesized [Pro^3]TL analogues.

Peptide	Sequence[a]
TL, **1**[b]	F-V-Q-W-F-S-K-F-L-G-R-I-L-NH_2
[Pro^3]TL, **2**[b]	F-V-**Pro**-W-F-S-K-F-L-G-R-I-L-NH_2
3	F-V-(***cis*-4F-Pro**)-W-F-S-K-F-L-G-R-I-L-NH_2
4	F-V-(**4,4-diF-Pro**)-W-F-S-K-F-L-G-R-I-L-NH_2
5	F-V-(***cis*-4CF_3-Pro**)-W-F-S-K-F-L-G-R-I-L-NH_2
6	F-V-(***cis*-4MeS-Pro**)-W-F-S-K-F-L-G-R-I-L-NH_2
7	F-V-(***cis*-4NH_2-Pro**)-W-F-S-K-F-L-G-R-I-L-NH_2
8	F-V-(***trans*-4Chx-Pro**)-W-F-S-K-F-L-G-R-I-L-NH_2
9	F-V-(***trans*-4Ph-Pro**)-W-F-S-K-F-L-G-R-I-L-NH_2
10	F-V-(***trans*-4Bn-Pro**)-W-F-S-K-F-L-G-R-I-L-NH_2
11	F-V-(***cis*-4PhO-Pro**)-W-F-S-K-F-L-G-R-I-L-NH_2

[a] Residue variations relative to **1** are highlighted in bold. [b] Described previously by Carotenuto et al.[29]

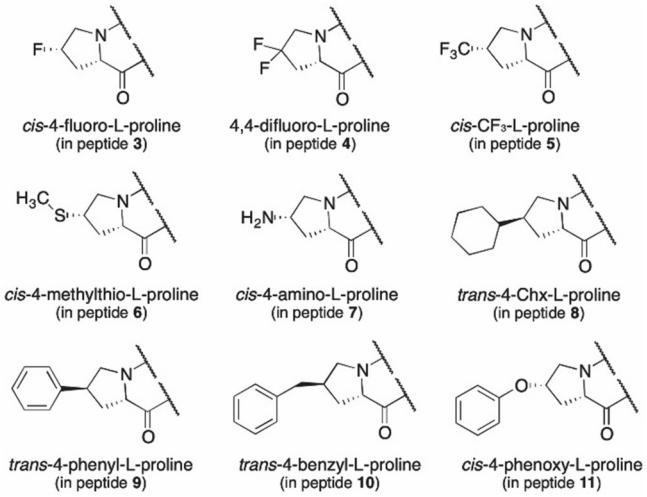

Figure 1. Proline derivatives used in this study.

Results and Discussion

Synthesis

Synthesis of peptides **1**–**11** was manually performed by microwave-assisted solid-phase peptide synthesis (SPPS) and using Fmoc/*t*Bu chemistry. After cleavage from the solid support, crude peptides were purified and characterized by reversed-phase high-performance liquid chromatography (RP-HPLC) and ESI-MS (Table S1 and Figure S1, see Supporting Information).

Biological activity

Antimicrobial activity

The primary structures of the designed temporin L analogues are listed in Table 1, where position 3 was replaced with several proline residues (Figure 1) decorated with various chemical groups at position 4 of the pyrrolidine ring. In particular, polar electron-withdrawing (fluoro, trifluoromethyl), apolar (methylthio), positively charged (amino), aliphatic (cyclohexyl), or aromatic (phenyl and benzyl) groups were used, as these groups can interact with the microbial membrane envisaged as the biological target of TL and its derivatives.[30]

The antimicrobial activity against some reference bacterial and *Candida* strains was evaluated by broth microdilution assay to determine the MIC (Table 2). All synthesized compounds displayed good antimicrobial activity toward the Gram-positive bacterial strains considered in this study, with MIC values similar to those of **1** and **2**. Notably, almost all compounds displayed efficacy against *C. albicans* ATCC 24433 similar to that of compound **2**. Peptide **3**, in which the Pro^3 residue was replaced with *cis*-4-fluoroproline, showed antibacterial activity similar to that of the parent peptide **2** on both Gram-negative and Gram-positive bacterial strains. In addition, the

Table 2. Antimicrobial activity of designed compounds **3**–**11**.[a]

Microorganisms	MIC [μM][b]										
	1	**2**	**3**	**4**	**5**	**6**	**7**	**8**	**9**	**10**	**11**
Gram-negative bacteria											
E. coli ATCC 25922	12.5	12.5	12.5	12.5	12.5	12.5	3.12	50.0	12.5	25.0	25.0
P. aeruginosa ATCC 27853	12.5	25.0	12.5	25.0	25.0	25.0	12.5	100	50.0	50.0	50.0
Gram-positive bacteria											
B. megaterium Bm11	3.12	3.12	3.12	3.12	3.12	3.12	3.12	3.12	3.12	3.12	3.12
S. epidermidis ATCC 12228	3.12	6.25	3.12	3.12	3.12	3.12	3.12	3.12	3.12	3.12	3.12
Yeasts											
C. albicans ATCC 24433	6.25	12.5	12.5	12.5	12.5	6.25	12.5	25.0	12.5	25.0	12.5

[a] Aliquots (50 μL) of bacteria in mid-log phase at a concentration of 2×10^6 colony-forming units (CFU) per mL (5×10^4 CFU mL^{-1} for *C. albicans*) in culture medium (Müller–Hinton (MH) broth for bacteria, Winge broth for *C. albicans*) were added to 50 μL of MH broth (Winge broth for *C. albicans*) containing the peptide in twofold serial dilutions. [b] The minimal inhibitory concentration (MIC) is the concentration of peptide at which 100% inhibition of microbial growth is observed, after an incubation of 16–18 h at 37 °C (30 °C for *C. albicans*); values are the average of at least three independent experiments.

activity toward *C. albicans* resulted to be 2-fold lower with respect to TL. Peptides **5** and **6**, featuring *cis*-trifluoromethyl-Pro and *cis*-methylthio-Pro, respectively, showed similar behavior. In fact, they were found to be 2-fold less active than TL toward *P. aeruginosa* ATCC 27853, while the activity on *E. coli* ATCC 25922 was unchanged. The addition of another fluorine atom on the pyrrolidine in peptide **4** (4,4-difluoro-Pro) had little effect on antimicrobial activity, compared with either **5** (*cis*-4-trifluoromethyl-Pro TL) or to the parent [Pro^3]TL (**2**). In contrast, peptide **7**, characterized by a *cis*-4-amino-Pro residue, displayed a significantly lower MIC (3.12 μM) on *E. coli* ATCC 25922, while maintaining similar activity against *P. aeruginosa* ATCC 27853. Furthermore, the anticandidal activity was slightly decreased with respect to **1**. Surprisingly, by replacing the Pro^3 with its *trans*-4-cyclohexyl-Pro derivative, the resulting peptide **8** showed a dramatic decrease in activity on *E. coli* ATCC 25922 and lost effect on *P. aeruginosa* ATCC 27853. In addition, the activity toward *C. albicans* resulted to be 2-fold lower than the parent peptide **2**. Finally, analogues **9**–**11**, all characterized by an aromatic functionality at position 4 of the pyrrolidine ring, *trans*-4-phenyl-Pro (**9**), *trans*-4-benzyl-Pro (**10**), and *cis*-4-phenoxy-Pro (**11**) were found to be poorly active on *P. aeruginosa* ATCC 27853 (MIC 50 μM), while the activity on *E. coli* ATCC 25922 was 2-fold lower for compounds **10** and **11**, relative to both reference peptides TL (**1**) and [Pro^3]TL (**2**). However, the anticandidal activity remained almost unchanged with respect to **2**, except for compound **10**, showing a MIC of 25.0 μM.

Subsequently, the peptides were evaluated for their activity against some veterinary bacterial strains, namely *E. coli* and *Proteus mirabilis* (Gram-negative), *Staphylococcus pseudintermedius* (Gram-positive), *Malassezia pachydermatis* (yeast). The veterinary clinical isolates were first analyzed by disc diffusion test for the occurrence of antibiotic resistance, demonstrating a strong resistance to most common antibiotics used in the therapy of pet animals (data not shown). Regarding the activity on Gram-negative strains, only compounds **6** and **7** showed notable activity on *E. coli*. In particular, compound **7** was found to be the most potent, with a MIC of 3.12 μM. In contrast, all other synthesized compounds were inactive against *P. mirabilis* (MIC $>$100 μM). Importantly, this strain was resistant to almost all classes of antibiotics tested by disc diffusion test (data not shown). Further interesting results were obtained on *S. pseudintermedius*. With the sole exception of compounds **4** and **5**, all peptides showed good activity. Specifically, compounds **3** and **11** displayed the best activity against both methicillin-sensitive (MSSP) and methicillin-resistant *S. pseudintermedius* (MRSP) with a MIC of 1.56 μM. Additionally, the compounds were tested on the yeast *M. pachydermatis*. Good activity was shown for all compounds, especially for **6**, **9**, and **11** with a MIC of 12.5 μM. Overall, compound **11** showed the best activity on both *M. pachydermatis* and *S. pseudintermedius*. Because both strains can be etiological agents in canine pyoderma and otitis, compound **11** can be considered a potential lead compound for combined therapy in the care of pet animals.

Taking into account the antimicrobial activity against reference strains and clinical isolates, the compounds that showed a better activity than compound **2** were found to be **6**, **7**, and **11**; for this reason they were selected for further characterization in the hemolysis assay.

Hemolytic activity

The compounds with the best antimicrobial activity (**6**, **7**, and **11**) were tested for their effect on circulating blood cells (i.e., erythrocytes), and the percentages of hemolysis are reported in Figure 2 and are compared with those of the parent peptide **2**. Compound **11** showed a potent hemolytic effect even at low concentrations ($>$40% at 3.12 or 6.25 μM). In comparison, compound **6** was found to be less hemolytic than compounds **11** and **2** at a concentration range from 3.12 to 25.0 μM, but

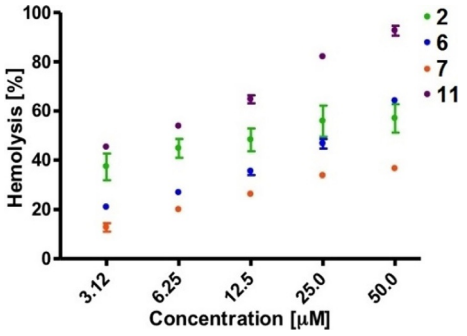

Figure 2. Hemolytic activity of compounds **6**, **7**, and **11** compared with parent peptide **2**. Percentages of hemolysis ± SEM were calculated with respect to the complete lysis of erythrocytes in distilled water.

more active than the parent peptide **2** at the highest concentration (i.e., 50 μM). Interestingly, compound **7** was less toxic than compound **2** ($p < 0.01$) and all the other tested analogues at all concentrations tested. This makes peptide **7** the compound with the best biological profile.

Structural studies

CD analysis

To explore the conformational changes of TL analogues synthesized in this study, we performed CD spectroscopy studies in phosphate buffer (PB, pH 7.4), sodium dodecyl sulfate (SDS), dodecylphosphocholine (DPC), and DPC/SDS 9:1 micelle solution (Figure 3). These micelles were used as rough mimetics of bacterial, mammalian, and yeast membranes, respectively.[31–33]

Secondary structure content (see Table 4 below) was evaluated from CD spectra by the Bestsel method.[34] CD spectra in PB revealed the prevalence of disordered conformers for all compounds characterized by a minimum close to 200 nm (Figure 3a and Table 4). For some analogues (**8**, **10**, and **11**) a relatively intense minimum at 228 and maximum at 200 nm were observed. These spectral features were associated by Bestsel prediction with an increase in β-sheet and/or β-turn structure content (Table 4).

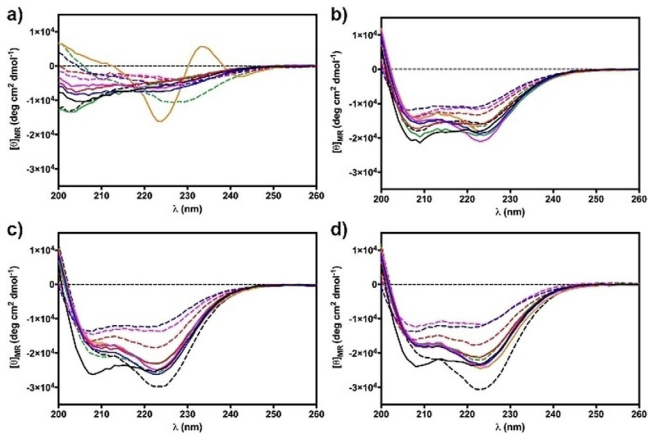

Figure 3. CD spectra of peptide **1** and its analogues **2**–**11** in a) PB, b) SDS, c) DPC, and d) DPC/SDS 9:1 micelle solution. **1**, black solid line; **2**, blue solid line; **3**, magenta solid line; **4**, red solid line; **5**, green solid line; **6**, orange solid line; **7**, black dashed line; **8**, blue dashed line; **9**, magenta dashed line; **10**, red dashed line; **11**, green dashed line.

In SDS, DPC, and DPC/SDS 9:1 membrane mimetic solutions, CD spectra indicated more structured peptides (Figure 3b–d). In all cases, two minima close to 208 and 222 nm were obtained, indicating helical propensity. Indeed, helical percentage of the peptides varied from 21 to 52% in SDS and from 24 to 60% in DPC/SDS according to Bestsel prediction (Table 4). Nonetheless, antibacterial activity on Gram-positive strains and antifungal activity were almost identical regardless of helical content. For example, peptides **7** (42.7% helix in SDS) and **8** (21.3% helix in SDS) had the same activity on both *B. megaterium* and *S. epidermidis* (Table 2). This is in accordance with our previous finding that the helical percentage of TL derivatives has only a minor effect on their antibacterial activity.[35]

The relationships between the conformations of the synthesized peptides and the antibacterial activity on Gram-negative bacteria is more intriguing. Three peptides (**8**, **10**, and **11**) showed lower activity than the parent **2** against both the human Gram-negative bacteria tested (Table 2). Those peptides had different degrees of helical content in SDS (from 21 to 48%), thus, again, there is not a clear correlation between antibacterial activity and helical content. Interestingly enough, peptides **8**, **10**, and **11** showed a relatively high propensity to the β-sheet or turn formation in PB solution, which could indicate their tendency to aggregate in amyloid-like structures. It can be hypothesized that this aggregation tendency increases in contact with the external membrane of the Gram-negative bacteria, in particular, in the presence of lipopolysaccharides (LPS). This possibility was tested by acquiring the CD spectrum of peptide **8**, which was almost inactive against Gram-negative bacteria, in the presence of LPS micelles (Figure S2, Supporting Information).

The spectrum displayed a minimum at 220 nm and a maximum at 196 nm, and its deconvolution by Bestsel algorithm gave a β-sheet content higher than 40%, a situation often associated with amyloid-like peptide oligomers.[35] Therefore, peptide **8** inactivity against Gram-negative bacteria could be due to its oligomeric state induced by contact with LPS. The large size of the oligomer makes it more difficult for the peptide to diffuse through the cell wall into the target cytoplasmic membrane.[36] Notably, TL, in contrast to peptide **8**, has a high helical propensity under the same experimental conditions.[35,37]

Compound **7** showed very high activity against *E. coli*, being 4-fold higher than both its parent **2** and the native TL (**1**). Notably, the activity of peptide **7** against *E. coli* was also confirmed on a veterinary strain (Table 3). Therefore, this peptide conformation was more thoroughly investigated by solution NMR spectroscopy (see below).

Considering the effect of the conformational propensities of the peptides on their hemolytic effect, peptide **11** showed the highest hemolytic effect (Figure 2) and also the highest helical content (Table 4) in the eukaryotic mimetic DPC solution. This result is in accordance with our previous result correlating peptide helicity in DPC with its hemolytic effect.[35,38] Peptides **2**, **6**,

Table 3. Antimicrobial activity of designed compounds **3**–**11** on veterinary strains.[a]

Microorganisms	MIC [μM][b]										
	1	**2**	**3**	**4**	**5**	**6**	**7**	**8**	**9**	**10**	**11**
Gram-negative bacteria											
E. coli	12.5	12.5	>100	>100	>100	12.5	3.12	>100	>100	>100	>100
P. mirabilis	>100	>100	>100	>100	>100	>100	>100	>100	>100	>100	>100
Gram-positive bacteria											
MSSP	3.12	3.12	1.56	>100	>100	3.12	6.25	3.12	3.12	3.12	1.56
MRSP	3.12	3.12	1.56	>100	>100	3.12	6.25	3.12	6.25	3.12	1.56
Yeasts											
M. pachydermatis	25	25	25	25	25	12.5	25	25	12.5	25	12.5

[a] Aliquots (50 μL) of bacteria in mid-log phase at a concentration of 2×10^6 colony-forming units (CFU) per mL (5×10^4 CFU mL^{-1} for yeasts) in culture medium (Müller–Hinton (MH) broth for bacteria, Sabouraud broth for *M. pachydermatis*) were added to 50 μL of MH broth (Sabouraud broth for *M. pachydermatis*) containing the peptide in twofold serial dilutions. [b] The minimal inhibitory concentration (MIC) is the concentration of peptide at which 100% inhibition of microbial growth is observed, after an incubation of 16–18 h at 37 °C (30 °C for yeasts); values are the average of at least three independent experiments.

Table 4. Secondary structure[a] percentages of TL analogues.

Peptide	PB solution				DPC solution				SDS solution				DPC/SDS Solution			
	h	β	t	r	h	β	t	r	h	β	t	r	h	β	t	r
1	12.7	31.5	14.2	41.5	62.2	2.0	9.5	26.4	47.7	8.7	11.0	32.6	60.5	3.7	11.1	24.7
2	9.6	19.1	18.7	52.7	42.8	16.2	11.2	29.8	45.6	3.4	15.0	36.0	43.2	14.5	12.7	29.5
3	11.9	25.1	16.3	46.7	42.2	9.9	12.8	35.2	42.0	10.9	14.3	32.8	43.5	8.4	13.8	34.3
4	12.3	26.9	16.2	44.5	40.2	17.1	11.0	31.7	43.5	5.9	12.0	38.6	41.0	16.5	11.2	31.3
5	15.3	17.9	14.8	51.9	39.5	13.4	11.3	35.9	51.7	2.8	12.4	33.1	40.9	14.5	11.9	32.7
6	0.0	51.7	13.1	35.2	42.6	8.1	12.4	36.9	44.1	2.3	16.1	37.5	45.3	5.1	13.0	36.7
7	14.9	14.5	16.1	54.5	44.3	16.1	12.0	27.5	42.7	9.4	12.8	35.2	45.1	15.2	11.5	28.2
8	6.1	36.7	16.1	41.0	25.0	13.4	13.5	48.2	21.3	15.8	13.6	49.3	24.4	21.2	12.3	42.1
9	13.3	31.0	16.1	39.7	28.8	17.9	13.4	39.9	32.3	6.7	14.7	46.3	26.5	15.2	16.6	41.7
10	4.8	35.8	18.0	41.3	39.4	6.1	12.9	41.6	30.9	4.2	14.3	50.6	35.8	12.5	12.4	39.3
11	5.5	22.1	27.6	44.8	51.8	6.8	10.8	30.6	48.4	4.2	12.7	34.8	49.9	8.0	13.9	28.2

[a] h: helix, β: beta-sheet, t: turn, r: random coil; peptide **8** in LPS: h 1.6, β 41.3, t 13.9, r 43.2.

and **7** displayed similar helical content (Table 4). The lower hemolytic potency of peptide **7** could be tentatively explained by considering our previous result on the mechanism of the hemolytic action of TL (**1**) and its derivatives. In fact, studying the interaction between **1** and zwitterionic DPC micelles by NMR[29] and MD simulations, [30] we found that **1** inserts into the micelle, perpendicular to the membrane, with the N terminus deeply buried in the micelle hydrophobic core, thus unveiling the barrel-stave mechanism.[30] The presence of a hydrophilic group on Pro^3 within the N-terminal region, such as the amino group of **7**, probably prevents the peptide from exerting the above-described mechanism, thus explaining its low toxicity.

NMR analysis of peptides 7 and 8

Considering the very interesting antimicrobial activity of compound **7**, in particular against Gram-negative bacteria, and its low hemolytic effect, it was also investigated by NMR spectroscopy. Moreover, peptide **8,** which was almost inactive against Gram-negative, was also investigated by NMR for comparison. NMR spectroscopy was performed in SDS micellar solution. Complete ^{1}H NMR chemical shift assignments were effectively achieved for both peptides according to the Wüthrich procedure (see Supporting Information, Tables S2–S3).[39]

Peptide **7** in SDS solution exhibited NMR spectral features pointing to helical propensity. Upfield shift of the Hα NMR signals and temperature coefficients of many amide protons (Table S2), and diagnostic NOEs (Table S4) indicated that many residues in the central and C-terminal region are in a helical conformation. Structure calculation gave an ensemble of 20 structures (Figure 4a) satisfying the NMR-derived constraints (violations smaller than 0.10 Å). The backbone is well defined, with RMSD = 0.34 Å. An inverse γ-turn centered on the amino-Pro^3 can be observed at the N terminus followed by an α-helix from Trp^4 to Leu^{13} (Figure 4a). Also, the side chains are well defined, apart from those of Phe^1, which is very flexible, and Phe^8, which shows both *trans* and *gauche*+ orientations. Interestingly, the peptide assumes an amphipathic structure with a positive side (upper side in Figure 4a) and a hydrophobic side (lower side).

In particular, the *cis*-4-amino group on Pro^3 points toward the other positively charged groups (Lys^7 amino and Arg^{11} guanidinium groups) enlarging the charged peptide surface. Diagnostic NMR parameters observed for **8** also indicated confor-

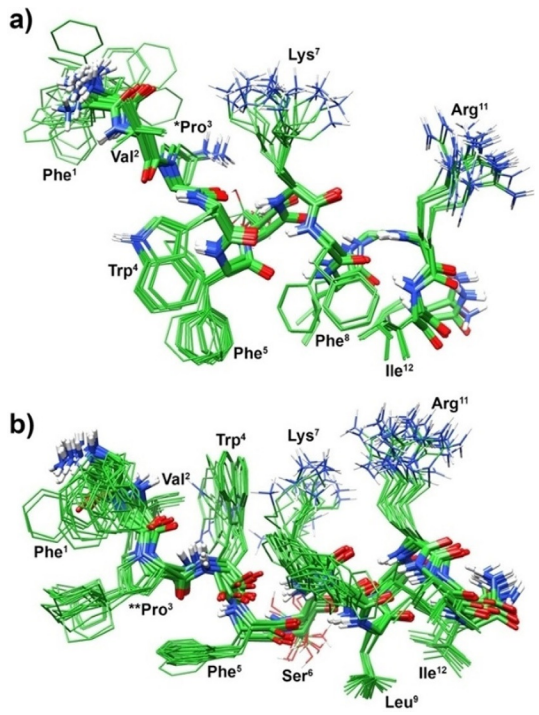

Figure 4. Superposition of the 20 lowest-energy conformers of a) **7** (PDB ID: 6QXB) and b) **8** (PDB ID: 6QXC) in SDS. Structures were superimposed using the backbone heavy atoms. Only heavy backbone atoms are shown for clarity, and are shown in ribbon format. Heavy atoms are shown in atom-type coloring (carbon, green; nitrogen, blue; oxygen, red). *Pro: *cis*-4-aminoproline; **Pro: *trans*-4-cyclohexylproline.

mational propensity toward helical or turn structures, but with higher flexibility (Tables S3 and S5). In fact, the upfield shifts of the Hα NMR signals were less intense than those observed for **2** and **7**. Calculated structures, shown in Figure 4b, were less defined than those obtained for **7** (backbone heavy atoms RMSD = 0.72 Å), which is in accordance with the CD result indicating minor helical structure content relative to **1**, **2**, and **7** (Table 4).

A helix structure is observable from residue 5 to 12 in many structures of the ensemble (18/20), while the N-terminal region is in extended conformation. Notably, the cyclohexyl group is positioned near the phenyl rings of Phe[1] and Phe[5] forming a hydrophobic cluster. The overall structure is amphipathic, with the cyclohexyl cluster oriented on the same side of Phe[8], Leu[9], and Ile[12] (lower side in Figure 4b). Different from peptides **7** and **8**, parent peptide **1** showed a tendency to the amphipathic α-helix along the entire sequence in SDS solution (Figure S3, Supporting Information) except some flexibility at the N and C termini.[29] However, the loss of the N-terminal helical segment, observed in **7** and **8**, does not affect the antimicrobial activity of the TL derivatives, as already demonstrated for peptide **2**.[29,30]

Therefore, both peptides **7** and **8** keep the amphipathic character of their parent peptides **1** and **2**, irrespective of the chemical modification on Pro[3]. This is due to the high flexibility of the N-terminal region of these peptides, which allows optimal orientation of the additional group on the proline for membrane interactions. Extending this result to all the developed peptides (Table 1), this could explain the high activity against Gram-positive bacteria and good activity against fungi observed for all of them (Table 2). In the same way, a proper orientation of the positively charged amino group of **7** can explain its increased activity against many Gram-negative strains.

On the other hand, decrease or loss of activity against Gram-negative bacteria observed in some of the novel peptides is likely due to peptide aggregation as stated above. In fact, the hydrophobic cluster found in the structure of peptide **8** (Figure 4b), but also predictable in other peptides such as **10** and **11**, can work as an aggregation point leading to oligomerization.

Conclusions

Peptide **1** has unique anti-yeast and anti-Gram-negative activity among the temporins. These activities were maintained by its analogue **2**, which also showed decreased cytotoxicity against red blood cells. By decorating the Pro[3] residue in **2**, we have now obtained interesting candidates for antimicrobial clinical studies. In particular, peptide **7**, characterized by a *cis*-4-amino-Pro residue, has shown improved activity over the parent peptide **2** against human and veterinary Gram-negative bacterial strains, and, at the same time, it has preserved the activity of **2** on Gram-positive bacteria and yeasts and low toxicity toward red blood cells. Peptide **11** is also interesting due to its activity against veterinary strains; however, because of its toxicity, it can be considered as a starting point for further chemical alterations.

More in general, we demonstrated that the decoration of Pro[3] on peptide **2** is a successful strategy to obtain active antimicrobial peptides, because the flexibility of the N-terminal peptide region allows the additional group to orient adequately for membrane interactions.

Experimental Section

Chemistry

Materials and general methods. N$^{\alpha}$-Fmoc-protected amino acids, Fmoc-Phe, Fmoc-Val, Fmoc-Gln(Trt), Fmoc-Pro, Fmoc-Trp(Boc), Fmoc-Ser(*t*Bu), Fmoc-Lys(Boc), Fmoc-Leu, Fmoc-Gly, Fmoc-Arg(Pbf), Fmoc-Ile, all were purchased from NovaBiochem. Other non-natural N$^{\alpha}$-Fmoc-amino acids, namely Fmoc-L-Pro(4,4-diF$_2$), Fmoc-L-Pro(*cis*-4-F), Fmoc-L-Pro(*cis*-4-CF$_3$), Fmoc-L-Pro(*cis*-4-OPh), Fmoc-L-Pro(-*trans*-4-Bz), Fmoc-L-Pro(*trans*-4-Ph), Fmoc-L-Pro(*trans*-4-Chx), and Fmoc-L-Pro(*cis*-4-SMe), were purchased from Polypeptide Laboratories. Fmoc-L-Pro(*cis*-4-NHBoc) was purchased from 3B Scientific Corp. The Rink amide resin was purchased from Chem-Impex. Coupling reagents were purchased as follows: *N*,*N*′-diisopropylcarbodiimide (DIC) from Sigma–Aldrich, ethyl cyano(hydroxyimino)acetate (Oxyma Pure®) from Chem-Impex, 1-hydroxy-7-azabenzotriazole (HOAt) from CreoSalus. *N*,*N*-Diisopropylethylamine (DIEA), piperidine and trifluoroacetic acid (TFA) were purchased from Sigma–Aldrich. Peptide synthesis solvents and reagents were purchased as follows: *N*,*N*-dimethylformamide (DMF), CH_2Cl_2, *tert*-butyl methyl ether (MTBE), MeOH, and CH_3CN HPLC grade were all from Sigma–Aldrich; Et_2O was from ITW Reagents; and *N*-methyl-2-pyrrolidone (NMP) was from Merck Millipore. All were reagent grade acquired from commercial sources and used without further purification.

Peptide synthesis. The synthesis of peptides **1**–**11** was performed by solid-phase peptide synthesis (SPPS) using Fmoc/*t*Bu chemistry. All peptides were assembled on a Rink amide PS resin 100–200 mesh, (0.2 mmol scale with 0.47 mmol g^{-1} of loading). The synthesis of peptides **1** and **2** was performed manually using a Microwave CEM Accent instrument. Amino acids (3 equiv) were acylated using equimolar amounts of DIC and Oxyma as activators. Double coupling conditions: 75 °C, 170 W, 15 min, then 90 °C, 30 W, 110 min, were used for all amino acids. The synthesis of all other peptides was performed on a Liberty Blue microwave synthesizer (CEM corporation) using a 5-fold excess of amino acids and equimolar amounts of DIC and Oxyma. The synthesis proceeded on the synthesizer up to Trp^4, followed by acylation with the different pyrrolidine analogues for each sequence by manual synthesis using three equivalents of each amino acid and equimolar amounts of activators DIC and HOAt in DMF. The last two residues Val^2 and Phe^1 were acylated by double acylation with DIC and HOAt as activators. The final peptide resins were washed and dried with CH_2Cl_2, MeOH, and Et_2O. Peptide **1** and its analogues **2**–**11** were cleaved from the resin using a solution of TFA/TIS/phenol/H_2O 87:3:5:5 for 2 h. The resins were filtered, and peptide solutions were precipitated with MTBE. The peptide precipitates were centrifuged and washed with fresh MTBE. The peptide pellets were dried dissolved in 50:50 H_2O/CH_3CN + 0.1 % TFA and lyophilized.

Purification of peptides was performed by preparative reversed-phase chromatography on a Waters 2545 HPLC system equipped with a 2489 UV detector on a Waters XBridge™ C18 preparative column (130 Å, 5 μm, 150×50 mm) using as eluents (A) 0.1 % TFA in water and (B) 0.1 % TFA in CH_3CN. All fractions with the highest purity were collected and lyophilized, obtaining peptides with a purity >95 % (20–65 % overall yield). Purified peptides were characterized on an Acquity UPLC Waters chromatograph, using a Waters BEH130 C18 Acquity column (2.1×100 mm, 1.7 μm, at 45 °C) for compounds **1**–**6** and an Aeris PEPTIDE XB-C18 100 Å column (2.1×100 mm, 2.6 μm, at 45 °C) for compounds **7**–**11**, using as eluents (A) 0.1 % TFA in water and (B) 0.1 % TFA in CH_3CN, and by ESI on an Acquity SQ2 Mass Detector (Table S1 and Figure S1, Supporting Information).

Biology

Microorganisms. The strains used for the antimicrobial assays were the following: Gram-negative bacteria, *Escherichia coli* ATCC 25922 and *Pseudomonas aeruginosa* ATCC 27853; Gram-positive bacteria, *Bacillus megaterium* Bm11 and *Staphylococcus epidermidis* ATCC 12228; yeast, *Candida albicans* ATCC 24433.

Veterinary clinical strains of *E. coli*, *P. mirabilis*, *S. pseudintermedius*, and *M. pachydermatis* were isolated from pet animals and processed at the Microbiology Laboratory of the Department of Veterinary Medicine and Animal Production, University of Naples Federico II (Italy). The strains were identified by matrix-assisted laser desorption ionization-time of flight mass spectrometry (MALDI-TOF MS) (Bruker Daltonik). For this study, multidrug-resistant bacterial strains were selected. Furthermore, two *S. pseudintermedius* strains were chosen, one methicillin-resistant (MRSP) and the other was methicillin-susceptible (MSSP).[40]

Antimicrobial assay. The MIC values were obtained by adapting the microbroth dilution method outlined by the Clinical and Laboratory Standards Institute, using sterile 96-well plates (Falcon NJ, USA). Aliquots (50 μL) of bacteria in mid-log phase at a concentration of 2×10^6 colony-forming units (CFU) per mL (5×10^4 CFU mL^{-1} for *C. albicans*) in culture medium (Mueller–Hinton, MH or Winge broth, WB, for *C. albicans*, and Sabouraud broth for *M. pachydermatis*) were added to 50 μL of MH/WB containing the peptide in serial 2-fold dilutions in water. Peptide dilutions ranged from 0.1 to 100 μM. MICs were considered as the peptide concentration at which 100 % inhibition of microbial growth is visually observed after 18–20 h of incubation at 37 °C (30 °C for yeasts). Each MIC value is the average of at least three independent experiments.[38]

Hemolytic assay. The hemolytic activity was measured on sheep red blood cells (OXOID, SR0051D). Briefly, aliquots of erythrocyte suspension (1×10^8 cells mL^{-1}) in 0.9 % (*w*/*v*) NaCl were incubated with serial 2-fold dilutions of the peptides in water for 40 min at 37 °C with gentle shaking. The samples were then centrifuged for 5 min at 900×*g* and the absorbance of the supernatant was measured at 415 nm using a microplate reader (Infinite M200; Tecan, Salzburg, Austria). The complete lysis of red blood cells was measured by suspending erythrocytes in distilled water.[31]

Conformational analyses

Circular dichroism spectroscopy. Circular dichroism spectra were recorded at 25 °C using quartz cells of 0.1 cm path length with a JASCO J-710 CD spectropolarimeter (JASCO International Co. Ltd.). Measurements were run in the 260–185 nm spectral range, 1 nm bandwidth, 16 s response time, and 2 nm min^{-1} scanning speed. The concentration of peptides was 100 μM in 10 mM sodium phosphate buffer (pH 7.4), SDS (20 mM), DPC (20 mM), or DPC/SDS (18/2 mM) micellar solutions. The Bestsel algorithm was used to extract secondary structure content.[34] A CD spectrum of peptide **8** was also acquired in LPS 100 μM.

NMR spectroscopy. The samples for NMR spectroscopy were prepared by dissolving the appropriate amount of peptides **7** and **8** in 0.55 mL of ^1H_2O, 0.05 mL of ^2H_2O to obtain a concentration of 1–2 mM peptides and 200 mM $[D_{25}]$SDS. The NMR experiments were performed at pH 5.0. NMR spectra were recorded on a Varian Unity INOVA 700 MHz spectrometer equipped with a *z*-gradient 5 mm triple-resonance probe head. All spectra were recorded at a temperature of 25 °C. The spectra were calibrated relative to TSP (0.00 ppm) as internal standard. One-dimensional (1D) NMR spectra were recorded in the Fourier mode with quadrature detection. Two-dimensional (2D) DQF-COSY,[41,42] TOCSY,[43] and NOESY spectra[44] were recorded in the phase-sensitive mode using the method from States et al.[45] Data block sizes were 2048 addresses in t2 and 512 equidistant t1 values. A mixing time of 80 ms was used for the TOCSY experiments. NOESY experiments were run with mixing times in the range of 100–200 ms. The water signal was suppressed by gradient echo.[46] The 2D NMR spectra were processed using the NMRPipe package.[47] Before Fourier transformation, the time domain data matrices were multiplied by shifted sin2 functions in both dimensions, and the free induction decay size was doubled in F1 and F2 by zero filling. The qualitative and quantitative analysis of DQF-COSY, TOCSY, and NOESY spectra were obtained using the interactive program package XEASY.[48] $^3J_{HN}$-Hα couplings were difficult to measure probably because of a combination of small coupling constants and broad lines. The temperature coefficients of the amide proton chemical shifts were calculated from 1D ^1H NMR and 2D TOCSY experiments performed at different temperatures in the range 298–320 K by means of linear regression.

Structure determinations. The NOE-based distance restraints were obtained from NOESY spectra collected with a mixing time of 100 ms. The NOE cross-peaks were integrated with the XEASY program and were converted into upper distance bounds using the CALIBA program incorporated into the program package CYANA.[49]

Only NOE-derived constraints were considered in the annealing procedures. For each examined peptide, an ensemble of 200 structures was generated with the simulated annealing of the program CYANA. Nonstandard *cis*-4-amino-Pro and *trans*-4-cyclohexyl-Pro residues were added to CYANA residue library using the Biopolymer module of Insight II (Accelrys, San Diego, CA, USA). Then, 20 structures were chosen, whose interproton distances best fitted NOE derived distances, and refined through successive steps of restrained and unrestrained energy minimization calculations using the Discover algorithm (Accelrys) and the consistent valence force field.[50] The minimization lowered the total energy of the structures; no residue was found in the disallowed region of the Ramachandran plot. The final structures were analyzed using the Insight II program (Accelrys). Molecular graphics images were realized using the UCSF Chimera package.[51]

Statistical analyses. Quantitative data were expressed as the mean ± standard error of the mean (SEM). Statistical analyses were performed using Student's t-test with the Prism software package (GraphPad, San Diego, CA, USA). Differences were considered to be statistically significant for $p < 0.05$.

Acknowledgements

This work was supported by grants from Regione Campania, Progetti Retrospettivi Coerenti con la Misura 3.5 del FET Campania 2007–2013 (art.41 del Reg. (CE) 1198/2006); and Finanziamento della ricerca di Ateneo—Università degli Studi di Napoli Federico II—Annualità 2016, prot. N. 16503 and Sapienza University of Rome (project RM11816436113D8A).

Conflict of interest

The authors declare no conflict of interest.

Keywords: antimicrobial peptides · biological activity · conformational studies · synthesis · temporin L analogues

[1] J. Davies, D. Davies, *Microbiol. Mol. Biol. Rev.* **2010**, *74*, 417 – 433.
[2] S. C. Davies, T. Fowler, J. Watson, D. M. Livermore, D. Walker, *Lancet* **2013**, *381*, 1606 – 1609.
[3] P. Butaye, M. A. Argudín, J. Threlfall in *Antimicrobial Resistance and Food Safety: Methods and Techniques*, (Eds.: C. Y. Chen, X. Yan, C. R. Jackson), Academic Press, Cambridge, **2015**, pp. 1 – 18.
[4] C. Elias, L. Moja, D. Mertz, M. Loeb, G. Forte, N. Magrini, *BMJ Open.* **2017**, 7.
[5] C. L. Ventola, *J. Clin. Pharm. Ther.* **2015**, *40*, 277 – 283.
[6] S. Sengupta, M. K. Chattopadhyay, H. P. Grossart, *Front. Microbiol.* **2013**, *4*.
[7] L. Morata, J. Mensa, A. Soriano, *Curr. Opin. Pharmacol.* **2015**, *24*, 45 – 51.
[8] H. Moisan, M. Pruneau, F. Malouin, *J. Antimicrob. Chemother.* **2010**, *65*, 713 – 716.
[9] R. G. Wunderink, M. S. Niederman, M. H. Kollef, A. F. Shorr, M. J. Kunkel, A. Baruch, W. T. Mcgee, A. Reisman, J. Chastr, *Clin. Infect. Dis.* **2012**, *54*, 621 – 629.
[10] R. J. Fair, Y. Tor, *Perspect. Medicin. Chem.* **2014**, *6*, 25 – 64.
[11] R. Maviglia, R. Nestorini, M. Pennisi, *Curr. Drug. Targets.* **2009**, *10*, 895 – 905.
[12] R. I. Aminov, *Front. Microbiol.* **2010**, *1*, 134.
[13] N. Mookherjee, R. E. W. Hancock, *Cell. Mol. Life Sci.* **2007**, *64*, 922 – 933.
[14] A. T. Y. Yeung, S. L. Gellatly, R. E. W. Hancock, *Cell. Mol. Life Sci.* **2011**, *68*, 2161 – 2176.
[15] R. E. Hancock, *Lancet Infect. Dis.* **2001**, *1*, 156 – 164.
[16] G. Wang, *Methods Mol. Biol.* **2015**, *1268*, 43 – 66.
[17] M. Mahlapuu, J. Håkansson, L. Ringstad, C. Björn, *Front. Cell. Infect. Microbiol.* **2016**, *6*, 194.
[18] D. Heimlich, A. Harrison, K. Mason, *Antibiotics (Basel)* **2014**, *3*, 645 – 676.
[19] G. Diamond, N. Beckloff, A. Weinberg, K. Kisich, *Curr. Pharm. Des.* **2009**, *15*, 2377 – 2392.
[20] R. E. W. Hancock, H. G. Sahl, *Nat. Biotechnol.* **2006**, *24*, 1551 – 1557.
[21] K. A. Brogden, *Nat. Rev. Microbiol.* **2005**, *3*, 238 – 250.
[22] K. E. Greber, M. G. Dawgul, *Curr. Top. Med. Chem.* **2016**, *17*, 620 – 628.
[23] J. L. Fox, *Nat. Biotechnol.* **2013**, *31*, 379 – 382.
[24] M. L. Mangoni, A. C. Rinaldi, A. D. Giulio, G. Mignogna, A. Bozzi, D. Barra, M. Simmaco, *Eur. J. Biochem.* **2000**, *267*, 1447 – 1454.
[25] M. L. Mangoni, *Cell. Mol. Life Sci.* **2006**, *63*, 1060 – 1069.
[26] M. L. Mangoni, Y. Shai, *Biochim. Biophys. Acta.* **2009**, *1788,* 1610 – 1619.
[27] A. C. Rinaldi, M. L. Mangoni, A. Rufo, C. Luzi, D. Barra, H. Zhao, P. K. Kinnunen, A. Bozzi, A. D. Giulio, M. Simmaco, *Biochem. J.* **2002**, *368*, 91 – 100.
[28] Y. Chen, C. T. Mant, S. W. Farmer, R. E. W. Hancock, M. L. Vasil, R. S. Hodges, *J. Biol. Chem.* **2005**, *280*, 12316 – 12329.
[29] A. Carotenuto, S. Malfi, M. R. Saviello, P. Campiglia, I. Gomez-Monterrey, M. L. Mangoni, L. M. Gaddi, E. Novellino, P. Grieco, *J. Med. Chem.* **2008**, *51*, 2354 – 2362.
[30] M. R. Saviello, S. Malfi, P. Campiglia, A. Cavalli, P. Grieco, E. Novellino, A. Carotenuto, *Biochemistry* **2010**, *49*, 1477 – 1485.
[31] F. Merlino, A. Carotenuto, B. Casciaro, F. Martora, M. R. Loffredo, R. Di Grazia, A. M. Yousif, D. Brancaccio, L. Palomba, E. Novellino, M. Galdiero, M. R. Iovene, M. L. Mangoni, P. Grieco, *Eur. J. Med. Chem.* **2017**, *139*, 750 – 761.
[32] P. Grieco, V. Luca, L. Auriemma, A. Carotenuto, M. R. Saviello, P. Campiglia, D. Barra, E. Novellino, M. L. Mangoni, *J. Pept. Sci.* **2011**, *17*, 358 – 365.
[33] P. Grieco, A. Carotenuto, L. Auriemma, A. Limatola, S. Di Maro, F. Merlino, M. L. Mangoni, V. Luca, A. Di Grazia, S. Gatti, P. Campiglia, I. Gomez-Monterrey, E. Novellino, A. Catania, *PLoS One* **2013**, *8*, e61614.
[34] A. Micsonai, F. Wien, L. Kernya, Y. H. Lee, Y. Goto, M. Refrégiers, J. Kardos, *Proc. Natl. Acad. Sci. USA* **2015**, *112*, 3095 – 3103.
[35] M. L. Mangoni, A. Carotenuto, L. Auriemma, M. R. Saviello, P. Campiglia, I. Gomez-Monterrey, S. Malfi, L. Marcellini, D. Barra, E. Novellino, P. Grieco, *J. Med. Chem.* **2011**, *54*, 1298 – 1307.
[36] M. Lindberg, J. Jarvet, U. Langel, A. Gräslund, *Biochemistry* **2001**, *40*, 3141 – 3149.
[37] Y. Rosenfeld, D. Barra, M. Simmaco, Y. Shai, M. L. Mangoni, *J. Biol. Chem.* **2006**, *281*, 28565 – 28574.
[38] P. Grieco, A. Carotenuto, L. Auriemma, M. R. Saviello, P. Campiglia, I. Gomez-Monterrey, L. Marcellini, V. Luca, D. Barra, E. Novellino, M. L. Mangoni, *Biochim. Biophys. Acta.* **2013**, *1828*, 652 – 660.
[39] K. Wütrich in *NMR of Proteins and Nucleic Acids*, John Wiley & Sons, New York, **1986**.
[40] J. S. Weese, E. van Duijkeren, *Vet. Microbiol.* **2010**, *140*, 418 – 429.
[41] U. Piantini, O. W. Soerensen, R. R. Ernst, *J. Am. Chem. Soc.* **1982**, *104*, 6800 – 6801.
[42] D. Marion, K. Wüthrich, *Biochem. Biophys. Res. Commun.* **1983**, *113*, 967 – 974.
[43] L. Braunschweiler, R. R. Ernst, *J. Magn. Reson.* **1983**, *53*, 521 – 528.
[44] J. Jeener, B. H. Meier, P. Bachmann, R. R. Ernst, *J. Chem. Phys.* **1979**, *71*, 4546 – 4553.
[45] D. J. States, R. A. Haberkorn, D. J. Ruben, *J. Magn. Reson.* **1982**, *48*, 286 – 292.
[46] T. L. Hwang, A. J. Shaka, *J. Magn. Reson.* **1995**, *112*, 275 – 279.
[47] F. Delaglio, S. Grzesiek, G. W. Vuister, G. Zhu, J. Pfeifer, A. Bax, *J. Biomol. NMR* **1995**, *6*, 277 – 293.
[48] C. Bartels, T. H. Xia, M. Billeter, P. Güntert, K. Wüthrich, *J. Biomol. NMR* **1995**, *6*, 1 – 10.
[49] P. Güntert, L. Buchner, *J. Biomol. NMR* **2015**, *62*, 453 – 471.
[50] J. R. Maple, U. Dinur, A. T. Hagler, *Proc. Natl. Acad. Sci. USA* **1988**, *85*, 5350 – 5354.
[51] E. F. Pettersen, T. D. Goddard, C. C. Huang, G. S. Couch, D. M. Greenblatt, E. C. Meng, T. E. Ferrin, *J. Comput. Chem.* **2004**, *25*, 1605 – 1612.

Manuscript received: April 8, 2019
Revised manuscript received: May 12, 2019
Accepted manuscript online: May 14, 2019
Version of record online: June 3, 2019

toxins

MDPI

Article

Nigritanine as a New Potential Antimicrobial Alkaloid for the Treatment of *Staphylococcus aureus*-Induced Infections

Bruno Casciaro [1], Andrea Calcaterra [2], Floriana Cappiello [3], Mattia Mori [4], Maria Rosa Loffredo [3], Francesca Ghirga [1,*], Maria Luisa Mangoni [3,*], Bruno Botta [2] and Deborah Quaglio [2]

1 Center For Life Nano Science@Sapienza, Istituto Italiano di Tecnologia, Viale Regina Elena 291, 00161 Rome, Italy
2 Department of Chemistry and Technology of Drugs, "Department of Excellence 2018–2022", Sapienza University of Rome, P.le Aldo Moro 5, 00185 Rome, Italy
3 Laboratory affiliated to Pasteur Italia-Fondazione Cenci Bolognetti, Department of Biochemical Sciences, Sapienza University of Rome, P.le Aldo Moro 5, 00185 Rome, Italy
4 Department of Biotechnology, Chemistry and Pharmacy, "Department of Excellence 2018–2022", University of Siena, via Aldo Moro 2, 53100 Siena, Italy
* Correspondence: francesca.ghirga@iit.it (F.G.); marialuisa.mangoni@uniroma1.it (M.L.M.)

Received: 24 July 2019; Accepted: 30 August 2019; Published: 1 September 2019

Abstract: *Staphylococcus aureus* is a major human pathogen causing a wide range of nosocomial infections including pulmonary, urinary, and skin infections. Notably, the emergence of bacterial strains resistant to conventional antibiotics has prompted researchers to find new compounds capable of killing these pathogens. Nature is undoubtedly an invaluable source of bioactive molecules characterized by an ample chemical diversity. They can act as unique platform providing new scaffolds for further chemical modifications in order to obtain compounds with optimized biological activity. A class of natural compounds with a variety of biological activities is represented by alkaloids, important secondary metabolites produced by a large number of organisms including bacteria, fungi, plants, and animals. In this work, starting from the screening of 39 alkaloids retrieved from a unique *in-house* library, we identified a heterodimer β-carboline alkaloid, nigritanine, with a potent anti-*Staphylococcus* action. Nigritanine, isolated from *Strychnos nigritana*, was characterized for its antimicrobial activity against a reference and three clinical isolates of *S. aureus.* Its potential cytotoxicity was also evaluated at short and long term against mammalian red blood cells and human keratinocytes, respectively. Nigritanine showed a remarkable antimicrobial activity (minimum inhibitory concentration of 128 μM) without being toxic in vitro to both tested cells. The analysis of the antibacterial activity related to the nigritanine scaffold furnished new insights in the structure–activity relationships (SARs) of β-carboline, confirming that dimerization improves its antibacterial activity. Taking into account these interesting results, nigritanine can be considered as a promising candidate for the development of new antimicrobial molecules for the treatment of *S. aureus*-induced infections.

Keywords: natural products; alkaloids; plant secondary metabolites; β-carboline; *Staphylococcus aureus*; antimicrobial activity; cytotoxicity

Key Contribution: Starting from the screening of 39 alkaloids, we biologically characterized a heterodimer β-carboline alkaloid, named nigritanine, with potent anti-*Staphylococcus* activity and non-toxic to mammalian red blood cells and human keratinocytes at its bioactive concentration.

This manuscript is dedicated to the memory of Professor Maurizio Botta (University of Siena, Department of Biotechnology, Chemistry and Pharmacy) who prematurely passed away on 2 August 2019. During his successfully scientific career, he synthesized a huge number of small bioactive molecules for the development of new pharmaceutical agents for cancer therapy and/or treatment of microbial infections, thus providing an invaluable contribution in the field of medicinal chemistry and drug discovery, worldwide.

1. Introduction

The discovery of antibiotics in the 1900s led to a medical revolution in the fight against bacterial infections. However, during the years, bacteria have developed different mechanisms to resist the killing activity of antibiotics [1]. The human pathogen *Staphylococcus aureus* is a microorganism with high adaptability and tenacity, as highlighted by its abundance in the environment and in the normal flora, the variety of virulence factors that it produces, and the capability to colonize various human organs such as nose, pharynx, and skin [2–4]. Furthermore, multidrug-resistant *S. aureus* is one of the major microorganisms causing bloodstream infections associated with high levels of morbidity and mortality worldwide [5]. Considering that *S. aureus* has successfully evolved numerous strategies to resist the activity of practically all antibiotics, new alternative compounds able to defeat *S. aureus*-induced infections are urgently needed [6]. Notably, a significant portion of the commercial drugs occurs in nature or is derived from natural products by means of chemical transformations or de novo synthesis [7]. Alkaloids are a group of important secondary metabolites which are produced by a wide variety of organisms including bacteria, fungi, plants, and animals. Chemically, alkaloids are a large and structurally diverse group of nitrogen-containing compounds (one or more nitrogen atoms within a heterocycle ring) [8]. Alkaloids can occur as monomers, dimers (bisalkaloids), trimers, or tetramers. According to their chemical structure, alkaloids are classified in heterocyclic alkaloids (also known as typical alkaloids), containing nitrogen in the heterocycle and originating from amino acids, and nonheterocyclic alkaloids (also known as atypical or proto-alkaloids), containing a nitrogen atom derived from an amino acid which is not a part of the heterocyclic ring [9]. Heterocyclic alkaloids are divided according to their ring structure in several classes of monomeric alkaloids (e.g., pyrrole, pyrrolidine, pyridine, piperidine, indole, quinoline, isoquinoline alkaloids). Since 1940, large-scale efforts have been made to evaluate the antibacterial effects of naturally occurring alkaloids. Several potent monomer and dimer alkaloids were identified, and synthetic modifications were investigated to improve their biological activity [8–11]. However, a tremendously wide discrepancy between their historical significance and their occurrence in modern drug development exists, and no alkaloids are available in the market as antibacterial drugs [12]. In this work, an in-house library of about 1000 natural products and their derivatives was used as a unique source of lead compounds to identify new potential antibacterial alkaloids. From the screening of all the alkaloids present in this library, the rare β-carboline heterodimer nigritanine was identified and showed a potent antistaphylococcal activity. Therefore, it was thoroughly characterized for its antimicrobial and cytotoxic activities.

2. Results and Discussion

2.1. Alkaloids Collection

Natural products remain the most productive source of leads in antibacterial drug discovery, often providing novel mechanism(s) and chemical structures as useful platforms for the development of drugs. A unique in-house library of about 1000 natural compounds, mostly isolated from several plants used in traditional medicine of South America and collected over the years, is available at the Organic Chemistry Laboratory of the Department of Chemistry and Technology of Drugs (Sapienza University of Rome, Italy). This library consists of natural products belonging to different classes of organic compounds which were previously published and fully characterized [13,14]. It was then enlarged by the addition of other natural small molecules from commercially available sources and

synthetic or semi-synthetic derivatives. Currently, all components of our collection are incorporated into a virtual library, and their chemical and physicochemical features are analyzed by means of cheminformatics tools, showing a satisfactory chemical diversity. Therefore, our *in-house* library is a valid source of chemotypes for the modulation of biomolecular targets, and it was successfully screened in silico and in vitro for the identification of hit and lead compounds in previous early-stage drug discovery projects [15]. One of the largest and most intriguing classes of natural occurring compounds within the library are the alkaloids, which consist of isoquinoline (**1**–**11**), quinoline (**12**–**15**), and indole (**16**–**39**) alkaloids (Table 1).

Table 1. List of alkaloids tested in this study.

Mol.	Common Name	Chemical Structure	M.W.	Molecular Formula	Source	Ref.
		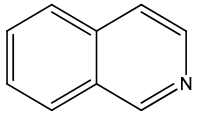 Isoquinoline Alkaloids				
1	Dihydroberberine·HCl	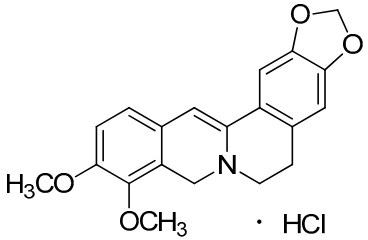	337.37 373.83 (+ HCl)	$C_{20}H_{19}NO_4$·HCl	*Berberis* species: *Berberis aristata, Berberis lyceum, Berberis petiolaris, Berberis tinctoria* (Berberidaceae family)	[16]
2	Bulbocapnine·HCl	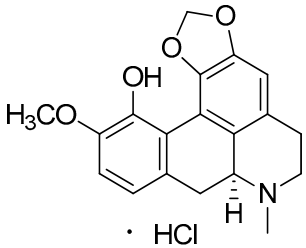	325.36 361.82 (+ HCl)	$C_{19}H_{19}NO_4$·HCl	Species: *Corydalis cava* (Papaveraceae family)	[17]
3	Boldine	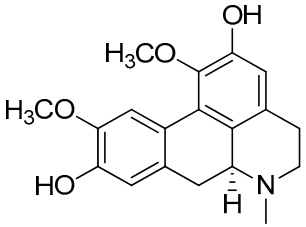	327.37	$C_{19}H_{21}NO_4$	Species: *Peumus boldus* (Monimiaceae family)	[18]

Table 1. *Cont.*

Mol.	Common Name	Chemical Structure	M.W.	Molecular Formula	Source	Ref.
4	Cotarmine·HCl	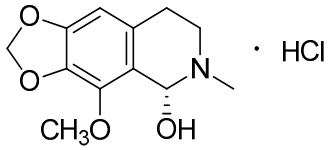	237.25 273.71	$C_{12}H_{15}NO_4$·HCl	Synthetic	[19]
5	Chelidonine	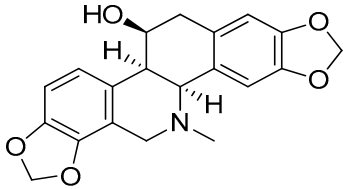	353.37	$C_{20}H_{19}NO_5$	Species: *Chelidonium majus* L. (Papaveraceae family)	[20]
6	Emetine·HCl	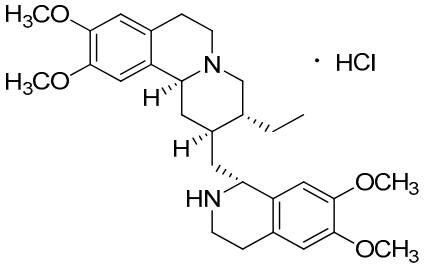	480.64 517.10 (+HCl)	$C_{29}H_{40}N_2O_4$	Species: *Psychotria ipecacuanha* Stokes (Rubiaceae family)	[21]
7	(*S*)-Glaucine	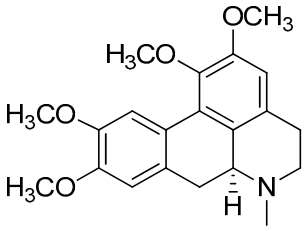	355.43	$C_{21}H_{25}NO_4$	Species: *Glaucium luteum* L. (Papaveraceae family)	[22]

Table 1. *Cont.*

Mol.	Common Name	Chemical Structure	M.W.	Molecular Formula	Source	Ref.
8	Hydrastine	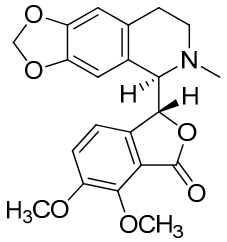	383.39	$C_{21}H_{21}NO_6$	Species: *Hydrastis canadensis* L. (Ranunculaceae family)	[23]
9	Noscapine (Narcotine)	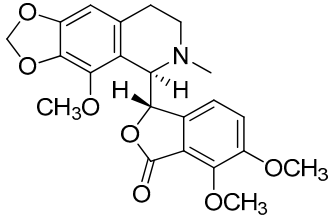	413.42	$C_{22}H_{23}NO_7$	Species: *Papaver somniferum* (Papaveraceae family)	[24]
10	Papaverine	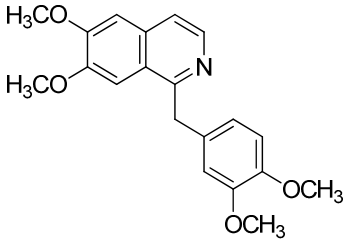	339.39	$C_{20}H_{21}NO_4$	Species: *P. somniferum* (Papaveraceae family)	[24]
11	Tubocurarine Chloride·HCl	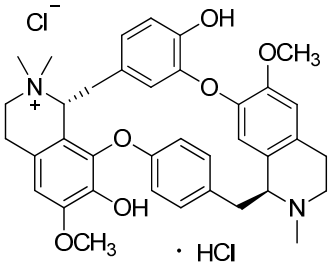	609.73 681.65 (+Cl^-+HCl)	$C_{37}H_{41}N_2O_6$·HCl + Cl^-	Species: *Liana Chondrodendron* (Menispermaceae family)	[25]

Table 1. *Cont.*

Mol.	Common Name	Chemical Structure	M.W.	Molecular Formula	Source	Ref.
12	Cinchonine	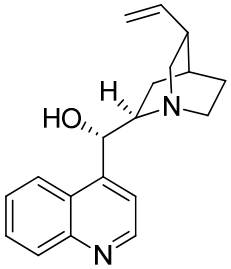	294.39	$C_{19}H_{22}N_2O$	Species: *Cinchona ledgeriana*, *Remijia peruviana* (Rubiaceae family)	[26]
13	Kokusaginine	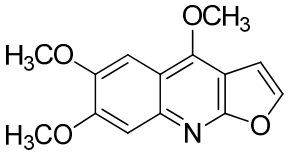	259.26	$C_{14}H_{13}NO_4$	Species: *Esenbeckia leiocarpa* (Rutaceae family)	[27]
14	Maculine	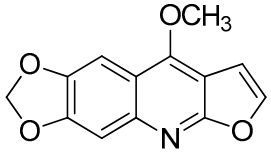	243.21	$C_{13}H_9NO_4$	Species: *E. leiocarpa* (Rutaceae family)	[27]
15	4-methoxy-2-(1-ethylpropyl)-quinoline	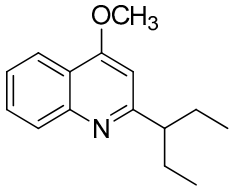	229.32	$C_{15}H_{19}NO$	Species: *E. leiocarpa* (Rutaceae family)	[27]
		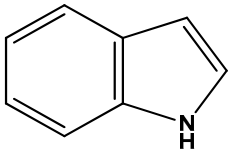				
		Indole Alkaloids				

Table 1. *Cont.*

Mol.	Common Name	Chemical Structure	M.W.	Molecular Formula	Source	Ref.
16	Aspidospermine	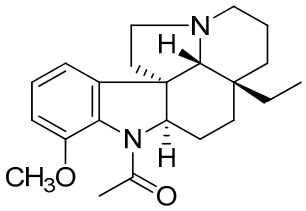	354.49	$C_{22}H_{30}N_2O_2$	*Aspidosperma* species: *Aspidosperma album*, *Aspidosperma australe*, *Aspidosperma exalatum*, *Aspidosperma peroba*, *Aspidosperma polyneuron*, *Aspidosperma pyricollum*, *Aspidosperma pyrifolium*, *Aspidosperma quebracho-blanco*, *Aspidosperma quirandy*, *Aspidosperma sessiflorum*, *Aspidosperma rhombeosignatum* (Apocynaceae family)	[28]
17	Brucine	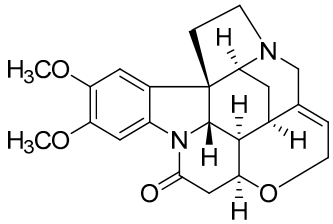	394.47	$C_{23}H_{26}N_2O_4$	Species: *Strychnos nux-vomica* (Apocynaceae family)	[29]
18	Diaboline	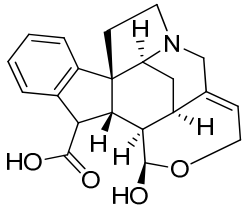	353.41	$C_{21}H_{23}NO_4$	Species: *Strychnos castelneana* (Loganiaceae family)	[27]
19	Physostigmine (Eserine)	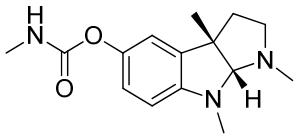	275.35	$C_{15}H_{21}N_3O_2$	*Physostigma venenosum* (Fabaceae family)	[30]

Table 1. *Cont.*

Mol.	Common Name	Chemical Structure	M.W.	Molecular Formula	Source	Ref.
20	Holstiine	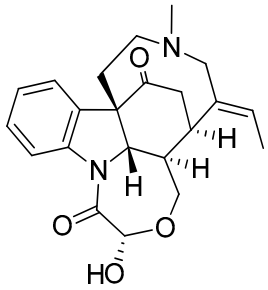	382.45	$C_{22}H_{26}N_2O_4$	Species: *Strychnos henningsii* Gilg (Loganiaceae family)	[31]
21	Pseudobrucine	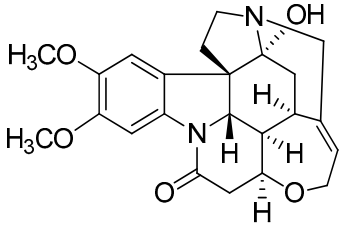	410.46	$C_{23}H_{26}N_2O_5$	Species: *S. nux-vomica* (Loganiaceae family)	[29]
22	Retuline	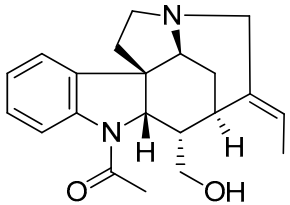	338.44	$C_{21}H_{26}N_2O_2$	*Strychnos* species: *Strychnos camptoneura*, *S. henningsii* (Loganiaceae family)	[31]
23	Serotonin	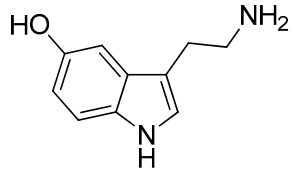	176.22	$C_{10}H_{12}N_2O$	Species: *Laphophora williamsii* (Cactaceae family)	[32]

Table 1. *Cont.*

Mol.	Common Name	Chemical Structure	M.W.	Molecular Formula	Source	Ref.
24	Triptamine·HCl	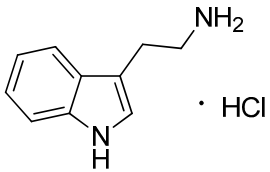	160.22 196.68 (+HCl)	$C_{10}H_{12}N_2$ HCl	*Acacia* species (Fabacee family)	[33]
25	Vomicine·HC1	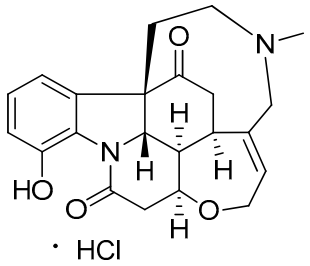	380.44 416.90 (+HCl)	$C_{22}H_{24}N_2O_4$ HCl	*Strychnos icaja* (Loganiaceae family)	[27,31]
26	Vindoline	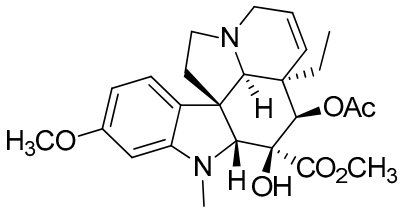	456.53	$C_{25}H_{32}N_2O_6$	*Catharanthus roseus* (Apocynaceae family)	[34]
		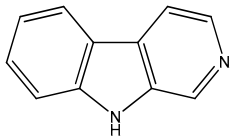				
		Carboline Alkaloids (Indole Subclass)				

Table 1. *Cont.*

Mol.	Common Name	Chemical Structure	M.W.	Molecular Formula	Source	Ref.
27	Akagerine	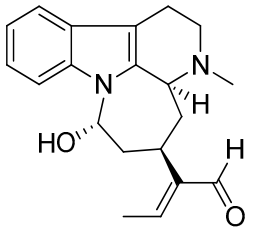	324.42	$C_{20}H_{24}N_2O_2$	*Strychnos* species: *Strychnos barteri* Solered, *S. camptoneurine*, *Strychnos nigritana* Bak (Loganiaceae family)	[31]
28	Canthin-6-one	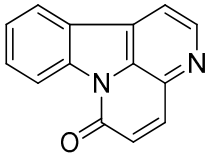	220.23	$C_{14}H_8N_2O$	Species: *Simaba ferruginea* (Simaroubaceae family)	[35]
29	α-Carboline	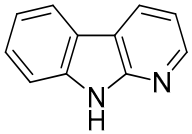	168.19	$C_{11}H_8N_2$	Synthetic	[36]
30	Harmane	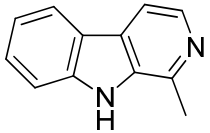	182.22	$C_{12}H_{10}N_2$	Species: *Chimarrhis turbinata*, *Ophiorrhiza communis*, *Ophiorrhiza liukiuensis*, *Ophiorrhiza tomentosa*, *Psychotria barbiflora* (Rubiaceae family)	[26]
31	Norharmane	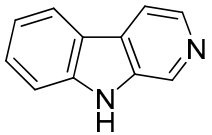	168.19	$C_{11}H_8N_2$	Species: *Hygrophorus eburneus* (Tricholomataceae family)	[37]

Table 1. *Cont.*

Mol.	Common Name	Chemical Structure	M.W.	Molecular Formula	Source	Ref.
32	Harmine	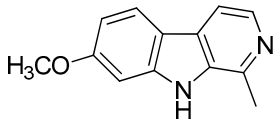	212.25	$C_{13}H_{12}N_2O$	Species: *Banisteriopsis caapi* (Malpighiaceae family), *Grewia bicolor* (Malvaceae family), *Passiflora edulis* f. *flavicarpa* O. Deg., *Passiflora incarnata* L. (Passifloraceae family), *Tribulus terrestris* L., *Peganum harmala* L. (Zygophyllaceae family)	[37]
33	Ibogaine	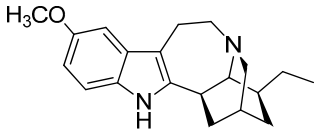	310.43	$C_{20}H_{26}N_2O$	Species: *Tabernanthe iboga* (Apocynaceae family)	[38]
34	Mitragynine	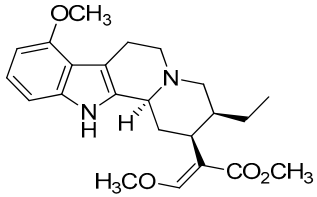	398.50	$C_{23}H_{30}N_2O_4$	Species: *Mitragyna speciosa* (Rubiaceae family)	[39]
35	Nigritanine	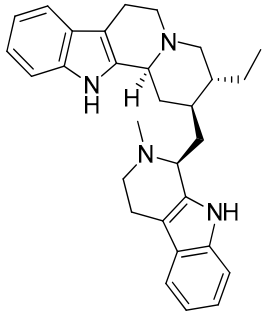	452.63	$C_{30}H_{36}N_4$	*Strychnos* species: *Strychnos borteri*, *S. nigritana* Bak. (Loganiaceae family)	[31]

Table 1. *Cont.*

Mol.	Common Name	Chemical Structure	M.W.	Molecular Formula	Source	Ref.
36	Paynantheine	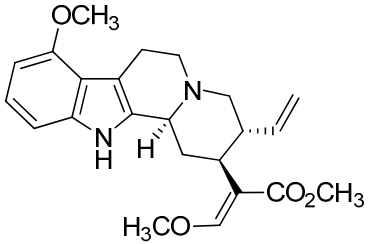	396.48	$C_{23}H_{28}N_2O_4$	Species: *M. speciosa* (Rubiaceae family)	[40]
37	Rhynchophylline	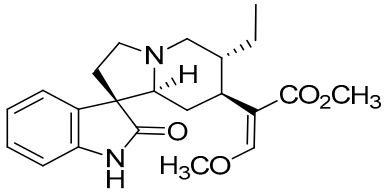	384.47	$C_{22}H_{28}N_2O_4$	Species: *M. speciosa*, *Uncaria rhynchophylla* (Rubiaceae family)	[40]
38	Speciociliatine	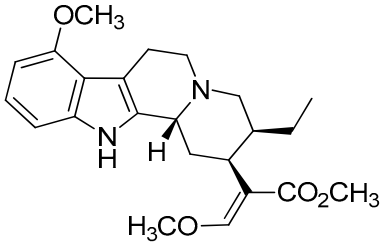	398.50	$C_{23}H_{30}N_2O_4$	Species: *M. speciosa* (Rubiaceae family)	[41]
39	Yohimbine·HCl	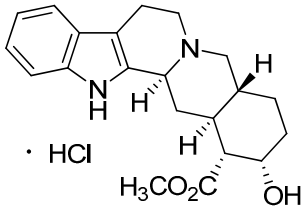	354.44 390.90 (+HCl)	$C_{21}H_{26}N_2O_3$ HCl	*Apocynaceae* species: *Aspidosperma discolor* A. DC., *Aspidosperma excelsum* Benth, *Aspidosperma eburneum* F. Allem, *Aspidosperma marcgravianum* Woodson, *Aspidosperma oblongum* A. DC.	[37]

Mol.: molecule number; M.W.: molecular weight; Ref.: references.

Considering the chemical structures of isoquinoline alkaloids, this group can be divided in two major categories: simple isoquinolines, which are composed of a benzene ring fused to a pyridine ring, and benzylisoquinolines, which contain a second aromatic ring [42]. In contrast, indole alkaloids are bicyclic structures consisting of a six-membered benzene ring fused to a five-membered nitrogen-containing pyrrole ring and are among the most numerous (at least 4100 known molecules) and complex alkaloids. In our library, the group of indole alkaloids covers several subclasses, the largest of which is represented by β-carbolines featuring a common tricyclic pyrido[3,4-b]indole ring structure (Table 1). According to the saturation of the N-containing six-membered ring, β-carbolines are categorized in fully aromatic (βCs), dihydro- (DHβCs), and tetrahydro- (THβCs) β-carbolines [43]. Alkaloids from the in-house library belonging to more than 10 plant families (e.g., Apocynaceae, Loganiaceae, Berberidaceae, Papaveraceae, Rubiaceae) are known to occur in several species (Table 1). With the aim to identify new potential antistaphylococcal agents, the in-house library of alkaloids was initially screened towards Gram(+) and Gram(-) reference bacterial strains. For the biological characterization, all the compounds were dissolved in dimethyl sulfoxide (DMSO).

2.2. Antimicrobial Activity

2.2.1. Inhibition Zone Assay

The antimicrobial activity of all collected compounds was initially tested on a reference strain of the Gram(+) *S. aureus* (*S. aureus* ATCC 25923) by the inhibition zone assay. The Gram(-) bacterial strain *Escherichia coli* ATCC 25922 was also included for comparison (Table 2). Most of the compounds resulted to be inactive against both classes of bacteria (data not shown). The only exception was the already characterized methylated derivative of β-carboline, i.e., harmane, which was able to inhibit the growth of both *S. aureus* and *E. coli* strains in an agar diffusion assay [44–46], with diameters of the inhibition zone of 4.36 and 8.46 mm, respectively (Table 2).

Table 2. Diameters of the inhibition zone of all the active tested compounds against the reference Gram(+) and Gram(-) bacterial strains.

Inhibition Zone Assay	**Diameter of Inhibition Zone (mm)** [1]	
Compound	**Gram-Positive *Staphylococcus aureus* ATCC 25923**	**Gram-Negative *Escherichia coli* ATCC 25922**
Dihydroberberine·HCl (**1**)	7.800	n.a.
(*S*)-Glaucine (**7**)	7.600	n.a.
Canthin-6-one (**28**)	6.100	n.a.
Harmane (**30**)	4.360	8.640
Harmine (**32**)	n.a.	6.250
Mytragine (**34**)	5.420	n.a.
Nigritanine (**35**)	10.39	n.a.
Paynantheine (**36**)	8.440	n.a.
Speciociliatine (**38**)	8.240	n.a.

[1] Data represent the mean of three independent experiments with standard deviation (SD) not exceeding 0.2; n.a.: not active.

Interestingly, a greater selectivity towards the human pathogen *S. aureus* was noted, especially for the β-carboline alkaloids. In fact, the rare heterodimer alkaloid nigritanine (compound **35**) as well as some of its analogues (i.e., speciociliatine, mytragine, and paynantheine) showed a powerful activity against the reference strain of *S. aureus* ATCC 25923, with a diameter of growth inhibition zone ranging from 8.24 to 10.39 mm. Mytragine was previously characterized for its selective anti-Gram(+) efficacy [47]; in contrast, no microbiological data have been provided so far for speciociliatine, paynantheine, and rhyncophylline. Because of these reasons, we decided to examine the activity of nigritanine, mytragine, and the other three abovementioned molecules against three multidrug-resistant

clinical isolates of *S. aureus*. As reported in Table 3, nigritanine was the sole compound that retained a potent activity against the clinical isolates of *S. aureus* (i.e., *S. aureus* 1a, 1b, 1c). This was indicated by the similar diameters of inhibition zones. In contrast, all the others molecules completely or almost completely lost their activity towards *S. aureus* 1a, 1b, and 1c strains.

Table 3. Diameters of the inhibition zone of some active alkaloids against the reference and clinical isolates of *S. aureus* strains.

Inhibition Zone Assay	**Diameter of Inhibition Zone (mm)** [1]			
Compound	***S. aureus* ATCC 25923**	***S. aureus* 1a**	***S. aureus* 1b**	***S. aureus* 1c**
Mytragine (**34**)	5.420	4.000	n.a.	n.a.
Nigritanine (**35**)	10.39	11.20	8.440	9.100
Paynantheine (**36**)	8.440	3.800	n.a.	n.a.
Speciociliatine (**38**)	8.240	4.520	4.340	4.580

[1] Data represent the mean of three independent experiments with SD not exceeding 0.2.

A representative image of the antibacterial activity of these compounds is shown in Figure 1. The growth inhibition zone of nigritanine (zone #1) is clearly evident compared to that of the other alkaloids tested. These results are in line with other published data of alkaloids extracted from *Anabasis articulata*, showing a potent anti-Gram(+) activity when evaluated by the inhibition zone assay [48].

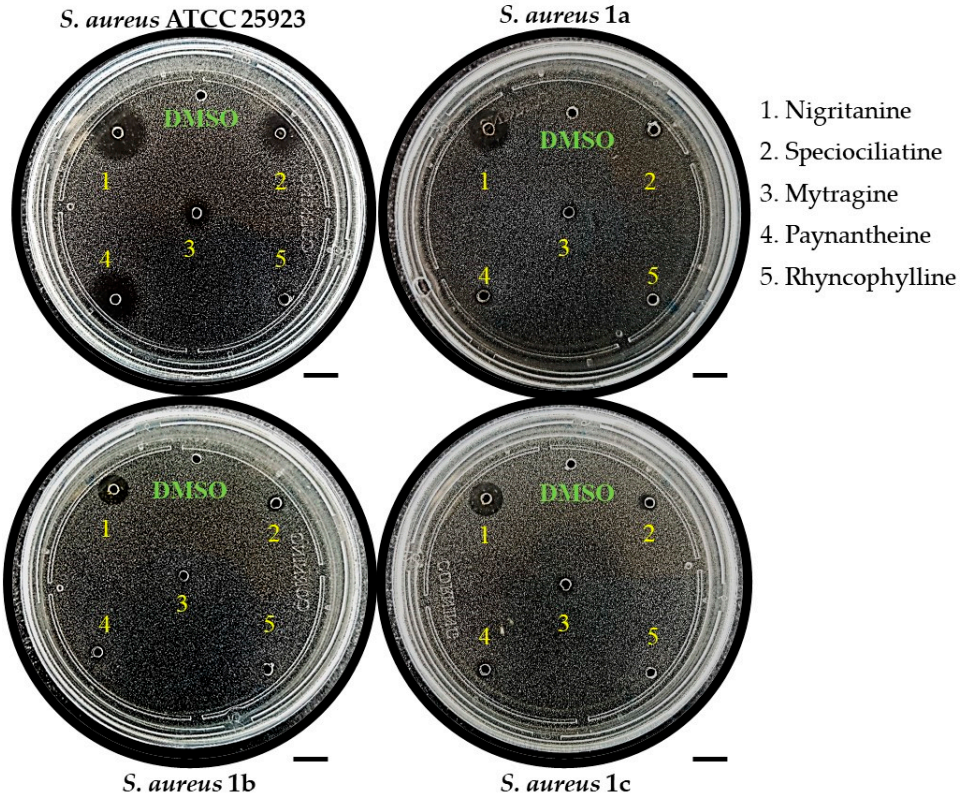

Figure 1. Representative image of the inhibition zone assays of nigritanine (**35**) and some other alkaloids against the reference strain and the three clinical isolates of *S. aureus*. Scale bars represent 1 cm.

2.2.2. Determination of the Minimum Inhibitory Concentration

The antibacterial activity of nigritanine, speciociliatine, mytragine, paynantheine, and rhyncophylline was also evaluated by the microdilution broth assay to determine the minimum inhibitory concentration (MIC) against the reference strain of *S. aureus* and the three clinical isolates after 16 hours of treatment

(Table 4). Remarkably, although the MIC of nigritanine against the reference strain of *S. aureus* was higher than the MIC of other alkaloids reported in the literature (i.e., 128 μM, 56.5 μg/mL versus 2–16 μg/mL for vincamine, atropine, allantoin, or trigonelline [49]), the ability to inhibit the growth of the clinical isolates was maintained at the same concentration of 128 μM. This is in contrast with what observed for the aforementioned compounds which completely lost activity when tested against clinical isolates [49]. Similar MIC values were also obtained with alkaloids from leaves of *Eclipta alba* [50].

Table 4. Minimum inhibitory concentration (MIC) (μM) of nigritanine, speciociliatine, mytragine, paynantheine, and rhyncophylline against the reference and clinical isolates of *S. aureus* strains. MICs are the values obtained from three identical readings out of four independent experiments.

Strains	Nigritanine	Speciociliatine	Mytragine	Paynantheine	Rhyncophylline
S. aureus ATCC 25923	128 μM	> 256 μM	> 256 μM	> 256 μM	> 256 μM
S. aureus 1a	128 μM	> 256 μM	> 256 μM	> 256 μM	> 256 μM
S. aureus 1b	128 μM	> 256 μM	> 256 μM	> 256 μM	> 256 μM
S. aureus 1c	128 μM	> 256 μM	> 256 μM	> 256 μM	> 256 μM

Notably, the MICs of nigritanine were found to correspond to the minimum bactericidal concentration (MBC) which is defined as the minimum concentration of drug causing ≥3 log killing of bacteria after 16 hours of incubation. Indeed, about five log reduction in the number of viable cells of the reference and clinical isolates of *S. aureus* were detected after treatment with nigritanine at its MIC (i.e., 128 μM) (Figure 2). Note that other plant alkaloid extracts had similar or even higher MIC and MBC values against *S. aureus* and other Gram(+) bacterial strains. For example, alkaloid extracts from the aerial part of *Sida acuta* gave MIC and MBC values ranging from 80 to >400 μg/mL against *Staphylococcus* strains [51], while the MIC of alkaloid extracts of *Mahonia aquifolium* ranged from 100 to 500 μg/mL against *Staphylococcus epidermidis* and *Staphylococcus hominis* strains [52]. Very high MIC values (>500 μg/mL) were obtained with alkaloids isolated from aerial parts of *Hypecoum erectum* L. (i.e., protopine and allocryptopine) against *S. aureus*, *Bacillus cereus*, and *Bacillus subtilis* strains [53]. Since alkaloids extracts with MICs ranging from 100 to 1000 μg/mL are considered to be compounds endowed with antimicrobial activity [54,55], nigritanine (MIC = 56.5 μg/mL) would represent a highly potential antimicrobial molecule.

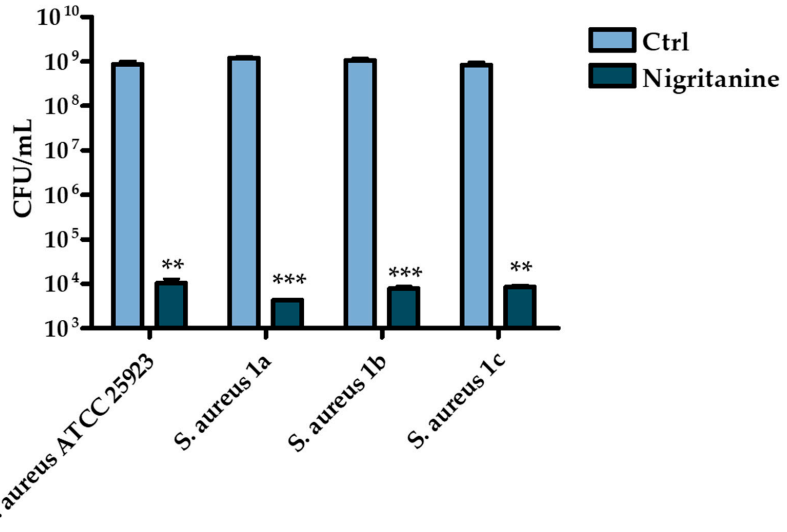

Figure 2. Reduction in the number of viable bacterial cells (evaluated by colony forming unit (CFU) counting) of the reference and clinical isolates of *S. aureus* strains after 16 hours treatment with nigritanine at the MIC (128 μM) compared to control (Ctrl) samples consisting in vehicle-treated bacterial cells. The data represent the mean of three independent experiments ± SD. The levels of statistical significance versus the Ctrl samples were $p < 0.01$ (**); $p < 0.001$ (***).

2.3. Structure–Activity Relationships (SARs) of Nigritanine for Its Antibacterial Activity

Taking into account all these microbiological data, the new β-carboline alkaloid nigritanine (**35**) emerged as a promising antibacterial agent against *S. aureus*. Nigritanine is a rare β-carboline heterodimer from different African *Strichnos* species. In particular, the interest for the *Strichnos* genus, due to the large variety of alkaloids and their use in traditional medicine, led Nicoletti et al. to isolate compound **35**, along with other alkaloids, from the leaves of *Strichnos nigritana* Bak and from the stem bark of *Strichnos barteri* Solered, two species rather common in West Africa. From a chemical standpoint, nigritanine is a heterodimer alkaloid formed by the union of a corynane (Figure 3a) and a tryptamine unit. Interestingly, this corynane heterodimer displays a substantially higher antibacterial activity than the monomeric analogs, confirming the trend observed for the β-carboline homodimer [43,56]. The structure–activity relationships (SARs) were investigated for nigritanine (**35**) and its monomeric analogs (Figure 3b). Accordingly, the analysis of the antibacterial activity related to the corynane scaffolds indicated that: (1) the tetrahydro-β-carboline scaffold exhibits good activity; (2) the methoxyl group at C9 position, the double bond at C19–C18, and the stereochemistry of C3 and C20 do not affect the activity; (3) the corynane heterodimer shows a substantially higher activity than the monomeric analogs, highlighting that the presence of the tryptamine unit is essential. Notably, for β-carboline indoles, dimerization improves the antibacterial activity possibly because the larger molecule is less susceptible to bacterial efflux [43].

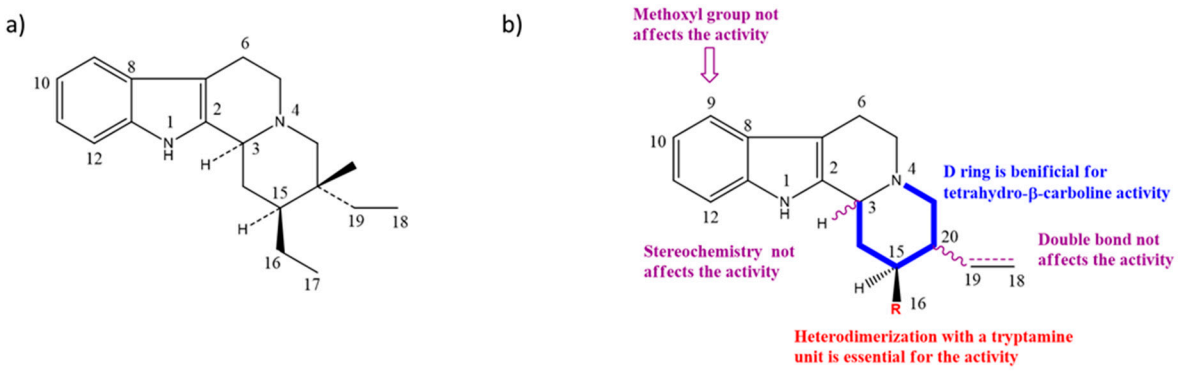

Figure 3. (**a**) Chemical structure of corynane. (**b**) Structure–activity relationship (SARs) analysis of tetrahydro-β-carboline alkaloids with respect to antibacterial activity.

2.4. Cytotoxicity

2.4.1. Hemolytic Assay

The short-term cytotoxic effect of nigritanine was tested against mammalian red blood cells after 40 minutes treatment at its MIC (128 μM), 2 × MIC (256 μM), and 4 × MIC (512 μM). The least active compound speciociliatine was tested at the same concentrations for comparison. As reported in Figure 4, both compounds displayed a weak toxic effect, causing about 30% hemolysis at the highest concentrations, while nigritanine gave rise to about 20% lysis of erythrocytes at its active concentration (128 μM). These results confirmed the potential safety of nigritanine in mammalian cells at a short term.

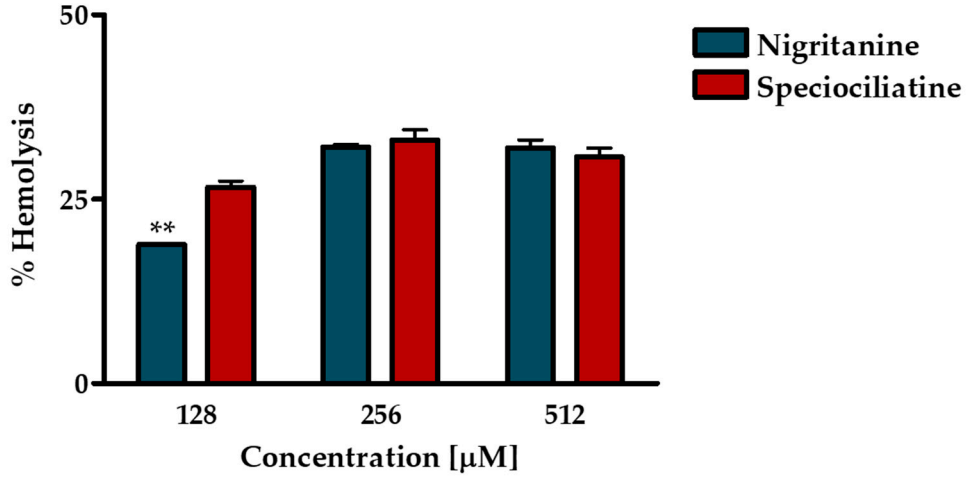

Figure 4. Hemolytic activity of nigritanine at 128 μM (MIC), 256 μM (2 × MIC), and 512 μM (4 × MIC) after 40 minutes of treatment compared to the least active speciociliatine. The data represent the mean ± standard error of the mean (SEM) of three independent experiments. The level of statistical significance between the two compounds was $p < 0.01$ (**).

2.4.2. Cytotoxic Effect on HaCaT Cells

Since the most common site of *S. aureus* infection is the skin, and keratinocytes represent the major cell type in the epidermis [57], the long-term cytotoxic effect of nigritanine was evaluated by the 3-(4,5-dimethylthiazol-2-yl)-2,5-diphenyltetrazolium bromide (MTT) assay on human immortalized keratinocytes (HaCaT) after 24 h treatment. As indicated in Figure 5, nigritanine did not induce any marked reduction in the percentage of viable keratinocytes after 24 h incubation at a concentration range between 2 μM and 200 μM. Note that other natural alkaloids were cytotoxic at much lower concentrations than 2 μM [49,58,59], which contrasts with the maximum non-toxic concentration tested for nigritanine (200 μM = 88.3 μg/mL). Moreover, the MICs of nigritanine (**35**) against reference and clinical isolates of *S. aureus* were equal to 128 μM. These results support the use of this compound as an antibacterial agent harmless to mammalian cells at its active antibacterial concentration.

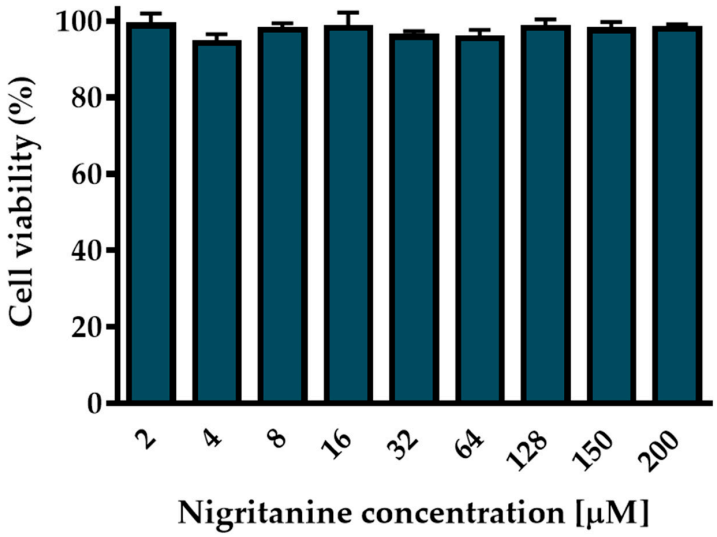

Figure 5. Effect of nigritanine on the viability of HaCaT cells determined by the MTT assay. Cell viability is expressed as a percentage with respect to the control. All data are the means of three independent experiments ± SEM.

3. Conclusions

With the increasing occurrence of multidrug-resistant bacterial infections and the low number of new antimicrobial agents on the market, the discovery of new natural compounds with antibiotic action is extremely necessary. In this work, we characterized the antibacterial profile of the heterodimer alkaloid nigritanine (isolated in the 1980s from *Strychnos* species), against *S. aureus* strains including clinical isolates. Interestingly, nigritanine resulted to have a potent anti-staphylococcal activity without being toxic to mammalian red blood cells and human keratinocytes at its active concentration. More importantly, it retained its antibacterial activity against three multidrug-resistant clinical isolates of *S. aureus*, a feature that was not observed for the other tested carboline alkaloids. Thus, the heterodimer alkaloid nigritanine has emerged as a promising scaffold for the design and development of potent and selective antibacterial compounds with low cytotoxicity.

4. Material and Methods

4.1. Chemistry

All the tested compounds (namely, **1**–**39**) are known structures belonging to our in-house library of natural products. The chemical identity of compounds was assessed by re-running Nuclear magnetic resonance spectroscopy (NMR) experiments and proved to be in agreement with the literature data reported below for each compound. The purity of all compounds, checked by reversed-phase High Performance Liquid Chromatography (HPLC), was always higher than 95%.

Compound **1** (dihydroberberine hydrochloride or 9,10-dimethoxy-6,8-dihydro-5*H*-[1,3]dioxolo[4,5-*g*]isoquinolino[3,2-*a*]isoquinoline hydrochloride) was purchased from Fluka (CAS: 483-15-8, St. Louis, MO, USA) and used without further purification.

Compound **2** (bulbocapnine hydrochloride or (*S*)-11-methoxy-7-methyl-6,7,7a,8-tetrahydro-5*H*-[1,3]dioxolo[4′,5′:4,5]benzo[1,2,3-*de*]benzo[*g*]quinolin-12-ol hydrochloride) was purchased from Sigma-Aldrich (CAS: 632-47-3, St. Louis, MO, USA) and used without further purification.

Compound **3** (boldine or (6a*S*)-1,10-dimethoxy-6-methyl-5,6,6a,7-tetrahydro-4*H*-dibenzo[*de,g*]quinoline-2,9-diol) was purchased from Sigma-Aldrich (CAS: 476-70-0, St. Louis, MO, USA) and used without further purification.

Compound **4** (cotarmine hydrochloride or (*R*)-4-methoxy-6-methyl-5,6,7,8-tetrahydro-[1,3]dioxolo[4,5-*g*]isoquinolin-5-ol) was purchased from MolPort (CAS: 82-54-2, Beacon, NY, USA) and used without further purification.

Compound **5** (chelidonine or (5b*R*,6*S*,12b*S*)-13-Methyl-5b,6,7,12b,13,14-hexahydro[1,3]dioxolo[4′,5′:4,5]benzo[1,2-*c*][1,3]dioxolo[4,5-*i*]phenanthridin-6-ol) was purchased from Sigma-Aldrich (CAS: 476-32-4, St. Louis, MO, USA) and used without further purification.

Compound **6** (emetine hydrochloride or (2*S*, 3 *R*, 11b *S*)-2-(((*R*)-6, 7-dimethoxy-1, 2, 3, 4-tetrahydroisoquinolin-1-yl)methyl)-3-ethyl-9,10-dimethoxy-2,3,4,6,7,11b-hexahydro-1*H*-pyrido[2,1-*a*]isoquinoline hydrochloride) was purchased from MolPort (CAS: 14198-59-5, Beacon, NY, USA) and used without further purification.

Compound **7** ((*S*)-Glaucine or (6a*S*)-1,2,9,10-tetramethoxy-6-methyl-5,6,6a,7-tetrahydro-4*H*-dibenzo[*de,g*]quinoline) was purchased from MolPort (CAS: 475-81-0, Beacon, NY, USA) and used without further purification.

Compound **8** (hydrastine or (*R*)-6,7-dimethoxy-3-((*R*)-6-methyl-5,6,7,8-tetrahydro-[1,3]dioxolo[4,5-g]isoquinolin-5-yl)isobenzofuran-1(3*H*)-one) was purchased from Sigma-Aldrich (CAS: 118-08-1, St. Louis, Mo., USA) and used without further purification.

Compound **9** (noscapine or narcotine or (3*S*)-6,7-dimethoxy-3-((5*R*)-4-methoxy-6-methyl-5,6,7,8,9,9a-hexahydro-[1,3]dioxolo[4,5-*g*]isoquinolin-5-yl)isobenzofuran-1(3*H*)-one) was purchased from Sigma-Aldrich (CAS: 128-62-1, St. Louis, MO, USA) and used without further purification.

Compound **10** (papaverine or (6,7-dimethoxyisoquinolin-1-yl)(3,4-dimethoxyphenyl)methanone) was purchased from MolPort (CAS: 58-74-2, Beacon, NY, USA) and used without further purification.

Compound **11** (tubocurarine chloride hydrochloride or (1*S*,16*R*)-10,25-dimethoxy-15,15,30-trimethyl-7,23-dioxa-30-aza-15-azoniaheptacyclo[22.6.2.2^{3,6}.1^{8,12}.1^{18,22}.0^{27,31}.0^{16,34}]hexatriaconta-3(36),4,6(35),8(34),9,11,18(33),19,21,24,26,31-dodecaene-9,21-diol chloride hydrochloride) showed NMR spectra identical to those reported in the literature [25].

Compound **12** (cinchonine or (*S*)-quinolin-4-yl((1S,2R,4S,5R)-5-vinylquinuclidin-2-yl)methanol) was purchased from Sigma-Aldrich (CAS: 118-10-5, St. Louis, MO, USA) and used without further purification.

Compound **13** (kokusaginine or 4,6,7-trimethoxyfuro[2,3-*b*]quinoline) showed NMR spectra identical to those reported in the literature [27].

Compound **14** (maculine or 9-methoxy-[1,3]dioxolo[4,5-*g*]furo[2,3-*b*]quinoline) showed NMR spectra identical to those reported in the literature [27].

Compound **15** (4-methoxy-2-(1-ethylpropyl)-quinoline) showed NMR spectra identical to those reported in the literature [27].

Compound **16** (aspidospermine or 1-((3a*R*,5a*R*,10b*R*,12b*R*)-3a-Ethyl-7-methoxy-2,3,3a,5,5a,11,12,12b-octahydro-1*H*,4*H*-6,12a-diaza-indeno[7,1-*cd*]fluoren-6-yl)-ethanone) showed NMR spectra identical to those reported in the literature [28].

Compound **17** (brucine or (4a*R*,5a*S*,8a*R*,15b*R*)-10,11-dimethoxy-4a,5,5a,7,8,13a,15,15a,15b,16-decahydro-2*H*-4,6-methanoindolo[3,2,1-*ij*]oxepino[2,3,4-*de*]pyrrolo[2,3-*h*]quinolin-14-one) was purchased from Sigma-Aldrich (CAS: 357-57-3, St. Louis, MO, USA) and used without further purification.

Compound **18** (diaboline or (4b*R*,7a*S*,8a*R*,13*R*,13a*R*,13b*R*)-13-hydroxy-5,6,7a,8,8a,11,13,13a,13b,14-decahydro-7,9-methanoindeno[1,2-*d*]oxepino[3,4-*f*]indole-14-carboxylic acid) showed NMR spectra identical to those reported in the literature [60].

Compound **19** (physostigmine or eserine or ((3a*R*,8b*S*)-3,4,8b-trimethyl-2,3a-dihydro-1*H*-pyrrolo[2,3-*b*]indol-7-yl) *N*-methylcarbamate) was purchased from MolPort (CAS: 57-47-6, Beacon, NY, USA) and used without further purification.

Compound **20** (holstiine or (15*Z*)-15-Ethylidene-10-hydroxy-17-methyl-11-oxa-8,17-diazapentacyclo[12.5.2.11,8.02,7.013,22]docosa-2,4,6-triene-9,20-dione) showed NMR spectra identical to those reported in the literature [61].

Compound **21** (pseudobrucine or (4a*R*,4a^1*R*,5a*R*,8a*S*,8a^1*S*,15a*S*)-5a-hydroxy-10,11-dimethoxy-4a^1,5,5a,7,8,8a^1,15,15a-octahydro-2*H*-4,6-methanoindolo[3,2,1-*ij*]oxepino[2,3,4-*de*]pyrrolo[2,3-*h*]quinolin-14(4a*H*)-one) was purchased from Fisherpharma (CAS: 560-30-5, Beacon, NY, USA) and used without further purification.

Compound **22** (retuline or 1-((3a*S*,5*R*,6*S*,6a*S*,11b*R*,*E*)-12-ethylidene-6-(hydroxymethyl)-1,2,4,5,6,6a-hexahydro-3,5-ethanopyrrolo[2,3-*d*]carbazol-7(3a*H*)-yl)ethanone) showed NMR spectra identical to those reported in the literature [62].

Compound **23** (serotonin or 3-(2-aminoethyl)-1H-indol-5-ol) was purchased from Sigma-Aldrich (CAS: 50-67-9, St. Louis, MO, USA) and used without further purification.

Compound **24** (triptamine hydrochloride or 2-(1*H*-indol-3-yl)ethan-1-amine hydrochloride) was purchased from Sigma-Aldrich (CAS: 343-94-2, St. Louis, MO, USA) and used without further purification.

Compound **25** (vomicine hydrochloride or (4a*R*,4a^1*R*,6a*S*,6a^1*S*,13a*S*)-10-hydroxy-16-methyl-4a,5,13,13a-tetrahydro-2*H*-6a,4-(ethanoiminomethano)indolo[3,2,1-*ij*]oxepino[2,3,4-*de*]quinoline-6,12(4a^1*H*,6a^1*H*)-dione hydrochloride) was purchased from MolPort (5969-84-6, Beacon, NY, USA) and used without further purification.

Compound **26** (vindoline or (3a*R*,3a^1*R*,4*R*,5*S*,5a*R*,10b*R*)-methyl 4-acetoxy-3a-ethyl-5-hydroxy-8-methoxy-6-methyl-3a,3a^1,4,5,5a,6,11,12-octahydro-1*H*-indolizino[8,1-*cd*]carbazole-5-carboxylate) was purchased from MolPort (CAS: 2182-14-1, Beacon, NY, USA) and used without further purification.

Compound **27** (akagerine or (*E*)-2-((3a*S*,5*R*,7*S*)-7-hydroxy-3-methyl-1,2,3,3a,4,5,6,7-octahydro-3,7a-diazacyclohepta[*jk*]fluoren-5-yl)but-2-enal) showed NMR spectra identical to those reported in the literature [63].

Compound **28** (canthin-6-one or 6*H*-indolo[3,2,1-*de*][1,5]naphthyridin-6-one) was purchased from MolPort (CAS: 479-43-6, Beacon, NY, USA) and used without further purification.

Compound **29** (α-carboline or 9*H*-pyrido[2,3-*b*]indole) was purchased from MolPort (CAS: 244-76-8, Beacon, NY, USA) and used without further purification.

Compound **30** (harmane or 1-methyl-9*H*-pyrido[3,4-*b*]indole) was purchased from Sigma-Aldrich (CAS: 486-84-0, St. Louis, MO, USA) and used without further purification.

Compound **31** (norharmane or 9*H*-pyrido[3,4-*b*]indole) was purchased from Sigma-Aldrich (CAS Number: 244-63-3, St. Louis, MO, USA) and used without further purification.

Compound **32** (harmine or 7-methoxy-1-methyl-9*H*-pyrido[3,4-*b*]indole) was purchased from Sigma-Aldrich (CAS: 442-51-3, St. Louis, MO, USA) and used without further purification.

Compound **33** (ibogaine or (6*R*,7*S*,11*S*)-7-ethyl-2-methoxy-6,6a,7,8,9,10,12,13-octahydro-5*H*-6,9-methanopyrido[1′,2′:1,2]azepino[4,5-*b*]indole) showed NMR spectra identical to those reported in the literature [38].

Compound **34** (mitragynine or (*E*)-methyl 2-((2*S*,3*S*,12b*S*)-3-ethyl-8-methoxy-1,2,3,4,6,7,12,12b-octahydroindolo[2,3-*a*]quinolizin-2-yl)-3-methoxyacrylate) was purchased from BOC Sciences (CAS: 4098-40-2, Shirley, NY, USA) and used without further purification.

Compound **35** (nigritanine or (2*S*,3*R*,12b*S*)-3-ethyl-2-(((*S*)-2-methyl-2,3,4,9-tetrahydro-1*H*-pyrido [3,4-*b*]indol-1-yl)methyl)-1,2,3,4,6,7,12,12b-octahydroindolo[2,3-*a*]quinolizine) showed NMR spectra identical to those reported in the literature [64]. The chemical characterization of compound **35** is reported below: Brown solid, m.p. 202-204°C; ^{1}H-NMR ($CDCl_3$, 400 MHz): 0.93 (t, J = 7 Hz, 3H, Me-C), 2.46 (s, 3H, Me-N), 3.56 (m, 1H, H-3), 6.40 (s, 1H, H-1 or H-1′), 7.80 (s, 1H, H-1 or H-1′); ^{13}C-NMR ($CDCl_3$, 101 MHz): 11.2 (C18), 20.7 (C6′), 21.5 (C6), 23.7 (C19), 41.9 (C20), 42.7 (N-CH_3), 34.9 (C14), 35.0 (C16), 35.8 (C15), 51.3 (C5′), 53.0 (C5), 58.6 (C17), 59.1 (C3), 60.2 (C21), 107.1 (C7), 108.8 (C7′), 110.8 (C12), 110.9 (C12′), 117.5 (C9 or C9′), 117.7 (C9 or C9′), 118.8 (C10 or C10′), 119.3 (C10 or C10′), 120.4 (C11 or C11′), 121.4 (C11 or C11′), 126.7 (C8), 127.0 (C8′), 134.7 (C2), 135.5 (C2′), 135.6 (C13 or C13′), 135.7 (C13 or C13′); m/z (ESI+) 452 (M+, 82%), 437 (6), 408 (10), 267 (8), 253 (12), 199 (27), 185 (100).

Compound **36** (paynantheine or (*E*)-methyl 3-methoxy-2-((2*S*,3*R*,12b*S*)-8-methoxy-3-vinyl-1,2,3,4,6,7,12,12b-octahydroindolo[2,3-*a*]quinolizin-2-yl)acrylate) was purchased from BOC Sciences (CAS: 4697-66-9, Shirley, NY, USA) and used without further purification.

Compound **37** (rhynchophylline or (*E*)-methyl 2-((1′*R*,6′*R*,7′*S*,8a′*S*)-6′-ethyl-2-oxo-3′,5′,6′,7′,8′,8a′-hexahydro-2′*H*-spiro[indoline-3,1′-indolizin]-7′-yl)-3-methoxyacrylate) was purchased from BOC Sciences (CAS: 76-66-4, Shirley, NY, USA) and used without further purification.

Compound **38** (speciociliatine or (*E*)-methyl 2-((2*S*,3*S*,12b*R*)-3-ethyl-8-methoxy-1,2,3,4,6,7,12,12b-octahydroindolo[2,3-*a*]quinolizin-2-yl)-3-methoxyacrylate) was purchased from BOC Sciences (CAS: 14382-79-7, Shirley, NY, USA) and used without further purification.

Compound **39** (yohimbine hydrochloride or (1*R*,2*S*,4a*R*,13b*S*,14a*S*)-methyl 2-hydroxy-1,2,3,4,4a,5,7,8,13,13b,14,14a-dodecahydroindolo[2′,3′:3,4]pyrido[1,2-*b*]isoquinoline-1-carboxylate hydrochloride) was purchased from Sigma-Aldrich (CAS: 65-19-0, St. Louis, MO, USA) and used without further purification.

4.2. Microorganisms and Cell Line

The reference Gram(+) and Gram(-) strains used for the antimicrobial tests were *S. aureus* ATCC 25923 and *E. coli* ATCC 25922, respectively. The multidrug-resistant clinical isolates of *S. aureus* (1a, 1b, and 1c) were kindly provided by Professor Giammarco Raponi (Sapienza, University of Rome).

HaCaT cells (AddexBio, San Diego, CA, USA) were cultured in Dulbecco's modified Eagle's medium supplemented with 4 mM glutamine (DMEMg), 10% heat-inactivated fetal bovine serum (FBS), and 0.1 mg/mL of penicillin and streptomycin at 37 °C and 5% CO_2, in 25 cm^2 or 75 cm^2 flasks.

4.3. Antimicrobial Assays

A bacterial culture inoculum was incubated at 37 °C in Luria–Bertani (LB) broth until reaching an optical density (O.D.) of 0.8 at 590 nm. For the inhibition zone assay, the bacterial culture was diluted 1:2000 and plated in LB-agarose plates. An aliquot (3 µL) of each compound at 5 mM was loaded into holes previously made in the agarose plates [65,66]. Afterwards, the plates were incubated overnight at 30 °C. Afterwards, the diameters of the inhibition zone were measured and reported in Tables 2 and 3.

For the determination of the MICs, 50 µL of bacterial suspension (2×10^5 cells/mL) in Mueller–Hinton broth (MH) was added to 50 µL MH containing serial dilutions of the compounds (from 256 µM to 2 µM) previously prepared in a 96-well plate. Controls consisted of vehicle-treated bacterial cells [67]. The plate was then incubated for 16 hours at 37 °C, and MIC was defined as the lowest concentration causing 100% visible inhibition of microbial growth. Afterwards, aliquots from the wells corresponding to the MIC of nigritanine (**35**) and to the control were withdrawn and plated onto LB agar plates for colony forming unit (CFU) counting and MBC determination.

4.4. Cytotoxicity Assays

To evaluate short-term cytotoxicity, selected alkaloids were tested on sheep red blood cells (OXOID, SR0051D). Aliquots of erythrocyte suspension (O.D. of 0.5 at 500 nm) in 0.9 % (*w*/*v*) NaCl were incubated for 40 min at 37 °C with three different concentrations (MIC, 2 × MIC, and 4 × MIC) of nigritanine (**35**) or the same concentrations of speciociliatine (**38**). The treated samples were then centrifuged for 5 min at 900× g. The amount of hemoglobin released in the supernatant by lysed red blood cells was measured at 415 nm using a microplate reader (Infinite M200; Tecan, Salzburg, Austria). The complete lysis was obtained by suspending erythrocytes in distilled water according to [68–70].

To evaluate the in vitro long-term cytotoxicity of nigritanine (**35**), a colorimetric method was employed. This assay is based on the intracellular reduction of the yellow tetrazolium salt MTT (Sigma-Aldrich, St. Luis, MO, USA) to purple formazan crystals by mitochondrial dehydrogenases of metabolically active cells. Therefore, the amount of purple color is directly proportional to the number of viable cells. About 4×10^4 HaCaT cells resuspended in DMEMg supplemented with 2% FBS, without antibiotics, were plated in each well of a 96-well plate. After overnight incubation in a humidified atmosphere containing 5% CO_2 at 37 °C, the medium was removed, and fresh serum-free DMEMg containing the compound at different concentration was added in each well. For controls, cells were treated with vehicle. The plate was incubated for 24 h at 37 °C and 5% CO_2. Afterwards, the medium was discarded, and 0.5 mg/mL of MTT in Hank's buffer (136 mM NaCl, 4.2 mM Na_2HPO_4, 4.4 mM KH_2PO_4, 5.4 mM KCl, 4.1 mM $NaHCO_3$, pH 7.2, supplemented with 20 mM D-glucose) was added to each well. After 4 h incubation at 37 °C and 5% CO_2, 100 µL of acidified isopropanol was added to each well, in order to dissolve the formazan crystals [71,72]. Absorbance was measured by a microplate reader (Infinite M200; Tecan, Salzburg, Austria) at 570 nm, and cell viability was calculated with respect to the control (cells in medium supplemented with vehicle).

4.5. Statistical Analysis

All data are expressed as the mean ± SD or SEM. Statistical analyses were performed using Student's t-test with the Prism software package (GraphPad, 6.0, San Diego, CA, USA), and the differences were considered to be statistically significant for $p < 0.05$.

Author Contributions: B.C. performed the microbiological assays; F.C. performed the cytotoxicity assays, M.R.L. partially contributed to the biological experiments. D.Q. and A.C. performed the acquisition and interpretation of the magnetic resonance spectroscopy (NMR) spectra of bioactive compounds and the determination of purity by High Performance Liquid Chromatography (HPLC). M.M. revised and edited the manuscript. B.B. provided overall guidance. F.G. and M.L.M. conceived the project and wrote the manuscript.

Funding: This work was supported by Italian Ministry of Education, University and Research—Dipartimenti di Eccellenza—L.232/2016 and Italian Institute of Technology. This work was also supported by grants from Sapienza University of Rome (project RM11816436113D8A).

Acknowledgments: We are grateful to Giammarco Raponi, Department of Public Health and Infectious Diseases, Sapienza University of Rome, for providing the clinical isolates.

Conflicts of Interest: The authors declare no conflict of interest.

References

1. Reygaert, W.C. An overview of the antimicrobial resistance mechanisms of bacteria. *AIMS Microbiol.* **2018**, *4*, 482–501. [CrossRef] [PubMed]
2. Ansari, S.; Jha, R.K.; Mishra, S.K.; Tiwari, B.R.; Asaad, A.M. Recent advances in *Staphylococcus aureus* infection: Focus on vaccine development. *Infect. Drug Resist.* **2019**, *12*, 1243–1255. [CrossRef] [PubMed]
3. Gajdacs, M. The continuing threat of methicillin-resistant *Staphylococcus aureus*. *Antibiotics* **2019**, *8*. [CrossRef] [PubMed]
4. Mermel, L.A.; Cartony, J.M.; Covington, P.; Maxey, G.; Morse, D. Methicillin-resistant *Staphylococcus aureus* colonization at different body sites: A prospective, quantitative analysis. *J. Clin. Microbiol.* **2011**, *49*, 1119–1121. [CrossRef] [PubMed]
5. Keihanian, F.; Saeidinia, A.; Abbasi, K. Epidemiology of antibiotic resistance of blood culture in educational hospitals in Rasht, North of Iran. *Infect. Drug Resist.* **2018**, *11*, 1723–1728. [CrossRef]
6. Chung, P.Y. Novel targets of pentacyclic triterpenoids in *Staphylococcus aureus*: A systematic review. *Phytomedicine Int. J. Phytother. Phytopharm.* **2019**. [CrossRef] [PubMed]
7. Calcaterra, A.; D'Acquarica, I. The market of chiral drugs: Chiral switches versus de novo enantiomerically pure compounds. *J. Pharm. Biomed. Anal.* **2018**, *147*, 323–340. [CrossRef]
8. Debnath, B.; Singh, W.S.; Das, M.; Goswami, S.; Singh, M.K.; Maiti, D.; Manna, K. Role of plant alkaloids on human health: A review of biological activities. *Mater. Today Chem.* **2018**, *9*, 56–72. [CrossRef]
9. Cushnie, T.P.T.; Cushnie, B.; Lamb, A.J. Alkaloids: An overview of their antibacterial, antibiotic-enhancing and antivirulence activities. *Int. J. Antimicrob. Agents* **2014**, *44*, 377–386. [CrossRef]
10. Ingallina, C.; D'Acquarica, I.; Delle Monache, G.; Ghirga, F.; Quaglio, D.; Ghirga, P.; Berardozzi, S.; Markovic, V.; Botta, B. The pictet-spengler reaction still on stage. *Curr. Pharm. Des.* **2016**, *22*, 1808–1850. [CrossRef]
11. Ghirga, F.; Bonamore, A.; Calisti, L.; D'Acquarica, I.; Mori, M.; Botta, B.; Boffi, A.; Macone, A. Green routes for the production of enantiopure benzylisoquinoline alkaloids. *Int. J. Mol. Sci.* **2017**, *18*. [CrossRef] [PubMed]
12. Amirkia, V.; Heinrich, M. Alkaloids as drug leads—A predictive structural and biodiversity-based analysis. *Phytochem. Lett.* **2014**, *10*. [CrossRef]
13. Infante, P.; Alfonsi, R.; Ingallina, C.; Quaglio, D.; Ghirga, F.; D'Acquarica, I.; Bernardi, F.; Di Magno, L.; Canettieri, G.; Screpanti, I.; et al. Inhibition of hedgehog-dependent tumors and cancer stem cells by a newly identified naturally occurring chemotype. *Cell Death Dis.* **2016**, *7*, E2376. [CrossRef] [PubMed]
14. Mori, M.; Tottone, L.; Quaglio, D.; Zhdanovskaya, N.; Ingallina, C.; Fusto, M.; Ghirga, F.; Peruzzi, G.; Crestoni, M.E.; Simeoni, F.; et al. Identification of a novel chalcone derivative that inhibits Notch signaling in T-cell acute lymphoblastic leukemia. *Sci. Rep.* **2017**, *7*, 2213. [CrossRef] [PubMed]
15. Infante, P.; Mori, M.; Alfonsi, R.; Ghirga, F.; Aiello, F.; Toscano, S.; Ingallina, C.; Siler, M.; Cucchi, D.; Po, A.; et al. Gli1/DNA interaction is a druggable target for Hedgehog-dependent tumors. *EMBO. J.* **2015**, *34*, 200–217. [CrossRef] [PubMed]
16. Srivastava, S.; Srivastava, M.; Misra, A.; Pandey, G.; Rawat, A. A review on biological and chemical diversity in Berberis (*Berberidaceae*). *Excli J.* **2015**, *14*, 247–267. [CrossRef]
17. Meyer, A.; Imming, P. Benzylisoquinoline alkaloids from the *Papaveraceae*: The heritage of Johannes Gadamer (1867–1928). *J. Nat. Prod.* **2011**, *74*, 2482–2487. [CrossRef]
18. Urzúa, A.P.A. Alkaloids from the bark of *Peumus boldus*. *Fitoterapia* **1983**, *54*, 175–177.
19. Imaki, N.M.Y.; Shimpuku, T.; Shirasaka, T. *A Process for Preparing Cotarnine*; Technical Report No. 4,963,684; U.S. Patent and Trademark Office: Washington, DC, USA, 1986.
20. Colombo, M.L.; Bosisio, E. Pharmacological activities of *Chelidonium majus* L. (*Papaveraceae*). *Pharmacol. Res.* **1996**, *33*, 127–134. [CrossRef]
21. Akinboye, E.; Bakare, O. Biological activities of emetine. *Open Nat. Prod. J.* **2011**, *411*, 8–15. [CrossRef]
22. Lapa, G.P.; Sheichenko, O.; Serezhechkin, A.G.N.; Tolkachev, O. HPLC determination of glaucine in yellow horn poppy grass (*Glaucium flavum* Crantz). *Pharm. Chem. J.* **2004**, *38*, 441–442. [CrossRef]

23. Brown, P.N.; Roman, M.C. Determination of hydrastine and berberine in goldenseal raw materials, extracts, and dietary supplements by high-performance liquid chromatography with UV: Collaborative study. *J. AOAC Int.* **2008**, *91*, 694–701. [PubMed]
24. Ramanathan, V.S.; Chandra, P. Recovery, separation and purification of narcotine and papaverine from Indian opium. *Bull. Narc.* **1981**, *33*, 55–64.
25. Lee, M.R. Curare: The South American arrow poison. *J. R. Coll. Physicians Edinb.* **2005**, *35*, 83–92. [PubMed]
26. Martins, D.; Nunez, C.V. Secondary metabolites from *Rubiaceae* species. *Molecules* **2015**, *20*, 13422–13495. [CrossRef] [PubMed]
27. Dellemonache, F.; Dellemonache, G.; Souza, M.A.D.; Cavalcanti, M.D.; Chiappeta, A. Isopentenylindole derivatives and other components of *Esenbeckia leiocarpa*. *Gazz. Chim. Ital.* **1989**, *119*, 435–439.
28. Guimaraes, H.A.; Braz-Filho, R.; Vieira, I.J.C. H-1 and C-13-NMR data of the simplest plumeran indole alkaloids isolated from *Aspidosperma* species. *Molecules* **2012**, *17*, 3025–3043. [CrossRef]
29. Galeffi, C.; Ciasca-Rendina, M.A.; Miranda Delle Monache, E.; Villar Del Fresno, A.; Marini Bettòlo, G.B. Gradient method for the counter-current separation of alkaloids using a heavy organic phase. *J. Chromatogr.* **1969**, *45*, 407–414. [CrossRef]
30. Zhao, B.; Moochhala, S.M.; Tham, S.Y. Biologically active components of *Physostigma venenosum*. *J. Chromatogr. B* **2004**, *812*, 183–192. [CrossRef]
31. Ohiri, F.C.; Verpoorte, R.; Baerheim Svendsen, A. The African *Strychnos* species and their alkaloids: A review. *J. Ethnopharmacol.* **1983**, *9*, 167–223. [CrossRef]
32. Mohammad-Zadeh, L.F.; Moses, L.; Gwaltney-Brant, S.M. Serotonin: A review. *J. Vet. Pharm.* **2008**, *31*, 187–199. [CrossRef] [PubMed]
33. Kousar, S.; Noreen Anjuma, S.; Jaleel, F.; Khana, J.; Naseema, S. Biomedical significance of tryptamine: A review. *J. Pharmacovigil.* **2017**, *5*. [CrossRef]
34. Song, K.M.; Park, S.W.; Hong, W.H.; Lee, H.; Kwak, S.S.; Liu, J.R. Isolation of vindoline from *Catharanthus roseus* by supercritical fluid extraction. *Biotechnol. Prog.* **1992**, *8*, 583–586. [CrossRef] [PubMed]
35. Noldin, V.F.; de Oliveira Martins, D.T.; Marcello, C.M.; da Silva Lima, J.C.; Delle Monache, F.; Cechinel Filho, V. Phytochemical and antiulcerogenic properties of rhizomes from *Simaba ferruginea* St. Hill. (*Simaroubaceae*). *Zeitschrift für Naturforschung C* **2005**, *60*, 701–706. [CrossRef]
36. Kumar, A.S.; Nagarajan, R. Synthesis of alpha-carbolines via Pd-catalyzed amidation and Vilsmeier-Haack reaction of 3-acetyl-2-chloroindoles. *Org. Lett.* **2011**, *13*, 1398–1401. [CrossRef]
37. Claudia, F.; Amaral, A.; Ramos, A.D.S.; Ferreira, J.; Santos, A.D.S.; Cruz, J.D.S.; De Luna, A.V.M.; Nery, V.V.C.; de Lima, I.C.; Chaves, M.H.d.C.; et al. LC-HRMS for the Identification of β-carboline and canthinone alkaloids isolated from natural sources. *Mass Spectrometry* **2017**, *187*. [CrossRef]
38. Alper, K.R. Ibogaine: A review. *Alkaloids. Chem. Biol.* **2001**, *56*, 1–38.
39. Takayama, H. Chemistry and pharmacology of analgesic indole alkaloids from the rubiaceous plant, *Mitragyna speciosa*. *Chem. Pharm. Bull.* **2004**, *52*, 916–928. [CrossRef]
40. Leon, F.; Habib, E.; Adkins, J.E.; Furr, E.B.; McCurdy, C.R.; Cutler, S.J. Phytochemical characterization of the leaves of *Mitragyna speciosa* grown in USA. *Nat. Prod. Commun.* **2009**, *4*, 907–910. [CrossRef]
41. Cinosi, E.; Martinotti, G.; Simonato, P.; Singh, D.; Demetrovics, Z.; Roman-Urrestarazu, A.; Bersani, F.S.; Vicknasingam, B.; Piazzon, G.; Li, J.H.; et al. Following the roots of kratom (*Mitragyna speciosa*): The evolution of an enhancer from a traditional use to increase work and productivity in Southeast Asia to a recreational psychoactive drug in western countries. *Biomed. Res. Int.* **2015**, 968786. [CrossRef]
42. Evans, W.C. *Pharmacopoeial and Related Drugs of Biological Origin*, 16th ed.; Saunders—Elsevier: Amsterdam, The Netherlands, 2009; pp. 353–416.
43. Dai, J.K.; Dan, W.J.; Schneider, U.; Wang, J.R. β-Carboline alkaloid monomers and dimers: Occurrence, structural diversity, and biological activities. *Eur. J. Med. Chem.* **2018**, *157*, 622–656. [CrossRef] [PubMed]
44. Dai, J.K.; Dan, W.J.; Ren, S.Y.; Shang, C.G.; Wang, J.R. Design, synthesis and biological evaluations of quaternization harman analogues as potential antibacterial agents. *Eur. J. Med. Chem.* **2018**, *160*, 23–36. [CrossRef] [PubMed]
45. Nenaah, G. Antibacterial and antifungal activities of (β)-carboline alkaloids of *Peganum harmala* (L) seeds and their combination effects. *Fitoterapia* **2010**, *81*, 779–782. [CrossRef] [PubMed]
46. Mohammad Reza, V.R.; Hadjiakhoondi, A. Cytotoxicity and antimicrobial activity of harman alkaloids. *J. Pharmacol. Toxicol.* **2007**, *2*, 677–680. [CrossRef]

47. Parthasarathy, S.; Bin Azizi, J.; Ramanathan, S.; Ismail, S.; Sasidharan, S.; Said, M.I.; Mansor, S.M. Evaluation of antioxidant and antibacterial activities of aqueous, methanolic and alkaloid extracts from *Mitragyna speciosa* (*Rubiaceae* family) leaves. *Molecules* **2009**, *14*, 3964–3974. [CrossRef]
48. Benziane Maatalah, M.; Kambuche Bouzidi, N.; Bellahouel, S.; Merah, B.; Fortas, Z.; Soulimani, R.; Saidi, S.; Derdour, A. Antimicrobial activity of the alkaloids and saponin extracts of *Anabasis articulate*. *J. Biotechnol. Pharm. Res.* **2012**, *3*, 54.
49. Ozcelik, B.; Kartal, M.; Orhan, I. Cytotoxicity, antiviral and antimicrobial activities of alkaloids, flavonoids, and phenolic acids. *Pharm. Biol.* **2011**, *49*, 396–402. [CrossRef]
50. Gurrapu, S.; Estari, M. In vitro antibacterial activity of alkaloids isolated from leaves of *Eclipta alba* against human pathogenic bacteria. *Pharmacogn. J.* **2017**, *9*, 573–577. [CrossRef]
51. Karou, D.; Savadogo, A.; Canini, A.; Yameogo, S.; Montesano, C.; Simpore, J.; Colizzi, V.; Traore, A.S. Antibacterial activity of alkaloids from *Sida acuta*. *Afr. J. Biotechnol.* **2006**, *5*, 195–200.
52. Slobodnikova, L.; Kost'alova, D.; Labudova, D.; Kotulova, D.; Kettman, V. Antimicrobial activity of *Mahonia aquifolium* crude extract and its major isolated alkaloids. *Phytother. Res.* **2004**, *18*, 674–676. [CrossRef]
53. Su, Y.F.; Li, S.K.; Li, N.; Chen, L.L.; Zhang, J.W.; Wang, J.R. Seven alkaloids and their antibacterial activity from *Hypecoum erectum* L. *J. Med. Plants Res.* **2011**, *5*, 5428–5432.
54. Manosalva, L.; Mutis, A.; Urzua, A.; Fajardo, V.; Quiroz, A. Antibacterial activity of alkaloid fractions from *Berberis microphylla* G. Forst and study of synergism with ampicillin and cephalothin. *Molecules* **2016**, *21*, 76. [CrossRef] [PubMed]
55. Tegos, G.; Stermitz, F.R.; Lomovskaya, O.; Lewis, K. Multidrug pump inhibitors uncover remarkable activity of plant antimicrobials. *Antimicrob. Agents Chemother.* **2002**, *46*, 3133–3141. [CrossRef] [PubMed]
56. Locher, H.H.; Ritz, D.; Pfaff, P.; Gaertner, M.; Knezevic, A.; Sabato, D.; Schroeder, S.; Barbaras, D.; Gademann, K. Dimers of nostocarboline with potent antibacterial activity. *Chemotherapy* **2010**, *56*, 318–324. [CrossRef] [PubMed]
57. Soong, G.; Paulino, F.; Wachtel, S.; Parker, D.; Wickersham, M.; Zhang, D.; Brown, A.; Lauren, C.; Dowd, M.; West, E.; et al. Methicillin-resistant Staphylococcus aureus adaptation to human keratinocytes. *mBio* **2015**, *6*, e00289-15. [CrossRef] [PubMed]
58. Malikova, J.; Zdarilova, A.; Hlobilkova, A.; Ulrichova, J. The effect of chelerythrine on cell growth, apoptosis, and cell cycle in human normal and cancer cells in comparison with sanguinarine. *Cell Biol. Toxicol.* **2006**, *22*, 439–453. [CrossRef] [PubMed]
59. Zhou, Z.S.; Li, M.; Gao, F.; Peng, J.Y.; Xiao, H.B.; Dai, L.X.; Lin, S.R.; Zhang, R.; Jin, L.Y. Arecoline suppresses HaCaT cell proliferation through cell cycle regulatory molecules. *Oncol. Rep.* **2013**, *29*, 2438–2444. [CrossRef] [PubMed]
60. Delle Monache, F.C.; Rossi, E.; Cartoni, C.; Carpi, A.; Marini Bettolo, G.B. The alkaloids of *Strychnos castelneana*. *Strychnos Alkaloids* **1970**, *33*, 279–283.
61. Martin, G.E. Configuration and total assignment of the ^{1}H-and ^{13}C-NMR spectra of the alkaloid holstiine. *J. Nat. Prod.* **1990**, *53*, 793–800.
62. Tavernier, D.; Anteunis, M.; Tits, M.; Angenot, L. The 1H NMR spectra of the strychnos alkaloids retuline isoretuline, and their N-deacetyl compounds. *Bull. Des Sociétés Chim. Belg.* **2010**, *87*, 595–607. [CrossRef]
63. Cao, M.; Muganga, R.; Nistor, I.; Tits, M.; Angenot, L.; Frederich, M. LC–SPE–NMR–MS analysis of *Strychnos usambarensis* fruits from Rwanda. *Phytochem. Lett.* **2012**, *5*, 170–173. [CrossRef]
64. Nicoletti, M.; Oguakwa, J.U.; Messana, I. On the alkaloids of two African *Strychnos*: *Strychnos nigritana* bak and *Strychnos barteri* Sol. carbon-13 NMR spectroscopy of nigritanins. *Fitoterapia* **1980**, *87*, 595–607.
65. Islas-Rodriguez, A.E.; Marcellini, L.; Orioni, B.; Barra, D.; Stella, L.; Mangoni, M.L. Esculentin 1-21: A linear antimicrobial peptide from frog skin with inhibitory effect on bovine mastitis-causing bacteria. *J. Pept. Sci. Off. Publ. Eur. Pept. Soc.* **2009**, *15*, 607–614. [CrossRef] [PubMed]
66. Mangoni, M.L.; Fiocco, D.; Mignogna, G.; Barra, D.; Simmaco, M. Functional characterisation of the 1–18 fragment of esculentin-1b, an antimicrobial peptide from *Rana esculenta*. *Peptides* **2003**, *24*, 1771–1777. [CrossRef] [PubMed]
67. Falciani, C.; Lozzi, L.; Pollini, S.; Luca, V.; Carnicelli, V.; Brunetti, J.; Lelli, B.; Bindi, S.; Scali, S.; Di Giulio, A.; et al. Isomerization of an antimicrobial peptide broadens antimicrobial spectrum to gram-positive bacterial pathogens. *PLoS ONE* **2012**, *7*, e46259. [CrossRef] [PubMed]

68. Buommino, E.; Carotenuto, A.; Antignano, I.; Bellavita, R.; Casciaro, B.; Loffredo, M.R.; Merlino, F.; Novellino, E.; Mangoni, M.L.; Nocera, F.P.; et al. The outcomes of decorated prolines in the discovery of antimicrobial peptides from Temporin-L. *ChemMedChem* **2019**, *14*, 1283–1290. [CrossRef] [PubMed]
69. Merlino, F.; Carotenuto, A.; Casciaro, B.; Martora, F.; Loffredo, M.R.; Di Grazia, A.; Yousif, A.M.; Brancaccio, D.; Palomba, L.; Novellino, E.; et al. Glycine-replaced derivatives of [Pro(3),DLeu(9)]TL, a temporin L analogue: Evaluation of antimicrobial, cytotoxic and hemolytic activities. *Eur. J. Med. Chem.* **2017**, *139*, 750–761. [CrossRef]
70. Grieco, P.; Carotenuto, A.; Auriemma, L.; Saviello, M.R.; Campiglia, P.; Gomez-Monterrey, I.M.; Marcellini, L.; Luca, V.; Barra, D.; Novellino, E.; et al. The effect of d-amino acid substitution on the selectivity of temporin L towards target cells: Identification of a potent anti-Candida peptide. *Biochimica et Biophysica Acta* **2013**, *1828*, 652–660. [CrossRef]
71. Cappiello, F.; Di Grazia, A.; Segev-Zarko, L.A.; Scali, S.; Ferrera, L.; Galietta, L.; Pini, A.; Shai, Y.; Di, Y.P.; Mangoni, M.L. Esculentin-1a-derived peptides promote clearance of *Pseudomonas aeruginosa* internalized in bronchial cells of cystic fibrosis patients and lung cell migration: Biochemical properties and a plausible mode of action. *Antimicrob. Agents Chemother.* **2016**, *60*, 7252–7262. [CrossRef]
72. Di Grazia, A.; Luca, V.; Segev-Zarko, L.A.; Shai, Y.; Mangoni, M.L. Temporins A and B stimulate migration of HaCaT keratinocytes and kill intracellular *Staphylococcus aureus*. *Antimicrob. Agents Chemother.* **2014**, *58*, 2520–2527. [CrossRef]